Formation of ternary alkaline earth/uranium/carbonate complexes. Thermodynamic data and their influence on uranium speciation and solubility in different geochemical environments

Chengming Shang

THESE DE DOCTORAT

NNT : 2021UPASF058

université PARIS-SACLAY

Formation of ternary alkaline earth/uranium/carbonate complexes. Thermodynamic data and their influence on uranium speciation and solubility in different geochemical environments

Thèse de doctorat de l'université Paris-Saclay

École doctorale n°571, Sciences chimiques : molécules, matériaux, instrumentation et biosystèmes (2MIB)
Spécialité de doctorat: Chimie
Unité de recherche : Université Paris-Saclay, CEA, Service d'Études Analytiques et de Réactivité des Surfaces, 91191, Gif-sur-Yvette, France
Graduate School : Chimie. Référent : Faculté des sciences d'Orsay

Thèse présentée et soutenue à Paris-Saclay, le 15 décembre 2021, par

Chengming SHANG

Composition du Jury

Pascal PERNOT Directeur de Recherche, CNRS, Université Paris-Saclay	Président du jury
Mireille DEL NERO Chargée de recherche, HDR, IPHC, Université de Strasbourg	Rapporteure & Examinatrice
Xavier GAONA MARTINEZ Professeur, KIT - Karlsruhe Institute of Technology	Rapporteur & Examinateur
Gilles MONTAVON Directeur de recherche, CNRS, Université de Nantes	Examinateur
Lara DURO Docteure, Amphos XXI	Examinatrice
Stéphane BRASSINES Docteur, ONDRAF - NIRAS	Examinateur

Direction de la thèse

Pascal E. REILLER Directeur de recherche, CEA, Université Paris-Saclay	Directeur de thèse

université PARIS-SACLAY

ÉCOLE DOCTORALE
Sciences Chimiques: Molécules, Matériaux, Instrumentation et Biosystèmes (2MIB)

Titre : Formation des complexes ternaires alcalino-terreux/uranium/carbonate. Données thermodynamiques et influence sur la spéciation et la solubilité de l'uranium dans différents contextes géochimiques

Mots clés : Uranium, Métaux alcalino-terreux, Carbonate

Résumé : La formation des complexes carbonate d'uranyle(VI) est primordiale pour la compréhension de la chimie et du transport de l'uranium. Les complexes ternaires triscarbonato-uranyle d'alcalino-terreux, $M_n[UO_2(CO_3)_3]^{(4-2n)-}$ (M = Mg^{2+} et Ca^{2+}) mis en évidence depuis la fin des années 1990, sont susceptibles de contrôler la chimie de l'uranium – et donc sa solubilité ou ses propriétés d'adsorption – dans des environnements variés, depuis l'eau de mer jusqu'aux milieux géologiques de stockage. Les données thermodynamiques de ces complexes restent sujettes à controverses. En plus des alcalino-terreux, l'influences des cations alcalins n'est pas claires entre l'influence de la force ionique de la solution ou l'influence des ions alcalins sur la structure des complexes. Ce travail de thèse se propose de clarifier les domaines d'existence des complexes $M_n[UO_2(CO_3)_3]^{(4-2n)-}$ en fonction de la force ionique en étudiant l'influence additionnelle des cations alcalins. Le choix de la technique analytique s'est porté sur la spectrofluorimétrie laser à résolution temporelle (SLRT). La quantification des mesures de luminescence des complexes $M_n[UO_2(CO_3)_3]^{(4-2n)-}$ est faite pour les analyses laboratoires. La présence des complexes étudiées dans les échantillons synthétiques peut être vérifiée par les bandes caractéristiques et les temps de décroissance. Dans ce travail, les données thermodynamiques en réponse à la température et à la force ionique pour les complexes $(Mg/Ca)_nUO_2(CO_3)_3^{(4-2n)-}$ en milieux NaCl et $NaClO_4$ sont très utiles pour estimer les effets de la température et de la salinité sur la spéciation de l'U(VI), en particulier dans les dépôts de déchets nucléaires, et pour combler les lacunes dans la base de données thermodynamiques pour ces complexes étudiées.

Title : Formation of ternary alkaline earth/uranium/carbonate complexes. Thermodynamic data and their influence on uranium speciation and solubility in different geochemical environments

Keywords : Uranium, Alkaline earth metal, Carbonate

Abstract : The formation of carbonato complexes of uranyl(IV) is of great importance for the understanding of the chemistry and transport of uranium. The ternary alkaline-earth triscarbonato-uranyl complexes, $M_n[UO_2(CO_3)_3]^{(4-2n)-}$ (M = Mg^{2+} and Ca^{2+}), evidence in the late 1990's, can control the uranium chemistry – and its solubility and adsorption properties – in various environments, including deep geological disposal, surface waters, and seawater. Thermodynamic data for these ternary complexes are still a matter of debate. In addition of alkaline-earths, the influence of alkaline cations is not clearly settled between the ionic strength effect and the influence on the structure of complexes. The aim of this thesis is to clarify the existence domains of $M_n[UO_2(CO_3)_3]^{(4-2n)-}$ complexes as a function of ionic strength by studying the additional influence of alkali ions. Time- resolved laser spectrofluorimetry (TRLFS), a highly sensitive technique to probe the characteristic features of uranium species, was chosen as the analytical technique in this work. The quantification of $M_n[UO_2(CO_3)_3]^{(4-2n)-}$ complexes from luminescence measurements was done for laboratory analysis. The presence of the studied complexes in the synthetic samples can be verified by their characteristic bands and decay times. In this work, the thermodynamic data with respect to temperature and ionic strength for the $(Mg/Ca)_nUO_2(CO_3)_3^{(4-2n)-}$ complexes in NaCl et $NaClO_4$ media are very useful for estimating the effects of temperature and salinity on the speciation of U(VI), especially in nuclear waste repositories, and for filling in the gaps in the thermodynamic database for these complexes.

Remerciements

Le travail de recherche présenté dans ce manuscrit de thèse a été réalisé au Laboratoire de développement Analytique Nucléaire Isotopique et Elémentaire (LANIE) au sein de Service d'Etudes Analytiques et de Réactivité des Surfaces (SEARS) au CEA à Saclay. Cette thèse a bénéficié d'un financement de l'Organisme national des déchets radioactifs et des matières fissiles enrichies en Belgique (ONDRAF-NIRAS). Si cette thèse représente un travail personnel, je profite de cette occasion pour rendre hommage et remercier toutes les personnes qui ont contribué à la réalisation de cette recherche.

Mes premiers remerciements s'adressent naturellement à mon directeur et encadrant de thèse, M. Pascal E. Reiller pour la qualité de sa direction, ses compétences hautement spécialisées et sa disponibilité qui m'ont permis de mener à bien ce projet. Je lui suis également reconnaissante pour ses écoutes continues, ses conseils précieux, ses soutiens solides, son humour habituel et ses réelles qualités humaines qui m'ont permis de travailler dans les meilleures conditions, tout au long de la période de cette thèse, y compris celle de stage d'avant.

Mettre le remerciement pour Stéphane Brassinnes (ONDRAF-NIRAS) ici en tant que financeur de thèse, et peut-être aussi pour Michael Descostes pour avoir suivi le travail de thèse (et fourni fait fournir les échantillons

Je tiens aussi à remercier Mme Mireille Del Nero et M. Xavier Gaona Martinez d'avoir accepté de rapporter cette thèse. Je remercie également MM. Pascal Pernot et Gilles Montavon, et Mme Lara Duro pour avoir bien voulu faire partie de jury.

Je remercie MM. Lionel Gosmain et Thomas Vercouter pour leur accueil sympathique au sein du SEARS et du LANIE .

Mes remerciements vont aussi à Hélène Isnard et Michel Schlegel pour leurs nombreux conseils et avis qu'ils m'ont donnés ainsi qu'à Michel Tabarant et Erwan Dupuis pour l'aide technique qu'ils m'ont apporté.

J'adresse également mes sincères remerciements aux membres des Pigeons : Lana Abou Zeid, Thibault Vital, Florian Le Dantec, Anne-Sophie Pires de Almeida... et tous les membres du SEARS et du bâtiment 391 que je n'ai pas cités pour la sympathie qu'ils ont créée dans le bâtiment grâce à laquelle j'ai pu finaliser ce travail de thèse tranquillement.

Enfin, je remercie toute ma famille, mes amis, mes camarades, pour leur soutien et leurs encouragements lors des périodes difficiles pendent la réalisation de cette thèse.

Résumé étendu

La formation des complexes carbonate d'uranyl(VI) (UO_2^{2+}) est importante pour la compréhension de la chimie et du comportement de l'uranium dans la biosphère afin d'évaluer des risques sanitaires et environnementaux de l'industrie nucléaire. Le comportement de l'uranium en milieux aqueux est fortement associé à sa spéciation vis-à-vis d'un environnement spécifique, autrement dit la répartition entre ses différentes formes d'espèces physico-chimiques. Dans le procédé d'évaluation pour les environnements variés, dont l'eau de mer ou les milieux géologiques de stockage, l'uranium fait l'objet de nombreux contrôles analytiques notamment dans les milieux où ses teneurs sont comprises entre le µg L^{-1} et le mg L^{-1} qui permet à l'exploitant de prédire les évolutions de l'uranium ou suivre les contrôles environnementaux.

Cependant, si ces contrôles sont indispensables, les outils utilisés pour la prédiction de la spéciation de l'uranium, surtout les données thermodynamiques, ne répondent pas parfaitement aux besoins. De plus, la recherche faite au cours des années dans ce domaine permet de restreindre le sujet à la complexation de l'uranium par le carbonate et les éléments alcalino-terreux qui sont fréquemment rencontrés en teneurs importantes dans des environnements naturels. En effet, les complexes ternaires triscarbonato-uranyl d'alcalino-terreux $M_nUO_2(CO_3)_3^{(4-2n)-}$, découverts à la fin des années 1990, sont susceptibles de contrôler la chimie de l'uranium et donc sa solubilité ou ses propriétés d'adsorption en milieu naturel. Néanmoins, les données thermodynamiques de ces complexes restent sujettes à controverses. Les calculs d'équilibre thermodynamiques, permettant l'établissement de diagrammes de spéciation, à partir des constantes de complexation permet de définir les conditions analytiques de formation des complexes considérés. En plus des alcalino-terreux, l'influence des cations alcalins n'est pas claire entre l'influence de la force ionique de la solution ou l'influence des ions alcalins sur la structure des complexes.

Ce travail de thèse se propose de clarifier les constantes et fonctions thermodynamiques, ainsi que les domaines d'existence des complexes $M_nUO_2(CO_3)_3^{(4-2n)-}$ en fonction de la force ionique, en étudiant l'influence additionnelle des cations alcalins. De par les informations quantitatives et structurales que l'on peut obtenir, le choix de la technique analytique s'est porté sur la spectrofluorimétrie laser à résolution temporelle (SLRT) pour les études des complexes $M_nUO_2(CO_3)_3^{(4-2n)-}$.

La SLRT est développée depuis plusieurs années au Commissariat à l'Energie Atomique et aux Energies Alternatives à Saclay, dernièrement au Laboratoire de développement Analytique

Nucléaire Isotopique et Elémentaire (LANIE). Le principe de la fluorescence est fondé sur les propriétés de luminescence de l'uranium au degré d'oxydation +VI. Lorsqu'il est soumis à une excitation lumineuse, l'uranium(VI) peut émettre une fluorescence (émission de l'état singulet excité à différents niveaux vibrationnels de l'état fondamental) caractéristique de couleur allant du bleu au jaune (majoritairement verte). Pour les atomes lourds comme les lanthanides[*] et actinides,[†] la phosphorescence (émission de l'état triplet à différents niveaux vibrationnels de l'état fondamental)peut se produire en même temps que la fluorescence. Ainsi, le terme luminescence s'utilisera dans ce travail de thèse pour décrire le processus de désexcitation de l'uranium(VI). La mesure de luminescence à proprement parlé consiste à détecter le signal de luminescence émis par les complexes d'uranium étudiés et à relier l'intensité de ce signal à la variation de concentration en complexe d'uranium(VI).

Cette mesure se réalise à l'aide d'un spectrofluorimètre. La quantification des mesures de luminescence d'uranium(VI) total se fait par la méthode des ajouts dosés en milieu acide phosphorique 5% pour les analyses de laboratoire. L'utilisation d'un laser pulsé présente l'avantage d'émettre une grande énergie d'excitation pendant une durée d'impulsion très courte et ainsi d'atteindre une limite de détection basse de l'ordre de 0.1 ng L^{-1} (≈ 23.8 ppt) pour l'uranium. Le principe consiste à détecter le signal de luminescence de l'uranium(VI) à un instant approprié après l'excitation pulsée qui permet de gagner en sélectivité en s'affranchissant les luminescences parasites à durée de vie courte.

Dans le cas de l'étude de complexes, tels que les complexes $M_nUO_2(CO_3)_3^{(4-2n)-}$, la présence des complexes étudiées dans les échantillons synthétiques peut être vérifiée par la variations des bandes de luminescence caractéristiques et les temps de décroissance. Cependant, la SLRT est très dépendante du milieu. Certains anions sont plutôt favorables à l'émission de luminescence de l'uranium grâce à l'effet complexant, par exemple PO_4^{3-} ou SO_4^{2-}. Cet effet peut également donner lieu à une inhibition de la luminescence vis-à-vis de l'uranyle chez certains anions, par exemple, les anions halogènes. Outre ces derniers, les anions perchlorates ClO_4^-, sous certaines conditions de concentration, possèdent la capacité complexant la moins forte à l'égard de l'uranyle, ce qui permet de diminuer la compétition entres les ligands inertes et les complexants en solution dans l'étude de complexation d'uranyle. Dans cette optique, cette thèse traite de la formation des complexes $M_nUO_2(CO_3)_3^{(4-2n)-}$ dans les électrolytes de fond NaCl et $NaClO_4$ dont le premier—l'ion chlorure—est l'ion le plus souvent trouvé en milieu naturel,

[*] Pr(III), Nd(III), Sm(III), Eu(II), Eu(III), Gd(III), Tb(III), Dy(III), Ho(III), Er(III), Tm(III)
[†] U(VI), Am(III) et Cm(III)

malgré son effet d'inhibition de la luminescence, et le second qui permet d'élargir le plus que possible le domaine expérimental de force ionique, ou d'interaction avec l'ion alcalin Na^+.

Le travail de thèse commence par étudier la formation de $Ca_nUO_2(CO_3)_3^{(4-2n)-}$ en milieu NaCl dans une gamme de force ionique la plus large que possible en tenant compte de la luminescence des espèces d'uranyle tricarbonate. Notre attention s'est focalisée sur l'application de la SLRT pour acquérir les propriétés caractéristiques de luminescence des complexes d'intérêt. Ce premier aspect est très important pour le déroulé des études suivantes. Son principal objectif est de vérifier l'efficacité de la méthode par titrage simultané du pH et du Ca^{2+} utilisée dans cette recherche qui est différente de la méthode classique du titrage à pH constant et concentration en Ca variable. L'introduction de coefficient de Ringböm permet de quantifier la teneur en $UO_2(CO_3)_3^{4-}$ en fonction du pH qui permet d'éviter la précipitation de calcite ($CaCO_3$) ou schoepite ($UO_3{:}2H_2O$) au cours du titrage de $UO_2(CO_3)_3^{4-}$ par Ca^{2+}. La limite supérieure en force ionique a été fixée à 1 mol kg_w^{-1} à cause de l'inhibition de luminescence de l'uranium(VI) par les ions chlorure. Lorsque la force ionique est élevée, son influence sur les attractions et répulsions entre ions, ainsi que les effets qui se produisent par suite d'une interaction collisionnelle, seront importants sur l'inhibition dynamique de luminescence. Néanmoins, vu l'importance environnementale des ions chlorure, les acquisitions des spectres de luminescence des complexes $Ca_nUO_2(CO_3)_3^{(4-2n)-}$ ont été effectuées pour la force ionique comprise entre 0,1 et 1 mol kg_w^{-1} NaCl.

Les spectres de luminescence des espèces d'uranyle tricarbonate sont généralement résolus en cinq bandes situées à environ 466, 485, 505, 526 et 549 nm, en bon accord avec les valeurs de la littérature. Il est évident que ces positions de pics sont décalées vers le bleu (déplacement hypsochrome) comparées à celles de l'uranyle. Les profiles spectraux de luminescence et les positions caractéristiques ne montrent aucun changement au cours du titrage en forces ioniques différentes à la résolution d'un spectromètre équipé d'un réseau à 300 traits mm^{-1}. Pour identifier la stœchiométrie du calcium, les analyses de pente, corrigées du coefficient de Ringböm de $UO_2(CO_3)_3^{4-}$, ont été appliquées dans ce travail. Des ajustements linéaires satisfaisants ont permis d'évaluer les constantes de formation conditionnelle de $Ca_nUO_2(CO_3)_3^{(4-2n)-}$ à chaque valeur de force ionique d'intérêt. Dans le cadre de cette thèse, la théorie de l'interaction spécifique (SIT) a été employé pour réaliser les extrapolations des constantes de formation à dilution infinie. Les résultats de $\log_{10}\beta°(Ca_nUO_2(CO_3)_3^{(4-2n)-})$ sont cohérents avec les données précédemment acquises dans la littérature. Cependant, les coefficients d'interactions spécifiques s'avèrent très différents des données estimées par

analogie—$\varepsilon(UO_2(CO_3)_2^{2-},Na^+) = \varepsilon(CaUO_2(CO_3)_3^{2-},Na^+)$—ou d'après les hypothèses classiques de la SIT—$\varepsilon(Ca_2UO_2(CO_3)_3,NaCl) = 0$. Cette différence souligne que la valeur conventionnellement adoptée de $\varepsilon(UO_2(CO_3)_2^{2-},Na^+) = -0.02$ kg_w mol^{-1} à $\varepsilon(CaUO_2(CO_3)_3^{2-}, Na^+)$, et la valeur nulle attribuée à $\varepsilon(Ca_2UO_2(CO_3)_3, Na^+)$ ne sont semblent pas valable.

Comme l'inhibition de la luminescence par les ions chlorures a limité notre première étude à des valeurs de force ionique de 1 mol kg_w^{-1} en NaCl, l'effort d'étendre cette méthode à des concentrations d'électrolyte plus élevés et d'acquérir plus de données expérimentales a été rendue nécessaire. Par conséquent, dans la deuxième partie, le milieu $NaClO_4$ moins inhibant de la luminescence de l'uranium(VI), a été utilisé pour obtenir l'extrapolation des constantes de formation à dilution infinie et les paramètres d'interaction spécifiques des complexes $Ca_nUO_2(CO_3)_3^{(4-2n)-}$ sur une échelle de force ionique plus large. La limite supérieure de la force ionique a été fixé à 2,46 mol kg_w^{-1} en raison de l'effet d'inhibition observé à plus forte concentration en perchlorate. D'après les analyses de pente et les extrapolations utilisant la formule SIT, les constantes de formation $\log_{10}\beta°(Ca_nUO_2(CO_3)_3^{(4-2n)-})$ sont en excellent accord avec notre détermination précédente en milieu NaCl. Cependant, les coefficients d'interactions spécifiques sont différentes entre NaCl et $NaClO_4$. Le changement d'anion du milieu aqueux de Cl^- à ClO_4^- conduit à une diminution notable des valeurs de ε pour le même complexe. Plusieurs modèles ont été testés pour décrire la tendance des données expérimentales avec une variation de ε en fonction de la force ionique qui permet de prédire les valeurs de $\log_{10}\beta(Ca_nUO_2(CO_3)_3^{(4-2n)-})$ jusqu'à 6 mol kg_w^{-1} en $NaClO_4$. Les résultats suggèrent que la formation de paires d'ions entre Ca^{2+} et ClO_4^- ou Cl^- peut exacerber la compétition pour Ca^{2+} entre $UO_2(CO_3)_3^{4-}$ et ClO_4^-/Cl^-. Il est fort probable que les interactions ioniques soient très complexes dans ce système, notamment en concentration d'électrolyte élevée où les interactions des ions constituant le milieu ne se limitent plus à la phase binaire— les ions inertes peuvent alors intervenir dans les réactions. Des questions sont ainsi soulevées pour estimer dans quelle mesure Na^+ est compétitif pour se lier à $UO_2(CO_3)_3^{4-}$ et $CaUO_2(CO_3)_3^{2-}$ par rapport à Ca^{2+}, et si Ca^{2+} est encombré par la formation de paires d'ions avec de anions comme ClO_4^-/Cl^-. Les discussions, détaillées dans le Chapitre 3, portent sur la nécessité de considérer attentivement les formations des paires d'ions et l'affinité de Na^+ avec $Ca_nUO_2(CO_3)_3^{(4-2n)-}$ à des forces ioniques élevées.

La troisième partie de ce document porte sur la détermination des données thermodynamiques des complexes $Mg_nUO_2(CO_3)_3^{(4-2n)-}$ dans les mêmes gammes de forces ioniques en NaCl et $NaClO_4$ que pour $Ca_nUO_2(CO_3)_3^{(4-2n)-}$. Cette partie vise à compléter la chimie de ces complexes d'intérêt. L'utilisation de la même approche est importante pour

éliminer les incertitudes systématiques et donc pour évaluer les résultats expérimentaux avec une fiabilité maximale. Deux réseaux de 300 et 1800 traits mm^{-1} ont été utilisés séparément pour acquérir les spectres de luminescence de $Mg_nUO_2(CO_3)_3^{(4-2n)-}$. A l'aide du réseau de 1800 traits mm^{-1}, nous avons pu détecter de faibles décalages des bandes caractéristiques vers le rouge (déplacement bathochrome) pour $Mg_nUO_2(CO_3)_3^{(4-2n)-}$, qui n'était pas visibles avec le réseau de 300 traits mm^{-1}. D'après l'analyse de pente, une seule espèce $MgUO_2(CO_3)_3^{2-}$ a été identifiée. De plus, il a été observé que la variation des constantes de formation conditionnelles en fonction de la force ionique se comportent de façon similaire à $CaUO_2(CO_3)_3^{2-}$ dans les deux types d'électrolyte—NaCl et $NaClO_4$—, ce qui se traduit par des valeurs des paramètres d'interaction ε très proches. Les résultats soulignent encore une fois l'importance des interactions ioniques à courte distance en solution concentrée. Les applications de ces données thermodynamiques des complexes $M_nUO_2(CO_3)_3^{(4-2n)-}$ ont été refaites pour plusieurs cas particuliers.

Cependant, un manque de connaissances sur les paramètres thermodynamiques avec la température pour ces complexes $M_nUO_2(CO_3)_3^{(4-2n)-}$ rend difficile la prédiction du comportement chimique de l'uranium dans le champ proche des dépôts de déchets radioactifs, où un gradient de température significatif s'impose au cours du temps. Donc, nous avons ensuite mesuré les constantes de formation à températures variables, et ajusté aux différents modèles d'approximation—l'équation de Van't Hoff, le modèle de capacité thermique constante, l'équation DQUANT et la modification isoélectrique—pour déduire leurs fonctions thermodynamiques—enthalpie $\Delta_rH°_m$, entropie $\Delta_rS°_m$, capacité thermique $\Delta_rC_p°_m$. En augmentant la température, l'évolution des positions des bandes spectrales avec l'augmentation de $[Mg^{2+}]/[Ca^{2+}]$ permet de distinguer les spectres individuels des espèces concernées, notamment à des températures plus élevées, c'est-à-dire 40, 45 et 50°C, où les décalages de bande étaient évidents.

Dans ce travail de thèse, les données thermodynamiques en réponse à la température et à la force ionique pour les complexes $M_nUO_2(CO_3)_3^{(4-2n)-}$ en milieux NaCl et $NaClO_4$ permettent d'estimer les effets de la température et de la salinité sur la spéciation de l'uranium(VI), en particulier dans les sites de stockage de déchets nucléaires, et pour combler les lacunes dans les bases de données thermodynamiques pour ces complexes. En outre, les spectres caractéristiques et les temps de décroissance expérimentaux peuvent servir à l'identification de ces espèces. Ainsi, dans la dernière partie, nous avons examiné les principales espèces dans les compositions d'eaux naturelles liées à l'activité minière de l'uranium, à la gestion des déchets radioactifs

(RWM), et d'autres milieux liés à l'uranium naturel avec les nouvelles données thermodynamiques déterminées pour les complexes $M_nUO_2(CO_3)_3^{(4-2n)-}$. Les contours de forme ellipsoïdale pour $UO_2CO_3(aq)$, $CaUO_2(CO_3)_3^{2-}$, et $Ca_2UO_2(CO_3)_3(aq)$ ont été déterminées à partir de la distribution des points d'échantillon dans le diagramme d'activité $\log_{10}(a(Ca^{2+})/a(H^+)^2)$-$\log_{10}(a(Na^+)/a(H^+))$-$\log_{10}(a(HCO_3^-)a(H^+))$ en 3D. Deux échantillons d'eau du site de Lodève ont été analysé pour leurs compositions chimiques et ensuite modélisés avec nos nouvelles données. Il est montré que la vérification des espèces dominantes pour les échantillons de Lodève est en accord avec les résultats du calcul de spéciation. On peut conclure que la détermination des ellipsoïdes pour les complexes $Ca_nUO_2(CO_3)_3^{(4-2n)-}$ est un outil approprié pour identifier rapidement les espèces majeures de carbonate d'uranyle (calcium) pour un échantillon d'eau naturelle donné, une fois que sa composition chimique est disponible. De plus, les propriétés de luminescence ont été acquises pour ces deux échantillons et comparées avec nos données expérimentales. Les performances de la technique de laser est ainsi testées pour les complexes $Ca_nUO_2(CO_3)_3^{(4-2n)-}$.

Contents

General Introduction

Context and issues

The evaluation of environmental consequences related to the extraction of uranium for nuclear power cycle – from exploration to recycling – has been an important consideration in any industrial project development, such as in the framework of the safety analysis of high-level waste (HLW) repositories, uranium mining activities, remediation of uranium-polluted soils and aquifers, as well as assessment of uranium toxicity in ecosystems. From the early days of the Manhattan Project to later development of civilian nuclear power, the demand for uranium mining has skyrocketed and thus produced considerable quantities of uranium-rich sediments or mining waste in the environment. Some of these contaminated sites are sources of local uranium contamination of groundwater. Uranium also contributes to the long-term radiotoxicity of nuclear fuel after reprocessing. The importance of uranium as a pollutant does not only depend on its quantities in nuclear waste and/or contaminated sediments, but also on the assessment of associated physico-chemical reactions that determine its mobility under specific conditions. However, it is quite limited and somewhat impossible at a laboratory scale to investigate processes that take long time to be followed by experiments, such as processes at a geological time scale.

Nuclear waste repositories

Multi-barrier nuclear waste repository systems are under consideration in the countries engaged in radioactive waste management. These systems involve first a natural barrier system, which includes the host rock and its surrounding subsurface environment, then the backfill system, which consists of bentonite in some disposal concepts[1,2] or mixtures with graphite and silica to enhance thermal conductivity in other concepts,[3] finally the waste canisters, which are considered as the most rigid barrier to prevent the release of uranium up to 10000 years.

Each repository has its own conditions and barrier properties, and their characteristics are under intense study. Currently, three types of host rock – clay/shale/argillite, crystalline/granite rocks, and geologic salt formations – have been most extensively considered throughout the world. Several underground research laboratories (URL) have been constructed to obtain extensive and comprehensive scientific knowledge and assess the long-term repository isolation performance of radioactive waste. Example of disposals in crystalline/granite geology are the Grimsel Test Site in Switzerland,[4] the Fennoscandian Shield in Sweden,[5] and the Beishan area

in China.[6] For clay/shale/argillite as the reference host rock for methodological studies on repository of radioactive waste, several URLs have made meaningful contributions, such as Boom clay at Mol in Belgium,[7,8] Callovo-Oxfordian clay at Bure in France,[9] and Opalinus Clay at Mont-Terri in Switzerland.[10] Out of the countries that are studying clay rock as host rock, Belgium, France, and Switzerland[11-13] are investigating pore water chemistry with relatively lower ionic strengths — e.g., from 0.02 mol kg_w^{-1} in Boom Clay to 0.5 mol kg_w^{-1} in Opalinus Clay —,[11] while Japan[14] and Canada[15] are studying sedimentary rocks with higher salinities in the pore waters, *e.g.*, > 200 g L^{-1} in the Canadian shield. Nevertheless, most of the research on radionuclide-water interactions have been conducted at low ionic strengths. Several nuclear waste repositories are at deep salt formations where groundwaters can have ionic strengths, such as the Waste Isolation Pilot Plant (WIPP) in Carlsbad, New Mexico in the USA,[16] and the Gorleben and Morsleben sites in Northern Germany[17] where the main ions Na^+, Mg^{2+}, Ca^{2+}, Cl^- give the important ionic strength.[18]

A potential radioactive waste repository has to conform to several criteria with the core requirements that the host rock as well as the backfill should be able to prevent radionuclides migration into biosphere for projected lifetime of the disposal facilities, which is typically set to 10,000 years. Properties of crystalline/granite rocks that are appreciated include low permeability (without fractures), mechanical stability, high thermal conductivity,[6] and those of clay/shale/argillite rock consist of low permeability, low diffusion coefficient and high adsorption capacity.

Importance of $Mg/Ca_nUO_2(CO_3)_3^{(4-2n)-}$ species

The most stable chemical form of uranium in the deep geological and reducing environment is U(IV) in the form of uraninite UO_2(s), which is also the major component of used-fuel pellets. During the oxidative dissolution of UO_2(s) as a result of continuing interactions with groundwater or with H_2O_2 formed by α-hydrolysis of H_2O[19], insoluble U(IV) can convert to soluble U(VI) resulting in the formation of uranyl hydroxides, commonly schoepite with general formula $UO_3{:}nH_2O$, $n \leq 2$ ($n = 2$ taken in this work).[20] For example, schoepite is selected as the controlling phase in early degradation of used-fuel waste packages,[21] where the role of bentonite backfill is essential because it can affect the dissolution of schoepite by the following reaction,

$$UO_3{:}2H_2O + 2H^+ \rightleftarrows UO_2^{2+} + 3H_2O \qquad (1)$$

with $\log_{10}K° = 5.96$[22] taken from the Giffaut *et al.* and Grivé *et al.*[23,24]

Once U(VI) formed in the environments related to uranium mining activities or released from the waste packages, it starts to migrate through geological materials, such as solid rocks and soils in which noticeable mineral phase changes occur on multiples time scales: the dissolution and precipitation of carbonate minerals such as calcite and dolomite then the dissolution of smectite and precipitation of illite known as the occurrence of illitization.[8] These processes are important in influencing the chemical conditions, *i.e.* aqueous pH value and concentrations of Ca^{2+} and HCO_3^-.

In the 1990's, the $Ca_2UO_2(CO_3)_3$ complex have been evidenced in seepage waters of mine waters of a uranium mine in Saxony, Germany.[25,26]

$$2Ca^{2+}+UO_2^{2+}+3CO_3^{2-}\rightleftarrows Ca_2UO_2(CO_3)_3$$

Latter the formation of the $CaUO_2(CO_3)_3^{2-}$ was also evidenced.[27]

$$Ca^{2+}+UO_2^{2+}+3CO_3^{2-}\rightleftarrows CaUO_2(CO_3)_3^{2-}$$

The studies on these complexes are increasing since then, and their existence was confirmed in natural environments.[28,29]

The solubility of shoepite can then result in the dominant Ca-UO_2-CO_3 aqueous complexes in pore waters by the following reactions.

$$UO_3{:}2H_2O+Ca^{2+}+3HCO_3^-\rightleftarrows H^++3H_2O+ CaUO_2(CO_3)_3^{2-} \quad (2)$$

$$UO_3{:}2H_2O+2Ca^{2+}+3HCO_3^-\rightleftarrows H^++3H_2O+ Ca_2UO_2(CO_3)_3 \quad (3)$$

Nevertheless, schoepite is not considered as stable phase in long term.[20,30]. In natural carbonate-rich regions, uranyl-carbonates are well known as the dominant aquatic uranyl(VI) species.[31] In the presence of alkali and alkaline-earth elements, it can transform into a sequence of secondary U(VI) phases and uranyl oxyhydroxides depending on other parameters like pH and water compositions, such as the liebigite group of the general formula $M_2[UO_2(CO_3)_3]{:}nH_2O$ where M stands for Mg, Ca, Na, K of different combinations and n ranges from 5 to 18.[32] The solubility and associated adsorption reactions of these minerals are important in controlling the source concentration of UO_2^{2+} for the uranium migration through geological materials.[33,34] However, the isolation of these secondary minerals as pure phase from the natural matrix is difficult to achieve. In particular, for the minerals within the liebigite group — *i.e.* liebigite $Ca_2[UO_2(CO_3)_3]{:}10H_2O$, swartzite $CaMg[UO_2(CO_3)_3]{:}12H_2O$, bayleyite $Mg_2[UO_2(CO_3)_3]{:}18H_2O$, and andersonite $Na_2Ca[UO_2(CO_3)_3]{:}6H_2O$ —, the published

synthesis methods raised some questions since the laboratory tests have shown the association of these minerals depending on the relative availabilities of Mg^{2+}, Ca^{2+}, Na^{+} in solution.[35,36] The lack of information on the uranium solubility associated with these important U(VI) phases imposes limitations on further investigations into the formation of aqueous $(Mg/Ca)_nUO_2(CO_3)_3^{(4-2n)-}$ species in geological context.

In addition, it was shown that the formation of $Ca_nUO_2(CO_3)_3^{(4-2n)-}$ species can lead to higher aqueous U(VI) concentrations within bentonite because of the surface complexation reactions occurred with exchangeable and adsorption sites of uranyl.[37] For example, the desorption of U(VI) on montmorillonite, which is the main constituent of bentonite, is illustrated as follows:

$$mon\_sOUO_2(OH)_2^- + 2Ca^{2+} + 3HCO_3^- \rightleftarrows mon\_sOH + 2H_2O + Ca_2UO_2(CO_3)_3 \quad (4)$$

However, out of the ongoing research in this field, the thermodynamic characters of Ca-UO_2-CO_3 complexes has not received enough attention, especially their complexations at varying temperatures and high ionic strengths that are common situations in heat-generating waste disposal modellings. In the scope of Nuclear Energy Agency Thermochemical Database project (NEA-TDB),[*] the equilibrium constants for $M_nUO_2(CO_3)_3^{(4-2n)-}$ (M = Mg, Ca, Sr, Ba) proposed in literature has only been recently accepted for the reasons detailed in the critical reviews.[38,39] The authors reanalyzed the experimental values from the literature and discussed the roles played by alkaline ions in the interactions between $UO_2(CO_3)_3^{4-}$ and M^{2+} (M are alkaline earth metal) of which the effects were not considered by the majority of researchers. The fact that the stability constant for the complex $MUO_2(CO_3)_3^{2-}$ (M = Mg, Ca, Sr, Ba) has a maximum for Ca^{2+} might be related to the geometric constraints of Mg^{2+}.[27] The extension of these results to include the structure of $M_nUO_2(CO_3)_3^{(4-2n)-}$ (M = Mg, Ca, Sr, Ba) in the analysis of coordination is necessary. There are two ways in which researchers have collected their structural properties: experimental measurement by spectroscopy and molecular dynamic simulation. Bernard *et al.*[26] and Kelly *et al.*[40] confirmed the presence of $Ca_nUO_2(CO_3)_3^{(4-2n)-}$ (n = 1, 2) by U L_{III}-edge EXAFS data, noting that the EXAFS signals suffers from an overlap of the calcium atoms and the distant oxygen atoms of the carbonate groups. Lee *et al.*[41] identified the existence of $Mg_nUO_2(CO_3)_3^{(4-2n)-}$ (n = 1, 2) complexes and reported their structural information by EXAFS data. Meanwhile, theoretical studies of the (magnesium/calcium) uranyl tricarbonate depend on the levels of theory, which determines the functional of the density. It demonstrates that the calculation of the aqueous ternary complexes needs to consider explicitly the counterions and

[*] https://www.oecd-nea.org/jcms/pl_22166/thermochemical-database-tdb-project

the water molecules in the hydration sphere, since the counterions are located very close to the uranyl moiety.[42,43]

Besides the investigation of their fundamental structural information, studies on thermodynamic properties at high ionic strengths and at varying temperatures to substantiate the actual formation of ternary uranium carbonate species have been scarcely conducted. In particular, the influence of background electrolyte effects on the ternary species received limited attention. To the best of our knowledge, the maximum investigated electrolyte concentrations in experiments are 0.509 mol kg_w^{-1} $NaNO_3$ for the Mg-UO_2-CO_3 system[44] and 3 mol kg_w^{-1} $NaClO_4$ for the Ca-UO_2-CO_3 system,[45] but there is a large scatter in the experimental data in the latter study. Some stability constants in 0.5 M NaCl were reported for the Mg/Ca-UO_2-CO_3 system by converting the values determined in 0.1 M NaCl.[46]

Such ionic strength (non-ideality) correction requires the choice of a model that could estimate the ion activity coefficients under the conditions other than the experimental electrolyte concentration. Out of the models proposed in literature, three models will be discussed: the Davies equation,[47], the specific ion interaction theory (SIT, used within the framework of the NEA-TDB reviews[38,39,48,49] and also in this work) and the Pitzer model.[50] The simple Davies equation, without any undetermined parameters, applies fairly well in describing the activity coefficient variations at low ionic strength under 0.3 mol kg_w^{-1}. The SIT and the Pitzer model are more appropriate for the extrapolation to higher ionic strength. Only the SIT model will be developed in the following — see Grenthe, *et al.*[49] for detailed analysis.

The SIT, allowing the extrapolation up to 3-4 mol kg_w^{-1}, requires the values of specific interaction parameters ε. However, the ε(Na^+, $M_nUO_2(CO_3)_3^{(4-2n)-}$) (M = Mg, Ca) for the investigated system have not been selected in Grenthe *et al*.[39] The review noted an inappropriate application of SIT to the experimental data from the work of Dong and Brooks,[44] which resulted in an unreasonably large interaction coefficient for (Na^+, $MgUO_2(CO_3)_3^{2-}$). Nevertheless, the lack of experimental points at high ionic strength (> 0.5 mol kg_w^{-1}) in literature adds difficulties to obtain the SIT parameters. Furthermore, the variation of $\log_{10}\beta$ in response to electrolyte concentration provides insights into the understanding of the electrolyte effects and the ligand effects, which is a particularly important aspect of ion paring formation in the sequential binding processes between Mg^{2+}/Ca^{2+} and $UO_2(CO_3)_3^{4-}$. Therefore, a systematical determination of formation constants and specific ion interaction coefficients for the Mg/Ca-UO_2-CO_3 system is crucial in clarifying the ion interaction mechanism as well as having a primary idea of the roles

of electrolyte ions by comparing the results obtained in two common background solutions — NaCl and $NaClO_4$.

Problematic questions and goals of this study

The complexation of alkaline earth metal ions with uranyl tricarbonate moiety has been studied mainly by titration of Mg^{2+}/Ca^{2+} at fixed pH value in literature.[26,41,46,51] However, the occurrence of mineral precipitation can occur if the initial pH value is low (pH < 7.8)[51] resulting in the formation of schoepite at the beginning of complexation and if the pH value is too high (pH > 8.5)[27,41,46] resulting in the formation of alkaline earth carbonate phases (magnesite, calcite) at the end of complexation. Fig. 1 (a) shows the predominance diagram of Ca-UO_2-CO_3 complexes at 0.1 mol kg_w^{-1} NaCl using the Thermochimie 10a database[52] with the implemented formation constants of $Ca_nUO_2(CO_3)_3^{(4-2n)-}$ species from the work of Lee *et al.*[41,51] One can observe that the predominance regions of Ca-UO_2-CO_3 complexes evolve with pH and calcium concentration. The species distribution at [U(VI)] = 50 µmol kg_w^{-1} for a series of solutions for which the pH values decrease and the calcium concentrations increase simultaneously were performed as preliminary calculations. Fig. 1 (b) shows that the fractions of $CaUO_2(CO_3)_3^{2-}$ and $Ca_2UO_2(CO_3)_3$(aq) could attain up to 50-85% in the middle and at the end of entire titration, respectively. Such approach—the change of pH as titration progresses—improves the degree of complexation of calcium and rules out the undesired precipitations that is better working with compared to conventional titration at fixed pH value.

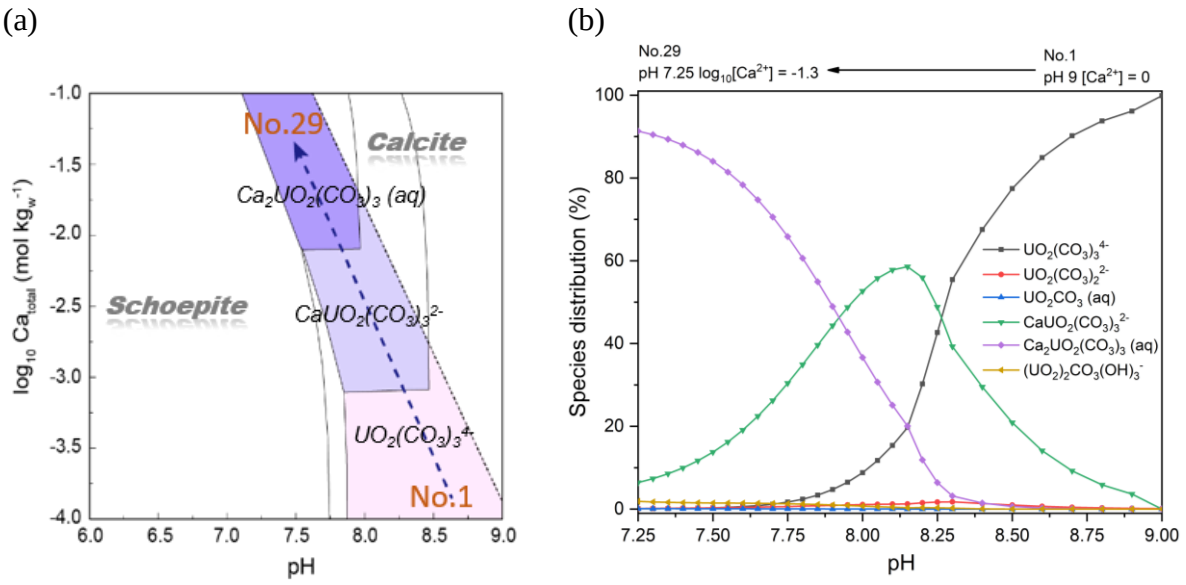

Fig. 1 Diagrams of the distribution of aqueous uranyl species in our solutions experimental, calculated from recommended thermodynamic data

Organization of this manuscript

This document is divided into six chapters.

Chapter I details the theoretical elements of thermodynamic in solution and a description of the methodology used in this work, including the calculation of Ringböm coefficient for uranyl carbonate at different pH values, the presentation of the TRLFS technique, the measurement of pH value with original/reconditioned combined glass electrodes in NaCl/$NaClO_4$ electrolytes and the calibration of pH-meter for the range of temperature from 5 to 50°C.

Chapter II and Chapter III present the results on the formation of $CaUO_2(CO_3)_3^{2-}$ and $Ca_2UO_2(CO_3)_3(aq)$ in NaCl and $NaClO_4$, respectively, at different ionic strengths. The luminescence quenching of chloride ions have limited our study to 1 mol L^{-1} NaCl ionic strength. The lesser quenching perchlorate ions slightly extended the range of ionic strength to 2.2 mol L^{-1} $NaClO_4$. The accurate determinations of formation constants at different ionic strengths, based on the quantitative analysis of the time-resolved luminescence spectra, allow deducing the formation constants at the ionic strength of the experiments ($\log_{10}K$), the extrapolations to infinite dilution giving the constant in standard conditions ($\log_{10}K°$), Gibbs energies of reaction ($\Delta_rG°_m$) and formation ($\Delta_fG°_m$), and specific ion interaction coefficients $\varepsilon((Mg/Ca)_nUO_2(CO_3)_3^{(4-2n)-},Na^+X^-)$. In particular, the results determined in NaCl are useful for predictive simulation of uranium simulation in a wide range of natural water compositions.[53] These chapters are mainly organized around the publications in Dalton Transactions: Shang and Reiller[54], and Shang, *et al.*[55]

Chapter IV concerns the complexation constants and specific ion interaction coefficients of $MgUO_2(CO_3)_3^{2-}$ species in NaCl and $NaClO_4$. Two gratings of different resolutions were used to acquire $MgUO_2(CO_3)_3^{2-}$ luminescence spectra. Thus far, consistent subsets of thermodynamic constants and ε values for $M_nUO_2(CO_3)_3^{(4-2n)-}$ (M = Mg, Ca) complexes are now available. The formation of ternary $M_nUO_2(CO_3)_3^{(4-2n)-}$ (M = Mg, Ca) complexes application in different geochemical contexts were examined. This chapter is organized around the publication in Dalton Transactions Shang and Reiller[56], and Inorganic Chemistry Oher, *et al.*[43]

Chapter V reports the complexation energetics of $Ca_nUO_2(CO_3)_3^{(4-2n)-}$ and $MgUO_2(CO_3)_3^{2-}$, based on measurements of their equilibrium constants at variable temperatures: 5-30°C for Mg^{2+} and 10-50°C for Ca^{2+}. The pure spectra were recovered at 50°C for $Ca_nUO_2(CO_3)_3^{(4-2n)-}$ and 30°C for $MgUO_2(CO_3)_3^{2-}$ using multivariate curve resolution alternating least squares analysis (MCR-ALS). Different computational methods were tested to fit the temperature-

dependent formation constants. This chapter is presented as a pre-print of a publication to be submitted in Dalton Transactions.

Chapter VI presents the analysis based on speciation calculation of the major species of water compositions linked to uranium mining activity, radioactive waste management (RWM), and of other more general interest related to natural uranium with the newly determined thermodynamic data for $(Mg/Ca)_nUO_2(CO_3)_3^{(4-2n)-}$ complexes described in previous chapters. Thermodynamic calculations and TRLFS analyses were also performed for two water samples collected from the Lodève site. The calculated dominant species corroborates well the experimental observations in terms of luminescence characteristics.

References

1. F. Huertas, *Full-Scale Engineered Barriers Experiment for a Deep Geological Repository for High-Level Radioactive Waste in Crystalline Host Rock (FEBEX project): Final Report*, Report 9282892859 9789282892855, Office for Official Publications of the European Communities, Luxembourg, 2000. http://op.europa.eu/fr/publication-detail/-/publication/f8579601-9bab-41e5-8e8f-cac382d93358
2. A. Hedin, *Long-Term Safety for KBS-3 Repositories at Forsmark and Laxemar - A First Evaluation. Main Report of the SR-Can Project*, Swedish Nuclear Fuel and Waste Management Co., Stockholm (Sweden), Stockholm, Sweden, 2006
3. JNC, *H12: Project to Establish the Scientific and Technical Basis for HLW Disposal in Japan*, Japan Nuclear Cycle Development Institute (JNC), International Atomic Energy Agency, Vienna, 2000
4. J. Hadermann and W. Heer, *J. Contam. Hydrol.*, 1996, **21**, 87-100.
5. D. Martin and R. Christiansson, *Int. J. Rock Mech. Min. Sci.*, 2009, **46**, 219-228.
6. X. Cao, L. Hu, J. Wang and J. Wang, *Hum. Ecol. Risk Assess.*, 2017, **23**, 2017-2032.
7. J.-D. Barnichon and G. Volckaert, *Hydrogeol. J.*, 2003, **11**, 193-202.
8. X. Cao, L. Zheng, D. Hou and L. Hu, *Chem. Geol.*, 2019, **525**, 46-57.
9. O. Fouché, H. Wright, J.-M. Cléac'h and P. Pellenard, *Appl. Clay Sci.*, 2004, **26**, 367-387.
10. P. Meier, T. Trick, P. Blümling and G. Volckaert, *Self-Healing of Fractures within the EDZ at the Mont Terri Rock Laboratory: Results after One Year of Experimental of work. Proceedings of International Workshop on Geomechanics, Hydromechanical and Thermohydro-Mechanical Behaviour of Deep Argillaceous Rocks: Theory and Experiment*, Paris, 2000
11. M. de Craen, L. Wang, M. Van Geet and H. Moors, *Geochemistry of Boom Clay pore water at the Mol site*, Report SCK•CEN-BLG-990, SCK•CEN, Mol, Belgium, 2004. http://jongeren.sckcen.be/~/media/Files/Science/disposal_radioactive_waste/Geochemistry_of_Boom_Clay_pore_Status_2004.pdf
12. F. J. Pearson, D. Arcos, A. Bath, J.-Y. Boisson, A. M. Fernández, H.-E. Gäbler, E. Gaucher and A. Gautschi, *Mont Terri Project – Geochemistry of Water in the Opalinus Clay Formation at the Mont Terri Rock Laboratory*, Federal Office for Water and Geology, Bern, Switzerland, 2003
13. A. Vinsot, S. Mettler and S. Wechner, *Phys. Chem. Earth*, 2008, **33**.
14. K. Hama, T. Kunimaru, R. Metcalfe and A. J. Martin, *Phys. Chem. Earth*, 2007, **32**, 170-180.

15. P. Fritz and S. K. Frape, *Chem. Geol.*, 1982, **36**, 179-190.
16. J. Conca, Environmental monitoring programs and public engagement for siting and operation of geological repository systems: experience at the Waste Isolation Pilot Plant, in *Geological Repository Systems for Safe Disposal of Spent Nuclear Fuels and Radioactive Waste, 2nd Edition*, eds. M. J. Apted and J. Ahn, Woodhead Publishing Series in Energy, 2017, DOI: 10.1016/B978-0-08-100642-9.00024-4, ch. 24, pp. 667-709.
17. M. Schwartz, *Hydrogeol. J.*, 2012, **20**.
18. D. A. Atwood, *Radionuclides in the Environment*, *EIC Books*, Wiley, Chichester, West Sussex, U.K. ; New York, 2010.
19. M. Odorowski, C. Jegou, L. De Windt, V. Broudic, G. Jouan, S. Peuget and C. Martin, *Geochim. Cosmochim. Acta*, 2017, **219**, 1-21.
20. J. Bruno, I. Casas, E. Cera, R. C. Ewing, R. J. Finch and L. O. Werme, The assessment of the long-term evolution of the spent nuclear fuel matrix by kinetic, thermodynamic and spectroscopic studies of uranium minerals, in *Symposium – Scientific Basis for Nuclear Waste Management XVIII*, eds. T. Murakami and R. C. Ewing, Materials Research Society, United States, 1995, vol. 353, p. 633.
21. P. Bernot, *Dissolved Concentration Limits of Radioactive Elements*, United States, 2005. www.osti.gov/biblio/883412
22. A. Sanding and J. Bruno, *Geochim. Cosmochim. Acta*, 1992, **56**, 4135-4145.
23. E. Giffaut, M. Grivé, P. Blanc, P. Vieillard, E. Colàs, H. Gailhanou, S. Gaboreau, N. Marty, B. Madé and L. Duro, *Appl. Geochem.*, 2014, **49**, 225-236.
24. M. Grivé, L. Duro, E. Colàs and E. Giffaut, *Appl. Geochem.*, 2015, **55**, 85-94.
25. G. Bernhard, G. Geipel, V. Brendler and H. Nitsche, *Radiochim. Acta*, 1996, **74**, 87-91.
26. G. Bernhard, G. Geipel, T. Reich, V. Brendler, S. Amayri and H. Nitsche, *Radiochim. Acta*, 2001, **89**, 511-518.
27. W. M. Dong and S. C. Brooks, *Environ. Sci. Technol.*, 2006, **40**, 4689-4695.
28. M. Maloubier, P. L. Solari, P. Moisy, M. Monfort, C. Den Auwer and C. Moulin, *Dalton Trans.*, 2015, **44**, 5417-5427.
29. O. Prat, T. Vercouter, E. Ansoborlo, P. Fichet, P. Perret, P. Kurttio and L. Salonen, *Environ. Sci. Technol.*, 2009, **43**, 3941-3946.
30. D. J. Wronkiewicz, J. K. Bates, T. J. Gerding, E. Veleckis and B. S. Tani, *J. Nucl. Mater.*, 1992, **190**, 107-127.
31. G. Meinrath and T. Kimura, *J. Alloys Compd.*, 1993, **202**, 89-93.
32. S. Amayri, T. Arnold, H. Foerstendorf, G. Geipel and G. Bernhard, *Can. Mineral.*, 2004, **42**, 953-962.
33. W. M. Murphy, *MRS on line Proc. Lib.*, 1996, **465**, 713-720.
34. M. C. A. Sandino and B. Grambow, *Radiochim. Acta*, 1994, **66-67**, 37-44.
35. A. K. Alwan and P. A. Williams, *Mineral. Mag.*, 1980, **43**, 665-667.
36. J. Y. Lee, S. Amayri, V. Montoya, D. Fellhauer, X. Gaona and M. Altmaier, *Appl. Geochem.*, 2019, **111**, 104374.
37. A. Meleshyn, M. Azeroual, T. Reeck, G. Houben, B. Riebe and C. Bunnenberg, *Environ. Sci. Technol.*, 2009, **43**, 4896-4901.
38. R. Guillaumont, T. Fanghänel, V. Neck, J. Fuger, D. A. Palmer, I. Grenthe and M. H. Rand, *Update of the Chemical Thermodynamics of Uranium, Neptunium, Plutonium, Americium and Technetium*, OECD Nuclear Energy Agency, Data Bank, Issy-les-Moulineaux, France, 2003.
39. I. Grenthe, X. Gaona, A. V. Plyasunov, L. Rao, W. H. Runde, B. Grambow, R. J. M. Koning, A. L. Smith and E. E. Moore, *Chemical Thermodynamics 14. Second Update on the Chemical Thermodynamics of Uranium, Neptunium, Plutonium, Americium and*

Technetium, *Chemical Thermodynamics Series*, OECD Nuclear Energy Agency Data Bank, Eds., OECD Publications, Paris, France, 2020.
40. S. D. Kelly, K. M. Kemner and S. C. Brooks, *Geochim. Cosmochim. Acta*, 2007, **71**, 821-834.
41. J. Y. Lee, M. Vespa, X. Gaona, K. Dardenne, J. Rothe, T. Rabung, M. Altmaier and J.-I. Yun, *Radiochim. Acta*, 2017, **105**.
42. S. Tsushima, Y. Uchida and T. Reich, *Chem. Phys. Lett.*, 2002, **357**, 73-77.
43. H. Oher, T. Vercouter, F. Réal, C. Shang, P. E. Reiller and V. Vallet, *Inorg. Chem.*, 2020, **59**, 15036-15049.
44. W. Dong and S. C. Brooks, *Environ. Sci. Technol.*, 2008, **42**, 1979-1983.
45. S. N. Kalmykov and G. R. Choppin, *Radiochim. Acta*, 2000, **88**, 603-606.
46. F. Endrizzi and L. F. Rao, *Chem.-Eur. J.*, 2014, **20**, 14499-14506.
47. C. W. Davies, *Ion Association*, Butterworths, London, UK, 1962.
48. I. Grenthe, L. Fuger, R. G. M. Konings, R. J. Lemire, A. B. Muller, C. Nguyen-Trung and H. Wanner, *Chemical Thermodynamics 1. Chemical Thermodynamics of Uranium*, *Chemical Thermodynamics Series*, North Holland Elsevier Science Publishers B. V., Amsterdam, The Netherlands, 1992.
49. I. Grenthe, A. V. Plyasunov and K. Spahiu, Chapter IX. Estimations of medium effects on thermodynamic data, in *Modelling in Aquatic Chemistry*, eds. I. Grenthe and I. Puigdomènech, OECD, Paris, France, 1997, ch. IX, pp. 325-426.
50. K. S. Pitzer, *Activity Coefficients in Electrolyte Solutions*, CRC Press, Boca Raton, 2nd edn., 1991.
51. J. Y. Lee and J. I. Yun, *Dalton Trans.*, 2013, **42**, 9862-9869.
52. Thermochimie, http://www.thermochimie-tdb.com/.
53. P. E. Reiller and M. Descostes, *Chemosphere*, 2020, **251**, 126301.
54. C. Shang and P. E. Reiller, *Dalton Trans.*, 2020, **49**, 466-481.
55. C. Shang, P. E. Reiller and T. Vercouter, *Dalton Trans.*, 2020, **49**, 15443-15460.
56. C. Shang and P. E. Reiller, *Dalton Trans.*, 2021, **50**, 4363-4379.

Chapter I. Bibliography

I - 1 Introduction

The aqueous chemistry of uranium refers to the various reactions taking place when uranium is contacting water. This term covers many different research directions due to its multifaceted chemical behaviour. Many chemical reactions can control the mobility of uranium in aquifers, depending on the oxidation state of the uranium and the physico-chemical conditions of the environment. The relative stability of the oxidation states of uranium depends on Eh, pH and complexing ligands. U(IV) and U(VI) are the most stable oxidation states of uranium in water. U(IV) is generally considered as immobile in the environment as a result of its low solubility, while U(VI) can potentially migrate through aquifers and into the biosphere by *e.g.*, complexation, polymerization and ion exchange.[1-3]

In aqueous solution, uranium (VI) exists in the form of trans-dioxo cations (UO_2^{2+}), called uranyl cations. The linear structure of the uranyl ion, *i.e.*, the distribution of electrons between uranium and the two oxygen atoms, gives uranium an "effective" charge of 3.3 ± 0.1 distributed in the equatorial plane of the molecule (plane perpendicular to the axis formed by the O-U-O alignment). Thus, uranyl ions are considered as hard acid according to the HSAB concept (abbreviation for "hard and soft (Lewis) acids and bases", also known as the Pearson acid-base concept[4-6]) and preferably form coordination with four/five/six hard base donor ligand in the equatorial plane.[7,8] The order of affinity of the uranyl ion reported for the predominant anions in natural waters is as follows: $OH^- > CO_3^{2-} > HPO_4^{2-} > SO_4^{2-} > NO_3^- > Cl^-$.[9] Choppin[10] has confirmed that the uranium dissolved in some groundwater is in the form of uranyl carbonate complexes.

This chapter gives some descriptions on uranyl-carbonate systems. The interpretation of experimental data of luminescence of uranyl ion complexed with carbonate and alkaline-earth metal ions require prior knowledge about:

(a) structural data and solution chemistry related to the studied ternary complexes.
(b) luminescent properties of uranium and determination of setup parameters.
(c) methodological analysis of luminescence data and extrapolation to infinite dilution.

I - 2 Electronic structure of UO_2^{2+}

A thorough description of the distribution of electrons in the uranium-oxygen binding orbitals is necessary for understanding the coordination properties in the uranyl ion UO_2^{2+}. The electron configurations in the fundamental state of oxygen (Z = 8) and uranium (Z = 92) are written as $1s^2 2s^2 2p^4$ and [Rn] $5f^3 6d^1 7s^2$, respectively, where [Rn] represents the electronic configuration of radon $1s^2 2s^2 2s^2 2p^6 3s^2 3p^6 4s^2 3d^{10} 4p^6 5s^2 4d^{10} 5p^6 4f^{14} 5d^{10} 6s^2 6p^6$. The electronic configuration of U^{6+} is [Rn] $5f^0 6d^0 7s^0$, and that of O^{2-} is $1s^2 2s^2 2p^6$. The uranyl dication is composed of two U≡O triple bonds, expressed as $[O{\equiv}U{\equiv}O]^{2+}$.[11] The U 5f/6d orbitals and the O 2p orbitals form the strong U≡O triple bonds containing 6 valence electrons, while U 7s shell remains nonbonding in U(VI) species due to its high orbital energy. It is noteworthy that 4/2 nonbonding orbitals ($f_{+\delta,-\delta}$, $f_{+\phi,-\phi}$)/($d_{+\delta,-\delta}$) in U 5f/6d do not participate in bonding because of their asymmetric structure towards the O 2p orbitals. However, these nonbonding orbitals are available for equatorial ligands by σ and π interactions, thus can modify U≡O bonds.[12,13] For uranyl carbonate complexes, a study using the density functional theory (DFT) calculations[14] confirmed that the coordination of carbonate can bend O≡U≡O from linear to about 176° and an orbital of uranyl-σ (5f/6d) character matched to the O 2p orbitals of the carbonate oxygens receives electrons from one of the four nonbonding U 5f orbitals in excitations.

I - 3 Structures of aqueous (Mg/Ca)-UO_2-CO_3 complexes

The structural data of (Mg/Ca)-UO_2-CO_3 complexes have been collected using different methods: experimental measurements *e.g.*, X-ray absorption spectroscopy,[15-17] X-ray powder diffraction;[18] and theoretical modelling *e.g.*, density functional theory (DFT),[19] hybrid DFT,[20-23] quantum mechanical/molecular mechanical (QM/MM) approach,[24,25] and classical molecular dynamics (MD) simulations.[19,26,27] According to the literature, the uranyl tricarbonate exhibits a 6-fold pattern with two of the three oxygen atoms in carbonate coordinating to the uranyl ion, though the coordination hexagon can be distorted due to an O-U-O angle < 60° to oxygen atoms of a carbonate ligand, as shown in Fig. I - 1.[7,20-23,28-32] However, a conversion of one carbonate from bidentate to monodentate binding that results in a 5-fold coordination in uranyl ion is assumed to be highly possible in aqueous conditions using the Quantum Mechanical Charge Field Molecular Dynamics (QMCF-MD) simulation.[24] The structural and dynamic data of uranyl carbonate are accordingly modified due to the protonation of one carbonate. The authors explained that this discrepancy comes from the explicit solvent effects in QM/MM simulation yielding more accurate results than other methods.

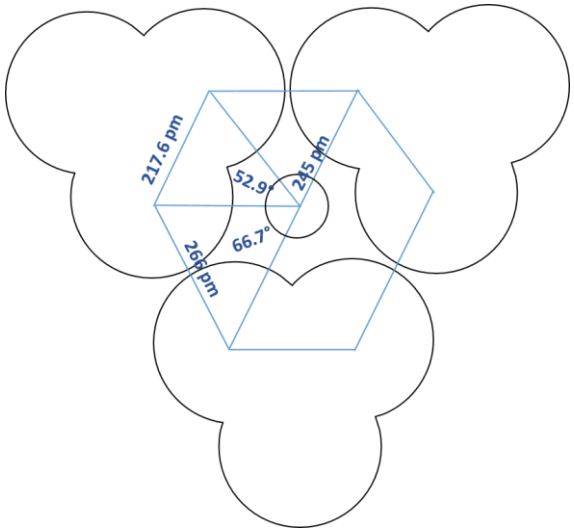

Fig. I - 1 Equatorial coordination of U(VI) in the $[UO_2(CO_3)_3^{4-}]$ complex.

Li *et al.*[27] explored the ways in which the UO_2^{2+} sequentially binds with three carbonates then with two calcium ions at the molecular level in pure water and in 0.1 mol L^{-1} NaCl using the QM/MM MD method. They concluded that the complexation of the first Ca^{2+} cannot stabilize the 6-fold coordination of $UO_2(CO_3)_3^{4-}$ group, whilst the secondary one finally contributes to a symmetric structure in the perpendicular plane of uranyl moiety in pure water. In comparison, the presence of sodium ion in NaCl medium distorts one carbonate group from bidentate to monodentate binding and destroys the symmetric structure of $UO_2(CO_3)_3^{4-}$ group. In fact, Na^+ play a competitive role in binding of Ca^{2+} with $UO_2(CO_3)_3^{4-}$ that renders the formation of $Ca_nUO_2(CO_3)_3^{(4-2n)-}$ complexes more difficult in 0.1 mol L^{-1} NaCl than in pure water. They reported the calculated binding free energy for the first Ca^{2+} ion binding with −36.9 kJ mol^{-1} in pure water and −20.0 kJ mol^{-1} in 0.1 mol L^{-1} NaCl, and for the second Ca^{2+} ion binding with −22.3 kJ mol^{-1} in pure water and −14.7 kJ mol^{-1} in 0.1 mol L^{-1} NaCl.

A parallel simulation study of $(Mg/Ca)_nUO_2(CO_3)_3^{(4-2n)-}$ complexation, limited to free solvent molecule environment, was conducted in our laboratory.[14] In order to reduce the computational costs and avoid undesired divergence, a charge-compensated model with aqueous counter ions — *i.e.* Na^+, Ca^{2+}, Mg^{2+} —, and symmetric structure hypothesis for $(Mg/Ca)_nUO_2(CO_3)_3^{(4-2n)-}$ complexes were maintained in the simulation. Within the framework of this study, we preferably consider the 6-fold coordination of uranyl tricarbonate group and analyze the luminescent properties based on this model. Nonetheless, any possible modification, such as conversion of coordination number from 6 to 5 within uranyl tricarbonate group as predicted in previous simulation studies, is not excluded, especially for experimental data obtained in concentrated electrolyte solutions.

I - 4 Time-resolved laser-induced fluorescence spectroscopy (TRLFS)

4.1 Electronic transitions and luminescence

4.1.1 Absorption

Luminescence refers to the emission of light after the excitation of molecules by photons of ultraviolet or visible light. It is formally divided into two categories: fluorescence and phosphorescence, depending on the electronic configuration of the excited state and the emission pathway. The typical Jablonski diagram shown in Fig. I - 2 illustrates the general case. At room temperature, the peripheral electrons are on the lowest energy level S_0 of spin multiplicity 1 (singlet state), called the fundamental state, whereas once excited, these electrons are propelled towards higher energy levels, first and second excitation states S_1 and S_2 called the excited states. Depending on the energy supplied in the form of photons, the excited level that an electron reaches satisfies the relation $\Delta E = h\nu$, where ΔE is the energy difference between the fundamental and excited levels, h is Planck's constant and ν is the frequency of the incident beam. Since the excitation of a molecule by light absorption normally occurs without any change in the electron spin-pairing, the excited state is also a singlet state.

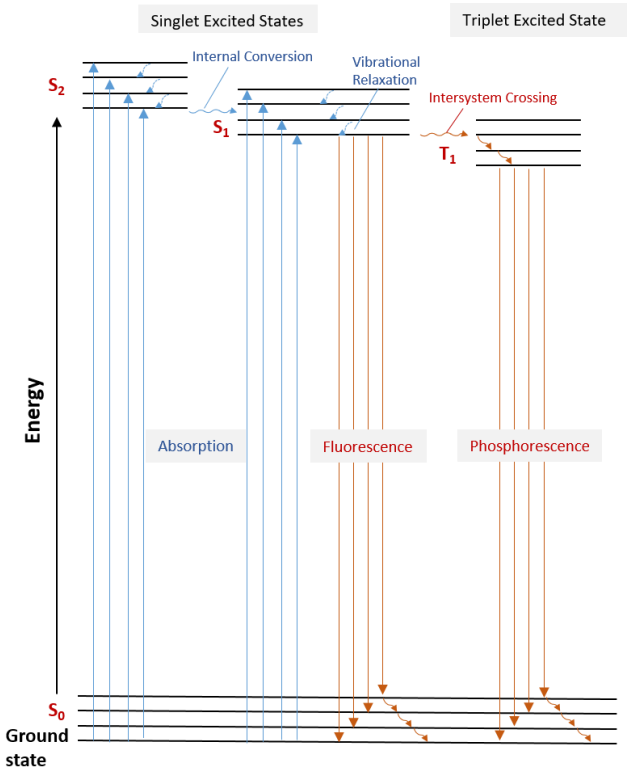

Fig. I - 2 Jablonski diagram including vibrational levels for absorbance, fluorescence, phosphorescence and non-radiative decay—internal conversion, vibrational relaxation, intersystem crossing.

Each electronic state is subdivided into a number of vibrational and rotational energy levels associated with atomic orbitals. In Fig. I - 2, the thicker lines represent the electronic energy levels (S_0, S_1, S_2 and T_1), while the thinner lines indicate the different vibrational energy states (the rotational energy states are ignored). Transitions between states are illustrated by straight or wavy arrows, depending on whether the transition is associated with the emission of photon (straight arrows) or the internal molecular conversion then non-radiative relaxation (wavy arrows). The light absorption takes place in approximately 10^{-15} s, the time necessary for the photon to run one wavelength. For a typical fluorophore, irradiation with a broad spectrum of wavelengths will generate a range of permitted transitions that populate different vibrational energy levels of the excited states. Some of these transitions will have a much higher degree of probability to occur, and constitute the absorption spectrum of the molecule.

4.1.2 De-excitation mechanisms

Immediately after the absorption of a photon, de-excitation processes will occur with different probabilities. A part of the absorbed energy is dissipated via a non-radioactive pathway to reach the lowest vibrational energy level of the first excited state ($S_1 = 0$; Fig. I - 2), during which the excess energy is transferred to the rotational and vibrational degrees of freedom. This process is known as internal conversion or vibrational relaxation (loss of energy in the absence of light emission) and is usually completed in a picosecond or less. This part of the dissipated energy can then be converted into heat, which is absorbed by the surrounding solvent molecules when colliding with the fluorophore in the excited state (dynamic inhibition). Although radiative de-excitation from S_2 to S_0 is also probable, the corresponding emission is of low energy with a very short decay-time, making detection often inaccessible. The loss of energy through a non-radiative transition is more evident at high temperatures, resulting in larger lines widths in the emission spectra.

The excited molecule exists in the lowest excited singlet state ($S_1 = 0$; Fig. I - 2) for periods on the order of nanoseconds before relaxing directly to the ground state (fluorescence) or changing to another excited state of spin multiplicity 3 (triplet state T_1) by spin change and inter-system crossing (phosphorescence), which is generally unfavorable and occur with longer decay-time. The phosphorescence can result either in photon emission from the triplet state T_1 or in transition back to the excited singlet state S_1 generating the delayed fluorescence. Transitions from the excited triplet state T_1 to the excited singlet ground state S_0 are normally prohibited due to selection rules, also the reason for which the rate constants for phosphorescence emissions are several orders of magnitude lower than those for fluorescence.

Nevertheless, these rules can be relaxed due to the intense spin-orbit coupling phenomenon, especially for molecules formed from heavy atoms such as lanthanides and actinides.

Table I - 1 lists the time range for different de-excitation processes. In practice, phosphorescence persists over a short period after shutting down photon supply — due to its unfavourable decay and long decay-time —, whereas fluorescence seems to stop immediately to the human eye. Indeed, the transitions most often involved in the radiative de-excitation of lanthanides and actinides are spin changes from the excited singlet state to the triplet state. However, the duration of this process is shorter than the characteristic times of phosphorescence. Thus, it is better to use the term luminescence, including fluorescence and phosphorescence, to describe de-excitation processes, even though fluorescence constitutes the majority of emission.

Table I - 1 Time dimensions for different de-excitation processes.

Transition	Processes	Rate constants	Time range (s)
$S_0 \rightarrow S_1$ or S_n	Absorption (Excitation)	Instantaneous	10^{-15}
$S_n \rightarrow S_1$	Internal conversion	k(ic)	from 10^{-14} to 10^{-10}
$S_1 \rightarrow S_1$	Vibrational relaxation	k(vr)	from 10^{-12} to 10^{-10}
$S_1 \rightarrow S_0$	Fluorescence	k(f)	from 10^{-9} to 10^{-7}
$S_1 \rightarrow T_1$	Intersystem crossing	k(pT)	from 10^{-10} to 10^{-8}
$S_1 \rightarrow S_0$	Radiative relaxation	k(nr), k(q)	from 10^{-7} to 10^{-5}
$T_1 \rightarrow S_0$	Phosphorescence	k(p)	from 10^{-3} to 100
$T_1 \rightarrow S_0$	Non radiative relaxation	k(nr), k(qT)	from 10^{-3} to 100

Generally, research on luminescence is performed with laser wavelengths ranging from ultraviolet to visible regions (250 to 700 nm). The vibrational energy levels of the ground state, when coupled with normal thermal motion, will produce a wide range of photon energies during emission. Therefore, fluorescence is practically observed as emission intensity over a band of wavelengths rather than sharp lines. Due to the difference in energy between the starting and ending levels, emission spectra can be used to identify compounds by their characteristic bands.

4.1.3 Stokes shift

Excitation and emission can be considered as processes where the luminescent species absorb photons of specific quantum energy and emit secondary photons in the form of fluorescence radiation. The emission spectra are generally independent of excitation wavelengths due to the very fast internal conversion processes. For most luminescent species, the spacing of vibrational energy levels is similar for excited and ground states, resulting in the emission spectrum strongly resembling the mirror image of the absorption spectrum.

The emitted photons contain generally less energy than the photons that are absorbed. Thus, the emission spectrum occurs at lower frequencies, or longer wavelengths, compared to the absorption spectrum. This phenomenon is known as the « Stokes shift ». The primary origin of Stokes shift is the energy loss in the rapid decay of excited electrons to the lower vibrational energy levels of the first excited state. In addition, luminescence emission is often accompanied by transitions to higher vibrational energy levels of the ground state, which will result in additional loss of excitation energy during vibrational relaxations to the lower energy levels of the ground state. Apart from the above-mentioned phenomena, excited state reactions, solvent orientation effects, and resonance energy transfer may also contribute to the increase in emission wavelengths.

4.1.4 Static and dynamic quenching

Quenching refers to the phenomenon that luminescence intensities and/or decay-times of luminescent species are reduced by interactions with other species in solution. This phenomenon can be either static or dynamic. Static quenching describes the formation of a non-luminescent species in the ground state. The efficiency of static quenching is correlated with the rate of the non-luminescent species formation and the concentration of quencher. Therefore, static quenching will result in decreased luminescence intensities because a part of luminescent species is converted to be non-luminescent, but the static quenching has no effect on the luminescence decay-times. In dynamic quenching, the formation of a non-luminescent species occurs during the de-excitation of luminescent species. This phenomenon depends on multiple factors: the viscosity of the solution, the concentration of quencher [Q], the lifetime of the excited state τ_0. Thus, dynamic quenching will induce a decrease not only in luminescence intensity, but also in luminescence decay-times. This can be summarized in the Stern-Volmer relationship.

$$\frac{\phi}{\phi_0} = \frac{1}{1+k_q\tau_0[Q]} \qquad \text{(I-1)}$$

where ϕ and ϕ_0 are the quantum yields of luminescence in the presence and absence of the quencher of which the concentration is noted as [Q]. k_q is the quencher rate coefficient.

4.1.5 Absorption phenomenon

Luminescent properties can be affected by different phenomena: absorption, quenching, and complexation.[33] The absorption phenomenon, containing the pre-filter effect and the post-filter effect, will be mainly addressed in this section. Usually, the pre-filter effect is the primary origin

of the nonlinearity of the dependence of the fluorescence intensity on the fluorophore concentration, especially in the case of high concentration of fluorophore (high absorbance).[34] These two common effects can be both ruled by the Beer-Lambert's law.

Beer-Lambert's law

The Beer-Lambert's law establishes a relationship between light attenuation and properties of the material through which the light travels. We consider a general case where a beam of monochromic light of intensity I_0 interact with a system: the optical path length is l cm, and the transmitted light intensity is noted as I. The Lambert's Law relates the intensity I to the original intensity I_0 by the formula as follows:

$$I = I_0 \cdot e^{-kl} \tag{I-2}$$

where k is the extinction coefficient of the material, expressed in cm^{-1}.

In solution, one can demonstrate that the extinction coefficient k is proportional to the concentration of solutes and depends on photon absorptivity of the attenuating species that is stated by the Beer's law,

$$k = \varepsilon \cdot C \tag{I-3}$$

where ε is the wavelength-dependent molar attenuation coefficient and depends on the incident wavelength λ. C is the concentration of the attenuating species.

The Beer-Lambert's law combines the two laws and is summerized as follows:

$$I = I_0 \cdot e^{-\epsilon Cl} \tag{I-4}$$

In spectroscopy, the absorbance A, a dimensionless parameter, relates the optical attenuation of a specific material containing attenuating species of concentration C to absorptivity ε of the species and the optical path length. The mathematical expression can be written as follows.

$$A = \log_{10} \frac{I_0}{I} = \varepsilon \cdot C \cdot l \tag{I-5}$$

With this relationship, light emission intensity can be used to quantitate the amount of the luminescing species in a sample. In practice, unknown concentrations of luminescing species are determined by quantitative measurement of luminescence intensity. However, many of the limitations of the Beer-Lambert's law can affect luminescence measurements, *e.g.*, inner-filter effects. These effects include pre-filter and post-filter effects.

Pre- and post-filter effects

Pre-filter effect describes the phenomenon that the excitation radiation is reduced by the absorption of species and interfering impurities before the exciting beam flux enters into the detection system. Similarly, post-filter effect refers to the decrease in the emission radiation by by the absorption of luminescing species. In order to eliminate the pre-filter and post-filter effects, a common method in spectroscopic analysis is to use diluted sample solutions.

Within the framework of this research, the concentration of uranium was controlled at 100 µmol L^{-1} or lower, which is consistent with the conditions where no polynuclear hydroxide species form. At such low concentrations, the systems can be assumed to show an acceptable proportionality between luminescence intensity and concentrations of luminescing substances and the inner-filter effects are small enough to be neglected.[35]

4.2 Temperature-dependent properties

The emission spectral properties of uranium are highly dependent on temperature because a multitude of factors that can affect luminescence emission spectra and quantum yields respond differently to temperature change. However, it can be difficult to decide which factor is dominant over others, and generally, more than one factor will simultaneously affect the luminescence. In this section, we will discuss major temperature effects on uranium luminescence in water surrounding environment.

The emission of any given fluorophore is theoretically affected by multiple interactions with the solvent molecules in their local environment. These interactions can have dramatic effects on emission spectra, such as spectral shifts to longer wavelengths or spectral deformation due to energy losses. The related factors possibly having major effects on the energy of the excited state are illustrated in Fig. I - 3.

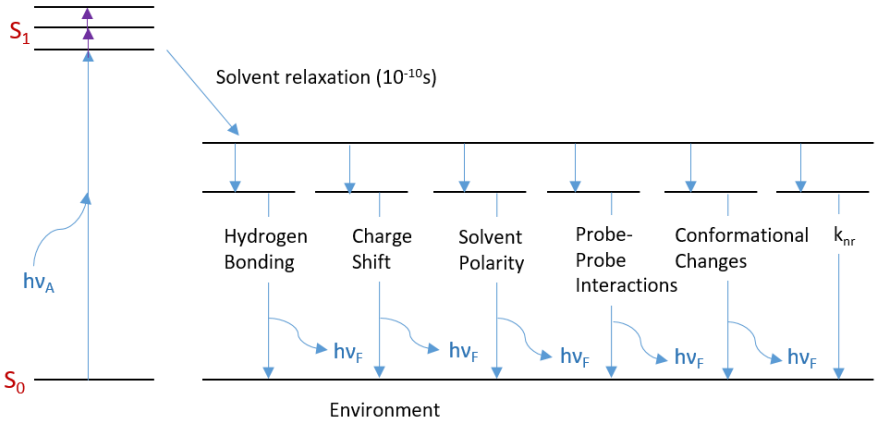

Fig. I - 3 Effects of environment on the energy of the excited state. The dashed arrows indicate the fluorophore can be fluorescent or nonfluorescent in the different states.

In the preceding sections, we illustrated dynamic processes that take place following light absorption in Jablonski diagram (Fig. I - 2). When discussing environmental effects, the solvent polarity and viscosity is often the first topic. In the excited state, the fluorophores often display a larger dipole moment (μ_E) then in the ground state (μ_G). The solvent dipoles can reorient or relax around μ_E following excitation, which lowers the energy of the excited state. As the water polarity is increased at low temperature, this effect can be more evident, which results in emission at lower energies or longer wavelengths. Fig. I - 4 shows the mechanism of this process. However, the water polarity and viscosity have opposite impacts on the emission spectrum though they display the same downward trend with temperature (Fig. I - 5).[36]

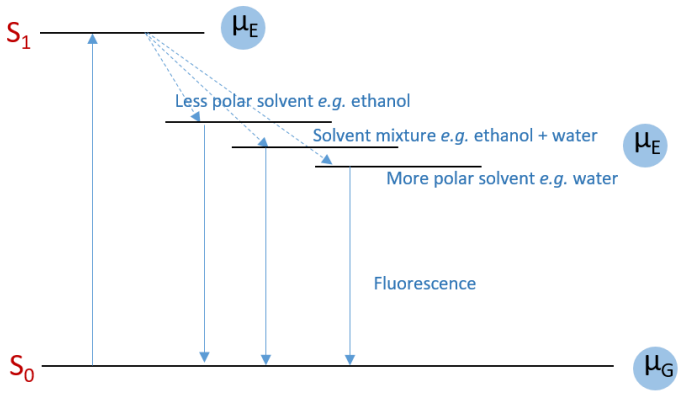

Fig. I - 4 Jablonski diagram for fluorescence with solvent relaxation

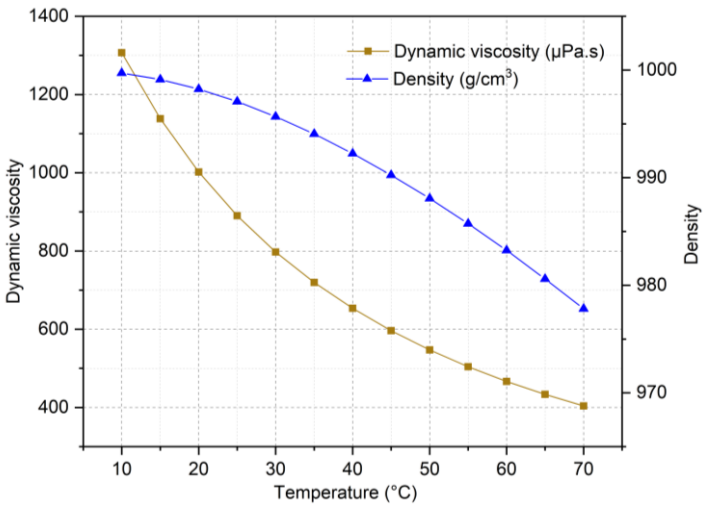

Fig. I - 5 Evolution of dynamic viscosity and density of water as a function of temperature.[36]

In polar solvent such as water, the molecules become more viscous at low temperatures thus the time for solvent relaxation increases accordingly.[37] The rapid decay of excited electrons from higher to the lowest vibrational energy level of the first excited state, the so-called vibrational relaxation, can also be strongly influenced by the temperature and viscosity of the solvent. In general, we assumed that these processes are completed prior to emission. However, if the solvent viscosity is large enough to prevent emission, then one expects to observe the blue-shifted emission spectrum of the unrelaxed F state (case at low temperature). If the relaxation is much faster than the emission, which occurs for fluid solvents, then one expects to observe the red-shifted emission spectrum of the relaxed R state (case at high temperature). When the relaxation rate is comparable to the emission rate, one can observe an emission spectrum of intermediate state. This is illustrated schematically in Fig. I - 6.

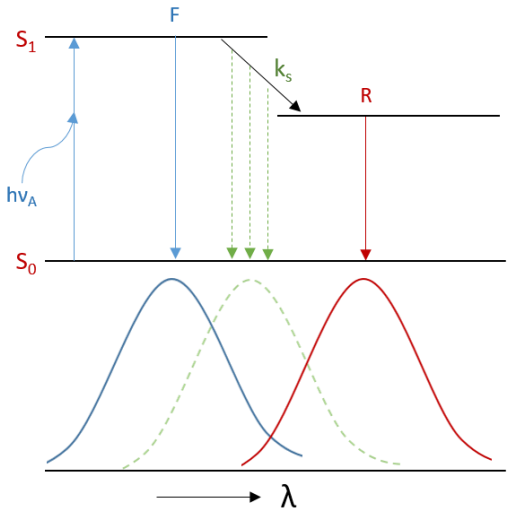

Fig. I - 6 Jablonski diagram for solvent relaxation.

In addition, the quantum yield (Q) is usually suggested to be tightly related to the non-radiative decay (k_{nr}). It has been observed in numerous fluorophores that the quantum yield is low in nonpolar solvents and increases when the solvent contains a polar additive. Eq. I-6 approximately expresses the relation between the quantum yield (Q) and the non-radiative decay (k_{nr}). As the water polarity is high at low temperature, it is reasonable that the value of rate k_{nr} decreases dramatically thus results in blue-shifted and better-resolved spectra due to high quantum yield. Regarding to changes in spectral shape, some states can be observed as a function of temperature, *e.g.*, the formation of an internal charge-transfer (ICT) states.[38] However, for the studied uranyl tricarbonate group, further research is needed to probe the complex luminescent properties of uranium.

$$k_{nr} = (1-Q)/T \quad \text{(I-6)}$$

$$G = Q/T \quad \text{(I-7)}$$

In summary, no single theory can help interpreting the effects of environmental factors on luminescence. In reality, previously mentioned factors should all be considered to account for the uranium luminescent behaviour with temperature, while it is beyond the scope of this work to go into detail about the various mechanisms of emission.

4.3 Experimental set-up

The experimental set-up used in the present work includes a nanosecond Nd:YAG laser oscillator (neodymium-doped yttrium-aluminium garnet laser, Continuum Surelight II) which delivers high pulse energy and the peak power required for the study. This laser source operates

at a repetition rate of 10 Hz with a pulse duration around 7 ns. The advantage of this type of laser source is to emit intense light beams of short duration compared to decay-times of the luminescing radionuclides, *e.g.*, lanthanides with oxidation degree +3, notably Eu(III)[39-42] — analog of Am(III) in the 5f series —, and actinides such as U(VI) and Cm(III) are the elements most often studied using laser because of their relatively high quantum yields. The wavelengths that can be emitted by a laser source (1064 nm, 532 nm, 355 nm, 266 nm) are applied depending on actual cases. In general, the fundamental output of 1064 nm is used for laser ablation or vaporization. The second and third harmonic generations (532 nm et 355 nm) are used to pump the pulsed dye laser or an optical parametric oscillator (only 355 nm). The third and fourth harmonic generations (355 nm et 266 nm) can be used as a photolysis laser in the production of free radicals, or direct excitation of U(VI).

By tripling the wavelength frequency to 1064 nm, the laser beam emitted from our laser source is of λ = 355 nm before entering an optical parametric oscillator (OPO), which can produce an excitation wavelength range from 192 to 2750 nm. The excitation wavelength is fixed at 450 nm in the present work. The laser beam passes through the studied sample that is placed in a cuvette holder cooled or heated by a water circuit thermostatted to a specific temperature to avoid temperature-dependent fluctuations in luminescence — morithis is particularly sensible for uranium(VI).[43] The luminescence light is collected at 90° to the incident beam in order to avoid the sample absorbance as a result of isotropic phenomenon of luminescence. A joulemeter is used to monitor possible drifts in the energy during acquisition. The output signal from the sample is then directed to a converging lens focusing the beam on a detector — the input slit of a spectrometer — which is composed of a monochromator equipped with 300, 600, 1800 lines mm^{-1} gratings in use and a charge-coupled device (CCD) camera. The camera, cooled by Peltier effect to -15°C, is controlled to convert the light signal into an electrical signal. A controller, connecting the camera, the laser source and the computer, allows the collection of luminescence spectra with varying delay time which are then processed to obtain the decay-time of the species under study.

Table I - 2 Operational conditions and acquisition parameters.

Optical quartz cuvette	111-QS, 117-QS with screw cap (Suprasil, Hellma Analytics)
Laser source	Laser Nd : YAG (Surelite, Continuum), 10Hz, impulse duration : 7 ns
OPO	Horizon, Continuum
Spectrometer	Acton 2358i
CCD camera	Princeton, Andor
Thermostat	Peter Huber Kältemaschinenbau AG
Joulemeter	RJP-734, Laser Probe Inc.
Excitation wavelength	450 nm
Delay	25 ns
Gate width	1 µs
Grating	300, 1800 lines mm^{-1}
Gain	245
Accumulation number	1000 for acquisitions at 300 lines mm^{-1}, 10000 for acquisitions at 1800 lines mm^{-1}

I - 5 Thermodynamics of aqueous solutions

The aim of this part is to explain the link between the conditional constants measured at different ionic strengths in experiments and the thermodynamic constants extrapolated to infinite dilution according to the chemical theory of aqueous solution.

5.1 Law of mass action

A chemical equation at equilibrium is generally written as follows:

$$aA + bB \rightleftarrows cC + dD \tag{I-8}$$

The influence of each species included in the equation is evaluated by the chemical potential terms, conventionally denoted by the symbol μ_i, which corresponds to the change in energy of a system following a variation of moles numbers of that species. The Gibbs energy $\Delta_r G$ is used to account for all these energy changes from different species with the following expression.

$$\Delta_r G = \sum_i n_i \mu_i \tag{I-9}$$

The chemical potential of a specific species, dependent on temperature T and pressure P, is composed of a standard chemical potential $\mu_i°$ and an activity term a_i (Eq. I-10). The equilibrium state corresponds to the state in which the Gibbs energy is minimal.

$$\mu_i(T,P) = \mu_i°(T,P) + RTln\left(\frac{a_i}{a°}\right) \tag{I-10}$$

where a° is the activity at standard state conditions, equivalent to 1 and R ≈ 8,31451 $J \cdot K^{-1} \cdot mol^{-1}$.

The equilibrium state requires that the Gibbs energy is minimal or its differential $\Delta_r G = 0$. This makes it possible to develop the expression $\Delta_r G$:

$$\Delta_r G = \sum_i n_i \mu_i = \sum_i n_i \mu_i^\circ + RT \ln \left(\frac{a_C^c \cdot a_D^d}{a_A^a \cdot a_B^b} \cdot \frac{a^{\circ a} a^{\circ b}}{a^{\circ c} a^{\circ d}} \right) = 0 \quad \text{(I-11)}$$

The standard chemical potentials μ_i° are grouped in $\Delta_r G^\circ$ with K° the thermodynamic constant in the reference state:

$$\frac{a_C^c \cdot a_D^d}{a_A^a \cdot a_B^b} \cdot \frac{a^{\circ a} a^{\circ b}}{a^{\circ c} a^{\circ d}} = \exp\left(- \frac{\Delta_r G^\circ}{RT} \right) = K^\circ \quad \text{(I-12)}$$

The infinite dilution state is conventionally chosen as the reference state, from which comes $a^\circ = 1$.

5.2 Real aqueous solutions

The experiments are most often carried out at a specific ionic strength and their activities are not easily accessible. A corrective term is then used in the law of mass action to account for the deviation from ideality. The activity coefficient can be written as follows.

$$a_i = \gamma_i [A]_i \quad \text{(I-13)}$$

With the above relationship, the law of mass action in equilibrium is expressed as follows:

$$K^\circ = \frac{a_C^c \cdot a_D^d}{a_A^a \cdot a_B^b} = \frac{\gamma_C^c \cdot \gamma_D^d}{\gamma_A^a \cdot \gamma_B^b} \cdot \frac{[C]^c [D]^d}{[A]^a [B]^b} \quad \text{(I-14)}$$

with the conditional equilibrium constant K defined as:

$$K = \frac{[C]^c [D]^d}{[A]^a [B]^b} \quad \text{(I-15)}$$

Hence, the formation constants at infinite dilution and at a specific ionic strength can be linked by the following relation:

$$\log_{10} K^\circ = \log_{10} \left(\frac{\gamma_C^c \cdot \gamma_D^d}{\gamma_A^a \cdot \gamma_B^b} \right) + \log_{10} K = \Delta \log_{10} \gamma + \log_{10} K \quad \text{(I-16)}$$

where the value of γ_i varies according to the estimation model.

5.3 Models for ionic strength correction

Activity coefficients cannot be directly experimentally accessible. Indeed, they are parameters to describe the difference between the standard state conditions (K°, also a

hypothetical condition where $a_i = 1$ et $\gamma_i = 1$) and the practical working state (*K*). Because the conditional equilibrium constant *K* determined at a specific ionic strength includes the coefficients γ_i, an estimate of *K*° can be achieved by measuring *K* at different electrolyte concentrations. The ionic strength is defined as follows:

$$I_m = \frac{1}{2}\sum_i m_i z_i^2 \qquad \text{(I-17)}$$

with z_i the charge of the species i. Several models relying on empirical and theoretical arguments have been developed to evaluate activity coefficients at different ionic strengths.

These models are in practice used to relate experimentally measured apparent constant *K* to equilibrium constant *K*° in ideal solution.[44,45]

The existing models used to evaluate activity coefficients all have the Debye-Hückel equation as starting point. The simple Debye-Hückel equation was firstly proposed with a firm theoretical basis to estimate the long-range electrostatic interactions between the ions of opposed charges.[46] However, experimental data exhibited deviations from estimated values of conditional constants with this equation outside the extreme dilution range. Different empirical parameters were introduced to extend the validity range of the simple Debye-Hückel equation.[47] The Davies model,[47,48] including an ion-size parameter with an ion-association approach, was developed to calculate activity coefficients at low ionic strengths. According to the Davies formula, activity coefficients depend only on the ionic strength within a small interval of I_m, but the nature of electrolyte is not taken into consideration. This model can be reduced to the simple Debye-Hückel equation at very low electrolyte concentrations since the supplementary term tends to zero with decreasing ionic strength. For this reason, the Davies equation can be applied to a slightly wider range of ionic strength than the simple Debye-Hückel equation.

The specific ion interaction formulations[49-52] are often applied in the cases of higher electrolyte solutions up to 3.5 mol kg_w^{-1} to estimate the activity coefficients of solutes. The SIT is specially employed when few experimental data are available to fit the ionic strength correction model, as in the case of actinide complex studies. This theory has been validated in previous studies and adopted in the NEA's critical review to justify the data selection — for uranium see Grenthe, *et al.*[49], Guillaumont, *et al.*[51], and Grenthe, *et al.*[52]. It will be detailed in the following section.

The Pitzer[45] model is applicable to a wider field than the SIT due to its more sophisticated formulation. Indeed, more adjustable parameters the model contains, more capable they are of

reproducing the experimental results. In comparison with the SIT, which has only one adjustable variable — the ion interaction coefficient —, the Pitzer formula has at least three parameters, made up of two binary and one ternary terms. Nevertheless, introducing a large number of variables is a disadvantage when some of them are unknown or difficult to estimate. In particular, the adjustment parameters are correlated with each other in the Pitzer theory, that makes the determination more complicated for solutions containing many chemical species.[45]

The SIT will be used throughout this document in order to both correct the ionic strength for the experimentally measured apparent constants *K* and intercompare the equilibrium constants *K*° extrapolated from different experimental sources in literature. Using the SIT formula, we will deduced the formation constants at infinite dilution and the interaction coefficients for the studied complexes in two different background electrolytes — NaCl and $NaClO_4$. As to the measurement of state functions of temperature, the osmotic coefficients ϕ and the water activity a_{H_2O} at different temperatures have been recalculated and used in the extrapolations with the values shown later. (*cf.* Table I - 6)

5.3.1 Davies equation

The Davies[48] equation, in its general form, depends only on the ionic strength of the inert solution. The estimation of activity coefficient for solutions of ionic strength lower to 0.3 mol L^{-1} can be written as follows:

$$\log_{10} \gamma_i = -Az_i^2 \left(\frac{\sqrt{I}}{1+\sqrt{I}} - 0.3I \right) \qquad \text{(I-18)}$$

where the quantity A has the same value for all ions and z_i is the charge on a particular ion *i*;

The way in which the activity coefficient corrections are performed is illustrated below for the general case of a complex formation reaction. The formation of ML_j complex, with j representing the number of ligand L varying from 1 to n, is expressed by Eq. I-19.

$$M + jL \rightleftarrows ML_j \qquad \text{(I-19)}$$

According to the mass action law, the conditional cumulative complexation constants are given by the following expression.

$$\beta_j = \frac{[ML_j]}{[M][L]^j} \qquad \text{(I-20)}$$

As stated in Eq. I-21, the logarithm of the formation constants $\log_{10}\beta_j°$ and $\log_{10}\beta_j$ are related by the following relationship:

$$\log_{10}\beta_j^\circ = \Delta\log_{10}\gamma + \log_{10}\beta_j \quad \text{(I-21)}$$

with $\Delta\log_{10}\gamma = \log_{10}\gamma\left(ML_j\right) - \log_{10}\gamma\left(M\right) - j\log_{10}\gamma\left(L\right)$

According to the Davies equation (Eq. I-18), the $\Delta\log_{10}\gamma$ can be calculated as following:

$$\Delta\log_{10}\gamma = -A\Delta z^2\left(\frac{\sqrt{I}}{1+\sqrt{I}} - 0.3I\right) \quad \text{(I-22)}$$

with $\Delta z^2 = z(ML_j)^2 - z(M)^2 - jz(L)^2$

5.3.2 Specific ion interaction theory

The estimation of activity coefficient in the SIT equation includes two terms: the first term corresponds to the Debye-Hückel equation and contains a single variable, ionic strength I_m, and the second term sums the contributions of aqueous ions. Moreover, the second I_m-dependent term comes from the first approximation of the virial expansion to describe the short-range, non-electrostatic interactions at higher concentrations. This term contains the specific ion interaction coefficients ε, which is considered correlated with the charge and size of the studied ions. The formulation of SIT is expressed as follows:

$$\log_{10}\gamma = -z_i^2 D + \sum_i(\varepsilon_{i,j}m_j) \quad \text{(I-23)}$$

with $\varepsilon_{i,j}$ (en $kg_w\ mol^{-1}$) the specific ion interaction coefficient between the ions i and j counterion in solution and m_j the molar concentration of ion j:

$$D = \frac{A(T)\sqrt{I}}{1+r_iB(T)\sqrt{I}} \quad \text{(I-24)}$$

where A(T) and B(T) are written as follows:[53]

$$A(T) = \frac{e^3}{8\pi ln10}\sqrt{\frac{2000N_A}{p(\varepsilon_0\varepsilon_W k_B T)^3}} \quad \text{(I-25)}$$

$$B(T) = e\sqrt{\frac{2000N_A}{p\varepsilon_0\varepsilon_W k_B T}} \quad \text{(I-26)}$$

with e the electron charge, N_A the Avogadro number, p the molarity-molality conversion coefficient, ε_0 the vacuum permittivity, ε_W the relative permittivity or dielectric constant of water relative to the vacuum permittivity, k_B the Boltzmann constant, T the absolute temperature (K), r_i the hydrated radius of ion i, estimated as a sphere shape.

These constants are all expressed in SI units. According to the approach of Brönsted, Guggenheim and Scarchard (abbreviated B-G-S equation),[44,54,55] A(T) and B(T) are considered independent of I_m, even if they depend on the constants p and ε_W that vary from pure water to a solution of non-zero ionic strength. These considerations support the fact that the Debye-Hückel term first term D_H considers mainly long-range electrostatic interactions when evaluating deviations from ideality of activity coefficients.

At 25°C and 1 bar, the values of A and B are respectively 0.5091 $L^{1/2}$ $mol^{-1/2}$ and $0.328.10^{10}$ $L^{1/2}$ $mol^{-1/2}$ m^{-1}.[56] In general, the product r_iB is an empirical choice and fixed to 1.5 at 25°C, which minimizes the variations of $\varepsilon_{i,j}$ with ionic strength for a number of electrolytes.[57] However, the hypothesis of $\varepsilon_{i,j}$ independence with respect to ionic strength does not seem to be always justified at low ionic strengths experimentally and theoretically.[45] Nonetheless, the term $\varepsilon_{i,j}m_j$ is negligible compared to the second term z_iD in dilute concentrations. Finally, assuming that $\varepsilon_{i,j}= \varepsilon_{j,I}$, validated for strong electrolytes in the development of the second virial term, one can still obtain $\log_{10}\gamma_i = \log_{10}\gamma_j$. It is known that the extrapolated values according to the SIT equation is not always in good agreement with the best experimental data, notably at dilute electrolyte concentrations, but the differences are often too small.[49,51,52]

The basic assumptions in SIT formulations have to be outlined here. First, the summations in the second term extend over all aqueous ions j. Nevertheless, the concentrations of the electrolyte ions X^+ and Y^- are generally much larger than those of reactions species. Thus, the medium ions make the main contribution to the value of activity factors γ_i. For this reason, the summations are often simplified so that only ion interaction coefficients between the ionic medium ions X^+ and Y^- and involved reactants/products are included:

$$\log_{10}\gamma = -z_i^2 D + \varepsilon_{i,\ X^+ ou\ Y^-}[XY] \qquad \text{(I-27)}$$

Secondly, the ion interaction coefficients are usually expected to be small for ions of the same charge sign due to electrostatic repulsion. Similarly, they should also be small for the electrostatic interactions between uncharged species, for which the SIT equation is reduced to only one term. One of the assumptions in SIT proposes a nil value for the interaction coefficients of uncharged complexes. However, Ciavatta tabulated a number of non-nil interaction coefficients for neutral species.[58] For organic ligand, Hummel, *et al.*[59] proposed $\varepsilon(EdtaH_4(aq),NaCl)$ and $\varepsilon(EdtaH_4(aq),KCl)$ values, and Fromentin and Reiller[40] proposed

$\varepsilon(AdipateH_2(aq), NaCl)$ values.[*] The results in these studies suggested that the numerical values of interaction coefficients could be inconsistent with those estimated from the assumptions of the SIT model.

Ion interaction coefficient of a given complex can be estimated by direct determination from the variation of equilibrium constants with ionic strength or by analogy with those of the ions of the same charge and size. It is noted in the NEA-TDB reviews that one should be prepared to verify the validity of corresponding assumptions when analyzing experimental data measured at high electrolyte concentrations or with the use of high precision techniques. Especially, it may be possible that the value of $\Delta\varepsilon$ can significantly varies from one ionic medium to another. Hence, the specific ion interaction coefficients should be specified with the medium in which the values are obtained.

Temperature influence on SIT parameters and interaction coefficients

The effect of temperature on the Debye-Hückel term requires supplementary approximations. In this study, the values of the Debye-Hückel parameter A(T) at different temperatures below 70°C are the values used in the NEA TDB reviews.[49,51,52] With regards to the values of r_iB, this product will be maintained at 1.5 $kg_w^{1/2}$ $mol^{-1/2}$ at any temperature in this study. In fact, the values of ε and r_iB are strongly correlated, as previously discussed in relation to the variations of interaction coefficients and parameter B(T) with temperature.[60-64] In other words, the variation of r_iB with temperature is included in the interaction coefficient, but the latter is an empirical term of which the physical signification is not well known. In the temperature interval of 0-100°C, the variation of the Debye-Hückel term D_H is extremely weak, even negligible. Therefore, the values of ε and r_iB will be taken as constant in the determination of formation constants of $MgCa_nUO_2(CO_3)_3^{(2n-4)-}$ over the experimental temperatures — see Chapter V for further details.

Modified versions of the SIT equation

As stated in the preceding section, ion interaction coefficients are assumed constant within a certain range of ionic strength. However, they are not strictly constant but vary slightly with ionic strength. In general, variation of ε is often neglected for 1:1, 1:2 or 2:1 electrolytes of concentrations less than 3.5 mol kg_w^{-1}, supported by an amount of experimental material.[55] For high-charge type electrolytes, the concentration-dependent ε should be used to calculate the

[*] $COOH–(CH_2)_4–COOH$

activity coefficient.[65] Several equations based on the SIT model have been proposed to evaluate ε as a function of ionic strength. The approach proposed by Ciavatta[58] has been used in some cases in previous studies, expressed in Eq. I-28.

$$\varepsilon(j, k, I_m) = \varepsilon_1 + \varepsilon_2 \log_{10} I_m \quad \text{(I-28)}$$

However, this relationship was not recommended by the NEA TDB for the reason that the interaction coefficient ε tends to negative infinity when the ionic strength tends to zero due to the introduction of logarithm in the expression of interaction coefficient.[65] Nevertheless, the complete expression of activity coefficient justifies the validity of this description at infinite dilution because the first term of $(\varepsilon_1 + \varepsilon_2 \log_{10} I_m)\, I_m = \varepsilon_1\, I_m + \varepsilon_2\, I_m \log_{10} I_m$. tends to zero when decreasing ionic strength[52] and the second one tends also to zero knowing that $\lim_{I_m \to 0} I_m \, ln \, I_m \to 0$.

Bretti *et al*.[66,67] added a term that takes into account the formation of weak ion pairs as follows.

$$\varepsilon(j, k, I_m) = \varepsilon_\infty + \frac{\varepsilon_0 - \varepsilon_\infty}{I_m + I} \quad \text{(I-29)}$$

By considering association of the ion pairs with the formation constant K, Eq. I-30 can be written as the approximation:

$$\varepsilon(j, k, I_m)\, I_m = \varepsilon I_m - log_{10}(1 + K\, I_m) \quad \text{(I-30)}$$

5.3.3 Pitzer equation

Apart from the above-mentioned ionic strength correction approaches, some other formulations have been developed in literature to describe the measured formations constants with high precision over a large concentration range, *e.g.*, the Pitzer and Brewer equation,[60] the Pitzer equations,[68-73] and the Baes and Mesmer equations.[74] The Pitzer equations consists of three terms involving a Debye-Hückel-like term, a term describing binary interactions and a term describing ternary interactions. Compared to the SIT equation considering only interactions between ions of opposite sign, the Pitzer equations also take into account cation-cation, anion-anion and cation/anion-neutral interactions. However, the main problem in using the Pitzer equations is the determination of the concentration-dependent second virial coefficient. In addition to that, the use of the Pitzer equations requires an amount of experimental data over a sufficiently large range of ionic strength to deduce reliable values for

salt-specific parameters that is often difficult to realize in experiments, especially using radioactive materials.

5.4 Temperature functions — enthalpy and entropy calculations

Evaluation of equilibrium constants from a specified temperature to any other desired temperature can be done by using the general thermodynamic relationships. Once the values of $\Delta_r H_m°$ or $\Delta_r S_m°$ at the reference temperature and their temperature dependence are available, the estimation of formation constants at other temperatures is straightforward. However, complete thermodynamic data of this kind is rarely available for complexes formations in aqueous solution because experiments only provide information about the species that are detectable in the laboratory systems. Therefore, difference approximation methods are necessary to recalculate equilibrium constants at any desired temperature.

Appearance of new species is one of the complications in the modelling of aqueous speciation at different temperatures. Thus, the modelling of such systems is supposed to be based on experimental evidence of change in speciation. Moreover, physical properties of solvent water change strongly with temperature that influence the relative amounts of charged complexes. For instance, the dielectric constant of water — the force between the ions to separate from each other — decreases significantly with increasing temperature — Fig. I - 7 shows the variation of dielectric water as a function of temperature following the equation of Malmberg and Maryott.[75] This decrease in water dielectric constant favours the formation of low or zero charge complexes but hinders that of polynuclear and high charges complexes. The acidity of water also decreases with increasing temperature that aggregates hydrolysis of metal ions.

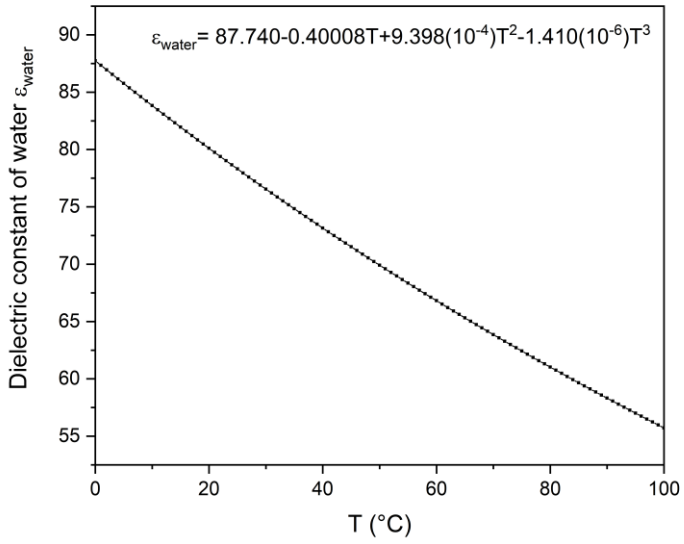

Fig. I - 7 Variation of dielectric water as a function of temperature

In practice, the approximation models used to determine temperature dependencies of chemical equilibria are based on oversimplified electrostatic models, which take the participating ionic species as point-charges and the solvent water as a homogeneous dielectric continuum. Two models named second- and third-law methods are generally adopted in extrapolating experimental data determined at a specific temperature to different temperatures. The third-law model is generally applied to equilibria between different phases over a large temperature range since this model requires accurately estimated heat capacities and relative enthalpies for reactants and products of pure phase. The second-law exploration model is generally used for accurate calculations over relatively small temperature ranges in aqueous environments with heat capacities estimated around the temperature of interest. In the frame of this work, we will use the second-law extrapolation to deduce the temperature functions of $(Mg/Ca)_nUO_2(CO_3)_3^{(2n-4)-}$ complexes.

5.4.1 Second-law extrapolations

The relationship between standard molar Gibbs energy, enthalpy, and entropy at a given temperature can be expressed as follows:

$$\Delta_r H_m^\circ = \Delta_r G_m^\circ + T\Delta_r S_m^\circ$$

where the enthalpy is the sum of the Gibbs free energy and the energy “dispersed” by the reaction, or more commonly as follows.

$$\Delta_r G_m^\circ = \Delta_r H_m^\circ - T\Delta_r S_m^\circ \quad \text{(I-31)}$$

The temperature dependence of the Gibbs energy is expressed as follows.

$$\left(\frac{\partial \Delta_r G_m^\circ}{\partial T}\right)_p = -\Delta_r S_m^\circ \quad \text{(I-32)}$$

$$\left(\frac{\partial \Delta_r G_m^\circ / T}{\partial T}\right)_p = \frac{-\Delta_r H_m^\circ(T)}{T^2} \quad \text{(I-33)}$$

Using the temperature derivatives of enthalpy and entropy, one can obtain:

$$\left(\frac{\partial \Delta_r H_m^\circ}{\partial T}\right)_p = \Delta_r C_{p,m}^\circ \quad \text{(I-34)}$$

$$\left(\frac{\partial \Delta_r S_m^\circ}{\partial T}\right)_p = \frac{\Delta_r C_{p,m}^\circ}{T} \quad \text{(I-35)}$$

It is possible to relate the temperature dependence of the Gibbs energy to the entropy and the heat capacity function at the reference temperature of 298.15K, expressed in the following:

$$\Delta_r G_m^\circ(T) = \Delta_r H_m^\circ(T_0) + \int_{T_0}^{T} \Delta_r C_{p,m}^\circ dT - T\left(\Delta_r S_m^\circ(T_0) + \int_{T_0}^{T} \frac{\Delta_r C_{p,m}^\circ}{T} dT\right) \quad \text{(I-36)}$$

with T_0 being the reference temperature.

From the relationship between the Gibbs energy and the equilibrium constants, one can write the temperature dependence of equilibrium constant as a function of the enthalpy and the heat capacity as follows:

$$\log_{10} K°(T) = \log_{10} K°(T_0) - \frac{\Delta_r H_m^\circ(T_0)}{R\ln(10)}\left(\frac{1}{T} - \frac{1}{T_0}\right) - \frac{1}{RT\ln(10)}\int_{T_0}^{T} \Delta_r C_{p,m}^\circ dT + \frac{1}{RT\ln(10)}\int_{T_0}^{T} \frac{\Delta_r C_{p,m}^\circ}{T} dT \quad \text{(I-37)}$$

with R the gas constant (8.31451 J K^{-1} mol^{-1}).

Equilibrium constant at any temperature T can thus be estimated with the Eq. I-37 when $\log_{10}K°(T_0)$, $\Delta_r C_{p,m}°$ and $\Delta_r H_m°(T_0)$ (or $\Delta_r S_m°(T_0)$) are known. The temperature dependence of heat capacity is not available for most aqueous species. Therefore, one can make some approximations in several situations such as extrapolations over a relatively small temperature interval assuming $\Delta_r C_{p,m}°$ constant or even zero as discussed below.

5.4.2 Approximations based on the second-law method

For the chemical species of which the heat capacity is not available, some estimations are necessary to be made in order to deduce $\log_{10}K°(T)$ using Eq. I-37. We will only introduce the models used in this work.

Assumption of constant enthalpy

This assumption greatly simplifies Eq. I-37 since the standard enthalpy does not vary with temperature and the heat capacity can be assumed zero at all temperatures. The reduced equation is the integrated Van't Hoff expression:

$$\log_{10} K°(T) = \log_{10} K°(T_0) - \frac{\Delta_r H_m^\circ(T_0)}{R\ln(10)}\left(\frac{1}{T} - \frac{1}{T_0}\right) \quad \text{(I-38)}$$

This equation is applicable to experimental systems of a single phase or multiphase at constant total pressure with no further constraint placed on the system. For the studies of temperature dependence of solubility products, the simplification in this model should be accordingly modified. Furthermore, for an extrapolation over a temperature range equal or less than 10 K,[76] the error introduced in the resulted $\log_{10}K°(T)$ using this equation will be within its uncertainty limits.

Assumption of constant heat capacity

For a temperature range slightly larger than about 20 K,[76] we choose another approach often used in conjunction with Eq. I-37 assuming constant heat capacity with temperature. Eq. I-37 becomes

$$\log_{10} K°(T) = \log_{10} K°(T_0) - \frac{\Delta_r H_m^\circ(T_0)}{R\ln(10)}\left(\frac{1}{T} - \frac{1}{T_0}\right) + \frac{\Delta_r C_{p,m}^\circ}{R\ln(10)}\left[\left(\frac{T_0}{T}\right) - 1 + \ln\left(\frac{T}{T_0}\right)\right] \quad \text{(I-39)}$$

Accordingly, the Gibbs energy can be expressed as follows:

$$\Delta_r G_m^\circ(T) = \Delta_r G_m^\circ(T_0) - (T - T_0)\Delta_r S_m^\circ(T_0) + \Delta_r C_{p,m}^\circ\left[T - T_0 - T\ln\left(\frac{T}{T_0}\right)\right] \quad \text{(I-40)}$$

The obtained equilibrium constants are more reliable than those obtained with the constant enthalpy assumption. The assumption of constant heat capacity is useful to calculate the Gibbs energy at higher temperatures specifically in the range 273 to 473 K. It should be noted that in some cases, the heat capacity term can be neglected if the entropy and the heat capacity are comparable in magnitude because $\Delta_r C_{p,m}^\circ[\Delta T - T\ln(T/T_0)]$ is less important than $\Delta_r S_m^\circ \Delta T$ over the temperature range of 273 to 473 K.

Isoelectric reactions

Isoelectric reactions are defined for the chemical reactions of the following form: the sum of positive charges among the reactants equals the sum of positive charges among the products, and the same for the negative charges among the reactants and the products. The reactions of this kind can largely balance out the electrostatic contributions to the temperature dependence of enthalpy, thus the heat capacity of reaction can be assumed constant with temperature. Using the isoelectric reaction modification, the constant enthalpy estimation model is reliable over a greatly larger temperature range up to $T \leq 473$ K and the constant heat capacity estimation model up to $T \leq 623$ K.[76] In this study, we can try to convert the original complexation to isoelectric reactions and fit the experimental data with the constant enthalpy estimation model.

5.5 Available speciation software and thermodynamic databases

To meet the industrial requirements of radioactive waste management, several predictive transport models have been currently developed by coupling physico-chemical knowledge of uranium and computer algorithms. The use of geochemical modelling codes have advantages and disadvantages. On one hand, such calculations can reach a high precision with results reported to even 6 significant digits. Therein comes out the disadvantage of the calculations codes as the precise results can camouflage the reliability of data sources especially to a non-expert geochemist or environmental scientist. For some species of which no experimental data exist at all, their implementing data are sometimes estimated by correlations or analogy until sufficient experimental data are available. However, the widespread use of computational codes has to make predictions in some critical societal fields of *e.g.*, the management of nuclear waste and remediation of toxic radioactive or conventional waste plumes. Thus, a critical assessment of literature data including tracking down their original sources, and understanding the limitations of the data being used, is essential prior to calculations because missing, or badly estimated, compounds can result in completely different speciation.

The final speciation results strongly rely on the algorithms of the used software and overall of the choice of the thermodynamic database file. Nowadays, PhreeqC (pH redox equilibrium in C),[77,78] CHESS (Chemical equilibrium of species and surfaces, http://chess.geosciences.mines-paristech.fr) and GWB (the Geochemists' WorkBench, http://www.gwb.com) are among the commonly used codes that allow a rapid calculation of solute speciation and mineral solubility in a variety of geochemical systems. For each of them several specific thermodynamic database files are provided.

For safety and assessment of radioactive waste management, a variety of databases has been developed, such as the Swiss Nagra/PSI TDB,[79] the American Lawrence Livermore National Laboratory TDB,[80,81] the Japanese JNC TDB,[82] the British HATCHES,[83] and the French ThermoChimie TDB[84-86] originally developed by ANDRA (France, Agency for radioactive waste management). The latter database is now covering the need for ANDRA, ONDRAF-NIRAS (Belgium), and RWM (Great Britain). The above databases share the same source of main uranium data that are critically selected and reviewed by experts participating in the NEA-TDB, then published in a series of *Chemical Thermochemistry* books.[49,51,56,59,87-91] Establishing this type of compilation requires an enormous amount of critical work, which necessarily reduces the number of data compilations as well as the number of species.

The second law of thermodynamics is the key to any geochemical solubility and speciation calculations: the chemical system attempts to attain the lowest energy state, which means minimizing the Gibbs free energy. The Gibbs free energy, as well as other thermodynamic properties, depends on multiple factors, notably temperature and pressure. The standard states (25°C, 1 bar) are adopted in calculations, as in many natural systems the temperature and pressure are often fixed. For this reason, the compiled constants in database file are defined in some limiting conditions, such as infinite dilution, and then extrapolated to the specified experimental conditions. Some computer programs allow generating equilibrium constants at higher ionic strengths with ionic correction functions: the truncated Davies model, the extended Debye-Hückel equation, the B-dot equation or the Pitzer's model (explained later on). For example, the program SUPCRT92[92] and EQ3/6 (https://ipo.llnl.gov/technology/software/softwaretitles/eq36.php), which was then adopted to other programs, *e.g.*, the CHESS and PhreeqC codes, broadly used with different database options: llnl, minteq, phreeqc, *etc*.

The correction functions determine the maximum ionic strength to which the extrapolation is valid. For dilute to moderately concentrated solutions, activity coefficients are sufficient to perform explorations, while Pitzer's ion interaction approach is necessary in dealing with highly concentrated solutions. This model is generally preferred over the one-parameter extrapolation one and has been incorporated into Eq3/6, PhreeqC[77,78], ToughReact,[93] and GWB. However, the lack of Pitzer's interaction parameters for minor or trace elements and incomplete description of thermodynamic behaviour at elevated temperature for a handful of common elements constitute a barrier to accurate calculations, though efforts have been made in compiling the Pitzer parameters.[94]

Apart from the ThermoChimie TDB,[84,85] which is dedicated to modelling the near field of disposal facilities for radioactive waste in the framework of Cigéo Project (Centre industriel de stockage géologique), an in-house database PRODATA TDB specifically used in the modelling of the Orano group's mining and post-mining activities[95] has been built with CEA. Among the above-mentioned databases, PRODATA TDB, based in priority on the recommendations of CODATA and NEA TDB and supplemented with data from literature, is a comprehensive thermodynamic database with 38 aqueous species of uranium (VI) compared to 32 species in ThermoChimie TDB. These two databases have the main body of compiled data, and the main difference relates to the constants of $M_nUO_2(CO_3)_3^{(4-2n)-}$ (n = {1, 2}, M = Ca, Ba; n = {1}, M = Mg, Sr) and $UO_2CO_3F_n^{n-}$ (n = {1, 2}) that are included in PRODATA TDB but absent in ThermoChimie TDB. The PRODATA base can also be exportable to the main software: PhreeqC, CHESS, and GWB.

I - 6 Complex formation equilibria

6.1 Uranyl hydrolysis products

The formation reaction of uranyl hydrolysis products and the associated formation constants $\beta_{q.m}$ are written as follows:

$$mUO_2^{2+} + qH_2O = (UO_2)_m(OH)_q^{2m-q} + qH^+ \quad \text{(I-41)}$$

$$\beta_{q.m}^0 = \frac{((UO_2)_m(OH)_q^{2m-q})\,(H^+)^q}{(UO_2^{2+})^m} \quad \text{(I-42)}$$

where $((UO_2)_m(OH)_q^{2m-q})$, (H^+), (UO_2^{2+}) are activities of hydroxy complexes, hydrogen ion and uranyl ion, respectively; m and q are the stoichiometric coefficients of hydrolysis complexes.

The formation constants as well as the existence of several uranyl hydrolysis species have been and still are discussed in the literature. To illustrate the discrepancies between published studies on uranyl hydrolysis species, Table I - 3 compares two selected thermodynamic databases: one recommended by the Nuclear Energy Agency (NEA)[49,51] and the other by the International Atomic Energy Agency (IAEA) from literature reviews carried out by international expert groups.[96] The selection of Guillaumont *et al.*[51] is the updated version of Grenthe *et al.*[49] including the estimated values different from those reported in the selection of Fuger *et al.*[96] This is the case for $(UO_2)_2OH^{3+}$ and $UO_2(OH)_2(aq)$ complexes, also for some other species that are not listed there. Overall, these selections agree only on the values of the formation constants of UO_2OH^+, $(UO_2)_2(OH)_2^{2+}$, $(UO_2)_3(OH)_5^+$. Fuger[97] then discussed the

values of the equilibrium constants of the two selections and noted that the data recommended by Grenthe *et al.*[49] and validated by the NEA were from deeper research, *i.e.* internal calculation — one can note that Jean Fuger participated in both programs.

Table I - 3 Hydrolysed uranyl species formation reactions and selected formation constants in different databases.

Reaction	$\log_{10} K^{\circ}$		
	Grenthe *et al.*[49]	Fuger *et al.*[96]	Guillaumont *et al.*[51]
$UO_2^{2+} + H_2O \rightleftarrows UO_2(OH)^+ + H^+$	-5.2 ± 0.3	-5.76 ± 0.10	-5.25 ± 0.24
$UO_2^{2+} + 2H_2O \rightleftarrows UO_2(OH)_2(aq) + 2H^+$	≤ -10.3[a]	-13.00 ± 0.25	-12.15 ± 0.07
$3UO_2^{2+} + 5H_2O \rightleftarrows (UO_2)_3(OH)_5^+ + 5H^+$	-15.55 ± 0.12	-15.44 ± 0.10	-15.55 ± 0.12
$2UO_2^{2+} + CO_2(g) + 4H_2O \rightleftarrows (UO_2)_2CO_3(OH)_3^- + 5H^+$	-19.01 ± 0.50		-19.01 ± 0.50

[a] this value was proposed as an upper value

The data recommended by Grenthe *et al.*[49] for the formation constants of UO_2OH^+, and $(UO_2)_3(OH)_5^+$ have been confirmed in subsequent studies and selections.[51,52] Choppin and Mathur[98] established that the equilibrium constant of UO_2OH^+ is equal to -(5.91 ± 0.08) in $NaClO_4$ at 0.1 mol L^{-1} ionic strength. Recently, Drobot, *et al.*[99] questioned the value of UO_2OH^+ from the NEA-TDB selections. Bruno and Sandino[100] have determined values of equilibrium constants at standard state conditions to -(15.6 ± 0.01) for $(UO_2)_3(OH)_5^+$. The determination of the formation constant of $UO_2(OH)_2(aq)$ complex has also been the subject of several studies since 1992. The results are compatible with the upper values recommended by Grenthe *et al.*[49] and Fuger *et al.*[96] Choppin and Mathur[98] have proposed a value less than -12 for formation constant of $UO_2(OH)_2$ which is close to that proposed by Fuger *et al.*[96] Silva[101] and Torrero *et al.*[102] reported a value less than or equal to -11.5 for the same complex. Guillaumont *et al.*[51] finally selected -(12.15 ± 0.17) for $UO_2(OH)_2$ in the updated version of 2003, which was confirmed in the last update by Grenthe, *et al.*[52].

The choice of values for the formation constants of the uranyl hydrolysis species remains delicate, due to the disparities between published data. The formation constants of the uranyl hydrolysis products used in this work to perform calculations of aqueous uranyl ion species distribution are taken from Guillaumont *et al.*[51] It can be emphasized that the recent update of Grenthe, *et al.*[52] does not change the core of these data.

6.2 Uranyl carbonate complexes

The aqueous carbonate system is important in analyzing environmental problems since the carbon dioxide and the alkaline earth carbonate-containing minerals — *e.g.*, calcite ($CaCO_3$) and dolomite ($CaMg(CO_3)_2$), and to a lesser extend nesquehonite ($MgCO_3{:}3H_2O$), are of high abundance in nature.[103] The principal equilibrium reactions of aqueous carbonate systems are given in Eq. I-43 – Eq. I-45,[104,105] with the Henry's Law constant $\log_{10}K^{\circ}_{H}$ describing the equilibrium between the atmospheric $CO_2(g)$ and dissolved $CO_2(aq)$ and $\log_{10}K^{\circ}_{eq}$ representing the formation of the carbonic acid, H_2CO_3 due to the dissolution of carbon dioxide gas in solution.

$$CO_2(g) \rightleftharpoons CO_2(aq) \qquad \log_{10}K^{\circ}_{H} = -1.47 \qquad \text{(I-43)}$$

$$CO_2(aq) + H_2O \rightleftharpoons H^+ + HCO_3^- \qquad \log_{10}K^{\circ}_{1} = -6.35 \qquad \text{(I-44)}$$

$$HCO_3^- \rightleftharpoons H^+ + CO_3^{2-} \qquad \log_{10}K^{\circ}_{2} = -10.33 \qquad \text{(I-45)}$$

In an open system, the total carbonate concentration is correlated with the amount of atmospheric CO_2 that dissolves into solution.[106] Thus the concentrations of HCO_3^- and CO_3^{2-} are dependent on the partial pressure of $CO_2(g)$ to which the solution is exposed. As an example, Fig. I - 8 gives the distribution of $CO_2(aq)$, HCO_3^- and CO_3^{2-} as a function of pH in 0.1 M $NaNO_3$ at $P(CO_2)= 10^{-3.5}$ atm. Under these conditions, HCO_3^- predominates over the range of pH 4-9 with the concentration increasing from about 10^{-6} M at pH 4 to 10^{-2} M at pH 8 and CO_3^{2-} is always in the minority compared to HCO_3^- at the same pH.

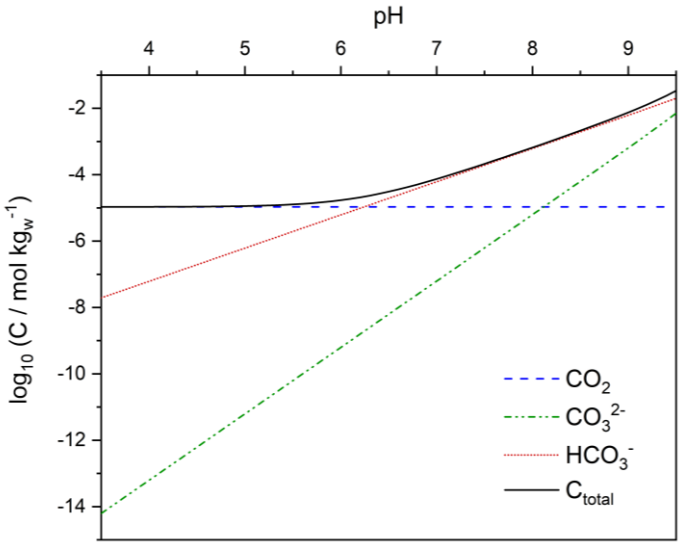

Fig. I - 8 Distribution of carbonate species in equilibrium with air ($P(CO_2)= 10^{-3.5}$atm) as a function of pH. The thick line represents the total dissolved carbonate concentration. (Electrolyte solution: 0.1 mol kg_w^{-1} NaCl)

It is therefore necessary to control the CO_2(g) source when studying carbonate systems. Equations expressed in terms of CO_2(g), shown in Eq. I-46 and Eq. I-47, are more useful for studies on open systems by rearranging the Eq. I-43 – Eq. I-45.

$$CO_2(g) + H_2O \rightleftharpoons 2H^+ + CO_3^{2-} \qquad \log_{10}K_3^\circ = -18.15 \tag{I-46}$$

$$CO_2(g) + H_2O \rightleftharpoons H^+ + HCO_3^- \qquad \log_{10}K_4^\circ = -7.82 \tag{I-47}$$

In the presence of dissolved carbonates, the formations of uranyl carbonate complexes are expressed as follows:

$$mUO_2^{2+} + qCO_3^{2-} = (UO_2)_m(CO_3)_q^{2m-2q} \tag{I-48}$$

$$\beta_{q.m}^0 = \frac{((UO_2)_m(CO_3)_q^{2m-2q})}{(UO_2^{2+})^m(CO_3^{2-})^q} \tag{I-49}$$

where $((UO_2)_m(CO_3)_q^{2m-2q})$, (UO_2^{2+}) and (CO_3^{2-}) are activities of uranyl carbonate complexes, uranyl ion and carbonate, respectively; m and q are stoichiometric coefficients of complexation reactions.

Table I - 4 gives the formation constants of uranyl carbonate complexes used in our study to calculate the distribution of aqueous uranyl ion species. Another complication of the aqueous carbonate systems is that the hydrolysis reactions are also present, and three ligands — OH^-, HCO_3^- and CO_3^{2-} — are always present in carbonated solutions. One cannot investigate metal-carbonate reactions without considering the metal ion hydrolysis chemistry because the

individual concentration of the three ligands does not vary independently due to the intimately connected hydrolysis and carbonate equilibria. For this reason, the uranyl carbonate system should be formally understood as a three-component system of uranyl, hydroxide, and carbonate.

Table I - 4 Formation constants of uranyl carbonate complexes at standard state conditions (I_m= 0, T= 298 K) from Guillaumont, et al.[51]

Reaction	$\log_{10}\beta^{\circ}$
$UO_2^{2+} + CO_3^{2-} \rightleftarrows UO_2(CO_3)(aq)$	9.94 ± 0.03
$UO_2^{2+} + 2CO_3^{2-} \rightleftarrows UO_2(CO_3)_2^{2-}$	16.61 ± 0.09
$UO_2^{2+} + 3CO_3^{2-} \rightleftarrows UO_2(CO_3)_3^{4-}$	21.84 ± 0.04

6.3 Ringböm coefficient calculations

The concept of Ringböm coefficient — also called side-reaction coefficient or α coefficient — was first introduced by Schwarzenbach[107] to simplify equilibrium calculations in analytical chemistry. Ringböm *et al.*[108-110] later suggested that practically all occurring side reactions with the responsible interfering species should be accounted to estimate their influence on a certain main reaction.

Considering the formation of a mononuclear complex ML by a metal ion M with a ligand L, the main reaction may be affected by hydrogen or hydroxide ions in three ways: the hydrolysis side reaction of M forming $M(OH)_n$, the side reaction of L with hydrogen ions forming H_nL, and the side reactions of ML with hydrogen or hydroxide ions forming MH_nL or $M(OH)_nL$. In the usual expression of Ringböm coefficient, the sums of the concentrations of the original species and the interfering species are denoted by primed symbols. For instance, [(ML)'] denotes the sum of [M] and $[MH_nL]$ or $[M(OH)_nL]$. Thus, the Ringböm coefficient α_{ML} of ML is defined by the expression

$$\alpha_{ML} = \frac{[(ML)']}{[ML]} \tag{I-50}$$

It is advantageous in this study to determine the stability constants of $M_nUO_2(CO_3)_3^{(4-2n)-}$ complexes in a way different from the ones commonly used in dealing with $UO_2(CO_3)_3^{4-}$ complex. The determination of these constants seems a rather complicated problem. In literature, to know the existence of $M_nUO_2(CO_3)_3^{(4-2n)-}$ complexes, solutions containing a constant $UO_2(CO_3)_3^{4-}$ complex at fixed pH value were examined varying the concentration of alkaline earth metal ion M^{2+} and determining the ratio of the number of metal

ions M^{2+} complexed to $UO_2(CO_3)_3^{4-}$.[111-115] The complexation can be described with the conditional equilibrium constants $K_{n.1.3}$ in the following,

$$nM^{2+} + UO_2(CO_3)_3^{4-} \rightleftarrows M_nUO_2(CO_3)_3^{(4-2n)-} \quad \text{(I-51)}$$

$$K_{n.1.3} = \frac{[M_nUO_2(CO_3)_3^{(4-2n)-}]}{[M^{2+}]^n[UO_2(CO_3)_3^{4-}]} \quad \text{(I-52)}$$

where squared brackets indicate concentration in molality (mol kg_w^{-1}). However, such approaches are restricted to avoid the occurrence of schoepite and magnesite/calcite that will be detailed in the following chapter. Therefore, the titration of M^{2+} at varying pH values is used in this work with the need to determine the influence of side reactions at different pH values on the concentration of $UO_2(CO_3)_3^{4-}$.

As presented in Eq. I-53, n stands for the stoichiometric number of calcium, R is the concentration ratio between complexed and non-complexed $UO_2(CO_3)_3^{4-}$ by M^{2+}, α is the Ringböm constant of $UO_2(CO_3)_3^{4-}$ considering all possible side reactions at different pH values and the intercept $\log_{10}K_{n.1.3}$ refers to the conditional stepwise formation constants of $M_nUO_2(CO_3)_3^{(4-2n)-}$ complexes at a given ionic strength.

$$\log_{10}R = \log_{10}\frac{\left[M_nUO_2(CO_3)_3^{(4-2n)-}\right]}{\left[UO_2(CO_3)_3^{4-}\right]/\alpha} = \log_{10}K_{n.1.3} + n\log_{10}[M^{2+}] \quad \text{(I-53)}$$

From an experimental point of view, the concentration of complexed $M_nUO_2(CO_3)_3^{(4-2n)-}$ is estimated based on their luminescent properties, *i.e.* luminescence intensity and decay time. Thus, Eq. I-54 can be converted in the following form.

$$\log_{10}R = \log_{10}\frac{FI_0\left(M_nUO_2(CO_3)_3^{(4-2n)-}\right)}{FI_0\left(UO_2(CO_3)_3^{4-}\right)/\alpha} = \log_{10}K_{n.1.3} + n\log_{10}[M^{2+}] \quad \text{(I-54)}$$

where $FI_0(M_nUO_2(CO_3)_3^{(4-2n)-})$ is the luminescence intensity extrapolated at $D = 0$ of the complexed species at variable pH values, $FI_0(UO_2(CO_3)_3^{4-})$ is that of the non-complexed triscarbonatouranyl complex at pH 9.

The rationale behind the use of Ringböm coefficient species is actually comprehensible due to the fact that the proportion of $UO_2(CO_3)_3^{4-}$ in uranyl carbonate system suffers a crucial decrease when the aqueous conditions change from alkaline to neutral. Fig. I - 9 shows the speciation diagram of U(VI) at the concentration of 50 µmol kg_w^{-1} in a solution of I_m = 0.1 mol kg_w^{-1} NaCl at T = 298 K and in equilibrium with the partial pressure of carbon dioxide of $10^{-3.5}$

atm, calculated using the PhreeqC software and the Thermochimie 10a database.[86] One can conclude that the distribution of uranyl carbonate complexes strongly depends on the pH value. Under the present aqueous conditions, the dominant species $UO_2(CO_3)_3^{4-}$ at pH 9 is successively substituted by the less-complexed species— *e.g.*, $UO_2(CO_3)_2^{2-}$ and $UO_2CO_3(aq)$ —, the hydroxo species — *e.g.*, $UO_2(OH)^+$ and $UO_2(OH)_2(aq)$ — and the polynuclear species — e.g., $(UO_2)_2CO_3(OH)_3^-$, $(UO_2)_3(OH)_5^+$… — when the pH value decreases.

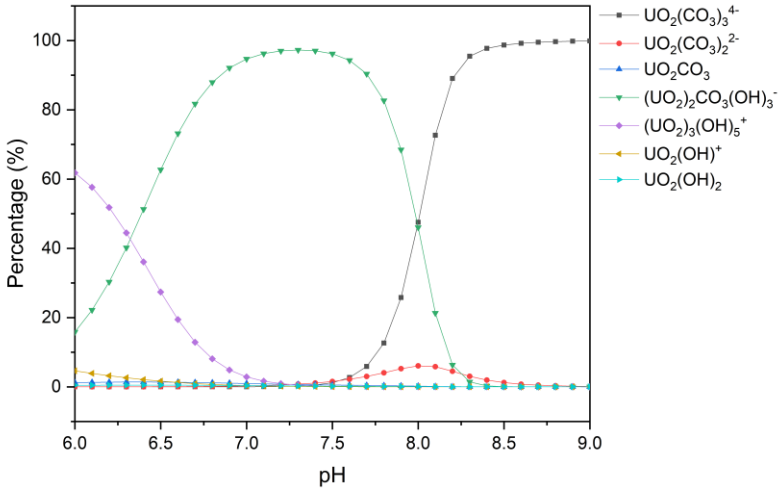

Fig. I - 9 Speciation diagram of [U(VI)] = 50 µ mol kg_w^{-1} in a solution of I_m = 0.1 mol kg_w^{-1} NaCl at T = 298 K, $P(CO_2) = 10^{-3.5}$ atm.

Because of the rich speciation of uranium(VI) driven by hydrolysis and oligomerization, even possible precipitation of $UO_3{:}2H_2O(cr)$, the prediction of individual concentration for all the involved species becomes difficult. For this reason, direct luminescence measurement of $UO_2(CO_3)_3^{4-}$ solutions prepared at pH values different from 9 in the absence of alkaline earth metal ions is untenable, as characteristic luminescence properties would be inevitably interfered by (polynuclear) hydroxo uranyl species. Fig. I - 10 presents the luminescence decay spectra of a sample prepared at pH 7.6, acquired over a large range of delay time. The spectral profiles of $UO_2(CO_3)_3^{4-}$ species were significantly affected as shown by the red line at D = 20 ns in Fig. I - 10 (b).

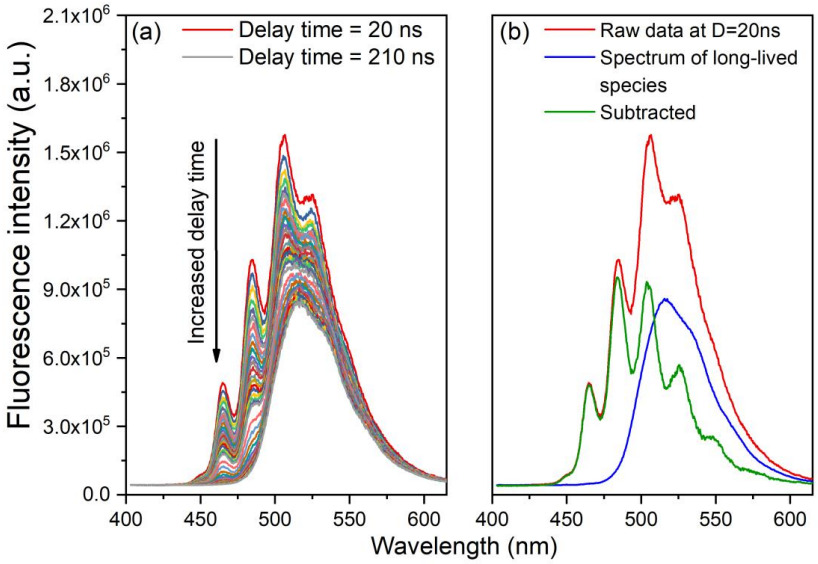

Fig. I - 10 (a) Fluorescence decay spectra of the sample at [U(VI)] = 50 µmol kg_w^{-1}, pH = 7.6 equilibrated with atmospheric CO_2(g), recorded with λ_{ex} = 450 nm from D = 20 ns to D = 210 ns. (b) Red line: spectrum recorded at D = 20 ns. Blue line: spectrum at D = 210 ns. Green line: subtraction of the blue line from the red one, also characteristic spectrum of $UO_2(CO_3)_3^{4-}$ species.

The typical description and thermodynamic formation constant of hydrolysis-carbonation equilibria with $UO_2(CO_3)_3^{4-}$ are often written relative to $UO_2(CO_3)_3^{4-}$ and CO_3^{2-} as follows.

$$m\ UO_2(CO_3)_3^{4-} + n\ H_2O \leftrightarrow (UO_2)_m(CO_3)_q(OH)_n^{(2m-n-2q)+} + (3m-q)\ CO_3^{2-} + n\ H^+ \quad \text{(I-55)}$$

Varying pH values means that CO_3^{2-} concentrations should be recalculated. In our case, it seems more convenient to express the complexation relative to $UO_2(CO_3)_3^{4-}$ and the partial pressure of CO_2(g) because $P(CO_2)$ is maintained constant throughout the experiments. Using Eq. I-56, the relationship between CO_3^{2-} and CO_2(g), the hydrolysis of $UO_2(CO_3)_3^{4-}$ can be expressed in CO_2(g), as shown in Eq. I-57 instead.

$$(3m-q)CO_3^{2-} + 2(3m-q)H^+ \leftrightarrow (3m-q)\ CO_2(g) + (3m-q)H_2O \quad \text{(I-56)}$$

$$m\ UO_2(CO_3)_3^{4-} + (6m-2q-n)H^+ \leftrightarrow$$
$$(UO_2)_m(CO_3)_q(OH)_n^{(2m-n-2q)+} + (3m-q)CO_2(g) + (3m-q-n)H_2O \quad \text{(I-57)}$$

with the expression of equilibrium constant:

$${}^*\beta''_{m.n.q} = \frac{\left((UO_2)_m(CO_3)_q(OH)_n^{(2m-n-2q)+}\right)\cdot P(CO_2)^{(3m-q)}\cdot a(H_2O)^{(3m-q-n)}}{\left(UO_2(CO_3)_3^{4-}\right)^m\cdot(H^+)^{(6m-2q-n)}} \quad \text{(I-58)}$$

also written as:

$$\log_{10}{}^{*}\beta^{\circ\prime\prime}{}_{m.n.q} = \log_{10}{}^{*}\beta^{\circ}{}_{m.n.q} - m\log_{10}\beta^{\circ}{}_{1.0.3} - (3m-q)\log_{10}\beta^{\circ}{}_{0.1.1} \quad \text{(I-59)}$$

with $\log_{10}\beta^{\circ}{}_{m.n.q}$ the global formation constant of $(UO_2)_m(CO_3)_q(OH)_n^{(2m-n-2q)+}$. According to the SIT approach, the relationship between the conditional formation constant $\log_{10}{}^{*}\beta''{}_{m.n.q}$ and $\log_{10}{}^{*}\beta^{\circ}{}_{m.n.q}$ at infinite dilution is expressed as follows:

$$\log_{10}{}^{*}\beta''{}_{m.n.q} = \log_{10}{}^{*}\beta^{\circ\prime\prime}{}_{m.n.q} + m\log_{10}\gamma_{UO_2(CO_3)_3^{4-}} + (6m-2q-n)\log_{10}\gamma_{H^+} - \log_{10}\gamma_{m.n.q} - (3m-q-n)\log_{10} a(H_2O) \quad \text{(I-60)}$$

In the scope of this research, we will consider the interfering species, listed in Table I - 5, in side reactions of $UO_2(CO_3)_3^{4-}$.

Table I - 5 Side reactions of $UO_2(CO_3)_3^{4-}$ and calculated stability constants of the interfering species.

Species	m	n	q	Reactions
$UO_2(CO_3)_2^{2-}$	1	0	2	$UO_2(CO_3)_3^{4-} + 2H^+ \rightleftarrows UO_2(CO_3)_2^{2-} + CO_2(g) + H_2O$
				$\log_{10}{}^{*}\beta^{\circ\prime\prime}{}_{1.0.2} = \log_{10}{}^{*}\beta^{\circ}{}_{1.0.2} - \log_{10}\beta^{\circ}{}_{1.0.3} - \log_{10}\beta^{\circ}{}_{1.0.1}$
				$\log_{10}{}^{*}\beta^{\circ\prime\prime}{}_{1.0.2} = 12.92 \pm 0.15$
$UO_2CO_3(aq)$	1	0	1	$UO_2(CO_3)_3^{4-} + 4H^+ \rightleftarrows UO_2CO_3(aq) + 2CO_2(g) + 2H_2O$
				$\log_{10}{}^{*}\beta^{\circ\prime\prime}{}_{1.0.1} = \log_{10}{}^{*}\beta^{\circ}{}_{1.0.1} - \log_{10}\beta^{\circ}{}_{1.0.3} - 2\log_{10}\beta^{\circ}{}_{1.0.1}$
				$\log_{10}{}^{*}\beta^{\circ\prime\prime}{}_{1.0.1} = 24.40 \pm 0.21$
$(UO_2)_2CO_3(OH)_3^-$	2	3	1	$2UO_2(CO_3)_3^{4-} + 7H^+ \rightleftarrows (UO_2)_2CO_3(OH)_3^- + 5CO_2(g) + 2H_2O$
				$\log_{10}{}^{*}\beta^{\circ\prime\prime}{}_{2.3.1} = \log_{10}{}^{*}\beta^{\circ}{}_{2.3.1} - \log_{10}\beta^{\circ}{}_{1.0.3} - 5\log_{10}\beta^{\circ}{}_{0.1.1}$
				$\log_{10}{}^{*}\beta^{\circ\prime\prime}{}_{2.3.1} = 46.21 \pm 0.70$
$(UO_2)_3(OH)_5^+$	3	5	0	$3UO_2(CO_3)_3^{4-} + 13H^+ \rightleftarrows (UO_2)_3(OH)_5^+ + 9CO_2(g) + 4H_2O$
				$\log_{10}{}^{*}\beta^{\circ\prime\prime}{}_{3.5.0} = \log_{10}{}^{*}\beta^{\circ}{}_{3.5.0} - \log_{10}\beta^{\circ}{}_{1.0.3} - 9\log_{10}\beta^{\circ}{}_{0.1.1}$
				$\log_{10}{}^{*}\beta^{\circ\prime\prime}{}_{3.5.0} = 82.28 \pm 0.84$
$UO_2(OH)^+$	1	1	0	$UO_2(CO_3)_3^{4-} + 5H^+ \rightleftarrows UO_2(OH)^+ + 3CO_2(g) + 2H_2O$
				$\log_{10}{}^{*}\beta^{\circ\prime\prime}{}_{1.1.0} = \log_{10}{}^{*}\beta^{\circ}{}_{1.1.0} - \log_{10}\beta^{\circ}{}_{1.0.3} - 3\log_{10}\beta^{\circ}{}_{0.1.1}$
				$\log_{10}{}^{*}\beta^{\circ\prime\prime}{}_{1.1.0} = 27.36 \pm 0.12$
$UO_2(OH)_2(aq)$	1	2	0	$UO_2(CO_3)_3^{4-} + 4H^+ \rightleftarrows UO_2(OH)_2(aq) + 3CO_2(g) + H_2O$
				$\log_{10}{}^{*}\beta^{\circ\prime\prime}{}_{1.2.0} = \log_{10}{}^{*}\beta^{\circ}{}_{1.2.0} - \log_{10}\beta^{\circ}{}_{1.0.3} - 3\log_{10}\beta^{\circ}{}_{0.1.1}$
				$\log_{10}{}^{*}\beta^{\circ\prime\prime}{}_{1.2.0} = 20.46 \pm 0.20$

If C_T is the analytical concentration of uranium, then a mass balance on uranium is:

$$C_T = \left[UO_2(CO_3)_3^{4-}\right] + \left[UO_2(CO_3)_2^{2-}\right] + [UO_2CO_3] + [UO_2(OH)^+] + [UO_2(OH)_2(aq)] + 2[(UO_2)_2CO_3(OH)_3^-] (+3\,[(UO_2)_3(OH)_5^+]) \quad \text{(I-61)}$$

Substituting in terms of the formation constants listed above gives:

$$C_T = \left[UO_2(CO_3)_3^{4-}\right] + \sum_m \sum_n \sum_q m\,{}^{*}\beta''{}_{m.n.q} \frac{\left[UO_2(CO_3)_3^{4-}\right]^{m-1} \cdot [H^+]^{(6m-2q-n)}}{P(CO_2)^{(3m-q)}} \quad \text{(I-62)}$$

$$C_T=\left[UO_2(CO_3)_3^{4-}\right]\left(1+\ {}^*\beta''_{1.0.2}\frac{[H^+]^2}{P(CO_2)}+{}^*\beta''_{1.0.1}\frac{[H^+]^4}{P(CO_2)^2}+{}^*\beta''_{1.1.0}\frac{[H^+]^5}{P(CO_2)^3}+{}^*\beta''_{1.2.0}\frac{[H^+]^4}{P(CO_2)^3}\right)+2$$

$${}^*\beta''_{2.3.1}\frac{\left[UO_2(CO_3)_3^{4-}\right]^2\cdot[H^+]^7}{P(CO_2)^5}\left(+3\ {}^*\beta''_{3.5.0}\frac{\left[UO_2(CO_3)_3^{4-}\right]^3\cdot[H^+]^{13}}{P(CO_2)^9}\right) \quad \text{(I-63)}$$

Then Eq. I-63 is a quadratic equation than can be arranged in standard form as $ax^2 + bx + c = 0$ with

$$a= 2\ {}^*\beta''_{2.3.1}\frac{[H^+]^7}{P(CO_2)^5} \quad \text{(I-64)}$$

$$b=\left(1+\ {}^*\beta''_{1.0.2}\frac{[H^+]^2}{P(CO_2)}+{}^*\beta''_{1.0.1}\frac{[H^+]^4}{P(CO_2)^2}\right) \quad \text{(I-65)}$$

$$c= -C_T \quad \text{(I-66)}$$

$$x = \left[UO_2(CO_3)_3^{4-}\right] \quad \text{(I-67)}$$

Hence, the roots of the quadratic equation, $[UO_2(CO_3)_3^{4-}]$, is expressed in Eq. I-71 with the known values of $[H^+]$, $P(CO_2)$, C_T as well as the involved formation constants ${}^*\beta''_{m.n.q.}$

$$\Delta = b^2 - 4ac \quad \text{(I-68)}$$

$$\Delta =\left(1+\ {}^*\beta''_{1.0.2}\frac{[H^+]^2}{P(CO_2)}+{}^*\beta''_{1.0.1}\frac{[H^+]^4}{P(CO_2)^2}\right)^2+8\ {}^*\beta''_{2.3.1}\frac{[H^+]^7}{P(CO_2)^5}\ C_T \quad \text{(I-69)}$$

$$\left[UO_2(CO_3)_3^{4-}\right] = \frac{-b \pm \sqrt{\Delta}}{2a} \quad \text{(I-70)}$$

$$\left[UO_2(CO_3)_3^{4-}\right]= \frac{-\left(1+\ {}^*\beta''_{1.0.2}\frac{[H^+]^2}{P(CO_2)}+{}^*\beta''_{1.0.1}\frac{[H^+]^4}{P(CO_2)^2}\right)\pm\sqrt{\left(1+\ {}^*\beta''_{1.0.2}\frac{[H^+]^2}{P(CO_2)}+{}^*\beta''_{1.0.1}\frac{[H^+]^4}{P(CO_2)^2}\right)^2+8\ {}^*\beta''_{2.3.1}\frac{[H^+]^7}{P(CO_2)^5}\ C_T}}{\left(4\ {}^*\beta''_{2.3.1}\frac{[H^+]^7}{P(CO_2)^5}\right)} \quad \text{(I-71)}$$

The values of water activity and the osmotic coefficients at investigated ionic strengths in NaCl and $NaClO_4$ used in the calculation of Ringböm coefficients are listed in Table I - 6.

Table I - 6 Values of water activity and the osmotic coefficients[116] at investigated ionic strengths in NaCl and $NaClO_4$ used in the calculation of Ringböm coefficients.

I_m (mol L^{-1}) NaCl	ρ (g/cm^3)	ρ/ρ_e	1-ϕ	ϕ	a_{H2O}

0	0.9974	1.0000	\	\	\
0.1	0.9995	1.0020	0.0649	0.9351	0.9966
0.2	1.0014	1.0010	0.0725	0.9275	0.9933
0.5	1.0071	1.0097	0.0723	0.9277	0.9831
0.75	1.0117	1.0143	0.0656	0.9344	0.9742
1.0	1.0161	1.0187	0.0568	0.9432	0.9651
I_m (mol L^{-1}) $NaClO_4$	ρ (g/cm^3)	ρ/ρ_e	1-ϕ	ϕ	a_{H2O}
0	0.9974	1.0000	\	\	\
0.1	1.0052	1.0077	0.0672	0.9328	0.9966
0.5	1.0358	1.0385	0.0841	0.9159	0.9832
1.0	1.0738	1.0766	0.0808	0.9192	0.9658
1.5	1.1116	1.1145	0.0735	0.9265	0.9475
2.0	1.1492	1.1522	0.0625	0.9350	0.9282
2.2	1.1642	1.1672	0.0613	0.9387	0.9202
3.0	1.2239	1.2271	0.046	0.9540	0.8866

I - 7 Preparatory experiments

7.1 Estimation of detection limit

The detection limit of U(VI) varies from one to another in different complexing media. Numerous studies have been carried out in various media, such as sulfuric, phosphoric, pyrophosphate, perchloric and nitric acids,[117] in order to better understand uranium luminescence and improve limit of detection. The criterion of medium selection relies upon its quenching effect on the uranyl ion, which affects both luminescence intensity and lifetime. For example, chloride is known as a classical strong quencher.[118,119]

It is demonstrated that the phosphoric acid is the most convenient medium in which the detection limit of uranium remarkably decreases. Moulin *et al.*[120] showed that in phosphoric acid, the detection limit of uranium could be in the ng L^{-1} range (4.2 10^{-12} mol L^{-1}), even lower, but this limit could be higher for *in-situ* determinations of uranium in groundwater where strong chloride quencher is present. With the aim to determine uranium sensitivity of our apparatus, a series of different U(VI) concentrations solutions from 10^{-8} to 10^{-10} mol kg_w^{-1} in 5% H_3PO_4 medium were prepared and excited at 429 nm excitation wavelength.

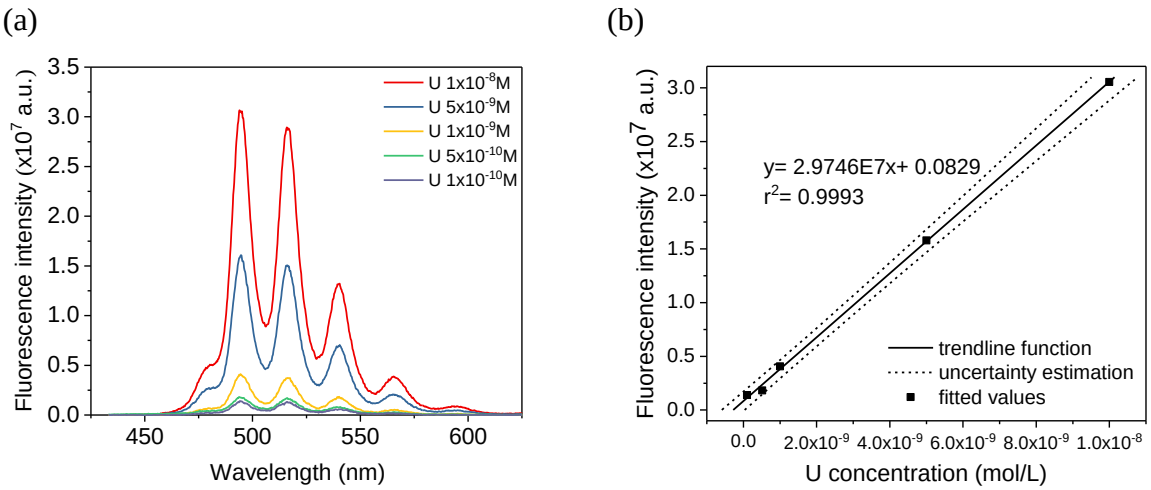

Fig. I - 11 (a) Luminescence spectra of UO_2^{2+} in 5% H_3PO_4 medium at different uranium concentrations from 10^{-8} to 10^{-10}M, recorded at excitation wavelength of 429 nm. (b) Linear dependence of luminescence peak intensities at 485.4 nm on uranium concentration.

An extension of integration time up to 1 ms was done in order to record as much signal as possible. The characteristic peaks of uranyl ions were found at 494, 516, 546, 565 nm. Compared with the spectroscopic data obtained by Scapolan *et al.*[121], the main aqueous species was identified as $UO_2H_2PO_4^+$. They also reported bathochromic shifts of luminescent spectra when increasing the pH value due to the consecutive formations of UO_2HPO_4 and $UO_2PO_4^-$ species. In Fig. I - 11 (b), the luminescence intensity is plotted versus uranium concentration in the range from 10^{-10} to 10^{-8} mol kg_w^{-1}. Dotted lines represent the relative standard deviation of 5% with the experimental points found in the 95% confidence interval. It can be served as a calibration curve as long as the experimental parameters (laser energy, delay time, gate width, integration time) remain constant.

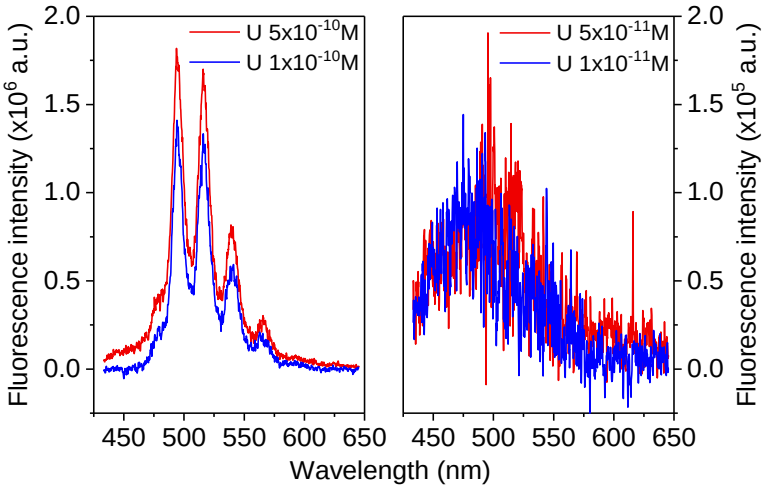

Fig. I - 12 Luminescence spectra collected for uranium concentrations down to 10^{-11} M in phosphoric medium.

The luminescence spectra were collected for uranium concentrations down to 10^{-11} mol kg_w^{-1}, as shown in Fig. I - 12. It is clear that the characteristic peaks cannot be distinguished at [U(VI)] = 10^{-11} mol kg_w^{-1}. Thus, the uranium detection limit of our apparatus is estimated at 10^{-10} mol kg_w^{-1}, or 23.8 ppt in phosphoric medium. Although the uranium concentration in further experiments will not decrease to such low levels, the determination of detection limit of the apparatus is still necessary as a part of preparatory experiments.

7.2 Determination of excitation wavelength

According to the work of Meinrath *et al.*[122], the highest molar absorbance was observed at 450.2 nm under the conditions where the $UO_2(CO_3)_3^{4-}$ gives the main contribution to the spectrum. Thus, the excitation wavelength is reasonable to be set at 450 nm for maximizing the efficiency.

7.3 pH Measurements

This section is dedicated to clarifying the principles of pH measurements with combined glass electrodes that will be used throughout the experiments. We will discuss the factors involved in measurements and the magnitude of effect that each factor has on measured results. This chapter is intended to understand the thermodynamic principles involved in the pH measurements, also to relate the measured potential values to the real hydrogen concentration for electrolyte solutions of different ionic strengths and at different temperatures.

7.3.1 Defining pH

The pH value is a measure of acidity and defined in terms of the hydrogen ion activity as follows:

$$pH = -log_{10}a_{H^+} = -log_{10}\gamma_{H^+}C_{H^+} \quad \text{(I-72)}$$

where γ_{H^+} is the activity coefficient of the hydrogen ion H^+ and C_{H^+} is its concentration.

Since the pH glass electrode is sensitive to the actual hydrogen ion activity, the factors correlated with its definition is important. In dilute solutions, the activity coefficient can be assumed to be unity, then activity equals to concentration and the effective pH values measured by the pH meter is equal to the actual acidity. However, the difference between effective and actual concentrations increases when moving toward less dilute solutions in which the activity coefficient becomes progressively more important. In other words, samples with the same H^+

concentration are expected to have different measured pH values if the ionic strengths of the samples greatly vary.

In addition to ionic strength, temperature also affects a_{H^+}, even the original speciation of the studied sample solutions. Thus, a sample pH value should not be extrapolated to another ionic strength or temperature. This means that if the pH value of a prepared solution is known at 50°C, its pH value at 25°C is not automatically known. The standard buffer solutions should be studied at the desired temperature, and the corresponding calibration curve will be naturally redefined.

Another effect that influences the pH measurements is the medium effect. This effect describes the electrostatic and chemical interactions between H^+ and solvent. For example, the a_{H^+} in ethanol is much more important than in water. In practice, the exact a_{H^+} in non-aqueous solution is usually unknown, thus the correlation between the measured value in a non-aqueous sample and the pH values obtained in the calibration with aqueous pH buffer solutions is not valid. Since all the samples in this work are prepared in aqueous solutions, the medium effect will not be discussed here.

Overall, the pH measurements of activity can be principally influenced by the ionic strength, the temperature and the type of solvent. This determines that the experimental conditions and the studied sample compositions need to be clarified when stating its measured pH value. The only valid comparison of pH values must be from the same measurement conditions and duplication of results by another person should also be performed under the originally measured conditions.

7.3.2 pH measuring system

A pH measuring system consists of a glass electrode, a reference and a pH meter. In the present work, a combination electrode is used to carry out all pH measurements. This electrode combines the glass and reference electrodes into a single probe. The objective of this section is to describe the functioning and parameters for glass and reference electrodes.

The combination electrode is normally constructed with the reference surrounding the glass as shown in Fig. I - 13.[123,124] With the glass electrode alone, it is not sufficient to conduct the potential measurements, because the measuring circuit needs to be completed by a reference electrode. In combination electrode, the shielding is completed by the reference filling solution. For example, saturated potassium chloride solution is often used as the filling solution to make

contact with the sample solution through a junction. An Ag/AgCl internal instead of a traditional calomel internal is used in this type of electrode to make its diameter small that allows the measurements of samples in limited access containers.

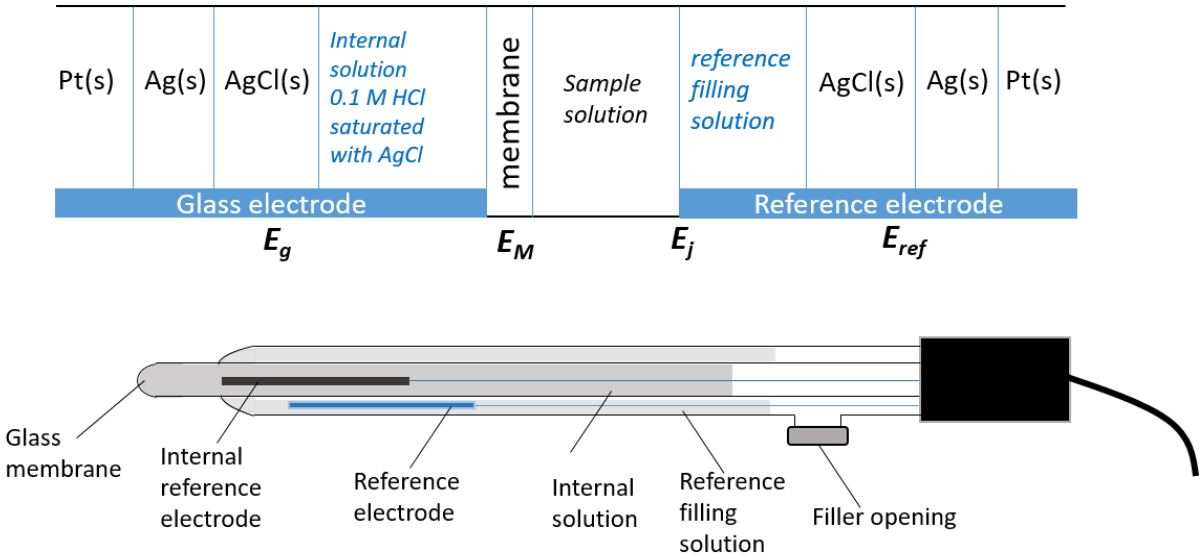

Fig. I - 13 The overall galvanic cell of a typical combination glass electrode.

When immersing the pH-sensitive bulb in the sample solution, an exchange equilibrium is established between the hydrogen ion in the measured solution and the ions in the glass. The reference electrode provides a stable potential against the potential from the glass electrode, between which the difference is the source of the potential displayed on the pH meter. The measured potential difference can be expressed as follows as a function of the potential differences at each interface of galvanic chain.

$$E_{mes} = E_{ref} + E_j + E_M - E_g \tag{I-73}$$

where E_{ref} and E_g are respectively the potential differences of Ag/AgCl in reference and glass electrodes which are stable and reproducible. E_M is the potential difference between inside and outside glass membrane that is established by the hydrogen ion activity of the sample solution. E_j is the liquid junction potential that will be discussed in detail because it varies with different reference filling solutions and inevitably causes many problems encountered in the pH measurements. According to the Nernst equation, the potential differences can be expressed as follows:

$$E_{ref} = E^{\circ}_{Ag/AgCl} + A_0 \log_{10} a_{Cl^-,ref} \tag{I-74}$$

$$E_g = E^{\circ}_{Ag/AgCl} + A_0 \log_{10} a_{Cl^-,g} \tag{I-75}$$

$$E_M = rA_0 \log_{10}(a_{H^+,solution}/a_{H^+,g}) \quad \text{(I-76)}$$

$$E_j \propto f(I_{solution}) - f(I_{ref}) \quad \text{(I-77)}$$

where A_0 = ln(10)RT/F with F the number of Faraday (A_0 = 59.16 mV/pH at 25°C), and r is a coefficient generally close to 1 that measures the deviation of the membrane response form the theoretical response. The activities $a_{Cl^-,ref}$, $a_{Cl^-,g}$, and $a_{H^+,ref}$ are intrinsic parameters that are related to the electrode solutions and normally known to users. The liquid junction potential E_j can be approximately described by a certain function f, which will be evaluated further for different reference filling solutions. With these variables and approximations, the measured potential can be written in the following form.

$$E_{mes} = rA_0 \log_{10} a_{H^+,solution} + f(I_{solution}) + B + C \quad \text{(I-78)}$$

with

$$B = A_0 \log_{10} a_{Cl^-,ref} - f(I_{ref}) \quad \text{(I-79)}$$

$$C = -A_0(r \log_{10} a_{H^+,g} + \log_{10} a_{Cl^-,g}) \quad \text{(I-80)}$$

where B and C will be determined in calibration. B is needed to be measured for each specific reference filling solution if it is replaced by user. C contains the values associated with the glass electrode that cannot be modified. In the cases where the ionic strength of the sample solution is comparable to the reference solution, the liquid junction potential becomes negligible. However, for sample solutions of which the ionic strengths are different from that of the reference solution, liquid junction potentials are needed to be estimated individually. Considering two solutions of the same concentration on H^+ but of different ionic strengths I_1 and I_2, the potentials measured by the same electrode are noted as E_{mes1} and E_{mes2}. According to the Eq. I-78, we have:

$$E_{mes2} - E_{mes1} = rA_0 \log_{10}(a_{H^+,solution2}/a_{H^+,solution1}) + f(I_{solution2}) - f(I_{solution1}) \quad \text{(I-81)}$$

From the measurements of $E_{mes2} - E_{mes1}$, the term $f(I_{solution2}) - f(I_{solution1})$ can thus be determined with the estimation of hydrogen ion activity using the SIT formulations.

7.3.3 Electrode calibration

Conditioning of electrodes

Two combination electrodes with saturated potassium chloride as reference filling solutions are used in the present work. One of them was reconditioned with a refilled reference solution

of 3 mol L^{-1} $NaClO_4$ + 0.01 mol L^{-1} NaCl and applied to solutions of inert electrolyte being $NaClO_4$. The other one was used in the inert solutions of NaCl. The conditioning of electrode was carried out in the following way:

(a) The reference electrode was cleaned with distilled water, then with a solution of 0.01 mol L^{-1} NaCl and finally with the new reference solution in order to eliminate the K^+ present in the original reference solution (saturated KCl) which may cause the precipitation of $KClO_4$ inside the liquid junction.
(b) The freshly prepared reference solution was added into the reference electrode with several grains of AgCl.
(c) The electrode was immersed in a solution of 3 mol L^{-1} $NaClO_4$ + 0.01 mol L^{-1} NaCl slightly acidified to pH ≈ 2-3 during 24h.
(d) The stability of this electrode can be verified if the response for one pH measurement does not exceed 10 s.

Buffer solution compositions

The buffer solutions used in this work are the pH 1.679 oxalate buffer, the pH 4.005 phthalate buffer, the pH 6.865 phosphate buffer, and the pH 9.18 borax buffer (SI Analytics, Mainz, Germany). All these buffers, except the pH 1.679 oxalate buffer, are primary buffers that are recommended by the National Bureau of Standards for their greater accuracy compared with other buffers of similar pH value. The pH 1.679 buffer has a composition of 0.05 mol kg_w^{-1} potassium hydrogen oxalate ($KH_3C_4O_8$). The pH 4.005 buffer has a composition of 0.05 mol kg_w^{-1} potassium hydrogen phthalate ($KHC_8H_4O_4$). This buffer is stable to dilution and change in temperature. The pH 6.865 buffer has a composition of 0.025 mol kg_w^{-1} potassium dihydrogen phosphate (KH_2PO_4) and 0.025 mol kg_w^{-1} disodium hydrogen phosphate (Na_2HPO_4). This buffer can be moderately affected by dilution and temperature. The pH 9.18 buffer has a composition of 0.01 mol kg_w^{-1} sodium tetraborate decahydrate ($Na_2B_4O_7{:}10H_2O$). The salt in this buffer hydrolyzes to form boric acid and sodium borate. Theoretically, this buffer should be protected from atmospheric CO_2 in use for maximum accuracy.

Calibration curve at different temperatures

A four-point calibration method is applied in this study with aforementioned buffer solutions. The 95% confidence limits are readily estimated by means of ordinary least squares regression, which allowed the uncertainties of pH determination below 0.05 pH units. The

calibration curves are shown in Fig. I - 14 for the reconditioned electrode used in $NaClO_4$ and the original electrode used in NaCl.

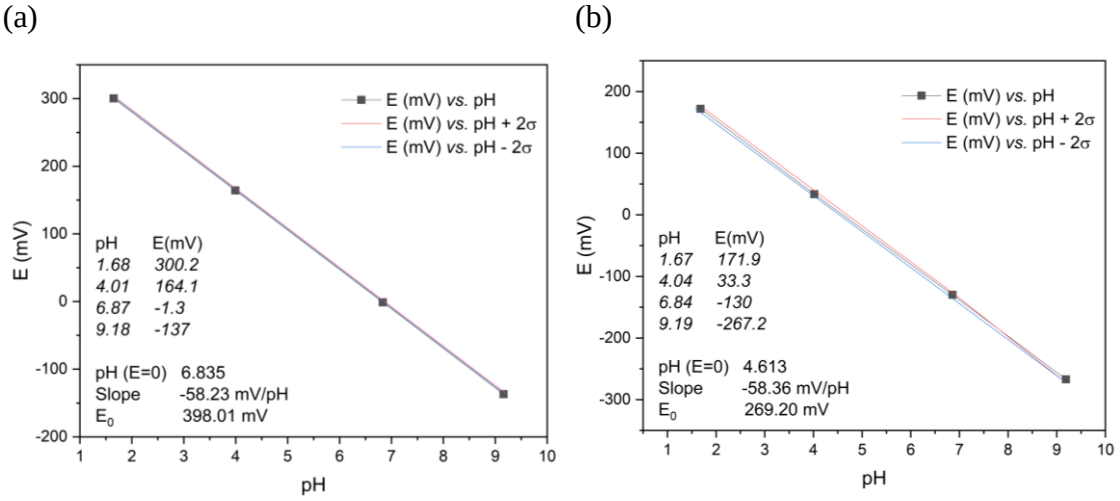

Fig. I - 14 Calibration curves for (a) the reconditioned electrode used in $NaClO_4$ and (b) the original electrode used in NaCl.

Table I - 7 Recalculated pH values of buffer solutions at investigated temperatures and potential values E_{mes} read on pH-meter.

Temp	pH	E(mV)	pH	E(mV)	pH	E(mV)	pH	E(mV)	Slope	Intercept
5°	1.67	299.1	4.00	166.9	6.95	1.8	9.39	-133.4	-56.01	391.81
10°	1.67	299.5	4.00	166.2	6.92	0.8	9.33	-135.1	-56.72	393.69
15°	1.67	302.2	4.00	165.5	6.90	-0.5	9.28	-135.2	-57.45	396.79
22°	1.68	304.2	4.00	164.9	6.88	-1.4	9.23	-136.1	-58.24	400.18
30°	1.68	308.2	4.01	165.6	6.85	-3.3	9.14	-138.8	-59.86	407.39
35°	1.69	311.2	4.02	167.1	6.84	-3.2	9.11	-139.5	-60.70	412.58
40°	1.69	314	4.03	168.7	6.84	-3	9.07	-140.2	-61.49	417.38
45°	1.70	318.2	4.04	171.4	6.83	-3.1	9.04	-140	-62.44	423.97
50°	1.71	321.2	4.06	171.9	6.83	-3.3	9.02	-140.4	-63.16	428.74

Table I - 8 Composition and properties of standard buffer solutions.[125]

pH value at 25°	1.68	4.01	6.87	9.18
Composition[125]	0.05 mol kg_w^{-1} potassium tetraoxalate ($KH_3C_4O_8$)	0.05 mol kg_w^{-1} potassium hydrogen phthalate ($KHC_8H_4O_4$)	0.025 mol kg_w^{-1} KH_2PO_4 and 0.025 mol kg_w^{-1} (Na_2HPO_4)	0.01 mol kg_w^{-1} $Na_2B_4O_7{:}10H_2O$
Temperature range	0-95	0-95	0-95	0-50
Temperature coefficient *d*pH/*dt*	--	+0.0012	-0.0028	-0.0028

A change in temperature will change the buffer pH value due to the influence on the hydrogen ion activity. The temperature coefficient dpH/dt are shown in Table I - 8, with which the pH values for each buffer are recalculated to different temperatures. It should be noted that the default temperature on the pHmeter should be reset before performing the new calibration at different temperature from 22°C. All the buffer solutions used in this work are valid within the experimental temperature range. The Fig. I - 15 illustrates the calibration curves using the normal combination electrode (saturated KCl as reference filling solution). The slopes and intercepts are listed in Table I - 7 at different temperatures.

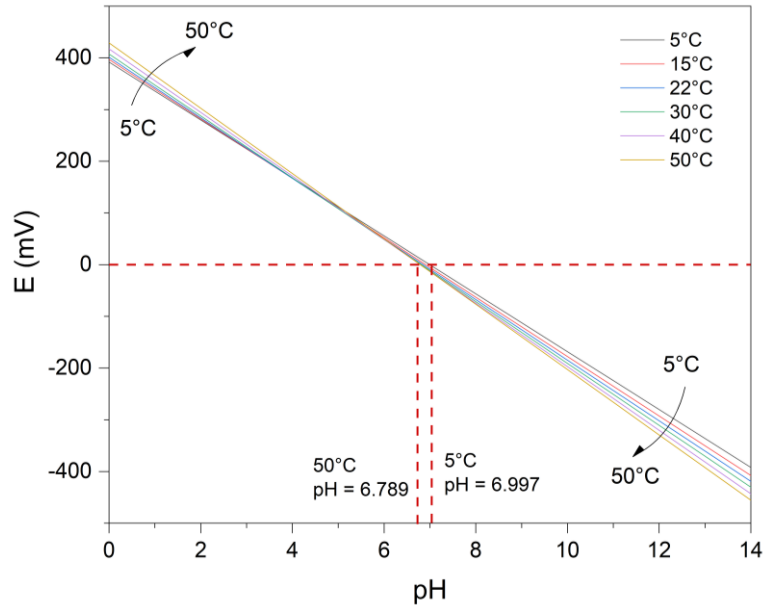

Fig. I - 15 Calibration lines in the temperature range of 5-50°C and the pH values corresponding to the zero point of electrode at 5°C and 50°C.

7.3.4 Measurements of liquid junction potential at different ionic strengths

The liquid junction potentials for the reconditioned and the original glass electrodes have been measured with $NaClO_4$/NaCl solutions of different ionic strengths. These solutions are specially prepared at the same $[H^+]$ being 0.01 mol L^{-1} of ionic strength from 0.01 to 3 mol L^{-1}. The difference ΔE_j is calculated from the Eq. I-81 from which the measured potential of a specific ionic strength solution is compared to that of the solution of I = 3 mol L^{-1}. Due to the strong dependency of activity on ionic strength, pcH ($= -\log_{10}[H^+]$) is used instead of pH ($= -\log_{10}a(H^+)$) throughout the experiments. The aqueous information and experimental measurements of E_{mes} are reported in Table I - 9. These measures allow establishing, for the reconditioned/original glass electrode with 3 mol L^{-1} $NaClO_4$/KCl as electrode filling solutions:

$\Delta E_j - rA_0 \log_{10}(a_2/a_1) = 19.20 \log_{10}(3.50/I_m) + 7.04$ / $\Delta E_j - rA_0 \log_{10}(a_2/a_1) = 11.86 \log_{10}(3.19/I_m)$

+ 12.03, thus defining the function f($I_{solution}$) with respect to ionic strength, as shown in Fig. I - 16.

Table I - 9 Potential values E_{mes} read on pH-meter for $NaClO_4$ solutions of I_m = 0.01 to 3.5 mol kg_w^{-1} at pcH = 2 using the reconditioned electrode of 3.5 mol kg_w^{-1} $NaClO_4$ reference solution and for NaCl solutions of I_m = 0.12 to 3.19 mol kg_w^{-1} at pcH = 2 using the combined-glass electrode with the filling solution of saturated KCl: liquid junction potentials ΔE_{mes} calculated to estimate the potential differences between the solutions of a specific $I_m \geq 0.1$ mol kg_w^{-1} and of I_m = 0.01 mol kg_w^{-1}; ⊿Emes then used in the four-point calibration with commercial buffer solution of pH 1.64, 4.01, 6.87, 9.18, assumed as diluted solutions of Im ≈ 0.01 mol kg_w^{-1}; the uncertainties of ± 0.05 pH in text included this non-significant experimental bias.

Solution	**I_m (mol kg_w^{-1})**	**Debye-Hückel term**	**$\log_{10}\gamma$**	**Emes**	**$\Delta Ej = Emes_1 - Emes_2$**	**$\Delta Ej - rA_0\log_{10}(a_2/a_1)$**
HCl 0.01M + $NaClO_4$ 2.99 M	3.50	0.2498	-0.24812	175.5	0	0
HCl 0.01M + $NaClO_4$ 2.49 M	2.85	0.2431	-0.2415	168	7.5	7.29
HCl 0.01M + $NaClO_4$ 1.99 M	2.22	0.2343	-0.2328	163.6	11.9	11.56
HCl 0.01M + $NaClO_4$ 1.49 M	1.62	0.2225	-0.2210	158.9	16.6	16.269
HCl 0.01M + $NaClO_4$ 0.99 M	1.05	0.2057	-0.2042	155.1	20.4	20.39
HCl 0.01M + $NaClO_4$ 0.49 M	0.51	0.1750	-0.1735	150.2	25.3	26.32
HCl 0.01M + $NaClO_4$ 0.19 M	0.20	0.1392	-0.1378	146.6	28.9	31.81
HCl 0.01M	0.01	0.0441	-0.0427	130.2	45.3	53.32
HCl 0.01M + NaCl 2.97 M	3.19	0.2471	-0.2458	299.5	0.0	0
HCl 0.01M + NaCl 1.49 M	1.56	0.2212	-0.2200	286	13.5	14.2
HCl 0.01M + NaCl 0.99 M	1.04	0.2051	-0.2039	280.8	18.7	20.0
HCl 0.01M + NaCl 0.74 M	0.76	0.1924	-0.1911	279.7	19.8	21.7
HCl 0.01M + NaCl 0.59 M	0.61	0.1832	-0.1820	277.9	21.6	24.0
HCl 0.01M + NaCl 0.49 M	0.51	0.1754	-0.1742	277.8	21.7	24.5

Solution	I_m (mol kg_w^{-1})	Debye-Hückel term	$\log_{10}\gamma$	Emes	$\Delta Ej = Emes_1 - Emes_2$	$\Delta Ej - rA_0\log_{10}(a_2/a_1)$
HCl 0.01M + NaCl 0.41 M	0.42	0.1674	-0.1662	276.7	22.8	26.0
HCl 0.01M + NaCl 0.29 M	0.30	0.1533	-0.1521	276.5	23.0	27.0
HCl 0.01M + NaCl 0.19 M	0.20	0.1363	-0.1351	276.4	23.1	28.0
HCl 0.01M + NaCl 0.10 M	0.12	0.1150	-0.1137	275.4	24.1	30.2
HCl 0.01M	0.01	0.0453	-0.0441	275	24.5	34.7

(a) (b)

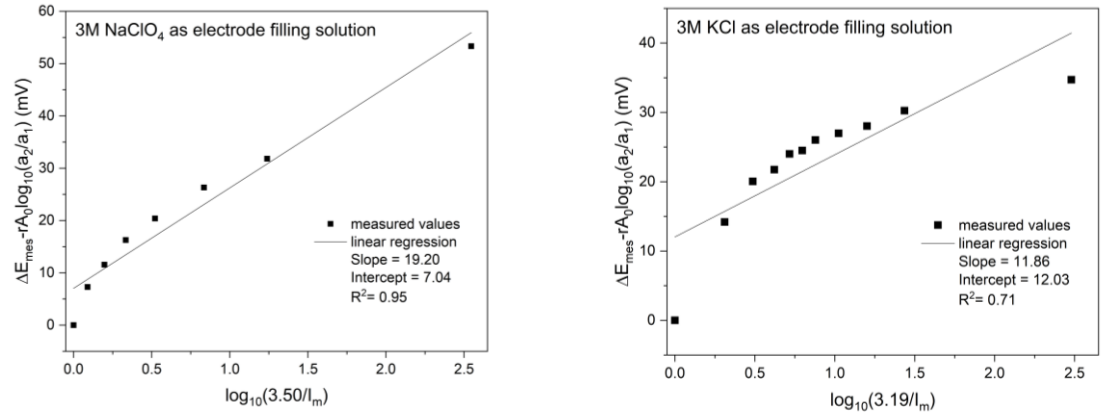

Fig. I - 16 Influence of ionic strength on the junction potential (a) with 3 mol L^{-1} $NaClO_4$ as electrode filling solution in the reconditioned glass electrode and (b) with 3 mol L^{-1} KCl as electrode filling solution in the original glass electrode.

I - 8 Reference

1. A. Meleshyn, M. Azeroual, T. Reeck, G. Houben, B. Riebe and C. Bunnenberg, *Environ. Sci. Technol.*, 2009, **43**, 4896-4901.
2. C. Tournassat, R. M. Tinnacher, S. Grangeon and J. A. Davis, *Geochim. Cosmochim. Acta*, 2018, **220**, 291-308.
3. B. D. Stewart, M. A. Mayes and S. Fendorf, *Environ. Sci. Technol.*, 2010, **44**, 928-934.
4. W. L. Jolly, *J. Chem. Educ.*, 1985, **62**, A137.
5. R. G. Pearson, *J. Am. Chem. Soc.*, 1963, **85**, 3533-3539.
6. R. G. Pearson, *J. Chem. Educ.*, 1968, **45**, 581.
7. P. G. Allen, D. K. Shuh, J. J. Bucher, N. M. Edelstein, T. Reich, M. A. Denecke and H. Nitsche, *Inorg. Chem.*, 1996, **35**, 784-787.
8. H. A. Thompson, G. E. Brown and G. A. Parks, *Am. Mineral.*, 1997, **82**, 483-496.
9. R. J. Silva and H. Nitsche, *Radiochim. Acta*, 1995, 377-396.
10. G. R. Choppin, *Mar. Chem.*, 1989, **28**, 19-26.
11. R. G. Denning, *J. Phys. Chem. A*, 2007, **111**, 4125-4143.
12. J. Su, P. D. Dau, Y.-H. Qiu, H.-T. Liu, C.-F. Xu, D.-L. Huang, L.-S. Wang and J. Li, *Inorg. Chem.*, 2013, **52**, 6617-6626.
13. A. R. Bubas, E. Perez, L. J. Metzler, S. D. Rissler and M. J. Van Stipdonk, *J. Mass Spectrom.*, 2021, **56**, e4720.
14. H. Oher, T. Vercouter, F. Réal, C. Shang, P. E. Reiller and V. Vallet, *Inorg. Chem.*, 2020, **59**, 15036-15049.
15. P. J. Kelly, *Public Health Nurs.*, 2005, **22**, 65-73.
16. S. D. Kelly, K. M. Kemner and S. C. Brooks, *Geochim. Cosmochim. Acta*, 2007, **71**, 821-834.
17. G. Bernhard, G. Geipel, T. Reich, V. Brendler, S. Amayri and H. Nitsche, *Radiochim. Acta*, 2001, **89**, 511-518.
18. S. Amayri, T. Reich, T. Arnold, G. Geipel and G. Bernhard, *J. Solid State Chem.*, 2005, **178**, 567-577.
19. S. Doudou, K. Arumugam, D. J. Vaughan, F. R. Livens and N. A. Burton, *Phys. Chem. Chem. Phys.*, 2011, **13**, 11402-11411.
20. J. D. Kubicki, G. P. Halada, P. Jha and B. L. Phillips, *Chem. Cent. J.*, 2009, **3**, 10.
21. W. A. de Jong, E. Aprà, T. L. Windus, J. A. Nichols, R. J. Harrison, K. E. Gutowski and D. A. Dixon, *J. Phys. Chem. A*, 2005, **109**, 11568-11577.
22. F. Schlosser, L. Moskaleva, A. Kremleva, S. Krüger and N. Rösch, *Dalton Trans.*, 2010, **39 24**, 5705-5712.
23. J. Vázquez, C. Bo, J. M. Poblet, J. de Pablo and J. Bruno, *Inorg. Chem.*, 2003, **42**, 6136-6141.
24. A. O. Tirler and T. S. Hofer, *J. Phys. Chem. B*, 2014, **118**, 12938-12951.
25. A. O. Tirler and T. S. Hofer, *Dalton Trans.*, 2016, **45**, 4983-4988.
26. W. Wu, C. Priest, J. Zhou, C. Peng, H. Liu and D. E. Jiang, *J. Phys. Chem. B*, 2016, **120**, 7227-7233.
27. B. Li, J. Zhou, C. Priest and D. E. Jiang, *J. Phys. Chem. B*, 2017, **121**, 8171-8178.
28. G. Meinrath, R. Klenze and J. I. Kim, *Radiochim. Acta*, 1996, **74**, 81-86.
29. T. I. Docrat, J. F. Mosselmans, J. M. Charnock, M. W. Whiteley, D. Collison, F. R. Livens, C. Jones and M. J. Edmiston, *Inorg. Chem.*, 1999, **38**, 1879-1882.
30. L. Gagliardi, I. Grenthe and B. O. Roos, *Inorg. Chem.*, 2001, **40**, 2976-2978.
31. A. Coda, A. Giusta and V. Tazzoli, *Acta Crystallogr. B*, 1981, **37**, 1496-1500.
32. S. Amayri, T. Arnold, T. Reich, H. Foerstendorf, G. Geipel, G. Bernhard and A. Massanek, *Environ. Sci. Technol.*, 2004, **38**, 6032-6036.

33. C. Moulin, P. Decambox and L. Trecani, *Anal. Chim. Acta*, 1996, **321**, 121-126.
34. A. V. Fonin, A. I. Sulatskaya, I. M. Kuznetsova and K. K. Turoverov, *Plos One*, 2014, **9**, e103878.
35. E. C. Jung, H. R. Cho, M. H. Baik, H. Kim and W. Cha, *Dalton Trans.*, 2015, **44**, 18831-18838.
36. J. Kestin, M. Sokolov and W. A. Wakeham, *J. Phys. Chem. Ref. Data*, 1978, **7**, 941-948.
37. J. R. Lakowicz, *Principles of fluorescence spectroscopy*, Springer, New York, 3rd edn., 2006.
38. M. Viard, J. Gallay, M. Vincent, O. Meyer, B. Robert and M. Paternostre, *Biophys. J.*, 1997, **73**, 2221-2234.
39. E. Fromentin, D. Lebeau, A. Bergounioux, M. Ferry and P. E. Reiller, *Radiochim. Acta*, 2020, **108**, 383-395.
40. E. Fromentin and P. E. Reiller, *Inorg. Chim. Acta*, 2018, **482**, 588-596.
41. Y. Z. Kouhail, M. F. Benedetti and P. E. Reiller, *Environ. Sci. Technol.*, 2016, **50**, 3706-3716.
42. Y. Z. Kouhail, M. F. Benedetti and P. E. Reiller, *Chem. Geol.*, 2019, **522**, 175-185.
43. M. Moriyasu, Y. Yokoyama and S. Ikeda, *J. Inorg. Nucl. Chem.*, 1977, **39**, 2211-2214.
44. J. N. Brönsted, *J. Am. Chem. Soc.*, 1922, **44**, 938-948.
45. K. S. Pitzer, *Activity Coefficients in Electrolyte Solutions*, CRC Press, Boca Raton, 2nd edn., 1991.
46. P. Debye, *Phys. Z.*, 1923, **24**, 185-206.
47. C. W. Davies, *J. Chem. Soc.*, 1938, DOI: 10.1039/JR9380002093, 2093-2098.
48. C. W. Davies, *Ion Association*, Butterworths, London, UK, 1962.
49. I. Grenthe, L. Fuger, R. G. M. Konings, R. J. Lemire, A. B. Muller, C. Nguyen-Trung and H. Wanner, *Chemical Thermodynamics 1. Chemical Thermodynamics of Uranium, Chemical Thermodynamics Series*, North Holland Elsevier Science Publishers B. V., Amsterdam, The Netherlands, 1992.
50. I. Grenthe, A. V. Plyasunov and K. Spahiu, Chapter IX. Estimations of medium effects on thermodynamic data, in *Modelling in Aquatic Chemistry*, eds. I. Grenthe and I. Puigdomènech, OECD, Paris, France, 1997, ch. IX, pp. 325-426.
51. R. Guillaumont, T. Fanghänel, V. Neck, J. Fuger, D. A. Palmer, I. Grenthe and M. H. Rand, *Update of the Chemical Thermodynamics of Uranium, Neptunium, Plutonium, Americium and Technetium*, OECD Nuclear Energy Agency, Data Bank, Issy-les-Moulineaux, France, 2003.
52. I. Grenthe, X. Gaona, A. V. Plyasunov, L. Rao, W. H. Runde, B. Grambow, R. J. M. Koning, A. L. Smith and E. E. Moore, *Chemical Thermodynamics 14. Second Update on the Chemical Thermodynamics of Uranium, Neptunium, Plutonium, Americium and Technetium, Chemical Thermodynamics Series*, OECD Nuclear Energy Agency Data Bank, Eds., OECD Publications, Paris, France, 2020.
53. H. C. Helgeson and D. H. Kirkham, *Am. J. Sci.*, 1974, **274**, 1199-1261.
54. G. Scatchard, *Chem. Rev.*, 1931, **8**, 321-333.
55. E. A. Guggenheim, *Applications of Statistical Mechanics*, Oxford, Clarendon Press, 1966.
56. R. J. Lemire, J. Fuger, H. Nitsche, P. Potter, M. Rand, J. Rydberg, K. Spahiu, J. C. Sullivan, W. J. Ullman, P. Vitorge and H. Wanner, *Chemical Thermodynamics 4. Chemical Thermodynamics of Neptunium and Plutonium, Chemical Thermodynamics*, North Holland Elsevier Science Publishers B. V., Amsterdam, The Netherlands, 2001.
57. G. Scatchard, *Equilibrium in Solutions and Surface and Colloid Chemistry*, Harvard University Press, 2013.
58. L. Ciavatta, *Ann. Chim. (Rome)*, 1990, **80**, 255-263.

59. W. Hummel, G. Anderegg, L. F. Rao, I. Puigdomènech and O. Tochiyama, *Chemical Thermodynamics 9. Chemical Thermodynamics of Compounds and Complexes of U, Np, Pu, Am, Tc, Se, Ni and Zr with Selected Organic Ligands*, *Chemical Thermodynamics Series*, North Holland Elsevier Science Publishers B. V., Amsterdam, The Netherlands, 2005.
60. G. N. Lewis, M. Randall, K. S. Pitzer and L. Brewer, *Thermodynamics*, McGraw-Hill, New York, 1961.
61. A. G. Dickson and M. Whitfield, *Mar. Chem.*, 1981, **10**, 315-333.
62. H. C. Helgeson, D. H. Kirkham and G. C. Flowers, *Am. J. Sci.*, 1981, **281**, 1249.
63. E. H. Oelkers and H. C. Helgeson, *Geochim. Cosmochim. Acta*, 1990, **54**, 727-738.
64. I. Grenthe and A. Plyasunov, *Pure Appl. Chem.*, 1997, **69**, 951-958.
65. I. Grenthe, F. Mompean, K. Spahiu and H. Wanner, *Guidelines for the extrapolation to zero ionic strength*, Report TDB-2, OECD NEA, Issy-les-Moulineaux, France, 2013. http://www.oecd-nea.org/upload/docs/application/pdf/2020-09/tdb2_2020-09-02_11-51-54_735.pdf
66. C. Bretti, C. Foti and S. Sammartano, *Chem. Spec. Bioavailab.*, 2004, **16**, 105-110.
67. C. Bretti, C. Foti, N. Porcino and S. Sammartano, *J. Solution Chem.*, 2006, **35**, 1401-1415.
68. K. S. Pitzer and J. J. Kim, Thermodynamics of Electrolytes.: IV. Activity and Osmotic Coefficients for Mixed Electrolytes, in *Molecular Structure and Statistical Thermodynamics*, 1974, DOI: 10.1142/9789812795960_0060, pp. 413-419.
69. K. S. Pitzer and G. Mayorga, Thermodynamics of Electrolytes.: III. Activity and Osmotic Coefficients for 2–2 Electrolytes, in *Molecular Structure and Statistical Thermodynamics*, 1974, DOI: 10.1142/9789812795960_0059, pp. 405-412.
70. K. S. Pitzer, *J. Solution Chem.*, 1975, **4**, 249-265.
71. K. S. Pitzer and G. Mayorga, *J. Phys. Chem.*, 1973, **77**, 2300-2308.
72. K. S. Pitzer, *J. Phys. Chem.*, 1973, **77**, 268-277.
73. K. S. Pitzer, J. R. Peterson and L. F. Silvester, *J. Solution Chem.*, 1978, **7**, 45-56.
74. C. F. Baes and R. S. Mesmer, *The Hydrolysis of Cations*, John Wiley & Sons, New York, 1976.
75. C. G. Malmberg and A. A. Maryott, *J. Res. Nat. Bur. Std.*, 1956, **56**, 2641.
76. I. Puigdomènech, A. V. Plyasunov, J. A. Rard and I. Grenthe, Chapter X. Temperature correction to thermodynamic data and enthalpy calculations, in *Modelling in Aquatic Chemistry*, eds. I. Grenthe and I. Puigdomènech, OECD, Paris, 1997, pp. 427-493.
77. D. L. Parkhurst and C. A. J. Appelo, *User's Guide to PHREEQC (Version 2) — A Computer Program for Speciation, Batch-Reaction, One-Dimensional Transport, and Inverse Geochemical Calculations*, Report 99-4259, U.S. Geological Survey, Water-Resources Investigations, Lakewood, Colorado, USA, 1999. http://wwwbrr.cr.usgs.gov/projects/GWC_coupled/phreeqci/
78. D. L. Parkhurst and C. A. J. Appelo, *Description of Input and Examples for PHREEQC Version 3 — A Computer Program for Speciation, Batch-Reaction, One-Dimensional Transport, and Inverse Geochemical Calculations. Chapter 43 of Section A, Groundwater Book 6, Modeling Techniques*, U.S. Geological Survey, Denver, Colorado, USA, 2013. http://pubs.usgs.gov/tm/06/a43/pdf/tm6-A43.pdf
79. W. Hummel, U. Berner, E. Curti, F. Pearson and T. Thoenen, *Nagra/PSI Chemical Thermodynamic Data Base 01/01*, 2002.
80. T. Wolery, *EQ3/6, A Software Package for Geochemical Modeling of Aqueous Systems: Package Overview and Installation Guide (Version 7.0)*, Report UCRL-MA-110662-Pt.1, Lawrence Livermore National Lab. (LLNL), Livermore, CA, USA, 1992. http://doi.org/10.2172/138894

81. T. Wolery and M. Sutton, *Generic Natural Systems Evaluation - Thermodynamic Database Development and Data Management*, Report LLNL-TR-500113, Lawrence Livermore National Lab. (LLNL), Livermore, CA, USA, 2011. http://doi.org/10.2172/1035958
82. M. Yui, J. Azuma and M. Shibata, *JNC Thermodynamic Database for Performance Assessment of High-Level Radioactive Waste Disposal System*, Japan, 1999. http://inis.iaea.org/search/search.aspx?orig_q=RN:31060738
83. J. E. Cross and F. T. Ewart, *Radiochim. Acta*, 1991, **52-53**, 421-422.
84. E. Giffaut, M. Grivé, P. Blanc, P. Vieillard, E. Colàs, H. Gailhanou, S. Gaboreau, N. Marty, B. Madé and L. Duro, *Appl. Geochem.*, 2014, **49**, 225-236.
85. M. Grivé, L. Duro, E. Colàs and E. Giffaut, *Appl. Geochem.*, 2015, **55**, 85-94.
86. Thermochimie, http://www.thermochimie-tdb.com/.
87. R. J. Silva, G. Bidoglio, P. B. Robouch, I. Puigdomenech, H. Wanner and M. Rand, *Chemical Thermodynamics 2. Chemical Thermodynamics of Americium*, *Chemical Thermodynamics Series*, North Holland Elsevier Science Publishers B. V., Amsterdam, The Netherlands, 1995.
88. H. Gamsjäger, J. Bugajski, T. Gajda, R. J. Lemire and W. Preis, *Chemical Thermodynamics 6. Chemical Thermodynamics of Nickel*, *Chemical Thermodynamics Series*, North Holland Elsevier Science Publishers B. V., Amsterdam, The Netherlands, 2005.
89. Å. Olin, B. Noläng, E. Osadchii, L.-O. Öhman and E. Rosén, *Chemical Thermodynamics 7. Chemical Thermodynamics of Selenium*, OECD Nuclear Energy Agency, Data Bank, Issy-les-Moulineaux, France, 2005.
90. P. Brown, E. Curti, B. Grambow and C. Ekberg, *Chemical Thermodynamics 8. Chemical Thermodynamics of Zirconium*, *Chemical Thermodynamics Series*, North Holland Elsevier Science Publishers B. V., Amsterdam, The Netherlands, 2005.
91. M. Rand, J. Fuger, I. Grenthe, V. Neck and D. Rai, *Chemical Thermodynamics 11. Chemical Thermodynamics of Thorium*, *Chemical Thermodynamics Series*, OECD Nuclear Energy Agency Data Bank, Eds., OECD Publications, Paris, France, 2009.
92. J. W. Johnson, E. H. Oelkers and H. C. Helgeson, *Comput. Geosci.*, 1992, **18**, 899-947.
93. G. Zhang, N. Spycher, E. Sonnenthal and C. Steefel, presented in part at the TOUGH Symposium, Lawrence Berkeley National Laboratory, May 15-17, 2006, 2006. http://tough.lbl.gov/assets/files/02/documentation/proceedings/2006-Zhang_Pitzer.pdf.
94. T. Wolery, C. Jove-Colon, J. A. Rard and A. Wijesinghe, *Pitzer Database Development: Description of the Pitzer Geochemical Thermodynamic Database data0.ypf. Appendix I in In-Drift Precipitates/Salts Model (P. Mariner)*, Las Vegas, Nevada, 2004
95. P. E. Reiller and M. Descostes, *Chemosphere*, 2020, **251**, 126301.
96. J. Fuger, I. L. Khodakovsky, E. I. Sergeyeva, V. A. Medvedev and J. D. Navratil, *The Chemical Thermodynamics of Actinide Elements and Compounds: Part 12. The Actinide Aqueous Inorganic Complexes*, IAEA, Vienna, 1992.
97. J. Fuger, *Radiochim. Acta*, 1992, **58-59**, 81-92.
98. G. R. Choppin and J. N. Mathur, *Radiochim. Acta*, 1991, **52-53**, 25-28.
99. B. Drobot, A. Bauer, R. Steudtner, S. Tsushima, F. Bok, M. Patzschke, J. Raff and V. Brendler, *Anal. Chem.*, 2016, **88**, 3548-3555.
100. J. Bruno and A. Sandino, *MRS on line Proc. Lib.*, 1988, **127**, 871-878.
101. R. J. Silva, *MRS on line Proc. Lib.*, 1991, **257**, 323-330.
102. M. E. Torrero, I. Casas, J. de Pablo, M. C. A. Sandino and B. Grambow, *Radiochim. Acta*, 1994, **66-67**, 29-36.
103. W. Stumm and J. J. Morgan, *Aquatic Chemistry : Chemical Equilibria and Rates in Natural Waters*, Wiley, New York, 3rd edn., 1996.

104. D. D. Perrin, *Ionisation constants of inorganic acids and bases in aqueous solution*, *IUPAC chemical data series*, Pergamon Press, Oxford, 2nd edn., 1982.
105. D. A. Palmer and R. Van Eldik, *Chem. Rev.*, 1983, **83**, 651-731.
106. D. L. Clark, D. E. Hobart and M. P. Neu, *Chem. Rev.*, 1995, **95**, 25-48.
107. G. Schwarzenbach, *Complexometric titrations*, Interscience Publishers, New York, 2nd edn., 1957.
108. A. Ringböm, *Complexation in Analytical Chemistry: A Guide for the Critical Selection of Analytical Methods Based on Complexation Reactions*, Interscience Publishers, New York, NY, USA, 1963.
109. A. Ringbom and E. Still, *Anal. Chim. Acta*, 1972, **59**, 143-146.
110. A. Ringbom and L. Harju, *Anal. Chim. Acta*, 1972, **59**, 33-47.
111. W. M. Dong and S. C. Brooks, *Environ. Sci. Technol.*, 2006, **40**, 4689-4695.
112. F. Endrizzi and L. F. Rao, *Chem.-Eur. J.*, 2014, **20**, 14499-14506.
113. J. Y. Lee and J. I. Yun, *Dalton Trans.*, 2013, **42**, 9862-9869.
114. G. Bernhard, G. Geipel, V. Brendler and H. Nitsche, *Radiochim. Acta*, 1996, **74**, 87-91.
115. S. N. Kalmykov and G. R. Choppin, *Radiochim. Acta*, 2000, **88**, 603-606.
116. P. Novotny and O. Sohnel, *J. Chem. Eng. Data*, 1988, **33**, 49-55.
117. H. Deniau, P. Decambox, P. Mauchien and C. Moulin, *Radiochim. Acta*, 1993, **61**, 23-28.
118. Y. Yokoyama, M. Moriyasu and S. Ikeda, *J. Inorg. Nucl. Chem.*, 1976, **38**, 1329-1333.
119. M. Moriyasu, Y. Yokoyama and S. Ikeda, *J. Inorg. Nucl. Chem.*, 1977, **39**, 2199-2203.
120. C. Moulin, C. Beaucaire, P. Decambox and P. Mauchien, *Anal. Chim. Acta*, 1990, **238**, 291-296.
121. S. Scapolan, E. Ansorborlo, C. Moulin and C. Madic, *Radiat. Prot. Dosim.*, 1998, **79**, 505-508.
122. G. Meinrath and M. Schweinberger, *Radiochim. Acta*, 1996, **75**, 205.
123. G. G. Manov, N. J. Delollis and S. F. Acree, *J. Res. Nat. Bur. Std.*, 1945, **34**, 115-127.
124. *A guide to pH measurement: Theory and practice of pH applications*, Report 630-321-9646, Alliance Technical Sales, Switzerland, 2013
125. Y. C. Wu, W. F. Koch and R. A. Durst, *Standardization of pH measurements*, Report 260-53, US Department. of Commerce, National Bureau of Standards, 1988. http://nvlpubs.nist.gov/nistpubs/Legacy/SP/nbsspecialpublication260-53e1988.pdf

Chapter II. Determination of Formation Constants and Specific Ion Interaction Coefficients for $Ca_nUO_2(CO_3)_3^{(4-2n)-}$ Complexes in NaCl Solution by Time-Resolved Laser-Induced Luminescence Spectroscopy.

*Chengming Shang, Pascal E. Reiller**

[1] Den – Service d'Études Analytiques et de Réactivité des Surfaces (SEARS), CEA, Université Paris-Saclay, F-91191, Gif-sur-Yvette, France
*Corresponding author. Tel.: +33 1 6908 4312; fax: +33 1 6908 9475. E-mail address: pascal.reiller@cea.fr

Dalton Transactions **49** (2), 466-481.

http://doi.org/10.1039/C9DT03543E

II - 1 Abstract

The formation constants of $CaUO_2(CO_3)_3^{2-}$ and $Ca_2UO_2(CO_3)_3(aq)$ were determined in NaCl medium at ionic strengths between 0.1 and 1 mol kg_w^{-1} using time-resolved laser-induced luminescence spectroscopy (TRLS). Spectroluminescence titration of $UO_2(CO_3)_3^{4-}$ complex by Ca^{2+} were conducted at atmospheric $CO_2(g)$ and varying pH values in order to eliminate the eventual precipitation of both schoepite ($UO_3{:}2H_2O$) and calcite ($CaCO_3$) in aqueous solutions. To identify the stoichiometry of calcium, the slope analyses corrected by the Ringböm coefficient for $UO_2(CO_3)_3^{4-}$ relative to pH and $CO_2(g)$ — instead of typical expression relative to UO_2^{2+} and CO_3^{2-} — was applied in this work. Satisfactory linear fits assessed the conditional stepwise formation constants in the range of ionic strength employed in this work, the values of which are in good agreement with literature data at comparable ionic strengths. Extrapolations to infinite dilution were realized in the framework of the specific ion interaction theory (SIT), also providing the evaluation of the specific ion interaction coefficients. The cumulative stability constants at infinite dilution was determined to be $\log_{10}\beta^\circ(CaUO_2(CO_3)_3^{2-}) = 27.20 \pm 0.04$ and $\log_{10}\beta^\circ(Ca_2UO_2(CO_3)_3(aq)) = 30.49 \pm 0.05$, which are in good agreement with extrapolation proposed elsewhere in literature using a different extrapolation framework. The specific ion interaction coefficients were found to be $\varepsilon(CaUO_2(CO_3)_3^{2-},Na^+) = (0.29 \pm 0.11)$ and $\varepsilon(Ca_2UO_2(CO_3)_3(aq),NaCl) = (0.66 \pm 0.12)$ $kg_w\ mol^{-1}$. Integration of alkali metals into the ternary species may explain these positive and relatively large interaction coefficients. Implications on the speciation of uranium in clay groundwaters, representative of radioactive waste repositories, and in seawater are discussed.

II - 2 Introduction

The speciation of uranium is of great significance for a reliable prediction of its transport from disposal and storage sites of radioactive waste towards geosphere and biosphere. A variety of oxidation states and high coordination number complicates the chemical properties of uranium.[1,2] Hence, primary geochemical reactions — *e.g.*, oxido-reduction, complexation with natural and anthropogenic ligands, and adsorption onto minerals — need to be carefully considered.[3] In particular, the ubiquitous presence of calcium and carbonate in natural water systems renders the formation and chemical behaviour of uranium in Ca-CO_3 rich waters important to be elucidated.[4] The $Ca_nUO_2(CO_3)_3^{(4-2n)-}$ complexes have been studied since their first identification in a seepage water from a uranium mine in Saxony, Germany.[5] Since then, several analytical methods were used to explore their chemical structures and behaviour, such as time-resolved laser-induced luminescence spectroscopy (TRLS),[5-11] anion exchange method,[12,13] potentiometry — using Ca-specific electrode —,[14] ultraviolet-visible (UV-Vis) absorption spectroscopy,[15] and extended X-ray absorption spectroscopy (EXAFS).[7,8,16-18] The interaction between Ca^{2+} and $UO_2(CO_3)_3^{4-}$ seems slightly more important compared to the other alkaline earth elements,.[12,13] but the typically more important concentration of calcium yield to a prevalence of $Ca_nUO_2(CO_3)_3^{(4-2n)}$ complexes over the other ternary species under environmental conditions in general, and potentially under envisaged disposal sites of nuclear waste in particular.[2,19] Adsorption experiments have showed that the formation of $Ca_nUO_2(CO_3)_3^{(4-2n)-}$ can influence U(VI) adsorption on minerals,[20,21] and enhance the mobility of uranium.[22,23] Therefore, the properties of $Ca_nUO_2(CO_3)_3^{(4-2n)-}$ complexes should be studied in detail, especially their thermodynamic binding constants, which are primordial for predictive modelling.

Among the methods mentioned above, TRLS is a highly sensitive technique to probe the characteristic features of luminescent species with limited disturbance of the aqueous equilibrium. The application to uranyl systems at low concentrations has proven the suitability and appropriateness in trace analysis of uranium.[24,25] The investigations of uranium(VI) hydrolysis have shown individual spectroscopic signatures of principle components after spectral decomposition of a series of experimental spectra as a function of pH.[26-28] However, uranyl complexation by carbonate has been considered faintly detectable by TRLS for a long time, which was attributable to the weak luminescence of UO_2-CO_3 at room temperature as a result of the quenching effects of carbonates.[29] More recently, authors have been able to collect the luminescence emission spectra of uranyl carbonate complexes and measure their decay-

time,[6,30] even in a pronounced quenching environment like seawater.[17] The achievable acquisition of binary species spectrum permitted determining quantitatively the stability constants of ternary species with steadily enhanced luminescence intensity upon the association with alkaline earth cations.

Authors reported the stability constants of $Ca_nUO_2(CO_3)_3^{(4-2n)-}$ species in different electrolyte media based on similar thermodynamic considerations.[6,8,9,14] Titrations by calcium ion, generally at a fixed pH value, starting from a specific alkaline condition, where $UO_2(CO_3)_3^{4-}$ was dominating, to where the ternary species would take precedence. However, further investigations of experimental ranges suggest that aqueous conditions in literature may result in varying degrees of oversaturation with regard to calcite ($CaCO_3$) or schoepite ($UO_3{:}2H_2O$) in solution depending on the pH value — for calcite this was clearly shown by Dong and Brooks.[12] Endrizzi and Rao performed potentiometric titration at pH 10 in 0.1 mol L^{-1} NaCl using Ca^{2+} ion selective electrode.[14] The interfering effects of Na^+ and minor Mg^{2+} on the stability of electrode were confirmed to be absent in their work. Nevertheless, one can notice that another principal source of bias might emerge from the potential oversaturation of calcite at the reported pH value — even if this was clearly not observed. Similarly, in Kalmykov and Choppin,[9] onset of calcite precipitation might have occurred at pH 8.1 in 0.1 mol L^{-1} $NaClO_4$ because the end of spectroluminescent titration was conducted near the saturation limit of calcite. Moreover, Lee and Yun determined the formation constants at three pH values of 7.4, 8.1, and 9 in 0.1 mol L^{-1} $NaClO_4$.[6] Combined with an EDTA titration, it was found that $CaUO_2(CO_3)_3^{2-}$ was predominantly present at pH 8.1, and 9, and $Ca_2UO_2(CO_3)_3(aq)$ at pH 7.4 and higher Ca concentration. Their results could have also suffered from the same bias as the occurrence of schoepite (pH 7.4) and calcite (pH 8.1 and 9) were possible at different stages of titration.

Even though several thermodynamic constants have previously been reported, discrepancies in measured values and resulting theoretical calculations are worth mentioning. Up to now, none of these values have been selected in the critical review commissioned by the Thermochemical DataBase project of the Nuclear Energy Agency-Organization from the Economic Co-operation and Development (NEA-OECD, https://www.oecd-nea.org/dbtdb/)[31,32] — the implication of alkaline metal ions was suggested in Guillaumont, *et al.*[32] It should be noted that the relevant formation constants are must-have parameters for modelling the species distribution.[19]

The influence of background electrolyte effects on the ternary species received limited attention. Within the NEA-OECD selection of data, this particular aspect is dealt with using the specific interaction theory (SIT) — see Guillaumont, *et al.*[32] for details — through specific ion interaction coefficients ε between a complex and the oppositely charged ion from the background electrolyte. Equivocal implications of the reported ε values have been rarely assessed. To the best of our knowledge, only Dong and Brooks[13] proposed $\varepsilon(MgUO_2(CO_3)_3^{2-},Na^+) = -(3.0 \pm 0.3)\ kg_w\ mol^{-1}$ and re-evaluated $\varepsilon(Ca_2UO_2(CO_3)_3(aq),NaClO_4) = -2.7\ kg_w\ mol^{-1}$ from Kalmykov and Choppin.[9] Other authors postulated that $\varepsilon(MUO_2(CO_3)_3^{2-},Na^+)$ could be approximated in analogy to $\varepsilon(UO_2(CO_3)_2^{2-},Na^+) = -0.02 \pm 0.09\ kg_w\ mol^{-1}$, and that $\varepsilon(Ca_2UO_2(CO_3)_3(aq),MX)$ was nil as commonly stated for non-charged species.[31,32] The very high ε values sometimes reported are reminiscent of theoretical calculation on the integration of alkaline ions into the structure of the $Ca_nUO_2(CO_3)_3^{(4-2n)-}$ complexes,[33] which remains to be demonstrated experimentally.

The scarcity of systematically determined specific ion interaction coefficients for this system is a major obstacle to the accurate speciation of uranium in natural media, and to specify whether the alkaline ions are capable of integrating into the manifold structures of ternary species at high ionic strengths.

To help answering these remaining questions, the aim of this work is to determine the thermodynamic formation constants of $Ca_nUO_2(CO_3)_3^{(4-2n)-}$ in NaCl using TRLS. The NaCl medium is chosen, instead of typical $NaClO_4$ for inert background electrolyte, for its relevance for natural waters, particularly for radioactive waste management sites.[34,35] It is also worthy to notice that these complex are of primordial importance in the context of uranium extraction from seawater.[14] The experiments are covering a large pH range excluding any possible precipitation of solid phases by modifying the total calcium concentration. The slope analyses of spectroluminescent titrations are used to identify the respective stability fields of the species and give information about their spectroscopic properties. The stepwise formation constants measured at various ionic strengths allow proposing the thermodynamic formation constants at infinite dilution, and the specific ion interaction coefficients $\varepsilon(CaUO_2(CO_3)_3^{2-},Na^+)$ and $\varepsilon(Ca_2UO_2(CO_3)_3(aq),NaCl)$, in the SIT framework. Practical application of the thermodynamic constants and specific ion interaction coefficients of the complexes will then be done for the estimation of uranium speciation in water compositions representative of radioactive waste management sites, and in seawater contexts as well.

II - 3 Experimental Section

3.1 Materials

A stock solution of natural U(VI) was prepared after dissolution of U_3O_8 in 37 % hydrochloric acid (Sigma-Aldrich, ACS reagent) during one week. The aqueous concentration of uranium is measured by inductively coupled plasma mass spectroscopy (ICP-MS). The total uranium concentration in the experiments is maintained at 50 µmol kg_w^{-1} by diluting in NaCl solutions of different ionic strengths (0.1, 0.25, 0.5, 0.75 and 1 mol kg_w^{-1}), prepared with anhydrous NaCl (Sigma-Aldrich, ACS reagent, ≥ 99 %) and Millipore deionized water (Alpha-Q, 18.2 MΩ/cm). The observed spectral behaviour of U(VI), assumed to be the cumulative contribution of aqueous species, under saturated with respect to schoepite and calcite, is therefore an essential prerequisite for further acquisition. No precipitation effects has occurred at the present concentration of U(VI).

The pH values of the sample solutions were controlled in the range 7.4–9.0 with sodium hydroxide (Analytical Grade, Fisher) and diluted hydrochloric acid — the pH measurement protocol are detailed afterwards. The desired pH value is regularly checked and maintained unvaried in each analysed system throughout the experiments. The last measurement of pH value is done before TRLS analysis. Carbonate is introduced by adding appropriate amounts of freshly prepared $NaHCO_3$ solution (Analytical Grade, Fisher), calculated on the basis of equilibrium between aqueous solution and atmospheric CO_2(g). Calcium chloride (Sigma-Aldrich, ACS reagent, ≥ 99 %) is used to control the concentration of calcium. Sample solution is prepared in 15 mL polyethylene bottle and titrated with adequate amount of $CaCl_2$ solution. The volume of each required reagent is controlled as small as possible with the aim to maintain the ionic strength at the set value. All dilution are performed by weighing.

3.2 Determination of pH values and liquid junction potential

The measurements of pH values are performed at 22 °C. A combined-glass electrode (Mettler Toledo, USA) is calibrated routinely using four commercial solutions of pH 1.68, 4.01, 6.87 and 10.01 (SI Analytics, Mainz, Germany). A series of NaCl solutions of ionic strength from 0.1 to 3 mol kg_w^{-1} acidified by HCl to pcH (= $-\log_{10}[H^+]$) 2 was prepared to estimate the liquid junction potential.[36] The responses of potential read on the pH-meter against ionic strengths of NaCl solution were analysed in linear regression (not shown). The multi-point calibration method is applied in this study with aforementioned buffer solutions, the electrolyte concentrations of which are known.[37] The 95 % confidence limits are readily estimated by

means of ordinary least squares,[38] which allowed the uncertainty of pH determination below 0.05 pH units.

For each measuring sample, the first pH adjustment is performed after introducing $NaHCO_3$ solution into the aqueous system. Then, the samples are let opened to the atmosphere during two hours. The values of pH would be slightly adjusted and checked for the second time, if there were any modifications. The final pH determination is carried out just before spectrum acquisition. The equilibrium with $CO_2(g)$ can be confirmed by the fact that the pH values were almost unvarying after the additions of $NaHCO_3(aq)$.

3.3 Time-Resolved Laser-Induced Luminescence Spectroscopy

A 2 mL solution of U(VI) is taken from the 15 mL polyethylene bottle and placed in a 1 cm quartz cuvette (QS101, Suprasil, Hellma Analytics). Prior to data acquisition, the cuvette is pre-equilibrated thermally at least 10 min in a controlled-temperature sample holder, connected to a thermostat (Peter Huber Kältemaschinenbau AG, Germany) with circulating water. A 355 nm tripled Nd:YAG laser (Surelite, Continiuum, USA) delivering about 170 mJ of energy is used as the laser excitation source, pulsed at 10 Hz with 5 ns pulse. An optical parametric oscillator system (Horizon, Continiuum, USA) is set at λ_{ex} = 450 nm. The fluorescence cuvette is placed in a thermostated holder during measurements in order to minimize the temperature influence on uranyl luminescence.[39] The energy is monitored by a RJP-734 Joule-meter (Laser Probe, Inc.). The fluorescence signal is focused into a monochromator spectrometer (Acton) using a 300 lines mm^{-1} grating. An intensified CCD camera (Andor, UK) cooled by the Peltier effect (-10 °C) is used to detect the time-resolved fluorescence signal. Emission spectra are recorded as a function of gate delay D ($\geq$ 25 ns, minimum for preventing the Raman scatter peak of H_2O) at the fixed gate width W = 1 μs. Following the expression of fluorescence signal in Eq. (II - 1), the collected spectra are then integrated over the same wavelength span to deduce the fluorescence intensity at various delay time. The concentration of U(VI) is low enough to eliminate the absorption effect of excitation and emission wavelength, *i.e.* the pre- and post-filter effects.

$$FI = \sum_i FI_0 \, \tau_i \exp\left(-\frac{D}{\tau_i}\right)\left(1 - \exp\left(-\frac{W}{\tau_i}\right)\right) \qquad \text{(II - 1)}$$

where τ_i is fluorescence lifetime of species *i*, W is the gate width, FI represents fluorescence intensity at any given delay time and FI_0 is that at D = 0.

Spectral data management and analysis are carried out with Origin 9.0 software (OriginLab Corporation, USA) by a specially created data processing procedure. The Levenberg-Marquardt algorithm is used in least-square fitting method. The fluorescence intensities *FI* obtained at various delay time are fitted to an exponential decay function in order to derive the luminescence decay-time as well as the luminescence intensity at $D = 0$.[40-43] It is found that the decay time of Ca-UO_2-CO_3 species and delay time *D* are in the same order of magnitude. One prominent cause is that the luminescence intensity at $D = 25$ ns differed greatly from FI_0 and *FI*, thus should not be used in the analytical procedure for the sake of accuracy.

3.4 Correction for slope analysis

The methodological approach in this paper is based on the broader implications of previous studies.[5-15] As mentioned earlier, complexation of calcium with uranyl carbonate moiety has been investigated mainly by titration of calcium at fixed pH value. Such approaches, however, are restricted by the occurrence of schoepite and calcite. In spite of possible precipitation of minerals with actual concentrations of calcium(II) and uranium(VI), the speciation from literature improved our understanding of the Ca-UO_2-CO_3 system.

The predominance regions of calcium(II) and dicalcium(II) triscarbonatouranyl complexes are shown to evolve with pH and calcium concentration. More precisely, $CaUO_2(CO_3)_3^{2-}$ occurs at relatively high pH and low calcium concentration, while lower pH and higher calcium concentration favours $Ca_2UO_2(CO_3)_3(aq)$. For ruling out the undesired precipitations, a titration of calcium at varying pH values is used in this study. The degree of complexation is estimated by the variation of fluorescence intensity as a function of the free Ca^{2+} concentration. By these means, the stoichiometry of ternary species is identified by the so-called slope analysis, which provided an approach to investigate separately their properties. Preliminary calculations are performed with literature data.[12] It appears that simultaneously changed pH values and Ca^{2+} concentrations allow the successive complexation to such an extent that the fractions of $CaUO_2(CO_3)_3^{2-}$ and $Ca_2UO_2(CO_3)_3(aq)$ could attain up to 50-85 % in the middle and at the end of entire titration, respectively — see Fig. II - S1, and the aqueous conditions are listed in Table II - S1 of the Supplementary Information (SI). Stepwise formations of $CaUO_2(CO_3)_3^{2-}$ and $Ca_2UO_2(CO_3)_3(aq)$ are described with the stepwise equilibrium constants $K_{n.1.3}$ at a given ionic strength expressed as follows,

$$nCa^{2+} + UO_2(CO_3)_3^{4-} \rightleftarrows Ca_nUO_2(CO_3)_3^{(4-2n)-}$$

$$K_{n,1,3} = \frac{[Ca_nUO_2(CO_3)_3^{(4-2n)-}]}{[Ca^{2+}]^n\,[UO_2(CO_3)_3^{4-}]} \qquad \text{(II - 2)}$$

where squared brackets indicate concentration on molality scale (mol kg_w^{-1}).

As represented in Eq. (II - 4), the slope n stands for the stoichiometric number of calcium ion involved, *R* is the concentration ratio between complexed and non-complexed uranyl carbonate moiety by calcium considering the influence of pH, and the intercepts $\log_{10}K_{n.1.3}$ refer to the stepwise formation constants of $Ca_nUO_2(CO_3)_3^{(4-2n)-}$ and $Ca_2UO_2(CO_3)_3$(aq) at a particular ionic strength value.

$$\log_{10}R = \log_{10}\frac{[Ca_nUO_2(CO_3)_3^{(4-2n)-}]}{[UO_2(CO_3)_3^{4-}]/\alpha} = \log_{10}K_{n,1,3} + n\log_{10}[Ca^{2+}] \qquad \text{(II - 3)}$$

This latter expression can be expressed as luminescence intensity,

$$\log_{10}R = \log_{10}\frac{FI_0(Ca_nUO_2(CO_3)_3^{(4-2n)-})}{FI_0(UO_2(CO_3)_3^{4-})/\alpha} = \log_{10}K_{n.1.3} + n\log_{10}[Ca^{2+}] \qquad \text{(II - 4)}$$

where $FI_0(Ca_nUO_2(CO_3)_3^{(4-2n)-})$ is the fluorescence intensity extrapolated at $D = 0$ of the complexed species at variable pH values, $FI_0(UO_2(CO_3)_3^{4-})$ is that of the non-complexed triscarbonatouranyl moiety at pH 9, and α represents the Ringböm[44] coefficient of $UO_2(CO_3)_3^{4-}$. It is calculated to assess the variation of aqueous content of triscarbonatouranyl with pH (vide infra), since the denominator of *R* refers to the amount of $UO_2(CO_3)_3^{4-}$ at the same pH value with the numerator sample but at $[Ca^{2+}] = 0$ conditions.

3.5 Calculation of the Ringböm coefficient relative to $UO_2(CO_3)_3^{4-}$

The investigated pH range varied from a circum neutral condition about pH 7.4 to a mildly alkaline condition at pH *ca*. 9.0. The highest pH value leads to the predominance of $UO_2(CO_3)_3^{4-}$ in atmospherically-equilibrated aqueous solution, owing to the dissolution of CO_2(g) in H_2CO_3(aq), HCO_3^-, and CO_3^{2-}. In contrast, in neutral to mildly alkaline conditions without calcium, complicated speciation of uranium(VI) driven by hydrolysis and oligomerization, even possible precipitation of $UO_3{:}2H_2O$(cr), would render the prediction of individual concentration for all the involved species difficult. For this reason, direct fluorescence measurement of uranyl-carbonate solutions prepared at investigated pH values without calcium is untenable, as characteristic fluorescence properties would be inevitably interfered by hydroxo uranyl species. Fluorescence decay spectra of a sample prepared at pH 7.6 were acquired over a large range of delay time, where the spectral profiles were significantly affected as shown in Fig. II - S2 of the SI.

Many previous studies of uranyl carbonate system showed that when the solution suffered a decrease in pH, starting from a highly alkaline condition, the proportion of $UO_2(CO_3)_3^{4-}$ crucially decreased as the less-complexed species — *e.g.*, $UO_2(CO_3)_2^{2-}$, $UO_2CO_3(aq)$ —, the hydroxo species — *e.g.*, $UO_2(OH)^+$, $UO_2(OH)_2(aq)$ — and the polynuclear species — *e.g.*, $(UO_2)_2CO_3(OH)_3^-$, $(UO_2)_3(OH)_5^+$… — increased.[28,29,45-47] To reconcile these aqueous features of hydroxo and carbonato uranyl complexes, we postulated that $UO_2(CO_3)_3^{4-}$ contributed primarily to the variation of non-complexed by calcium species as a function of pH, over other hydroxides and carbonates species in calcium-uranium(VI)-carbonate system. Consequently, evaluation of the Ringböm[44] coefficient α at different pH values in free-calcium conditions sufficed to estimate the impact of pH values. The assumption is then validated by speciation calculation with determined thermodynamic data in this work.

The typical description and thermodynamic formation constant of hydrolysis-carbonation equilibria are often written relative to uranyl(VI) species UO_2^{2+} and CO_3^{2-} as follows.

$$m\mathrm{UO_2^{2+}} + n\mathrm{H_2O} + q\mathrm{CO_3^{2-}} \rightleftarrows (\mathrm{UO_2})_m(\mathrm{CO_3})_q(\mathrm{OH})_n^{(2m-n-2q)+} + n\mathrm{H^+}$$

$$\log_{10}\beta^\circ_{m.n.q} = \frac{[(\mathrm{UO_2})_m(\mathrm{CO_3})_q(\mathrm{OH})_n^{(2m-n-2q)+}]\,[\mathrm{H^+}]^n}{[\mathrm{UO_2^{2+}}]^m\,[\mathrm{CO_3^{2-}}]^q} \qquad \text{(II - 5)}$$

Varying pH values means that CO_3^{2-} concentrations should be recalculated. In our case, it seems more convenient to express the complexation relative to $UO_2(CO_3)_3^{4-}$ and partial pressure of $CO_2(g)$ as follows instead.

$$m\mathrm{UO_2(CO_3)_3^{4-}} + (6m-2q-n)\mathrm{H^+} \rightleftarrows (\mathrm{UO_2})_m(\mathrm{CO_3})_q(\mathrm{OH})_n^{(2m-n-2q)+} + (3m-q)\mathrm{CO_2(g)} + (3m-q-n)\mathrm{H_2O}$$

$$\log_{10}\beta^\circ_{m.n.q} = \frac{[(\mathrm{UO_2})_m(\mathrm{CO_3})_q(\mathrm{OH})_n^{(2m-n-2q)+}]\,P(\mathrm{CO_2})^{(3m-q)}}{[\mathrm{UO_2(CO_3)_3^{4-}}]^m\,[\mathrm{H^+}]^{(6m-2q-n)}} \qquad \text{(II - 6)}$$

The thermodynamic constant can be calculated from the selected thermodynamic data from Guillaumont, *et al*.[32] as follows,

$$\log_{10}\beta'^\circ_{m.n.q} = \log_{10}\beta^\circ_{m.n.q} - \mathrm{m}\,\log_{10}\beta^\circ_{1.0.3} - (3m-q)\,\log_{10}\beta^\circ_{0.1.1} \qquad \text{(II - 7)}$$

or directly form the Gibbs energy of formation, $\Delta_f G^\circ_m$.

The concentration of $UO_2(CO_3)_3^{4-}$ at each pH value can then be expressed only as a function of $[H^+]$ and $P(CO_2)$ using the constants calculated from the known $\Delta_f G^\circ_m$ taken from the NEA-OECD database,[32] as listed in Table II - 1 and Table II - 2, using the mass action law.

The Ringböm coefficient is introduced to quantify the fraction of U(VI) present as the $UO_2(CO_3)_3^{4-}$ complex with the mass balance on $UO_2(CO_3)_3^{4-}$ expressed in Eq. (II - 8). The

mathematical form is slightly simplified to a quadratic equation with one unknown as $UO_2(CO_3)_3^{4-}$ by neglecting lesser contributing terms from hydrolysed species $(UO_2)_n(OH)_m^{(2n-m)+}$.

$$C_T = [UO_2(CO_3)_3^{4-}] + \left(1 + \beta_{1.0.2}\frac{[H^+]}{P(CO_2)} + \beta_{1.0.1}\frac{[H^+]^4}{P(CO_2)^2}\right) + 2\beta_{2.3.1}\frac{[UO_2(CO_3)_3^{4-}]^2\,[H^+]^7}{P(CO_2)^5} \quad \text{(II - 8)}$$

where $\alpha = C_T/[UO_2(CO_3)_3^{4-}]$, $P(CO_2) = 10^{-3.5}$ atm, and $[H^+]$ is converted from (H^+), measured by pH-meter. The calculation of $\beta_{m.n.l}$ required a correction of the water activity a_{H_2O} for each ionic strength — see Eq. B.9 from Guillaumont, *et al.*[32] Ringböm coefficient was calculated for each sample at specified values of pH and ionic strength (Table II - S2 of the SI).

Table II - 1 Stability constants of U(VI) complexes at 25 °C and I_m = 0, used in the work.

Reaction	$\log_{10} K^\circ$	References
$CO_2(g) + H_2O \rightleftarrows CO_3^{2-} + 2H^+$	-18.15 ± 0.06	[32]
$UO_2^{2+} + H_2O \rightleftarrows UO_2(OH)^+ + H^+$	-5.25 ± 0.24	[32]
$UO_2^{2+} + 2H_2O \rightleftarrows UO_2(OH)_2(aq) + 2H^+$	-12.15 ± 0.07	[32]
$3\,UO_2^{2+} + 5H_2O \rightleftarrows (UO_2)_3(OH)_5^+ + 5H^+$	-15.55 ± 0.12	[32]
$UO_2^{2+} + CO_3^{2-} \rightleftarrows UO_2(CO_3)(aq)$	9.94 ± 0.03	[32]
$UO_2^{2+} + 2\,CO_3^{2-} \rightleftarrows UO_2(CO_3)_2^{2-}$	16.61 ± 0.09	[32]
$UO_2^{2+} + 3\,CO_3^{2-} \rightleftarrows UO_2(CO_3)_3^{4-}$	21.84 ± 0.04	[32]
$2\,UO_2^{2+} + CO_2(g) + 4H_2O \rightleftarrows (UO_2)_2CO_3(OH)_3^- + 5H^+$	-19.01 ± 0.50	[32]
$UO_2(CO_3)_3^{4-} + 4H^+ \rightleftarrows UO_2(CO_3)(aq) + 2CO_2(g) + 2H_2O$	24.40 ± 0.21*	Recalculated from[32]
$UO_2(CO_3)_3^{4-} + 2H^+ \rightleftarrows UO_2(CO_3)_2^{2-} + CO_2(g) + H_2O$	12.92 ± 0.15*	Recalculated from[32]
$2\,UO_2(CO_3)_3^{4-} + 7\,H^+ \rightleftarrows (UO_2)_2CO_3(OH)_3^- + 5CO_2(g) + 2H_2O$	46.21 ± 0.70*	Recalculated from[32]
$Ca^{2+} + UO_2(CO_3)_3^{4-} \rightleftarrows CaUO_2(CO_3)_3^{2-}$	5.26 ± 0.01	This work
$2Ca^{2+} + UO_2(CO_3)_3^{4-} \rightleftarrows Ca_2UO_2(CO_3)_3(aq)$	8.65 ± 0.02	This work
$Ca^{2+} + UO_2^{2+} + 3\,CO_3^{2-} \rightleftarrows CaUO_2(CO_3)_3^{2-}$	27.20 ± 0.04	This work
$2Ca^{2+} + UO_2^{2+} + 3\,CO_3^{2-} \rightleftarrows Ca_2UO_2(CO_3)_3(aq)$	30.49 ± 0.05	This work

Table II - 2 Gibbs energies of formation from the main species considered within this work.

Species	$\Delta_f G°_m$ (kJ mol^{-1})	References
H_2O	-237.140 ± 0.041	[32]
CO_2(g)	-394.373 ± 0.133	[32]
CO_3^{2-}	-527.900 ± 0.390	[32]
UO_2^{2+}	-952.551 ±1.747	[32]
$UO_2(CO_3)_3^{4-}$	-2 660.914 ± 2.116	[32]
$(UO_2)_2CO_3(OH)_3^-$	-3 139.526 ± 4.517	[32]
Ca^{2+}	-552.806 ± 1.050	[32]
$CaUO_2(CO_3)_3^{2-}$	-3 244.316 ± 2.361	This work
$Ca_2UO_2(CO_3)_3$(aq)	-3 815.901 ± 2.985	This work

3.6 Specific ion interaction theory (SIT)

The SIT approach,[32] used to extrapolate the thermodynamic constants to infinite dilution, is applicable to a wider range of ionic strength compared to the Davies equation.[48] Thus, the SIT is employed to extrapolate the conditional formation constants to infinite dilution condition, and determine the specific ion interaction coefficients $\varepsilon(CaUO_2(CO_3)_3^{2-},Na^+)$ and $\varepsilon(Ca_2UO_2(CO_3)_3(aq),NaCl)$. The activity coefficient is expressed as follows,

$$\log_{10}\gamma = -z_j^2 D_H + \varepsilon(j,k,I_m)\, m_k \qquad \text{(II - 9)}$$

with D_H the Debye-Hückel term,

$$D_H = \frac{A\sqrt{I_m}}{1 + 1.5\sqrt{I_m}} \qquad \text{(II - 10)}$$

where I_m is the ionic strength on the molal scale, ε represents the ion interaction coefficient (kg$_w$ mol^{-1}) and m_k is the concentration of background electrolyte k in molality.

The value of 0.507 kg$^{1/2}$ mol$^{-1/2}$ is assigned to A at 22 °C.[32] The correlation between stepwise formation constants and ionic strengths can be drawn by the following relationship:

$$\log_{10}K_{n.1.3} = \log_{10}K°_{n.1.3} + \Delta z^2 D_H - \Delta\varepsilon\, I_m \qquad \text{(II - 11)}$$

where

$$\Delta z^2 = z\left(Ca_nUO_2(CO_3)_3^{(4-2n)-}\right)^2 - n\, z(Ca^{2+})^2 - z\left(UO_2(CO_3)_3^{4-}\right)^2 \qquad \text{(II - 12)}$$

($\Delta z^2 = -16$ for n = 1 and $\Delta z^2 = -24$ for n = 2)

and

$$\Delta\varepsilon = \varepsilon(Ca_nUO_2(CO_3)_3^{(4-2n)-},Na^+) - n\,\varepsilon(Ca^{2+},Cl^-) - \varepsilon(UO_2(CO_3)_3^{4-},Na^+) \qquad \text{(II - 13)}$$

The main specific ion interaction coefficients used in this work are reported in Table II - 3.

Table II - 3 Main specific ion interaction coefficients used in this work.

Specific ion interaction coefficient	Value (± 1σ)	Reference
$\varepsilon(H^+,Cl^-)$	0.12 ± 0.01	[32]
$\varepsilon(Na^+,CO_3^{2-})$	-0.08 ± 0.03	[32]
$\varepsilon(UO_2^{2+},Cl^-)$	0.21 ± 0.02	[32]
$\varepsilon(Ca^{2+},Cl^-)$	0.14 ± 0.01	[32]
$\varepsilon(UO_2(CO_3)_2^{2-},Na^+)$	-0.02 ± 0.09	[32]
$\varepsilon(UO_2(CO_3)_3^{4-},Na^+)$	-0.01 ± 0.11	[32]
$\varepsilon(CaUO_2(CO_3)_3^{2-},Na^+)$	0.29 ± 0.11	This work
$\varepsilon(Ca_2UO_2(CO_3)_3(aq),NaCl)$	0.66 ± 0.12	This work

II - 4 Results and discussion

4.1 Evolution of luminescence spectra

The upper limit of aqueous electrolyte concentration is imposed to 1 mol kg_w^{-1} NaCl considering the noticeable quenching effect of chloride ions.[49] Five series of solutions are separately prepared at designed ionic strengths. The fluorescence spectra of aqueous Ca-UO_2-CO_3 complexes at I_m = 0.5 mol kg_w^{-1} NaCl are shown in Fig. II - 1 — those of the four other series are shown in Fig. II - S3 of the SI. A total of 100 sample fluorescence spectra acquired at D = 25 ns were imported into Origin 9.0 software for Gaussian-based peak separation analysis. Characteristic peak wavelengths found at 464.31 ± 0.38, 483.30 ± 0.30, 503.18 ± 0.29, 524.26 ± 0.76 and 546.96 ± 2.25 nm (weighed average of all peak maxima with 2σ uncertainties) are in agreement with literature values.[6,8,9] Hypsochromic-shifted peak positions compared with those of uranyl ions (470.07, 487.31, 509.31, 533.38 and 559.86 nm) in acidic conditions provide evidence for the inner-sphere substitution of carbonate groups for water molecules (Fig. II - S4 of the SI).[50] Fluorescence spectral profiles and band positions do not show any change irrespective of varying aqueous conditions, *i.e.* Ca^{2+} concentration and pH value. This observation indicates that energy transfer between excited electronic state and distinct vibrational levels of ground electronic state is less susceptible to the binding of additional Ca^{2+} ions.

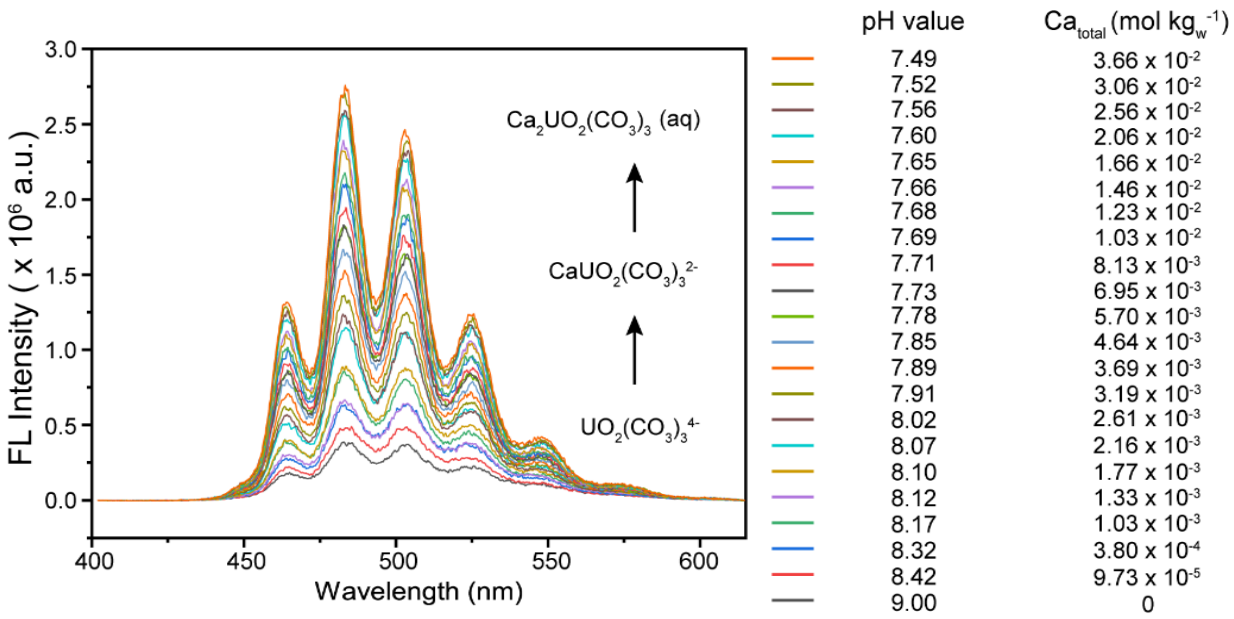

Fig. II - 1 Measured luminescence emission spectra of uranium(VI) at various calcium concentrations and pH values, $P(CO_2) = 10^{-3.5}$ *atm, and* $I_m = 0.5$ *mol* kg_w^{-1} *NaCl; initial delay time of* D *= 25 ns and gate width W = 1 μs, number of accumulation is 1000.*

Successive complexation reactions of calcium ions with triscarbonatouranyl moiety give information about the characters of the studied complexes, resulting from gradually enhanced fluorescence intensity, better-resolved spectrum, and slower luminescence decay-time. Similar trend of spectral and temporal features are observed for every measuring series. The continuously increasing luminescence intensity and decay-time illustrate the progressive complexation of calcium ions. The observed tendency is in line with the sequentially conformational change from $CaUO_2(CO_3)_3^{2-}$ to $Ca_2UO_2(CO_3)_3(aq)$ in aqueous solution.

Luminescence decay-times are determined by fitting the integrated time-resolved luminescence intensities to exponential decay functions. The slope analysis results are used to clarify the borderlines of predominant regions of $CaUO_2(CO_3)_3^{2-}$ and $Ca_2UO_2(CO_3)_3(aq)$ complexes.

Graphical representation of $\log_{10}R$ vs. $\log_{10}[Ca^{2+}]$ allows a straightforward examination of complexation. The aqueous calcium ion is assumed to be present as free Ca^{2+}, since the analytical concentration of calcium is at least 10 times as large as that of U(VI). This simplification is attended by the fact that the amount of calcium consumed in the complexation is negligible with regard to its initial concentration.[51] The experimental data are fitted to straight lines using a least square method,[52] the slopes representing the stoichiometry of Ca^{2+} ions bound to triscarbonatouranyl complex, the intercepts are assigned to the stepwise equilibrium

constants at specific background electrolyte concentration. Linear relationships between $\log_{10}R$ and $\log_{10}[Ca^{2+}]$ are obtained with slopes changing from ca. 1 to ca. 2 as Ca^{2+} is added into the solution (Fig. II - 2). This also demonstrates conclusive evidence for successive formations of $CaUO_2(CO_3)_3^{2-}$ then $Ca_2UO_2(CO_3)_3(aq)$.

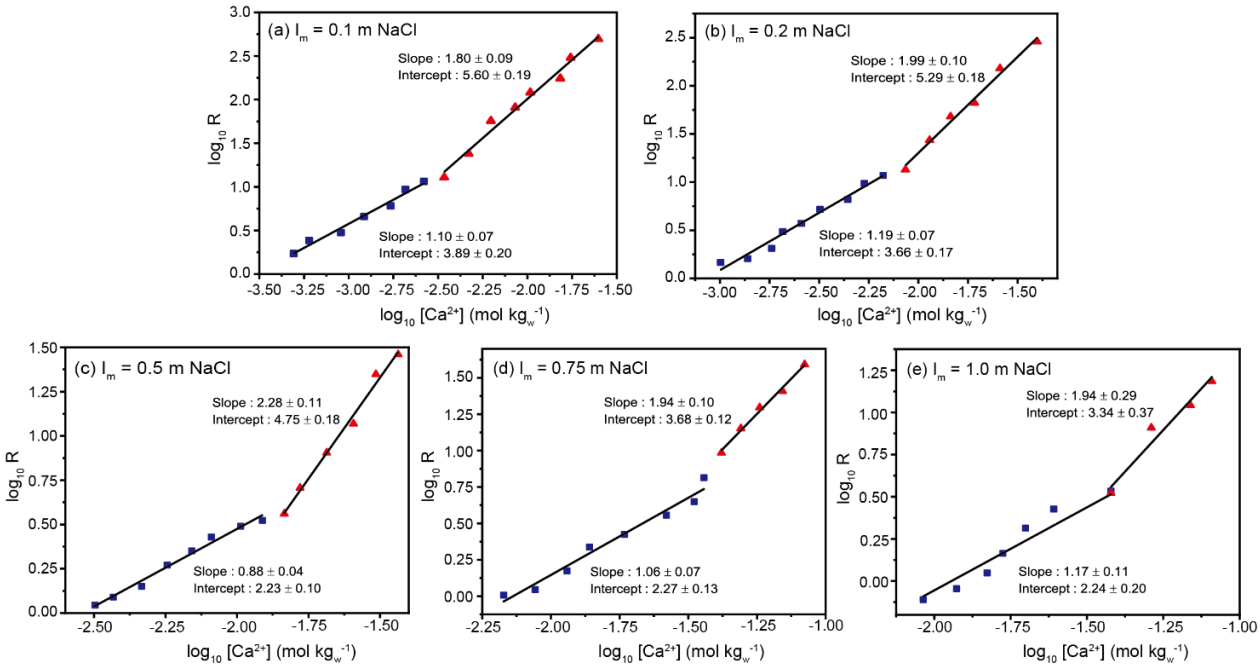

Fig. II - 2 . Logarithmic ratio R in terms of luminescence intensity and Ringböm coefficient plotted as a function of $log_{10}[Ca^{2+}]$ (mol kg_w^{-1}) at investigated NaCl ionic strengths: $[U]_{total}$ = 50 µmol kg_w^{-1}, $P(CO_2) = 10^{-3.5}$ atm

The respective decay-times are deduced by averaging the measured decay-times of correspondent sample solutions. It is assessed that in 0.1 mol kg_w^{-1} NaCl medium, $UO_2(CO_3)_3^{4-}$ is showing a fast decay-time of $\tau(UO_2(CO_3)_3^{4-})$ =(11.04 ± 0.11) ns, compared with $\tau(CaUO_2(CO_3)_3^{2-})$ = (28.30 ± 0.57) ns and $\tau(Ca_2UO_2(CO_3)_3(aq))$ = (46.7 ± 2.7) ns. The possible quenching effect of chloride on luminescence decay-time make it moderately meaningful to compare our results with those in literature, generally in non-complexing medium (0.1 mol L^{-1} $Na/HClO_4$),[6,8] albeit measured decay-times are numerically comparable with each other. In addition, a noticeable suppression of Ca-UO_2-CO_3 complexes decay-times is observed at larger NaCl concentrations that gives a clue to information such as quenching rate constant, which would require deeper attention in further works.

Only mono-exponential functions are needed to fit the intensity decay curves, though at least two calcium triscarbonatouranyl complexes are expected to exist in the majority of the samples. Two representative exponential fits at ionic strength of 0.1 mol kg_w^{-1} NaCl are shown in Fig. II

- 3. Single exponential decay generally suggests that either only one luminescent species is observed, or the rate of de-excitation process is faster than that of ligand exchange. Nevertheless, for such a complex system containing rather complicated fluorophores, luminescence decay behaviour cannot be simply settled. Our observations are in accordance with previous studies as the same decay mode has been observed otherwise for Ca-UO_2-CO_3 ternary system.[6,8] However, a recent study showed clear multi-exponential decays in Mg-UO_2-CO_3 system, from which the characteristic decay times for principle U(VI) species were determined.[7]

Numerous mutually exclusive mechanisms, especially in photochemistry, have been proposed to interpret the inconsistencies in decay mode between Ca/Mg-UO_2-CO_3 systems, *e.g.*, hydrogen abstraction,[53] formation of exciplex,[54] and reversible intersystem crossing.[55] Unfortunately, these mechanisms are not likely to explain the discrepancy between experimental results, as the complexation of Ca/Mg is likely to occur outside the first coordination sphere. It seems more likely that the shorter distance of U-Mg (3.84 Å) compared to that of U-Ca (4.15 Å) could reason out the difference in fluorescent properties.[7]

Several emission spectra of different compositions in binary/ternary species at I_m = 0.2 and 1 mol kg_w^{-1} are normalized to their total area in order to compare the spectroscopic changes (Fig. II - 4). The percentage of species are calculated with the determined formation constants (vide post) for $CaUO_2(CO_3)_3^{2-}$ and $Ca_2UO_2(CO_3)_3$(aq). Unambiguously, the increase in Ca^{2+} concentration makes no distinctive difference in peak positions but results in clearly better resolved spectra and narrow peak widths. The similar spectral trends have been observed elsewhere.[6,7] It must be noted that the use of the 300 lines mm^{-1} grid favours convolution of the different components with the parameters of the optical set-up. The use of a grid with a higher resolution could help in the deconvolution of the signal and identifying spectral differences.[56]

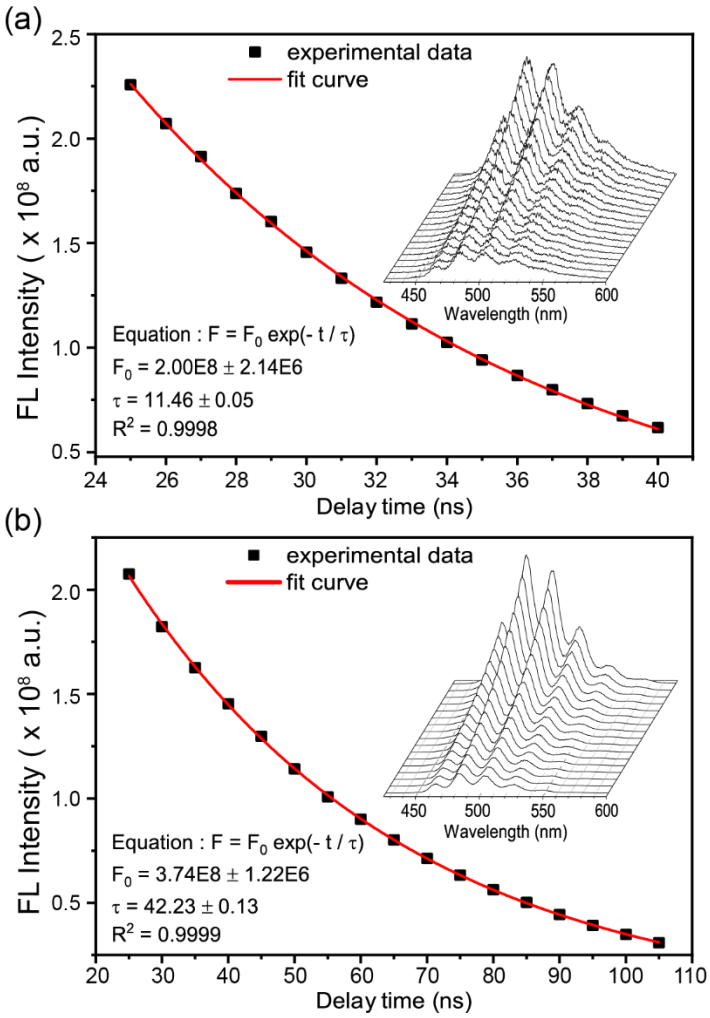

Fig. II - 3 Mono-exponential fits of luminescence intensity decay of (a) $UO_2(CO_3)_3^{4-}$ at [U(VI)] = 50 µmol kg_w^{-1} and pH = 9.0, and (b) Ca-UO_2-CO_3 complexes at [U(VI)] = 50 µmol kg_w^{-1}, $log_{10}[Ca^{2+}]$ = -2.06, pH = 7.60 and I_m = 0.1 mol kg_w^{-1} NaCl. The insets show the waterfall plots of luminescence emission spectra as a function of delay time.

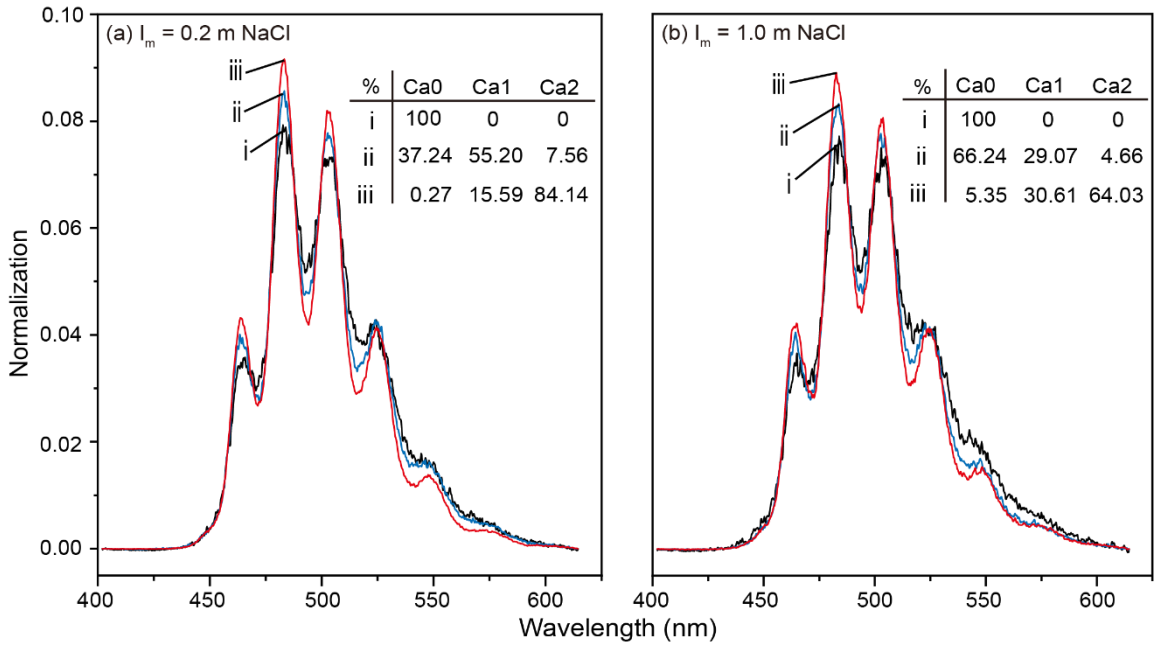

Fig. II - 4 Luminescence emission spectra normalized to the same area at D = 25 ns of (Ca-)UO_2-CO_3 species at (a) I_m = 0.2 mol kg_w^{-1}, and (b) 1 mol kg_w^{-1}; Ca0, Ca1, and Ca2 stand for $UO_2(CO_3)_3^{4-}$, $CaUO_2(CO_3)_3^{2-}$, and $Ca_2UO_2(CO_3)_3(aq)$, respectively.

4.2 Evaluation of equilibrium constants and specific ion interaction coefficients

The graphical results in previous section provide insights into the fluorescence behaviour and complexation mechanism of the investigated system. The quenching effect of chloride is susceptible to affect the applicability of slope analysis method at high concentration, *ca.* 1 mol kg_w^{-1} NaCl, given that the experimental points at $\log_{10}([Ca^{2+}]$ mol $kg_w^{-1}) \geq -1.1$ deviates from the linear trend — not shown in Fig. II - 2. A possible explanation is probably associated with some artefacts altering the measurements of emission spectra. Because of the concentrated electrolyte, the system required a raising quantity of calcium to overcome the electrostatic force for the formation of the ternary species. This fact led to a significant increase in the actual ionic strength as a result of the contribution of $[Ca^{2+}]$, which in turn made the impact of polarization and viscosity on fluorescence too important to be neglected.[57] However, it is yet unclear to which extent the spectral features are influenced. Notwithstanding the sparse experimental points, acceptable linear fits were retained at I_m = 1 mol kg_w^{-1}.

The calcium concentrations for predominance regions of the $Ca_nUO_2(CO_3)_3^{(4-2n)-}$ species can be read directly from Fig. II - 4. Table II - 4 summarizes the detailed solution information of calcium concentrations and pH values for every species being predominantly present. Converting back from the logarithmic form, one can infer that the predominance range of

$CaUO_2(CO_3)_3^{2-}$ enlarges with ionic strength, as a result of increasing interionic attraction between Ca^{2+} and Cl^-.

Table II - 4 Values of decimal logarithm of calcium concentration (mol kg_w^{-1}) extracted from the slope analysis in Fig. II - 4, and pH values measured before luminescence acquisition.

I_m (mol kg_w^{-1})	$CaUO_2(CO_3)_3^{2-}$	$Ca_2UO_2(CO_3)_3$(aq)
0.10	$-3.35 \le \log_{10}[Ca^{2+}] \le -2.58$ $8.10 \le pH \le 7.85$	$-2.58 \le \log_{10}[Ca^{2+}] \le -1.52$ $7.85 \le pH \le 7.45$
0.20	$-3.00 \le \log_{10}[Ca^{2+}] \le -2.15$ $8.14 \le pH \le 7.75$	$-2.15 \le \log_{10}[Ca^{2+}] \le -1.41$ $7.75 \le pH \le 7.40$
0.50	$-2.50 \le \log_{10}[Ca^{2+}] \le -1.87$ $7.91 \le pH \le 7.68$	$-1.87 \le \log_{10}[Ca^{2+}] \le -1.43$ $7.68 \le pH \le 7.49$
0.75	$-2.20 \le \log_{10}[Ca^{2+}] \le -1.44$ $7.79 \le pH \le 7.52$	$-1.44 \le \log_{10}[Ca^{2+}] \le -1.07$ $7.52 \le pH \le 7.39$
1.00	$-2.12 \le \log_{10}[Ca^{2+}] \le -1.40$ $7.86 \le pH \le 7.54$	$-1.40 \le \log_{10}[Ca^{2+}] \le -1.08$ $7.54 \le pH \le 7.40$

The binding constants of Ca^{2+} ion to $CaUO_2(CO_3)_3^{2-}$, noted as $\Delta\log_{10}K$, are 2.43, 2.13, 1.79, 1.59, and 1.51 by subtracting $\log_{10}K_{1.1.3}$ from $\log_{10}K_{2.1.3}$. It is found that $\Delta\log_{10}K$ is lower than $\log_{10}K_{1.1.3}$ at each ionic strength, revealing that the binding of Ca^{2+} to $CaUO_2(CO_3)_3^{2-}$ is more difficult than that of Ca^{2+} to $UO_2(CO_3)_3^{4-}$. This is expected because the electrostatic interaction is stronger between $Ca^{2+}/UO_2(CO_3)_3^{4-}$ than that between $Ca^{2+}/CaUO_2(CO_3)_3^{2-}$ due to the stepwise charge neutralization.

The resulting conditional equilibrium constants after rounding off the slope values to their nearest integers are given in Table II - S3 of the SI. By comparing the different ionic strength series, one can immediately assess the tendency of the stability of ternary species. The dependence of $\log_{10}K_{1.1.3} + 16D$ and $\log_{10}K_{2.1.3} + 24D$ vs. the molal ionic strength in NaCl is represented in Fig. II - 5. The two plots both give a linear relationships over the entire range of ionic strength, which allow determining the ion interaction coefficients and the stepwise formation constants by extrapolating to infinite dilution using the SIT to $\log_{10}K°_{1.1.3} = 5.36 \pm 0.02$ and $\log_{10}K°_{2.1.3} = 8.65 \pm 0.02$. For $CaUO_2(CO_3)_3^{2-}$ and $Ca_2UO_2(CO_3)_3$(aq), the cumulative formation constants are $\log_{10}\beta°_{1.1.3} = 27.20 \pm 0.04$ and $\log_{10}\beta°_{2.1.3} = 30.49 \pm 0.05$, respectively — see Table II - 1, and see $\Delta_f G°_m$ in Table II - 2. The ion interaction coefficients are evaluated to be $\varepsilon(CaUO_2(CO_3)_3^{2-},Na^+) = (0.29 \pm 0.11)$ and $\varepsilon(Ca_2UO_2(CO_3)_3(aq),NaCl) = (0.66 \pm 0.12)$ kg_w mol^{-1}. The mean values and respective uncertainties for $\log_{10}\beta°$ and ε are estimated using the weighed linear regression with reciprocals of the squared standard deviation ($1/\sigma_i^2$) as weights,[58] determined from the slope analysis. The uncertainty range is assessed by propagating the uncertainties from $I_m = 0$ up to 1 mol kg_w^{-1}. The successive calcium complexes

display increasing overall formation constants, which mirrors the stability of the ternary complexes. The obtained values for $\log_{10}\beta^{\circ}_{1.1.3}$ and $\log_{10}\beta^{\circ}_{2.1.3}$ are consistent with literature data[12,14] within the uncertainty limits.

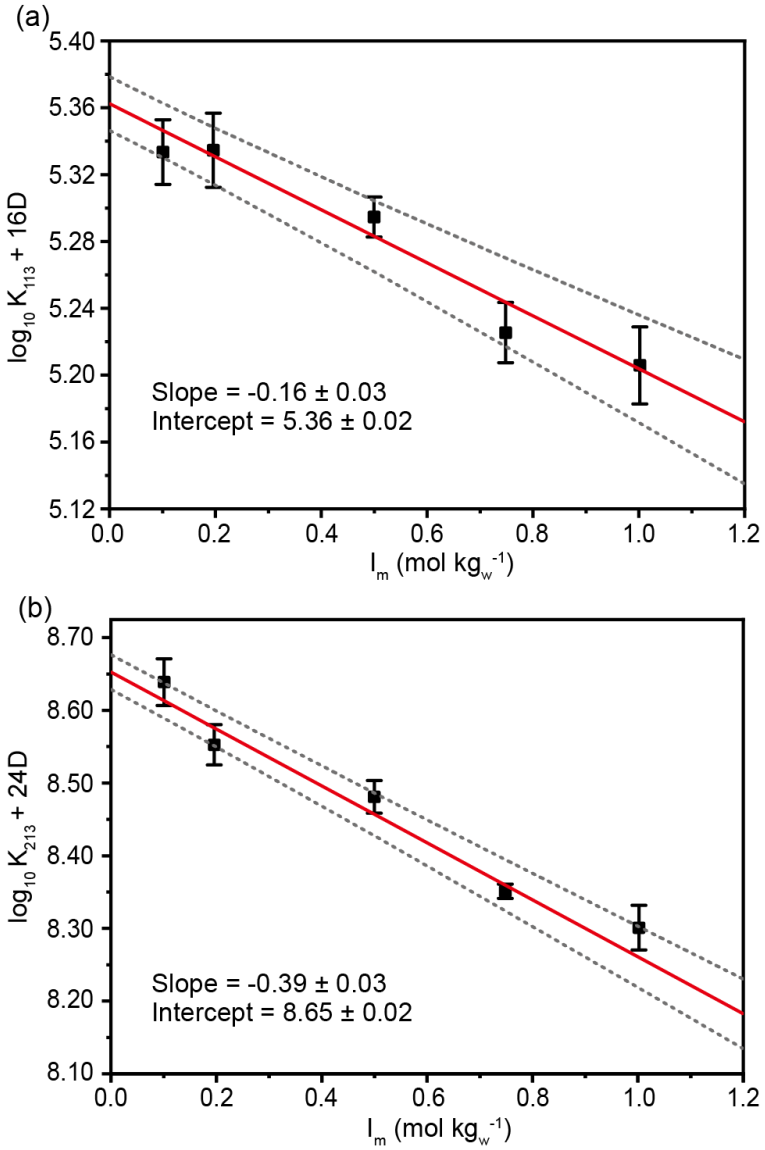

Fig. II - 5 Extrapolation to infinite dilution of the experimental data of (a) $\log_{10}K_{1.1.3}$ + 16D and (b) $\log_{10}K_{2.1.3}$ + 24D as a function of molal ionic strength.

The predominance diagram at I_m = 0.2 mol kg_w^{-1} NaCl in Fig. II - 6 is constructed from our newly determined $\log_{10}\beta^{\circ}_{n.1.3}$ and ε values using PhreePlot,[59,60] which includes PhreeqC[61,62] that handles the SIT. The apparent precipitation region of calcite, limited by the black dashed line, is imposed by the equilibrium between the atmospheric CO_2(g) and the aqueous solution — the four other series are shown in Fig. II - S5 of the SI. As expected, the increase of calcium concentration impedes the precipitation of UO_3:$2H_2O$(cr) — schoepite. It was observed that the

boundaries found by simulation corresponded pretty well to the experimental results. It can also be verified that the more charged species, *i.e.* $UO_2(CO_3)_3^{4-}$ and $CaUO_2(CO_3)_3^{2-}$, see their predominance domains increase with ionic strength.

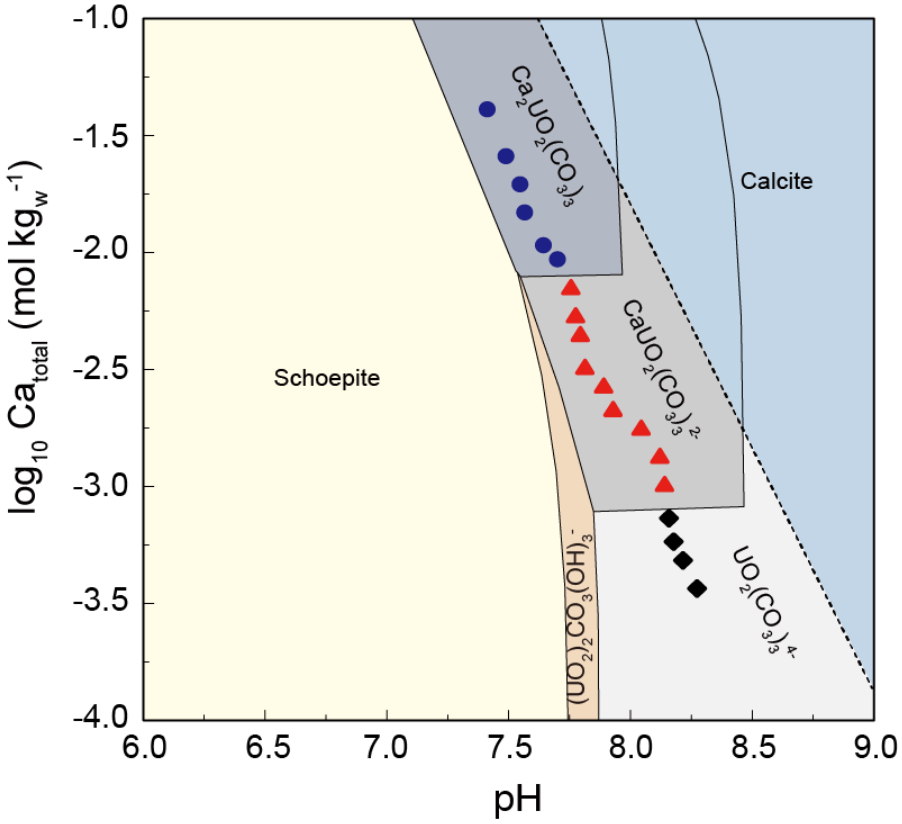

Fig. II - 6 Predominance plots of Ca-UO_2-CO_3 system at [U(VI)] = 50 µmol kg_w^{-1}, $P(CO_2) = 10^{-3.5}$ atm and I_m = 0.2 mol kg_w^{-1} NaCl. Experimental points giving slopes ca. 1 and 2 are highlighted with red triangles and blue filled circles, respectively. The black diamond represents the beginning of titration where the $UO_2(CO_3)_3^{4-}$ complex dominates.

4.3 Discussion on the values of ε and $\log_{10}\beta°$

The $\log_{10}\beta°$ values that we have determined are comparable to other determination in the literature, specific ion interaction coefficients determined in this work are different from literature data,[9,13] and different from other -2 bearing charge complexes — see Table II - S4 of the SI. It is often considered in literature that like-charged ions do share comparable ε values in analogy. This was specifically the case for $CaUO_2(CO_3)^{2-}$,[6,14] and also for other cases — see *e.g.* Table B-4 and B-5 in Guillaumont, *et al.* [32]. After an analysis from tabulated data in Na^+ media, the highest found negative value is $\varepsilon(EdtaH_2^{2-},Na^+) = -(0.37 \pm 0.14)$ kg_w mol^{-1};[63] the highest positive value is $\varepsilon(Cu(OH)_4^{2-},Na^+) = (0.19 \pm 0.05)$ kg_w mol^{-1}.[64] Even it has no physical meaning, a grand average of the available data yields to $\varepsilon(X^{2-},Na^+) = -(0.09 \pm 0.12)$ kg_w mol^{-1}, illustrated by the repartition of the data in Fig. II - S6 of the SI. Our value for

$\varepsilon(CaUO_2(CO_3)_3^{2-},Na^+) = 0.29 \pm 0.11$ is higher than any other observed values — and markedly higher than $\varepsilon(UO_2(CO_3)_2^{2-},Na^+) = -(0.02 \pm 0.09)$ —; only $\varepsilon(Cu(OH)_4^{2-},Na^+)$ or $\varepsilon(UO_2F_4^{2-},Na^+)$ are contained in the standard deviation. Other multi-centred complexes as, *e.g.*, UO_2Edta^{2-}, are showing negative values. This clearly shows that the analogy between like-charged ions is limited.

Ciavatta[65] proposed empirical relationships to estimate missing ε values of a product from the known ε values of the other reactants. In the case of $CaUO_2(CO_3)_3^{2-}$ one can postulate a 1:1 stoichiometry from Eq. (II - 2) and it comes

$$\varepsilon(CaUO_2(CO_3)_3^{2-},Na^+) = \frac{\varepsilon(UO_2(CO_3)_3^{4-},Na^+) + \varepsilon(Ca^{2+},Cl^-)}{2} \qquad (14)$$

$$\varepsilon(CaUO_2(CO_3)_3^{2-},Na^+) = (0.07 \pm 0.06)\ kg_w\ mol^{-1}$$

that is showing a positive value, slightly higher, yet not significantly different from the grand average. It seems though that no other type of -2 charge bearing complex can be compared with $CaUO_2(CO_3)_3^{2-}$, and thus using other ε values in analogy seems not justified.

The case of $Ca_2UO_2(CO_3)_3(aq)$ is more challenging as there are only a few data on globally neutral species. Even if the common hypothesis of a nil value is used very often,[31,32] Ciavatta[65] proposed ε values for chloride, bromide, iodide, thiocyanate, and hydroxide complexes of Cd^{2+}, Hg^{2+}, and Pb^{2+} in perchlorate media; Zhang and Muhammed proposed a value for $Zn(OH)_2(aq)$ complex.[66] The grand average value of $\varepsilon(M(aq),NaClO_4) = -(0.01 \pm 0.06)\ kg_w\ mol^{-1}$ seems to confirm the common hypothesis of a nil value.

Nevertheless, other determinations of inorganic complexes do not follow this general trend. Ciavatta[65] determined $\varepsilon(Hg(OH)_2(aq),NaClO_4) = 0.2\ kg_w\ mol^{-1}$, and proposed that this positive value was linked to the formation of a hydrated oxocation complex $HgO(H_2O)_x$. Plyasunova, *et al.*[67] proposed $\varepsilon(Co(OH)_2(aq),NaClO_4) = -(0.15 \pm 0.10)\ kg_w\ mol^{-1}$. One can also note the $\Delta\varepsilon = (0.14 \pm 0.36)\ kg_w\ mol^{-1}$ $Cu(OH)_2(aq)$ in $NaClO_4$,[68] which would yield in $\varepsilon(Cu(OH)_2(aq), NaClO_4) = (0.18 \pm 0.36)\ kg_w\ mol^{-1}$ using ε from Guillaumont, *et al.*[69] and Ciavatta.[65] Powell, *et al.*[70] proposed $\Delta\varepsilon = -(0.05 \pm 0.03)\ kg_w\ mol^{-1}$ for the formation of $Zn(SO_4)(aq)$ in $LiClO_4$ media, which would yield in $\varepsilon(Zn(SO_4)(aq),LiClO_4) = (0.25 \pm 0.06)\ kg_w\ mol^{-1}$ using ε from Guillaumont, *et al.*[69] Otherwise, Ciavatta,[65] Hummel, *et al.*,[63] and Fromentin and Reiller[42] proposed ε values for globally neutral organic species that range from the zwitterion ethylenediaminetetracetic acid, $\varepsilon(EdtaH_4(aq),NaClO_4) = -(0.29 \pm 0.14)\ kg_w\ mol^{-1}$, to the adipic

acid, ε(AdipateH$_2$(aq),NaCl) = (0.105 ± 0.005) kg$_w$ mol^{-1}. It is also noteworthy that for adipic acid, the specific ion interaction coefficients proposed by Fromentin and Reiller[42] is significantly different in NaCl and $NaClO_4$ — the perchlorate case being close to the nil value hypothesis. From this analysis, it seems that the hypothesis of a nil value for the ε values of neutral species is not always justified.

Considering that $Ca_2UO_2(CO_3)_3$(aq) is a 1:2 complex regarding Eq. (II - 2), and using the empirical relationship from Ciavatta[65] it comes,

$$\varepsilon(Ca_2UO_2(CO_3)_3(aq),NaCl) = \frac{\varepsilon(UO_2(CO_3)_3^{4-},Na^+) + 2\varepsilon(Ca^{2+},Cl^-)}{3}$$

$$\varepsilon(Ca_2UO_2(CO_3)_3(aq),NaCl) = (0.09 \pm 0.04)\ kg_w\ mol^{-1} \qquad \text{(II - 14)}$$

which is positive but is not giving a value as high as the one we are obtaining.

It can be inferred that for $Ca_2UO_2(CO_3)_3$(aq) the common hypothesis of a nil value for ε does not seem to be justified either. It is noteworthy that Ciavatta[65] proposed another empirical relationship based on ionic radius, the values of which are not easy to retrieve for the $Ca_nUO_2(CO_3)_3^{(4-2n)-}$ complexes.

The implications of the different thermodynamic constants and specific interaction coefficients can be seen as a function of I_m through the variation of the activity coefficients (Fig. II - S7(a)), and thermodynamic constants (Fig. II - S7(b)). It is clearly shown that our results and extrapolations for $CaUO_2(CO_3)_3^{2-}$ are perfectly in agreement with the determinations in $NaNO_3$,[12] NaCl,[14,15] and $NaClO_4$.[15] For $Ca_2UO_2(CO_3)_3$(aq), there is a very good agreement with other obtained data,[8,12,15] when there is slight overestimation of Bernhard, *et al.*,[5] and a slight underestimation of Endrizzi and Rao.[14] Up to 1 mol kg$_w^{-1}$ one can notice that the values that we are proposing allows a very good representation of the $Ca_nUO_2(CO_3)_3^{(4-2n)-}$ complexes comportment. The comparison with the estimation of Kalmykov and Choppin[9] shows that our estimation is in agreement until I_m = 0.5 mol kg$_w^{-1}$, but do not allow understanding the comportment in more concentrated $NaClO_4$ medium, which would require further works accounting for the discussion in Guillaumont, *et al.*,[32] and recent theoretical modeling.[33,71] The same comment applies to the evolution of $MgUO_2(CO_3)_3^{2-}$ proposed in Dong and Brooks,[13] as the influence of ionic strength seems very high and does not compare favourably with our results on $CaUO_2(CO_3)_3^{2-}$, which would be considered as an analogue component. Further works are clearly required to decipher these comportments, for instance in high ionic strength medium containing magnesium.[72,73]

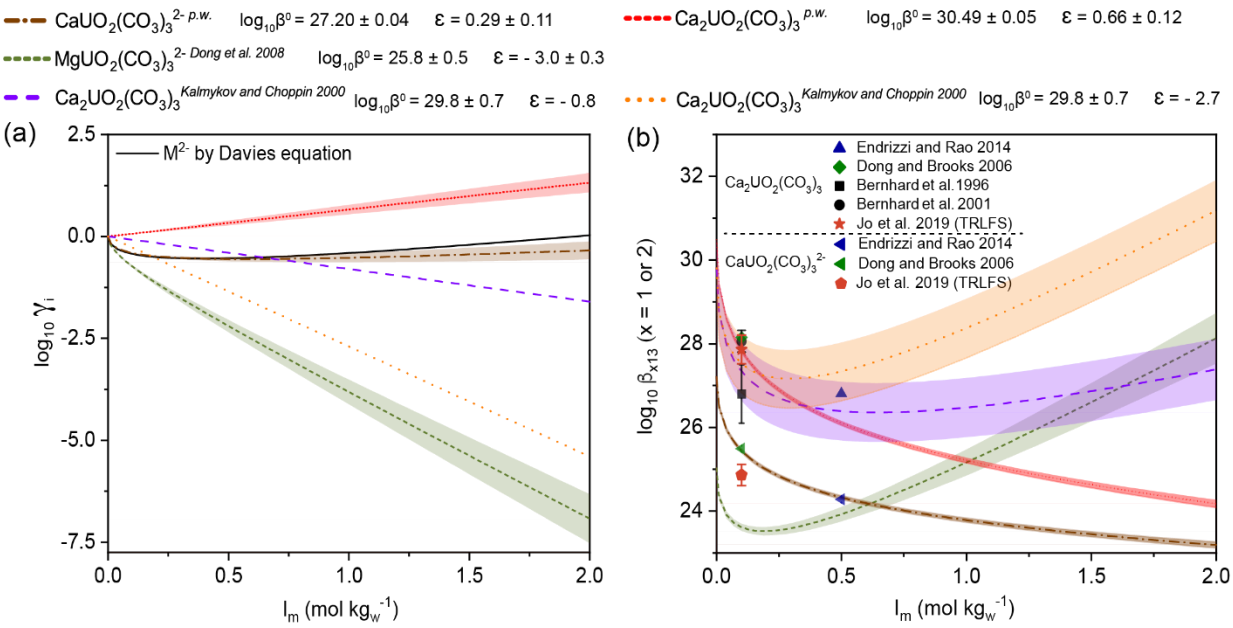

Fig. II - 7 Variations of activity coefficients (a) and formation constants (b) for the $M_nUO_2(CO_3)_3^{(4-2n)-}$ complexes (M being Mg or Ca) as a function of molal ionic strength.

4.4 Structural implications for ternary species

The difference between these species, and other -2 charge bearing complexes, drew our attention to the molecular structures and actual electric charges of these species. Actually, complexation by alkali and alkaline earth metals is generally considered as weak ligand binding since the attraction between opposite-charged ions is marginally stronger than that of simple electrostatic interaction.[74] A specific term is used in SIT to describe this (partial) association, and it should be noted that the extent to which cations form complexes varies widely in solution.[75] For $Ca_nUO_2(CO_3)_3^{(4-2n)-}$ species, the alkaline earth ions is locating in the second shell outside the inner shell for the three carbonates. Several EXAFS studies reported close bond distances for U-Ca shell, structurally exhibiting the manifold patterns of Ca-UO_2-CO_3 species.[7,8,16-18] Lee, *et al.*,[7] and Kelly, *et al.*,[16] respectively reported 4.15 and 4.1 Å for U-Ca in aqueous solution, which are in agreement with a previous study that proposed the value for R(U-Ca) = 4.05 Å in the corresponding solid — *i.e.* liebigite $Ca_2UO_2(CO_3)_3(aq):10H_2O$.[18] These results confirmed the similar structures existing in $Ca_2UO_2(CO_3)_3(aq)$ complex independent of its state. However, the principal limitation of EXAFS is that the interpretation of data is often interfered by the very close distances of R(U-Ca) and R(U-O_{dist}).[7]

The role of cation in complexation has been investigated through theoretical modelling. The counter-ion effects of Ca^{2+} were proven to help stabilizing the fourfold negatively charged complex $UO_2(CO_3)_3^{4-}$ in aqueous environment with hybrid quantum mechanical/molecular

mechanical molecular dynamics simulations.[76,77] Furthermore, classical molecular dynamics simulations have successfully described the impact of Na^+ on the binding between $UO_2(CO_3)_3^{4-}$ and Ca^{2+} ions by simulating the effect of 0.1 mol L^{-1} NaCl as background electrolyte.[71] The presence of sodium provoked a distortion of carbonate denticity and thus yielded space for entering one water molecule in the primary coordination sphere in $CaUO_2(CO_3)_3^{2-}$. As a consequence, an alteration in coordination number was induced in the equatorial plan of UO_2^{2+}, whereas in $Ca_2UO_2(CO_3)_3(aq)$, sodium solely exacerbated the asymmetry of two calcium ions without changing the coordination number.

These findings provide indication for detectable influence of Na^+ on the structures of ternary species, which may give reasons for the positive and relatively large ε values in our study. Ion-pair formation most likely accounts for the strong dependence of ε on electrolyte concentration. The results of this study further indicate that the conventionally adopted value of $\varepsilon(UO_2(CO_3)_2^{2-},Na^+)$ to $\varepsilon(CaUO_2(CO_3)_3^{2-},Na^+)$ by analogy is questionnable. The affinity of Na^+ with globally neutral complex could yield a globally positively charged-complex, which has been proposed by theoretical calculations,[33] and maybe suggested by our experimental results. Besides, as suggested by previous investigators, the nil value of ε for like-charged ions should be treated carefully, because the ion-solvent interaction is underestimated according to the assumption of SIT.[78,79]

II - 5 Practical applications

5.1 Practical application to the case of radioactive waste management

Once the determined thermodynamic constants of $Ca_nUO_2(CO_3)_3^{(4-2n)-}$ complexes allow predicting aqueous speciation accurately up to I_m = 1 mol kg_w^{-1} in NaCl-based medium, the first application is the calculation of the uranium speciation in a water composition representative of a clay host rock for a geological repository for radioactive wastes. Compositions of water in equilibrium with a clay rock, which can be the host rock of a radioactive waste repository, were proposed in the Belgian context of the Boom clay,[34] and in the French context of the Callovo-Oxfordian clay.[35] Using thermodynamic data from Guillaumont, *et al.*,[32] if one considers that uranium is mostly under its +IV redox state under these conditions, the solid phase controlling the solubility is either UO_2(am,hyd) for the most soluble one, or UO_2(cr) for the most insoluble one. The very low solubility of these two phases, and the concentration of carbonate in these systems, prevents the formation of polynuclear species.

Up to now, the available data in the framework of the SIT[32] are not sufficiently complete to perform a calculation in a real situation. It would require the addition of thermodynamic data from other sources. Hence, we have used the Thermochimie 9b database — the sit.dat database file — provided with PhreeqC,[61,62] which contains the data from Guillaumont, *et al.*[32] for uranium, to perform the theoretical speciation calculation — the selection of data can be found on the web pages.[80] In this version of the database, $Ca_nUO_2(CO_3)_3^{(4-2n)-}$ complexes from Dong and Brooks[12] are present, with no ε values, which mean that the ε values are nil. The Mg^{2+}, Sr^{2+}, and Ba^{2+} complexes are not implemented.[7,10,12,13] We have made the choice to implement the Mg^{2+} and Sr^{2+} complexes from Dong and Brooks[12] as an estimation of their potential importance in the input PhreeqC file with no ε values.

The redox potentials — Eh_{SHE} = –274 mV, t = 16°C, pH 8.5 for the Mol reference water in de Craen, *et al.*[34], and Eh_{SHE} = –163 mV at pH 7.1 for solution A in Gaucher, *et al.*[35] — are fixed by a partial pressure of dioxygen calculated from the Eh_{SHE} and temperature of the water — $P(O_2) = 10^{-68.67}$ and $10^{-65.83}$ atm for de Craen, *et al.*[34] and Gaucher, *et al.*[35], respectively.

The solubility and aqueous speciation of uranium between pH 7 and 9 for the two water compositions are shown in Fig. II - 8. The speciation results are markedly different because of the differences in total carbonate, calcium and magnesium concentrations, and Eh values. In the case of the Boom Clay water (Fig. II - 8(a), (b)),[34] even with a lower Eh value, the carbonate concentration in the Boom Clay water stabilizes the different triscarbonatouranyl complexes at the expenses of $U(OH)_4(aq)$. The marked change in uranium speciation between $CaUO_2(CO_3)_3^{2-}$ and $UO_2(CO_3)_3^{4-}$ at pH 8.2 corresponds to the precipitation of dolomite ($CaMg(CO_3)_2$), which also affects the $MgUO_2(CO_3)_3^{2-}$ and $Ca_2UO_2(CO_3)_3(aq)$ complexes. In the case of the Callovo-Oxfordian water (Fig. II - 8(c), (d)),[35] the lower carbonate content but high calcium concentration yields to the predominance of $M_nUO_2(CO_3)_3^{(4-2n)-}$ complexes at pH values lower than 8.5, and to the predominance of $U(OH)_4(aq)$ at higher pH values. In both cases, the $MgUO_2(CO_3)_3^{2-}$ complex should be minor; the $SrUO_2(CO_3)_3^{2-}$ complex should be even minor.

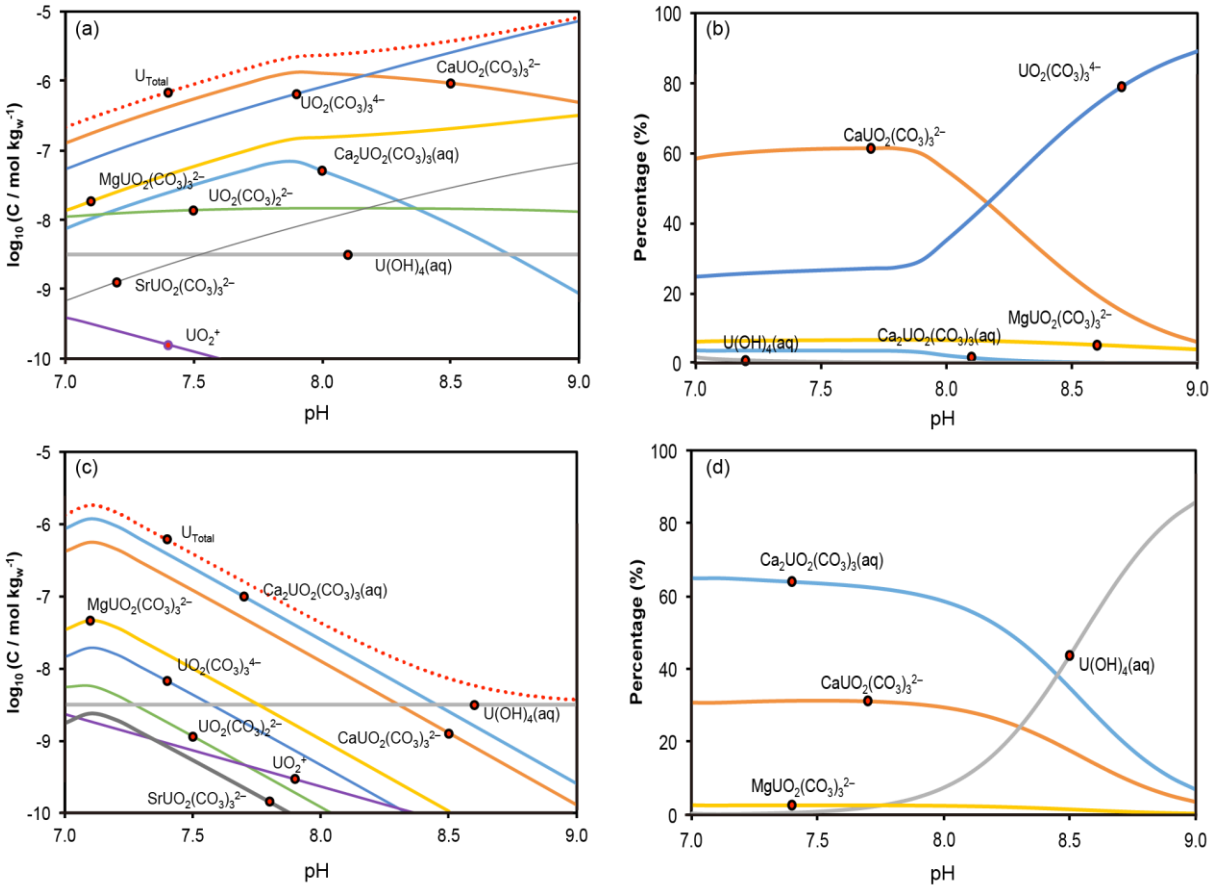

Fig. II - 8 Solubility of UO_2(am,hyd) (a,c) and aqueous speciation of uranium (b,d) between pH 7 and 9 for Boom[34] (a,b) and Callovo-Oxfordian[35] (c,d) clay equilibrium waters using thermodynamic data from the Thermochime 9b database,[80] implementing $MgUO_2(CO_3)_3^{2-}$ and $SrUO_2(CO_3)_3^{2-}$,[12] correcting the $Ca_nUO_2(CO_3)_3^{(4-2n)-}$ data with thermodynamic constants values from Table II - 1, and implementing specific ion interaction coefficient from Table II - 3: $P(O_2) = 10^{-68.67}$ (a,b) and $10^{-65.83}$ (c,d) atm.

5.2 Practical application to the case of uranium speciation in seawater

Another application is the distribution of ternary species as well as the effects of solvent ions in seawater. Different compositions of seawater were proposed in the literature. Large amounts of calcium and magnesium led to the predominance of $M_nUO_2(CO_3)_3^{(4-2n)-}$ complexes after theoretical speciation calculations.[7,14,17] Knowing the particular dependence observed for the $MgUO_2(CO_3)_3^{2-}$ complex as a function of $NaClO_4$ ionic strength,[13] and the lack of information on the corresponding comportment in NaCl, we will only focus our discussion on $Ca_nUO_2(CO_3)_3^{(4-2n)-}$ complexes in the following.

Authors proposed theoretical speciation calculations using either the data from Dong and Brooks[12] in an average Mediterranean seawater,[17] or their own determinations using simplified seawater compositions.[7,14] The predominance of either the neutral $Ca_2UO_2(CO_3)_3$(aq)

complex,[14,17] or the -2 charge bearing $CaUO_2(CO_3)_3^{2-}$ complex,[7] was obtained. However, the water composition is relatively unbalanced — electrical balance is 4.15 10^{-2} eq using PhreeqC — and the activity correction is not clearly specified, but guessed as done through a simplified Debye-Hückel approximation — which is not applicable in seawater — in the former case;[17] in the latter case,[7,14] the water composition — simplified from Millero, *et al.*[81] — is equilibrated and SIT with the nil hypothesis for the ε values, which seems not justified (vide ante), was used. It seems awkward to assess which complex dominates the uranium speciation in seawater.

Millero, *et al*. proposed the composition of a standard seawater,[81] which can be used to perform a similar exercise, applying the thermodynamic constants (Table II - 1) and specific ion interaction coefficients (Table II - 3) determined in this work — the $UO_2CO_3F^-$ complex,[32] absent from Thermochimie 9b database, is implemented. We are proposing the theoretical speciation calculation in Fig. II - 9, where $CaUO_2(CO_3)_3^{2-}$ is dominating the speciation at pH > 7, and $Ca_2UO_2(CO_3)_3(aq)$ is a significant secondary species — in this example, the partial pressure of $CO_2(g)$ is calculated from the total carbonate concentration in Millero, *et al*.,[81] *i.e.* $10^{-3.24}$ atm. This speciation is reminiscent of the one proposed by Lee, *et al.*[7], but with a slightly less important proportion of the $Ca_2UO_2(CO_3)_3(aq)$ complex. It is noteworthy that dolomite ($CaMg(CO_3)_2$) and calcite ($CaCO_3$) are showing positive saturation indices at pH values above 7.6 and 7.8, respectively (Fig. II - S7 of the SI). This means that the initial seawater composition is oversaturated with regards of these two phases. For this exercise, the precipitation of the carbonate phases of alkaline earth metals was not required.

This exercise confirms the general predominance of $Ca_nUO_2(CO_3)_3^{(4-2n)-}$ in seawater and enlightens the need of comparable studies on the $Mg_nUO_2(CO_3)_3^{(4-2n)-}$ complexes at varying ionic strengths. As Mg/Ca concentration ratio is ca. 5 from Millero, *et al*. seawater composition,[81] and $\beta^\circ\left(CaUO_2(CO_3)_3^{2-}\right)/\beta^\circ\left(MgUO_2(CO_3)_3^{2-}\right)$ is ca. 12 according to the estimation from Dong and Brooks,[12] $MgUO_2(CO_3)_3^{2-}$ should be significantly present in seawater — see the theoretical speciation proposed in Lee, *et al.*[7] Further works on the $Mg_nUO_2(CO_3)_3^{(4-2n)-}$ complexes vs. ionic strength are necessary to reduce the uncertainties on thermodynamic constants, and avoid the approximations for the specific ion interaction coefficients values.

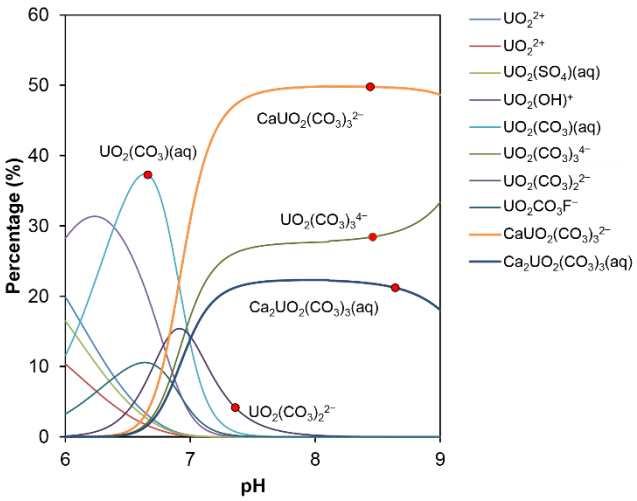

Fig. II - 9 Theoretical speciation of uranium in a standard seawater composition,[81] $P(CO_2) = 10^{-3.24}$ atm from the total carbonate concentration, and using the thermodynamic data from the Thermochimie 9b database,[80] correcting the $Ca_nUO_2(CO_3)_3^{(4-2n)-}$ data with thermodynamic constants values (Table II - 1) and implementing the specific ion interaction coefficients (Table II - 3) proposed in this work.

II - 6 Conclusion

The thermodynamic constants $\log_{10}\beta°$ and Gibbs energies of formation $\Delta_fG°_m$ of $CaUO_2(CO_3)_3^{2-}$ and $Ca_2UO_2(CO_3)_3(aq)$ have been extrapolated to infinite dilution from TRLS experiments in NaCl medium from I_m = 0.1 up to 1 mol kg_w^{-1}. The characteristics of the luminescence spectra are strikingly similar for all species, with gradually narrowed peak widths with complexation of calcium. The pH-dependent slope analysis was necessarily corrected with the Ringböm coefficient relative to $UO_2(CO_3)_3^{4-}$ complex according to the experimental methodology. As expected, no precipitation of schoepite or calcite was observed during the experiments. The stability constants are consistent with previously reported data. Conversely, the values of the specific ion interaction coefficients $\varepsilon(CaUO_2(CO_3)_3^{2-},Na^+)$ and $\varepsilon(Ca_2UO_2(CO_3)_3(aq),NaCl)$ are strongly positive and markedly different from the previous estimation by analogy from like-charged ions, which may suggest a high affinity of Na^+ with $Ca_nUO_2(CO_3)_3^{(4-2n)-}$ species in solution. Similar studies at higher ionic strength and other background electrolyte such as sodium perchlorate media, and comparable studies on Mg^{2+} are highly desirable.

Acknowledgment

This work was financed by ONDRAF-NIRAS (contract DEN4857-CCHO 2018-0456/00/00). Dr. Hélène Isnard is acknowledged for her help during the dissolution of U_3O_8.

II - 7 References

1. S. Cotton, *Lanthanide and Actinide Chemistry*, Wiley, Rutland, UK, 2006.
2. K. Maher, J. R. Bargar and G. E. Brown, Jr., *Inorg. Chem.*, 2013, **52**, 3510-3532.
3. J. I. Kim and B. Grambow, *Eng. Geol.*, 1999, **52**, 221-230.
4. M. Altmaier and T. Vercouter, in *Radionuclide Behaviour in the Natural Environment - Science, Implications and Lessons for the Nuclear Industry*, eds. C. Poinssot and H. Geckeis, Woodhead Publishing, Oxford, UK, 2012, DOI: 10.1533/9780857097194.1.44, ch. 3, pp. 44-69.
5. G. Bernhard, G. Geipel, V. Brendler and H. Nitsche, *Radiochim. Acta*, 1996, **74**, 87-91.
6. J. Y. Lee and J. I. Yun, *Dalton Trans.*, 2013, **42**, 9862-9869.
7. J.-Y. Lee, M. Vespa, X. Gaona, K. Dardenne, J. Rothe, T. Rabung, M. Altmaier and J.-I. Yun, *Radiochim. Acta*, 2017, **105**.
8. G. Bernhard, G. Geipel, T. Reich, V. Brendler, S. Amayri and H. Nitsche, *Radiochim. Acta*, 2001, **89**, 511-518.
9. S. N. Kalmykov and G. R. Choppin, *Radiochim. Acta*, 2000, **88**, 603-606.
10. G. Geipel, S. Amayri and G. Bernhard, *Spectrochim. Acta. A, Mol. Biomol. Spectrosc.*, 2008, **71**, 53-58.
11. C. Götz, G. Geipel and G. Bernhard, *J. Radioanal. Nucl. Chem.*, 2010, **287**, 961-969.
12. W. M. Dong and S. C. Brooks, *Environ. Sci. Technol.*, 2006, **40**, 4689-4695.
13. W. Dong and S. C. Brooks, *Environ. Sci. Technol.*, 2008, **42**, 1979-1983.
14. F. Endrizzi and L. F. Rao, *Chem.-Eur. J.*, 2014, **20**, 14499-14506.
15. Y. Jo, A. Kirishima, S. Kimuro, H.-K. Kim and J.-I. Yun, *Dalton Trans.*, 2019, **48**, 6942-6950.
16. S. D. Kelly, K. M. Kemner and S. C. Brooks, *Geochim. Cosmochim. Acta*, 2007, **71**, 821-834.
17. M. Maloubier, P. L. Solari, P. Moisy, M. Monfort, C. Den Auwer and C. Moulin, *Dalton Trans.*, 2015, **44**, 5417-5427.
18. S. Amayri, T. Reich, T. Arnold, G. Geipel and G. Bernhard, *J. Solid State Chem.*, 2005, **178**, 567-577.
19. M. Grivé, L. Duro, E. Colàs and E. Giffaut, *Appl. Geochem.*, 2015, **55**, 85-94.
20. M. H. Bradbury and B. Baeyens, *Applied Clay Science*, 2011, **52**, 27-33.
21. M. Marques Fernandes, N. Vér and B. Baeyens, *Appl. Geochem.*, 2015, **59**, 189-199.
22. W. M. Dong, W. P. Ball, C. X. Liu, Z. M. Wang, A. T. Stone, J. Bai and J. M. Zachara, *Environ. Sci. Technol.*, 2005, **39**, 7949-7955.
23. O. Prat, T. Vercouter, E. Ansoborlo, P. Fichet, P. Perret, P. Kurttio and L. Salonen, *Environ. Sci. Technol.*, 2009, **43**, 3941-3946.
24. C. Moulin, C. Beaucaire, P. Decambox and P. Mauchien, *Anal. Chim. Acta*, 1990, **238**, 291-296.
25. T. Vercouter, P. Vitorge, B. Amekraz and C. Moulin, *Inorg. Chem.*, 2008, **47**, 2180-2189.
26. C. Moulin, I. Laszak, V. Moulin and C. Tondre, *Appl. Spectrosc.*, 1998, **52**, 528-535.
27. C. Moulin, P. Decambox, V. Moulin and J. G. Decaillon, *Anal. Chem.*, 1995, **67**, 348-353.
28. G. Meinrath, *Radiochim. Acta*, 1997, **77**, 221-234.
29. Y. Kato, G. Meinrath, T. Kimura and Z. Yoshida, *Radiochim. Acta*, 1994, **64**, 107-111.
30. E. C. Jung, H. R. Cho, M. H. Baik, H. Kim and W. Cha, *Dalton Trans.*, 2015, **44**, 18831-18838.
31. I. Grenthe, L. Fuger, R. G. M. Konings, R. J. Lemire, A. B. Muller, C. Nguyen-Trung and H. Wanner, *Chemical Thermodynamics 1. Chemical Thermodynamics of Uranium*, North Holland Elsevier Science Publishers B. V., Amsterdam, The Netherlands, 1992.

32. R. Guillaumont, T. Fanghänel, V. Neck, J. Fuger, D. A. Palmer, I. Grenthe and M. H. Rand, *Update of the Chemical Thermodynamics of Uranium, Neptunium, Plutonium, Americium and Technetium*, OECD Nuclear Energy Agency, Data Bank, Issy-les-Moulineaux, France, 2003.
33. W. Wu, C. Priest, J. Zhou, C. Peng, H. Liu and D. E. Jiang, *J. Phys. Chem. B*, 2016, **120**, 7227-7233.
34. M. de Craen, L. Wang, M. Van Geet and H. Moors, *Geochemistry of Boom Clay pore water at the Mol site*, Report SCK•CEN-BLG-990, SCK•CEN, Mol, Belgium, 2004.
35. E. C. Gaucher, C. Tournassat, F. J. Pearson, P. Blanc, C. Crouzet, C. Lerouge and S. Altmann, *Geochim. Cosmochim. Acta*, 2009, **73**, 6470-6487.
36. I. Feldman, *Anal. Chem.*, 1956, **28**, 1859-1866.
37. G. G. Manov, N. J. Delollis and S. F. Acree, *J. Res. Nat. Bur. Stand.*, 1945, **34**, 115-127.
38. R. de Levie, *Adanced Excel for Scientific Data Analysis*, Oxford University Press, New York, 2005.
39. M. Moriyasu, Y. Yokoyama and S. Ikeda, *J. Inorg. Nucl. Chem.*, 1977, **39**, 2211-2214.
40. P. Moreau, S. Colette-Maatouk, P. Vitorge, P. Gareil and P. E. Reiller, *Inorg. Chim. Acta*, 2015, **432**, 81-88.
41. Y. Z. Kouhail, M. F. Benedetti and P. E. Reiller, *Environ. Sci. Technol.*, 2016, **50**, 3706-3716.
42. E. Fromentin and P. E. Reiller, *Inorg. Chim. Acta*, 2018, **482**, 588-596.
43. Y. Z. Kouhail, M. F. Benedetti and P. E. Reiller, *Chem. Geol.*, 2019, **522**, 175-185.
44. A. Ringböm, Complexation in Analytical Chemistry: A Guide for the Critical Selection of Analytical Methods Based on Complexation Reactions, Interscience Publishers, New York, NY, USA, 1963.
45. L. Maya, *Inorg. Chem.*, 1982, **21**, 2895-2898.
46. K. Muller, V. Brendler and H. Foerstendorf, *Inorg. Chem.*, 2008, **47**, 10127-10134.
47. I. Grenthe, D. Ferri, F. Salvatore and G. Riccio, *J. Chem. Soc., Dalton Trans.*, 1984, **0**, 2439-2443.
48. C. W. Davies, *Ion Association*, Butterworths, London, UK, 1962.
49. Y. Yokoyama, M. Moriyasu and S. Ikeda, *J. Inorg. Nucl. Chem.*, 1976, **38**, 1329-1333.
50. C. Ekberg and L. P. Brown, *Hydrolysis of Metal Ions*, Wiley-VCH, Weinheim, Germany, 2016.
51. V. Eliet, G. Bidoglio, N. Omenetto, L. Parma and I. Grenthe, *J. Chem. Soc., Faraday Trans.*, 1995, **91**, 2275-2285.
52. H. Anton and R. C. Busby, *Contemporary Linear Algebra*, Wiley & Sons, Inc., Pennsylvania, USA, 2002.
53. M. Moriyasu, Y. Yokoyama and S. Ikeda, *J. Inorg. Nucl. Chem.*, 1977, **39**, 2205-2209.
54. M. D. Marcantonatos, *J. Chem. Soc., Faraday Trans. I*, 1980, **76**, 1093-1115.
55. S. J. Formosinho, M. D. M. Miguel and H. D. Burrows, *J. Chem. Soc., Faraday Trans. I*, 1984, **80**, 1717-1733.
56. P. E. Reiller and J. Brevet, *Spectrochim. Acta, Part A*, 2010, **75**, 629-636.
57. B. Valeur, *Molecular Fluorescence: Principles and Applications*, Wiley-VCH, Weinheim, Germany, 2001.
58. D. J. Leggett, Computational Methods for the Determination of Formation Constants, Plenum Press, New York, USA, 1985.
59. D. G. Kinniburgh and D. M. Cooper, *Environ. Sci. Technol.*, 2004, **38**, 3641-3648.
60. D. C. Kinniburgh and D. M. Cooper, *PhreePlot: Creating Graphical output with PHREEQC*, http://www.phreeplot.org, 2011.
61. D. L. Parkhurst and C. A. J. Appelo, User's Guide to PHREEQC (Version 2) — A Computer Program for Speciation, Batch-Reaction, One-Dimensional Transport, and

Inverse Geochemical Calculations, Report 99-4259, U.S. Geological Survey, Water-Resources Investigations, Lakewood, Colorado, USA, 1999.
62. D. L. Parkhurst and C. A. J. Appelo, Description of Input and Examples for PHREEQC Version 3 — A Computer Program for Speciation, Batch-Reaction, One-Dimensional Transport, and Inverse Geochemical Calculations. Chapter 43 of Section A, Groundwater Book 6, Modeling Techniques, U.S. Geological Survey, Denver, Colorado, USA, 2013.
63. W. Hummel, G. Anderegg, L. F. Rao, I. Puigdomènech and O. Tochiyama, Chemical Thermodynamics 9. Chemical Thermodynamics of Compounds and Complexes of U, Np, Pu, Am, Tc, Se, Ni and Zr with Selected Organic Ligands, North Holland Elsevier Science Publishers B. V., Amsterdam, The Netherlands, 2005.
64. N. V. Plyasunova, M. S. Wang, Y. Zhang and M. Muhammed, *Hydrometallurgy*, 1997, **45**, 37-51.
65. L. Ciavatta, *Ann. Chim. (Rome)*, 1990, **80**, 255-263.
66. Y. Zhang and M. Muhammed, *Hydrometallurgy*, 2001, **60**, 215-236.
67. N. V. Plyasunova, Y. Zhang and M. Muhammed, *Hydrometallurgy*, 1998, **48**, 153-169.
68. K. J. Powell, P. L. Brown, R. H. Byrne, T. Gajda, G. Hefter, S. Sjoberg and H. Wanner, *Pure Appl. Chem.*, 2007, **79**, 895-950.
69. R. Guillaumont, T. Fanghänel, J. Fuger, I. Grenthe, V. Neck, D. A. Palmer and M. Rand, *Chemical Thermodynamics 5. Update on the Chemical Thermodynamics of Uranium, Neptunium, Plutonium, Americium and Technetium*, North Holland Elsevier Science Publishers B. V., Amsterdam, The Netherlands, 2003.
70. K. J. Powell, P. L. Brown, R. H. Byrne, T. Gajda, G. Hefter, A.-K. Leuz, S. Sjöberg and H. Wanner, *Pure Appl. Chem.*, 2013, **85**, 2249-2311.
71. B. Li, J. Zhou, C. Priest and D. E. Jiang, *J. Phys. Chem. B*, 2017, **121**, 8171-8178.
72. J. F. Ranville, M. J. Hendry, T. N. Reszat, Q. L. Xie and B. D. Honeyman, *J. Contam. Hydrol.*, 2007, **91**, 233-246.
73. P. E. Reiller, L. Marang, D. Jouvin and M. F. Benedetti, in *The New Uranium Mining Boom. Challenge and Lessons Learned*, eds. B. Merkel and M. Schipek, Springer-Verlag, Berlin, Germany, 2012, DOI: 10.1007/978-3-642-22122-4_65, pp. 565-572.
74. J. N. Butler and D. R. Cogley, *Ionic Equilibrium: Solubility and pH Calculations*, Wiley & Sons, Inc., New York, USA, 1998.
75. Y. Marcus and G. Hefter, *Chem. Rev.*, 2006, **106**, 4585-4621.
76. A. O. Tirler and T. S. Hofer, *J. Phys. Chem. B*, 2014, **118**, 12938-12951.
77. A. O. Tirler and T. S. Hofer, *Dalton Trans.*, 2016, **45**, 4983-4988.
78. C. J. Downes, *J. Phys. Chem.*, 1970, **74**, 2153-2160.
79. M. H. Panckhurst and J. B. Macaskill, *J. Solution Chem.*, 1976, **5**, 469-482.
80. Thermochimie, http://www.thermochimie-tdb.com/).
81. F. J. Millero, R. Feistel, D. G. Wright and T. J. McDougall, *Deep-Sea Res. Pt. I*, 2008, **55**, 50-72.

II - 8 Supporting Information

This supporting information contains 7 Figures and 4 Tables: the measured fluorescence emission spectra at atmospheric $CO_2(g)$, various Ca concentration and pH values, and 5 different ionic strength values; the predominance plots of the Ca-UO_2-CO_3 system under the experimental conditions; frequency distribution of the $\varepsilon(X^{2-}, Na^{+})$ values from literature compared to the $\varepsilon(CaUO_2(CO_3)_3^{2-}, Na^{+})$ determined in this work; and evolution of the saturation indices of calcite $(CaCO_3)$, nesquehonite $(MgCO_3{:}3H_2O)$, and dolomite $(CaMg(CO_3)_2)$ from the theoretical speciation in Fig. II - 9 of the main text; the stepwise formation constants values from Fig. II - 5 of the main text; the $\varepsilon(X^{2-},Na^{+})$ values from literature.

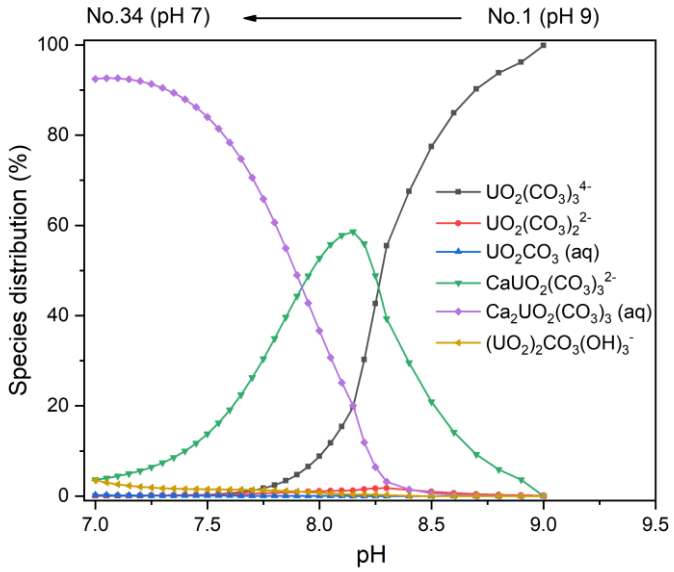

Fig. II - S1 Species distribution at [U(VI)] = 50 μmol kg_w^{-1} in preliminary calculations with stability constants for $UO_2(CO_3)_3^{4-}$, $UO_2(CO_3)_2^{2-}$, $UO_2(CO_3)_3$(aq), and $(UO_2)_2CO_3(OH)_3^{-}$ listed in Table II - 1, and those for $Ca_nUO_2(CO_3)_3^{4-2n}$ taken from the work of Lee and Yun.[1] Other aqueous information is in Table II - S1.

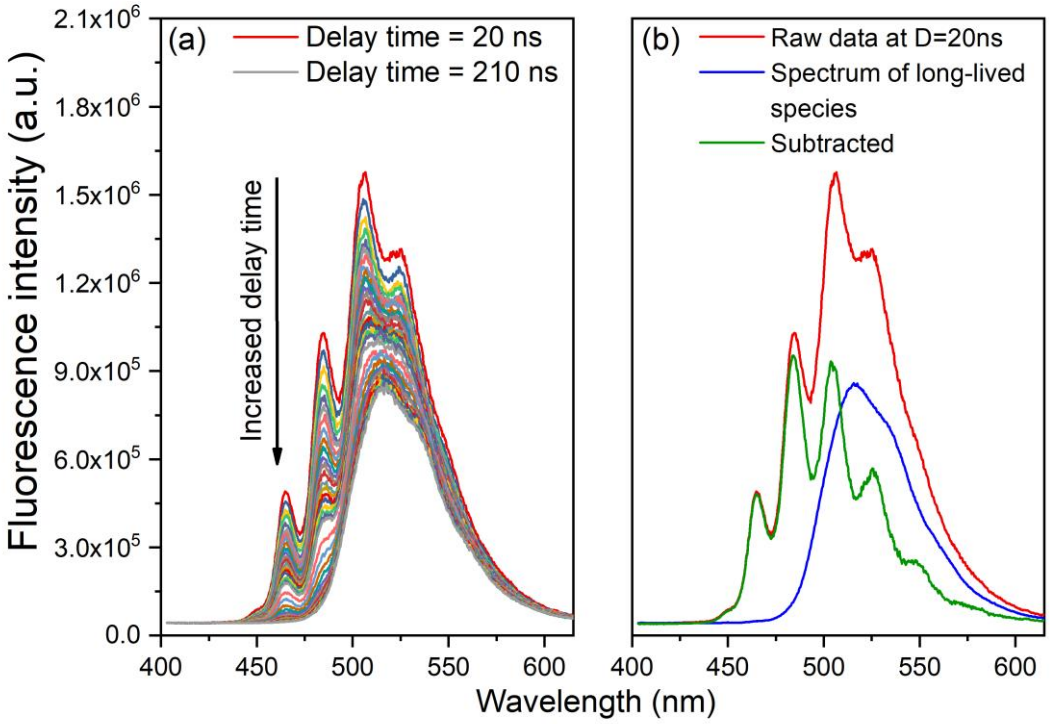

Fig. II - S2 (a) Fluorescence decay spectra of the sample at [U(VI)] = 50 µmol kg_w^{-1}, pH = 7.6 equilibrated with atmospheric $CO_2(g)$, recorded with λ_{ex} = 450 nm from D = 20 ns to D = 210 ns. (b) Red line: spectrum recorded at D = 20 ns. Blue line: spectrum at D = 210 ns. Green line: subtraction of the blue line from the red one, also characteristic spectrum of UO_2-CO_3 species.

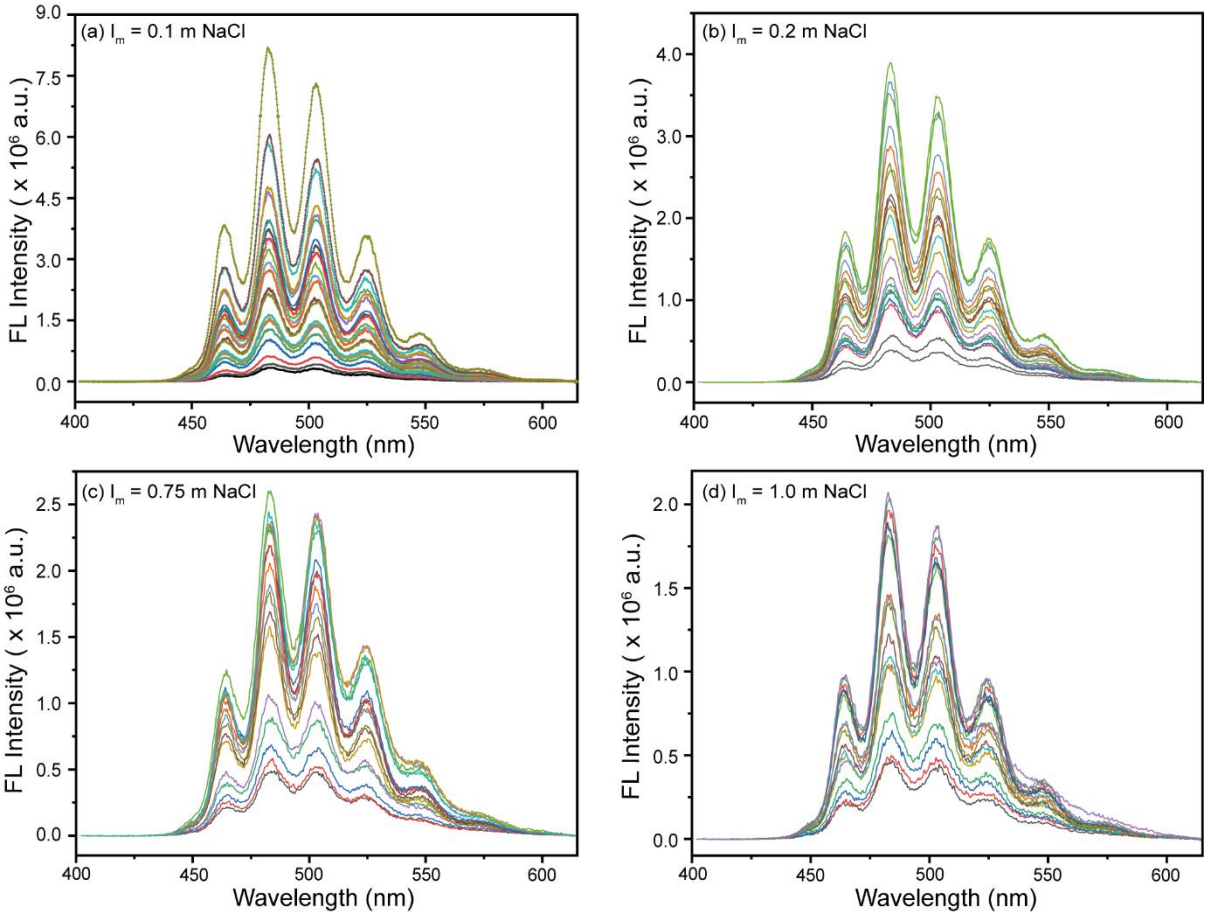

Fig. II - S3 Measured fluorescence emission spectra of binary and ternary species at various calcium concentrations and pH values of (a) I_m = 0.1 mol kg_w^{-1}, (b) I_m = 0.2 mol kg_w^{-1}, (c) I_m = 0.75 mol kg_w^{-1}, and (d) I_m = 1.0 mol kg_w^{-1} NaCl series. Initial delay time D = 25 ns and gate width W = 1 μs, and 1000 accumulations fixed for all acquisitions.

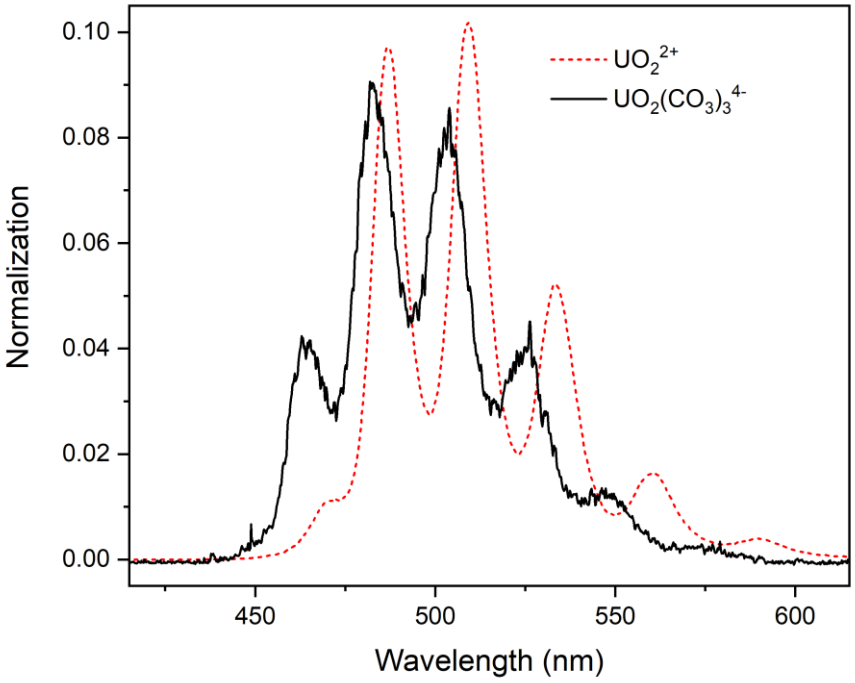

Fig. II - S4 Hypsochromic-shifted fluorescence spectrum of $UO_2(CO_3)_3^{4-}$ ([U(VI)] = 50 μmol kg_w^{-1}, pH = 9, I_m = 0.1 mol kg_w^{-1} NaCl) compared with that of UO_2^{2+} ([U(VI)] = 0.1 mmol kg_w^{-1}, pH = 1) in $HClO_4$.

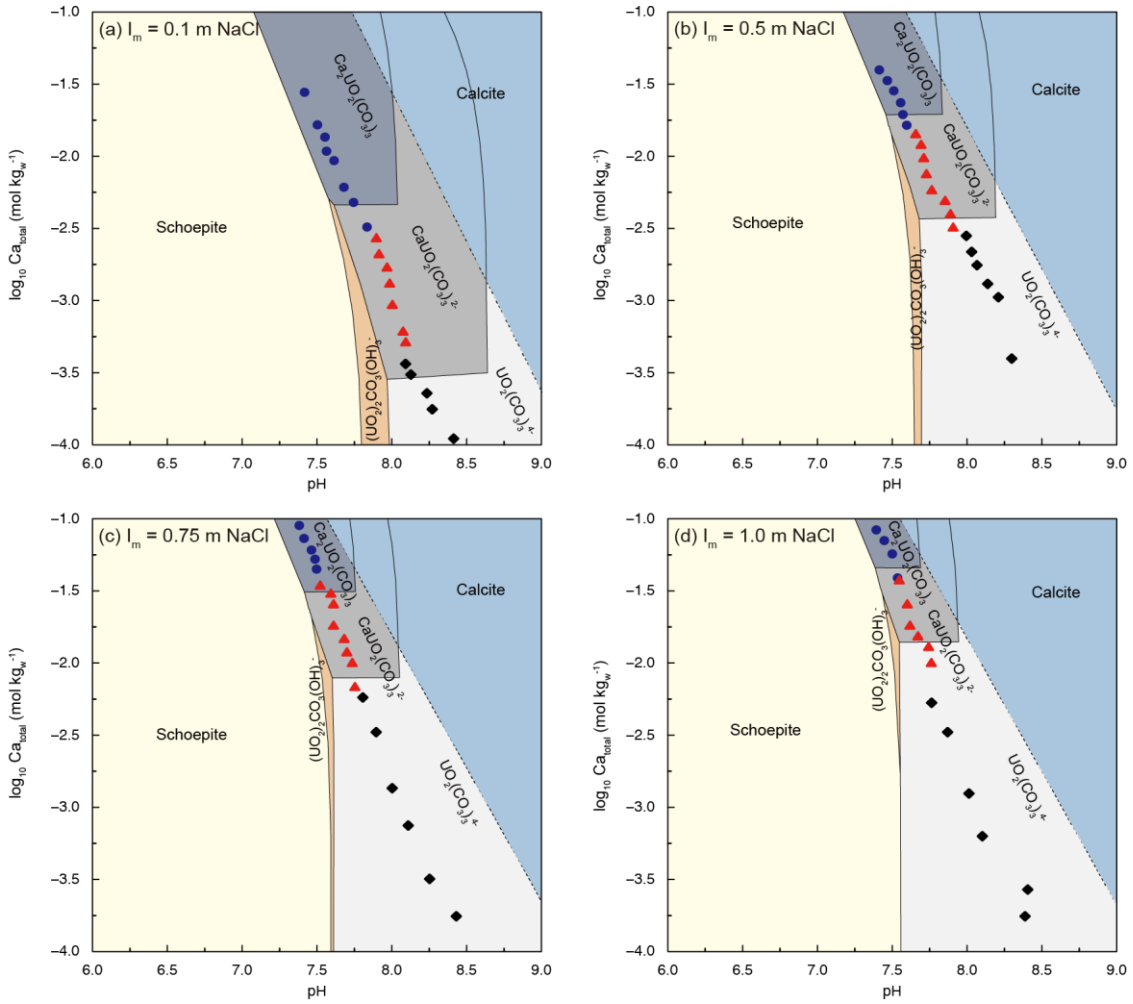

Fig. II - S5 Predominance plots of Ca-UO_2-CO_3 system at [U(VI)] = 50 µmol kg_w^{-1}, P(CO_2) = $10^{-3.5}$ atm and (a) I_m = 0.1 mol kg_w^{-1}, (b) I_m = 0.5 mol kg_w^{-1}, (c) I_m = 0.75 mol kg_w^{-1}, and (d) I_m = 1.0 mol kg_w^{-1} NaCl. Experimental points giving slopes of 1 and 2 are highlighted with red triangles and blue filled circles, respectively. The black diamond represents the beginning of titration where the binary complexes dominated.

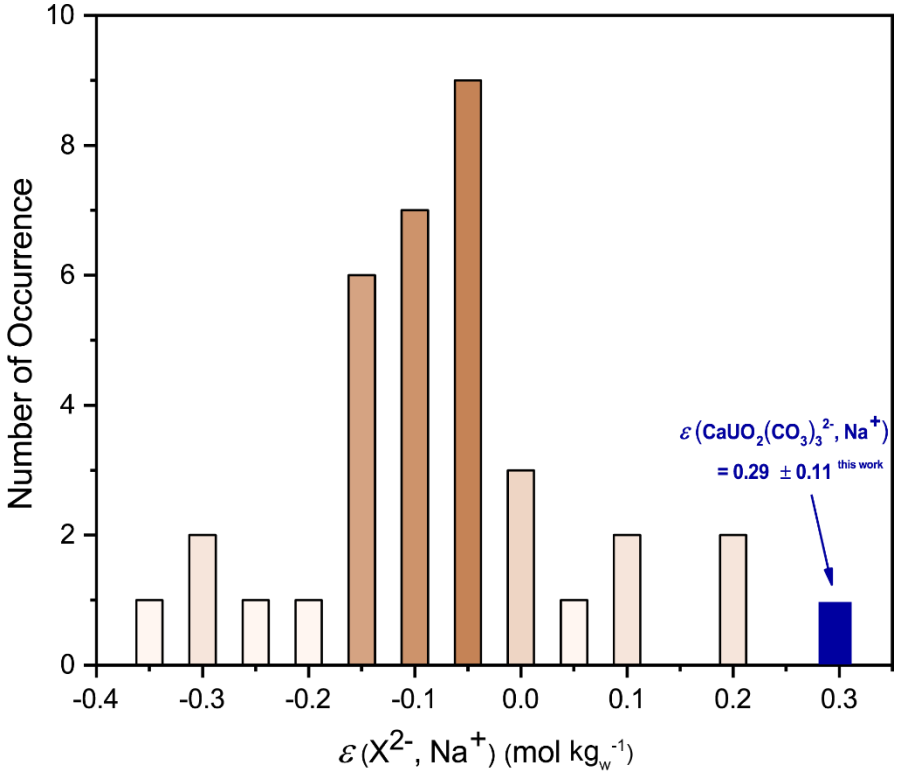

Fig. II - S6 Frequency of the $\varepsilon(X^{2-}, Na^{+})$ *from literature (Table II - S2); the values for* $\varepsilon\left(Th(OH)_y(CO_3)_z^{4-y-2z}, Na^{+}\right)$ *complexes*[2] *were not taken into account as they as they were proposed in analogy to like-charged complexes in Altmaier, et al.*[3] *from data in NEA-OECD.*[4-6]

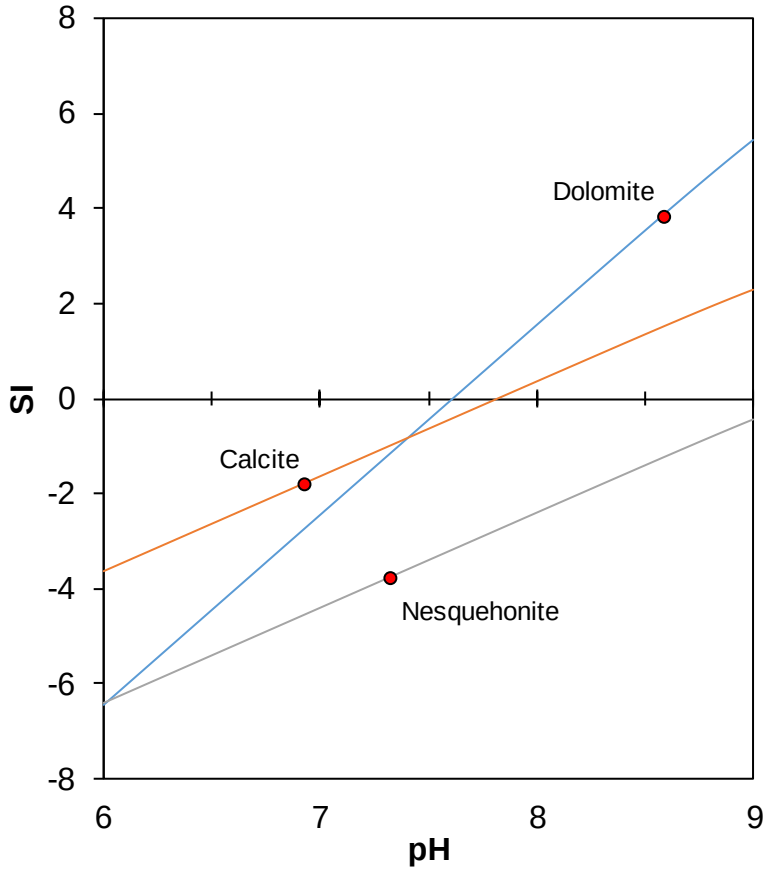

Fig. II - S7 Evolution of the saturation indices of calcite ($CaCO_3$), *nesquehonite* ($MgCO_3{:}3H_2O$), *and dolomite* ($CaMg(CO_3)_2$) *from the theoretical speciation in Fig. II - 9 of the main text.*

Table II - S1 Aqueous conditions in preliminary calculations.

Sample No.	***pH***	***$log_{10}([Ca^{2+}]$ /mol $kg_w^{-1})$***	***$[Ca^{2+}]$ (mol kg_w^{-1})***
1	9.00	---	1.00×10^{-5}
2	8.90	-4.90	1.26×10^{-5}
3	8.80	-4.70	2.00×10^{-5}
4	8.70	-4.50	3.16×10^{-5}
5	8.60	-4.30	5.01×10^{-5}
6	8.50	-4.10	7.94×10^{-5}
7	8.40	-3.90	1.26×10^{-4}
8	8.30	-3.70	2.00×10^{-4}
9	8.25	-3.50	3.16×10^{-4}
10	8.20	-3.30	5.01×10^{-4}
11	8.15	-3.10	7.94×10^{-4}
12	8.10	-3.00	1.00×10^{-3}
13	8.05	-2.90	1.26×10^{-3}
14	8.00	-2.80	1.58×10^{-3}
15	7.95	-2.70	2.00×10^{-3}
16	7.90	-2.60	2.51×10^{-3}
17	7.85	-2.50	3.16×10^{-3}
18	7.80	-2.40	3.98×10^{-3}
19	7.75	-2.30	5.01×10^{-3}
20	7.70	-2.20	6.31×10^{-3}

Sample No.	*pH*	*$\log_{10}([Ca^{2+}]$ /mol $kg_w^{-1})$*	*$[Ca^{2+}]$ (mol kg_w^{-1})*
21	7.65	-2.10	7.94×10^{-3}
22	7.60	-2.00	1.00×10^{-2}
23	7.55	-1.90	1.26×10^{-2}
24	7.50	-1.80	1.58×10^{-2}
25	7.45	-1.70	2.00×10^{-2}
26	7.40	-1.60	2.51×10^{-2}
27	7.35	-1.50	3.16×10^{-2}
28	7.30	-1.40	3.98×10^{-2}
29	7.25	-1.30	5.01×10^{-2}
30	7.20	-1.20	6.31×10^{-2}
31	7.15	-1.10	7.94×10^{-2}
32	7.10	-1.00	1.00×10^{-1}
33	7.05	-0.90	1.26×10^{-1}
34	7.00	-0.80	1.58×10^{-1}

Table II - S2 Calculated Ringböm coefficients α for experimental samples.

	I_m = 0.1 mol kg_w^{-1}		**I_m = 0.2 mol kg_w^{-1}**		**I_m = 0.5 mol kg_w^{-1}**		**I_m = 0.75 mol kg_w^{-1}**		**I_m = 1 mol kg_w^{-1}**	
Sample	pH value	α	pH value	α	pH value	α	pH value	α	pH value	α
1	9.00	1.00	8.98	1.00	9.00	1.00	9.05	1.00	8.94	1.00
2	8.66	1.06	8.45	1.00	8.42	1.01	8.45	1.00	8.40	1.01
3	8.42	1.04	8.28	1.02	8.32	1.03	8.24	1.01	8.44	1.04
4	8.26	1.10	8.21	1.04	8.17	1.04	8.10	1.01	8.12	1.03
5	8.23	1.12	8.18	1.04	8.12	1.02	8.02	1.02	8.04	1.03
6	8.15	1.24	8.16	1.06	8.10	1.03	7.90	1.06	7.85	1.04
7	8.11	1.37	8.14	1.06	8.07	1.05	7.83	1.12	7.77	1.13
8	8.10	1.34	8.13	1.07	8.02	1.05	7.79	1.19	7.83	1.06
9	8.08	1.51	8.05	1.10	7.91	1.11	7.75	1.29	7.73	1.20
10	8.00	2.06	7.93	1.59	7.89	1.15	7.70	1.53	7.66	1.46
11	7.97	2.52	7.90	1.88	7.83	1.27	7.62	2.28	7.60	1.85
12	7.92	3.30	7.85	2.42	7.76	1.63	7.57	2.94	7.55	2.38
13	7.87	4.79	7.82	2.90	7.72	1.97	7.53	3.94	7.52	3.04
14	7.85	5.51	7.77	4.05	7.69	2.31	7.50	4.85	7.48	3.86
15	7.81	7.07	7.75	4.73	7.67	2.57	7.45	6.95	7.36	9.08
16	7.75	11.55	7.73	5.42	7.66	2.73	7.40	10.15	7.32	12.31
17	7.63	28.25	7.64	10.60	7.65	2.91	7.35	14.87	7.28	16.98
18	7.60	37.08	7.57	18.27	7.60	4.01	7.31	20.34	--	--
19	7.55	53.34	7.54	23.09	7.54	6.16	7.28	25.78	--	--
20	7.52	70.02	7.44	50.93	7.49	8.89	7.24	35.42	--	--
21	7.50	79.91	7.36	98.01	7.41	16.67	--	--	--	--
22	7.48	96.30	--	--	7.38	21.02	--	--	--	--

Table II - S3 Stepwise formation constants derived from the rounded off slopes through the linear dependence of $\log_{10}R$ on $\log_{10}[Ca^{2+}]$ (mol·kg_w^{-1}).

I_m (mol·kg_w^{-1})	**$\log_{10}K_{113}$**	**$\log_{10}K_{213}$**
0.10	3.58 ± 0.02	6.01 ± 0.03
0.20	3.17 ± 0.02	5.30 ± 0.03
0.50	2.50 ± 0.01	4.29 ± 0.02
0.75	2.16 ± 0.02	3.75 ± 0.01
1.00	1.95 ± 0.02	3.41 ± 0.03

Table II - S4 Values of the $\varepsilon(X^{2-}, Na^{+})$ from literature.

Species	$\varepsilon(X^{2-},Na^{+})$ $kg_w\ mol^{-1}$	References
$EdtaH_2^{2-}$	-0.37 ± 0.14	[7]
$UO_2F_4^{2-}$	-0.3 ± 0.06	[4]
ThF_6^{2-}	-0.3 ± 0.06	[2]
$Ni(Oxalate)_2^{2-}$	-0.26 ± 0.03	[7]
$UO_2(Edta)^{2-}$	-0.22 ± 0.18	[7]
$UO_2(Oxalate)_2^{2-}$	-0.18 ± 0.07	[7]
HPO_4^{2-}	-0.15 ± 0.06	[4]
ZrF_6^{2-}	-0.15 ± 0.06	[8]
$Mg(Oxalate)_2^{2-}$	-0.15 ± 0.03	[7]
$Si_2O_3(OH)_4^{2-}$	-0.15 ± 0.06	[4]
$Si_2O_3(OH)_4^{2-}$	-0.15 ± 0.06	[4]
$(UO_2)_2(OH)_2(SO_4)_2^{2-}$	-0.14 ± 0.22	[4]
$UO_2(SO_4)_2^{2-}$	-0.12 ± 0.06	[4]
SO_4^{2-}	-0.12 ± 0.06	[4]
$UO_2(N_3)_4^{2-}$	-0.1 ± 0.1	[4]
$Zr(OH)_6^{2-}$	-0.1 ± 0.1	[8]
$NpO_2(HPO4)_2^{2-}$	-0.1 ±	[4]
$SiO_2(OH)_2^{2-}$	-0.1 ± 0.07	[4]
$Th(SO4)_3^{2-}$	-0.091 ± 0.038	[2]
CO_3^{2-}	-0.08 ± 0.03	[4]
$Oxalate^{2-}$	-0.08 ± 0.01	[7]
SO_3^{2-}	-0.08 ± 0.05	[4]
$S_2O_3^{2-}$	-0.08 ± 0.05	[4]
CrO_4^{2-}	-0.06 ± 0.04	[4]
$Co(OH)_4^{2-}$	-0.06 ± 0.02	[9]
$NpO_2(Citrate)^{2-}$	-0.06 ± 0.03	[7]
$Fe(CO_3)_2^{2-}$	-0.05 ± 0.05	[10]
$CitrateH^{2-}$	-0.04 ± 0.02	[7]
$UO_2(CO_3)_2^{2-}$	-0.02 ± 0.09	[4]
$Mg(Edta)^{2-}$	-0.01 ± 0.15	[7]
$Zn(OH)_4^{2-}$	0.05 ± 0.04	[11]
$NpO_2(EdtaH)^{2-}$	0.07 ± 0.16	[7]
$Zn_2(OH)_6^{2-}$	0.1 ± 0.08	[11]
$Ni(CN)_4^{2-}$	0.185 ± 0.081	[12]
$Cu(OH)_4^{2-}$	0.19 ± 0.05	[13]

References

1. J. Y. Lee and J. I. Yun, *Dalton Trans.*, 2013, **42**, 9862-9869.
2. M. Rand, J. Fuger, I. Grenthe, V. Neck and D. Rai, *Chemical Thermodynamics 11. Chemical Thermodynamics of Thorium*, *Chemical Thermodynamics Series*, OECD Nuclear Energy Agency Data Bank, Eds., OECD Publications, Paris, France, 2009.
3. M. Altmaier, V. Neck, R. Muller and T. Fanghänel, *Radiochim. Acta*, 2005, **93**, 83-92.
4. R. Guillaumont, T. Fanghänel, V. Neck, J. Fuger, D. A. Palmer, I. Grenthe and M. H. Rand, *Update of the Chemical Thermodynamics of Uranium, Neptunium, Plutonium, Americium and Technetium*, OECD Nuclear Energy Agency, Data Bank, Issy-les-Moulineaux, France, 2003.

5. I. Grenthe, L. Fuger, R. G. M. Konings, R. J. Lemire, A. B. Muller, C. Nguyen-Trung and H. Wanner, *Chemical Thermodynamics 1. Chemical Thermodynamics of Uranium*, *Chemical Thermodynamics Series*, North Holland Elsevier Science Publishers B. V., Amsterdam, The Netherlands, 1992.
6. R. J. Lemire, J. Fuger, H. Nitsche, P. Potter, M. Rand, J. Rydberg, K. Spahiu, J. C. Sullivan, W. J. Ullman, P. Vitorge and H. Wanner, *Chemical Thermodynamics 4. Chemical Thermodynamics of Neptunium and Plutonium*, *Chemical Thermodynamics*, North Holland Elsevier Science Publishers B. V., Amsterdam, The Netherlands, 2001.
7. W. Hummel, G. Anderegg, L. F. Rao, I. Puigdomènech and O. Tochiyama, *Chemical Thermodynamics 9. Chemical Thermodynamics of Compounds and Complexes of U, Np, Pu, Am, Tc, Se, Ni and Zr with Selected Organic Ligands*, *Chemical Thermodynamics Series*, North Holland Elsevier Science Publishers B. V., Amsterdam, The Netherlands, 2005.
8. P. Brown, E. Curti, B. Grambow and C. Ekberg, *Chemical Thermodynamics 8. Chemical Thermodynamics of Zirconium*, *Chemical Thermodynamics Series*, North Holland Elsevier Science Publishers B. V., Amsterdam, The Netherlands, 2005.
9. N. V. Plyasunova, Y. Zhang and M. Muhammed, *Hydrometallurgy*, 1998, **48**, 153-169.
10. R. J. Lemire, U. Berner, C. Musikas, D. A. Palmer, P. Taylor and O. Tochiyama, *Chemical Thermodynamics 13a. Chemical Thermodynamics of Iron. Part 1*, *Chemical Thermodynamics Series*, OECD Nuclear Energy Agency Data Bank, Eds., OECD Publications, Paris, France, 2013.
11. Y. Zhang and M. Muhammed, *Hydrometallurgy*, 2001, **60**, 215-236.
12. H. Gamsjäger, J. Bugajski, T. Gajda, R. J. Lemire and W. Preis, *Chemical Thermodynamics 6. Chemical Thermodynamics of Nickel*, *Chemical Thermodynamics Series*, North Holland Elsevier Science Publishers B. V., Amsterdam, The Netherlands, 2005.
13. N. V. Plyasunova, M. S. Wang, Y. Zhang and M. Muhammed, *Hydrometallurgy*, 1997, **45**, 37-51.

Chapter III. Spectroluminescence Measurements of Stability Constants of $Ca_nUO_2(CO_3)_3^{(4-2n)-}$ Complexes in $NaClO_4$ Medium and Investigation of Interaction Effects.

Chengming Shang, Pascal E. Reiller and Thomas Vercouter*
[1] Den – Service d'Études Analytiques et de Réactivité des Surfaces (SEARS), CEA, Université Paris-Saclay, F-91191, Gif-sur-Yvette, France
*Corresponding author. Tel.: +33 1 6908 4312; fax: +33 1 6908 9475. E-mail address: pascal.reiller@cea.fr

Dalton Transactions **49** (43), 15443-15460.

http://doi.org/10.1039/D0DT03164J

III - 1 Abstract

The stability constants of ternary calcium uranyl tricarbonate complexes, $CaUO_2(CO_3)_3^{2-}$ and $Ca_2UO_2(CO_3)_3(aq)$, were determined in $NaClO_4$ medium at various ionic strengths using time-resolved laser-induced luminescence spectroscopy (TRLS) – also known as time-resolved laser-induced fluorescence spectroscopy (TRLFS). As in a previous study, the potential precipitation of schoepite ($UO_3 \cdot 2H_2O$) and calcite ($CaCO_3$) were avoided *via* titration of triscarbonatouranyl complex by Ca^{2+} at varying pH values. The Ringböm coefficients relative to $UO_2(CO_3)_3^{4-}$ were individually evaluated for test sample conditions. Steadily enhanced luminescence intensity and increased decay-times were representative of complexation processes. The stoichiometry of calcium was quantified by slope analysis, the measured intensity of which was corrected by the corresponding Ringböm coefficient. The conditional formation constants, *i.e.* $\log_{10} K_{n.1.3}$, were then assessed after rounding off the slope values to their nearest integers. Determinations of cumulative formation constants at infinite dilution $\log_{10} \beta^\circ_{n.1.3}$, and specific ion interaction parameters ε were based on the experimental origin and slope values, respectively, over the range 0.1-2.46 mol kg_w^{-1} $NaClO_4$ using the specific ion interaction theory (SIT) approach. The cumulative stability constants $-\log_{10} \beta^\circ(CaUO_2(CO_3)_3^{2-}) = 27.26 \pm 0.04$ and $\log_{10} \beta^\circ(Ca_2UO_2(CO_3)_3(aq)) = 30.53 \pm 0.06$. The specific ion interaction coefficients are estimated to be $\varepsilon(CaUO_2(CO_3)_3^{2-},Na^+) = (0.02 \pm 0.04)$ kg_w mol^{-1} and $\varepsilon(Ca_2UO_2(CO_3)_3(aq),NaClO_4) = (0.18 \pm 0.07)$ kg_w mol^{-1}. These latter values are different from the ones that were our previously obtained in NaCl, and underlying causes are discussed from different aspects. This work provides valuable information to address the interaction effects between Ca-UO_2-CO_3 species and 1:1 type electrolytes. It is suggested that

the affinity of the cation in background electrolyte with $Ca_nUO_2(CO_3)_3^{(4-2n)-}$ (n = {1;2}) are to be taken into consideration at high ionic strengths, especially for the globally non-charged species.

III - 2 Introduction

The first identification of $Ca_nUO_2(CO_3)_3^{(4-2n)-}$ species was published in 1996 by Bernhard, *et al.*[1] in a report of seepage water analyses from a uranium mine tailing in Saxony, Germany. Since then, there has been a surge of interests in the chemical properties of ternary complexes of the type $M_nUO_2(CO_3)_3^{(4-2n)-}$ (M = alkaline earth metal elements, *i.e.* Mg^{2+}, Ca^{2+}, Sr^{2+}, Ba^{2+}, n = {1;2}), their chemical structures and behaviour in solution. Various analytical methods and techniques have been employed, such as time-resolved laser-induced luminescence spectroscopy (TRLS)[1-8], anion exchange method[9,10], calcium(II)-selective potentiometry[11], ultraviolet-visible (UV-vis) absorption spectroscopy[12] and extended X-ray absorption spectroscopy (EXAFS)[3,7,13-15]. Results from earlier studies demonstrate the necessity and the importance of clarifying physical and chemical characteristics of these ternary complexes, as they have been proven influential on the U(IV)/U(VI) bio-oxidation/reduction[16,17] and U(VI) adsorption-absorption on minerals.[18-23] Moreover, the $Ca_nUO_2(CO_3)_3^{(4-2n)-}$ complexes have been found as principal species in Ca-CO_3 rich waters—*e.g.*, in the vadose zone at Hanford site, USA[24-27] and from drilled wells in Southern Finland[22]—and proposed in other instances.[28]

Among the research perspectives mentioned above, experimental determination of thermodynamic constants of Ca-UO_2-CO_3 complexes draws our major attention. For predictive modelling of species distribution, particularly in the field of radioactive waste management, the formation constants are must-have parameters, as well as specific ion interaction coefficients in the framework of the specific ion interaction theory (SIT).[29] To date, none of the reported formation constants have been selected by the Thermochemical Database project of the NEA-OECD—the Nuclear Energy Agency from the Organization for the Economic Co-operation and Development (https://www.oecd-nea.org/jcms/pl_20079/tdb-project-publications-chemical-thermodynamics-series).[29,30] One of the main reasons is the difficulty to experimentally and accurately investigate the stability domains of such ternary species, which has led to differences in the complex formation constants. In past studies, the conventional titration of triscarbonatouranyl complex ($UO_2(CO_3)_3^{4-}$) by Ca^{2+} at fixed pH values has been widely used,[2,9,11] starting from alkaline conditions – where $UO_2(CO_3)_3^{4-}$ predominates. The resulting analyses were based on the measures of complexation degree with increasing calcium

concentration. However, the principal source of bias might emerge from the different extents of oversaturation of schoepite ($UO_3 \cdot nH_2O$) and calcite ($CaCO_3$) depending on the pH value.

In our previous study,[8] we used a spectroluminescence titration at varying pH values in order to circumvent the possible schoepite and calcite precipitation. Satisfactory linear fits in the slope analysis proved the feasibility of the experimental methodology. The successful collection of luminescence spectra and decay-time measurements of the calciumtriscarbonato-uranyl species in the investigated range of I_m = 0.1 to 1 mol kg_w^{-1} NaCl (hereafter noted *m*), have demonstrated the high performance of TRLS technique and implied further applications. Nevertheless, the quenching effect of chloride ion has prevented the use of ionic strength media above 1 *m*. The obtained specific ion interaction coefficients $\varepsilon(Na^+,CaUO_2(CO_3)_3^{2-})$ and $\varepsilon(Ca_2UO_2(CO_3)_3(aq),NaCl)$ were both surprisingly positive – *i.e.* 0.29 and 0.66 $kg_w\ mol^{-1}$, respectively – and could not be compared with the coefficients of other like-charged dissolved species. According to the general hypothesis of the SIT,[29] interactions between anionic complexes and Na^+ are often characterized by negative values of ε, while those for neutral complexes are considered as nil. The results in our previous paper questioned these classical assumptions. [8] Furthermore, research on this subject raised important issues that rely on restricted available references. The selected value[29] of $\varepsilon(UO(CO_3)_2^{2-},Na^+)$ = -(0.02 ± 0.09) $kg_w\ mol^{-1}$ was commonly taken as an analogy for $\varepsilon(MUO_2(CO_3)_3^{2-},Na^+)$, and $\varepsilon(M_2UO_2(CO_3)_3,NaX)$ was estimated to be nil, as postulated in SIT for non-charged species.[29,30] Comparison with other data – *i.e.* $\varepsilon(MgUO_2(CO_3)_3^{2-},Na^+)$ = (-3.0 ± 0.3) $kg_w\ mol^{-1}$ proposed by Dong and Brooks[10] and $\varepsilon(Ca_2UO_2(CO_3)_3,NaClO_4)$ = -2.7 $kg_w\ mol^{-1}$ evaluated from the work of Kalmykov and Choppin[2] –, produces equivocal implications of involved ion interaction processes, which led to the non-selection in Guillaumont, *et al.*[29]

What also remains ambiguous is whether the affinity of Na^+ with $Ca_nUO_2(CO_3)_3^{(4-2n)-}$ complexes is capable of yielding globally positively-charged complexes that may contribute to the relatively large and the positive values of ε in NaCl evidenced in Shang and Reiller,[8] as suggested in theoretical calculations.[31-33] For the sake of an exhaustive consideration, variations of the reaction constants should be measured in a larger range of ionic strength in which the potentially strong ion interaction processes could be better described. It is hoped that the completeness of reliable information with respect to thermodynamic constants in specific conditions would contribute to a deeper understanding of ion interaction mechanisms and fill the knowledge gap in the thermodynamic data.

Sodium perchlorate, when dissolved in water, can hardly react through coordination, or in any other manner, with different aqueous species.[34] The lack of chemical reactivity in solutions allows its extensive use as an inert background salt in the reactions of ionic materials. To the best of our knowledge, Kalmykov and Choppin[2] have used $NaClO_4$ as the supporting electrolyte, and extended the ionic strength up to 3 *m*. The authors evidenced a noticeable deviation from the theoretical linear trend of $\log_{10} \beta_{2.1.3}$ *vs.* the ionic strength when using SIT.[29] However, only $Ca_2UO_2(CO_3)_3(aq)$ was postulated, and the monocalciumtriscarbonatouranyl complex was not identified. Furthermore, the lack of experimental points between 1 and 3 *m* $NaClO_4$ ionic strength also adds difficulties to separate the electrolyte effects from the ligand effects, particularly important aspect of ion paring formation in the sequential binding processes between Ca^{2+} and $UO_2(CO_3)_3^{4-}$.

With increasing electrolyte concentration, the aqueous ions interactions are reinforced by the increasing mutually electrostatic effects disturbing the inner- and outer-sphere water molecules of solute and solvent ions and forming ion-pairs.[35] The cation-anion pairs can be divided into three categories according to the varying extents of ionic association: (i) the solvent-separated ion-pairs (SSIP) involve generally two layers of water molecules between the ion partners of the pair, and (ii) the solvent-shared ion pairs (SIP) contain one; (iii) the contact ion-pairs (CIP) are used to describe the situation where the desolvation of the inner-sphere water layer of both ions is inevitable. Several studies reported the hydration of Ca^{2+}, Na^+, ClO_4^- and Cl^- in aqueous solution and their tendencies to form different types of ion-pairs as a function of electrolyte concentration. It has been shown that the hydration layers of Na^+ and Ca^{2+} can be depicted as $Na^+(H_2O)_4(H_2O)_9(H_2O)_5$ and $Ca^{2+}(H_2O)_{6\text{-}8}(H_2O)_{12}$, respectively. Na^+ is less hydrated in its first hydration sphere than Ca^{2+}. The hydration of the larger anions ClO_4^- and Cl^- are – reported to be 3.8 H_2O and 6 H_2O, respectively.[36-41] More specifically, Tu, *et al.*[42] attributed the broadening bands of ClO_4^- in Raman spectra when increasing the $Ca(ClO_4)_2$ concentration to the growing number of SIPs. They also assumed that the oppositely charged ions are more likely to form CIPs if they are comparatively hydrated, suggesting the easier association between Ca^{2+} and Cl^- than between Ca^{2+} and ClO_4^-. The fundamental properties and chemical behaviour of the ions from the electrolyte would help us to clarify the ion interactions mechanism at high electrolyte concentrations and gain an in-depth explanation for the experimental results in NaCl and $NaClO_4$.

The aim of this work is to determine the thermodynamic formation constants of $Ca_nUO_2(CO_3)_3^{(4-2n)-}$ complexes in $NaClO_4$ media using TRLS. Despite the intricate approaches,

it seems that the effects of electrolyte ions may have no noticeable impact on the luminescence results over a certain range of ionic strength. The upper limit of $NaClO_4$ ionic strength will be evaluated at the concentration above which the analysis of uranyl luminescence for speciation is no more valid. By analysing the evolution of formation constants within the I_m range, this study is expected to clarify the $Ca_nUO_2(CO_3)_3^{(4-2n)-}$-$ClO_4^-$ interaction mechanisms. These results will be discussed considering former observations in NaCl medium.[8] Variations of specific ion interaction coefficients as a function of electrolyte concentration will be described and predicted by different models proposed in the literature. Extension of the SIT approach would also be feasible to much higher ionic strength based on the present results.

Moreover, as regards to photophysical and radiochemical processes that possibly occurred when exciting UO_2^{2+} in perchloric environment, the most debated problem prevails on the reactivity of UO_2^{2+} in different states – *i.e.* excited or ground state.[43-53] It was proposed that the influence of perchlorate and hydrogen ions, especially the effect of quenching, was occurring at high ClO_4^- concentrations.[51-53] However, what is less clear is the degree to which the luminescence mechanisms proposed in these studies can be transposable to the Ca-UO_2-CO_3 systems, as well as the sensibility of the overall packing scheme in the UO_2-CO_3 structure towards perchlorate interaction. The results in this work may raise intriguing questions about the quenching effect of perchlorate ions on triscarbonatouranyl units.

III - 3 Experimental Section

3.1 Materials

An appropriate quantity of high purity U_3O_8 solid was dissolved in 60-70% perchloric acid (ACS reagent) to prepare the stock solution of U(VI). A brilliant greenish-yellow U(VI) liquid solution was obtained at the end of 48 hours. Inductively coupled plasma mass spectroscopy (ICP-MS) was used to measure the aqueous concentration of uranium after multiple dilutions of the concentrated U(VI) solution. Seven series of $NaClO_4$ solutions of different ionic strengths (*i.e.* 0.1, 0.51, 1.05, 1.62, 2.21, 2.46, and 3.5 *m*) were prepared by dissolving anhydrous $NaClO_4$ (Sigma-Aldrich, ACS reagent, ≥ 99%) in Millipore deionized water (Alpha-Q, 18.2 MΩ cm^{-1}). All measurements were performed at the same uranium concentration of 50 μ*m*.

Sodium hydroxide (Analytical Grade, Fisher) and diluted perchloric acid were used to adjust the aqueous pH values. The introduction of carbonate was performed with freshly prepared sodium bicarbonate solution ($NaHCO_3$, Analytical Grade, Fisher). As all the sample solutions were open to the atmosphere during the preparation, carbon dioxide in the air equilibrated with

CO_2(aq), hydrogen and bicarbonate in solution. Therefore, the amounts of added $NaHCO_3$ were calculated based on the equilibrium between the pH-fixed solution and atmospheric CO_2(g) in the absence of calcium. In order to maintain the electrolyte concentrations at constant values, the volumes of reagents were kept small compared to that of the solution. Calcium perchlorate ($Ca(ClO_4)_2$:$4H_2O$, Sigma-Aldrich, ACS reagent, ≥ 99%) solutions of various concentrations were prepared to control the concentration of calcium for each sample. All reagent preparations were conducted by weighing. Concentrations of involved species are expressed in molality units (mol kg_w^{-1} or *m*) with squared-brackets in this work. Necessary prerequisite for further measurement—no variation of Ca concentrations has been verified at the present U(VI) concentration (data not shown). For every sample the saturation indices of UO_3:$2H_2O$(cr) and calcite are negative, which means that precipitation is unlikely.

3.2 Modification of pH electrode and measurements of liquid junction potential

A hydrogen ion-sensitive glass electrode (type, Mettler Toledo, USA) was used to perform the measurements of pH values. Considering the particular electrolyte anion in this work, the saturated KCl solution in the reference electrode was replaced with 3.5 *m* $NaClO_4$ (2.99 M $NaClO_4$ + 0.01 M NaCl), to avoid the $KClO_4$ precipitation inside the liquid junction. The electrode was carefully handled in this procedure and then properly conditioned for reuse. The change of the reference inert solution generates a systematic deviation of potential difference between the electrodes. The potential gradient between the silver chloride electrode and the buffer solution in the pH electrode would remain constant, whereas that between the reference electrode and the test sample, separated by a semi-permeable membrane, needs to be re-determined for each electrolyte concentration. For this reason, a series of $NaClO_4$ solutions of from 0.01 to 3.5 *m* acidified by HCl to pcH 2 (= $-\log_{10}[H^+]$) were prepared to measure the junction potentials with the reconditioned electrode of 3.5 *m* $NaClO_4$ reference solution.[54] The potential values E_{mes} read on pH-meter for the $NaClO_4$ solutions of the same acidity ($-\log_{10}[H^+]$ = 2) but different ionic strengths are reported in Table III - S1 of the Supplementary Information (SI). For a given inert electrolyte concentration, the difference between the value of E_{mes} measured at I_m = 0.01M and that at other I_m is including the liquid junction potential of the reconditioned electrode and the activity coefficient of H^+. Therefore, the experimentally measured ΔE_{mes} were taken to correct the pH value of sample solutions at specific electrolyte concentrations.

A four-point calibration using the commercial buffer standard solutions of known and fixed pH values, respectively of 1.68, 4.01, 6.87 and 9.18 (SI Analytics, Mainz, Germany) was daily

required to maintain the accuracy.[55] The method of ordinary least squares was employed to estimate the 95% confidence limits, corresponding to 0.05 pH units of maximum uncertainties.[56]

Measurements of pH values were performed in triplicate at 22°C. For each test sample, the pH value was regularly checked and adjusted if necessary. The first pH measurement was carried out after adding appropriate quantities of $NaHCO_3$(aq). The samples were then let open to air. After two hours, the pH value was checked for the second time and slightly adjusted if necessary. The pH never evolved after the nest additions of calcium perchlorate into the sample solution. The pH was then measured prior to each spectrum acquisition.

3.3 Time-resolved laser-induced luminescence spectroscopy

A 1 cm quartz cuvette (QS101, Suprasil, Hellma Analytics) containing a 2 mL aliquot of U(VI) test sample was used to measure the luminescence spectra in the wavelength range from 415 to 615 nm. The fluorescence cuvette was placed in the thermostated sample holder, connected to the thermostat (Peter Huber Kältemaschinenbau AG, Germany) with circulating water, during at least 10 min before data acquisition. The cooling water temperature was set at 22ºC for minimizing the temperature fluctuation on uranyl fluorescence. A frequency-tripled Nd:YAG laser at 355 nm (Surelite, Continuum, USA) working with 5 ns pulse at 10 Hz of about 170 mJ as energy was used as the pump laser of an optical parametric oscillator system (Horizon, Continuum, USA). The excitation wavelength was set at 450 nm for all luminescence measurements. This wavelength represents the better compromise between the selective excitation of uranium(VI) and the excitation energy delivered by the optical parametric oscillator. A RJP-734 Joule-meter (Laser Probe, Inc.) was used to monitor the excitation energy. The 300 lines mm^{-1} grating, favouring the convolution of various fluorescing components with the detection apparatus, was selected in the monochromator spectrometer (Acton 300i, Roper Scientific, U.S.A.). The resulting measured fluorescence signal was detected by an intensified CCD camera (Andor, U.K.) maintained at -10°C by a Peltier effect. All emission spectra acquisitions started at the delay time of 25 ns with the gate width fixed at 1 μs.

The present concentration of U(VI) was low enough not to generate any pre- and post-filter effects. The observed fluorescent behaviour was thus assumed to be the cumulative contribution of aqueous U(VI) complexes, on the condition that neither precipitation nor colloidal aggregation occurred in solution. The recorded spectra were integrated over the emission wavelength span to evaluate the fluorescence intensity at various delay times. The luminescence

intensity at D = 0, as well as luminescence decay-time, were derived by fitting the intensity results to the exponential fluorescence decay function, expressed as follows,[57-60]

$$FI = \sum_i FI_0\ \tau_i\ \exp\left(-\frac{D}{\tau_i}\right)\left(1 - \exp\left(-\frac{W}{\tau_i}\right)\right) \qquad \text{(III - 1)}$$

where FI and FI_0 are respectively the fluorescence intensity at a specific delay time and at D = 0. The gate width W equals to 1 μs and τ_i represents the decay-time of species i.

Origin 9.0 software (OriginLab Corporation, USA) was used to analyse experimental data. The background noise was recorded and subtracted from measured fluorescence emission spectra for each series prior to subsequent peak analysis. The trapezoidal integration method was used to calculate the fluorescence intensity. The least-square fitting process was then evaluated by the Levenberg-Marquardt algorithm.

3.4 Correction for slope analysis and calculation of related Ringböm coefficient.

For explanatory purposes, the equations used for the slope analysis and the meanings of the corrective factor α, also the Ringböm[61] coefficient relative to $UO_2(CO_3)_3^{4-}$, are recalled here. The calculation procedure for α has been exemplified in our previous study.[8] The Ringböm coefficient – calculated using the thermodynamic constants from Table III - 1 and specific ion interaction coefficients from Table III - 2– corresponding to each specified aqueous condition in this work was listed in the Table III - S2 of the SI. The sequential binding of Ca^{2+} with $UO_2(CO_3)_3^{4-}$ is described by the following equations,

$$n\,Ca^{2+} + UO_2(CO_3)_3^{4-} \rightleftarrows Ca_nUO_2(CO_3)_3^{(4-2n)-}$$

$$K_{n.1.3} = \frac{\left[Ca_nUO_2(CO_3)_3^{(4-2n)-}\right]}{\left[Ca^{2+}\right]^n\left[UO_2(CO_3)_3^{4-}\right]} \qquad n = 1, 2 \qquad \text{(III - 2)}$$

where the concentrations are expressed in molality (m).

Table III - 1 Stability constants of U(VI) complexes at 25 °C and I_m = 0, used in the work

Reaction	$\log_{10} K^\circ$	References
$CO_2(g) + H_2O \rightleftarrows CO_3^{2-} + 2H^+$	-18.15 ± 0.06	[29]
$CO_3^{2-} + 2H^+ \rightleftarrows CO_2(aq) + H_2O$	16.68 ± 0.05	[29]
$CO_3^{2-} + H^+ \rightleftarrows HCO_3^-$	10.33 ± 0.05	[29]
$UO_2^{2+} + H_2O \rightleftarrows UO_2(OH)^+ + H^+$	-5.25 ± 0.24	[29]
$UO_2^{2+} + 2H_2O \rightleftarrows UO_2(OH)_2(aq) + 2H^+$	-12.15 ± 0.07	[29]
$3\ UO_2^{2+} + 5H_2O \rightleftarrows (UO_2)_3(OH)_5^+ + 5H^+$	-15.55 ± 0.12	[29]
$UO_2^{2+} + CO_3^{2-} \rightleftarrows UO_2(CO_3)(aq)$	9.94 ± 0.03	[29]
$UO_2^{2+} + 2CO_3^{2-} \rightleftarrows UO_2(CO_3)_2^{2-}$	16.61 ± 0.09	[29]
$UO_2^{2+} + 3CO_3^{2-} \rightleftarrows UO_2(CO_3)_3^{4-}$	21.84 ± 0.04	[29]
$2UO_2^{2+} + CO_2(g) + 4H_2O \rightleftarrows (UO_2)_2CO_3(OH)_3^- + 5H^+$	-19.01 ± 0.50	[29]
$UO_2(CO_3)_3^{4-} + 4H^+ \rightleftarrows UO_2(CO_3)(aq) + 2CO_2(g) + 2H_2O$	24.40 ± 0.21*	Recalculated from[29]
$UO_2(CO_3)_3^{4-} + 2H^+ \rightleftarrows UO_2(CO_3)_2^{2-} + CO_2(g) + H_2O$	12.92 ± 0.15*	Recalculated from[29]
$2UO_2(CO_3)_3^{4-} + 7H^+ \rightleftarrows (UO_2)_2CO_3(OH)_3^- + 5CO_2(g) + 2H_2O$	46.21 ± 0.70*	Recalculated from[29]
$Ca^{2+} + UO_2(CO_3)_3^{4-} \rightleftarrows CaUO_2(CO_3)_3^{2-}$	5.36 ± 0.01[a]	[8] in NaCl
$2Ca^{2+} + UO_2(CO_3)_3^{4-} \rightleftarrows Ca_2UO_2(CO_3)_3(aq)$	8.65 ± 0.02	[8] in NaCl
	$\log_{10}\beta^\circ$	References
$Ca^{2+} + UO_2^{2+} + 3CO_3^{2-} \rightleftarrows CaUO_2(CO_3)_3^{2-}$	27.20 ± 0.04	[8] in NaCl
	27.26 ± 0.08	p.w. $NaClO_4$ individual regression
	27.22 ± 0.04	p.w. multilinear regression
$2Ca^{2+} + UO_2^{2+} + 3CO_3^{2-} \rightleftarrows Ca_2UO_2(CO_3)_3(aq)$	30.49 ± 0.05	[8] in NaCl
	30.53 ± 0.12	p.w. $NaClO_4$ individual regression
	30.51 ± 0.06	p.w. multilinear regression

[a] an error occurred in Table II - 1 from Shang and Reiller.[8] The correct value was reported in the text.

Table III - 2 Main specific ion interaction coefficients used in this work.

Specific ion interaction coefficient	Value (± 1σ) $kg_w\ mol^{-1}$	Ref.
$\varepsilon(H^+,ClO_4^-)$	0.14 ± 0.02	[29]
$\varepsilon(Na^+,CO_3^{2-})$	-0.08 ± 0.03	[29]
$\varepsilon(UO_2^{2+},ClO_4^-)$	0.46 ± 0.03	[29]
$\varepsilon(Ca^{2+},ClO_4^-)$	0.27 ± 0.03	[29]
$\varepsilon(UO_2(CO_3)_2^{2-},Na^+)$	-0.02 ± 0.09	[29]
$\varepsilon(UO_2(CO_3)_3^{4-},Na^+)$	-0.01 ± 0.11	[29]
$\varepsilon(CaUO_2(CO_3)_3^{2-},Na^+)$ (in NaCl)	0.29 ± 0.11	[8]
$\varepsilon(Ca_2UO_2(CO_3)_3,NaCl)$	0.66 ± 0.22	[8]
$\varepsilon(CaUO_2(CO_3)_3^{2-},Na^+)$ (in $NaClO_4$)	0.02 ± 0.04	this work individual regression
$\varepsilon(Ca_2UO_2(CO_3)_3,NaClO_4)$	0.18 ± 0.07	this work individual regression
$\varepsilon(CaUO_2(CO_3)_3^{2-},Na^+)$ (in NaCl)	0.32 ± 0.12	this work multilinear regression
$\varepsilon(Ca_2UO_2(CO_3)_3,NaCl)$	0.66 ± 0.15	this work multilinear regression
$\varepsilon(CaUO_2(CO_3)_3^{2-},Na^+)$ (in $NaClO_4$)	0.00 ± 0.10	this work multilinear regression
$\varepsilon(Ca_2UO_2(CO_3)_3,NaClO_4)$	0.17 ± 0.12	this work multilinear regression

Following the expression of $K_{n.1.3}$, the fluorescence intensity of $UO_2(CO_3)_3^{4-}$ should be measured at the same pH as in the sample of $Ca_nUO_2(CO_3)_3^{(4-2n)-}$. However, the fluorescence spectrum of a free-calcium triscarbonatouranyl sample under weakly basic conditions (pH < 8) is interfering inevitably with hydroxo, less-complexed carbonatouranyl, and polynuclear species – *e.g.*, $UO_2(CO_3)_2^{2-}$, $UO_2CO_3(aq)$, $UO_2(OH)^+$, $UO_2(OH)_2(aq)$, $(UO_2)_2CO_3(OH)_3^-$. As an

illustration, fluorescence decay spectra of UO_2-CO_3 sample at pH 7.6 were shown in the Fig. III - S2 in our previous study.[8] The spectral evidence indicated that FI_0 ($UO_2(CO_3)_3^{4-}$) cannot be directly measured at lower pH values (pH < 8). The Ringböm coefficient α was therefore introduced to deduce FI_0 ($UO_2(CO_3)_3^{4-}$) at desirable pH values (7 < pH ≤ 9), because there is no difficulty to acquire FI_0 ($UO_2(CO_3)_3^{4-}$) at pH 9 at the investigated ionic strengths (0.1 $m \leq I_m \leq$ 3.5 m). We expressed the slope analysis as in eqn 3), R is the concentration ration between the $[Ca_nUO_2(CO_3)_3^{(4-2n)-}]$ and $[UO_2(CO_3)_3^{4-}]$ with the factor α to evaluate the amount of $UO_2(CO_3)_3^{4-}$ at the pH values different from pH 9, at which the $FI_0(UO_2(CO_3)_3^{4-})$ was measured. The slope n represents the stoichiometric number of calcium ion and the intercepts $\log_{10} K_{n.1.3}$ stand for the formation constants of $Ca_nUO_2(CO_3)_3^{(4-2n)-}$.

$$\log_{10} R = \log_{10} \frac{\left[Ca_nUO_2(CO_3)_3^{(4-2n)-}\right]}{\left[UO_2(CO_3)_3^{4-}\right]/_{\alpha}}$$

$$\log_{10} R = \log_{10} \frac{FI_0\left(Ca_nUO_2(CO_3)_3^{(4-2n)-}\right)}{FI_0(UO_2(CO_3)_3^{4-})/_{\alpha}} = = \log_{10} K_{n.1.3} + n \log_{10}\left[Ca^{2+}\right] \qquad \text{(III - 3)}$$

3.5 Specific ion interaction Theory (SIT)

The SIT approach is used to extrapolate the conditional stability constants to infinite dilution, as the long-range and short-range forces are both considered in this model.[29] According to the specific ion interaction theory, the expression for the activity coefficient is in the form of Eq. III - 4:

$$\log_{10} \gamma_j = -z_j^2 D_H + \varepsilon(j, k, I_m)\, m_k \qquad \text{(III - 4)}$$

with D_H the Debye-Hückel term,

$$D_H = \frac{A\sqrt{I_m}}{1+1.5\sqrt{I_m}} \qquad \text{(III - 5)}$$

where $\varepsilon_{(j,k)}$ ($kg_w\ mol^{-1}$) represents the ion interaction coefficient between the aqueous ion j and either the cation or the anion k of background electrolyte (depending on the whether the ion j is cationic or anionic) of concentration I_m on the molal scale.

The value of 0.507 $kg^{1/2}\ mol^{-1/2}$ was chosen for Debye-Hückel constant A, instead of 0.509 $kg^{1/2}\ mol^{-1/2}$ calculated for 25°C, because the measurements were conducted at 22°C.[29] The relationship between conditional formation constants and ionic strengths is expressed by Eq. III - 6.

$$nCa^{2+} + UO_2^{2+} + 3CO_3^{2-} \rightleftarrows Ca_nUO_2(CO_3)_3^{(4-2n)-}$$

$$\beta_{n.1.3} = \frac{\left[Ca_nUO_2(CO_3)_3^{(4-2n)-}\right]}{\left[Ca^{2+}\right]^n\left[UO_2^{2+}\right]\left[CO_3^{2-}\right]^3} \qquad n = 1, 2$$

$$log_{10}\,\beta_{n.1.3} = log_{10}\,\beta_{0.1.3} + log_{10}\,K_{n.1.3} = log_{10}\,\beta^{\circ}_{n.1.3} + \Delta z^2 D_H - \Delta\varepsilon\, I_m \quad \text{(III - 6)}$$

where

$$\Delta z^2 = z\left(Ca_nUO_2(CO_3)_3^{(4-2n)-}\right)^2 - nz\left(Ca^{2+}\right)^2 - z\left(UO_2^{2+}\right)^2 - 3z\left(CO_3^{2-}\right)^2 \quad \text{(III - 7)}$$

($\Delta z^2 = -16$ for n = 1 and $\Delta z^2 = -24$ for n = 2) and

$$\Delta\varepsilon = \varepsilon\left(Ca_nUO_2(CO_3)_3^{(4-2n)-}, Na^+\right) - n\varepsilon\left(Ca^{2+}, ClO_4^-\right) - \varepsilon\left(UO_2^{2+}, ClO_4^-\right) - 3\varepsilon(Na^+, CO_3^{2-}) \quad \text{(III - 8)}$$

Table III - 2 summarizes the specific ion interaction coefficients used in calculations. It should be noted that in Guillaumont, *et al.*, [29] the value of $\varepsilon(UO_2(CO_3)_3^{4-},Na^+)$ = (0.08 ± 0.11) $kg_w\ mol^{-1}$ was assigned using the interaction coefficient $\varepsilon(UO_2^{2+},ClO_4^-)$ = 0.46 $kg_w\ mol^{-1}$, and not from $\varepsilon(UO_2^{2+},Cl^-)$ = 0.21 $kg_w\ mol^{-1}$, since the complexation of chloride towards dioxouranium(VI), though very weak, should be taken into consideration. In our previous study of NaCl medium, the use of $\varepsilon(UO_2^{2+},Cl^-)$ = 0.21 $kg_w\ mol^{-1}$ was avoided by applying the linear regression to the variation of $\log_{10} K_{n.1.3}$ *vs.* I_m, as an alternative to $\log_{10} \beta_{n.1.3}$.[8] Therefore, the thermodynamic constants and ion interaction coefficients in these two works are both deduced with $\varepsilon(UO_2^{2+},ClO_4^-)$ = 0.46 $kg_w\ mol^{-1}$.

III - 4 Results and discussion

4.1 Evaluation of equilibrium constants and specific ion interaction coefficients

The upper limit of investigated ionic strength is enlarged to 3.5 *m* $NaClO_4$, also in the I_m range of application of SIT. Seven series of solutions are separately prepared at 0.1, 0.51, 1.05, 1.62, 2.21, 2.46, and 3.5 *m* $NaClO_4$ with between 14 and 19 samples per series (Table III - S1 of the SI). Out of 114 luminescence spectra, 96 were used to estimate the specific ion interaction coefficients and stability constants by linear regression analysis. The results at the highest ionic strength of this work, *i.e.* 3.5 *m* $NaClO_4$, were excluded due to the lack of the second slope of two in slope analysis – *vide post* and Fig. III - S1 in the SI.

As shown in Fig. III - 1, the emission spectra at *D* = 25 ns illustrate the successive complexations of calcium ions with triscarbonatouranyl moiety. The expected spectral and temporal characteristics – better resolved spectrum, continuously enhanced luminescence

intensity and slower decay-times –, agree well with the changes of stoichiometry from monocalcium- to dicalciumtriscarbonatouranyl complexes in aqueous solution.

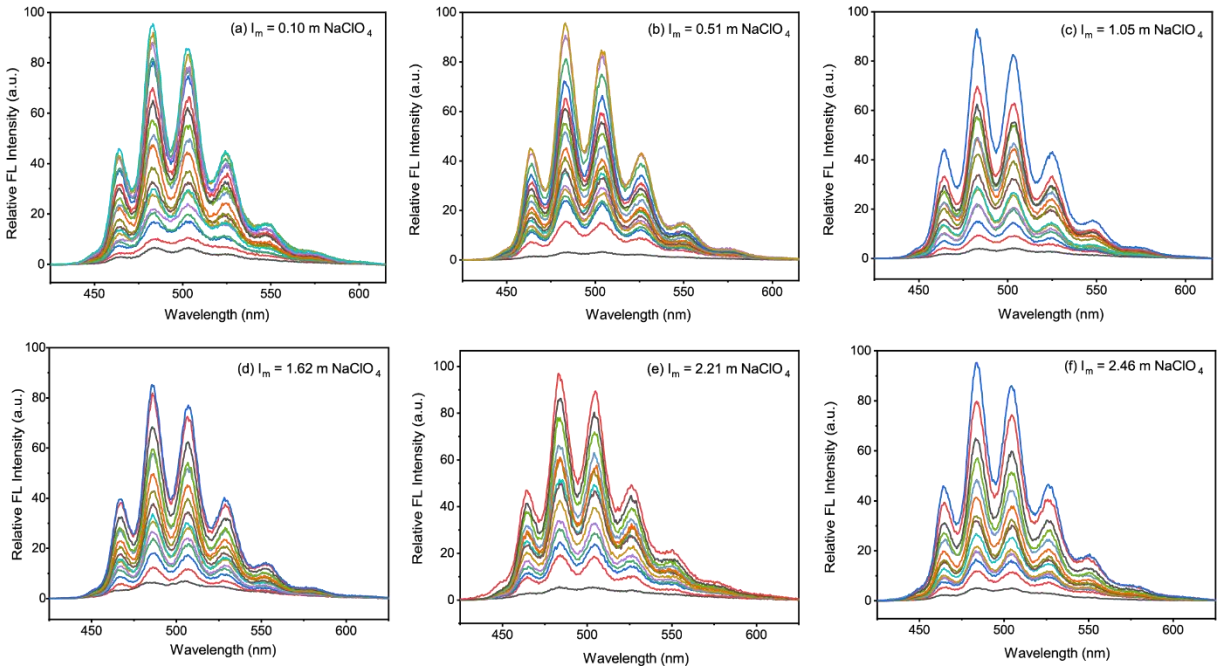

Fig. III - 1 Evolution of luminescence emission spectra during complexation of Ca(II) with $UO_2(CO_3)_3^{4-}$ at different ionic strengths: the aqueous conditions where the ternary species dominate are listed in Table III - 3.

The graphical representations of experimental data at investigated electrolyte concentrations are shown in Fig. III - 2. The error bars representing 2σ, albeit evaluated for each experimental point, are too small to be presented, due to the use of trapezoidal rule in the numerical integration method to deduce FI_0 (the fluorescence intensity at D = 0). Weighted least-squares regression analysis was used to perform all linear fits and subsequently to determine the related parameters, *i.e.* slope and intercept mean values with 95% uncertainties. On account that the analytical calcium concentration is much larger than that of uranium, the aqueous Ca^{2+} is considered as free calcium ion in linear plots. According to the meanings of parameters in linear regression analysis, the slope values, *ca.*1 and 2, correspond to the ratio of coordinated calcium towards the triscarbonatouranyl moiety. After rounding off the slope values to the integers of 1 and 2, the associated intercepts represent the formation constants of $CaUO_2(CO_3)_3^{2-}$ and $Ca_2UO_2(CO_3)_3(aq)$ at a specific ionic strength. It is noteworthy that the fixed slopes intrinsically influence the uncertainties of associated intercepts. In the further analysis, the deduced uncertainties after imposing the slope values to integers would be adopted for the aim of consistency.

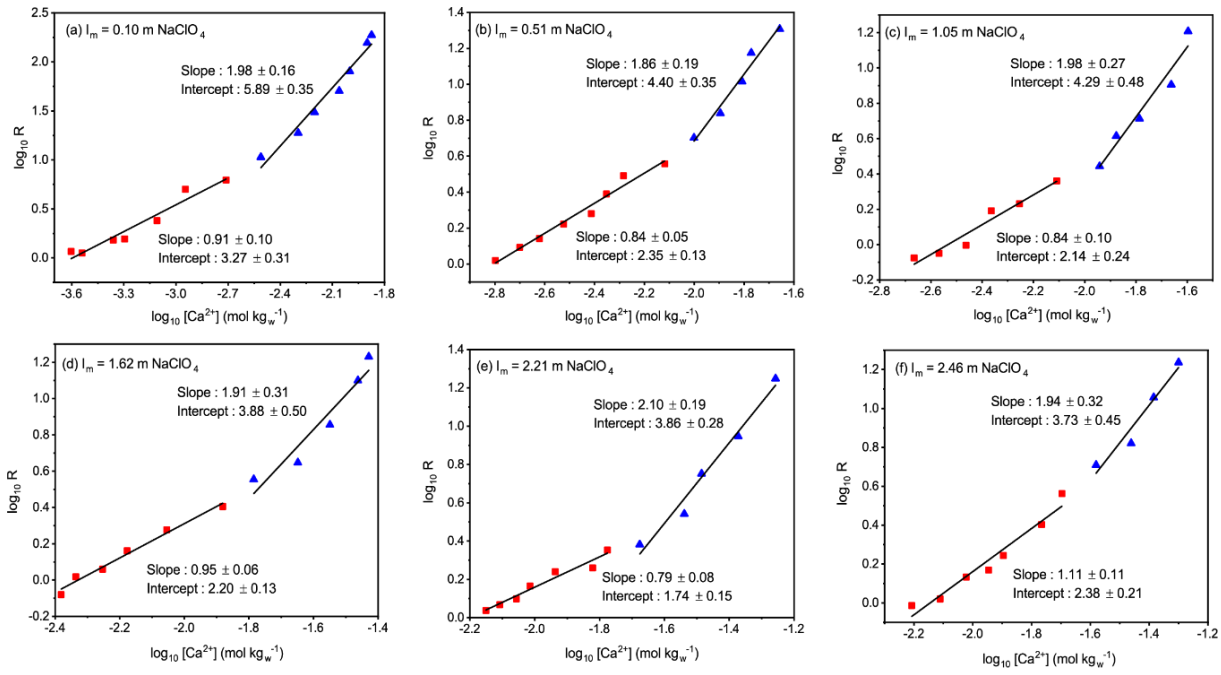

Fig. III - 2 Plot of logarithmic ratio R as a function of $log_{10}[Ca^{2+}]$ (m) at (a) I_m = 0.10 m $NaClO_4$ (b) I_m = 0.51 m $NaClO_4$ (c) I_m = 1.05 m $NaClO_4$ (d) I_m = 1.62 m $NaClO_4$ (e) I_m = 2.21 m $NaClO_4$ (e) I_m = 2.46 m $NaClO_4$: $[U]_{total}$ = 50 μm, $P(CO_2) = 10^{-3.5}$ atm.

In Table III - 3 are gathered the complete information of aqueous calcium concentrations transformed to decimal logarithms and pH values for $CaUO_2(CO_3)_3^{2-}$ and $Ca_2UO_2(CO_3)_3(aq)$ being predominant in solution. The data were satisfactorily fitted with two straight lines with slopes of 1 and 2 for the ionic strengths of from 0.10 to 2.46 *m* $NaClO_4$ (Fig. III - 2), whereas a unique straight line with a slope of one was used to fit the data for I_m = 3.50 *m* $NaClO_4$ (Fig. III - S1 in the SI). At the highest ionic strength, the addition of Ca^{2+} does not give rise to the enhanced fluorescence intensity, or the second slope. For the sake of conformity, the results of I_m = 3.50 *m* $NaClO_4$ would not be included in the linear regression for evaluating the global stability constants and specific ion interaction coefficients – *vide post* for discussion.

Table III - 3 Values of $log_{10}[Ca^{2+}]$ extracted from the slope analysis in Fig. III - 2, and pH values measured before luminescence acquisition.

I_m	$CaUO_2(CO_3)_3^{2-}$ ($\log_{10}$ [Ca^{2+}], pH)	$Ca_2UO_2(CO_3)_3(aq)$ ($\log_{10}$ [Ca^{2+}], pH)
0.10 *m*	(-3.60, 8.21) → (-2.71, 7.87)	(-2.51, 7.80) → (-1.87, 7.46)
0.51 *m*	(-2.80, 7.84) → (-2.12, 7.64)	(-2.00, 7.60) → (-1.66, 7.44)
1.05 *m*	(-2.67, 7.78) → (-2.11, 7.56)	(-1.94, 7.52) → (-1.60, 7.34)
1.62 *m*	(-2.38, 7.72) → (-1.88, 7.52)	(-1.79, 7.48) → (-1.43, 7.32)
2.21 *m*	(-2.15, 7.82) → (-1.78, 7.50)	(-1.68, 7.48) → (-1.26, 7.22)
2.46 *m*	(-2.21, 7.58) → (-1.70, 7.34)	(-1.58, 7.30) → (-1.30, 7.18)

According to the experimental results listed in Table III - 3, one can conclude that higher concentrated electrolytes require a larger quantity of Ca^{2+} to the formation of ternary species. This fact results from the increased electrostatic attraction between the salt ions and oppositely charged particles at higher ionic strengths. The conditional formation constants derived from the rounded off slopes in linear regression analysis are given in Table III - 4. The difference between $\log_{10} K_{1.1.3}$ and $\log_{10} K_{2.1.3}$ represents the stepwise binding constant, noted $\Delta\log_{10} K$, for Ca^{2+} complexing to $CaUO_2(CO_3)_3^{2-}$. One of the reason of the non-selection of the $Ca_nUO_2(CO_3)_3^{(4-2n)-}$ data in Guillaumont, *et al.*[29] was that the obtained $\Delta\log_{10} K$ was higher than $\log_{10} K_{1.1.3}$, which is unlikely. In order to make the first comparison with the results of NaCl medium, the values of $\Delta\log_{10} K$ are calculated for each ionic strength of $NaClO_4$ medium. The stepwise binding constants are determined as 2.37, 1.91, 1.81, 1.70, 1.55, and 1.65 at 0.10, 0.51, 1.05, 1.62, 2.21, and 2.46 *m* $NaClO_4$, respectively. The lower values of $\Delta\log_{10} K$ compared with the $\log_{10} K_{1.1.3}$ confirm that the coordination of the second Ca^{2+} towards the $CaUO_2(CO_3)_3^{2-}$ is more difficult than the first Ca^{2+} to $UO_2(CO_3)_3^{4-}$, as expected from electrostatic interactions. Moreover, it is noteworthy that the value of $\Delta\log_{10} K^{2.46\ m} = 1.65$, is slightly higher than that $\Delta\log_{10} K^{2.21\ m} = 1.55$.

Table III - 4 Formation constants $\log_{10} K_{n.1.3}$ derived from the rounded off to integer slopes in Fig. III - 2. Values of $\log_{10} \beta_{0.1.3}$ were calculated with $\log_{10} \beta^\circ_{0.1.3} = 21.84 \pm 0.20$ and $\Delta\varepsilon = -0.23$.[29] Stepwise binding constants $\Delta\log_{10} K$ were obtained by subtracting $\log_{10} K_{1.1.3}$ from $\log_{10} K_{2.1.3}$.

I_m (m)	$\log_{10} K_{1.1.3}$	$\log_{10} K_{2.1.3}$	$\log_{10} \beta_{0.1.3}$	$\log_{10} \beta_{1.1.3} + 16D_H$	$\log_{10} \beta_{2.1.3} + 24D_H$	$\Delta\log_{10} K$
0.10	3.56 ± 0.03	5.93 ± 0.03	21.86 ± 0.04	27.17 ± 0.05	30.42 ± 0.05	2.37
0.51	2.75 ± 0.02	4.66 ± 0.02	21.96 ± 0.04	27.52 ± 0.04	30.84 ± 0.04	1.91
1.05	2.51 ± 0.02	4.32 ± 0.03	22.08 ± 0.04	27.89 ± 0.05	31.34 ± 0.05	1.81
1.62	2.32 ± 0.01	4.03 ± 0.04	22.21 ± 0.04	28.09 ± 0.04	31.58 ± 0.05	1.71
2.21	2.15 ± 0.01	3.70 ± 0.02	22.35 ± 0.04	28.25 ± 0.04	31.68 ± 0.05	1.55
2.46	2.17 ± 0.02	3.82 ± 0.03	22.41 ± 0.04	28.38 ± 0.04	31.94 ± 0.05	1.65
3.50	1.88 ± 0.02	/	22.65 ± 0.04	28.52 ± 0.04	/	/

Specifically, the values of $\Delta\log_{10} K$ at 0.1, 0.5, and 1 *m* $NaClO_4$ can be compared with the corresponding ones in NaCl medium. In the most dilute supporting electrolyte (0.1 *m*), there is nearly no difference in results, $\Delta\log_{10} K^{0.1\ m} = 2.37$ in $NaClO_4$ compared to $\Delta\log_{10} K^{0.1\ m} = 2.43$ in NaCl. With increasing electrolyte concentration, the difference becomes evident: $\Delta\log_{10} K^{0.5\ m} = 1.91$ in $NaClO_4$ compared to $\Delta\log_{10} K^{0.5\ m} = 1.79$ in NaCl, and $\Delta\log_{10} K^{1.0\ m} = 1.81$ in $NaClO_4$ compared to $\Delta\log_{10} K^{1.0\ m} = 1.51$ in NaCl. This tendency indicates that the association between Ca^{2+} and $CaUO_2(CO_3)_3^{2-}$ is more likely to occur in $NaClO_4$ than in NaCl, since the values of $\Delta\log_{10} K$ are more important in $NaClO_4$.

The extrapolation of the cumulative constants to infinite dilution is shown in Fig. III - 3(a,b) with the variation of $\log_{10} \beta_{1.1.3} + 16D_H$ and $\log_{10} \beta_{2.1.3} + 24D_H$ *vs.* ionic strength in $NaClO_4$ medium (red circles). The cumulative formation constants, *i.e.* $\log_{10} \beta_{1.1.3}$ and $\log_{10} \beta_{2.1.3}$, were calculated by adding $\log_{10} \beta_{0.1.3}$ from Guillaumont, *et al.*[29] to either $\log_{10} K_{1.1.3}$ or $\log_{10} K_{2.1.3}$, with uncertainties determined by propagation of error – the values of $\log_{10} \beta_{0.1.3}$ at different I_m were calculated using the SIT approach and listed in Table III - 4. The linear relationships enable the evaluations of $\log_{10} \beta^\circ$ (intercept, $I_m = 0$) and $\Delta\varepsilon$ (slope) within the SIT framework. Systematically, propagation of errors is applied to assess the uncertainty range from infinite dilution up to 3 *m* $NaClO_4$. The resulting stability constants are $\log_{10} \beta^\circ_{1.1.3} = 27.26 \pm 0.08$ and $\log_{10} \beta^\circ_{2.1.3} = 30.53 \pm 0.12$; the Gibbs energies of reaction are $\Delta_r G^\circ_m(CaUO_2(CO_3)_3^{2-}) = -(155.601 \pm 0.457)$ kJ mol^{-1} and $\Delta_r G^\circ_m(Ca_2UO_2(CO_3)_3(aq)) = -(174.267 \pm 0.685)$ kJ mol^{-1}; and the Gibbs energies of formation are $\Delta_f G^\circ_m(CaUO_2(CO_3)_3^{2-}) = -(3\,244.658 \pm 2.394)$ kJ mol^{-1} and $\Delta_f G^\circ_m(CaUO_2(CO_3)_3(aq)) = -(3\,816.130 \pm 3.050)$ kJ mol^{-1}. These values are in excellent agreement with our previous work in NaCl[8] – see Table III - 5 and blue squares in Fig. III - 3(a,b) –, and with other literature data within uncertainty limits.[2,3,6,9,11]

Table III - 5 Gibbs energies of formation from the main species considered.

Species	$\Delta_f G^\circ_m$ kJ mol^{-1}	Ref.
H_2O	-237.140 ± 0.041	[29]
CO_2(g)	-394.373 ± 0.133	[29]
CO_3^{2-}	-527.900 ± 0.390	[29]
UO_2^{2+}	-952.551 ± 1.747	[29]
$UO_2(CO_3)_3^{4-}$	-2 660.914 ± 2.116	[29]
Ca^{2+}	-552.806 ± 1.050	[29]
$CaUO_2(CO_3)_3^{2-}$	-3 244.316 ± 2.361	[8]
	-3 244.658 ± 2.394	p.w.
	-3 244.430 ± 2.361	p.w. multilinear regression
$Ca_2UO_2(CO_3)_3$(aq)	-3 815.901 ± 2.985	[8]
	-3 816.130 ± 3.050	p.w.
	-3 816.015 ± 2.991	p.w. multilinear regression

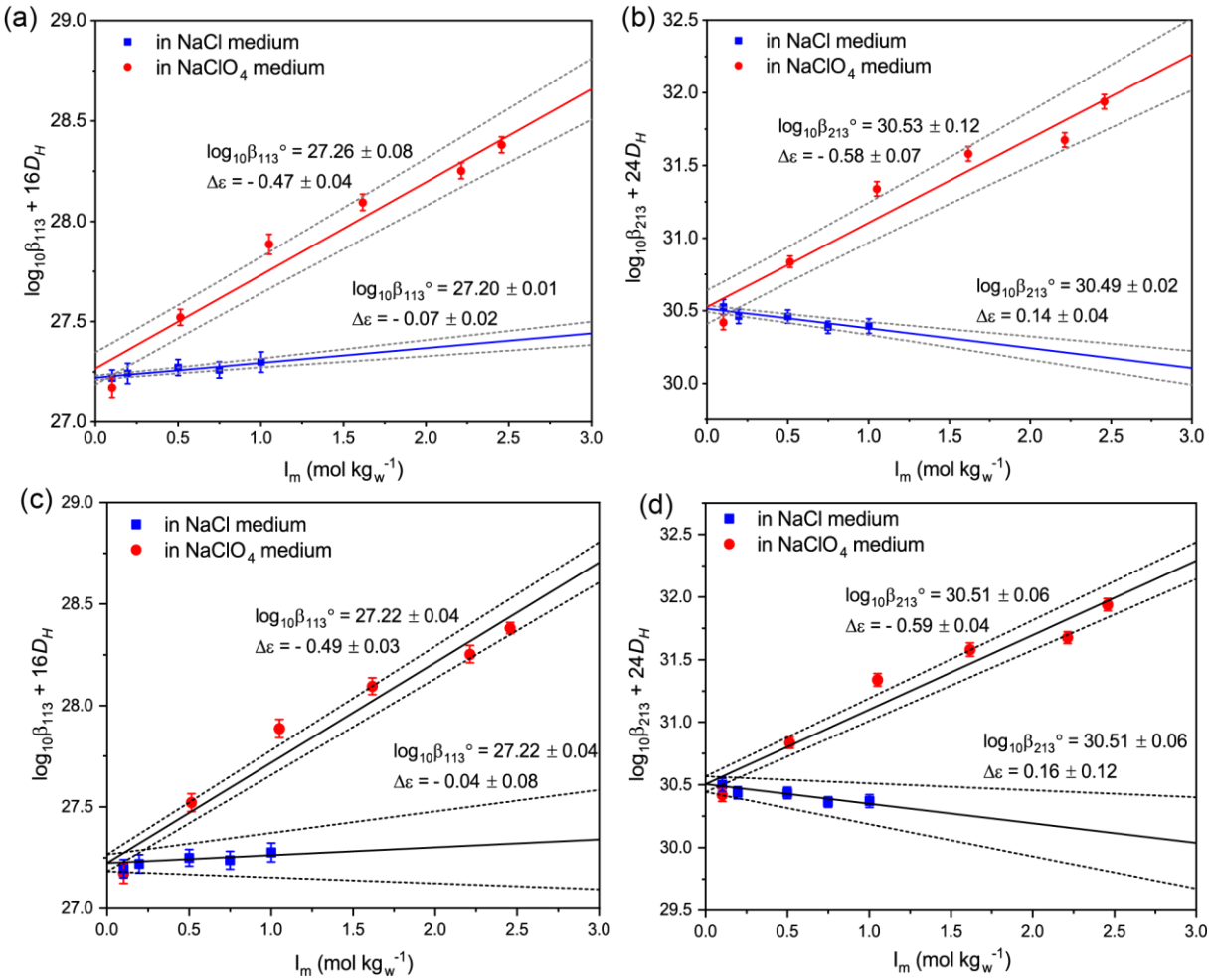

Fig. III - 3 Specific ion interaction theory extrapolation to infinite dilution of the experimental data of (a,c) $\log_{10}\beta_{1.1.3} + 16D_H$ and (b,d) $\log_{10}\beta_{2.1.3} + 24D_H$, for $CaUO_2(CO_3)_3^{2-}$ and $Ca_2UO_2(CO_3)_3(aq)$, respectively, as a function of molal ionic strength for different ionic media: NaCl data (blue squares) are from Shang and Reiller[8]; (a,b) extrapolation in individual ionic media (red line, present work; blue line from Shang and Reiller[8]); (c,d) multilinear regression of $NaClO_4$ and NaCl[8] data; dashed line are the propagation of errors from infinite dilution to 3 m, using the different regressions.

From the slope in Fig. III - 3 (a,b) and ε values in Table III - 2, the specific ion interaction coefficients are estimated to be $\varepsilon(CaUO_2(CO_3)_3^{2-},Na^+)$ = (0.02 ± 0.04) $kg_w\ mol^{-1}$ and $\varepsilon(Ca_2UO_2(CO_3)_3,NaClO_4)$ = (0.18 ± 0.07) $kg_w\ mol^{-1}$, which are somewhat different from the NaCl case.[8] This will be discussed afterwards.

4.2 Comparison and interpretation of $\log_{10}\beta^\circ$ and ε determined in NaCl and $NaClO_4$

The comparison of $\log_{10}\beta_{1.1.3} + 16D_H$ and $\log_{10}\beta_{2.1.3} + 24D_H$ *vs.* I_m in NaCl[8] – from our previous work using the same experimental method – and $NaClO_4$ in Fig. III - 3 shows that the $\log_{10}\beta^\circ_{n.1.3}$ values are so similar that a weighted average would give $\log_{10}\beta^\circ_{1.1.3}$ = 27.20 ± 0.01 and $\log_{10}\beta^\circ_{2.1.3}$ = 30.49 ± 0.01. A multilinear regression — as in Hummel, *et al.*[62] — is leading

to the plots in Fig. III - 3 (c,d) that give common $\log_{10} \beta^{\circ}_{n.1.3}$ values for NaCl and $NaClO_4$, and the ε values for the ionic media. The common values of $\log_{10} \beta^{\circ}_{1.1.3} = 27.22 \pm 0.04$ and $\log_{10} \beta^{\circ}_{2.1.3} = 30.51 \pm 0.06$ can be proposed.

The deduced values of $\varepsilon(CaUO_2(CO_3)_3^{2-},Na^+)$ and $\varepsilon(Ca_2UO_2(CO_3)_3(aq),NaX)$ – X being either ClO_4^- or Cl^- in all hypothesis – are summarized in Table III - 2. The sets of data were satisfactory fitted within the SIT framework. The stability constants at infinite dilution were virtually the same in both media, whatever the hypothesis considering the uncertainties. The increasing tendency of $\log_{10} \beta_{2.1.3} + 24D_H$ *vs.* I_m in $NaClO_4$ is comparable with that reported by Kalmykov and Choppin.[2] Conversely, the slopes that represents $-\Delta\varepsilon$, are different in NaCl and $NaClO_4$. The ion interaction parameters of the ternary complexes were determined from these values and the change of aqueous medium anion from Cl^- to ClO_4^- leads to a noticeable decrease in the values of ε for the same complex.

The variations of specific ion interaction coefficients do show some interesting patterns that are tightly related to ionic strength and inert medium. The discussion of inconsistencies in ε values for the same counter-ion in different background electrolyte can conveniently starts by examining the appropriateness of the SIT model to explain the observed evolution. The Debye-Hückel theory is basically a theory of weak interactions, considering the long-range interaction in dilute binary solutions between homogeneously charged spherical ions.[63] The specific ion-interaction contribution arises from an I_m-dependent second virial coefficient-type expression, originally proposed to account for the interactions between pairs of molecules for gases.[32,64] Nevertheless, ion association caused by ion-solvent and short-range interactions should not be ignored at high electrolyte concentrations. The enhanced formation of ion-pairs between Ca^{2+} and ClO_4^- or Cl^- could enhance the competition with the interaction between Ca^{2+} and $UO_2(CO_3)_3^{4-}$. In this respect, the binding processes of Ca^{2+} with structurally asymmetric $UO_2(CO_3)_3^{4-}$ group, calculated with theoretical methods,[65,66] are more complicated at higher I_m, because the less evenly distributed charges can distort and polarize the immediate electron cloud of $UO_2(CO_3)_3^{4-}$ that confronts the assumption of SIT.

The quantitative comparison of $\Delta\varepsilon$ in different media draws our attention to the relevant factors that influence the activity of calcium during coordination. In our studied systems, the existing binary interactions implicate Ca^{2+}-$UO_2(CO_3)_3^{4-}$, Na^+-$UO_2(CO_3)_3^{4-}$, Ca^{2+}-$CaUO_2(CO_3)_3^{2-}$, Na^+-$CaUO_2(CO_3)_3^{2-}$, and Ca^{2+}-ClO_4^-/Cl^-. Questions are raised about to which extent Na^+ is competitive to bind with $UO_2(CO_3)_3^{4-}$ and $CaUO_2(CO_3)_3^{2-}$compared with

Ca^{2+}, and whether Ca^{2+} is encumbered by the ion-pair formation with large anions. Li, *et al.*[31] examined the role of Na^+ on solvation of $UO_2(CO_3)_3^{4-}$ and $Ca_nUO_2(CO_3)_3^{(4-2n)-}$ by classical molecular dynamics simulations. They reported that the presence of Na^+ is capable of alternating the coordination number of uranyl moiety and probably resulting in changes of global charge for $UO_2(CO_3)_3^{4-}$ and $CaUO_2(CO_3)_3^{2-}$, but not likely to provoke a substitution from $CaUO_2(CO_3)_3^{2-}$ to $NaUO_2(CO_3)_3^{3-}$. They provided indication for the Na^+ influence on inner-sphere level of uranyl unit and shed light on its key role of common ions in formation processes of $Ca_nUO_2(CO_3)_3^{(4-2n)-}$.

Regarding the ion association of Ca^{2+}-ClO_4^-/Cl^-, SIPs are possibly the most predominant for Ca^{2+}-ClO_4^- at the investigated ionic strengths, as the inner hydration shell of Ca^{2+} was observed intact up to 6 *m* in the work of Rudolph and Irmer.[67] These authors also concluded that for Ca^{2+}-Cl^-, the ion association is slightly stronger than that of Ca^{2+}-ClO_4^-, which can contribute to an increasing amount of CIPs. These interactions cannot be discounted in treating experimental data obtained in concentrated solutions. The differences in $\Delta\varepsilon$ in NaCl and $NaClO_4$ may partly be explained by the ion triplet interactions of Na^+-Ca^{2+}-ClO_4^-/Cl^- that could reduce the activity of Ca^{2+} to different degrees depending on the kind of anion with increasing ionic strengths. It would be instructive to consider the Pitzer[64] model to calculate the activity coefficient for this intractable system. Unfortunately, the fitting parameters for the ion partners of the pairs, especially for the $UO_2(CO_3)_3^{4-}$ species, are not completely available. Even if estimations of $\beta^{(0)}$, $\beta^{(1)}$, and C^{Φ} have been proposed from SIT parameters,[68,69] the $\beta^{(2)}$ coefficient in Pitzer expression used to describe the ion pairing effects was questioned for its degree of sophistication.[70] Therefore, the effort to extend this method to higher I_m and acquire additional experimental data could be helpful. It would be interesting to perform measurements in a liquid medium supposed to be less complexing than ClO_4^- and exhibit weaker quenching effect than Cl^- – *e.g.*, sodium triflate.[71,72]

Another aspect concerning the affinity of Na^+ with $Ca_nUO_2(CO_3)_3^{(4-2n)-}$ can also make a distinction between $\Delta\varepsilon$ in NaCl and $NaClO_4$. In previous theoretical calculations, the close-by Na^+ was suggested to indirectly interact with $Ca_nUO_2(CO_3)_3^{(4-2n)-}$, which may result in alternation of global apparent charge of the ternary complexes. The complex-forming tendencies could give rise to the formation of $Na[Ca_2UO_2(CO_3)_3]^+$ under high I_m conditions.[33]

Ciavatta[73] stressed the role of water molecules rearrangements in solvation sphere during complexation for interpreting chemical behaviour of metal ions at high ionic strengths. By

comparing the interaction coefficients of a series of metal ions in several common salts, it was stated that the values of ε between oppositely charged ions usually have lower values if the ion partners are of similar size, because of the more easily occurred desolvation in both hydration shells, and further facilitated association between them. Considering its larger size, ClO_4^- should be more likely to interact than Cl^- with a potentially large-sized $Na[Ca_2UO_2(CO_3)_3]^+$ species. The comparison of ε values well supports the hypothesis that the interaction between the $Ca_nUO_2(CO_3)_3^{(4-2n)-}$ and background electrolyte ions is likely impacted by the integration of Na^+ implying that the neutral or positively charged quaternary complexes would more likely interact with the increasing concentrations of medium anions rather than with alkali cations. Otherwise, the interaction coefficients determined respectively in NaCl and $NaClO_4$ solutions should not significantly differ from each other. Nevertheless, there is a need of more direct evidences, *e.g.* based on charge determinations.

4.3 Evolution of spectral- and temporal-luminescence parameters

The evolutions of emission spectra of aqueous Ca-UO_2-CO_3 ternary species are illustrated in Fig. III - 1. The spectra were decomposed using a Gaussian distribution function. As already observed for the NaCl electrolyte, no apparent shift in peak positions was observed in $NaClO_4$ using the 300 lines mm^{-1} grid. Moreover, the relatively high ionic strength in the case of I_m = 3.5 *m* $NaClO_4$ did not induce any shift in wavelength. Peak maxima were determined at 464.4 ± 0.7 nm, 483.6 ± 0.7 nm, 503.8 ± 1.1 nm, 525.4 ± 1.9 nm, and 547.9 ± 4.9 nm (2σ) by averaging all peak maxima of 114 sample spectra, and agree well with literature values.[2,3,6,8] The luminescence of the triscarbonatouranyl corresponds to transitions from non-bonding 5f orbitals of uranium to a mixed orbital with uranyl-σ (5f, 6d) and oxygen-2p character.[74,75] The energy levels of the excited and ground states are almost insensitive – at least at the resolution of the apparatus using the 300 lines mm^{-1} grid, which gives a difference of 0.2 nm between each pixel of the camera – to the presence of calcium located out of the first coordination sphere, composed of three bidentate carbonate ligands.[15]

In order to probe the role of long-range solvent anions and examine the effects of electrolyte concentration, a comparison of several normalized emission spectra is shown in Fig. III - 4. The species percentages of sample solution were calculated using the $\log_{10}\beta^\circ$ and ε determined in this work for $NaClO_4$ medium and the results determined in our earlier work for NaCl medium.[8] Four solutions that contain nearly identical composition in binary/ternary species are selected from test samples prepared at I_m = 0.1 *m* NaCl/$NaClO_4$ and 1 *m* NaCl/1.05 *m* $NaClO_4$. As shown

in Fig. III - 4, the normalized spectra display mostly the same profile in the entire acquisition range when the composition of aqueous solutions are nearly identical. This observation indicates that the principle spectral parameters are mainly determined by the proportion of aqueous binary/ternary species and not affected by the type or the concentration of solvent anion – at least at the resolution of the spectroscopic set-up.

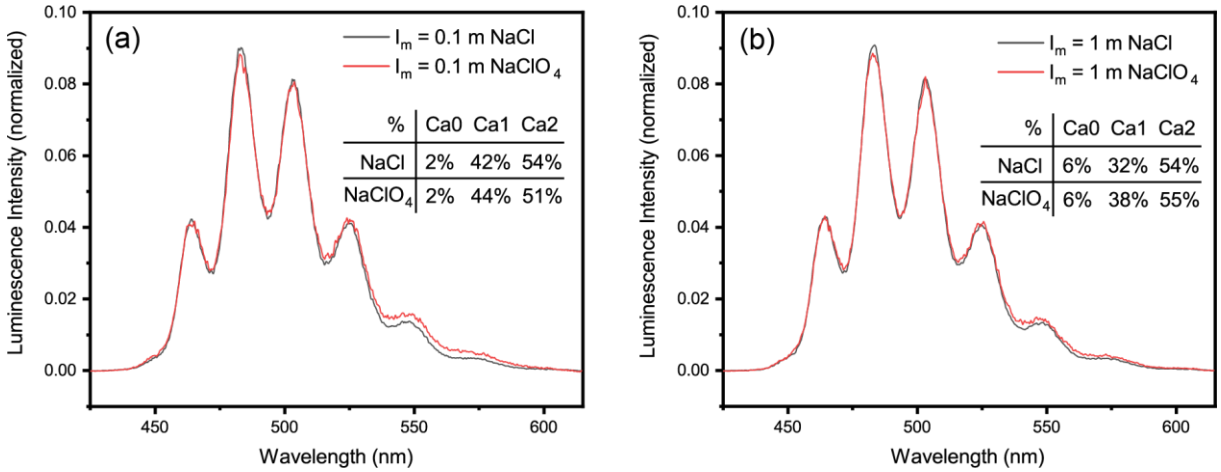

Fig. III - 4 Luminescence emission spectra normalized to the same area at D = 25 ns, W = 1 μs of binary and ternary species at (a) I_m = 0.1 m, and (b) I_m = 1 m. Ca0, Ca1 and Ca2 stand for $UO_2(CO_3)_3^{4-}$, $CaUO_2(CO_3)_3^{2-}$, $Ca_2UO_2(CO_3)_3(aq)$, respectively.

Fig. III - 5 shows normalized spectra of chosen samples of equal calcium concentration (*ca.* 6×10^{-3} *m*) at increasing ionic strengths from 0.1 to 2.46 *m* $NaClO_4$. The Gaussian-peak shape was used to fit the emission bands with Levenberg-Marquardt method and to perform the spectrum decomposition. As expected, the increase of I_m hinders the complexation of calcium and results in a decrease of the proportion of aqueous calcium(II)triscarbonatouranyl(VI) complexes. Table III - 6 lists the percentages of major U(VI) complexes in selected solutions. Subtle spectral differences have been observed when comparing these spectra. The dicalcium(II) complex contributes to better resolved spectra and narrower peak widths than the monocalcium(II)triscarbonatouranyl(VI) complex, as observed elsewhere,[3,6] and also in our previous work in NaCl medium.[8] In particular, the ratio of maximum heights between the second (*ca.* 484 nm) and the third peak (*ca.* 504 nm) varies as a function of complexed calcium concentration, as illustrated in Fig. III - 6. These two peaks represent the luminescence transitions from the lowest triplet excited state (10) to different vibrational levels of singlet ground state (0υ), with υ = 0 for the peak *ca.* 484 nm and υ = 1 for *ca.* 504 nm.[76,77] The decreasing trend of ratio values, though relatively weak, suggests that the 483.6 nm peak (10 → 00 at 20,680 cm^{-1}) is more sensitive to the calcium complexation than the 503.8 nm (10 →

01 at 19,850 cm^{-1}) peak. The vibronic frequency corresponding to the symmetrical U-O stretching mode can be determined from the difference in energy between the 10 → 0υ (υ = 0—3, 483.6 nm, 503.8 nm, 525.4 nm, 547.9 nm) transitions, and was found to be about 810 ± 19 cm^{-1} which is in good accordance with the symmetrical stretching υ_s values measured by Raman/IR spectroscopies.[78]

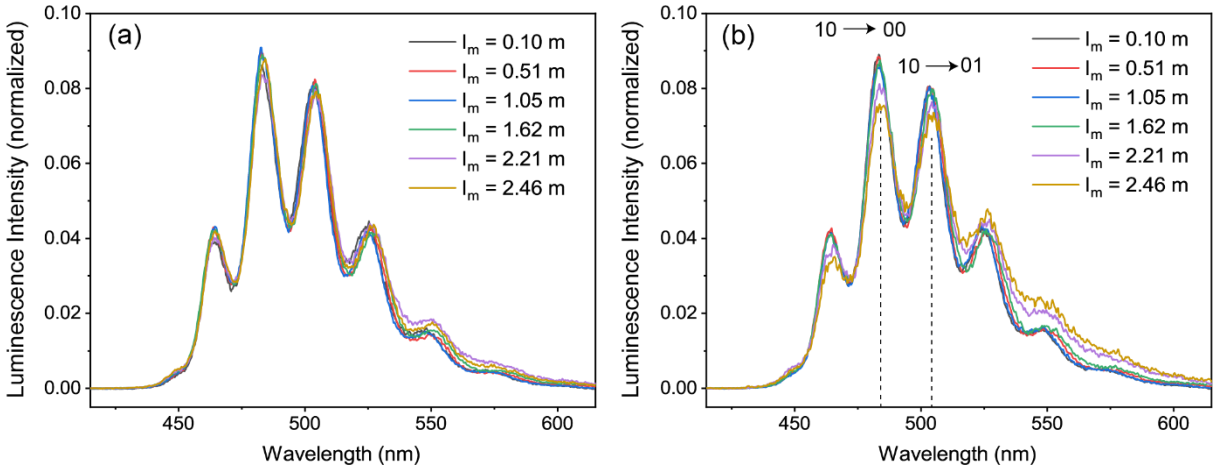

Fig. III - 5 Luminescence emission spectra normalized to the same area at D = 25 ns of Ca-UO_2-CO_3 species: the aqueous compositions are listed in Table III - 6; (a) the sample solutions having the similar composition are specifically selected at different ionic strengths; (b) the Ca(II) concentration is fixed at 6 ×10^{-3} m; the variation of spectral feature vs. ionic strength was shown in Fig. III - 6.

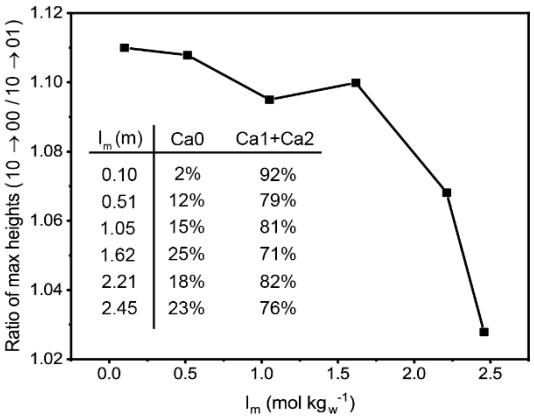

Fig. III - 6 Maximum heights of the peaks of 10⟶00 (484 nm) and 10⟶01 (503 nm) transitions are obtained from the spectra in Fig. 5 (b) using Gaussian decomposition: Ca0, Ca1+Ca2 stand for $UO_2(CO_3)_3^{4-}$, the sum of $CaUO_2(CO_3)_3^{2-}$, $Ca_2UO_2(CO_3)_3(aq)$, respectively.

Table III - 6 Aqueous composition in binary/ternary species for specifically selected sample solutions, of which luminescence emission spectra are shown in Fig. III - 5.

	$UO_2(CO_3)_3^{4-}$		$CaUO_2(CO_3)_3^{2-}$		$Ca_2UO_2(CO_3)_3(aq)$	
I_m (m)	(a)	(b)	(a)	(b)	(a)	(b)
0.10	2%	2%	43%	37%	50%	55%
0.51	7%	12%	42%	50%	42%	29%
1.05	6%	15%	31%	51%	42%	30%
1.62	8%	25%	38%	45%	48%	26%
2.21	8%	18%	35%	66%	44%	16%
2.46	9%	23%	36%	66%	41%	10%

The decay-times of $CaUO_2(CO_3)_3^{2-}$ and $Ca_2UO_2(CO_3)_3(aq)$ are respectively assessed by averaging the measured decay-times of the sample solutions giving the slopes of 1 and 2 (Fig. III - 2). Whereas the decay-time of $UO_2(CO_3)_3^{4-}$ is evaluated by measuring the sample prepared at [U(VI)] = 50 μ*m*, pH = 9 and $P(CO_2) = 10^{-3.5}$ atm at each ionic strength. The exact values of the three species are listed in Table III - S4. Contrary to the series of NaCl medium,[8] where the intensity decay curves were fitted by mono-exponential function, two exponential functions containing two sets of parameters, *i.e.* intensities FI_1, FI_2 and decay-times τ_1, τ_2, fit much better the sets of experimental data in $NaClO_4$ series. A typical example of the decay-time analysis is presented in Fig. III - 7. The more parametric bi-exponential function yields two decay-times of which the fast decay one (5.68 ns) has a very high initial fluorescence intensity (1.19×10^9 counts) governing the total *FI* in short delay times (D < 25 ns) and the slow decay one have similar results as the mono-exponential fitting. It was verified *a posteriori* that in all bi-exponential fitting cases, one of the two components always have a much shorter decay-time and a higher initial intensity compared to the other one. However, the contribution of the fast decay component is nearly negligible (below 10%) and is only due to one data point at low delay after the laser flash – *D* = 25 ns. Thus, this fast-decay component is possibly an artefact in the acquisition process and should not be considered as a meaningful species in the decay-time analysis. The estimation for decay-times of the studied species is consequently based on single exponential decay fit in this study.

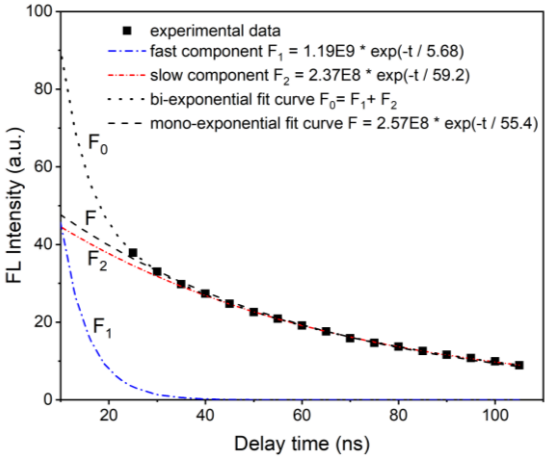

Fig. III - 7 Mono-exponential and bi-exponential fits of luminescence intensity decay of Ca-UO_2-CO_3 complexes at [U(VI)] = 50 µm, $log_{10}[Ca^{2+}]$ = -1.88, pH = 7.48 and I_m = 1.05 m $NaClO_4$.

Fig. III - 8 shows the decay-time variations of (Ca-)UO_2-CO_3 complexes over the ionic strength range of 0.1 to 2.46 *m* $NaClO_4$. For the ternary species, the decay-time measurements present slight fluctuations within the applied ionic strength up to 2.21 *m* $NaClO_4$ and an increase at I_m = 2.46 *m* $NaClO_4$, whereas the variation of $UO_2(CO_3)_3^{4-}$ is very weak in the entire I_m range. The decay-time $\tau(UO_2(CO_3)_3^{4-})$ = (10.0 ± 1.0) ns is finally assessed by averaging the measured decay-times at 0.10 to 2.46 *m* $NaClO_4$. The value of $\tau(CaUO_2(CO_3)_3^{2-})$ and $\tau(Ca_2UO_2(CO_3)_3(aq))$ are determined to be (34.20 ± 2.24) ns and (59.21 ± 4.15) ns, respectively, excluding the values measured at 2.46 *m* $NaClO_4$.

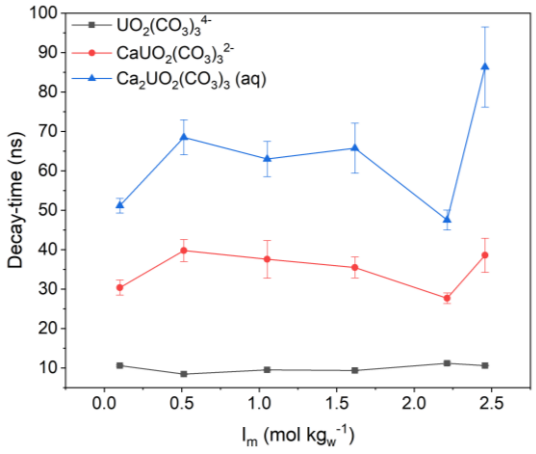

Fig. III - 8 Averaged decay-times of sample solutions giving the slopes of 1 (red circles) and 2 (blue triangles) at investigated $NaClO_4$ ionic strengths; the values for $UO_2(CO_3)_3^{4-}$ complex are decay-times of the sample prepared at [U(VI)] = 50 µm, pH = 9 and $P(CO_2)$ = $10^{-3.5}$ atm at each I_m; the error bars of $UO_2(CO_3)_3^{4-}$ are too small to be shown; Exact values are listed in Table III - S4 of the SI.

In our previous study,[8] the suppression of decay-times was evident with increasing concentration of electrolyte NaCl due to the quenching effect of chloride. The values of τ measured at I_m = 0.1 *m* NaCl – *i.e.* $\tau(UO_2(CO_3)_3^{4-})$ = (11.04 ± 0.11) ns, $\tau(CaUO_2(CO_3)_3^{2-})$ = (28.30 ± 0.57) ns, and $\tau(Ca_2UO_2(CO_3)_3(aq))$ = (46.7 ± 2.7) ns – are somewhat comparable with the averaged results in this study.[8] Particularly, the moderately longer decay-times of $CaUO_2(CO_3)_3^{2-}$ and $Ca_2UO_2(CO_3)_3(aq)$ (several nanoseconds) determined to be (30.41 ± 1.90) ns and (51.19 ± 1.94) ns at I_m = 0.1 *m* $NaClO_4$ provide evidences of less quenched luminescent properties of Ca(II)-bound species by ClO_4^- than Cl^-. Nonetheless, the possible quenching effect of ClO_4^- was not avoided at higher $NaClO_4$ concentrations in this study, supported by the non-presence of the second slope of 2 at I_m = 3.5 *m* $NaClO_4$.

4.4 Implications of luminescence behaviour at I_m = 3.50 m $NaClO_4$ for quenching effect

Fig. III - S1 of the SI shows the slope analysis at I_m = 3.50 *m*. Although the calcium concentrations are considered sufficient for the second complexation to occur, only the slope of 1 is obtained using the least-squares adjustment to our data. In the predominance plot (Fig. III - S2 of the SI), the test samples (red square) at the end of complexation could be affected by the onset of calcite precipitation, induced by the practical failure of fixing the pH values overly close to the steep plunge of pH near the neutral zone. One can note that 17 sample solutions have primarily satisfied the formation conditions of $Ca_2UO_2(CO_3)_3(aq)$ in terms of calcium concentration and pH value. A striking fact is that the 13 experimental points giving the slope of one are all found set in the predominance region of $Ca_2UO_2(CO_3)_3(aq)$. In addition, the last three points in slope analysis seem to reach a plateau in terms of intensity (Fig S1 in the SI), while the decay-times increased with the addition of Ca^{2+}. For this reason, the intercept value obtained at I_m = 3.50 *m* was not taken in the evaluation of $\log_{10} \beta^\circ$ and ε. Nevertheless, the resulting constant would be included as an indicative point in the fits using different predictive models in an extended range of I_m in the next section.

Regarding the question of quenching effect of perchlorate ions, the research to date has mostly been focused on the spectral and temporal behaviours of the aqueous uranyl ions in $HClO_4/NaClO_4$ environment.[51,52,71] It was reported that the decay-time of UO_2^{2+} depends significantly on the acidity and perchlorate concentration. The increase of $[ClO_4^-]$ would lead to a decrease of decay-time at constant pH value, while the increase of acidity would contribute to longer decay-times of UO_2^{2+} except at very high concentration of $HClO_4$ (> 10 M).[71] In the work of Rustenholz *et al.*[52] the concomitantly decreasing trends of fluorescence intensity and

decay-time were observed for the uranyl ion when increasing perchlorate concentration at the same [H^+]. Interestingly, the decreases of fluorescence parameters *FI* and τ, both exhibit an obvious steep at [ClO_4^-] = 2.75 M, *i.e.* 3.14 *m*.[79] The discussion on these results typically examines the quality of fit by chemical- or physical-based models. However, the conclusions in literature also could seem arguable to apply directly to the Ca-UO_2-CO_3 system since the published research mainly focuses on free uranyl ions in an extremely acid environment in which the perchlorate ion approaches closer to the UO_2^{2+} central entity. The present luminescence results for $Ca_nUO_2(CO_3)_3^{(4-2n)-}$ (n = {0; 1; 2}) does not sit on a sufficiently wide basis of evidence to justify the impact of aqueous acidity. The quenching effect of ClO_4^- still remains as a plausible reasoning for interpreting the different variations of *FI* and τ observed at I_m = 3.50 *m* $NaClO_4$, even though its influence on U(VI) luminescence behaviour might be very subtle due to the protection of three carbonates around the uranyl moiety.

As shown in Fig. III - 8, the invariance of $UO_2(CO_3)_3^{4-}$ decay-time *ca.* 10 ns *vs.* I_m provides evidence for its insensitivity of deexcitation processes to the [ClO_4^-]. For the ternary species, the decay-time of $Ca_2UO_2(CO_3)_3$(aq) manifests higher increasing tendency than $CaUO_2(CO_3)_3^{2-}$ at I_m = 2.46 *m* $NaClO_4$. We could infer that under mildly alkaline environment (pH = 9), luminescence properties of the large negative ion $UO_2(CO_3)_3^{4-}$, caged by Na^+ in its surrounding environment and undergoing repelling forces with ClO_4^-, is less likely to be affected by ClO_4^-. In the presence of calcium, the earlier mentioned hypothesis that the affinity of Na^+ is capable of altering the global apparent charge seems to reconcile with our experimental results and should be reconsidered in the light of molecular dynamics modelling.[31,33]

A case in point is proposed formation of the positively like-charged $Na[Ca_2UO_2(CO_3)_3]^+$. If occurring, the effective distance between aqueous U(VI) complexes and ClO_4^- would be shortened due to the attractive force between them. This could give the reason for the experimental observations that the quenching effect of ClO_4^- started to be noticeable at high I_m. As illustrated in Fig. III - S1 of the SI, the suppression of fluorescence intensity is more evident than decay-time on addition of $Ca(ClO_4)_2$ into the system of I_m= 3.5 *m* to the extent that the intensity levelled off and the second slope no longer appeared, but meanwhile the decay-times showed a continuous increase. It is thus suggested that the quenching effect of ClO_4^- is more effective in diminishing fluorescence intensity than decay-time.

4.5 Description of equilibrium constants variation by different models

Using our newly determined constants and parameters ($\log_{10}\beta^{\circ}$ and ε), the predominance diagrams at studied ionic strengths are constructed using PhreePlot[80] – which is including the program PhreeqC[81,82] that contains the ThermoChimie database,[83] developed for SIT ionic strength correction. Fig. III - 9 depicts the distribution of experimental points on the [Ca]-pH plan of each series. The equilibrium between the atmospheric CO_2(g) ($P(CO_2) = 10^{-3.5}$ atm) and the aqueous solution is calculated to identify the precipitation region of calcite, imposed by the black dashed line. It seems evident that the increase of ionic strength enlarges the predominance domain of $UO_2(CO_3)_3^{4-}$ and narrows those of the ternary and polynuclear complexes – $CaUO_2(CO_3)_3^{2-}$, $Ca_2UO_2(CO_3)_3$(aq), and $(UO_2)_2CO_3(OH)_3^-$ – illustrating the hindrance of ionic strength to the formation the calcium(II)triscarbonatouranyl(VI) complex. The domain limits are reflecting the experimental results. Nevertheless, it should be noted that at relatively high electrolyte concentrations (from 1.05 to 2.46 *m* $NaClO_4$), the sample solutions giving the desired slopes cross the boundaries to some extent at the beginning of complexation.

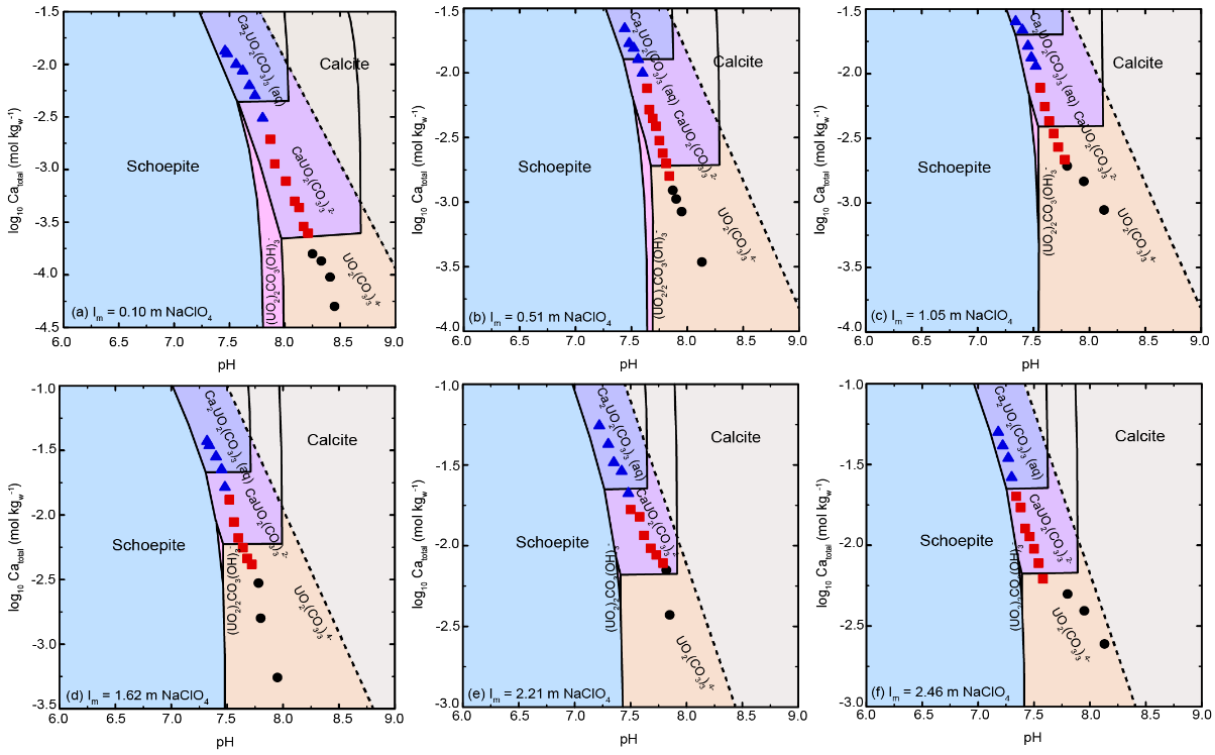

Fig. III - 9 Predominance plots obtained using PHREEPLOT[80] of Ca-UO_2-CO_3 system at [U(VI)] = 50 µm, $P(CO_2) = 10^{-3.5}$ atm at ionic strength from 0.1 to 2.46 m $NaClO_4$: experimental points giving slopes of 1 and 2 are highlighted with red squares and blue triangles, respectively; the black circles represent the beginning of titration where the binary complex dominates; dashed lines represents the line of predominance between Ca^{2+} and calcite.

This differences between simulations and experimental results may suggest the possible variation of ε as a function of ionic strength, since the specific ion interaction coefficients, implemented in the ThermoChimie database, are taken as invariable up to the upper limit of validity of the SIT approach, *ca.* I_m = 3-4 *m*, in the PhreeqC calculations. The back extrapolation from infinite dilution using $\log_{10} \beta^\circ_{n.1.3}$ and constant ε to deduce $\log_{10} \beta_{n.1.3}$ at specific ionic strengths could be questioned for high I_m situations. Several modified models based on the SIT approach are applied to better represent our experimental data and examine the dependence of interaction coefficients on ionic strength. The fit results of the one-parameter SIT model are compared with those of two-parameter models in Fig. III - 10. Considering the significant suppression in terms of fluorescence intensity at I_m = 3.50 *m*, only the conditional formation constants determined in the range of 0.1 to 2.46 *m* are fitted to the models. The relationships used to fit the data set are expressed as follows:

$$\varepsilon(j, k, I_m)\ m_k = \varepsilon I_m - \log_{10}(1 + K I_m) \quad \text{(III - 9)}$$

$$\varepsilon(j, k, I_m) = \varepsilon_\infty + \frac{\varepsilon_0 - \varepsilon_\infty}{I_m + 1} \quad \text{(III - 10)}$$

$$\varepsilon(j, k, I_m) = \varepsilon_1 + \varepsilon_2 \log_{10} I_m \quad \text{(III - 11)}$$

where Eq. III - 9 and Eq. III - 10 are reported by Bretti and co-workers,[84,85] and Eq. III - 11 is proposed by Ciavatta,[73] and also reported in *e.g.* Guillaumont et al.[29] and used by Brown and Ekberg.[86]

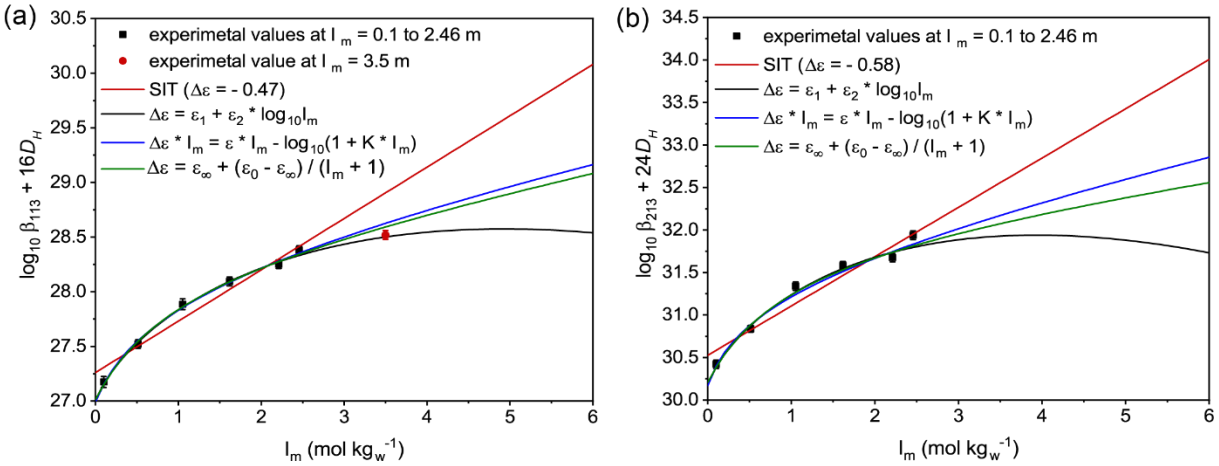

Fig. III - 10 Fits of experimental data (a) $\log_{10} \beta_{113} + 16D_H$ and (b) $\log_{10} \beta_{213} + 24D_H$ by different models and extrapolation to 6 m.

Table III - 7 summarizes the results of fitting parameters in different models. The inspection of individual parameters shows no obvious incorrectness and the residual sum-of-squares (*RSS*) is reasonably lower than that of one-parameter SIT model. The convergence of model fitting is

finally attained even with the limitation of number of experimental points. It is therefore suggested that the new parameters in two-parameter models are viable to generate trend lines for current data to higher ionic strengths. With the mainly illustrative purpose, the range of electrolyte concentration is extended to 6 *m*, at which the use of two-parameter model has been proven compatible with the traditional one-parameter SIT model for classical 1:1 type electrolytes.[85] One can observe that no important inconsistencies are identified over the ionic strength from 0.1 to 2.46 *m*. The general trend can be well fitted by the one-parameter SIT model over this range, but the quality of the fit is degraded compared to the two-parameter models. In a larger range of ionic strength up to 6 *m*, the difference between the two models proposed by Bretti, *et al.*,[84,85] is almost negligible. In their papers, this approximation was also verified and considered acceptable within a certain electrolyte concentration. However, the difference between the model proposed by Ciavatta[73] and the simplified SIT equation increases considerably for ionic strength above 3 *m*. The dependence of ion interaction coefficient on ionic strength would give rise to more significant differences in resulting conditional stability constants at higher electrolyte concentration.

Table III - 7 Parameter values by fitting the experimental results at ionic strengths from 0.1 to 2.46 m $NaClO_4$ to the models under consideration.

Ref.	SIT Eq. III - 4				Ciavatta[73] Eq. III - 11			
	$\log_{10}\beta°_{n.1.3}$	$\Delta\varepsilon(NaClO_4)$		*RSS**	$\log_{10}\beta°_{n.1.3}$	ε_1	ε_2	*RSS**
$CaUO_2(CO_3)_3^{2-}$	27.26 ± 0.08	-0.47 ± 0.04		19.97	27.02 ± 0.05	-0.81 ± 0.06	0.67 ± 0.12	1.86
$Ca_2UO_2(CO_3)_3(aq)$	30.53 ± 0.12	-0.58 ± 0.07		40.10	30.21 ± 0.13	-1.03 ± 0.16	0.92 ± 0.32	10.42
	SIT multilinear							
	$\log_{10}\beta°_{n.1.3}$	$\Delta\varepsilon(NaClO_4)$	$\Delta\varepsilon(NaCl)$					
$CaUO_2(CO_3)_3^{2-}$	27.22 ± 0.04	-0.49 ± 0.03	-0.04 ± 0.02					
$Ca_2UO_2(CO_3)_3(aq)$	30.51 ± 0.06	-0.59 ± 0.04	0.16 ± 0.12					
Ref.	Bretti *et al.*[84] Eq. III - 9				Bretti *et al.*[85] Eq. III - 10			
	$\log_{10}\beta°_{n.1.3}$	ε	*K*	*RSS**	$\log_{10}\beta°_{n.1.3}$	ε_0	ε_∞	*RSS**
$CaUO_2(CO_3)_3^{2-}$	27.02 ± 0.07	-0.14 ± 0.03	3.63 ± 1.18	2.00	27.03 ± 0.05	-1.40 ± 0.17	-0.19 ± 0.05	1.76
$Ca_2UO_2(CO_3)_3(aq)$	30.18 ± 0.21	-0.21 ± 0.08	5.78 ± 4.71	11.79	30.23 ± 0.12	-1.83 ± 0.43	-0.19 ± 0.14	10.40

* Residual Sum of Square RSS = $\sum_{i=1}^{n} w_i(y_i - \hat{y}_i)^2$, with $w_i = 1/\sigma^2$. The values of σ_i are the uncertainties associated with $\log_{10}\beta_{1.1.3} + 16D_H$ for $CaUO_2(CO_3)_3^{2-}$, $\log_{10}\beta_{2.1.3} + 24D_H$ for $Ca_2UO_2(CO_3)_3(aq)$ in Table III - 4 and $\hat{y}_i$ are estimated values by weighted least squares regression for the datasets (I_m, $\log_{10}\beta_{1.1.3} + 16D_H$ /$\log_{10}\beta_{2.1.3} + 24D_H$).

Concerning the residual sum-of-squares, generally used to quantify the goodness-of-fit, it is shown that the two-parameter models fit the same data set better than the linear model. Typically, multi-parametric nonlinear regressions give more flexibility to the curve fitting and

thus cover the data better than one-parameter model, which generates a linear trend. Therefore, the goodness-of-fit, estimated by the sum of squares of distances between the data points and the best fit curvature, is naturally and technically better in more complicated models than that in the simpler model.[87] To discriminate one model from another among the current two-parameter models, the value of $\log_{10} \beta_{1.1.3}$ determined at I_m = 3.50 *m* is added in the figure to help predicting and choosing the best trend line. It appears that the model proposed by Ciavatta better describes the data.[73] Nonetheless, there is a possibility that the value of $\log_{10} \beta_{1.1.3}$ has been somewhat underestimated, because of the unclear quenching mechanisms at this ionic strength. This is also the reason why we did not take this value into the evaluations of $\log_{10} \beta°$ and ε. It seems now possible to state that the model constructed by Bretti, *et al.*[84,85] could serve as a trade-off between the one-parameter SIT model and that of Ciavatta.[73]

III - 5 Conclusion

The stability constants $\log_{10} \beta°$ and specific ion interaction coefficients ε were evaluated for $CaUO_2(CO_3)_3^{2-}$ and $Ca_2UO_2(CO_3)_3(aq)$ in $NaClO_4$ by extrapolating the experimentally measured $\log_{10} K_{n.1.3}$ at I_m = 0.1 to 2.46 *m* to infinite dilution using the specific ion interaction theory. The use of $NaClO_4$ as inert electrolyte allowed the measurements of $UO_2(CO_3)_3^{4-}$ luminescence signal over an extended range of ionic strength, compared to our previous study of NaCl medium suffering from strong quenching effect above 1 *m*.[8] However, suppression of luminescence intensity was obvious at high $[ClO_4^-]$ *ca.* 3.50 *m* in experiments, which suggests quenching effect. The values of $\varepsilon(CaUO_2(CO_3)_3^{2-},Na^+)$ and $\varepsilon(Ca_2UO_2(CO_3)_3(aq),NaClO_4)$ differ greatly from those measured in NaCl, while the resulting $\log_{10} \beta°_{n.1.3}$ interestingly agree with previous values. The discussions of ion-pairing formations and quenching effect of ClO_4^- both suggest the need for careful considerations of the affinity of Na^+ with $Ca_nUO_2(CO_3)_3^{(4-2n)-}$ ($n = \{1; 2\}$) at high ionic strengths. Several models were tested to describe the trending of experimental data with varying ε as a function of I_m. A reliable prediction of thermodynamic constants could be done up to 3 *m*.

Acknowledgments

This work was financed by CEA and ONDRAF-NIRAS (contract DEN4857-CCHO 2018-0456/00/00). Dr. Hélène Isnard is acknowledged for her help in the dissolution of U_3O_8.

III - 6 References

1. G. Bernhard, G. Geipel, V. Brendler and H. Nitsche, *Radiochim. Acta*, 1996, **74**, 87-91.

2. S. N. Kalmykov and G. R. Choppin, *Radiochim. Acta*, 2000, **88**, 603-606.
3. G. Bernhard, G. Geipel, T. Reich, V. Brendler, S. Amayri and H. Nitsche, *Radiochim. Acta*, 2001, **89**, 511-518.
4. G. Geipel, S. Amayri and G. Bernhard, *Spectrochim. Acta. Part A*, 2008, **71**, 53-58.
5. C. Götz, G. Geipel and G. Bernhard, *J. Radioanal. Nucl. Chem.*, 2010, **287**, 961-969.
6. J. Y. Lee and J.-I. Yun, *Dalton Trans.*, 2013, **42**, 9862-9869.
7. J. Y. Lee, M. Vespa, X. Gaona, K. Dardenne, J. Rothe, T. Rabung, M. Altmaier and J.-I. Yun, *Radiochim. Acta*, 2017, **105**.
8. C. Shang and P. E. Reiller, *Dalton Trans.*, 2020, **49**, 466-481.
9. W. M. Dong and S. C. Brooks, *Environ. Sci. Technol.*, 2006, **40**, 4689-4695.
10. W. Dong and S. C. Brooks, *Environ. Sci. Technol.*, 2008, **42**, 1979-1983.
11. F. Endrizzi and L. F. Rao, *Chem.-Eur. J.*, 2014, **20**, 14499-14506.
12. Y. Jo, A. Kirishima, S. Kimuro, H.-K. Kim and J.-I. Yun, *Dalton Trans.*, 2019, **48**, 6942-6950.
13. S. D. Kelly, K. M. Kemner and S. C. Brooks, *Geochim. Cosmochim Acta*, 2007, **71**, 821-834.
14. M. Maloubier, P. L. Solari, P. Moisy, M. Monfort, C. Den Auwer and C. Moulin, *Dalton Trans.*, 2015, **44**, 5417-5427.
15. S. Amayri, T. Reich, T. Arnold, G. Geipel and G. Bernhard, *J. Solid State Chem.*, 2005, **178**, 567-577.
16. J. Wan, T. K. Tokunaga, E. Brodie, Z. Wang, Z. Zheng, D. Herman, T. C. Hazen, M. K. Firestone and S. R. Sutton, *Environ. Sci. Technol.*, 2005, **39**, 6162-6169.
17. S. C. Brooks, J. K. Fredrickson, S. L. Carroll, D. W. Kennedy, J. M. Zachara, A. E. Plymale, S. D. Kelly, K. M. Kemner and S. Fendorf, *Environ. Sci. Technol.*, 2003, **37**, 1850-1858.
18. G. P. Curtis, P. Fox, M. Kohler and J. A. Davis, *Appl. Geochem.*, 2004, **19**, 1643-1653.
19. E. El Hayek, C. Torres, L. Rodriguez-Freire, J. M. Blake, C. L. De Vore, A. J. Brearley, M. N. Spilde, S. Cabaniss, A.-M. S. Ali and J. M. Cerrato, *Environ. Sci. Technol.*, 2018, **52**, 13089-13098.
20. M. H. Bradbury and B. Baeyens, *Appl. Clay Sci.*, 2011, **52**, 27-33.
21. M. Marques Fernandes, N. Vér and B. Baeyens, *Appl. Geochem.*, 2015, **59**, 189-199.
22. O. Prat, T. Vercouter, E. Ansoborlo, P. Fichet, P. Perret, P. Kurttio and L. Salonen, *Environ. Sci. Technol.*, 2009, **43**, 3941-3946.
23. W. M. Dong, W. P. Ball, C. X. Liu, Z. M. Wang, A. T. Stone, J. Bai and J. M. Zachara, *Environ. Sci. Technol.*, 2005, **39**, 7949-7955.
24. Z. M. Wang, J. M. Zachara, W. Yantasee, P. L. Gassman, C. X. Liu and A. G. Joly, *Environ. Sci. Technol.*, 2004, **38**, 5591-5597.
25. Z. M. Wang, J. M. Zachara, P. L. Gassman, C. X. Liu, O. Qafoku, W. Yantasee and J. G. Catalano, *Geochim. Cosmochim Acta*, 2005, **69**, 1391-1403.
26. Z. Wang, J. M. Zachara, J. P. McKinley and S. C. Smith, *Environ. Sci. Technol.*, 2005, **39**, 2651-2659.
27. C. Liu, J. M. Zachara, O. Qafoku, J. P. McKinley, S. M. Heald and Z. Wang, *Geochim. Cosmochim Acta*, 2004, **68**, 4519-4537.
28. K. H. Williams, P. E. Long, J. A. Davis, M. J. Wilkins, A. L. N'Guessan, C. I. Steefel, L. Yang, D. Newcomer, F. A. Spane, L. J. Kerkhof, L. McGuinness, R. Dayvault and D. R. Lovley, *Geomicrobiol. J.*, 2011, **28**, 519-539.
29. R. Guillaumont, T. Fanghänel, V. Neck, J. Fuger, D. A. Palmer, I. Grenthe and M. H. Rand, *Update of the Chemical Thermodynamics of Uranium, Neptunium, Plutonium, Americium and Technetium*, OECD Nuclear Energy Agency, Data Bank, Issy-les-Moulineaux, France, 2003.

30. I. Grenthe, L. Fuger, R. G. M. Konings, R. J. Lemire, A. B. Muller, C. Nguyen-Trung and H. Wanner, *Chemical Thermodynamics 1. Chemical Thermodynamics of Uranium, Chemical Thermodynamics Series*, North Holland Elsevier Science Publishers B. V., Amsterdam, The Netherlands, 1992.
31. B. Li, J. Zhou, C. Priest and D. E. Jiang, *J. Phys. Chem. B*, 2017, **121**, 8171-8178.
32. A. O. Tirler and T. S. Hofer, *Dalton Trans.*, 2016, **45**, 4983-4988.
33. W. Wu, C. Priest, J. Zhou, C. Peng, H. Liu and D. E. Jiang, *J. Phys. Chem. B*, 2016, **120**, 7227-7233.
34. E. T. Urbansky, *Perchlorate in the Environment*, Springer, United States Environmental Protection Agency, Cincinnati, Ohio, 2000.
35. M. C. Bellissent-Funel and G. W. Neilson, *The Physics and Chemistry of Aqueous Ionic Solutions*, *NATO Science Series C*, D. Reidel Pub. Co., Dordrecht, Holland; Boston; Norwell, MA, U.S.A., 1987.
36. X.-F. Pang, *Water: Molecular Structure and Properties*, World Scientific, Hackensack, New Jersey, 2014.
37. C. W. Bock, G. D. Markham, A. K. Katz and J. P. Glusker, *Theor. Chem. Acc.*, 2006, **115**, 100-112.
38. P. A. Bergström, J. Lindgren and O. Kristiansson, *J. Phys. Chem.*, 1991, **95**, 8575-8580.
39. R. Mancinelli, A. Botti, F. Bruni, M. A. Ricci and A. K. Soper, *J. Phys. Chem. B*, 2007, **111**, 13570-13577.
40. F. Jalilehvand, D. Spångberg, P. Lindqvist-Reis, K. Hermansson, I. Persson and M. Sandström, *J. Am. Chem. Soc.*, 2001, **123**, 431-441.
41. T. Megyes, I. Bakó, S. Bálint, T. Grósz and T. Radnai, *J. Mol. Liq.*, 2006, **129**, 63-74.
42. S. Tu, S. S. Lobanov, J. M. Bai, H. Zhong, J. Gregerson, A. D. Rogers, L. Ehm and J. B. Parise, *J. Phys. Chem. B*, 2019, **123**, 9654-9667.
43. Y. Yokoyama, M. Moriyasu and S. Ikeda, *J. Inorg. Nucl. Chem.*, 1976, **38**, 1329-1333.
44. M. Moriyasu, Y. Yokoyama and S. Ikeda, *J. Inorg. Nucl. Chem.*, 1977, **39**, 2205-2209.
45. M. Moriyasu, Y. Yokoyama and S. Ikeda, *J. Inorg. Nucl. Chem.*, 1977, **39**, 2211-2214.
46. M. D. Marcantonatos, M. Deschaux, F. Celardin and M. Levental, *Chem. Phys. Lett.*, 1979, **65**, 316–321.
47. M. D. Marcantonatos, *J. Chem. Soc., Faraday Trans. 1*, 1980, **76**, 1093-1115.
48. H. Burrows, A. Cardoso, S. Formosinho and M. Miguel, *J. Chem. Soc., Faraday Trans. 1*, 1985, **81**, 49-60.
49. S. J. Formosinho, M. D. M. Miguel and H. D. Burrows, *J. Chem. Soc., Faraday Trans. 1*, 1984, **80**, 1717-1733.
50. A. Cardoso and H. Burrows, *J. Chem. Soc., Faraday Trans. 1*, 1984, **80**.
51. I. Billard, A. Rustenholtz, L. Sémon and K. Lützenkirchen, *Chem. Phys.*, 2001, **270**, 345-354.
52. A. Rustenholz, I. Billard, G. Duplâtre, K. Lützenkirchen and L. Sémon, *Radiochim. Acta*, 2001, **89**.
53. I. Billard and K. Lützenkirchen, *Radiochim. Acta*, 2003, **91**, 285-294.
54. I. Feldman, *Anal. Chem.*, 1956, **28**, 1859-1866.
55. G. G. Manov, N. J. Delollis and S. F. Acree, *J. Res. Natl. Bur. Stand.*, 1945, **34**, 115-127.
56. R. de Levie, *Adanced Excel for Scientific Data Analysis*, Oxford University Press, New York, 2005.
57. P. Moreau, S. Colette-Maatouk, P. Vitorge, P. Gareil and P. E. Reiller, *Inorg. Chim. Acta*, 2015, **432**, 81-88.
58. Y. Z. Kouhail, M. F. Benedetti and P. E. Reiller, *Environ. Sci. Technol.*, 2016, **50**, 3706-3716.

59. E. Fromentin and P. E. Reiller, *Inorg. Chim. Acta*, 2018, **482**, 588-596.
60. Y. Z. Kouhail, M. F. Benedetti and P. E. Reiller, *Chem. Geol.*, 2019, **522**, 175-185.
61. A. Ringböm, Complexation in Analytical Chemistry: A Guide for the Critical Selection of Analytical Methods Based on Complexation Reactions, Interscience Publishers, New York, NY, USA, 1963.
62. W. Hummel, G. Anderegg, L. F. Rao, I. Puigdomènech and O. Tochiyama, Chemical Thermodynamics 9. Chemical Thermodynamics of Compounds and Complexes of U, Np, Pu, Am, Tc, Se, Ni and Zr with Selected Organic Ligands, Chemical Thermodynamics Series, North Holland Elsevier Science Publishers B. V., Amsterdam, The Netherlands, 2005.
63. J. S. Newman and K. E. Thomas-Alyea, *Electrochemical Systems*, J. Wiley, Hoboken, N.J., 3rd edn., 2004.
64. K. S. Pitzer, *Activity Coefficients in Electrolyte Solutions*, CRC Press, Boca Raton, 2nd edn., 1991.
65. S. Tsushima, Y. Uchida and T. Reich, *Chem. Phys. Lett.*, 2002, **357**, 73-77.
66. D. Majumdar, S. Roszak, K. Balasubramanian and H. Nitsche, *Chem. Phys. Lett.*, 2003, **372**, 232-241.
67. W. W. Rudolph and G. Irmer, *Dalton Trans.*, 2013, **42**, 3919-3935.
68. I. Grenthe, A. V. Plyasunov and K. Spahiu, in *Modelling in Aquatic Chemistry*, eds. I. Grenthe and I. Puigdomènech, OECD, Paris, France, 1997, ch. IX, pp. 325-426.
69. A. Plyasunov, T. Fanghanel and I. Grenthe, *Acta Chem. Scand.*, 1998, **52**, 250-260.
70. Y. Marcus and G. Hefter, *Chem. Rev.*, 2006, **106**, 4585-4621.
71. M. Bouby, I. Billard, A. Bonnenfant and G. Klein, *Chem. Phys.*, 1999, **240**, 353-370.
72. L. Sémon, C. Boehme, I. Billard, C. Hennig, K. Lützenkirchen, T. Reich, A. Roßberg, I. Rossini and W. Georges, *ChemPhysChem*, 2001, **2**, 591-598.
73. L. Ciavatta, *Ann. Chim.*, 1980, **70**, 551–562.
74. H. Oher, T. Vercouter, F. Réal, C. Shang, P. E. Reiller and V. Vallet, *Inorg. Chem.*, 2020, DOI: 10.1021/acs.inorgchem.0c01986.
75. C. Görller-Walrand, S. De Houwer, L. Fluyt and K. Binnemans, *Phys. Chem. Chem. Phys.*, 2004, **6**, 3292-3298.
76. J. T. Bell and R. E. Biggers, *J. Mol. Spectrosc.*, 1968, **25**, 312-329.
77. A. Brachmann, G. Geipel, G. Bernhard and H. Nitsche, *Radiochim. Acta*, 2002, **90**, 147-153.
78. A. Anderson, C. Chieh, D. Irish and J. Tong, *Can. J. Chem.*, 2011, **58**, 1651-1658.
79. P. Novotny and O. Sohnel, *J. Chem. Eng. Data*, 1988, **33**, 49-55.
80. D. G. Kinniburgh and D. M. Cooper, *Creating Graphical Output with PHREEQC*, 2011. http://www.phreeplot.org
81. D. L. Parkhurst and C. A. J. Appelo, User's Guide to PHREEQC (Version 2) — A Computer Program for Speciation, Batch-Reaction, One-Dimensional Transport, and Inverse Geochemical Calculations, Report 99-4259, U.S. Geological Survey, Water-Resources Investigations, Lakewood, Colorado, USA, 1999. http://wwwbrr.cr.usgs.gov/projects/GWC_coupled/phreeqci/
82. D. L. Parkhurst and C. A. J. Appelo, Description of Input and Examples for PHREEQC Version 3 — A Computer Program for Speciation, Batch-Reaction, One-Dimensional Transport, and Inverse Geochemical Calculations. Chapter 43 of Section A, Groundwater Book 6, Modeling Techniques, U.S. Geological Survey, Denver, Colorado, USA, 2013. http://pubs.usgs.gov/tm/06/a43/pdf/tm6-A43.pdf
83. E. Giffaut, M. Grivé, P. Blanc, P. Vieillard, E. Colàs, H. Gailhanou, S. Gaboreau, N. Marty, B. Madé and L. Duro, *Appl. Geochem.*, 2014, **49**, 225-236.
84. C. Bretti, C. Foti and S. Sammartano, *Chem. Spec. Bioavailab.*, 2004, **16**, 105-110.

85. C. Bretti, C. Foti, N. Porcino and S. Sammartano, *J. Solution Chem.*, 2006, **35**, 1401-1415.
86. P. L. Brown and C. Ekberg, *Hydrolysis of Metal Ions*, Wiley-VCH Verlag GmbH & Co., Weinheim, Germany, 2016.
87. H. Motulsky and A. Christopoulos, *Fitting Models to Biological Data Using Linear and Nonlinear Regression*, Oxford University Press, New York, 2004.

III - 7 Supporting Information

This supporting information contains four Tables: the liquid junction potentials measured for $NaClO_4$ solutions of different ionic strengths ($0.01\ m \leq I_m \leq 3.5\ m$) using the reconditioned electrode; experimental samples information – pH value, calculated Ringböm coefficients α, $[Ca^{2+}]$ ($mol \cdot kg_w^{-1}$) and deduced F_0; information for samples in Fig. III - 4; Decay-times of $Ca_nUO_2(CO_3)_3^{(4-2n)-}$ determined at each I_m ; and two Figures: the slope analysis results of I_m = 3.5 *m*; the predominance plot of the 3.5 *m* experiment.

Table III - S1 Potential values E_{mes} read on pH-meter for $NaClO_4$ solutions of I_m = 0.01 to 3.5 m at pcH = 2 using the reconditioned electrode of 3.5 m $NaClO_4$ reference solution: liquid junction potentials ΔE_{mes} calculated to estimate the potential differences between the solutions of a specific $I_m \geq 0.1$ m and of I_m = 0.01 m; ΔE_{mes} then used in the four-point calibration with commercial buffer solution of pH 1.64, 4.01, 6.87, 9.18, assumed as diluted solutions of $I_m \approx$ 0.01 m; the uncertainties of ± 0.05 pH in text included this non-significant experimental bias.

Solution	Conversion factor (from molarity M to molality *m*)	I_m ($mol\ kg_w^{-1}$)	E_{mes} (mV)	$\Delta E_{mes} = E_{mes} - E_{mes}$ (I_m = 0.01 *m*)
HCl 0.01 M + $NaClO_4$ 2.99 M	1.1678	3.50	172.2	31.3
HCl 0.01 M + $NaClO_4$ 2.49 M	1.1361	2.84	168	27.1
HCl 0.01 M + $NaClO_4$ 2.19 M	1.1196	2.46	165.5	24.6
HCl 0.01 M + $NaClO_4$ 1.99 M	1.1062	2.21	163.6	22.7
HCl 0.01 M + $NaClO_4$ 1.49 M	1.0780	1.62	158.9	18
HCl 0.01 M + $NaClO_4$ 0.99 M	1.0515	1.05	155.1	14.2
HCl 0.01 M + $NaClO_4$ 0.49 M	1.0265	0.51	150.2	9.3
HCl 0.01 M + $NaClO_4$ 0.19 M	1.0098	0.20	146.6	5.7
HCl 0.01 M + $NaClO_4$ 0.09 M	1.0075	0.10	144.5	3.6
HCl 0.01 M	1.0000	0.01	140.9	0
For the solution of I_m < 0.1 M, the conversion factor taken as 1. The factor values for $I_m \geq 0.1$ M taken from Guillaumont et al.[1]				

Table III - S2 Experimental samples information – pH value, calculated Ringböm coefficients α, $[Ca^{2+}]$ ($mol \cdot kg_w^{-1}$) and deduced F_0.

I_m ($mol \cdot kg_w^{-1}$)	0.10				0.51			
Sample	pH value	α	$[Ca^{2+}]$ ($mol \cdot kg_w^{-1}$)	F_0 (counts)	pH value	α	$[Ca^{2+}]$ ($mol \cdot kg_w^{-1}$)	F_0 (counts)
1	9.00	1.00	0	1.49E+08	9.00	1.00	0	2.48E+08

2	8.45	1.02	5.03E-05	1.75E+08	8.13	1.02	3.44E-04	2.10E+08
3	8.41	1.03	9.51E-05	1.55E+08	7.95	1.09	8.46E-04	1.95E+08
4	8.33	1.06	1.35E-04	1.44E+08	7.90	1.17	1.06E-03	1.95E+08
5	8.25	1.12	1.58E-04	2.23E+08	7.87	1.24	1.24E-03	2.10E+08
6	*8.21*	*1.17*	*2.49E-04*	*1.48E+08*	*7.84*	*1.27*	*1.59E-03*	*2.05E+08*
7	*8.17*	*1.19*	*2.88E-04*	*1.41E+08*	*7.81*	*1.38*	*2.00E-03*	*2.23E+08*
8	*8.13*	*1.29*	*4.36E-04*	*1.76E+08*	*7.78*	*1.54*	*2.39E-03*	*2.24E+08*
9	*8.09*	*1.45*	*5.06E-04*	*1.61E+08*	*7.75*	*1.73*	*2.99E-03*	*2.40E+08*
10	*8.01*	*2.03*	*7.77E-04*	*1.77E+08*	*7.72*	*2.00*	*3.86E-03*	*2.36E+08*
11	*7.91*	*3.69*	*1.13E-03*	*2.03E+08*	*7.69*	*2.36*	*4.45E-03*	*2.58E+08*
12	*7.87*	*4.84*	*1.94E-03*	*1.92E+08*	*7.66*	*2.83*	*5.20E-03*	*2.72E+08*
13	***7.80***	***8.04***	***3.08E-03***	***1.98E+08***	*7.64*	*3.21*	*7.61E-03*	*2.79E+08*
14	***7.73***	***13.67***	***5.05E-03***	***2.06E+08***	***7.60***	***4.21***	***9.97E-03***	***2.97E+08***
15	***7.68***	***20.17***	***6.27E-03***	***2.27E+08***	***7.56***	***5.59***	***1.27E-02***	***3.06E+08***
16	***7.62***	***32.36***	***8.69E-03***	***2.33E+08***	***7.52***	***7.54***	***1.56E-02***	***3.41E+08***
17	***756***	***52.16***	***1.00E-02***	***2.30E+08***	***7.48***	***10.22***	***1.69E-02***	***3.63E+08***
18	***7.48***	***98.99***	***1.26E-02***	***2.35E+08***	***7.44***	***13.97***	***2.20E-02***	***3.60E+08***
19	***7.46***	***116.8***	***1.34E-02***	***2.40E+08***				
I_m (mol·kg$_w^{-1}$)	1.05				1.62			
Sample	pH value	α	[Ca^{2+}] (mol·kg$_w^{-1}$)	F_0 (counts)	pH value	α	[Ca^{2+}] (mol·kg$_w^{-1}$)	F_0 (counts)
1	9.00	1.00	0	2.27E+08	9.00	1.00	0	5.45E+08
2	8.13	1.01	8.81E-04	1.71E+08	7.95	1.04	5.53E-04	4.01E+08
3	7.95	1.04	1.46E-03	1.55E+08	7.80	1.09	1.59E-03	3.91E+08
4	7.80	1.08	1.94E-03	1.54E+08	7.78	1.12	2.97E-03	3.75E+08
5	*7.78*	*1.11*	*2.16E-03*	*1.73E+08*	*7.72*	*1.22*	*4.15E-03*	*3.71E+08*
6	*7.72*	*1.20*	*2.70E-03*	*1.69E+08*	*7.68*	*1.36*	*4.61E-03*	*4.19E+08*
7	*7.68*	*1.32*	*3.45E-03*	*1.70E+08*	*7.64*	*1.56*	*5.58E-03*	*4.00E+08*
8	*7.64*	*1.51*	*4.32E-03*	*2.33E+08*	*7.60*	*1.88*	*6.65E-03*	*4.22E+08*
9	*7.60*	*1.80*	*5.57E-03*	*2.15E+08*	*7.56*	*2.33*	*8.82E-03*	*4.42E+08*
10	*7.56*	*2.22*	*7.77E-03*	*2.35E+08*	*7.52*	*2.97*	*1.31E-02*	*4.68E+08*
11	***7.52***	***2.81***	***1.14E-02***	***2.24E+08***	***7.48***	***3.86***	***1.64E-02***	***5.07E+08***
12	***7.48***	***3.64***	***1.33E-02***	***2.57E+08***	***7.45***	***4.79***	***2.25E-02***	***5.05E+08***
13	***7.45***	***4.50***	***1.64E-02***	***2.60E+08***	***7.40***	***6.95***	***2.83E-02***	***5.61E+08***
14	***7.40***	***6.52***	***2.18E-02***	***2.80E+08***	***7.34***	***11.08***	***3.45E-02***	***6.18E+08***
15	***7.34***	***10.36***	***2.53E-02***	***3.53E+08***	***7.32***	***15.00***	***3.73E-02***	***6.13E+08***
I_m (mol·kg$_w^{-1}$)	2.21				2.46			
Sample	pH value	α	[Ca^{2+}] (mol·kg$_w^{-1}$)	F_0 (counts)	pH value	α	[Ca^{2+}] (mol·kg$_w^{-1}$)	F_0 (counts)
1	9.06	1.00	0	3.02E+08	8.80	1.00	0	4.77E+08
2	7.85	1.02	3.72E-03	2.81E+08	8.13	1.00	2.45E-03	4.61E+08
3	*7.82*	*1.05*	*7.07E-03*	*3.14E+08*	7.95	1.01	3.93E-03	4.34E+08
4	*7.79*	*1.05*	*7.80E-03*	*3.37E+08*	7.80	1.02	4.99E-03	4.30E+08
5	*7.73*	*1.07*	*8.77E-03*	*3.53E+08*	*7.58*	*1.17*	*6.20E-03*	*3.96E+08*
6	*7.68*	*1.11*	*9.67E-03*	*3.98E+08*	*7.54*	*1.28*	*7.74E-03*	*3.91E+08*
7	*7.62*	*1.19*	*1.16E-02*	*4.40E+08*	*7.50*	*1.45*	*9.51E-03*	*4.47E+08*
8	*7.58*	*1.24*	*1.51E-02*	*4.42E+08*	*7.46*	*1.69*	*1.13E-02*	*4.17E+08*
9	*7.50*	*1.60*	*1.68E-02*	*4.28E+08*	*7.42*	*2.06*	*1.27E-02*	*4.06E+08*
10	***7.48***	***1.75***	***2.11E-02***	***4.16E+08***	*7.38*	*2.60*	*1.72E-02*	*4.65E+08*
11	***7.42***	***2.38***	***2.89E-02***	***4.41E+08***	*7.34*	*3.34*	*2.01E-02*	*5.22E+08*
12	***7.35***	***3.71***	***3.27E-02***	***4.59E+08***	***7.30***	***4.42***	***2.63E-02***	***5.52E+08***
13	***7.30***	***5.29***	***4.24E-02***	***5.05E+08***	***7.27***	***5.50***	***3.46E-02***	***5.75E+08***
14	***7.22***	***9.62***	***5.54E-02***	***5.56E+08***	***7.22***	***7.97***	***4.13E-02***	***6.82E+08***
					7.18	***10.85***	***5.01E-02***	***7.59E+08***
I_m (mol·kg$_w^{-1}$)	3.50							
Sample	pH value	α	[Ca^{2+}] (mol·kg$_w^{-1}$)	F_0 (counts)				
1	8.94	1.00	0.00001	1.28E+08				

2	8.30	1.01	0.00097	2.39E+08	
3	8.10	1.03	0.00306	3.87E+08	
4	7.90	1.03	0.00719	1.92E+08	
5	7.70	1.06	0.01769	2.28E+08	
6	*7.60*	*1.11*	*0.02156*	*1.86E+08*	
7	*7.50*	*1.29*	*0.02623*	*2.04E+08*	
8	*7.44*	*1.49*	*0.03109*	*2.08E+08*	
9	*7.39*	*1.85*	*0.04189*	*2.18E+08*	
10	*7.33*	*2.58*	*0.05419*	*2.27E+08*	
11	*7.29*	*3.33*	*0.06825*	*2.07E+08*	
12	*7.27*	*3.84*	*0.09060*	*2.48E+08*	
13	*7.25*	*4.44*	*0.14429*	*2.79E+08*	
14	*7.22*	*5.56*	*0.21003*	*3.31E+08*	
15	*7.20*	*6.51*	*0.25634*	*3.57E+08*	
16	*7.17*	*8.23*	*0.32939*	*3.88E+08*	
17	*7.16*	*9.00*	*0.39816*	*4.09E+08*	
18	*7.15*	*9.85*	*0.50482*	*4.05E+08*	

Table III - S3 Information for samples in Fig. III - 4.

	0.1 m NaCl	0.1 m $NaClO_4$	1 m NaCl	1 m $NaClO_4$
pH value	7.82	7.78	7.43	7.56
$[Ca^{2+}]$ (mol kg_w^{-1})	5.98E-3	5.19E-3	7.80E-2	2.80E-2

Table III - S4 Decay-times of $Ca_nUO_2(CO_3)_3^{(4-2n)-}$ determined at each I_m.

I_m (mol·kg_w^{-1})	τ ($UO_2(CO_3)_3^{4-}$) (ns)	τ ($CaUO_2(CO_3)_3^{2-}$) (ns)	τ ($Ca_2UO_2(CO_3)_3$(aq)) (ns)
0.10	10.62 ± 0.22	30.41 ± 1.9	51.19 ± 1.85
0.51	8.46 ± 0.17	39.79 ± 2.78	68.53 ± 4.45
1.05	9.51 ± 0.11	37.57 ± 4.77	63.02 ± 4.45
1.62	9.39 ± 0.13	35.52 ± 2.66	65.76 ± 6.35
2.21	11.21 ± 0.40	27.72 ± 1.34	47.54 ± 2.53
2.46	10.61 ± 0.12	38.6 ± 4.33	86.36 ± 10.15
Averaged τ	10.0 ± 1.0 (τ measured from I_m = 0.1 to 2.46 *m*)	34.20 ± 2.24 (τ measured from I_m = 0.1 to 2.21 *m*)	59.21 ± 4.15 (τ measured from I_m = 0.1 to 2.21 *m*)

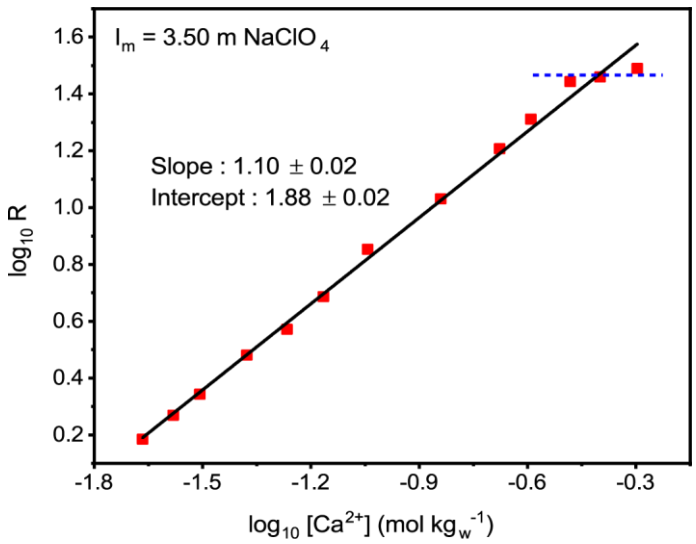

Fig. III - S1 Plot of logarithmic ratio R as a function of $log_{10}[Ca^{2+}]$ (mol kg_w^{-1}) at I_m = 3.50 m of $NaClO_4$ medium: $[U]_{total}$ = 50 µmol kg_w^{-1}, $P(CO_2) = 10^{-3.5}$ atm.

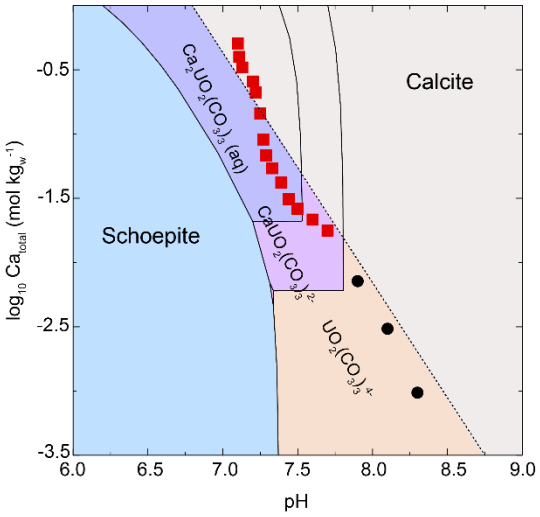

Fig. III - S2 Predominance plot obtained using PHREEPLOT[2] of Ca-UO_2-CO_3 system at [U(VI)] = 50 µm, $P(CO_2) = 10^{-3.5}$ atm at I_m = 3.50 m $NaClO_4$: experimental points giving slopes of one are highlighted with red squares; the black circles represent the beginning of titration where the binary complex dominates; dotted line represent the predominance line between Ca^{2+} and calcite.

References

1. R. Guillaumont, T. Fanghänel, V. Neck, J. Fuger, D. A. Palmer, I. Grenthe and M. H. Rand, *Update of the Chemical Thermodynamics of Uranium, Neptunium, Plutonium, Americium and Technetium*, OECD Nuclear Energy Agency, Data Bank, Issy-les-Moulineaux, France, 2003.
2. D. G. Kinniburgh and D. M. Cooper, *Creating Graphical Output with PHREEQC*, 2011. http://www.phreeplot.org

Chapter IV. Thermodynamic Constants of $MgUO_2(CO_3)_3^{2-}$ Complex in $NaClO_4$ and NaCl Media Using Time-Resolved Luminescence Spectroscopy, and Applications to Different Geochemical Contexts.

*Chengming Shang, Pascal E. Reiller**
[1] Den – Service d'Études Analytiques et de Réactivité des Surfaces (SEARS), CEA, Université Paris-Saclay, F-91191, Gif-sur-Yvette, France
*Corresponding author. Tel.: +33 1 6908 4312; fax: +33 1 6908 9475. E-mail address: pascal.reiller@cea.fr

Dalton Transactions **50** (12), 4363-4369.

http://doi.org/10.1039/D0DT04124F

IV - 1 Abstract

The formation constants and specific ion interaction coefficients of $MgUO_2(CO_3)_3^{2-}$ complex were determined in 0.1 to 1 mol kg_w^{-1} NaCl and 0.1 to 2.21 mol kg_w^{-1} $NaClO_4$ media in the framework of the specific ion interaction theory (SIT), using time-resolved laser-induced luminescence spectroscopy. The upper limits of ionic strength were chosen in order to limit luminescence quenching effects generated by high concentrations of Cl^- and ClO_4^-, already observed during our earlier studies on $Ca_nUO_2(CO_3)_3^{(4-2n)-}$ (Shang & Reiller, Dalton Trans. 49, 466; Shang *et al.*, *ibid* 49, 15443). The cumulative formation constant determined is $\log_{10}\beta°_{1.1.3}$ = 26.40 ± 0.07, and the specific ion interaction coefficients $\varepsilon(MgUO_2(CO_3)_3^{2-}, Na^+)$ = 0.19 ± 0.11 kg_w mol^{-1} in $NaClO_4$ and $\varepsilon(MgUO_2(CO_3)_3^{2-}, Na^+)$ = 0.09 ± 0.16 kg_w mol^{-1} in NaCl. The 300 and 1800 lines mm^{-1} gratings were both used to acquire $MgUO_2(CO_3)_3^{2-}$ luminescence spectra, where the high-resolution 1800 lines mm^{-1} grating detected slight spectral shifts for the principal luminescent bands relative to $Ca_nUO_2(CO_3)_3^{(4-2n)-}$. The application of the consistent set of thermodynamic constants and ε values for $M_nUO_2(CO_3)_3^{(4-2n)-}$ (M = Mg, Ca) are examined in different geochemical contexts, where Mg over Ca concentration ratio varies to help defining the relative importance of these species.

IV - 2 Introduction

The alkaline earth triscarbonatouranyl complexes $M_nUO_2(CO_3)_3^{(4-2n)-}$ – especially for Mg and Ca – seem to have an essential role in controlling the U(VI) speciation and mobility in mildly basic carbonate-rich groundwater by increasing U(VI) solubility and facilitating its migration.[1-8] Due to the importance of these species, their thermodynamic constants and

functions – $\log_{10}\beta°_{n.1.3}$, $\Delta_r G°_m$ $\Delta_r H°_m$, $\Delta_r S°_m$ –, as well as their ionic strength dependence, have been investigated by different methods such as time-resolved luminescence spectroscopy (TRLS),[1,2,9-13] ion-exchange, [14,15] UV-Visible spectroscopy,[16,17] and potentiometry.[18]

Even if the existence of the alkaline earth carbonate phases of uranium(VI) are known since the 19th century,[19,20] the first evidence of the Ca aqueous complexes is quite recent in uranium chemical history,[1] see *e.g.* in the critical compilations of thermochemical data commissioned by the Nuclear Energy Agency from the Organization for Economic Co-operation and Development – NEA-OECD[21-23]. The aqueous complexes had not been evidenced yet in Grenthe, *et al.*,[21] and were not selected in Guillaumont, *et al.*[22] A selection of thermodynamic functions and constants have been proposed recently in Grenthe, *et al.*, [23], based on determinations available before 2018 – the most recent reviewed work being Lee, *et al.*[10] The only works that were dealing with ionic strength variation are Kalmykov and Choppin[11] for Ca, and Dong and Brooks[15] for Mg, which have not been judged satisfying in Guillaumont, *et al.*[22] and Grenthe, *et al.*,[23] respectively. The selected data, obtained in a limited range of ionic strength, could not allow proposing both extrapolations of formation constants to infinite dilution ($\log_{10}\beta°$) and the specific ion interaction coefficients (ε), using the specific ion interaction theory (SIT), which is the framework of the proposition of thermodynamic constants for the NEA-OECD commissioned reviews.

In recent works, we reported the conditional formation constants for $Ca_nUO_2(CO_3)_3^{(4-2n)-}$ species at I_m = 0.1 to 1 mol kg_w^{-1} in NaCl,[24] and 0.1 to 2.21 mol kg_w^{-1} in $NaClO_4$,[25] which had led to the propositions of $\log_{10}\beta°(CaUO_2(CO_3)_3^{2-})$, $\log_{10}\beta°(Ca_2UO_2(CO_3)_3(aq))$, $\varepsilon(CaUO_2(CO_3)_3^{2-},Na^+)$, $\varepsilon(Ca_2UO_2(CO_3)_3(aq),NaCl)$, and $\varepsilon(Ca_2UO_2(CO_3)_3(aq),NaClO_4)$. These works could not have been included in the latter NEA-OECD review,[23] as they were published after the peer-review.

Particularly, we showed that two usual hypotheses concerning the value of ε for these complexes were not justified: (i) the charge-like analogy of $CaUO_2(CO_3)_3^{2-}$ and $UO_2(CO_3)_2^{2-}$ was not justified concerning their ε value towards Na^+; and (ii) the nil value of ε for neutral complexes could not be generalized for these large species – one can also notice that Ciavatta[26] already represented non-nil ε values for Cd(II) and Hg(II) neutral complexes.

The spectroluminescence titration of uranyl carbonate solutions with alkaline earth metal cations at varying pH values – in order to avoid the precipitation of schoepite and calcite – was proven feasible and robust to derive the $\log_{10}\beta°$ and ε values by extrapolating $\log_{10}\beta$ measured

at specific ionic strengths to infinite dilution using SIT. In NaCl,[24] the striking quenching effect of chloride impeded the acquisitions of well-resolved luminescence spectra at $I_m > 1$ mol kg_w^{-1}. In $NaClO_4$,[25] the more limited quenching effect of perchlorate still restricted the I_m upper limit to 2.46 mol kg_w^{-1}. The interaction coefficients of $Ca_nUO_2(CO_3)_3^{(4-2n)-}$ complexes exhibited drastically different patterns depending on the nature of the media. The positive interaction coefficient values were estimated to be $\varepsilon(Na^+,CaUO_2(CO_3)_3^{2-}) = (0.29 \pm 0.11)$ kg_w mol^{-1} and $\varepsilon(Ca_2UO_2(CO_3)_3(aq),NaCl) = (0.66 \pm 0.12)$ kg_w mol^{-1}. The change of background electrolyte to $NaClO_4$ gave rise to less positive values as $\varepsilon(Na^+,CaUO_2(CO_3)_3^{2-}) = (0.02 \pm 0.04)$ kg_w mol^{-1} and $\varepsilon(Ca_2UO_2(CO_3)_3(aq),NaClO_4) = (0.18 \pm 0.07)$ kg_w mol^{-1} – the value of the neutral complex being significantly different from 0.

Our previous results provided evidence for the medium-dependent interaction coefficients of a specific complex. The obtained ε values for $CaUO_2(CO_3)_3^{2-}$ and $Ca_2UO_2(CO_3)_3(aq)$ suggest that the hypothesis $\varepsilon(CaUO_2(CO_3)_3^{2-},Na^+) = \varepsilon(UO_2(CO_3)_2^{2-},Na^+) = (-0.02 \pm 0.09)$ kg_w mol^{-1} requires particular attention, as well as the nil value for $\varepsilon(Ca_2UO_2(CO_3)_3(aq), NX)$ – NX being the background electrolyte. In addition, the $\log_{10}\beta_{n.1.3}$ *vs.* I_m functions displayed remarkably different patterns in NaCl and $NaClO_4$ that are possibly accounted for by the tertiary ion-ion interactions as well as ion pairing at high ionic strengths. The interactions between Ca^{2+} and $UO_2(CO_3)_3^{4-}$ are suspected to be perturbed by the ion association of Ca^{2+} with other competing anions in the background solutions.[27] Moreover, the affinity of Na^+ can induce a distortion of carbonate denticity from bidentate to monodentate and thus change the first shell coordination number of U, as proposed by molecular dynamics simulations.[28,29] These findings for Ca-UO_2-CO_3 species strongly suggest the important influence of high ionic strengths on $Ca^{2+}/UO_2^{2+}/CO_3^{2-}$ complexation.

In this work, we propose new determinations of thermodynamic constants of formation for another environmentally relevant alkaline earth cation, Mg^{2+}, to form the $Mg_nUO_2(CO_3)_3^{(4-2n)-}$ complexes at ionic strength 0.1 to 1 mol kg_w^{-1} NaCl and 0.1 to 2.21 mol kg_w^{-1} $NaClO_4$ media, using slope analysis of the uranium(VI) spectra in time-resolved laser-induced luminescence spectroscopy. The conditional constants will be extrapolated to infinite dilution in the framework of SIT providing both $\log_{10}\beta°$ and ε values for the evidenced complexes.

Even if Mg^{2+} and Ca^{2+} are likely to have a similar role in uranyl carbonate complexes, different hydration structures of these two elements still lead to various degrees of difficulty in complexation with the $UO_2(CO_3)_3^{4-}$ moiety.[18,30-34] Especially the more difficult water exchange

between $Mg(H_2O)_6^{2+}$ – stable octahedral with perpendicular square plan[31,33,34] – and $UO_2(CO_3)_3^{4-}$. Jo, *et al.*[16,17] evidenced that the formation of Mg-UO_2-CO_3 complexes is subjected to endothermic reaction, whilst that of Ca-UO_2-CO_3 complexes is exothermic, which was also observed by Endrizzi and Rao. [18] Furthermore, as for other ligands – see Fig. IV - S1 of the supplementary information (SI) –, the stability constant of $MgUO_2(CO_3)_3^{2-}$ also presents a marked anomaly in comparison with the $\log_{10}\beta°$ ($MUO_2(CO_3)_3^{2-}$) for the other stable alkaline earth cations – M = Ca, Sr, and Ba in Dong and Brooks[14] in Fig. IV - S2 of the SI. The question raised here is whether the hydration structural nuances of Mg^{2+} and Ca^{2+} will be reflected in the formations of $M_nUO_2(CO_3)_3^{(4-2n)-}$ at high ionic strengths. The comparison of $\log_{10}\beta°$ and ε for similar types of $M_nUO_2(CO_3)_3^{(4-2n)-}$ complexes determined in different media allow achieving a clearer view of ion interaction mechanism, and help rationalizing the differences in interaction coefficients.

The thermodynamic functions of $Mg_nUO_2(CO_3)_3^{(4-2n)-}$ and $Ca_nUO_2(CO_3)_3^{(4-2n)-}$ could be important to account for when describing the geochemistry of representative cases where the concentration of magnesium is at least comparable or higher than that of calcium[7]. Using the estimation from Dong and Brooks[14] for $MgUO_2(CO_3)_3^{2-}$ and $CaUO_2(CO_3)_3^{2-}$ the equality of concentration of the two complexes should occur at $[Mg^{2+}]/[Ca^{2+}]$ *ca.* 12, and *ca.* 24 using the Dong and Brooks[15] constants extrapolated using Davies[35] equation for Mg.

Reiller and Descostes[7] identified some cases where the need of dedicated ionic strength determinations for both Ca and Mg complexes were stressed: the clay-rich minerals dedicated to geological repository for radioactive wastes – *e.g.* the Boom Clay in the Belgian context,[36] and the Callovo-Oxfordian Clay in the French context[37] –, and seawater.[38] We can select other instances as: a Canadian aquitard[39,40] characteristic of the spatially varying ratio Mg/Ca with depth; and in addition, the cases of uranium-rich Indian groundwaters[41,42], sources of local drinking water, as a part of discussion considering its humanistic and ecological significance.

Theoretical modelling using PhreeqC[43,44] are performed by implementing the newly measured $\log_{10}\beta°$ and ε and those for $Ca_nUO_2(CO_3)_3^{(4-2n)-}$ in our previous studies[24,25]. Clear differences in speciation results are analysed after comparing the modelling results with other available thermodynamic constants in literature.

IV - 3 Experimental Section

3.1 Materials

Stock solutions of U(VI) were separately prepared by dissolving appropriate quantities of U_3O_8 solid in 60-70% perchlorate acid (Sigma-Aldrich, ACS reagent) for two days, and in 37% hydrochloric acid (Sigma-Aldrich, ACS reagent) for one week. The concentrations of U(VI) were measured by inductively coupled plasma mass spectroscopy (ICP-MS). The final concentration of uranium was diluted to 50 µmol kg_w^{-1} in both ionic media for further experiments. Anhydrous $NaClO_4$ (Sigma-Aldrich, ACS reagent, ≥ 99%) and NaCl (Sigma-Aldrich, ACS reagent, ≥ 99%) were used to prepare the inert electrolytes with Millipore deionized water (Alpha-Q, 18.2 MΩ cm^{-1}) at varying ionic strengths, respectively 0.1, 0.51, 1.05, 1.62 and 2.21 mol kg_w^{-1} for $NaClO_4$ series, and 0.1, 0.25, 0.50, 0.75 and 1.0 mol kg_w^{-1} for NaCl series.

Freshly prepared $NaHCO_3$ (Analytical Grade, Fisher) solution was used to introduce carbonate into the aqueous solutions prior to the addition of alkaline earth metal ions. The amounts of added bicarbonate solution were previously calculated considering the equilibrium between the atmospheric carbon dioxide and the planning pH values. Magnesium perchlorate ($Mg(ClO_4)_2$, Sigma-Aldrich, ACS reagent, ≥ 99%) and magnesium chloride ($MgCl_2$, Sigma-Aldrich, ACS reagent, ≥ 99%) were used to control the concentration of magnesium. The addition of reagents was restricted to be in small volume so as not to disturb the electrolyte concentrations. The reagent preparations were performed by weighing. The species concentrations were expressed in molality units (mol kg_w^{-1} or *m* in the rest of the text). The saturation indices of $UO_3{:}2H_2O$(cr) and $MgCO_3$ from the ThermoChimie 10a database – see Grivé, *et al.*[45]; http://www.thermochimie-tdb.com – for every sample were checked as negative or near zero values, which suggested undersaturation of schoepite or magnesite during experiments.

The adjustment of aqueous pH value was conducted with NaOH (Analytical Grade, Fisher) and diluted HCl or $HClO_4$ solutions. Two hydrogen ion-sensitive glass electrodes (Mettler Toledo, USA) were used for pH measurements. As for the Ca-UO_2-CO_3 study,[25] the pH-electrode used in $NaClO_4$ was reconditioned by changing the filling solution from saturated KCl to 3.5 *m* $NaClO_4$ in order to avoid the precipitation of $KClO_4$ inside the frit. The junction potential for these two electrodes were estimated by measuring the potential values of specially prepared NaCl and $NaClO_4$ solutions of the same $\log_{10}[H^+]$ but different I_m. The establishment

of linear relationship between the measured potential values and the ionic strengths is important to correct and convert the measured potential to actual pH value for each sample solution.[46] The experimentally measured ΔE_{mes} (difference between E_{mes} measured at I_m = 0.01 *m* and that at other I_m) were reported in Table IV - S1 of the SI for NaCl medium. The results for $NaClO_4$ are available in Table IV - S1 of the SI in Shang, *et al.*[25] Commercial solutions of pH = 1.68, 4.01, 6.87 and 9.18 (SI Analytics, Mainz, Germany) were daily used to check the calibration and maintain the accuracy. A 95% confidence interval that corresponds to 0.05 pH units of uncertainties was obtained by the method of ordinary least squares. All pH measurements were performed in triplicate at 22°C.

3.2 Time-resolved laser-induced luminescence spectroscopy

The time-resolved luminescence apparatus was already described in details elsewhere. [24,25] The luminescence spectra were acquired at the excitation wavelength of 450 nm, assuring a selective excitation of U(VI),[47] using a frequency-tripled Nd:YAG laser at 355 nm (Surelite, Continuum, USA) as the pulsed laser beam and an optical parametric oscillator (OPO) system (Horizon, Continuum, USA). The excitation energy was monitored by a RTP-734 Joule-meter (Laser Probe, Inc.). The temperature of sample solutions was set at 22°C during all the measurements using the thermostated sample holder, connected to a thermostat (Peter Huber Kältemaschinenbau AG, Germany) with circulating cooling water to minimise the temperature influence on the U(VI) luminescence.[48] The luminescence signal was collected by an Andor monochromator spectrometer using either the 300 or the 1800 lines mm^{-1} grating. The U(VI) spectra were recorded in the emission wavelength range 415-615 nm using an intensified CCD camera (Acton).

The fluorescence behaviour was considered to be cumulative contribution of different U(VI) species. The time-resolved emission spectra acquisitions were acquired at different delay time *D* with the gate-width *W* fixed at 1 μs, and then analysed using Origin 9.0 software (OriginLab Corporation, USA), including subtraction of background noise, and peak integration with the trapezoidal rule. The intensity results were fitted to the exponential decay function to derive the luminescence intensity at *D* = 0 and the luminescence decay-time, expressed as already discussed,[24,25]

$$FI = \sum_i FI_0\ \tau_i \exp\left(-\frac{D}{\tau_i}\right)\left(1 - \exp\left(-\frac{W}{\tau_i}\right)\right) \qquad \text{(IV - 1)}$$

where FI is the fluorescence intensity at a specific delay time and FI_0 is at $D = 0$. The gate width $W = 1$ μs and τ_i is the decay-time of species i.

3.3 Correction for slope analysis and calculation of Ringböm coefficients

The introduction of Ringböm[49] coefficient α has been discussed in our previous studies.[24,25] We will simply recall here the equations used for the slope analysis and the meanings of α for explanatory purposes. The successive binding of Mg^{2+} with $UO_2(CO_3)_3^{4-}$ is described by Eq. IV - 2,

$$n Mg^{2+} + UO_2(CO_3)_3^{4-} \rightleftarrows Mg_nUO_2(CO_3)_3^{(4-2n)-}$$

$$K_{n.1.3} = \frac{\left[Mg_nUO_2(CO_3)_3^{(4-2n)-}\right]}{\left[Mg^{2+}\right]^n\left[UO_2(CO_3)_3^{4-}\right]} \qquad n = 1, 2 \qquad \text{(IV - 2)}$$

where the unit of concentration is molality (mol kg_w^{-1}).

The slope analysis, as expressed in Eq. IV - 3, is used to evaluate the conditional successive formation constants $\log_{10}K_{n.1.3}$ after rounding-off the slope n, representative of stoichiometric number of Mg^{2+}, to its nearest integer,

$$\log_{10} R = \log_{10} \frac{\left[Mg_nUO_2(CO_3)_3^{(4-2n)-}\right]}{\left[UO_2(CO_3)_3^{4-}\right]/_\alpha} = \log_{10} \frac{FI_0\left(Mg_nUO_2(CO_3)_3^{(4-2n)-}\right)}{FI_0(UO_2(CO_3)_3^{4-})/_\alpha}$$

$$\log_{10} R = \log_{10} K_{n.1.3} + n \log_{10}\left[Mg^{2+}\right] \qquad \text{(IV - 3)}$$

where R represents the concentration ratio between the $[Mg_nUO_2(CO_3)_3^{(4-2n)-}]$ and $[UO_2(CO_3)_3^{4-}]$ taking α into account.

The α coefficient allows calculating the amount of $UO_2(CO_3)_3^{4-}$ at pH values as a function of pH. The formation constants used to calculate α are given in Table IV - 1 and the calculated α values for each sample in this work are listed in Table IV - S2 of the SI.

Table IV - 1 Stability constants of U(VI) complexes at 25°C and I_m = 0, used in this work.

Reaction	$\log_{10} K^\circ$	References
$CO_2(g) + H_2O \rightleftarrows CO_3^{2-} + 2H^+$	-18.15 ± 0.06	Guillaumont, *et al.*[22]
$CO_3^{2-} + 2H^+ \rightleftarrows CO_2(aq) + H_2O$	16.68 ± 0.05	Guillaumont, *et al.*[22]
$CO_3^{2-} + H^+ \rightleftarrows HCO_3^-$	10.33 ± 0.05	Guillaumont, *et al.*[22]
$UO_2^{2+} + H_2O \rightleftarrows UO_2(OH)^+ + H^+$	-5.25 ± 0.24	Guillaumont, *et al.*[22]
$UO_2^{2+} + 2H_2O \rightleftarrows UO_2(OH)_2(aq) + 2H^+$	-12.15 ± 0.07	Guillaumont, *et al.*[22]
$3\ UO_2^{2+} + 5H_2O \rightleftarrows (UO_2)_3(OH)_5^+ + 5H^+$	-15.55 ± 0.12	Guillaumont, *et al.*[22]
$UO_2^{2+} + CO_3^{2-} \rightleftarrows UO_2(CO_3)(aq)$	9.94 ± 0.03	Guillaumont, *et al.*[22]
$UO_2^{2+} + 2CO_3^{2-} \rightleftarrows UO_2(CO_3)_2^{2-}$	16.61 ± 0.09	Guillaumont, *et al.*[22]
$UO_2^{2+} + 3CO_3^{2-} \rightleftarrows UO_2(CO_3)_3^{4-}$	21.84 ± 0.04	Guillaumont, *et al.*[22]
$2UO_2^{2+} + CO_2(g) + 4H_2O \rightleftarrows (UO_2)_2CO_3(OH)_3^- + 5H^+$	-19.01 ± 0.50	Guillaumont, *et al.*[22]
$UO_2(CO_3)_3^{4-} + 4H^+ \rightleftarrows UO_2(CO_3)(aq) + 2CO_2(g) + 2H_2O$	24.40 ± 0.21*	Recalculated from Guillaumont, *et al.*[22]
$UO_2(CO_3)_3^{4-} + 2H^+ \rightleftarrows UO_2(CO_3)_2^{2-} + CO_2(g) + H_2O$	12.92 ± 0.15*	Recalculated from Guillaumont, *et al.*[22]
$2UO_2(CO_3)_3^{4-} + 7H^+ \rightleftarrows (UO_2)_2CO_3(OH)_3^- + 5CO_2(g) + 2H_2O$	46.21 ± 0.70*	Recalculated from Guillaumont, *et al.*[22]
$Ca^{2+} + UO_2(CO_3)_3^{4-} \rightleftarrows CaUO_2(CO_3)_3^{2-}$	5.36 ± 0.01	Shang and Reiller[22] in NaCl
$2Ca^{2+} + UO_2(CO_3)_3^{4-} \rightleftarrows Ca_2UO_2(CO_3)_3(aq)$	8.65 ± 0.02	Shang and Reiller[22] in NaCl
	$\log_{10} \beta^\circ$	
$Ca^{2+} + UO_2^{2+} + 3CO_3^{2-} \rightleftarrows CaUO_2(CO_3)_3^{2-}$	27.20 ± 0.04	Shang and Reiller[24] in NaCl
	27.22 ± 0.04	multilinear regression
$2Ca^{2+} + UO_2^{2+} + 3CO_3^{2-} \rightleftarrows Ca_2UO_2(CO_3)_3(aq)$	30.49 ± 0.05	Shang and Reiller[24] in NaCl
	30.51 ± 0.06	multilinear regression
$Mg^{2+} + UO_2^{2+} + 3CO_3^{2-} \rightleftarrows MgUO_2(CO_3)_3^{2-}$	26.40 ± 0.07	p.w.

Table IV - 2 Thermodynamic functions of formation ($\Delta_f G°_m$ et $\Delta_f H^\circ_m$) for the main species considered.

Species	$\Delta_f G°_m$ (kJ mol^{-1})	$\Delta_f H°_m$ (kJ mol^{-1})
$CO_2(g)$	-394.373 ± 0.133[a]	-393.510 ± 0.130[a]
$CO_2(aq)$	-385.970 ± 0.270[a]	-413.260 ± 0.200[a]
HCO_3^-	-586.845 ± 0.251[a]	-689.930 ± 0.200[a]
CO_3^{2-}	-527.900 ± 0.390[a]	-675.230 ± 0.250[a]
UO_2^{2+}	-952.551 ± 1.747[a]	-1 019.000 ± 1.500[a]
$UO_2(CO_3)_3^{4-}$	-2 660.914 ± 2.116[a]	-3 083.890 ± 4.430[a]
$MgUO_2(CO_3)_3^{2-}$	-3 141.177 ± 2.740[b]	
	-3 142.318 ± 8.699 (p.w.)	
$Mg_2UO_2(CO_3)_3(aq)$	-3 601.689 ± 4.825[b]	
	Not evidenced in p.w.	
$CaUO_2(CO_3)_3^{2-}$	-3 243.174 ± 2.613[b]	-3 634.690 ± 6.310[b]
	-3 244.430 ± 2.361[c]	
$Ca_2UO_2(CO_3)_3(aq)$	-3 817.671 ± 3.747[b]	-4 177.690 ± 7.471[b]
	-3 816.015 ± 2.991[c]	/
Mg^{2+}	-455.375 ± 1.335[a]	-467.000 ± 0.600[a]
Ca^{2+}	-552.806 ± 1.050[a]	-543.000 ± 1.000[a]

a Guillaumont, *et al.*[22]; b Grenthe, *et al.*[23]; c Shang, *et al.*[24]

3.4 Specific ion interaction Theory (SIT)

The formation constants $\log_{10}K°_{n.1.3}$ were obtained by extrapolating the $\log_{10}K_{n.1.3}$ values at investigated ionic strengths with the SIT approach, in which the activity coefficient is expressed as follows,

$$\log_{10}\gamma_j = -z_j^2 D_H + \varepsilon(j, k, I_m)\, m_k \qquad \text{(IV - 4)}$$

where ε(j,k) ($kg_w\ mol^{-1}$) is the specific ion interaction coefficient between the aqueous ion j and the oppositely charge ion *k* in medium solution of ionic strength I_m. The Debye-Hückel term is expressed in Eq. IV - 5,

$$D_H = \frac{A\sqrt{I_m}}{1+1.5\sqrt{I_m}} \qquad \text{(IV - 5)}$$

where the value of 0.507 $kg^{1/2}\ mol^{-1/2}$ was assigned to Debye-Hückel constant *A*, corresponding to the actual temperature of 22°C.[22] In Eq. IV - 6, the relationship between the global conditional formation constants $\log_{10}\beta_{0.1.3}$ and ionic strengths is expressed,

$$\log_{10}\beta_{n.1.3} = \log_{10}\beta_{0.1.3} + \log_{10}K_{n.1.3} = \log_{10}\beta^{\circ}_{n.1.3} + \Delta z^2 D_H - \Delta\varepsilon I_m \qquad \text{(IV - 6)}$$

where

$$\Delta z^2 = z\left(Mg_nUO_2(CO_3)_3^{(4-2n)-}\right)^2 - nz\left(Mg^{2+}\right)^2 - z\left(UO_2^{2+}\right)^2 - 3z\left(CO_3^{2-}\right)^2 \qquad \text{(IV - 7)}$$

($\Delta z^2 = -16$ for n = 1 and $\Delta z^2 = -24$ for n = 2) and

$$\Delta\varepsilon = \varepsilon\left(Mg_nUO_2(CO_3)_3^{(4-2n)-}, Na^+\right) - n\varepsilon\left(Mg^{2+}, Cl^-/ClO_4^-\right) - \varepsilon\left(UO_2^{2+}, Cl^-/ClO_4^-\right) - 3\varepsilon(Na^+, CO_3^{2-}) \qquad \text{(IV - 8)}$$

The specific ion interaction coefficients used in calculations are summarized in Table IV - 3. It is noteworthy that $\varepsilon(UO_2^{2+},Cl^-)$ = 0.21 $kg_w\ mol^{-1}$ was not used in this study, because Guillaumont, *et al.*[22] proposed that the complexation between uranyl and chloride ion should not be ignored, though the interaction is rather weak. For the sake of consistency with our previous works, $\varepsilon(UO_2^{2+}, ClO_4^-)$ = 0.46 $kg_w\ mol^{-1}$ was used in this work.

Table IV - 3 Main specific ion interaction coefficients used in this work.

Specific ion interaction coefficient	Value (± 1σ)	Ref.
$\varepsilon(H^+,ClO_4^-)$	0.14 ± 0.02	Guillaumont, *et al.*[22]
$\varepsilon(H^+,Cl^-)$	0.12 ± 0.01	idem
$\varepsilon(Na^+,CO_3^{2-})$	-0.08 ± 0.03	idem
$\varepsilon(UO_2^{2+},ClO_4^-)$	0.46 ± 0.03	idem
$\varepsilon(UO_2^{2+},Cl^-)$	0.46 ± 0.03	idem
$\varepsilon(Mg^{2+},ClO_4^-)$	0.33 ± 0.03	idem
$\varepsilon(Mg^{2+},Cl^-)$	0.19 ± 0.02	idem
$\varepsilon(UO_2(CO_3)_2^{2-},Na^+)$	-0.02 ± 0.09	idem
$\varepsilon(UO_2(CO_3)_3^{4-},Na^+)$	-0.01 ± 0.11	idem
$\varepsilon(MgUO_2(CO_3)_3^{2-},Na^+)$ (in $NaClO_4$)	0.19 ± 0.11	p.w.
$\varepsilon(MgUO_2(CO_3)_3^{2-},Na^+)$ (in NaCl)	0.09 ± 0.16	p.w.
$\varepsilon(CaUO_2(CO_3)_3^{2-},Na^+)$ (in NaCl)	0.29 ± 0.11	Shang and Reiller[24]
$\varepsilon(Ca_2UO_2(CO_3)_3,NaCl)$	0.66 ± 0.22	idem
$\varepsilon(CaUO_2(CO_3)_3^{2-},Na^+)$ (in $NaClO_4$)	0.02 ± 0.04	idem
$\varepsilon(Ca_2UO_2(CO_3)_3,NaClO_4)$	0.18 ± 0.07	idem

IV - 4 Results and discussion

4.1 Evaluation of equilibrium constants and specific ion interaction coefficients

A series of solutions was prepared at desired ionic strengths with the maximum electrolyte concentrations fixed to 1 mol kg_w^{-1} in NaCl,[24] and 2.21 mol kg_w^{-1} in $NaClO_4$.[25] The luminescence intensities FI_0 at $D = 0$ and decay-times τ for individual sample solution were obtained by integrating time-resolved luminescence spectra with the trapezoidal rule then fitting the resulting intensities *FI* at various delay times to the exponential decay functions. Fig. IV - 1 shows the graphical relationship between $\log_{10}R$ and $\log_{10}[Mg^{2+}]$ at varying ionic strengths. The stoichiometric coefficients of Mg^{2+} are determined by the slope analysis according to the experimental methodology. The 2σ uncertainties resulting from the trapezoidal integration rule were evaluated in the values of $\log_{10}R$ and included in the linear fits by weighted least-squares regression analysis.

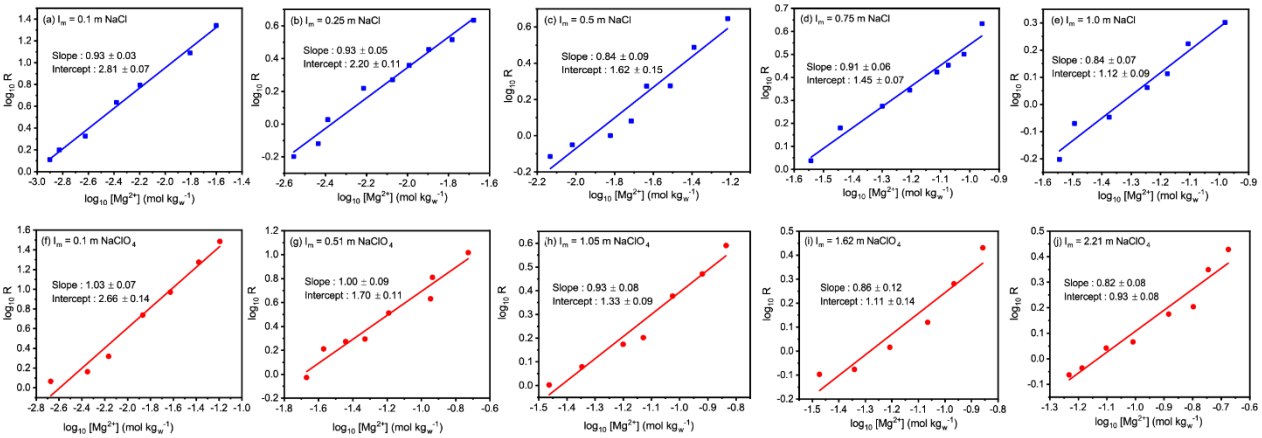

Fig. IV - 1 Plot of logarithmic ratio R as a function of $\log_{10}[Mg^{2+}]$ (mol kg_w^{-1}) at (a) – (e) I_m = 0.10 – 1.0 mol kg_w^{-1} of NaCl, (f) – (j) I_m = 0.10 – 2.21 mol kg_w^{-1} of $NaClO_4$: $[U]_{total}$ = 50 μmol kg_w^{-1}, $P(CO_2) = 10^{-3.5}$ atm.

A slope *ca.* 1 was obtained in the linear correlation at specific ionic strength in both media, indicating the formation of $MgUO_2(CO_3)_3^{2-}$. The expected presence of $Mg_2UO_2(CO_3)_3(aq)$, according to Lee, *et al.*,[10] cannot be identified, albeit relatively high final [Mg^{2+}]. The essential ingredient for application of α coefficient is the accurate description of $UO_2(CO_3)_3^{4-}$ variation as a function of pH and I_m in absence of Mg^{2+}. Failure to maintain the background electrolyte concentration when adding the alkaline metal ions to U(VI)-CO_3 systems may cause unpredictable results on conditional stability constants, especially for the investigated charge neutralization during which the highly charged ions could interact significantly.[50,51] This problematic situation was avoided by restricting the maximum concentration of Mg^{2+} within about 10% of actual ionic strengths at the end of complexation in most series (*c.f.* Table IV - S2 of the SI). Even though at relatively lower I_m, *i.e.*, 0.10 and 0.51 *m* $NaClO_4$ and 0.10 *m* NaCl, the last two or three samples exceed somewhat the limit of 10%, the including of these points did not give the second slope (Fig. IV - 1). For this reason, they were retained in the slope analysis.

Table IV - 4 lists the total magnesium concentration and aqueous pH values where the linear relationship is satisfied. The slope values of the fitting results in Fig. IV - 1 were rounded-off to unity, and the associated intercepts were assigned to the formation constants of $MgUO_2(CO_3)_3^{2-}$ at different ionic strengths in $NaClO_4$ and NaCl. Table IV - 5 summarizes the apparent successive constants $\log_{10}K_{1.1.3}$, the cumulative constants $\log_{10}\beta_{1.1.3}$, and the values of $\log_{10}\beta_{1.1.3} + 16D_H$ for the evaluations of $\log_{10}\beta°$ and $\varepsilon(MgUO_2(CO_3)_3^{2-},Na^+)$. The dependence of the conditional equilibrium constants on ionic strength is clearly shown. As I_m increases, the interaction between Mg^{2+} and $UO_2(CO_3)_3^{4-}$ is inevitably weakened as a result of the attraction

from the oppositely charged ions in solution, *i.e.* Cl^-/ClO_4^- and Na^+. This phenomenon can be numerically interpreted by the decreasing trend of $\log_{10}K_{1.1.3}$ *vs.* I_m, as shown in Table IV - 5.

Table IV - 4 Values of $\log_{10}[Mg^{2+}]$ and pH obtained from the slope analysis in Fig. IV - 1.

I_m ($NaClO_4$)	$MgUO_2(CO_3)_3^{2-}$ ($\log_{10}$ [Mg^{2+}], pH)	I_m (NaCl)	$MgUO_2(CO_3)_3^{2-}$ ($\log_{10}$ [Mg^{2+}], pH)
0.10 m	(-2.67, 8.20) → (-1.19, 7.73)	0.10 m	(-2.90, 8.07) → (-1.60, 7.74)
0.51 m	(-1.67, 8.09) → (-0.73, 7.53)	0.25 m	(-2.55, 8.00) → (-1.68, 7.70)
1.05 m	(-1.46, 7.67) → (-0.84, 7.48)	0.50 m	(-2.13, 7.75) → (-1.22, 7.55)
1.62 m	(-1.47, 7.78) → (-0.86, 7.47)	0.75 m	(-1.54, 7.82) → (-0.96, 7.55)
2.21 m	(-1.23, 7.85) → (-0.67, 7.43)	1.00 m	(-1.54, 7.71) → (-0.98, 7.50)

Table IV - 5 Formation constants $\log_{10}K_{1.1.3}$ derived from the rounded off slopes in Fig. IV - 1. Values of $\log_{10}\beta_{0.1.3}$ were calculated with $\log_{10}\beta_{0.1.3}^\circ = 21.84$ and $\Delta\varepsilon = -0.23$. $kg_w\ mol^{-1}$.

I_m ($NaClO_4$)	$\log_{10}K_{1.1.3}$	$\log_{10}\beta_{0.1.3}$	$\log_{10}\beta_{1.1.3} + 16D_H$	I_m (NaCl)	$\log_{10}K_{1.1.3}$	$\log_{10}\beta_{0.1.3}$	$\log_{10}\beta_{1.1.3} + 16D_H$
0.10 *m*	2.61 ±	21.86 ±	26.23 ± 0.05	0.10 *m*	2.98 ±	21.86 ±	26.59 ± 0.05
0.51 *m*	1.69 ±	21.96 ±	26.46 ± 0.04	0.25 *m*	2.35 ±	21.90 ±	26.58 ± 0.04
1.05 *m*	1.40 ±	22.08 ±	26.77 ± 0.05	0.50 *m*	1.88 ±	21.96 ±	26.63 ± 0.05
1.62 *m*	1.26 ±	22.21 ±	27.04 ± 0.04	0.75 *m*	1.56 ±	22.01 ±	26.64 ± 0.04
2.21 *m*	1.10 ±	22.35 ±	27.20 ± 0.04	1.00 *m*	1.33 ±	22.07 ±	26.66 ± 0.04

Fig. IV - 2(a) shows the variation of $\log_{10}\beta_{1.1.3} + 16D_H$ as a function of I_m in NaCl and $NaClO_4$, where the values of $\log_{10}\beta_{1.1.3}$ is the sum of $\log_{10}\beta_{0.1.3}$ and $\log_{10}K_{1.1.3}$ and D_H are recalculated with respect to the specific ionic strengths. Error propagation was used to evaluate the uncertainty ranges. The obtained equilibrium constants are determined as $\log_{10}\beta^\circ_{1.1.3} = 26.27 \pm 0.06$ in $NaClO_4$ and $\log_{10}\beta^\circ_{1.1.3} = 26.57 \pm 0.01$ in NaCl. The specific ion interaction coefficients are evaluated to be $\varepsilon(MgUO_2(CO_3)_3^{2-},Na^+) = 0.09 \pm 0.04\ kg_w\ mol^{-1}$ in $NaClO_4$ and $\varepsilon(MgUO_2(CO_3)_3^{2-},Na^+) = 0.31 \pm 0.02\ kg_w\ mol^{-1}$ in NaCl. However, from a theoretical point of view it seems difficult to understand that the extrapolation to infinite dilution, *i.e.* in the absence of salt, would depend on the type of background electrolyte.

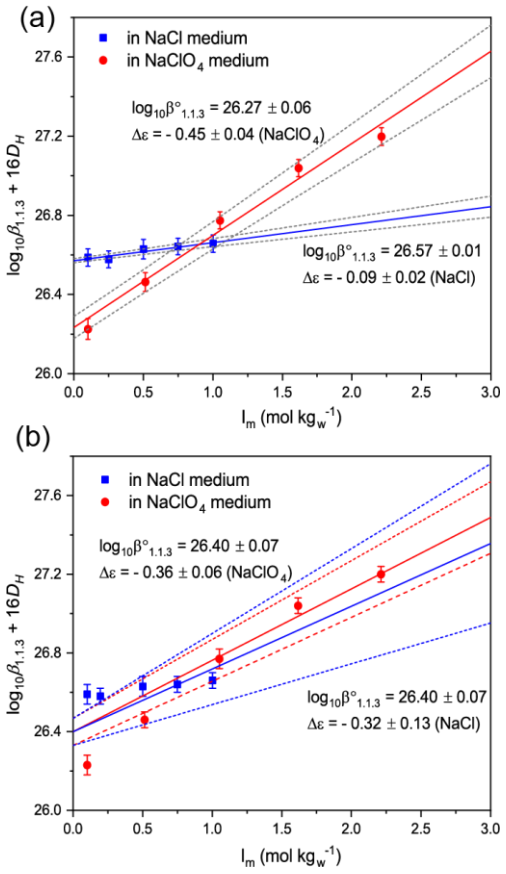

Fig. IV - 2 Extrapolation to infinite dilution of the experimental data of $log_{10}\beta_{1.1.3}$+ $16D_H$ as a function of ionic strength (a) by individual regression in NaCl and $NaClO_4$ and (b) by multilinear regression.

The simultaneous fitting with a common value of $\log_{10}\beta^\circ_{1.1.3}$ was performed on the two datasets of (I_m, $\log_{10}\beta_{1.1.3} + 16D_H$) in NaCl and $NaClO_4$ as shown in Fig. IV - 2(b). The common formation constant was determined as $\log_{10}\beta^\circ_{1.1.3}$ = 26.40 ± 0.07 with $\varepsilon(MgUO_2(CO_3)_3^{2-}, Na^+)$ = 0.19 ± 0.11 $kg_w\ mol^{-1}$ in $NaClO_4$ and $\varepsilon(MgUO_2(CO_3)_3^{2-},Na^+)$ = 0.09 ± 0.16 $kg_w\ mol^{-1}$ in NaCl. The earlier published stability constants of $MgUO_2(CO_3)_3^{2-}$ complex are listed in Table IV - 6. The obtained constants in the present work are slightly higher than those reported previously in the case of NaCl. It is worth noting that the value of $\log_{10}\beta^\circ_{1.1.3}$ depends on the extrapolation models used to describe the correlation between activity coefficient and ionic strength. For the previous propositions, the mainly used models were Davies,[35] applicable to I_m < 0.3 mol kg_w^{-1}, and SIT,[22] valid for a wider range of I_m < 3-4 mol kg_w^{-1}. In a systematic manner, Dong and Brooks[15] compared the values of $\log_{10}\beta^\circ_{1.1.3}$ using these two different models in $NaNO_3$. The authors mentioned that the use of Davies equation is not appropriate in their study in which the maximum ionic strength extended to 0.509 mol kg_w^{-1} $NaNO_3$ and also proposed the results for $\varepsilon(MgUO_2(CO_3)_3^{2-}, Na^+)$ estimated by SIT as -3.0 ± 0.3 $kg_w\ mol^{-1}$.

Table IV - 6 Formation constants of $MgUO_2(CO_3)_3^{2-}$ complex determined in literature and in this work.

$\log_{10}\beta°(MgUO_2(CO_3)_3^{2-})$	Medium and I_m correction	Ref
26.11 ± 0.04	0.1 mol L^{-1} $NaNO_3$ (Davies)	Dong and Brooks[14]
25.8 ± 0.5	Averaged from values in 0.101 to 0.509 mol kg_w^{-1} $NaNO_3$ (Davies)	Dong and Brooks[15]
25.02 ± 0.08	Extrapolated using SIT 0.101 - 0.509 mol kg_w^{-1} $NaNO_3$	Dong and Brooks[15]
26.25 ± 0.04	0.1 mol L^{-1} NaCl (SIT)	Endrizzi and Rao[18]
25.8 ± 0.3	0.15 mol L^{-1} NaCl (SIT)	Lee, *et al.*[10]
26.24 ± 0.13	0.1 mol L^{-1} $NaClO_4$ (Davies)	Geipel, *et al.*[12]
26.57 ± 0.01	0.1 – 1.0 mol kg_w^{-1} NaCl (SIT)	p.w.
26.27 ± 0.06	0.1 – 2.21 mol kg_w^{-1} $NaClO_4$ (SIT)	p.w.

4.2 Discussion on the values of $\log_{10}\beta°_{1.1.3}$ and ε

The value of $\log_{10}\beta°(MgUO_2(CO_3)_3^{2-})$, the Gibbs energy of formation, and specific ion interaction coefficients are reported in the Table IV - 1, 2 and 3, respectively. It can be seen that the values proposed in Grenthe, *et al.*[23] are very similar to the ones obtained here. Our data set presenting the advantage to provide the specific ion interaction coefficients, which could not be selected at the time of the review. The variations of $\log_{10}\beta_{1.1.3} + 16D_H$ *vs.* I_m for $MgUO_2(CO_3)_3^{2-}$ and $CaUO_2(CO_3)_3^{2-}$ in NaCl and $NaClO_4$ exhibited virtually identical behaviours and resulted in comparable values of interaction coefficients. In NaCl, $\varepsilon(CaUO_2(CO_3)_3^{2-}, Na^+)$ and $\varepsilon(MgUO_2(CO_3)_3^{2-}, Na^+)$ were determined to be 0.29 ± 0.11 kg_w mol^{-1} and 0.31 ± 0.02 kg_w mol^{-1}, respectively, and in $NaClO_4$, $\varepsilon(CaUO_2(CO_3)_3^{2-}, Na^+)$ and $\varepsilon(MgUO_2(CO_3)_3^{2-}, Na^+)$ were estimated to be 0.09 ± 0.04 kg_w mol^{-1} and 0.02 ± 0.04 kg_w mol^{-1}, respectively. Regardless of the type of alkaline earth cation, the ε values both presented obvious decrease when changing the supporting electrolyte from NaCl to $NaClO_4$. The behaviour of ε implies that the influence of ionic strength on the complexations of Mg^{2+} and Ca^{2+} with $UO_2(CO_3)_3^{4-}$ is more sensitively reflected by the change of medium anions than alkaline earth metal ions. At high electrolyte concentrations, the complexation of Mg^{2+} and Ca^{2+} with $UO_2(CO_3)_3^{4-}$ can be in all likelihood competed with cationic Na^+ as well as hampered by attraction of anionic ClO_4^- or Cl^- through ionic pairings. As a result, the binding processes of Mg^{2+} and Ca^{2+} with $UO_2(CO_3)_3^{4-}$ should not be estimated to the binary stage alone. Still, the ion-pairs formations between Mg^{2+}/Ca^{2+} and the medium anion are supposed to have comparable quantitative effects on the complexation of Mg^{2+}/Ca^{2+} with $UO_2(CO_3)_3^{4-}$, resulting in the close values of interaction coefficients for $MUO_2(CO_3)_3^{2-}$ in a given electrolyte.

For small ions of high charge density like M^{2+} (M = Mg, Ca), the ease of desolvation in their hydrated shells due to the attraction of large ions of small charge density like ClO_4^- or Cl^- is probably responsible for their ion-pairs association.[26,52] Nevertheless, the ionic attraction could not to overcome the first hydration shell of M^{2+} (M = Mg, Ca) in the investigated range of

electrolyte concentrations, and thus solvent-shared ion pairs are the most probable type where only one layer of water molecules between the ion partners of the pair exists.[53] Such ion-pairs formation makes the cation M^{2+} (M = Mg, Ca) effectively larger, also reduces their electric ability to approach and react with $UO_2(CO_3)_3^{4-}$.[54] Whereas once complexed with $UO_2(CO_3)_3^{4-}$, the integrity of inner sphere water molecules of alkaline earth cations is disrupted by partly replacing oxygen atoms of carbonates for water molecules.[28-30,55]

It is worth noting here that complexation of the first and the second alkaline earth cation exhibit slightly different configurations in molecular dynamic (MD) simulations. Under present experimental concentrations, *i.e.* 0.1-2.21 mol kg_w^{-1}, Ca^{2+} – IR_{VII} = 1.06 Å, in Shannon[56] – is most probably surrounded with 7 H_2O in its immediate environment giving a pentagonal bipyramid geometry[31,33,57]. While smaller Mg^{2+} – IR_{VI} = 0.72 Å, Shannon[56] – adopts an octahedral structure with perpendicular square plan, which is disadvantageous to the water exchange when coordinating to $UO_2(CO_3)_3^{4-}$.[34,58] Kerisit and Liu[33] reported the structural properties of $M_nUO_2(CO_3)_3^{(4-2n)-}$ (M = Mg, Ca, Sr, n = {1;2}) using the MD simulations, and observed that for $MgUO_2(CO_3)_3^{2-}$ and $M_nUO_2(CO_3)_3^{(4-2n)-}$ (M = Ca, Sr, n = {1;2}) species, at least two water molecules were substituted by carbonates in the first coordination shell of alkaline earth metal ions that promote stable complexation. However, for the $Mg_2UO_2(CO_3)_3(aq)$ complex, one of two Mg^{2+} exceptionally changed its configuration from bidentate to monodentate towards $UO_2(CO_3)_3^{4-}$ because of an additional H_2O in the inner sphere of Mg^{2+}. The intrinsic difficulty in the second Mg^{2+} complexation, induced by the solid square geometry in its equatorial plane, possibly contributes to this monodentate binding configuration, also the reason for the non-detection of $Mg_2UO_2(CO_3)_3(aq)$ complex in this work. It can also be reminded that Oher, *et al.*[47] stated that $MgUO_2(CO_3)_3^{2-}$ and $Mg_2UO_2(CO_3)_3(aq)$ are supposed to show almost indistinguishable luminescence spectra.

The steric hindrance effects of Mg^{2+} can be reflected by comparing the stability constants with various ligands with other elements in the alkaline earth group. The $\log_{10}\beta°$ values often present a regular sequence from Ca to Ba with an anomaly occurred for Mg (see Fig. IV - S1 of the SI). Another important evidence supporting the steric congestion of Mg^{2+} has to do with the energy balance obtained for the complexations of Mg^{2+} and Ca^{2+} with $UO_2(CO_3)_3^{4-}$. Indeed, the energy required to break the hydrogen bonds Mg-O(H_2O) is higher than the energy released by the formation of Mg-O(CO_3) bonds, leading to a net loss of energy.[17] The opposite situation instead applies for the Ca^{2+} complexation that gives rise to an exothermic reaction.[16,18]

In Fig. IV - S1 of the SI, the clearly discernible linear relationship between the formation constants of Mg and those of Ca with different ligands indicates that the highly charged counterparts generally form stable complexes (see Table IV - S4 of the SI for formation constants). However, with the same ligand, the stability constants pattern is less clear and exhibits two kinds of behaviour depending on the size of alkaline earth metal ions from Ca^{2+} to Ba^{2+}. For ligands of large charge density and anions of weak acids, *e.g.* F^-, OH^-, and CO_3^{2-}, the values of $\log_{10}K^o$ decreases generally with the ionic radius. On the contrary, for anions of strong oxoacids, *e.g.* SO_4^{2-}, $S_2O_3^{2-}$, the stability constants are usually small but present an increasing trend with the cation size (see Table IV - S5 of the SI). Interestingly, the evolution of $\log_{10}\beta°_{1.1.3}$ shows an unambiguous increase with decreasing size of cation, except the anomaly with Mg^{2+} as shown in Fig. IV - S1 and S2 of the SI. It is therefore suggested that the $UO_2(CO_3)_3^{4-}$ displays similar characteristics to weak acids in complexation.

4.3 Evolution of luminescence spectra and temporal properties

Fig. IV - 3 illustrates the complexation of Mg^{2+} with $UO_2(CO_3)_3^{4-}$ in spectral domain using the 300 lines mm^{-1} grating. The progressively enhanced luminescence intensities, better-resolved spectra and steadily narrowing bands evidenced the binding process of alkaline earth metal ions. The spectral evolution pattern for Mg-UO_2-CO_3 complexes are in line with previous observations on alkaline earth cations.[2,9,10,12,24,25] Gaussian-based peak separation analysis – implemented in Origin 9.0 software – was applied to the luminescence spectra at D = 25 ns.

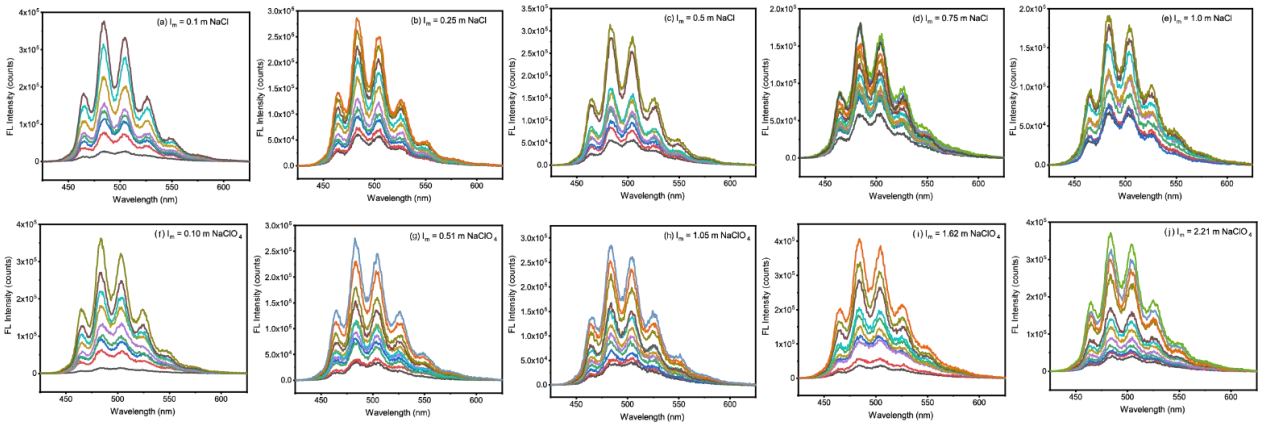

Fig. IV - 3 Graphical representations of luminescence emission spectra on complexation of Mg(II) with $UO_2(CO_3)_3^{4-}$ at investigated ionic strengths: (a) – (e) I_m = 0.10 – 1.0 mol kg_w^{-1} of NaCl, (f) – (j) I_m = 0.10 – 2.21 mol kg_w^{-1} of $NaClO_4$, acquired at D = 25 ns and gate width W = 1μs, number of accumulation is 1000. The aqueous conditions where the $MgUO_2(CO_3)_3^{2-}$ complex dominate were listed in Table IV - 4.

An example of peak decomposition was shown in Fig. IV - 4 (see Table IV - S3 of SI for detailed decomposition parameters). The variations of characteristic peak wavelengths are weak and stay within the uncertainties when favouring the formations of ternary species. The spectral peak positions are then weightily averaged with 2σ uncertainties and found at 464.98 ± 0.44 nm, 484.77 ± 0.22 nm, 503.50 ± 0.49 nm, 524.84 ± 1.11 nm and 542.28 ± 2.71 nm in $NaClO_4$ and 464.63 ± 0.32 nm, 483.77 ± 0.29 nm, 503.71 ± 0.33 nm, 525.08 ± 0.80 nm and 546.24 ± 2.21 nm in NaCl. No obvious shifts in characteristic peak positions emerged in Mg-UO_2-CO_3 spectra, irrespective of the nature of background electrolyte or ionic strength. This observation is consistent with the spectral results obtained for Ca-UO_2-CO_3 complexes in NaCl and $NaClO_4$ in our previous works.[24,25] Nonetheless, the use of 300 lines mm^{-1} grating is very limited to discriminate the spectral differences of Mg-UO_2-CO_3 and Ca-UO_2-CO_3 complexes because of their highly similar spectral fingerprints, and of the convolution of the bands with the optical parameters of the apparatus.

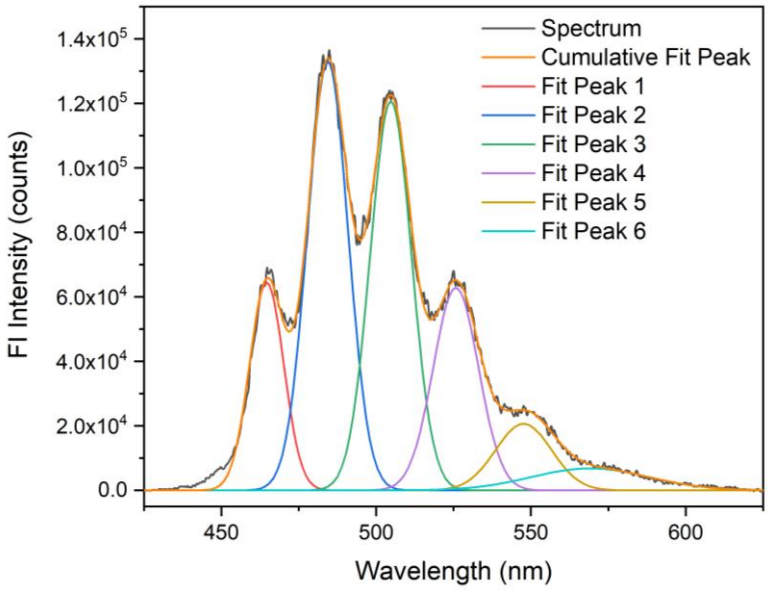

Fig. IV - 4 Gaussian decomposition of luminescence spectrum of the sample: U(VI) = 50 μmol kg_w^{-1}, Mg(II) = 0.00149 mol kg_w^{-1}, $P(CO_2) = 10^{-3.5}$ atm, pH = 8.05 at 0.1 mol kg_w^{-1} NaCl, acquired at delay time D = 25 ns and gate width W = 1μs, number of accumulation is 1000. The decomposition results were listed in Table IV - S3 of the SI.

In order to probe the possible spectral modifications, we specifically selected two samples at I_m = 0.1 and 1 *m* NaCl to focus on their specific characteristic peaks using the more resolutive 1800 lines mm^{-1} grating, as done in Oher, *et al.*[47] The wavelengths corresponding to maximum intensity were found at 465.63 nm, 484.84 nm, 504.66 nm, 527.61 nm and 548.65 nm, as shown in Fig. IV - 5. The peak shifts were not such apparent compared with the averaged peak

positions obtained by Gaussian-based decomposition of the spectra acquired with 300 lines mm^{-1} grating. A very slight bathochromic shift in the luminescence spectra when varying the principal aqueous component from Ca-UO_2-CO_3 to Mg-UO_2-CO_3 was already reported.[9,10,47]

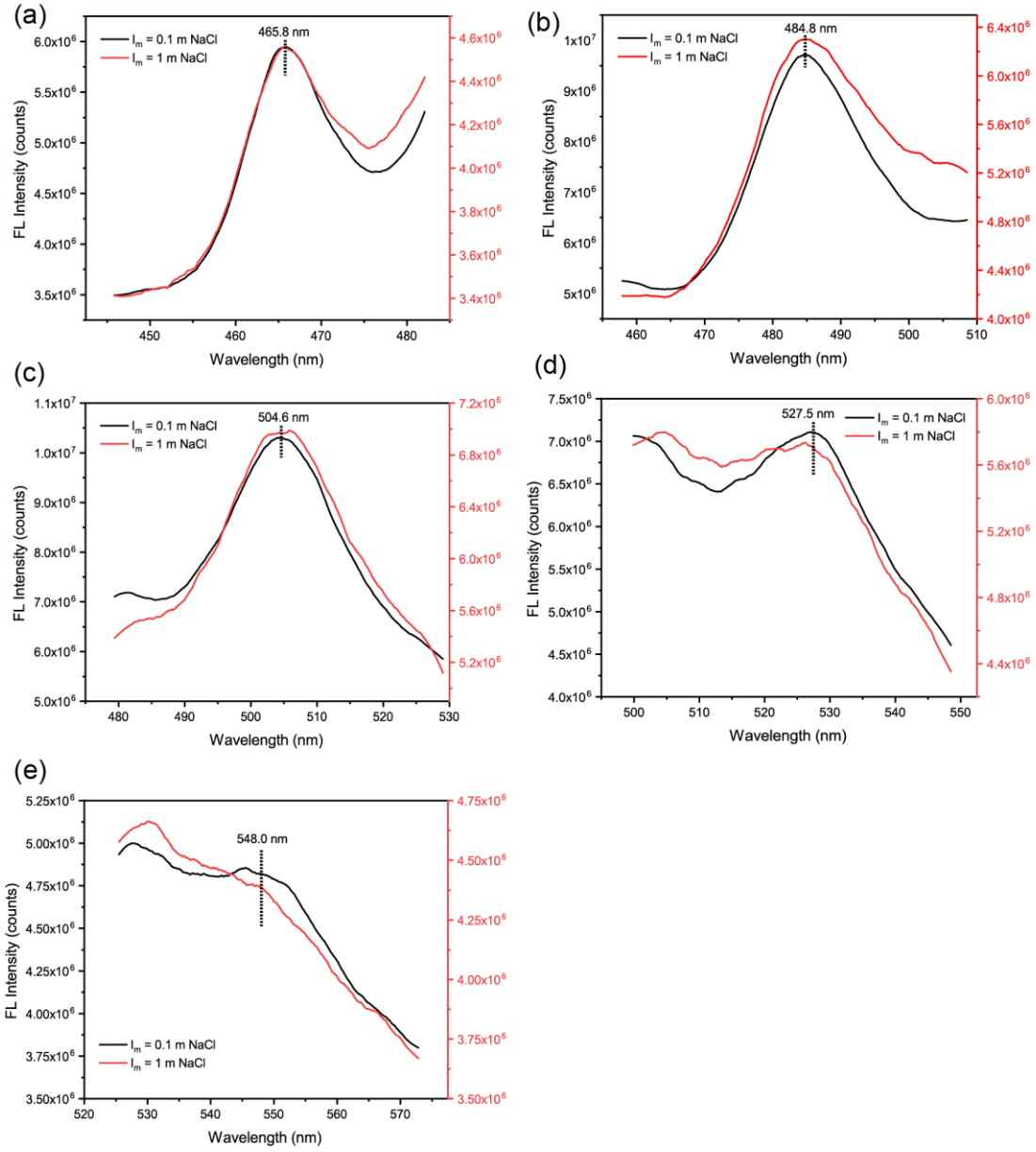

Fig. IV - 5 Measured luminescence emission spectra for each characteristic peak at: (a) 465.8 nm, (b) 484.78 nm, (c) 504.6 nm, (d) 527.5 nm et (e) 548 nm, acquired at delay time at D = 25 ns, gate width W = 1 µs and accumulation number 10000 using the 1800 lines mm^{-1} grating. The spectra were then smoothed for better comparison. The two samples are of U(VI) = 50 µmol kg_w^{-1}, Mg(II) = 0.0042 mol kg_w^{-1}, pH = 7.90 at I_m = 0.1 mol kg_w^{-1} NaCl and Mg(II) = 0.0442 mol kg_w^{-1}, pH = 7.65 at 1 mol kg_w^{-1} NaCl. The peak positions were averaged to be 464.63 ± 0.32 nm, 483.77 ± 0.29 nm, 503.71 ± 0.33 nm, 525.08 ± 0.80 nm and 546.24 ± 2.21 nm in NaCl using the 300 lines mm^{-1} grating.

The decay-times of $MgUO_2(CO_3)_3^{2-}$ are estimated by averaging the τ values of correspondent samples that give the slope of one in the slope analysis. Table IV - 7 lists the decay-times determined for $M_nUO_2(CO_3)_3^{(4-2n)-}$ (M = Mg, Ca) complexes in NaCl and $NaClO_4$. The possible quenching effect of Cl^- on temporal properties of $M_nUO_2(CO_3)_3^{(4-2n)-}$ complexes can be traced by comparing the decay-times measured at 0.1 mol kg_w^{-1} NaCl and $NaClO_4$ (see Table IV - 7). At higher NaCl concentrations, a notable decrease of decay-times is measured for $MgUO_2(CO_3)_3^{2-}$ as seen for $Ca_nUO_2(CO_3)_3^{(4-2n)-}$ complexes in Shang and Reiller.[24] Fig. IV - 6 shows that the characteristic decay-times decreased steeply in the investigated I_m range of NaCl, but varies around an average value of 22.6 ± 1.4 ns in $NaClO_4$, which is in relative good agreement with the values of 18.2 ± 2.7 ns reported by Geipel, *et al.*[12] and 17 ± 2 ns by Lee, *et al.*[10] These phenomena are significantly lower than previous results reported for $Ca_nUO_2(CO_3)_3^{(4-2n)-}$, with the average decay-times of 34.2 ± 2.2 ns for $CaUO_2(CO_3)_3^{2-}$ and 59.2 ± 4.2 ns for $Ca_2UO_2(CO_3)_3(aq)$ in $NaClO_4$.[25]

Table IV - 7 Decay-times determined for $M_nUO_2(CO_3)_3^{(4-2n)-}$ (M = Mg, Ca) complexes in NaCl and $NaClO_4$.

Decay-time (ns)	$MgUO_2(CO_3)_3^{2-}$	$CaUO_2(CO_3)_3^{2-}$	$Ca_2UO_2(CO_3)_3$
0.1 *m* NaCl	23.47 ± 1.57	28.30 ± 0.57	46.70 ± 2.70
0.1 *m* $NaClO_4$	27.99 ± 2.43	30.41 ± 1.90	51.19 ± 1.94
0.1 – 2.21 *m* $NaClO_4$	22.64 ± 1.40	34.20 ± 2.24	59.21 ± 4.15

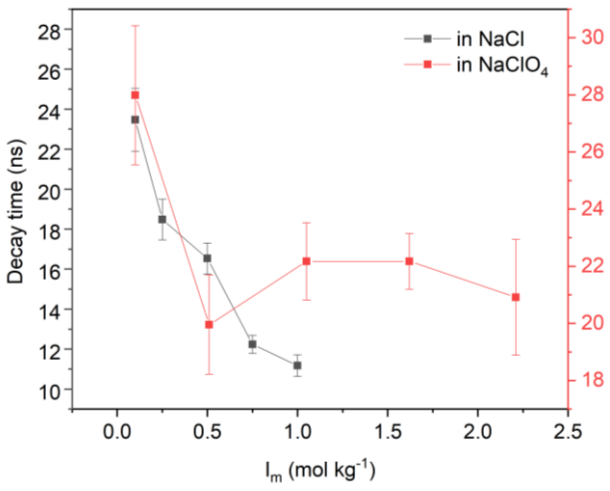

Fig. IV - 6 Variations of decay-times obtained by averaging the sample solutions giving the slopes of 1 at investigated NaCl and $NaClO_4$ ionic strengths.

The decay-time results demonstrate that the Ca(II)-bound U(VI) species are more fluorescent than the Mg(II)-bound U(VI) species in terms of the temporal proprieties. The fact that the

Ca-UO_2-CO_3 complexes have longer decay-times than Mg-UO_2-CO_3 complexes under similar conditions is probably related to the differences in their luminescent capacity.

IV - 5 Practical applications

5.1 Case of radioactive waste management

In Shang and Reiller,[24] the application of the experimentally measured $\log_{10}\beta°$ and ε values of $Ca_nUO_2(CO_3)_3^{(4-2n)-}$ was done in the case of water compositions of underground research laboratory for nuclear disposal facilities: the Boom clay rock in Belgium,[36] and the Callovo-Oxfordian clay rock in France.[37] The predictive calculations used the thermodynamic constants of Mg^{2+}, Sr^{2+} complexes from Dong and Brooks[14] with no ε values – *i.e.* $\varepsilon = 0$ using the ThermoChimie 9b database for PhreeqC[43,44] at the time of writing of Shang and Reiller.[24]

In this exercise, the ThermoChimie 10a database was used to theoretical speciation calculations. We implement the input PhreeqC file with the $\log_{10}\beta°_{n.1.3}$ and ε values of $M_nUO_2(CO_3)_3^{(4-2n)-}$ (M = Mg, Ca, n = {1;2}) determined in NaCl from our previous work for Ca,[24] and those for Mg in the present work. The origin of data is detailed on the web pages (http://www.thermochimie-tdb.com). It is worth noting that the originally implemented stability constants of $Ca_nUO_2(CO_3)_3^{(4-2n)-}$ (n = {1; 2}) in ThermoChimie 10a database were taken from Dong and Brooks,[14] whilst the $MgUO_2(CO_3)_3^{2-}$ constant from the same authors was not implemented; no ε values were included for the $M_nUO_2(CO_3)_3^{(4-2n)-}$ complexes, and were thus considered as nil in calculations.

As illustrated in Fig. IV - 7, the relative proportion of $MgUO_2(CO_3)_3^{2-}$ slightly increased *ca.* 0.5 unit (Fig. IV - 7 (a, c)) (7-8% in percentage, see Fig. IV - 7 (b, d)) in both contexts, compared with the results in our previous work – see Fig. 8 of Shang and Reiller.[24] However, general distribution pattern did not exhibit strong alternation of the concerned species. As noted in Reiller and Descostes,[7] the high concentration of carbonate – or activity of either HCO_3^- or CO_3^{2-} – in Boom Clay context assures the predominance of $M_nUO_2(CO_3)_3^{(4-2n)-}$ complexes (n = {0;1;2}) throughout the pH values, even with a lower redox potential. Whereas in Callovo-Oxfordian context the higher Ca and lower carbonate concentrations – or Ca^{2+}, and either HCO_3^- or CO_3^{2-} activities – assure the predominance of $Ca_2UO_2(CO_3)_3$(aq) complex at pH values lower than 8.5, and then of $U(OH)_4$(aq) in higher basicity because of a lower carbonate content. It can be seen in both cases that the proportions of $MgUO_2(CO_3)_3^{2-}$ in solution is significantly higher than in our previous exercise. This is more evident for the Boom clay context compared to the

Callovo-Oxfordian context where the ratio of Ca/Mg is higher – see water compositions in SI in Reiller and Descostes.[7]

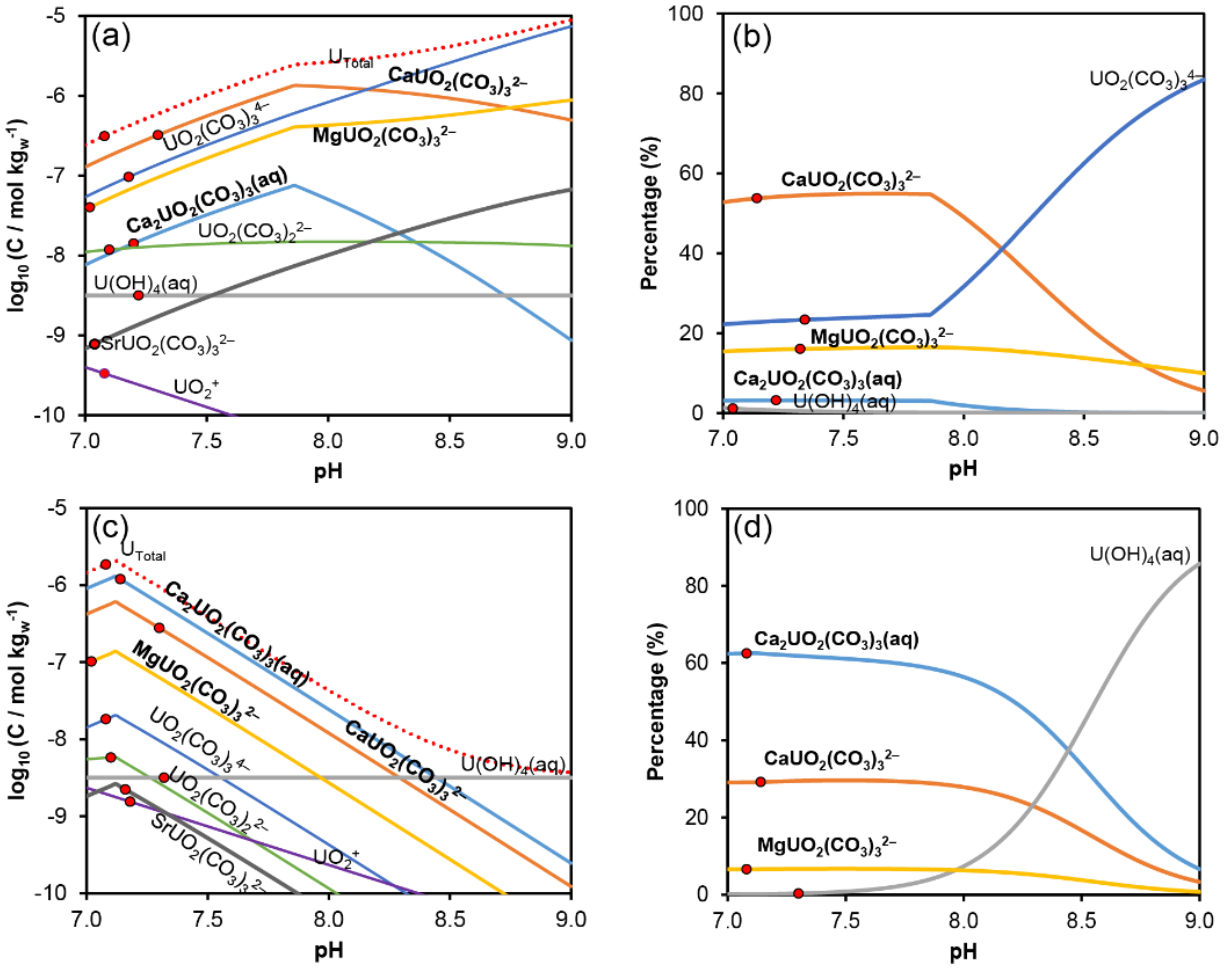

Fig. IV - 7 Solubility of UO_2(am,hyd) (a,c) and aqueous speciation of uranium (b,d) between pH 7 and 9 for Boom (a,b) and Callovo-Oxfordian (c,d) clay equilibrium waters using thermodynamic data from the Thermochime 10a database, implementing $SrUO_2(CO_3)_3^{2-}$,[14] correcting the $MgUO_2(CO_3)_3^{2-}$ and $Ca_nUO_2(CO_3)_3^{(4-2n)-}$ data with thermodynamic constants values from determined in this work and our earlier work,[24] and implementing specific ion interaction coefficient from Table IV - 3: (a,b) $P(O_2) = 10^{-68.67}$ atm and (c,d) $10^{-65.83}$ atm – see Shang and Reiller[24] for details.

5.2 Case of seawater

The second practical application to seawater in Shang and Reiller[24] is re-examined here with the newly measured $\log_{10}\beta°$ and ε values for $MgUO_2(CO_3)_3^{2-}$. Estimation of uranium speciation in seawater where provided by Maloubier, *et al.*[59] – using Dong and Brooks[14] constants and probably simplified Debye-Hückel ionic strength correction – and Lee, *et al.*,[10] using their determined $\log_{10}\beta°$ extrapolated using the $\varepsilon(MgUO_2(CO_3)_3^{2-},Na^+) = \varepsilon(UO_2(CO_3)_2^{2-},Na^+)$ hypothesis. The seawater composition, proposed by Millero, *et al.*[38] is described in the Table

IV - S6 of the SI. The initial seawater information, collected from upper ocean, is known to be supersaturated with respect to calcium and magnesium.[60] The natural concentration of U(VI) seems to be completely soluble under the seawater conditions and not controlled by any common uranyl carbonate minerals of alkaline or alkaline earth metals with the general formula $Na_jCa_kMg_m(UO_2)(CO_3)_3 \cdot xH_2O(cr)$ – *i.e.* liebigite, bayleyite, swartzite or andersonite, see Alwan and Williams,[61] Endrizzi, *et al.*,[62] Lee, *et al.*,[63] and references therein.

Fig. IV - 8 represents the distribution of uranium species as a function of pH in seawater. The $MgUO_2(CO_3)_3^{2-}$ and $CaUO_2(CO_3)_3^{2-}$ complexes share nearly equal proportions of 35% at pH values from 7.5 to 9, while the amounts of $UO_2(CO_3)_3^{4-}$ and $Ca_2UO_2(CO_3)_3(aq)$ represent less than one-third in total U(VI). The slight decrease of $Ca_nUO_2(CO_3)_3^{(4-2n)-}$ at pH > 9 was resulted from the decrease of $[Ca^{2+}]$ in solution as a consequence of dolomite and calcite formations at high pH conditions. Henceforth, It seems that the speciation of uranium in seawater is strongly influenced by both $MgUO_2(CO_3)_3^{2-}$ and $CaUO_2(CO_3)_3^{2-}$ complexes.

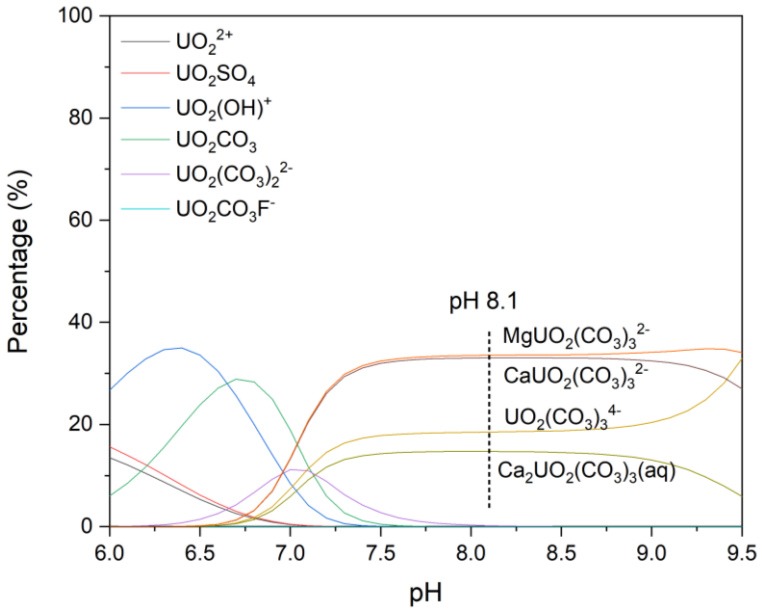

Fig. IV - 8 Theoretical speciation of uranium in a standard seawater composition,[38] $P(CO_2) = 10^{-3.5}$ atm from the total carbonate concentration, and using the thermodynamic data from the ThermoChimie 10a database, correcting the $MgUO_2(CO_3)_3^{2-}$, $Ca_nUO_2(CO_3)_3^{(4-2n)-}$ data with thermodynamic constants determined in this work (Mg) and our earlier work.[24,25]

We particularly performed calculations with the thermodynamic constants published earlier by Dong and Brooks,[14,15] and Lee and Yun[9] and Lee, et al.[10] listed in the Table IV - S7 of the SI. As shown in Fig. IV - S3 of the SI, the (M-)UO_2-CO_3 species differ considerably in distributions. The $CaUO_2(CO_3)_3^{2-}$ complex dominates the aqueous uranium distribution over 90% at pH values above 7.3 at the expenses of other triscarbonatouranyl species using the

constants from Dong and Brooks[14,15] (see Fig. IV - S3(b) of the SI), while its proportion decreased to 62% using the constants from Lee and Yun[9] and Lee, *et al.*[10] (see Fig. IV - S3(a) of the SI). This discrepancy can be attributed to the lower value of $\log_{10}\beta°(MgUO_2(CO_3)_3^{2-})$ = 25.02 and more negative interaction coefficient (-3 $kg_w\ mol^{-1}$) proposed in Dong and Brooks.[15] The use of these data – measured in $NaNO_3$ within the range of I_m = 0.1 mol kg_w^{-1} to 0.5 mol kg_w^{-1} – needs to be more carefully considered in high NaCl salinity environments.

Building on this exercise, the thermodynamic modelling of seawater contributes to predict and evaluate the competition of magnesium and calcium with triscarbonatouranyl. The distributions of (M-)UO_2-CO_3 species confirm the predominance of both the -2 bearing charge $MUO_2(CO_3)_3^{2-}$ regardless of the source of data: $\log_{10}\beta°_{n.1.3}$ and ε. Even through apparently showing low values,[16-18] it has been noticed that enthalpies of the studied complexations are needed in an effort to provide a thoughtful and rigorous evaluation of uranium in the ocean depending on the varying temperature.[64] The results in this work are expected to help addressing the issues in extraction of uranium from seawaters in which $Ca_2UO_2(CO_3)_3(aq)$ was conventionally considered to exceed $CaUO_2(CO_3)_3^{2-}$.[18,59,62,65,66] It is noteworthy to remember that Maloubier, *et al.*[59] questioned the result of their speciation calculation with regards to their determination of a too low decay-time results in TRLS in synthetic seawater, which was not in agreement with a predominance of $Ca_2UO_2(CO_3)_3(aq)$. From the evolution of decay time of the different complexes as a function of NaCl concentration in Shang and Reiller,[24] as well as in this work, the theoretical speciation and luminescence decay-times are now more consistent.

5.3 Case of Canadian aquitards

Another application of the obtained thermodynamic constants is connected with the aqueous speciation calculations in near-surface environments. The vertical variability over the depth of 2.3 to 29.0 meters in pore water compositions representative of smectite-rich clay aquitards in Saskatchewan (Canada) was reported by Hendry and Wassenaar[40] then specifically examined for the eventual uranium(VI)-natural organic matter associations (U(VI)-NOM) by Ranville, *et al.*[39]

The moderately basic and sulphate-type media exhibit regular depth profiles in terms of ionic strength, redox potential, ratio Mg/Ca, U concentration and total carbon (Fig. IV - S4 of the SI). The oxidized and fractured upper 3 meters of the till is more highly saline with elevated solute concentrations of total dissolved solids (TDS), SO_4^{2-}, Mg^{2+}, Na^+, and K^+ because of geochemical weathering. Essentially, the important SO_4^{2-} concentration has been attributed to

the oxidation of pyrite occurring at the shallower soil surface (< 3 meters) and the high Na^+ concentration is sourced from the favoured cation exchange of Ca^{2+} and Mg^{2+} for Na^+ after the dissolution of calcite and dolomite in clay minerals. Below 3 meters depth, the till is characterized as an unoxidized and non-fractured zone where the alkalinity decreases with depth until attaining the background concentration below 15 meters depth. The change of oxidation is also reflected by the fact that the total U concentration is reduced by nearly two orders of magnitude from 2.53 µmol L^{-1} at 2.3 meters depth to 0.084 µmol L^{-1} at 29.0 meters depth. Particularly, the dissolved salts (TDS, SO_4^{2-}, Mg^{2+}, Na^+ and K^+) display decreasing trends with depth, in contrast to the increasing trend for Ca^{2+}.[40] The resulting vertically decreasing ratio Mg/Ca implies an alteration of Mg and Ca speciation with depth so that the reasonable evaluation and the use of appropriate thermodynamic constants are necessary to make justifiable predictions of the real situations.

Reiller, *et al.*[67] confirmed the negligible proportions of U(VI)-NOM complexes at whatever depth in pore waters by theoretical calculations, but using the Davies[35] description of activity correction, which was clearly not appropriate, but inevitable in view of the U(VI)-NOM model, and software used. They proposed that the distribution of uranium species was majorly dominated by the ternary complexes $M_nUO_2(CO_3)_3^{(4-2n)-}$ (M = Mg, Ca, n = {0; 1; 2}) in the collected samples. For this reason, the U(VI)-NOM complexes are not considered in this exercise.

Given that the actual temperature of the site is much lower than 25°C, the implementation of $\Delta_f H°_m$ values would be appropriate to estimate the variation of $\log_{10}\beta$ ($M_nUO_2(CO_3)_3^{(4-2n)-}$) (M = Mg, Ca, n = {1; 2}) – see Figures S8-1 to S8-8 in the SI in Reiller and Descostes.[7] Because of scarce availability in literature, we decided to include the average of $\Delta_r H°_m$ values determined by Endrizzi and Rao[18] for the Ca- ternary complexes – which value has been selected by the latter NEA-OECD review[23] – and Jo *et al.*[16,17] for the Mg- and Ca-ternary complexes.

Previously, the particular case of Canadian aquitard has been tested by Reiller and Descostes[7] using PRODATA database – dedicated to uranium mining and environmental monitoring – with $M_nUO_2(CO_3)_3^{(4-2n)-}$ (M = Ca, Ba, n = {1;2}, M = Sr, n = 1) from Dong and Brooks[14] and $MgUO_2(CO_3)_3^{2-}$ from Dong and Brooks[15] and with the $\Delta_r H°_m$ reported by Endrizzi and Rao.[18] We specifically recalled the speciation calculation with PRODATA 1.1.0.4 database obtained in Reiller and Descostes[7] for comparison purposes in Fig. IV - 10(b). As illustrated in Fig. IV - 9, the distribution of U(VI) are showing similar patterns but with different amplitudes

for the different species, especially in oxidizing shallower depths, depending on the choice of $\log_{10}\beta°(M_nUO_2(CO_3)_3^{(4-2n)-})$ ($M = \{Mg^{2+},Ca^{2+}\}$, $n = \{1;2\}$) as well as the $\Delta_r H°_m$ values. The $MgUO_2(CO_3)_3^{2-}$ complex is calculated to be predominant using the data determined in our works (Fig. IV - 10(a), *i.e.* 61% at 2.3 meters depth, 59% at 3.8 meters depth, 53% at 5.3 meters depth, but less important using the PRODATA 1.1.0.4 database in which $\log_{10}\beta°(MgUO_2(CO_3)_3^{2-}) = 25.02$ and $\varepsilon(MgUO_2(CO_3)_3^{2-},Na^+) = -3.2$ kg_w mol^{-1} were selected (Fig. IV - 10(b)). At higher depths ($\geq$ 9.9 meters depth), both the $Ca_nUO_2(CO_3)_3^{(4-2n)-}$ complexes surpass all others, irrespective of the used databases. The clearly opposite evolutions of $MgUO_2(CO_3)_3^{2-}$ and $Ca_nUO_2(CO_3)_3^{(4-2n)-}$ are consistent with expectations as the ratio Mg/Ca decreased as a function of depth. It can be recalled that Reiller and Descostes[7] questioned the use of the value from Dong and Brooks[15] for Mg, and called for the type of determination done in this work.

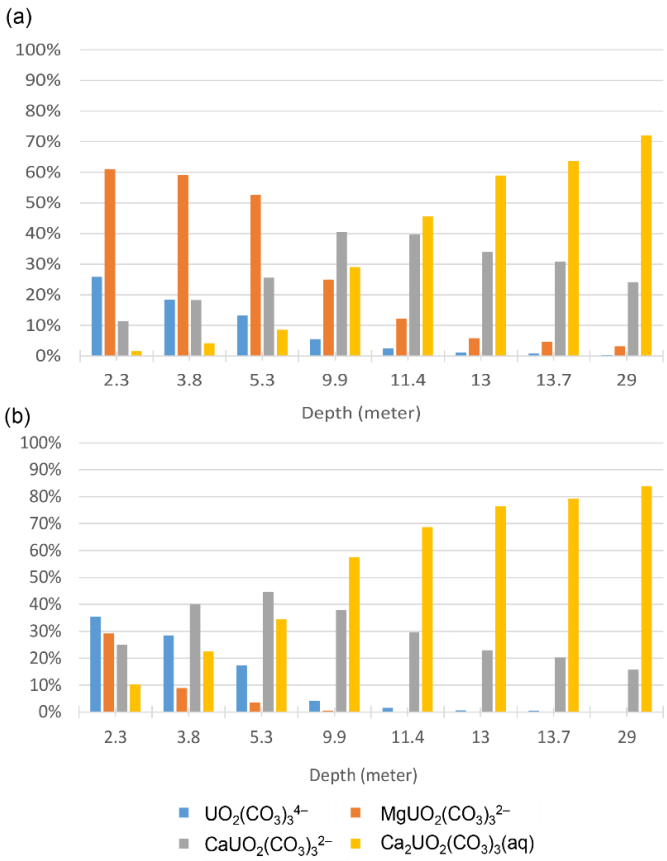

Fig. IV - 9 Evolution of repartitions of uranium species in selected Canadian aquitard waters at 5°C[39,40] as a function of depth: (a) using the ThermoChimie 10a database implemented with the $\log_{10}\beta°_{n.1.3}$ determined in this work; and (b) using the PRODATA 1.1.0.4 database.[7] The values for $\Delta_r H_m$ were listed in Table IV - S8 of the SI.

A series of predominance diagrams corresponding to the aqueous conditions of the collected samples at I_m = 0.06 to 1.38 mol kg_w^{-1} are constructed using the $\log_{10}\beta°(M_nUO_2(CO_3)_3^{(4-2n)-})$ ($M = \{Mg^{2+}, Ca^{2+}\}$, n = {1;2}) and ε determined in our work in Fig. IV - S5 of the SI. The activity of Mg^{2+} and Ca^{2+} values were fixed by $MgCl_2$ and $CaCl_2$ in calculations. The precipitation of calcite and dolomite were not requested, even though several waters were oversaturated relative to these phases. The boundaries plotted in dashed and solid lines represent the simulation results of 5 and 25°C, respectively. It is shown that the predominance domain of $UO_2(CO_3)_3^{4-}$ complex is obviously enlarged at the expenses of $M_nUO_2(CO_3)_3^{(4-2n)-}$ (n = {1;2}) when increasing the I_m from 0.06 to 1.38 mol kg_w^{-1} (from 29.0 m up to 2.3 m). The differences in the limits of each predominance domain *vs.* temperatures are illustrative of the weak values of the enthalpies of reaction.

In this example, the properties of $M_nUO_2(CO_3)_3^{(4-2n)-}$, especially their formation constants and interaction coefficients, are essential to have reliable appreciation of U(VI) equilibrium speciation that is driven by topography after the chemical weathering at the site. The $Ca_nUO_2(CO_3)_3^{(4-2n)-}$ species are proven to be responsible for the enhancement of U(VI) mobility by promoting its desorption from the clay minerals in literature.[68-74] Some emphasis should also be placed on Mg-concentrated natural conditions where the $MgUO_2(CO_3)_3^{2-}$ complex – similar to $Ca_nUO_2(CO_3)_3^{(4-2n)-}$ in terms of thermodynamic properties but did not receive sufficient attention – could take a large proportion of aqueous U(VI).

5.4 Case of Indian drinking water

Groundwater in India, including the water directly provided to consumers without treatment, suffers from numerous quality issues.[41,42,75] The prevailing uranium in groundwater could represent a serious concern to the local people, in addition to multiple high concentrations of inorganic contaminants such as arsenic and halides. Coyte, *et al.*[41] compiled uranium data from several states in North-Western India where the groundwater resources have been severely affected by over-exploitation and climate effects. In the shallower layers, the oxidizing and carbonate-rich conditions favour the formation of soluble uranyl carbonate complexes, which lead to high aqueous U(VI) concentration. The natural migration into deeper parts explains the observed considerable decrease in U(VI) with depth.

In the work of Coyte, *et al.*,[41] speciation modelling were done for some wells using the llnl database provided with the PhreeqC package,[43,44] where the $\log_{10}\beta°_{n.1.3}$ for Mg-, Ca-, Sr- uranyl carbonate complexes, taken from Dong and Brooks,[14] were manually added. The calculation

results were consistent with their prediction of predominant $Ca_nUO_2(CO_3)_3^{(4-2n)-}$ under these conditions. Despite this, awareness is raised to the fact that the formation constant of $UO_2(CO_3)_3^{4-}$ in llnl.dat – apparently chosen from the first NEA-OECD review[21] – is not the value selected by Dong and Brooks[14] in their estimation of cumulative constant from successive constants from the first NEA-OECD update.[22] Therefore, the successive formation constants $\log_{10}K°_{n.1.3}$ of $M_nUO_2(CO_3)_3^{(4-2n)-}$ species should have been integrated instead of the cumulative formation constants $\log_{10}\beta°_{n.1.3}$ using the llnl database. It is also noteworthy that the implemented activity corrections in the parameter file of llnl.dat – the extended Debye-Hückel equation with fitted b-dot parameters[76] – are not the SIT model used either in NEA-OECD review[21-23] or in ThermoChimie 10a database,[45] with which we are conducting the calculations.

For these reasons, we selected specific Mg-containing water information for five wells (see detailed information in Table IV - S9 of the SI) and performed speciation tests: (i) using llnl database with successive $\log_{10}K°_{n.1.3}$ for $M_nUO_2(CO_3)_3^{(4-2n)-}$ from Dong and Brooks;[14] and (ii) using ThermoChimie 10a database implemented with the cumulative $\log_{10}\beta°_{n.1.3}$ from the same work.[14] The speciation results displayed only minor even negligible differences (see

Table IV - S10 of the SI) and suggest that the use of $\log_{10}K°_{n.1.3}$ or $\log_{10}\beta°_{n.1.3}$ and the formalism of activity corrections did not generate too much of an inconsistency in this case when the calculations have the same source of formation constants for $M_nUO_2(CO_3)_3^{(4-2n)-}$ species.

Fig. IV - 10 compares the species percentages for the selected water samples using different constants for $\log_{10}\beta°(M_nUO_2(CO_3)_3^{(4-2n)-})$ ($M = \{Mg^{2+}, Ca^{2+}\}$, $n = \{1;2\}$). The higher $\log_{10}\beta°(MgUO_2(CO_3)_3^{2-})$ determined in this work than the one used by Coyte, *et al.*[41] leads to a more abundant $MgUO_2(CO_3)_3^{2-}$ and less abundant $Ca_nUO_2(CO_3)_3^{(4-2n)-}$ in modelling results.

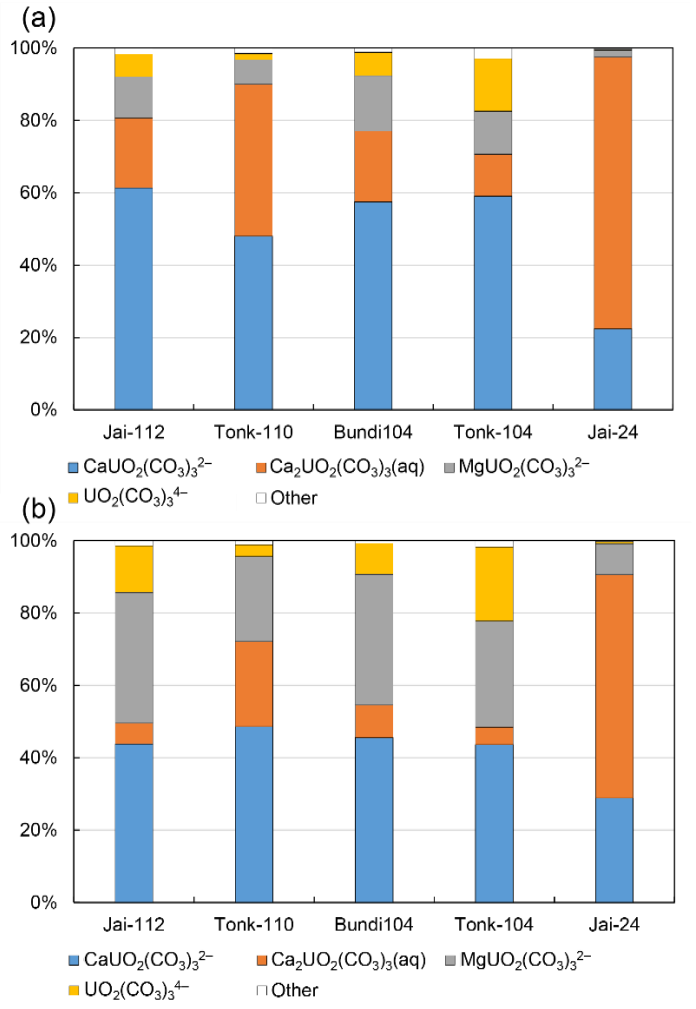

Fig. IV - 10 Evolution of the repartitions of uranium species in selected Indian groundwater calculated (a) using the llnl.dat in the work of Coyte, et al.[41] (b) using the Thermochimie 10a database with the $log_{10}\beta°_{n.1.3}$ determined in this work and our earlier work.

The water chemistry in North-Western India suggests that aqueous Mg/Ca uranyl carbonate complexes control the U(VI) distribution. However, the research to date on the bioavailability and toxicity of ternary $M_nUO_2(CO_3)_3^{(4-2n)-}$ complexes has tended to only focus on calcium rather than magnesium. For example, Carrière *et al.*[77,78] proposed negligible biological effects of $Ca_nUO_2(CO_3)_3^{(4-2n)-}$ complexes on cells. Prat, *et al.*[79] reported that no clinical manifestations were obtained among the population exposed to drinking water of high concentrations of natural uranium in Finland, when the importance of $M_nUO_2(CO_3)_3^{(4-2n)-}$ was evidenced experimentally and by theoretical speciation.[7,79] In plants, the uptake of uranium was also proven inhibited in calcium-carbonate solutions.[80] The actual uranium toxicity of these samples in India could be studied in light of the $M_nUO_2(CO_3)_3^{(4-2n)-}$ species-controlled distribution of U(VI).

IV - 6 Conclusion

The complexation behaviour of $MgUO_2(CO_3)_3^{2-}$ complex was studied in NaCl and $NaClO_4$ media by collecting the luminescence spectra and determining their thermodynamic constants $\log_{10}\beta°_{1.1.3}$ and specific ion interaction theory coefficients ε using TRLS. The luminescence spectra of $MgUO_2(CO_3)_3^{2-}$ complex showed slight hypochromic shifts compared with $CaUO_2(CO_3)_3^{2-}$, detectable using the 1800 lines mm^{-1} grating with our apparatus. The equilibrium constants measured $\log_{10}\beta°(MgUO_2(CO_3)_3^{2-}) = 26.40 \pm 0.07$ and the specific ion interaction coefficients represent similar features as $Ca_nUO_2(CO_3)_3^{(4-2n)-}$ complexes, *i.e.* different values in $NaClO_4$ – $\varepsilon(MgUO_2(CO_3)_3^{2-}, Na^+) = 0.19 \pm 0.11$ kg_w mol^{-1} – and in NaCl – $\varepsilon(MgUO_2(CO_3)_3^{2-}, Na^+) = 0.09 \pm 0.16$ kg_w mol^{-1}.

The underlying mechanisms in the ion interactions between M^{2+} (M = Mg, Ca) and $UO_2(CO_3)_3^{4-}$ were discussed and analysed from different aspects. The stable octahedral $Mg(H_2O)_6^{2+}$ structure may result in steric hindrance when coordinating to $UO_2(CO_3)_3^{4-}$ compared with the more hydrated $Ca(H_2O)_7^{2+}$, which facilitates the water exchange. This intrinsic characteristic of magnesium also gives reason for the anomaly in the stability constants for the $MUO_2(CO_3)_3^{2-}$ complexes (M = Mg, Ca, Sr, Ba) observed otherwise. Concerning the interaction coefficients, our results suggest that the ion associations occurring among Na^+, M^{2+}, Cl^- and ClO_4^- are supposed to be important at high I_m. This work is providing a complete thermodynamic constants set for the $M_nUO_2(CO_3)_3^{(4-2n)-}$ complexes, both in NaCl and $NaClO_4$ systems.

The applications to several representative geochemical contexts highlight the necessity to account for the $MgUO_2(CO_3)_3^{2-}$ complex in theoretical speciation calculation. Particularly when the ratio of magnesium over calcium approaches or overpasses the ratio of the formation constants.

Acknowledgment

This work was financed by CEA and ONDRAF-NIRAS (contract DEN4857-CCHO 2018-0456/00/00). Dr. Hélène Isnard is acknowledged for her help in the dissolution of U_3O_8.

IV - 7 References

1. G. Bernhard, G. Geipel, V. Brendler and H. Nitsche, *Radiochim. Acta*, 1996, **74**, 87-91.
2. G. Bernhard, G. Geipel, T. Reich, V. Brendler, S. Amayri and H. Nitsche, *Radiochim. Acta*, 2001, **89**, 511-518.

3. Z. M. Wang, J. M. Zachara, W. Yantasee, P. L. Gassman, C. X. Liu and A. G. Joly, *Environ. Sci. Technol.*, 2004, **38**, 5591-5597.
4. C. Liu, J. M. Zachara, O. Qafoku, J. P. McKinley, S. M. Heald and Z. Wang, *Geochim. Cosmochim. Acta*, 2004, **68**, 4519-4537.
5. K. H. Williams, P. E. Long, J. A. Davis, M. J. Wilkins, A. L. N'Guessan, C. I. Steefel, L. Yang, D. Newcomer, F. A. Spane, L. J. Kerkhof, L. McGuinness, R. Dayvault and D. R. Lovley, *Geomicrobiol. J*, 2011, **28**, 519-539.
6. W. M. Dong, W. P. Ball, C. X. Liu, Z. M. Wang, A. T. Stone, J. Bai and J. M. Zachara, *Environ. Sci. Technol.*, 2005, **39**, 7949-7955.
7. P. E. Reiller and M. Descostes, *Chemosphere*, 2020, **251**, 126301.
8. J. E. Lartigue, B. Charrasse, B. Reile and M. Descostes, *Chemosphere*, 2020, **251**, 126302.
9. J. Y. Lee and J. I. Yun, *Dalton Trans.*, 2013, **42**, 9862-9869.
10. J. Y. Lee, M. Vespa, X. Gaona, K. Dardenne, J. Rothe, T. Rabung, M. Altmaier and J.-I. Yun, *Radiochim. Acta*, 2017, **105**.
11. S. N. Kalmykov and G. R. Choppin, *Radiochim. Acta*, 2000, **88**, 603-606.
12. G. Geipel, S. Amayri and G. Bernhard, *Spectrochim. Acta, A*, 2008, **71**, 53-58.
13. C. Götz, G. Geipel and G. Bernhard, *J. Radioanal. Nucl. Chem.*, 2010, **287**, 961-969.
14. W. Dong and S. C. Brooks, *Environ. Sci. Technol.*, 2006, **40**, 4689-4695.
15. W. Dong and S. C. Brooks, *Environ. Sci. Technol.*, 2008, **42**, 1979-1983.
16. Y. Jo, A. Kirishima, S. Kimuro, H.-K. Kim and J.-I. Yun, *Dalton Trans.*, 2019, **48**, 6942-6950.
17. Y. Jo, H.-K. Kim and J.-I. Yun, *Dalton Trans.*, 2019, **48**, 14769-14776.
18. F. Endrizzi and L. F. Rao, *Chem.-Eur. J.*, 2014, **20**, 14499-14506.
19. J. L. Smith, *Am. J. Sci.*, 1848, **320**, 336-338.
20. J. L. Smith, *Am. J. Sci.*, 1851, **11**, 259.
21. I. Grenthe, L. Fuger, R. G. M. Konings, R. J. Lemire, A. B. Muller, C. Nguyen-Trung and H. Wanner, *Chemical Thermodynamics 1. Chemical Thermodynamics of Uranium, Chemical Thermodynamics Series*, North Holland Elsevier Science Publishers B. V., Amsterdam, The Netherlands, 1992.
22. R. Guillaumont, T. Fanghänel, V. Neck, J. Fuger, D. A. Palmer, I. Grenthe and M. H. Rand, *Update of the Chemical Thermodynamics of Uranium, Neptunium, Plutonium, Americium and Technetium*, OECD Nuclear Energy Agency, Data Bank, Issy-les-Moulineaux, France, 2003.
23. I. Grenthe, X. Gaona, A. V. Plyasunov, L. Rao, W. H. Runde, B. Grambow, R. J. M. Koning, A. L. Smith and E. E. Moore, *Chemical Thermodynamics 14. Second Update on the Chemical Thermodynamics of Uranium, Neptunium, Plutonium, Americium and Technetium, Chemical Thermodynamics Series*, OECD Nuclear Energy Agency Data Bank, Eds., OECD Publications, Paris, France, 2020.
24. C. Shang and P. E. Reiller, *Dalton Trans.*, 2020, **49**, 466-481.
25. C. Shang, P. E. Reiller and T. Vercouter, *Dalton. Trans*, 2020, **49**, 15443-15460.
26. L. Ciavatta, *Ann. Chim. Roma*, 1980, **70**, 551-567.
27. W. W. Rudolph and G. Irmer, *Dalton Trans.*, 2013, **42**, 3919-3935.
28. W. Wu, C. Priest, J. Zhou, C. Peng, H. Liu and D. E. Jiang, *J. Phys. Chem. B*, 2016, **120**, 7227-7233.
29. B. Li, J. Zhou, C. Priest and D. E. Jiang, *J. Phys. Chem. B*, 2017, **121**, 8171-8178.
30. A. O. Tirler and T. S. Hofer, *Dalton Trans.*, 2016, **45**, 4983-4988.
31. F. C. Lightstone, E. Schwegler, M. Allesch, F. Gygi and G. Galli, *ChemPhysChem*, 2005, **6**, 1745-1749.
32. C. Priest, Z. Tian and D.-e. Jiang, *Dalton Trans.*, 2016, **45**, 9812-9819.

33. S. Kerisit and C. Liu, *Geochim. Cosmochim. Acta*, 2010, **74**, 4937-4952.
34. T. Ikeda, M. Boero and K. Terakura, *J. Chem. Phys.*, 2007, **127**, 074503.
35. C. W. Davies, *Ion Association*, Butterworths, London, UK, 1962.
36. M. de Craen, L. Wang, M. Van Geet and H. Moors, *Geochemistry of Boom Clay pore water at the Mol site*, Report SCK•CEN-BLG-990, SCK•CEN, Mol, Belgium, 2004. http://jongeren.sckcen.be/~/media/Files/Science/disposal_radioactive_waste/Geochemistry_of_Boom_Clay_pore_Status_2004.pdf
37. E. C. Gaucher, C. Tournassat, F. J. Pearson, P. Blanc, C. Crouzet, C. Lerouge and S. Altmann, *Geochim. Cosmochim. Acta*, 2009, **73**, 6470-6487.
38. F. J. Millero, R. Feistel, D. G. Wright and T. J. McDougall, *Deep-Sea Res. Pt. I*, 2008, **55**, 50-72.
39. J. F. Ranville, M. J. Hendry, T. N. Reszat, Q. L. Xie and B. D. Honeyman, *J. Contam. Hydrol.*, 2007, **91**, 233-246.
40. M. J. Hendry and L. I. Wassenaar, *Water Resour. Res.*, 2000, **36**, 503-513.
41. R. M. Coyte, R. C. Jain, S. K. Srivastava, K. C. Sharma, A. Khalil, L. Ma and A. Vengosh, *Environ. Sci. Technol. Lett.*, 2018, **5**, 341-347.
42. R. Coyte, A. Singh, K. Furst, W. Mitch and A. Vengosh, *Sci. Total Environ.*, 2019, **688**.
43. D. L. Parkhurst and C. A. J. Appelo, *User's Guide to PHREEQC (Version 2) — A Computer Program for Speciation, Batch-Reaction, One-Dimensional Transport, and Inverse Geochemical Calculations*, Report 99-4259, U.S. Geological Survey, Water-Resources Investigations, Lakewood, Colorado, USA, 1999. http://wwwbrr.cr.usgs.gov/projects/GWC_coupled/phreeqci/
44. D. L. Parkhurst and C. A. J. Appelo, *Description of Input and Examples for PHREEQC Version 3 — A Computer Program for Speciation, Batch-Reaction, One-Dimensional Transport, and Inverse Geochemical Calculations. Chapter 43 of Section A, Groundwater Book 6, Modeling Techniques*, U.S. Geological Survey, Denver, Colorado, USA, 2013. http://pubs.usgs.gov/tm/06/a43/pdf/tm6-A43.pdf
45. M. Grivé, L. Duro, E. Colàs and E. Giffaut, *Appl. Geochem.*, 2015, **55**, 85-94.
46. G. G. Manov, N. J. Delollis and S. F. Acree, *J. Res. Nat. Bur. Std.*, 1945, **34**, 115-127.
47. H. Oher, T. Vercouter, F. Réal, C. Shang, P. E. Reiller and V. Vallet, *Inorg. Chem.*, 2020, **59**, 15036-15049.
48. M. Moriyasu, Y. Yokoyama and S. Ikeda, *J. Inorg. Nucl. Chem.*, 1977, **39**, 2211-2214.
49. A. Ringböm, *Complexation in Analytical Chemistry: A Guide for the Critical Selection of Analytical Methods Based on Complexation Reactions*, Interscience Publishers, New York, NY, USA, 1963.
50. Y. Marcus and G. Hefter, *Chem. Rev.*, 2006, **106**, 4585-4621.
51. J.-L. Burgot, *Ionic Equilibria in Analytical Chemistry*, Springer, New York, 2012.
52. J. L. Fulton, S. M. Heald, Y. S. Badyal and J. M. Simonson, *J. Phys. Chem. A*, 2003, **107**, 4688-4696.
53. S. Tu, S. S. Lobanov, J. M. Bai, H. Zhong, J. Gregerson, A. D. Rogers, L. Ehm and J. B. Parise, *J. Phys. Chem. B*, 2019, **123**, 9654-9667.
54. M. C. Bellissent-Funel and G. W. Neilson, *The Physics and Chemistry of Aqueous Ionic Solutions, NATO Science Series C*, D. Reidel Pub. Co., Dordrecht, Holland; Boston; Norwell, MA, U.S.A., 1987.
55. A. O. Tirler and T. S. Hofer, *J. Phys. Chem. B*, 2014, **118**, 12938-12951.
56. R. D. Shannon, *Acta Crystallogr., Sect. A*, 1976, **32**, 751-767.
57. N. A. Hewish, G. W. Neilson and J. E. Enderby, *Nature*, 1982, **297**, 138-139.
58. F. C. Lightstone, E. Schwegler, R. Q. Hood, F. Gygi and G. Galli, *Chem. Phys. Lett.*, 2001, **343**, 549-555.

59. M. Maloubier, P. L. Solari, P. Moisy, M. Monfort, C. Den Auwer and C. Moulin, *Dalton Trans.*, 2015, **44**, 5417-5427.
60. R. Chester and T. D. Jickells, *Marine Geochemistry*, Wiley, Chichester, West Sussex, UK Hoboken, NJ, Third edition. edn., 2012.
61. A. K. Alwan and P. A. Williams, *Mineral. Mag.*, 1980, **43**, 665-667.
62. F. Endrizzi, C. J. Leggett and L. F. Rao, *Ind. Eng. Chem. Res.*, 2016, **55**, 4249-4256.
63. J. Y. Lee, S. Amayri, V. Montoya, D. Fellhauer, X. Gaona and M. Altmaier, *Appl. Geochem.*, 2019, **111**, 104374.
64. F. J. Millero, *Chemical Oceanography*, Taylor & Francis, Boca Raton, 4th edn., 2013.
65. C. J. Leggett, F. Endrizzi and L. F. Rao, *Ind. Eng. Chem. Res.*, 2016, **55**, 4257-4263.
66. C. J. Leggett and L. Rao, *Polyhedron*, 2015, **95**, 54-59.
67. P. E. Reiller, L. Marang, D. Jouvin and M. F. Benedetti, Uranium (VI) binding to humic substances: speciation, estimation of competition, and application to independant data, in *The New Uranium Mining Boom. Challenge and Lessons Learned*, eds. B. Merkel and M. Schipek, Springer-Verlag, Berlin, Germany, 2012, DOI: 10.1007/978-3-642-22122-4_65, pp. 565-572.
68. A. Meleshyn, M. Azeroual, T. Reeck, G. Houben, B. Riebe and C. Bunnenberg, *Environ. Sci. Technol.*, 2009, **43**, 4896-4901.
69. T. Philipp, S. Shams Aldin Azzam, A. Rossberg, N. Huittinen, K. Schmeide and T. Stumpf, *Sci. Total Environ.*, 2019, **676**, 469-481.
70. V. Pirlet, P. Van Iseghem, A. Dierckx and J. F. Desreux, *J. Alloys Compd.*, 1998, **271-273**, 267-271.
71. Z. P. Zheng, T. K. Tokunaga and J. M. Wan, *Environ. Sci. Technol.*, 2003, **37**, 5603-5608.
72. Y. H. Wang, M. Frutschi, E. Suvorova, V. Phrommavanh, M. Descostes, A. A. A. Osman, G. Geipel and R. Bernier-Latmani, *Nature Communications*, 2013, **4**.
73. C. Tournassat, R. M. Tinnacher, S. Grangeon and J. A. Davis, *Geochim. Cosmochim. Acta*, 2018, **220**, 291-308.
74. X. L. Tan, M. Fang and X. K. Wang, *Molecules*, 2010, **15**, 8431-8468.
75. K. P. Singh, N. Kishore, N. Tuli, R. S. Loyal, M. Kaur and J. K. Taak, Uranium Contamination of Groundwater in Southwest Parts of Punjab State, India, with Special Reference to Role of Basement Granite, in *Clean and Sustainable Groundwater in India*, eds. D. Saha, S. Marwaha and A. Mukherjee, Springer Singapore, Singapore, 2018, DOI: 10.1007/978-981-10-4552-3_7, pp. 95-106.
76. I. Grenthe, I. Puigdomenech and B. Allard, *Modelling in Aquatic Chemistry*, OECD Publishing, Issy-les-Moulineaux, France, 1997.
77. M. Carrière, L. Avoscan, R. Collins, F. Carrot, H. Khodja, E. Ansoborlo and B. Gouget, *Chem. Res. Toxicol.*, 2004, **17**, 446-452.
78. M. Carriere, H. Khodja, L. Avoscan, F. Carrot and B. Gouget, *Radiochim. Acta*, 2005, **93**, 691-697.
79. O. Prat, T. Vercouter, E. Ansoborlo, P. Fichet, P. Perret, P. Kurttio and L. Salonen, *Environ. Sci. Technol.*, 2009, **43**, 3941-3946.
80. E. El Hayek, C. Torres, L. Rodriguez-Freire, J. M. Blake, C. L. De Vore, A. J. Brearley, M. N. Spilde, S. Cabaniss, A.-M. S. Ali and J. M. Cerrato, *Environ. Sci. Technol.*, 2018, **52**, 13089-13098.

IV - 8 Supporting Information

Number of tables: 10

Number of figures: 6

Table IV - S1 Potential values E_{mes} read on pH-meter for NaCl solutions of I_m = 0.01 m to 3.19 m at pcH = 2 using the combined-glass electrode with the filling solution of saturated KCl: liquid junction potentials ΔE_{mes} calculated to estimate the potential differences between the solution of I_m = 3.19 m and those of different I_m; ΔE_{mes} then used in the four-point calibration with commercial buffer solution of pH 1.64, 4.01, 6.87, 9.18, assumed as diluted solutions of $I_m \approx 0.01$ m.

Solution	*Conversion factor (from molarity M to molality m)*	*I_m (mol kg_w^{-1})*	*E_{mes} (mV)*	*$\Delta E_{mes} = E_{mes}$ (I_m = 3.19 m) – E_{mes}*
HCl 0.01 M + NaCl 2.99 M	1.0668[a]	3.19	*299.5*	0.0
HCl 0.01 M + NaCl 1.49 M	1.0319[a]	1.56	*286*	13.5
HCl 0.01 M + NaCl 0.99 M	1.0215[a]	1.04	*280.8*	18.7
HCl 0.01M + NaCl 0.74 M	1.0165[a]	0.76	*279.7*	19.8
HCl 0.01 M + NaCl 0.59 M	1.0135[b]	0.61	*277.9*	21.6
HCl 0.01 M + NaCl 0.49 M	1.0118[a]	0.51	*277.8*	21.7
HCl 0.01 M + NaCl 0.41 M	1.0092[b]	0.42	*276.7*	22.8
HCl 0.01M + NaCl 0.29M	1.0064[b]	0.30	*276.5*	23.0

Solution	*Conversion factor (from molarity M to molality m)*	I_m *(mol* kg_w^{-1}*)*	E_{mes} *(mV)*	$\Delta E_{mes} = E_{mes}$ *(*I_m *= 3.19 m)* $- E_{mes}$
HCl 0.01M + NaCl 0.19M	1.0040[b]	0.20	*276.4*	23.1
HCl 0.01M + NaCl 0.11M	1.0020[b]	0.12	*275.4*	24.1
HCl 0.01M	1.0000	0.01	*275.0*	24.5

The conversion factor was taken as 1 for the solution of I_m = 0.01 M,. The factor values for the solutions of $I_m \geq 0.1$ M were either [a] taken from Guillaumont *et al.*[1] or [b]extrapolated from these known values.

Table IV - S2 Experimental sample information – pH values, calculated Ringböm coefficients α, [Mg^{2+}*] (mol* kg_w^{-1}*) and deduced* F_0 *and τ; the sample solutions giving the slope of 1 are set in italics.*

I_m $NaClO_4$ (mol·kg_w^{-1})	**0.10**					**0.51**				
Sample	pH value	α	[Mg^{2+}] (mol·kg_w^{-1})	F_0 (counts)	τ (ns)	pH value	α	[Mg^{2+}] (mol·kg_w^{-1})	F_0 (counts)	τ (ns)
1	9.00	1.00	0	1.60E+07	8.59	9.00	1.00	0	2.23E+07	10.42
2	8.45	1.02	1.76E-04	1.83E+07	13.28	8.23	1.05	9.46E-03	3.68E+07	11.46
3	8.30	1.06	4.50E-04	2.29E+07	12.21	8.16	1.07	1.93E-02	3.17E+07	12.65
4	8.23	1.12	1.57E-03	1.58E+07	16.71	*8.09*	*1.03*	*2.14E-02*	*2.04E+07*	*14.74*
5	*8.20*	*1.17*	*2.12E-03*	*1.59E+07*	*16.24*	*7.89*	*1.15*	*2.69E-02*	*3.16E+07*	*13.79*
6	*8.09*	*1.45*	*4.45E-03*	*1.61E+07*	*23.44*	*7.82*	*1.34*	*3.61E-02*	*3.12E+07*	*15.75*
7	*8.06*	*1.62*	*6.82E-03*	*2.07E+07*	*27.92*	*7.71*	*2.11*	*4.69E-02*	*2.08E+07*	*19.50*
8	*8.01*	*3.71*	*1.35E-02*	*2.36E+07*	*28.39*	*7.66*	*2.82*	*6.45E-02*	*2.58E+07*	*20.56*
9	*7.84*	*6.17*	*2.36E-02*	*2.43E+07*	*31.61*	*7.62*	*3.65*	*1.13E-01*	*2.61E+07*	*23.21*
10	*7.76*	*10.78*	*4.18E-02*	*2.79E+07*	*33.48*	*7.58*	*4.81*	*1.16E-01*	*2.99E+07*	*25.55*
11	*7.73*	*14.18*	*6.41E-02*	*3.45E+07*	*34.83*	*7.53*	*6.91*	*1.87E-01*	*3.35E+07*	*26.53*
I_m $NaClO_4$ (mol·kg_w^{-1})	**1.05**					**1.62**				
Sample	pH value	α	[Mg^{2+}] (mol·kg_w^{-1})	F_0 (counts)	τ (ns)	pH value	α	[Mg^{2+}] (mol·kg_w^{-1})	F_0 (counts)	τ (ns)
1	9.00	1	0	3.33E+07	10.28	9.00	1.00	0	5.44E+07	8.19
2	8.45	1.01	1.00E-03	2.49E+07	12.43	8.70	1.01	9.38E-04	3.56E+07	11.35
3	8.30	1.02	5.12E-03	2.57E+07	13.38	8.22	1.02	2.37E-02	4.32E+07	15.04
4	8.23	1.05	1.60E-02	2.57E+07	13.38	8.18	1.05	5.52E-02	4.49E+07	17.32
5	8.16	1.06	2.02E-02	1.88E+07	16.22	8.09	1.06	1.43E-02	4.23E+07	14.30
6	7.70	1.27	2.68E-02	2.65E+07	15.07	7.98	1.02	2.32E-02	4.20E+07	15.54
7	*7.67*	*1.38*	*3.44E-02*	*2.36E+07*	*17.83*	7.89	1.02	2.60E-02	3.74E+07	17.42
8	*7.64*	*1.54*	*4.50E-02*	*2.51E+07*	*18.62*	*7.78*	*1.06*	*3.36E-02*	*4.13E+07*	*18.62*
9	*7.61*	*1.74*	*6.30E-02*	*2.75E+07*	*19.86*	*7.69*	*1.11*	*4.55E-02*	*4.11E+07*	*20.13*
10	*7.58*	*2.02*	*7.43E-02*	*2.52E+07*	*22.79*	*7.64*	*1.21*	*6.19E-02*	*4.67E+07*	*23.50*
11	*7.54*	*2.53*	*9.44E-02*	*3.18E+07*	*22.99*	*7.56*	*1.54*	*8.60E-02*	*4.67E+07*	*22.17*
12	*7.51*	*3.05*	*1.20E-01*	*3.27E+07*	*26.04*	*7.50*	*2.06*	*1.08E-01*	*5.05E+07*	*23.72*
13	*7.48*	*3.73*	*1.46E-01*	*3.54E+07*	*27.08*	*7.47*	*2.53*	*1.39E-01*	*5.80E+07*	*24.88*

I_m NaClO$_4$ (mol·kg$_w^{-1}$)	2.21				
Sample	pH value	α	[Mg^{2+}] (mol·kg$_w^{-1}$)	F_0 (counts)	τ (ns)
1	9.00	1.00	0	3.86E+07	9.27
2	8.30	1.02	3.11E-03	3.19E+07	10.77
3	8.23	1.05	1.53E-02	3.80E+07	10.40
4	8.16	1.06	4.31E-02	3.19E+07	12.31
5	*7.85*	*1.02*	*5.86E-02*	*3.27E+07*	*13.60*
6	*7.70*	*1.07*	*6.50E-02*	*3.32E+07*	*15.74*
7	*7.59*	*1.23*	*7.89E-02*	*3.47E+07*	*16.70*
8	*7.54*	*1.40*	*9.80E-02*	*3.23E+07*	*19.15*
9	*7.51*	*1.57*	*1.31E-01*	*3.71E+07*	*20.27*
10	*7.49*	*1.71*	*1.59E-01*	*3.64E+07*	*27.86*
11	*7.46*	*1.98*	*1.80E-01*	*4.38E+07*	*25.32*
12	*7.43*	*2.34*	*2.11E-01*	*4.45E+07*	*28.66*

I_m NaCl (mol·kg$_w^{-1}$)	0.10					0.25				
Sample	pH value	α	[Mg^{2+}] (mol·kg$_w^{-1}$)	F_0 (counts)	τ (ns)	pH value	α	[Mg^{2+}] (mol·kg$_w^{-1}$)	F_0 (counts)	τ (ns)
1	9.17	1.00	0	2.61E+07	9.16	9.00	1.00	0	4.82E+07	9.93
2	8.26	1.09	3.48E-04	2.82E+07	13.15	8.30	1.05	8.23E-04	4.52E+07	9.72
3	8.22	1.12	7.32E-04	2.37E+07	14.38	8.23	1.04	1.72E-03	2.49E+07	13.59
4	*8.07*	*1.49*	*1.25E-03*	*2.23E+07*	*18.58*	*8.00*	*1.20*	*2.79E-03*	*2.54E+07*	*15.33*
5	*8.05*	*1.64*	*1.49E-03*	*2.49E+07*	*19.11*	*7.95*	*1.31*	*3.66E-03*	*2.76E+07*	*15.61*
6	*8.00*	*2.08*	*2.38E-03*	*2.62E+07*	*20.35*	*7.88*	*1.70*	*4.08E-03*	*2.97E+07*	*15.79*
7	*7.90*	*3.80*	*4.16E-03*	*2.90E+07*	*23.99*	*7.81*	*2.42*	*6.10E-03*	*3.23E+07*	*15.60*
8	*7.87*	*4.80*	*6.36E-03*	*3.30E+07*	*25.72*	*7.79*	*2.73*	*8.46E-03*	*3.22E+07*	*18.31*
9	*7.78*	*8.90*	*1.56E-02*	*3.51E+07*	*28.22*	*7.77*	*3.16*	*1.02E-02*	*3.42E+07*	*20.05*
10	*7.74*	*12.13*	*2.50E-02*	*4.59E+07*	*28.30*	*7.75*	*3.50*	*1.27E-02*	*3.85E+07*	*20.36*
11						*7.73*	*4.03*	*1.65E-02*	*3.83E+07*	*22.22*
12						*7.70*	*5.01*	*2.10E-02*	*4.05E+07*	*23.07*

I_m NaCl (mol·kg$_w^{-1}$)	0.50					0.75				
Sample	pH value	α	[Mg^{2+}] (mol·kg$_w^{-1}$)	F_0 (counts)	τ (ns)	pH value	α	[Mg^{2+}] (mol·kg$_w^{-1}$)	F_0 (counts)	τ (ns)
1	9.00	1.00	0	7.96E+07	7.91	9.00	1.00	0	5.03E+07	9.48
2	8.45	1.01	8.50E-04	8.48E+07	8.97	8.45	1.01	8.19E-04	6.70E+07	9.59
3	7.95	1.09	5.91E-03	3.88E+07	11.65	8.30	1.02	3.17E-03	6.21E+07	9.63
4	7.87	1.19	6.34E-03	2.97E+07	13.09	7.90	1.08	6.39E-03	5.82E+07	9.93
5	*7.75*	*1.70*	*7.37E-03*	*3.60E+07*	*13.09*	*7.82*	*1.14*	*2.87E-02*	*4.83E+07*	*11.22*
6	*7.70*	*2.20*	*9.57E-03*	*3.22E+07*	*14.37*	*7.73*	*1.38*	*3.61E-02*	*5.51E+07*	*10.75*
7	*7.68*	*2.45*	*1.50E-02*	*3.25E+07*	*15.11*	*7.68*	*1.68*	*5.03E-02*	*5.64E+07*	*11.11*
8	*7.63*	*3.35*	*1.93E-02*	*2.86E+07*	*17.26*	*7.65*	*1.94*	*6.23E-02*	*5.74E+07*	*11.65*
9	*7.60*	*4.17*	*2.32E-02*	*3.58E+07*	*16.70*	*7.62*	*2.29*	*7.72E-02*	*5.83E+07*	*12.28*
10	*7.59*	*4.36*	*3.07E-02*	*3.44E+07*	*17.94*	*7.59*	*2.73*	*8.44E-02*	*5.23E+07*	*13.18*
11	*7.57*	*5.05*	*4.07E-02*	*4.85E+07*	*19.69*	*7.57*	*3.12*	*9.54E-02*	*5.12E+07*	*14.26*
12	*7.55*	*5.89*	*6.08E-02*	*5.98E+07*	*18.11*	*7.55*	*3.57*	*1.10E-01*	*6.07E+07*	*13.48*

I_m NaCl (mol·kg$_w^{-1}$)	1.00				
Sample	pH value	α	[Mg^{2+}] (mol·kg$_w^{-1}$)	F_0 (counts)	τ (ns)
1	9.00	1.00	0	1.16E+08	7.44
2	8.45	1.01	7.92E-04	7.43E+07	8.58
3	8.30	1.03	3.00E-03	6.40E+07	8.84
4	8.23	1.03	1.18E-02	6.22E+07	9.36
5	8.16	1.03	1.71E-02	4.17E+07	10.73

6	*7.71*	*1.14*	*2.85E-02*	*6.38E+07*	*10.16*	
7	*7.68*	*1.24*	*3.21E-02*	*7.95E+07*	*9.40*	
8	*7.65*	*1.38*	*4.22E-02*	*7.53E+07*	*10.44*	
9	*7.61*	*1.64*	*5.67E-02*	*8.12E+07*	*10.20*	
10	*7.53*	*2.59*	*6.65E-02*	*5.81E+07*	*12.89*	
11	*7.52*	*2.78*	*7.83E-02*	*6.96E+07*	*12.48*	
12	*7.50*	*3.20*	*1.05E-01*	*7.25E+07*	*12.65*	

Table IV - S3 Characteristic decomposition parameters of the luminescence spectrum in Fig. IV - 4 of the main text.

Peak Index	Area Fit	Center Max	Max Height	FWHM
1	8.94E+06	464.62	6.43E+04	13.06
2	2.19E+06	484.37	1.34E+05	15.50
3	2.02E+06	504.75	1.21E+05	15.74
4	1.16E+06	525.76	6.27E+04	17.29
5	4.68E+05	547.63	2.06E+04	21.32
6	3.25E+05	569.17	6.81E+03	44.75

Table IV - S4 Formation constants $log_{10}K^0$ used in Fig. IV - S1.

$log_{10}K^0$	Mg	Ca
$MCO_3(aq)$	2.98[a]	3.22[b]
MOH^+	2.32[c]	1.17[d]
MF^+	1.35[a]	0.68[a]
$MSO_4(aq)$	2.26[e]	2.02[f]
MPO_4^-	4.85[g]	6.46[g]
$MHPO_4(aq)$	2.88[g]	2.55[g]
$MH_2PO_4^+$	1.17[g]	1.40[g]
$MSeO_4(aq)$	2.2[h]	2[h]

[a] Sverjensky, *et al.*;[2] [b] Plummer and Busenberg;[3] [c] Palmer and Wesolowski;[4] [d] Shock, *et al.*,[5] [e] Wagman, *et al.*[6] [f] Yeatts and Marshall;[7]; [g] Turner, *et al.*,[8] [h] Olin, *et al.*[9]

Table IV - S5 Evolutions of $log_{10}K°$ values from Mg^{2+} to Ba^{2+} with different ligands, used in Fig. IV - S2.

$log_{10}K°_{1.1.3}$	Mg^{2+}	Ca^{2+}	Sr^{2+}	Ba^{2+}
F^-	1.35[a]	0.68[a]	0.14[a]	-0.18[a]
OH^-	2.32[b]	1.17[c]	0.69[c]	0.49[d]
CO_3^{2-}	2.98[a]	3.22[e]	2.81[f]	2.71[g]
Ox^{2-}	3.43[h]	3.19[h]	2.92[h]	2.93[h]
SO_4^{2-}	2.26[d]	2.02[i]	2.30[j]	2.70[k]
$S_2O_3^{2-}$	1.84[l]	2.02[l]	2.04[l]	2.3[l]
$UO_2(CO_3)_3^{4-}$	4.27[m] 4.73 p.w. in NaCl 4.43 p.w. in $NaClO_4$	5.34[m] 5.36 in NaCl[n] 5.42 in $NaClO_4$[n]	5.02[m]	4.84[m]

[a] Sverjensky, *et al.*;[2] [b] Palmer and Wesolowski;[4] [c] Shock, *et al.*;[5] [d] Wagman, *et al.*;[6] [e] Plummer and Busenberg;[3] [f] Busenberg, *et al.*;[10] [g] Busenberg and Plummer;[11] [h] Prapaipong, *et al.*;[12] [i] Yeatts and Marshall;[7] [j] Reardon and Armstrong;[13] [k] Reardon and Armstrong;[13] [l] Davies;[14] [m] Dong and Brooks;[15] [n] Shang and Reiller[16]

Table IV - S6 Seawater composition from Millero, et al.[17]

Temp	25°C
pH	8.1
pe	4
Density (g/cm^3)	1.023
Units	mol kg$_w^{-1}$
Na	0.4861
Mg	0.0547
Ca	0.0106
K	0.0106
Sr	0.0001
Cl	0.5658
S(6)	0.0293
Br	0.0018
F	0.0001
U	1.386E-08

Table IV - S7 Thermodynamic constants used in theoretical speciation of seawater case in Fig. IV - 8 of the main text and in Fig. IV - S4.

		$CaUO_2(CO_3)_3^{2-}$	$Ca_2UO_2(CO_3)_3(aq)$	$MgUO_2(CO_3)_3^{2-}$	$Mg_2UO_2(CO_3)_3(aq)$
Fig. IV - 8	$\log_{10}\beta°$	27.20[a]	30.49[a]	26.57 p.w.	/
	ε	0.29 ± 0.11[a]	0.66 ± 0.12[a]	0.31 ± 0.02 p.w.	/
Fig. IV - S4(a)	$\log_{10}\beta°$	27.27[b]	29.81[b]	25.8[c]	27.1[c]
	ε	-0.02[b]	0[b]	-0.02[c]	0[c]
Fig. IV - S4(b)	$\log_{10}\beta°$	27.18[d]	30.70[d]	25.02[e]	/
	ε	-3[d]	0[d]	-3[e]	/

[a] Shang and Reiller;[16] [b] Lee and Yun;[18] [c] Lee, *et al.*;[19] [d] Dong and Brooks;[15] [e] Dong and Brooks[20]

Table IV - S8 Thermodynamic constants used in theoretical speciation of Canadian aquitard case in Fig. IV - 9 of the main text and in Fig. IV - S6.

		$CaUO_2(CO_3)_3^{2-}$	$Ca_2UO_2(CO_3)_3(aq)$	$MgUO_2(CO_3)_3^{2-}$
Fig. IV - 9(a) and Fig. IV - S6	$\log_{10}K°$	5.36[a]	8.65[a]	4.73 p.w.
	ε	0.29 ± 0.11[a]	0.66 ± 0.12[a]	0.31 ± 0.02 p.w.
	Δ_rH_m (KJ mol^{-1})	-8 ± 6[b]	-8 ± 7[b]	/
		-1.2 ± 0.3[c]	-3.1 ± 3.0[c]	4.3 ± 1.5[c]
		-4.6 (average)	-5.55 (average)	4.3 (average)
Fig. IV - 9(b)	$\log_{10}\beta°$	27.18[d]	30.70[d]	25.02[e]
	ε	0	0	-3.2
	Δ_rH_m (KJ mol^{-1})	-47[b]	-47[b]	/

[a] Shang and Reiller,[16] [b] Endrizzi and Rao;[21] [c] Jo *et al.*;[22,23] [d] Dong and Brooks;[15] [e] Dong and Brooks[20]

Table IV - S9 Compositions of selected Indian drinking water samples, collected from the work of Coyte, et al.[24]

Description	Units	Jai-112	Tonk-110	Bundi-104	Tonk-104	Jai-24
Temperature	°C	29.6	29.7	27.1	29.1	30.5
pH		7.4	7.15	7.68	7.55	6.83
F	mg/L	1.83	2.68	5.15	5.25	0
Cl	mg/L	293	314	388	1050	545
Br	mg/L	0.58	1.6	1.18	2.11	1.15
I	mg/L	0	0	1.512	0	0
N(5) as NO_3^-	mg/L	23.1	207	31.6	28.6	252
S(6) as SO_4^{2-}	mg/L	166	119	337	400	90.3
C(4) as HCO_3^-	mg/L	1530	737	970	1030	832
Ca	mg/L	13.9	38.9	20.5	14.9	212
Mg	mg/L	23	38	39.3	21.5	119
Sr	mg/L	0.99	1.45	0.92	1.58	2.89
Na	mg/L	800	484	700	1320	372
Fe	mg/L	0	0	0	0	0.53
Ba	mg/L	0.27	0.24	0.11	0.02	0.38
Mn	mg/L	0	0	0	0	0.45
Si	mg/L	10.5	26.8	12.4	6.31	23
Li	µg/L	0	11.26	30.35	31.33	13.28
B	µg/L	2310	754	2180	4140	893
V	µg/L	0	0	0	0	0
Cr	µg/L	0	0	0	0	0
Ni	µg/L	0	0	0	0	3.79
Cu	µg/L	0	0	0	0	20.69
Zn	µg/L	392.15	10.8	13.1	22.13	0
As	µg/L	0	0	0	0	0
Se	µg/L	0	0	0	0	0
Mo	µg/L	52.31	6.64	29.19	15.25	2.63
Pb	µg/L	0.69	0.52	0.63	1.06	0.34
U	µg/L	181.28	32.71	50.45	319.67	31.23

Table IV - S10 Modeling of uranium speciation for selected Indian underground water samples.

(a) Using llnl.dat[25,26] with $\log_{10}K°_{n.1.3}$ from Dong and Brooks[15,20] as follows:					
$\log_{10}K°_{1.1.3}$ ($CaUO_2(CO_3)_3^{2-}$) = 5.34			$\log_{10}K°_{1.1.3}$($MgUO_2(CO_3)_3^{2-}$) = 4.27		
$\log_{10}K°_{2.1.3}$($Ca_2UO_2(CO_3)_3$(aq)) = 8.86			$\log_{10}K°_{1.1.3}$($SrUO_2(CO_3)_3^{2-}$) = 5.02		
Sample	$CaUO_2(CO_3)_3^{2-}$	$Ca_2UO_2(CO_3)_3$(aq)	$MgUO_2(CO_3)_3^{2-}$	$UO_2(CO_3)_3^{4-}$	Other
Jai-112	54.9%	12.8%	13.0%	16.0%	3.4%
Tonk-110	47.9%	39.2%	6.6%	3.3%	2.9%
Bundi-104	54.6%	18.8%	14.4%	10.6%	1.7%
Tonk-104	51.6%	10.2%	10.3%	24.2%	3.7%
Jai-24	20.6%	76.7%	1.7%	0.4%	0.5%
(b) Using Thermochimie.dat (http://www.thermochimie-tdb.com) with $\log_{10}\beta°_{n.1.3}$ from Dong and Brooks[15,20] as follows:					
$\log_{10}\beta°_{1.1.3}$ ($CaUO_2(CO_3)_3^{2-}$) = 27.18			$\log_{10}\beta°_{1.1.3}$ ($MgUO_2(CO_3)_3^{2-}$) = 26.11		
$\log_{10}\beta°_{2.1.3}$ ($Ca_2UO_2(CO_3)_3$(aq)) = 30.7			$\log_{10}\beta°_{1.1.3}$ ($SrUO_2(CO_3)_3^{2-}$) = 26.86		
Sample	$CaUO_2(CO_3)_3^{2-}$	$Ca_2UO_2(CO_3)_3$(aq)	$MgUO_2(CO_3)_3^{2-}$	$UO_2(CO_3)_3^{4-}$	Other
Jai-112	58.5%	12.9%	13.9%	13.3%	1.4%
Tonk-110	50.0%	39.5%	6.9%	2.7%	0.9%
Bundi-104	56.0%	17.8%	15.4%	10.0%	0.8%
Tonk-104	55.7%	10.0%	11.4%	21.2%	1.8%
Jai-24	21.3%	76.5%	1.7%	0.3%	0.2%

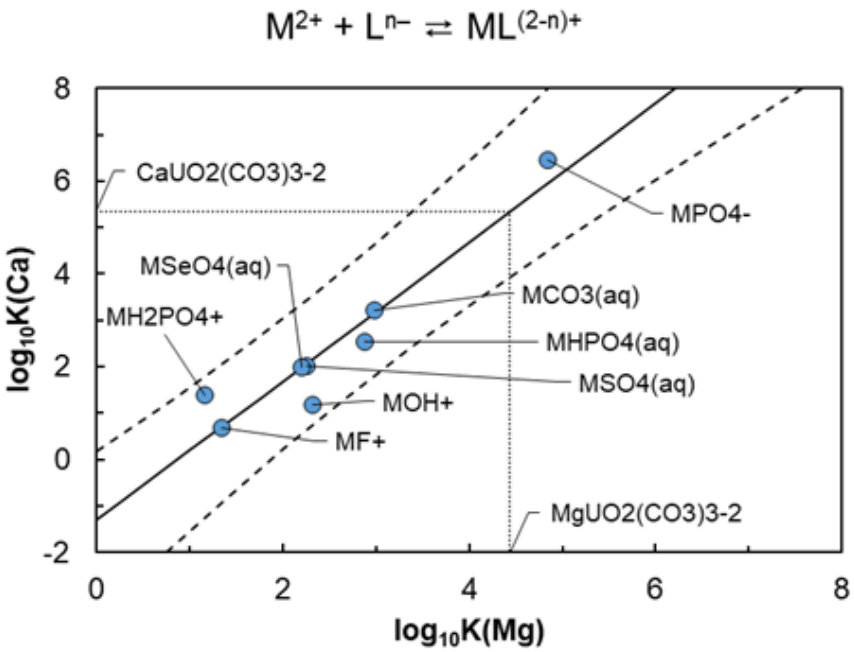

Fig. IV - S1 Linear relationship between the formation constants $log_{10}K°$ for Mg and Ca with different ligands. The values of $log_{10}K°$ are listed in Table IV - S4.

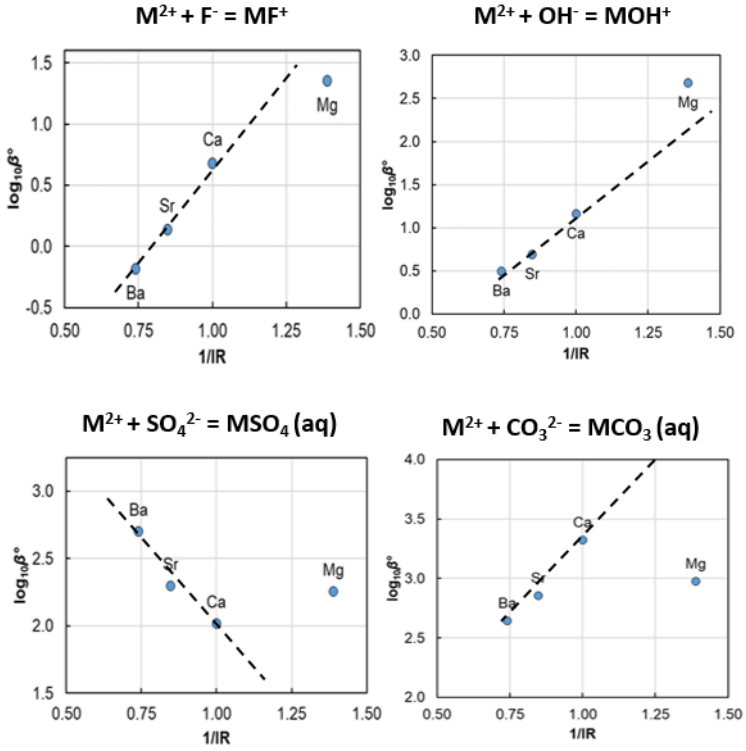

Fig. IV - S2 Stability constants of alkali earth metal ions and different ligands – F^-, OH^-, SO_4^{2-}, CO_3^{2-} – as a function of 1/R with R being the size of the ionic radius. The values of $log_{10}K°$ are listed in Table IV - S5.

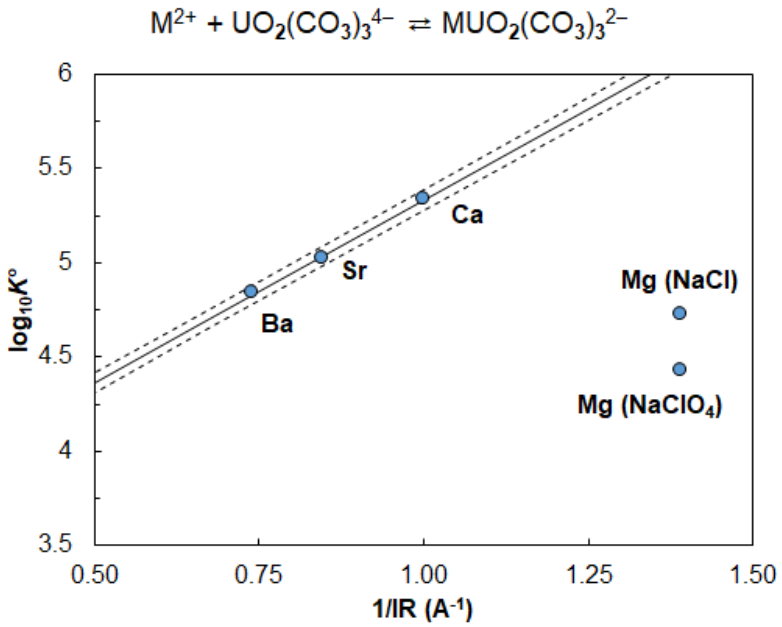

Fig. IV - S3 Stability constants of alkaline earth metal ions and $UO_2(CO_3)_3^{4-}$ as a function of 1/R with R being the size of the ionic radius. The values of $log_{10}K^o$ are listed in Table IV - S5.

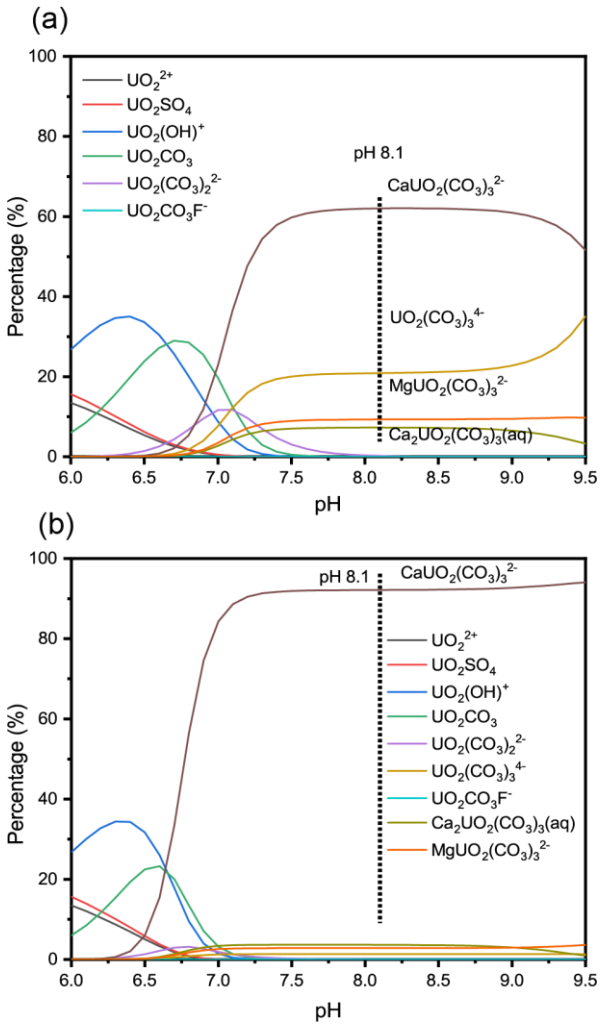

Fig. IV - S4 Theoretical speciation of uranium in standard seawater (composition listed in Table IV - S6) at $P(CO_2) = 10^{-3.5}$ atm. Thermochimie 10a database was used in calculations by implementing the thermodynamic constants of $MgUO_2(CO_3)_3^{2-}$, $Ca_nUO_2(CO_3)_3^{(4-2n)-}$ listed in Table IV - S7.

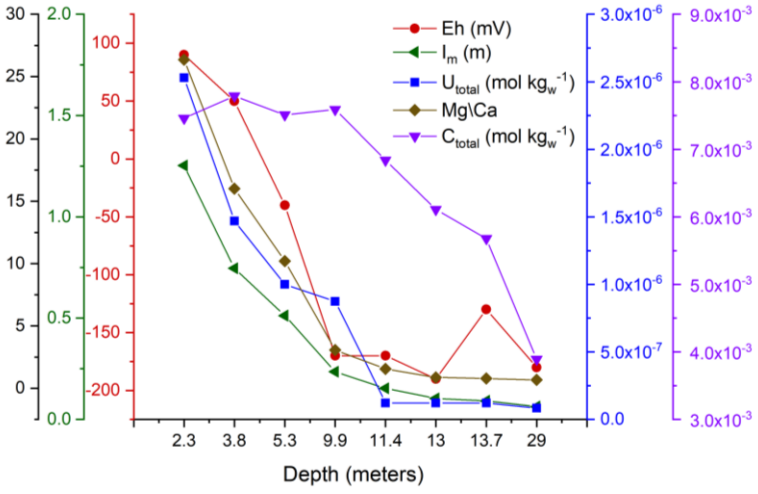

Fig. IV - S5 Evolutions of principal parameters in the selected Canadian aquitard waters.[27,28]

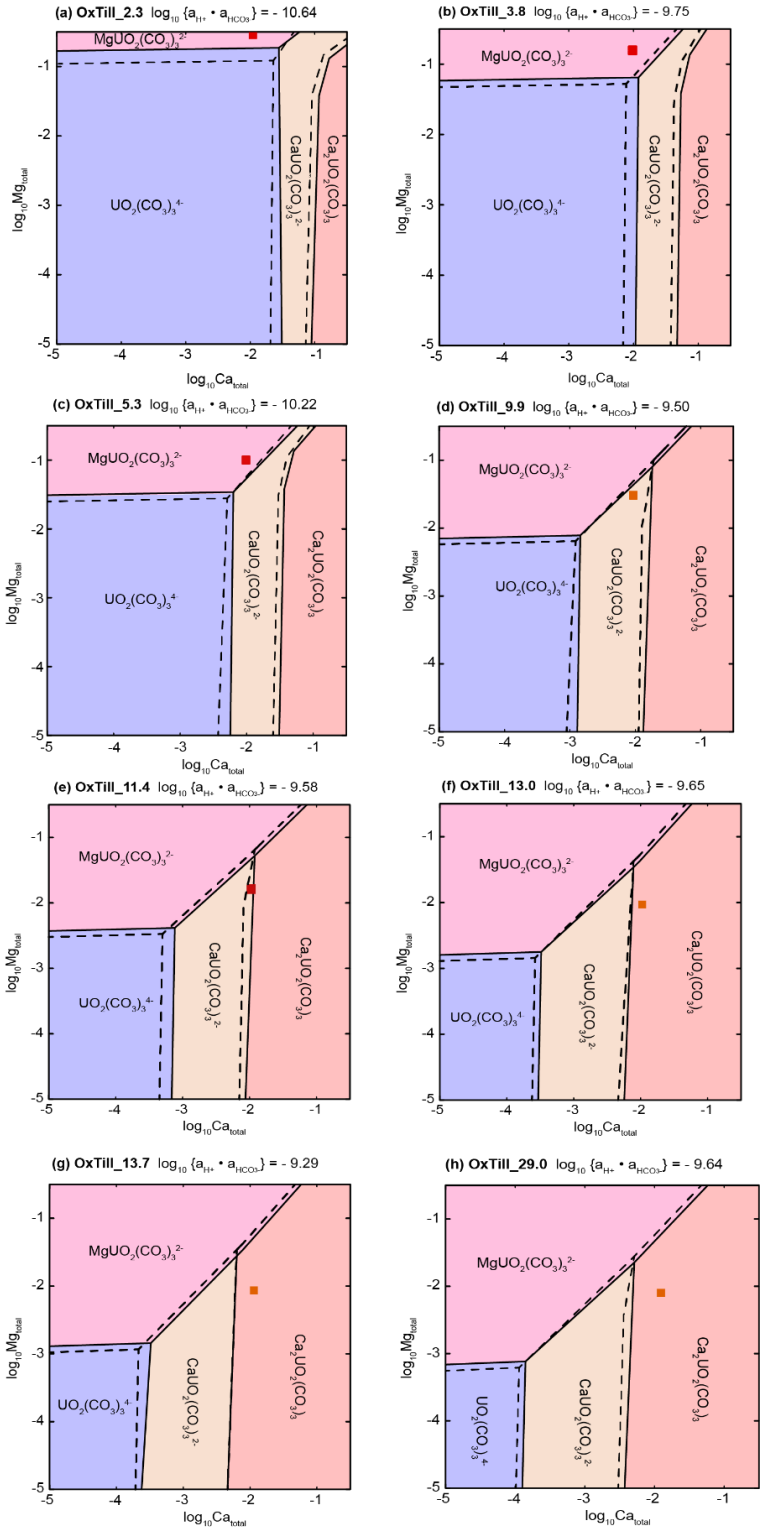

Fig. IV - S6 Predominance plots of uranium species at the fixed values of $log_{10}\{a_{H^+}\ a_{HCO_3^-}\}$ *corresponding to the aqueous conditions of the collected samples in Canadian aquitard site. Thermochimie 10a database file[29] and SIT ionic strength correction were used in calculations with implemented thermodynamic constants of* $MgUO_2(CO_3)_3^{2-}$, $Ca_nUO_2(CO_3)_3^{(4-2n)-}$ *listed in Table IV - S8. The boundaries plotted in dashed lines represent the simulation results at 5°C and the solid lines at 25°C. The ionic strength varies from 1.38 mol* kg_w^{-1} *at 29 m to 0.06 mol* kg_w^{-1} *to at 2.3 m.*

References

1. R. Guillaumont, T. Fanghänel, V. Neck, J. Fuger, D. A. Palmer, I. Grenthe and M. H. Rand, *Update of the Chemical Thermodynamics of Uranium, Neptunium, Plutonium, Americium and Technetium*, OECD Nuclear Energy Agency, Data Bank, Issy-les-Moulineaux, France, 2003.
2. D. A. Sverjensky, E. L. Shock and H. C. Helgeson, *Geochim. Cosmochim. Acta*, 1997, **61**, 1359-1412.
3. L. N. Plummer and E. Busenberg, *Geochim. Cosmochim. Acta*, 1982, **46**, 1011-1040.
4. D. A. Palmer and D. J. Wesolowski, *J. Solution Chem.*, 1997, **26**, 217-232.
5. E. L. Shock, D. C. Sassani, M. Willis and D. A. Sverjensky, *Geochim. Cosmochim. Acta*, 1997, **61**, 907-950.
6. D. D. Wagman, W. H. Evans, V. B. Parker, R. H. Schumm and I. Halow, *The NBS tables of chemical thermodynamic properties. Selected values for inorganic and C1 and C2 organic substances in SI units*, National Standard Reference Data System, 1982
7. L. B. Yeatts and W. L. Marshall, *J. Phys. Chem.*, 1969, **73**, 81-90.
8. D. R. Turner, M. Whitfield and A. Dickson, 1981.
9. Å. Olin, B. Noläng, E. Osadchii, L.-O. Öhman and E. Rosén, *Chemical Thermodynamics 7. Chemical Thermodynamics of Selenium*, OECD Nuclear Energy Agency, Data Bank, Issy-les-Moulineaux, France, 2005.
10. E. Busenberg, L. N. Plummer and V. B. Parker, *Geochim. Cosmochim. Acta*, 1984, **48**, 2021-2035.
11. E. Busenberg and L. N. Plummer, 1986.
12. P. Prapaipong, E. L. Shock and C. M. Koretsky, *Geochim. Cosmochim. Acta*, 1999, **63**, 2547-2577.
13. E. J. Reardon and D. K. Armstrong, *Geochim. Cosmochim. Acta*, 1987, **51**, 63-72.
14. C. W. Davies, Incomplete dissociation in aqueous salt solutions, in *The Structure of Electrolytic Solutions*, John Wiley and Sons, New York, 1959, pp. 19-34.
15. W. Dong and S. C. Brooks, *Environ. Sci. Technol.*, 2006, **40**, 4689-4695.
16. C. Shang and P. E. Reiller, *Dalton Trans.*, 2020, **49**, 466-481.
17. F. J. Millero, R. Feistel, D. G. Wright and T. J. McDougall, *Deep-Sea Res. Pt. I*, 2008, **55**, 50-72.
18. J. Y. Lee and J. I. Yun, *Dalton Trans.*, 2013, **42**, 9862-9869.
19. J. Y. Lee, M. Vespa, X. Gaona, K. Dardenne, J. Rothe, T. Rabung, M. Altmaier and J.-I. Yun, *Radiochim. Acta*, 2017, **105**.
20. W. Dong and S. C. Brooks, *Environ. Sci. Technol.*, 2008, **42**, 1979-1983.
21. F. Endrizzi and L. F. Rao, *Chem.-Eur. J.*, 2014, **20**, 14499-14506.
22. Y. Jo, A. Kirishima, S. Kimuro, H.-K. Kim and J.-I. Yun, *Dalton Trans.*, 2019, **48**, 6942-6950.
23. Y. Jo, H.-K. Kim and J.-I. Yun, *Dalton Trans.*, 2019, **48**, 14769-14776.
24. R. M. Coyte, R. C. Jain, S. K. Srivastava, K. C. Sharma, A. Khalil, L. Ma and A. Vengosh, *Environ. Sci. Technol. Lett.*, 2018, **5**, 341-347.
25. D. L. Parkhurst and C. A. J. Appelo, *Description of Input and Examples for PHREEQC Version 3 — A Computer Program for Speciation, Batch-Reaction, One-Dimensional Transport, and Inverse Geochemical Calculations. Chapter 43 of Section A, Groundwater Book 6, Modeling Techniques*, U.S. Geological Survey, Denver, Colorado, USA, 2013. http://pubs.usgs.gov/tm/06/a43/pdf/tm6-A43.pdf
26. D. L. Parkhurst and C. A. J. Appelo, *User's Guide to PHREEQC (Version 2) — A Computer Program for Speciation, Batch-Reaction, One-Dimensional Transport, and Inverse Geochemical Calculations*, Report 99-4259, U.S. Geological Survey, Water-

Resources Investigations, Lakewood, Colorado, USA, 1999. http://wwwbrr.cr.usgs.gov/projects/GWC_coupled/phreeqci/
27. M. J. Hendry and L. I. Wassenaar, *Water Resour. Res.*, 2000, **36**, 503-513.
28. J. F. Ranville, M. J. Hendry, T. N. Reszat, Q. L. Xie and B. D. Honeyman, *J. Contam. Hydrol.*, 2007, **91**, 233-246.
29. J. N. Brönsted, *J. Am. Chem. Soc.*, 1922, **44**, 877-898.

Chapter V. Effect of Temperature on the Complexation of Triscarbonatouranyl(VI) with Calcium and Magnesium in NaCl Aqueous Solution.

Chengming Shang and Pascal E. Reiller.*
Université Paris-Saclay, CEA, Service d'Études Analytiques et de Réactivité des Surfaces (SEARS), F-91191 Gif-sur-Yvette CEDEX, France.
Uranium; Carbonate; Ternary magnesium-uranyl-carbonate complexes; Luminescence.
*Email pascal.reiller@cea.fr

Dalton Transactions **50** (46), 17165-17180.

http://doi.org/10.1039/D1DT03204F

V - 1 Abstract

The complex formation of triscarbonatouranyl(VI) $UO_2(CO_3)_3^{4-}$ with alkaline earth metal ions Mg^{2+} and Ca^{2+} in 0.10 mol kg_w^{-1} NaCl were studied at variable temperatures: 5-30°C for Mg^{2+} and 10-50°C for Ca^{2+}. Under appropriate conditions, the ternary complexes ($M_nUO_2(CO_3)_3^{(4-2n)-}$ with n = 1 for Mg, n = {1;2} for Ca) were identified by time-resolved laser-induced luminescence spectrometry. Their pure spectra at 50°C for $Ca_nUO_2(CO_3)_3^{(4-2n)-}$ and 30°C for $MgUO_2(CO_3)_3^{2-}$ were recovered by multivariate curve resolution alternating least squares analysis. Approximation models were tested to fit the experimental data — the equilibrium constants of complexation measured at different temperatures — and deduce the thermodynamic functions, i.e., enthalpy, entropy, and heat capacity. The weak influence of temperature on complexation constants induces large uncertainties on thermodynamic functions. Assuming the enthalpy is constant with temperature using the Van't Hoff equation, the first stepwise complexation of $UO_2(CO_3)_3^{4-}$ by Ca^{2+} is estimated to be slightly endothermic with $\Delta_r{}^{VH}H°_m$ = (4.9 ± 5.9) kJ mol^{-1}, while the second stepwise complexation of $CaUO_2(CO_3)_3^{2-}$ by Ca^{2+} with is slightly exothermic $\Delta_r{}^{VH}H°_m$ = – (6.2 ± 13.3) kJ mol^{-1}. In contrary to Ca^{2+}, the complexation of $UO_2(CO_3)_3^{4-}$ by Mg^{2+} is slightly exothermic with $\Delta_r{}^{VH}H°_m$ = – (11.7 ± 10.3) kJ mol^{-1}. These values are not significantly different from nil inasmuch as the uncertainties are important due to a weak dependence of $\log_{10}K°$ values. The entropic character of the complexation is verified as $T\Delta_rS°_m$ = (36.5 ± 6.0) kJ mol^{-1} for the first stepwise complexation of $UO_2(CO_3)_3^{4-}$ by Ca^{2+}, $T\Delta_rS°_m$ = (13.8 ± 13.3) kJ mol^{-1} for the second stepwise complexation of $CaUO_2(CO_3)_3^{2-}$ by Ca^{2+}, and $T\Delta_rS°_m$ = (14.2 ± 10.3) kJ mol^{-1} for the complexation of $UO_2(CO_3)_3^{4-}$ by Mg^{2+}. The energetics of complexation and sensitivity analysis of model

estimates with temperature are discussed. The uranium speciation in the case of the safety of nuclear waste management, using the present thermodynamic functions, provides support to the assessment of underground nuclear waste repositories.

V - 2 Introduction

The migration of actinides in natural environments, especially uranium, is of great importance in the long-term performance assessment of nuclear waste processing and disposal.[1] It is thus necessary to acquire the environmental information of the geological repository — temperature, pH value, nature of solid phases, types of existing inorganic and organic complexing agents, *etc.* —, which influences the mobility of radionuclides. With this aim in mind, the thermodynamic constants — formation constant $\log_{10}K°$—, and functions — Gibbs energy $\Delta_r G°_m$, enthalpy $\Delta_r H°_m$, entropy $\Delta_r S°_m$, heat capacity $\Delta_r C_p°_m$, *etc*. — for involved reactions are mandatory for the predictive calculations. The complexation of actinides by major inorganic materials in underground waters at other temperatures than standard raises critical scientific interest, because the temperature in the nuclear waste storage casks could be up to 90°C because of radioactive decay.[2,3] However, a certain lack of knowledge on thermodynamic parameters of actinide complexation with temperature renders it difficult to predict chemical behaviour of actinides in the near-field of radioactive waste repositories, where a significant temperature gradient is estimated in timescale evolution.[4] The variation of water properties with temperature, *e.g.*, ion product and dielectric constants, can result in significant rearrangement of the solvation sphere of complexing ions, affecting the energetics of uranium complexation reactions.[5,6] Therefore, full thermodynamic data of uranium reactions with various common ligands like carbonate are of interest to accurately simulate the uranium transport in the near-field, as well as in the far field, of a repository.[7]

The nuclear waste repository isolation system consists typically of a natural barrier, mainly in clay or granite, depending on the country-specific rock formation, and an engineered barrier including in general waste canister, bentonite backfill, and concrete liner.[8] This multi-barrier system is extremely important in preventing the migration of actinides into the biosphere by means of pore-waters, which are similar in compositions with Cl^-, SO_4^{2-}, HCO_3^-, Ca^{2+}, Mg^{2+}, and Na^+ as the main ions at pH value ca. 8 in several envisaged geological formations.[9-14]

The triscarbonatouranyl(VI) complexes with alkaline earth metals (Mg^{2+}, Ca^{2+}) have been reported, or calculated, in the literature as one of the predominant U(VI) species under a variety of conditions at near-standard temperatures,[15-20] even if U(IV) phases are controlling the

solubility.[20] The formation constants of these complexes have been determined around standard temperature using different techniques, *e.g.*, time-resolved laser-induced luminescence spectrometry (TRLFS),[21-25] Ca^{2+} selective electrodes,[18] anion exchange,[26,27] and ultraviolet-visible (UV/Vis) absorption spectroscopy.[28,29] Their molecular structures have also been well defined by EXAFS[19,21,22,30,31] and molecular simulations.[32,33] In recent works,[34-36] we have reported the determinations of the stepwise thermodynamic constants $\log_{10}K°_{n}$ for the equilibria,

$$M^{2+} + UO_2(CO_3)_3^{4-} \rightleftarrows MUO_2(CO_3)_3^{2-}$$

$$M^{2+} + CaUO_2(CO_3)_3^{2-} \rightleftarrows M_2UO_2(CO_3)_2(aq)$$

where M^{2+} represents the divalent alkaline earth free ion Mg^{2+} and Ca^{2+}, and the cumulative thermodynamic constants $\log_{10}\beta°_{n.1.3}$ for the equilibria,

$$nM^{2+} + UO_2^{2+} + 3CO_3^{2-} \rightleftarrows M_nUO_2(CO_3)_3^{(4-2n)-} \text{ (n = 1 for Mg, and n = \{1;2\} for Ca)}$$

in NaCl and $NaClO_4$ electrolytes using TRLFS. We also obtained their specific interaction coefficients $\varepsilon(M_nUO_2(CO_3)_3^{(4-2n)-},Na^+X^-)$ (X^- being Cl^- and ClO_4^-) using the specific ion interaction theory (SIT) that were absent from compilation of data[37-39] — see our previous works[34-36] and references therein. Using these data, the thermodynamic functions of the ternary complexes under standard conditions are more complete and the speciation modelling should be more reliable.

However, very scarce data at varying temperature are available for $M_nUO_2(CO_3)_3^{(4-2n)-}$ complexes. Endrizzi and Rao[18] measured the complexation of $Ca_nUO_2(CO_3)_3^{(4-2n)-}$ complexes at 25°C using calorimetric titration. They concluded that the successive formations are entropy driven, and the contribution from enthalpy is rather small with $\Delta_r H° = -(7.6 \pm 5.8)$ and (0 ± 7) kJ mol^{-1} for $CaUO_2(CO_3)_3^{2-}$ and $Ca_2UO_2(CO_3)_3(aq)$, respectively, and statistically no different from nil. Similar conclusions were reported using calorimetry by Jo, *et al.*[28] with $\Delta_r H°_m = -(1.2 \pm 0.3)$ and $-(3.1 \pm 3.0)$ kJ mol^{-1} for $CaUO_2(CO_3)_3^{2-}$ for $Ca_2UO_2(CO_3)_3(aq)$, respectively. The latter authors reported the equilibrium constants at variable temperatures (10-70 °C) using TRLFS, Ca^{2+} selective electrode, UV/Vis absorption spectroscopy, and calorimetry. However, the experimental performance of the used techniques was limited to 70°C. For this reason, the experimental results measured in the temperature range of 10-50°C, though incomplete, were applied to the modified isoelectric reactions, as defined in Eq. V - 15 and Eq. V - 16, in order

to extrapolate the $\log_{10}K°_{n.1.3}$ to 70°C and derive the enthalpies using the Van't Hoff equation. The enthalpies of reaction were determined to be $\Delta_r H°_m$ = -1.2 kJ mol^{-1} and -1.7 kJ mol^{-1} for $CaUO_2(CO_3)_3^{2-}$ and $Ca_2UO_2(CO_3)_3$(aq), respectively, in satisfactory agreement with the results directly measured at 25°C by calorimetry. The application of isoelectric reaction to enlarge the validity of the Van't Hoff equation is particularly useful to predict the stability constants at non-standard temperature. The authors later applied the same analysis method to Mg-UO_2-CO_3 system and obtained $\Delta_r H°_m$ = (4.3 ± 1.5) kJ mol^{-1} for $MgUO_2(CO_3)_3^{2-}$.[29]

Recently, Maia, *et al.*[40] also using the Van't Hoff equation and a Schubert type method applied to an ion-exchange resin, reported $\Delta_r H°_m$ = (14.9 ± 5.1) kJ mol^{-1} and (36.5 ± 10.0) kJ mol^{-1} for $CaUO_2(CO_3)_3^{2-}$ for $Ca_2UO_2(CO_3)_3$(aq), respectively, slightly more important than the previous results.[18,28] One should question before any modelling the fulfilment of an important criterion of the Van't Hoff equation, the constant molar enthalpy in the investigated temperature range, as the derived parameters are very sensitive to the fitting values. Maia, *et al.*[40] also reviewed the data of Jo, *et al.*[28] by directly fitting the experimental values measured at 10-70°C to the Van't Hoff equation — not adopted in the original paper. Similar thermodynamic trends were obtained with the data of Jo, *et al.*[28] — $\Delta_r H°_m$ = (10.9 ± 9.5) kJ mol^{-1} and (23.5 ± 7.0) kJ mol^{-1} for $CaUO_2(CO_3)_3^{2-}$ and $Ca_2UO_2(CO_3)_3$(aq), respectively — that could be attributed to the constant enthalpy assumption in absence of modification to isoelectric reactions.

In the present work, we will focus on the complexation of triscarbonatouranyl(VI) with Ca^{2+} and Mg^{2+} by TRLFS in the temperature range 10-50°C and 5-30°C, respectively. Stability constants of $M_nUO_2(CO_3)_3^{(4-2n)-}$ will be determined at I_m = 0.1 mol kg_w^{-1} NaCl, with spectroluminescent titration by Ca^{2+} or Mg^{2+} at variable pH values, which has been successfully applied to determine formation constants and interaction coefficients in our previous studies.[34-36] The luminescence emission intensity and decay-times with increasing temperatures will also be studied. Different approximation models — the Van't Hoff equation, the constant heat capacity model, the DQUANT equation, and the isoelectric modification — will be adjusted to our experimental values. The molar enthalpy values obtained in different approaches will be compared with previously published values.[18,28,29,40] The implications in complexation mechanisms will be further discussed, in combination with our previous observations in concentrated electrolytes. These data can serve as parameters in the prediction of uranium migration in deep underground geological nuclear waste management context. Coupled

influence of temperature and ionic strength on $M_nUO_2(CO_3)_3^{(4-2n)-}$ complexation will be analysed for particular scenarios in combination with our previous data.[34-36]

V - 3 Experimental Section

3.1 Sample preparation

The stock solution of U(VI) was prepared by dissolving high purity U_3O_8 in 37% hydrochloric acid (Sigma-Aldrich, ACS reagent). Inductively coupled plasma mass spectroscopy (ICP-MS) was used to measure the stock concentration of U(VI). The concentration of U(VI) in all studied solutions was fixed at 50 μmol kg_w^{-1}. The ionic strength was maintained at 0.1 mol kg_w^{-1} with anhydrous NaCl (Sigma-Aldrich, ACS reagent, ≥ 99%) and Millipore deionized water (Alpha-Q, 18.2 MΩ cm). The addition of freshly prepared $NaHCO_3$ (Analytical Grade, Fisher) solution was previously calculated considering the equilibrium between the atmospheric CO_2 and the aqueous pH value at 25°C. Calcium chloride ($CaCl_2$, Sigma-Aldrich, ACS reagent, ≥ 99%) and magnesium chloride ($MgCl_2$, Sigma-Aldrich, ACS reagent, ≥ 99%) were used to control the concentrations of alkaline earth metal ions. Freshly prepared NaOH (Analytical Grade, Fisher) and diluted HCl solutions were used for the pH adjustments. The samples were under saturated with respect to uranium ($UO_3{:}2H_2O$ or β-$UO_2(OH)_2$),[39] and calcite[41] (for Ca-series) or magnesite[42] (for Mg-series). No obvious precipitation was observed throughout the experiments. The preparation of all samples was carried out by weighing under aerobic conditions.

The pH measurements were done using a combined hydrogen ion-sensitive glass electrode (Mettler Toledo, USA), filled with saturated potassium chloride (Radiometer Analytical, HACH). The recommended pH buffer solutions by National Institute of Standards and Technology (NIST) (pH 1.68, 4.01, 6.87, and 9.18 at 25°C, SI Analytics, Mainz, Germany) were used throughout the experiments. The detailed information of the commercial buffer solutions can be found in the literature[43] — see Table V - S1 of the Supplementary Information (SI) —, and the corresponding pH values at other temperatures are in Table V - S2 of the SI. The pH buffers and the sample solutions were maintained in a water bath (Lauda Ecoline E100, Germany) operating at the desired temperature. The default temperature on the pH meter (Mettler Toledo, USA) was manually reset before performing the calibration at other temperatures. Four-point calibrations based on the linear relationship between the pH values of buffer solutions and the potential read on the pH-meter were achieved in 5-50°C temperature range (see Fig. V - S1 of the SI). The sample bottle was placed in a beaker containing the water

at the desired temperature in order to maintain the solution temperature during pH measurements. The pH values were regularly adjusted if there were any modifications prior to the luminescent spectrum acquisition. The pH measurements were performed in triplicate for each sample.

3.2 Time-resolved laser-induced luminescence spectroscopy

The time-resolved luminescence apparatus has been already described.[34-36] The sample solution was added in a fluorescence quartz cuvette with a sealable cap (QS 117F, Suprasil, Hellma Analytics) leaving a minimum headspace to limit evaporation and CO_2 degassing. Before spectrum acquisition, the cuvette was placed in the thermostated sample holder during at least 20 min. The temperature was maintained at a constant value by circulating water through the thermostat (Peter Huber Kältemaschinenbau AG, Germany). The sample cuvette was thermally equilibrated with the circulating water throughout the measurements for minimizing the temperature fluctuation on uranyl fluorescence. The laser excitation source in this study is a frequency-tripled Nd:YAG laser at 355 nm (Surelite, Continuum, USA) providing a 5 ns pulse at 10 Hz of about 170 mJ as energy. An optical parametric oscillator system (Horizon, Continuum, USA) was used to tune the excitation wavelength at λ_{exc} = 450 nm. The fluorescence beam energy — average of 100 laser shots — was read on a Joule-meter RJP-734 (Laser Probe, Inc.). The 300 lines per mm grating was selected in monochromator spectrometer (Acton). The resulting measured fluorescence signal, recorded at a delay time D = 25 ns with the gate width W = 1 μs, was detected by an intensified CCD camera (Andor, UK) maintained at -10°C by Peltier effect.

The recorded spectra were integrated over the emission wavelength range at varying D values, with the trapezoidal method implemented in Origin 9.0 software (OriginLab Corporation, USA), to evaluate the fluorescence intensity at various delay times. The least-square fitting process (Levenberg-Marquardt algorithm) was used to calculate the luminescence intensity at $D = 0$ and decay-time τ by fitting the intensity results to the exponential fluorescence decay function, expressed as already discussed,[34-36]

$$FI = \sum_i FI_0\ \tau_i \exp\left(-\frac{D}{\tau_i}\right)\left(1 - \exp\left(-\frac{W}{\tau_i}\right)\right) \qquad \text{(V - 1)}$$

where FI and FI_0 are respectively the fluorescence intensity at a specific delay time and at $D = 0$. The gate width $W = 1$ μs and τ_i represents the decay-time of species i.

3.3 Equilibrium constants and ionic medium corrections

The stoichiometry of $M_nUO_2(CO_3)_3^{(4-2n)-}$ complexes is identified by the so-called slope analysis, which has been successfully applied in our previous studies,[34-36] to calculate the formation constants in NaCl and $NaClO_4$ electrolytes of different ionic strengths. The pH values and Mg^{2+}/Ca^{2+} concentrations are changed simultaneously in spectroluminescent titration i) to avoid the occurrence of $UO_3{:}2H_2O(cr)$[38,39] and calcite ($CaCO_3$)[41] or magnesite ($MgCO_3$)[42] compared to the typical pH-fixed experimental methodology, and ii) to allow the formation of ternary species to a great magnitude in solution.

Successive formations of $M_nUO_2(CO_3)_3^{(4-2n)-}$ are described with the conditional equilibrium constants $K_{n.1.3}$ expressed as follows,

$$nM^{2+} + UO_2(CO_3)_3^{4-} \rightleftarrows M_nUO_2(CO_3)_3^{(4-2n)-}$$

$$K_{n.1.3} = \frac{\left[M_nUO_2(CO_3)_3^{(4-2n)-}\right]}{\left[M^{2+}\right]^n\left[UO_2(CO_3)_3^{4-}\right]} \qquad n = \{1;2\} \qquad \text{(V - 2)}$$

where squared brackets indicate concentration in molality (mol kg_w^{-1}).

The logarithmic transformation of Eq. V - 2 in Eq. V - 3 allows calculating the $\log_{10}K_{n.1.3}$ value. The slope n in Eq. V - 3 stands for the stoichiometry of Mg^{2+}/Ca^{2+}, R_f is the concentration ratio between complexed and non-complexed $UO_2(CO_3)_3^{4-}$ by Mg^{2+}/Ca^{2+}. The intercept $\log_{10}K_{n.1.3}$ refers to the conditional stepwise formation constants of $M_nUO_2(CO_3)_3^{(4-2n)-}$ at a given ionic strength,

$$\log_{10}R_f = \log_{10}\frac{\left[M_nUO_2(CO_3)_3^{(4-2n)-}\right]}{\left[UO_2(CO_3)_3^{4-}\right]/\alpha} = \log_{10}K_{n.1.3} + n\log_{10}[M^{2+}] \qquad \text{(V - 3)}$$

which can be converted to luminescence intensity supposing it is proportional to the U(VI) concentrations.

$$\log_{10}R_f = \log_{10}\frac{FI_0\left(M_nUO_2(CO_3)_3^{(4-2n)-}\right)}{FI_0\left(UO_2(CO_3)_3^{4-}\right)/\alpha} = \log_{10}K_{n.1.3} + n\log_{10}[M^{2+}] \qquad \text{(V - 4)}$$

Here $FI_0(M_nUO_2(CO_3)_3^{(4-2n)-})$ is the fluorescence intensity extrapolated at D = 0. $FI_0(UO_2(CO_3)_3^{4-})$ is the one of the non-complexed $UO_2(CO_3)_3^{4-}$ at pH 9, and α represents the Ringböm coefficient[44] of $UO_2(CO_3)_3^{4-}$. The variation of $UO_2(CO_3)_3^{4-}$ with pH at $[M^{2+}] = 0$ conditions was calculated to assess the value of α — the reader is referred to previous papers for detailed explanation and specific calculation.[34-36] The α values were calculated using the thermodynamic data ($\log_{10}K°$ and $\Delta_rH°_m$) from Table V - S3 of the SI,[38] and specific ion

interaction coefficients from Table V - S4 of the SI.[34,36,38] As the H^+ activity was determined from the acidity measurement of the solutions, the dissociation constants of water pK_w, were used to evaluate the H^+ concentration at various temperatures.[5] The corresponding α values at each specified aqueous condition was listed in Table V - S5 of the SI.

The specific ion interaction theory (SIT) was used to correct the ionic strength effect in solution, as recommended in widely accepted Nuclear Energy Agency-Thermochemical Data Base (NEA-TDB) reviews.[37-39] The activity coefficient γ_i of an aqueous species i in the SIT approach is given by

$$\log_{10} \gamma_i = -z_j^2 D_H + \varepsilon(j, k, I_m)\, m_k \qquad \text{(V - 5)}$$

with $D_H(T)$ the temperature-dependent Debye-Hückel term expressed as,

$$D_H(T) = \frac{A(T)\sqrt{I_m}}{1+1.5\sqrt{I_m}} \qquad \text{(V - 6)}$$

where z_i is the charge of ion i, $\varepsilon(j,k,I_m)$ ($kg_w\ mol^{-1}$) is the ion interaction coefficient between the aqueous ion j and ion k of background electrolyte of concentration I_m at a given temperature — in this study no variation of ε with I_m was postulated and is thus considered $\varepsilon(j,k)$ in the following. The temperature influence on $\varepsilon(j,k)$ ($kg_w\ mol^{-1}$) is usually not available for the involved ions. However theoretically, $\varepsilon(j,k)(T) = \varepsilon(j,k)(T°)T°/T$ because $\varepsilon(j,k)m_k$ is a second virial expansion term.[45,46] In the experimental temperature range, the correction of $\varepsilon(j,k)m_k$ to temperature is not necessary as the correction should be too small to be considered. Values of the Debye-Hückel parameters A(T) at different temperatures are shown in Table V - S6 of the SI. The relationship between conditional formation constants and ionic strength is expressed by

$$\log_{10} K_{n.1.3} = \log_{10} K^{\circ}_{n.1.3} + \Delta z^2 D_H - \Delta\varepsilon I_m \qquad \text{(V - 7)}$$

where

$$\Delta z^2 = z\left(M_nUO_2(CO_3)_3^{(4-2n)-}\right)^2 - n\, z\left(M^{2+}\right)^2 - z\left(UO_2(CO_3)_3^{4-}\right)^2 \qquad \text{(V - 8)}$$

($\Delta z^2 = -16$ for n = 1 and $\Delta z^2 = -24$ for n = 2) and

$$\Delta\varepsilon = \varepsilon\left(M_nUO_2(CO_3)_3^{(4-2n)-}, Na^+\right) - n\varepsilon\left(M^{2+}, Cl^-\right) - \varepsilon\left(UO_2(CO_3)_3^{4-}, Cl^-\right) \qquad \text{(V - 9)}$$

with the used values of $\varepsilon(j,k)$ listed in Table V - S4 of the SI.

3.4 Temperature dependence modelling

The formation constants for many chemical species are tightly related to temperature. However, thorough understanding of the temperature-dependent chemical behaviour of

$M_nUO_2(CO_3)_3^{(4-2n)-}$ complexes has not yet been developed because of the scarcity of experimental results at higher than standard temperatures.[39] Nonetheless, computational methods such as the constant enthalpy equation, the constant heat capacity equation, the DQUANT model and the modification to isoelectric reactions have been proven adequate in a certain temperature range for evaluating temperature-dependent complexation constants. These four models were employed to describe the temperature-dependent $\log_{10}K°_{n.1.3}$ measured in the temperature range 10-50°C for $Ca_nUO_2(CO_3)_3^{(4-2n)-}$ and 5-30°C $MgUO_2(CO_3)_3^{2-}$ and used to cautiously extend their formation constants at higher temperatures. The simplified Van't Hoff equation, assuming constant $\Delta_rH°_m$ with temperature and zero heat capacity, is shown in Eq. V - 10.

$$\log_{10} K°(T) = \log_{10} K°(T_0) - \frac{\Delta_r H°_m(T_0)}{R\ln(10)}\left(\frac{1}{T} - \frac{1}{T_0}\right) \quad \text{(V - 10)}$$

with $K°$ the formation constant under standard conditions (infinite dilution), R the gas constant (8.31451 J K^{-1} mol^{-1}), T the absolute temperature in Kelvin, and $\Delta_rH°_m(T_0)$ the molar reaction enthalpy at standard temperature T_0. It should be noted that the validity of temperature range $(T–T_0) \leq 10$ K is quite narrow in this equation.[47] Extrapolation over a temperature range larger than 10 K will undoubtedly introduce greater uncertainties in the resulted $\log_{10}K°(T)$.

The constant non-nil heat capacity equation slightly extends the validity of temperature range to 20 K (Eq. V - 11).[47] The assumption of constant heat capacity is useful to calculate the equilibrium constant in the range 273-473 K. In some cases, the heat capacity term can be neglected if the entropy and the heat capacity are comparable in magnitude as the term of $\Delta_rC°_{p,m}[\Delta T–T\ln(T/T_0)]$ is less important than $\Delta_rS°_m\Delta T$.

$$\log_{10} K°(T) = \log_{10} K°(T_0) - \frac{\Delta_r H°_m(T_0)}{R\ln(10)}\left(\frac{1}{T} - \frac{1}{T_0}\right) + \frac{\Delta_r C°_{p,m}}{R\ln(10)}\left[\left(\frac{T_0}{T} - 1\right) + \ln(T/T_0)\right] \quad \text{(V - 11)}$$

Helgeson[48] reported the enthalpy- and entropy-based DQUANT model, as shown in Eq. V - 12.

$$\log_{10} K°(T) = \frac{\Delta_r S°_m}{RT\ln(10)}\left\{T_0 - \frac{\theta}{\omega}\left[1 - \exp\left(\exp(b + aT) - C + \frac{T - T_0}{\theta}\right)\right]\right\} - \frac{\Delta_r H°_m(T_0)}{RT\ln(10)} \quad \text{(V - 12)}$$

where $\Delta_rH°_m$ represents the molal reaction enthalpy, $\Delta_rS°_m$ denotes the molal reaction entropy, a = 0.01875 K^{-1}, b = 12.741, c = exp (b + aT_0), θ =219 K and ω = (1 + acθ). The uncertainties of the formation constants determined for various chemical reactions using the DQUANT equation show less than 1-9% error in 0-200°C temperature range.[47]

Isoelectric reactions are defined for the chemical reactions of the following form: the sum of positive charges among the reactants equals the total amount of positive charges among the products, and the same for the negative charges among reactants and products. The modifications of $M_nUO_2(CO_3)_3^{(4-2n)-}$ complexation to isoelectric reactions requires the additional equations Eq. V - 13 and Eq. V - 14 to balance out the charges in Eq. V - 2:

$$CO_2(aq) + H_2O \rightleftarrows CO_3^{2-} + 2H^+ \quad \text{(V - 13)}$$

$$UO_2^{2+} + 3CO_3^{2-} \rightleftarrows UO_2(CO_3)_3^{4-} \quad \text{(V - 14)}$$

The isoelectric forms of $M_nUO_2(CO_3)_3^{(4-2n)-}$ complexation are expressed as follows.

$$M^{2+} + UO_2^{2+} + 2CO_2(aq) + CO_3^{2-} + 2H_2O \rightleftarrows MUO_2(CO_3)_3^{2-} + 4H^+ \quad \text{(V - 15)}$$

$$2M^{2+} + UO_2^{2+} + 3CO_2(aq) + 3H_2O \rightleftarrows M_2UO_2(CO_3)_3(aq) + 6H^+ \quad \text{(V - 16)}$$

These kinds of reactions can cancel out the electrostatic contributions to the temperature dependence of enthalpy. The formation constants of the additional reactions Eq. V - 13 and V - 14 have been calculated for the temperature range of 5-90°C using the existing general formula,[49-51] as listed in Table V - S3 of the SI. The enthalpies for the isoelectric reactions Eq. V - 15 and V - 16 were calculated by the Van't Hoff equation with the assumption of constant enthalpy and zero heat capacity. In this study, the formation constants $\log_{10}K°_{n.1.3}(T)$ of $M_nUO_2(CO_3)_3^{(4-2n)-}$ were finally determined by subtracting the $\log_{10}K°(T)$ of Eq. V - 13 and Eq. V - 14 from the global equilibrium constants $\log_{10}\beta°_{n.1.3}(T)$ for the isoelectric reactions Eq. V - 15 and Eq. V - 16, estimated by the Van't Hoff equation at each temperature, as listed in Table V - S7 of the SI. The values of $\log_{10}K°_{n.1.3}(T)$ ascertained by different computational approximations were compared considering the individual uncertainties involved in each model.

V - 4 Results and discussion

4.1 Luminescent emission spectra analysis

Fig. V - 1 and Fig. V - 2 illustrate the evolutions of luminescent emission spectra of $M_nUO_2(CO_3)_3^{(4-2n)-}$ complexes. The formation constants for $CaUO_2(CO_3)_3^{2-}$ were measured in temperature range of 10-50°C, while those for $MgUO_2(CO_3)_3^{2-}$ were achieved in a relatively narrower temperature range (5-30°C), because of a pronounced decrease in the luminescence emission intensity, and a strong deformation of characteristic spectra at T > 30°C that caused difficulties in interpreting the luminescence evolution.

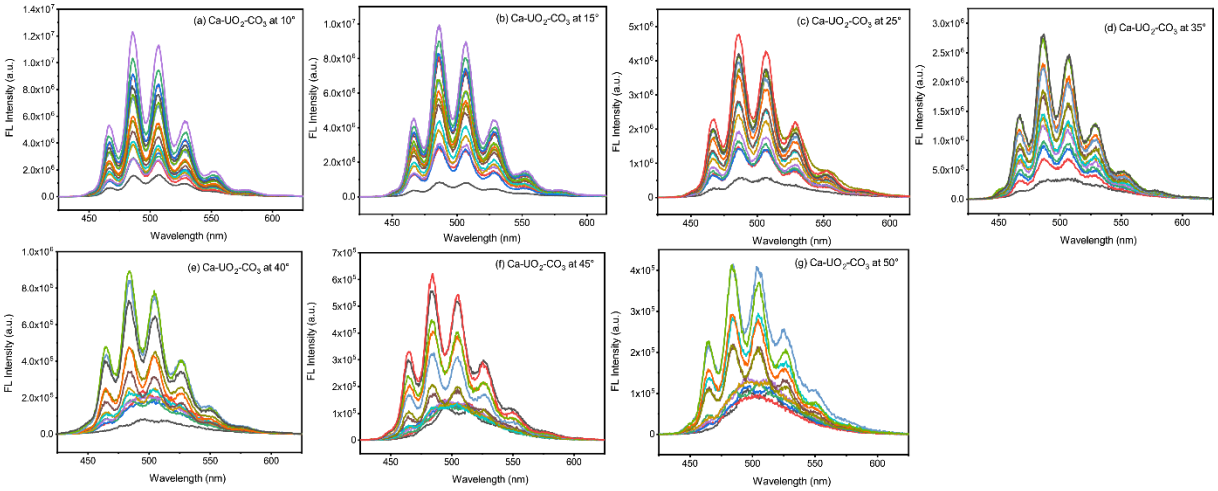

Fig. V - 1 Evolution of luminescence emission spectra during complexation of Ca(II) with $UO_2(CO_3)_3^{4-}$ at different temperature (a)-(f): 10-50°C.

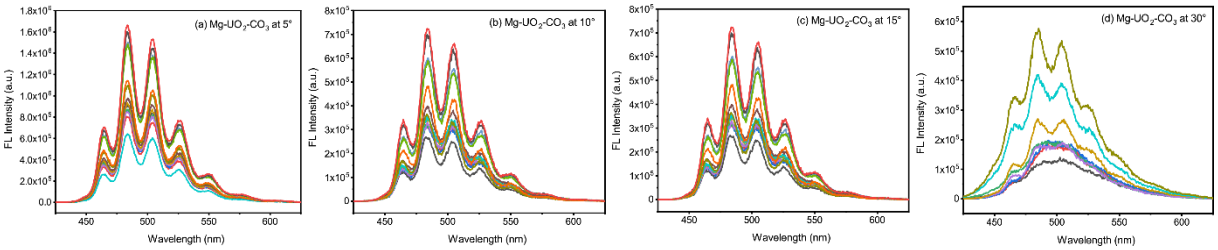

Fig. V - 2 Evolution of luminescence emission spectra during complexation of Mg(II) with $UO_2(CO_3)_3^{4-}$ at different temperature (a)-(d): 5-30°C.

At a specified temperature, the spectra showed an increase in the emission intensity with increasing alkaline earth metal concentrations, which indicates the successive complexation of Mg^{2+}/Ca^{2+} to $UO_2(CO_3)_3^{4-}$. As temperature increases, the global amplitude of intensity suffered a pronounced decrease. As shown in Fig. V - 3, the solution of fixed $[Ca^{2+}] = 6.13\ 10^{-4}$ mol kg_w^{-1} displays an obvious decrease in intensity when the temperature increases from 40 to 50°C. Apparently, the increase in temperature leads to slight shifts of the spectra to higher wavelengths also broader characteristic bands. The band shifts and broadening can become more significant at high temperatures even contributing to the deformation of spectra. One can observe that in the temperature range of 10-35°C, the samples exhibited well-defined characteristic spectra in the course of $Ca\text{-}UO_2\text{-}CO_3$ complexation, while outside this range, the spectra showed irregular evolution at the beginning of the complexation, *i.e.*, 40, 45, and 50°C. Specifically, we compared the area-normalized emission spectra of triscarbonatouranyl from 5 to 50°C in the absence of Mg^{2+}/Ca^{2+} in Fig. V - 4. The concentration of U(VI) varied from 50 to 250 µmol kg_w^{-1} in order to increase the luminescence at the highest temperatures. Indeed, the emission spectra contain features originating from vibronic transitions from the lowest excited

state to the ground state manifold, 11→00 of the hot band and 10→0ν (ν = 0, 1, 2, 3) of other peaks.[52] With the increase in temperature, the less-defined bands of $UO_2(CO_3)_3^{4-}$ were continuously red-shifted.

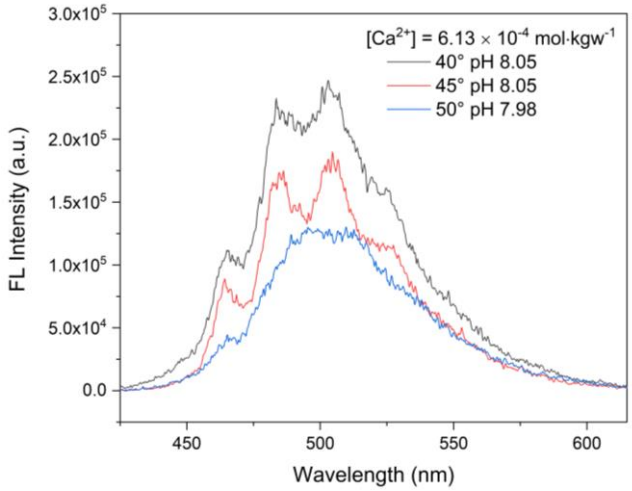

Fig. V - 3 Luminescence emission spectra at higher temperatures than the ambient of the sample: [U(VI)] = 50 μm, $[Ca^{2+}]$ = 6.13 10^{-4} mol kg_w^{-1}, pH ≈ 8 with the dominant species $CaUO_2(CO_3)_3^{2-}$ in solution.

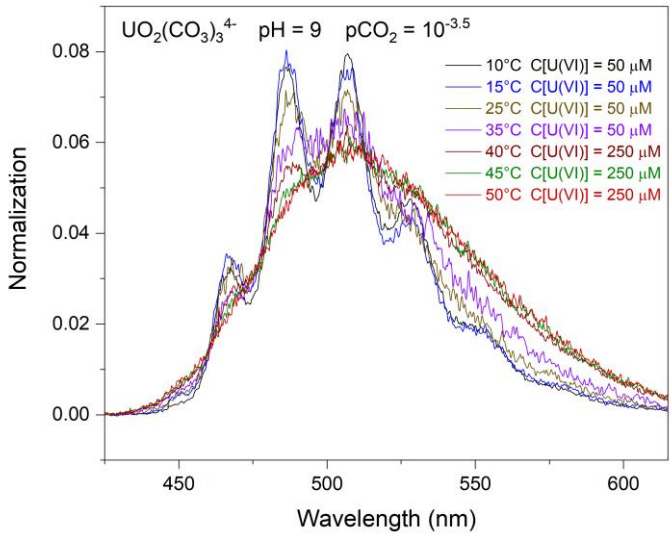

Fig. V - 4 Luminescence emission spectra of $UO_2(CO_3)_3^{4-}$ normalized to the same area at D = 25 ns; the concentration of [U(VI)] increased at high temperatures (40-50°C) to enhance the emission intensity.

Numerous reasons have been put forward in the application of laser techniques. The red-shifted and broadened with lower intensity emission spectra of $UO_2(CO_3)_3^{4-}$ may give impression that the non-radiative decay becomes more important at higher temperature, which

lowers the quantum yield (Q). It is also possible that a change in temperature will alter the rates of some reactions, *e.g.*, the formation of an internal charge-transfer (ICT) states, which hinders the radiative decay.[53] Further research is needed to probe the luminescent properties of triscarbonatouranyl(VI) with temperature.

The evolution of spectral band positions with increasing [Ca^{2+}] allows sorting out individual spectra of involved species, notably at higher temperatures, *i.e.*, 40, 45, and 50°C, where the band shifts were obvious. The data analysis method employed in the present study is the combination of Singular Value Decomposition (SVD),[54] used to assess the number of distinguishable components, and multivariate curve resolution alternating least squares (MCR-ALS)[55-57] used to recover the spectra. The analysed global data matrix at a specified temperature is composed of 1024 rows and *n* columns, with 1024 corresponding to the number of pixels of the CCD camera (416.46-633.81 nm wavelength range), and *n* corresponding to the sample number in each series. The calculations have been carried out with codes developed in-house in R environment (https://github.com/ppernot/SK-Ana). Unlike the routine application of the developed codes to spectro-kinetics matrices data — built by delay-varying measurements —, the global matrices in this work were constructed from the spectra of different [Ca^{2+}] concentrations, measured at D = 25 ns. By this means, the problem can be recast into a decomposable form that emphasizes the bilinearity between Ca^{2+}-dependent concentration and spectral properties, as expressed in the following equation:

$$F(\lambda, [Ca]) = \sum_k F_k(\lambda) C_k([Ca]) \qquad \text{(V - 17)}$$

where $F(\lambda, [Ca])$ (luminescent intensity), represents an additive result of pure spectra $F_k(\lambda)$, of k principal components determined by SVD weighted by their concentration profile as a function of $C_k([Ca])$. This interpretation of luminescent spectra evolution is also chemically meaningful. However, it was noted in Ruckebusch, *et al.*[55] that SVD can suffer from an excess of estimated rank towards the expected number of components when the pure spectrum of a single chemical compound shows a clear spectral shift, thus the sequential transformation of discrete components was applied in the decomposition in order to verify the concentration-wavelength separability.[58]

The global matrices data analysis was conducted for the Ca series at 50°C. The first spectrum [Ca^{2+}] = 0 was separately implemented as an external file serving as the reference shape, which can facilitate the calculation and improve the accuracy. The SVD analysis and the sequential transformation were tested for determining the number of components. The spectra and concentration profile were constrained to be positive. It was shown by both methods that there

are two distinguishable components, which is consistent with the hypothesis of $CaUO_2(CO_3)_3^{2-}$ and $Ca_2UO_2(CO_3)_3$(aq) occurrences. The MCR-ALS analysis with two species results in a lack-of-fit (LOF) of 3.73%. The recovered spectra of $CaUO_2(CO_3)_3^{2-}$ and $Ca_2UO_2(CO_3)_3$(aq) are shown in Fig. V - 5, compared to the experimentally acquired $UO_2(CO_3)_3^{4-}$ spectrum, see Fig. V - S2 of the SI for spectral decomposition. The spectrum decomposition was performed by fitting the emission bands into Gaussian-peak shape using Levenberg-Marquardt method to evaluate the uncertainties — for details of decomposition information, see Table V - S8 of the SI.

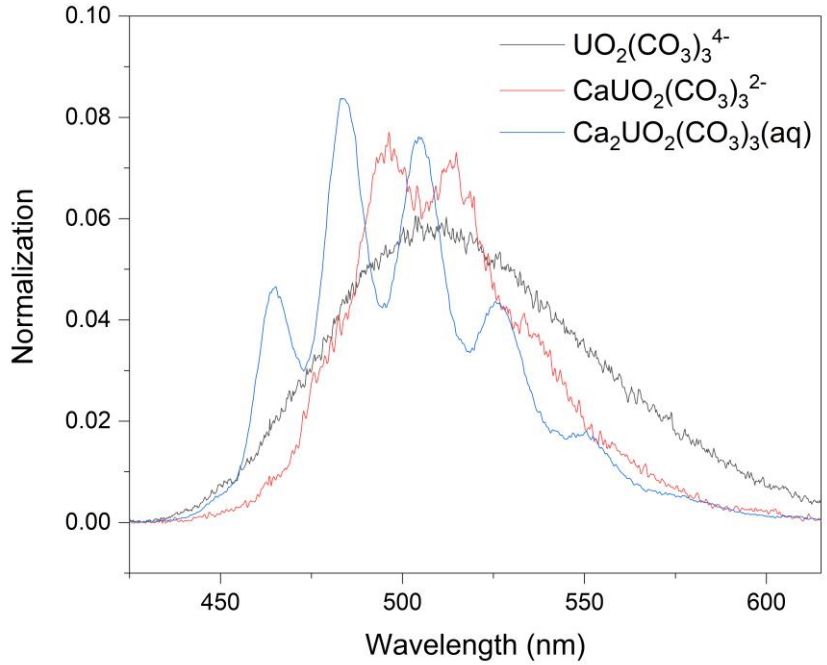

Fig. V - 5 Pure emission spectra obtained from MCR-ALS analysis of the complexation of Ca^{2+} with $UO_2(CO_3)_3^{4-}$ at 50°C.

One can observe that at 50°C, the energy losses in luminescence are intensified for the incomplete complexations, *i.e.*, $UO_2(CO_3)_3^{4-}$ and $CaUO_2(CO_3)_3^{2-}$, that contribute to the red-shifted and strongly deformed spectra. On the contrary, the neutral charged species $Ca_2UO_2(CO_3)_3$(aq) is more resistant to the temperature effect. The characteristic band positions were determined at 465, 484, 505, 526, and 549 nm for $Ca_2UO_2(CO_3)_3$(aq) that are consistent with our previous results,[34,35] whereas the pure spectrum of $CaUO_2(CO_3)_3^{2-}$ at 50°C exhibited obvious red-shifts with bands resolved at 480, 497, 515, 533, and 552 nm. The recovered spectra using the MCR-ALS analysis of $Ca_nUO_2(CO_3)_3^{(4-2n)-}$ at 40 and 45°C are not shown, but the

trends in the spectral features are similar. The same procedure was also applied to the Mg-series at 30°C. As shown in Fig. V - S3 of the SI, the pure spectrum of $MgUO_2(CO_3)_3^{2-}$ at 30°C did not show a shift compared to our previous measurements,[36] with band positions determined at 466, 485, 503, 523, and 546 nm. It is believed that the spectral properties of Mg/Ca-UO_2-CO_3 complexes reflect subtle differences in the coordination of alkaline metal ion to triscarbonatouranyl(VI), which also affect their thermodynamic properties. This will be pointed out with the analysis of their thermodynamic functions in the following section.

4.2 Evaluation of equilibrium constants at different temperatures

The graphical representations of linear regression results at different temperatures are shown in Fig. V - 6 for $Ca_nUO_2(CO_3)_3^{(4-2n)-}$ and in Fig. V - 7 for $MgUO_2(CO_3)^{2-}$. The stability constants at 22°C of $M_nUO_2(CO_3)_3^{(4-2n)-}$ had been measured during our previous studies.[34,36] The 2σ error bars are too small to be presented due to the trapezoidal integration method used to deduce the value of FI_0 (the fluorescence intensity at D = 0). Linear fits were achieved by weighted least-squares regression analysis with estimated parameters of slope and intercept mean values with 95% uncertainties. After rounding off the slope values to the integers of 1 and 2, *i.e.* the stoichiometry of coordinated Mg^{2+}/Ca^{2+}, we obtained the conditional formation constants of $M_nUO_2(CO_3)_3^{(4-2n)-}$ listed in Table V - 1 with the $\log_{10}K°_{n.1.3}$ extrapolated to infinite dilution by SIT.

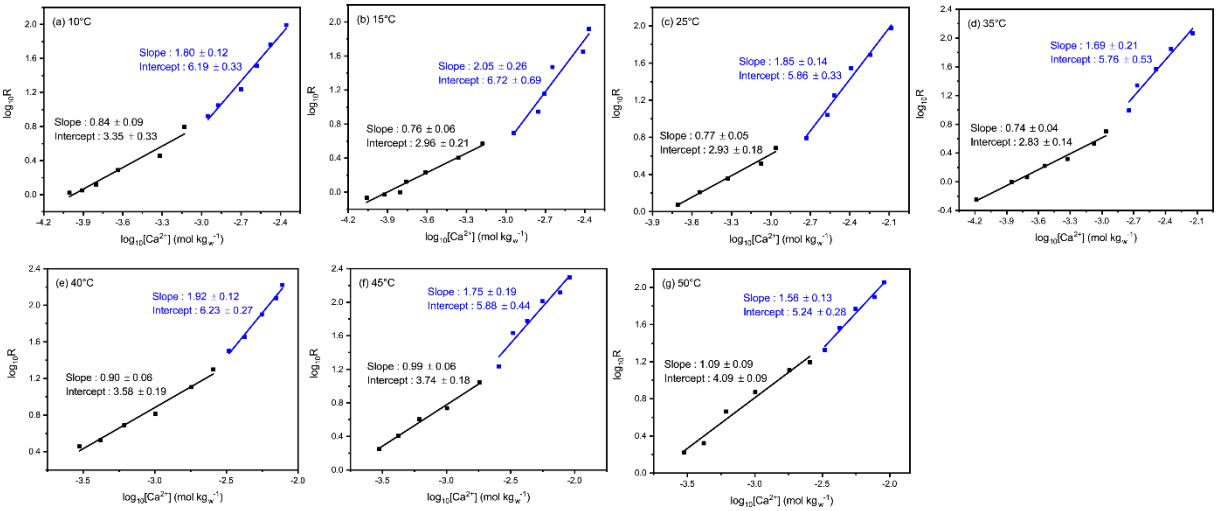

Fig. V - 6 Plot of logarithm ratio of R as a function of $log_{10}[Ca^{2+}]$ (m) at (a)-(f): 10-50°C: $[U]_{total}$ = 50 μm.

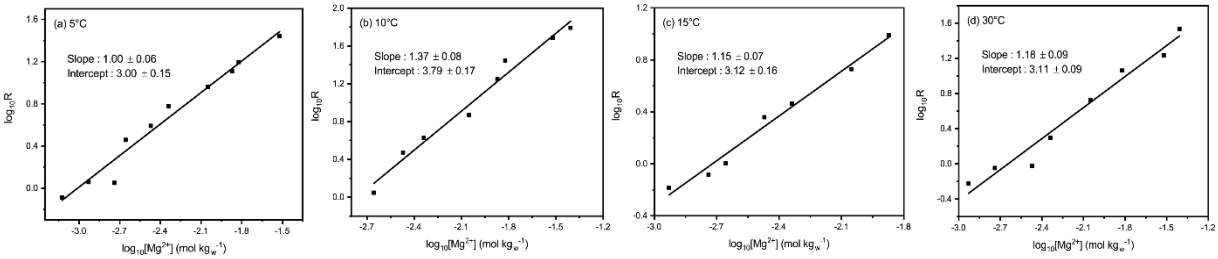

Fig. V - 7 Plot of logarithm ratio of R as a function of $log_{10}[Mg^{2+}]$ (m) at (a)-(d): 5-30°C: $[U]_{total}$ = 50 μm.

Table V - 1 Formation constants $log_{10}K_{n.1.3}$ derived from the rounded off slopes in Fig. V - 6 and Fig. V - 7 with values of $log_{10}K_{0.1.3}°$ taken from Götz et al.[49]

$Ca_nUO_2(CO_3)_3^{(4-2n)-}$							
T (°C)	$log_{10}K_{1.1.3}$	$log_{10}K_{2.1.3}$	$log_{10}K°_{1.1.3}$	$log_{10}K°_{2.1.3}$	$log_{10}K°_{0.1.3}$	$log_{10}\beta°_{1.1.3}$	$log_{10}\beta°_{2.1.3}$
10	3.92 ± 0.03	6.73 ± 0.03	5.62 ± 0.03	9.31± 0.03	22.28 ± 0.04	27.91 ± 0.04	31.59± 0.04
15	3.85 ± 0.03	6.58 ± 0.05	5.57 ± 0.03	9.17± 0.05	22.11 ± 0.04	27.68 ± 0.04	31.28± 0.05
22[34]	3.56 ± 0.02	5.93 ± 0.03	5.29 ± 0.02	8.55± 0.03	21.93 ± 0.04	27.22 ± 0.04	30.48± 0.05
25	3.69 ± 0.03	6.23 ± 0.03	5.43 ± 0.03	8.87± 0.03	21.81 ± 0.04	27.24 ± 0.04	30.68± 0.04
35	3.75 ± 0.05	6.52 ± 0.05	5.52 ± 0.05	9.18± 0.05	21.58 ± 0.04	27.10 ± 0.05	30.76 ± 0.04
40	3.89 ± 0.02	6.41 ± 0.02	5.68 ± 0.02	9.10± 0.02	21.48 ± 0.04	27.16 ± 0.04	30.58± 0.04
45	3.78 ± 0.01	6.46 ± 0.04	5.59 ± 0.01	9.17± 0.04	21.40 ± 0.04	26.99 ± 0.04	30.57± 0.04
50	3.80 ± 0.03	6.23 ± 0.04	5.63 ± 0.03	8.97± 0.04	21.33 ± 0.04	26.96 ± 0.04	30.30± 0.04
$MgUO_2(CO_3)_3^{2-}$							
T (°C)	$log_{10}K_{1.1.3}$	$log_{10}K°_{1.1.3}$	$log_{10}K°_{0.1.3}$	$log_{10}\beta°_{1.1.3}$			
5	3.00 ± 0.03	4.67 ± 0.03	22.48 ± 0.04	27.18 ± 0.04			
10	3.04 ± 0.07	4.72 ± 0.07	22.28 ± 0.04	27.03 ± 0.07			
15	2.76 ± 0.03	4.45 ± 0.03	22.11 ± 0.04	26.59 ± 0.04			
22[36]	2.98 ± 0.02	4.68 ± 0.02	21.93 ± 0.04	26.65 ± 0.04			
30	2.73 ± 0.05	4.46 ± 0.05	21.69 ± 0.04	26.32 ± 0.05			

4.3 Determination of enthalpy and entropy

The enthalpy of the formation of $M_nUO_2(CO_3)_3^{(4-2n)-}$ is the net thermal effect of three processes: i) the energy required for dehydration of Mg^{2+}/Ca^{2+} and $UO_2(CO_3)_3^{4-}$; ii) the energy released/required during the formation of $M_nUO_2(CO_3)_3^{(4-2n)-}$; and iii) the energy released/required during the formation of hydrogen bonding between dehydrated water molecules and the surrounding bulk water. The value of $\Delta_r H°_m$ is established by the competition between the energy-consuming and -generating processes in complexation and a net gain/loss in energy balance resulting in negative/positive value of $\Delta_r H°_m$, respectively. The stability constants of $M_nUO_2(CO_3)_3^{(4-2n)-}$ determined in this work did not show obvious variation in the investigated temperature range that made the model parameters sensible to adjustment and resulted in large errors. Four approximation approaches were tested to fit the experimental $log_{10}K°_{n.1.3}$: the Van't Hoff equation, the constant heat capacity equation, the DQUANT

equation, and the isoelectric modification. Notwithstanding the different assumptions of each estimated model, as well as their corresponding temperature range of validity, the four approximation approaches provide satisfactory fitting of experimental data and allow prediction of the formation constants with temperatures. It must be reminded here that two digits will be kept for thermodynamic constants and entropy values, and three digits will be kept in the values of the Gibbs energy and enthalpy values, in coherence with the selected data of the NEA-TDB,[37-39] even if they may not be significant.

With the values of $\log_{10}K°_{n.1.3}$ and $\Delta_r H°_m$ determined at 25°C using different approximation approaches, the temperature effect can be quantitatively estimated to predict the formation constants as a function of temperature. Fig. V - 8 shows that the approaches, including the Van't Hoff equation, the constant heat capacity equation, the DQUANT approach, and the isoelectric modification method, provide satisfactory description of the measured $\log_{10}K°_{n.1.3}$ in the temperature ranges of 5-30°C for $MgUO_2(CO_3)_3^{2-}$ and 10-50°C for $Ca_nUO_2(CO_3)_3^{(4-2n)-}$. However, deviations start to increase at elevated temperature, *i.e.*, 70-90°C, reaching several logarithm units, especially between the values evaluated by the Van't Hoff equation and the constant heat capacity equation. Fig. V - 9 presents the variation of $\log_{10}K°_{n.1.3}$ uncertainties bands with temperature using the Van't Hoff approach.

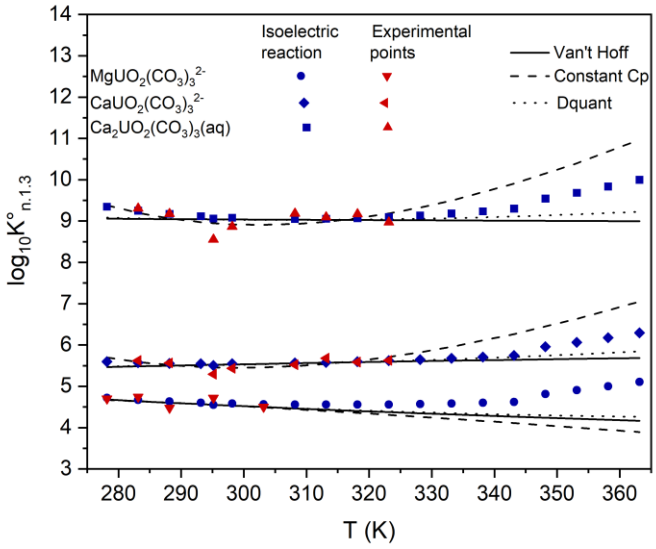

Fig. V - 8 Dependence on temperature of the thermodynamic constants for $M_nUO_2(CO_3)_3^{(4-2n)-}$ with lines: the fitted curves based on the Van't Hoff equation, the constant heat capacity equation and the DQUANT equation and red points: the values of $\log_{10}K°_{n.1.3}$ recalculated for each temperature with the isoelectric reaction, as listed in Table V - S7 of the SI.

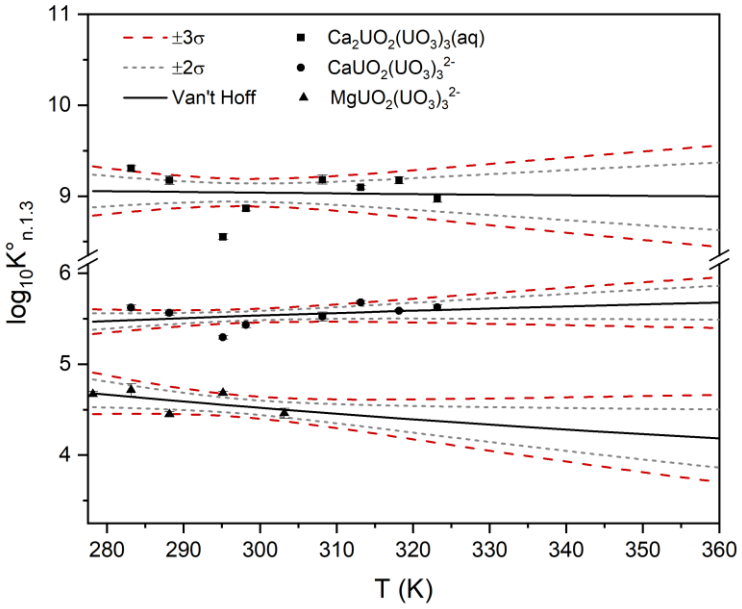

Fig. V - 9 Dependance on temperature of the thermodynamic constants for $Mg_n/Ca_nUO_2(CO_3)_3^{(4-2n)-}$ with lines represented fitted curves based on the Van't Hoff equation, grey short-dashed lines display the 95% confidence interval and red long-dashed lines show the 98% confidence level (see thermodynamic parameters in Table V - 2).

Table V - 2 Comparison of thermodynamic parameters for the formations of $M_nUO_2(CO_3)_3^{(4-2n)-}$ obtained by different approximation approaches.

	Model	$\log_{10}K°_{n.1.3} \pm 2\sigma$ at 25°C	$\log_{10}\beta°_{n.1.3} \pm 2\sigma$ at 25°C	$\Delta_r H°_m \pm 2\sigma$ (kJ mol^{-1}) at 25°C	$T\Delta_r S°_m \pm 2\sigma$ (kJ mol^{-1}) at
	[a] $Ca^{2+} + UO_2(CO_3)_3^{4-} = CaUO_2(CO_3)_3^{2-}$				
Ca(II)	Van't Hoff	5.53 ± 0.05	27.37 ± 0.06	4.882 ± 5.949	36.45 ± 5.96
	$\Delta_r^{VH}G°_m$ = -31.565 ± 0.285 kJ mol^{-1}				
	$\Delta_f^{VH}G°_m$ = -3 245.285 ± 4.550 kJ mol^{-1}				
	$\Delta_f^{VH}H°_m$ = -3 618.800 ± 7.484 kJ mol^{-1}				
	$^{VH}S°_f$ = 104.500 ± 24.663 J K^{-1} mol^{-1}				
	Constant C_p	5.45 ± 0.06	27.29 ± 0.07	-1.784 ± 6.145	29.32 ± 6.15
				$\Delta_r C°_{p.m}$ = 1.74 ± 0.93 kJ mol^{-1}	
	DQUANT	5.52 ± 1.38	27.36 ± 1.38	4.306 ± 5.599	35.81 ± 5.51
	Isoelectric	5.74 ± 0.05	27.58 ± 0.06	-5.001 ± 5.395	27.79 ± 5.40
	[b] $Ca^{2+} + CaUO_2(CO_3)_3^{2-} = Ca_2UO_2(CO_3)_3$				
	Van't Hoff	3.51 ± 0.11		-6.229 ± 13.285	13.80 ± 13.30
	$\Delta_r^{VH}G°_m$ = -572.842 ± 5.470 kJ mol^{-1}				
	Constant C_p	3.47 ± 0.15		-9.208 ± 15.427	10.60 ± 15.45
					$\Delta_r C°_{p.m}$ = 0.77 ± 2.33 kJ mol^{-1}
	DQUANT	3.51 ± 3.12		-6.440 ± 12.705	13.61 ± 12.50
	Isoelectric	3.62 ± 0.09		-11.208 ± 10.548	9.60 ± 10.56
	[c] $2Ca^{2+} + UO_2(CO_3)_3^{4-} = Ca_2UO_2(CO_3)_3$				
	Van't Hoff	9.04 ± 0.10	30.88 ± 0.11	-1.347 ± 11.879	50.25 ± 11.89
	$\Delta_r^{VH}G°_m$ = -51.601 ± 0.571 kJ mol^{-1}				
	$\Delta_f^{VH}G°_m$ = -3 818.127 ± 3.035 kJ mol^{-1}				
	$\Delta_f^{VH}H°_m$ = -4 169.290 ± 12.835 kJ mol^{-1}				
	$^{VH}S°_f$ = 94.585 ± 42.450 J K^{-1} mol^{-1}				
	Constant C_p	8.92 ± 0.14	30.76 ± 0.15	-10.992 ± 14.150	39.92 ± 14.17
					$\Delta_r C°_{p.m}$ = 2.51 ± 2.14 kJ mol^{-1}
	DQUANT	9.03 ± 2.80	30.87 ± 2.80	-2.134 ± 11.405	49.42 ± 11.22
	Isoelectric	9.39 ± 0.07	31.23 ± 0.08	-16.209 ± 9.064	37.39 ± 9.07
	[d] $Mg^{2+} + UO_2(CO_3)_3^{4-} = MgUO_2(CO_3)_3^{2-}$				
Mg(II)	Van't Hoff	4.53 ± 0.08	26.37 ± 0.09	-11.653 ± 10.300	14.22 ± 10.31
	$\Delta_r^{VH}G°_m$ = -25.876 ± 0.450 kJ mol^{-1}				
	$\Delta_f^{VH}G°_m$ = -3 142.170 ± 2.542 kJ mol^{-1}				
	$\Delta_f^{VH}H°_m$ = -3 562.540 ± 11.228 kJ mol^{-1}				
	$^{VH}S°_f$ = -50.859 ± 37.676 J K^{-1} mol^{-1}				
	Constant Cp	4.53 ± 0.10	26.37 ± 0.11	-13.477 ± 30.494	12.38 ± 30.50
	$\Delta_r C°_{p.m}$ = 0.224 ± 3.409 kJ mol^{-1}				
	DQUANT	4.53 ± 2.69	26.37 ± 2.69	-11.171 ± 10.683	14.70 ± 11.00
	Isoelectric	4.54 ± 0.09	26.38 ± 0.10	-12.025 ± 12.435	13.89 ± 12.45

As shown in Table V - 2, the enthalpies were calculated by the Van't Hoff equation to be $\Delta_r^{VH}H°_m$ = (4.882 ± 5.949) kJ mol^{-1} and – (1.347 ± 11.879) kJ mol^{-1} for $CaUO_2(CO_3)_3^{2-}$ and $Ca_2UO_2(CO_3)_3$(aq), respectively, indicating that the first complexation of Ca^{2+} to $UO_2(CO_3)_3^{4-}$ is slightly endothermic. Similar values were obtained with the DQUANT equation, $\Delta_r^{DQUANT}H°_m$ = (4.306 ± 5.599) and – (2.134 ± 11.405) kJ mol^{-1} for $CaUO_2(CO_3)_3^{2-}$ and $Ca_2UO_2(CO_3)_3$(aq), respectively. However, the constant heat capacity model and the isoelectric modification approach suggested slightly exothermic reaction for the formation of $CaUO_2(CO_3)_3^{2-}$ with $\Delta_r^{CHC}H°_m$ = – (1.784 ± 6.145) kJ mol^{-1} and $\Delta_r^{Exo}H°_m$ = – (5.001 ± 5.395)

kJ mol^{-1}, and for $Ca_2UO_2(CO_3)_3$(aq) with $\Delta_r^{CHC}H°_m$ = – (10.992 ± 14.150) kJ mol^{-1} and $\Delta_r^{Exo}H°_m$ = – (16.209 ± 9.064) kJ mol^{-1}. We specifically calculated the thermodynamic constants for the successive complexation of Ca^{2+} to $CaUO_2(CO_3)_3^{2-}$ by subtracting the values determined for $CaUO_2(CO_3)_3^{2-}$ from those for $Ca_2UO_2(CO_3)_3$(aq) (Table V - 2). The uncertainties were apparently too large, due to the very weak variation of the values of $\log_{10}K°_{n.1.3}$ in the investigated temperature ranges.

One can note that for the formation of $CaUO_2(CO_3)_3^{2-}$, the entropy term $T\Delta_rS°_m$ varies from (27.79 ± 5.40) kJ mol^{-1} to (36.45 ± 5.96) kJ mol^{-1} at room temperature depending on the fitting equation. It seems though that the formation of $CaUO_2(CO_3)_3^{2-}$ is entropy-driven, consistent with the trends observed both by Endrizzi and Rao[18] and Jo *et al.*[28], whilst the enthalpy value is closely related to the approximation approach. In comparison, the second complexation of $CaUO_2(CO_3)_3^{2-}$ by Ca^{2+} is always exothermic regardless of the approximation approach. The entropy term $T\Delta_rS°_m$ of this reaction — from (9.60 ± 10.56) kJ mol^{-1} to (13.80 ± 13.30) kJ mol^{-1} — shares nearly equal importance with the enthalpy term but is much less important than in the first complexation.

The decrease in entropy term for the first and second stepwise reactions may results principally from the degree of solvation and the polarity of surrounding water molecules of the reacting species and the complexes. The hydration shell of $UO_2(CO_3)_3^{4-}$ — highly charged and symmetric in structure — is much more ordered than that of the globally -2 bearing charge ion $CaUO_2(CO_3)_3^{2-}$. In the process of complexation, the ordered water molecules around $UO_2(CO_3)_3^{4-}$ have to be released to a disordered bulk solvent that allows a bidentate binding configuration for calcium. Therefore, the initial hydration shell of $UO_2(CO_3)_3^{4-}$ is inevitably perturbed by the first complexation, which explained the great entropy gain as a result of a large change in hydration sphere. The molecular calculations showed that the triscarbonatouranyl(VI) group can impose a specific geometry on the primary hydration sphere of calcium ion by reducing its coordination number from 7 to 5.[59] In this respect, the second complexation of Ca^{2+} to $CaUO_2(CO_3)_3^{2-}$ should be less favourable in terms of entropy because the distorted hydration shell of $CaUO_2(CO_3)_3^{2-}$ may be easier to accept the next Ca^{2+} than the first one, which would result in a lower entropy gain.[60] In addition, it was postulated in classical molecular dynamics simulations[61] that the presence of solvent ion Na^+ is able to distort one of the three equatorial carbonate groups in $CaUO_2(CO_3)_3^{2-}$ from bidentate to monodentate, while the second Ca^{2+} is able to stabilize the bidentate binding of the three CO_3^{2-} in $Ca_2UO_2(CO_3)_3$(aq). This conversion of denticity during the second complexation of $CaUO_2(CO_3)_3^{2-}$ by Ca^{2+} could partially

contribute to an exothermic process due to the bond formation of U-O_{CO_3}, and a less important entropy value due to the formation of $Ca_2UO_2(CO_3)_3$(aq), which agrees with our experimental results.

The reaction enthalpy and entropy values were determined for the formation of $MgUO_2(CO_3)_3^{2-}$ from the variation of stability constants in temperature range of 5-30°C with the four approximation approaches. The fitting results of the Van't Hoff equation and the DQUANT equation are of equal magnitude with slightly negative $\Delta_r^{VH}H°_m = -(11.653 \pm 10.300)$ kJ mol^{-1} and $\Delta_r^{DQUANT}H°_m = -(11.171 \pm 10.683)$ kJ mol^{-1}, while the constant heat capacity equation and isoelectric modification result in more exothermic process with $\Delta_r^{CHC}H°_m = -(13.477 \pm 30.494)$ kJ mol^{-1} and $\Delta_r^{Iso}H°_m = -(12.025 \pm 435)$ kJ mol^{-1}. In view of the high uncertainties, the enthalpy contribution to the formation of $MgUO_2(CO_3)_3^{2-}$ and $CaUO_2(CO_3)_3^{2-}$ may be both assumed to be almost nil. Our results are approximately consistent with the value directly measured at 25°C as $\Delta_rH°_m = (4.3 \pm 1.5)$ kJ mol^{-1} using calorimetry by Jo, *et al.*[29] It can be concluded that the entropy term contributes primarily to this reaction. However, unlike the comparable values of entropy term obtained for the formations of $MgUO_2(CO_3)_3^{2-}$ and $CaUO_2(CO_3)_3^{2-}$ in the work of Jo *et al.*,[28,29] the value of $T\Delta_rS°_m$ determined in this study for the complexation of Mg^{2+} is globally lower than that of Ca^{2+} by about 10-20 kJ mol^{-1}. The decrease in entropy value from $CaUO_2(CO_3)_3^{2-}$ to $MgUO_2(CO_3)_3^{2-}$ might very well be attributed to the more ordered bulk water structure of $MgUO_2(CO_3)_3^{2-}$, which would also explain the lower $\log_{10}K°_{1.1.3}$ value for the complexation of Mg^{2+} compared to Ca^{2+}. Because of its higher charge density, Mg^{2+} (charge denticity of 205 C mm^{-3} calculated from $ne/(4/3)\pi r^3$ with e = 1.60 10^{-19} C, IR_{VI} = 0.72 Å in Shannon[62] assuming Mg^{2+} six-coordinated by H_2O) exhibits a stronger polarizing effect than Ca^{2+} (charge denticity of 64 C mm^{-3} with IR_{VII} = 1.06 Å in Shannon[62] assuming Ca^{2+} seven-coordinated by H_2O) in aqueous solution. When complexing to large negative ion like $UO_2(CO_3)_3^{4-}$ the smaller Mg^{2+} should distort the electron cloud of $UO_2(CO_3)_3^{4-}$ to a larger degree, and even could favour partial covalence between Mg and O_{CO_3}, which leads to a more consequent deformation of originally symmetric structure of $UO_2(CO_3)_3^{4-}$. Therefore, $MgUO_2(CO_3)_3^{2-}$ should be less symmetric in electron distribution and exhibits stronger polarizing power than $CaUO_2(CO_3)_3^{2-}$ resulting in more ordered surrounding hydration sphere. This is in general agreement with the Hofmeister series, and kosmotrope character of Mg^{2+} relative to Ca^{2+}.[63] This subtle difference was detected in TRLFS using a more dispersing 1800 lines mm^{-1} grating.[36,52]

Discrepancies in enthalpies depend on numerous factors: experimental technique, approximation approach, and the inherent weakness of magnesium/calcium tricarbonatouranyl complexation, which gives rise to difficulties in measurements. Those factors finally render it difficult to accurately determine the enthalpy and yield a large scatter in results. Direct measurements of enthalpy by microcalorimetry could theoretically carry out more accurate data than the slope analysis and help explaining the observed discrepancy. Nonetheless, this method suffers from the fact that the uranium concentration should be high enough to detect any heat flow in the titration chamber of the microcalorimeter. This constraint on uranium concentration hinders its application to high temperatures because such conditions, *i.e.*, concentrated uranium at elevated temperature, are much favourable to the formation of U(VI) polynuclear species, e.g., $(UO)_2CO_3(OH)_3^-$, due to the decrease of dielectric constant of water. Alternatively, the capabilities of TRLFS, especially in speciation measurements, show interest in probing luminescent $M_nUO_2(CO_3)_3^{(4-2n)-}$ complexes. The identification of each species based on spectroscopic fingerprints gives more confidence in the stoichiometry of Mg and Ca and thermodynamic constants and functions.

V - 5 Practical applications

5.1 Case of nuclear waste repositories

The Boom clay and the Callovo-Oxfordian (COx) clay, identified as high-level long-lived radioactive waste repositories in Belgium and France,[64,65] respectively, had been characterized with the chemical compositions of equilibrium waters given in de Craen, *et al.*[9] and in Gaucher *et al.*[11] In our previous calculations using the experimentally determined constants $\log_{10}K°_{n.1.3}$ and ε at near standard conditions,[34,36] it has been concluded that the high carbonate concentration in the Mol reference water in the Boom clay contributes to the formation of $M_nUO_2(CO_3)_3^{(4-2n)-}$ at 25°C, though U(IV) should dominate the solubility and control the mobility of uranium because of the reducing redox potential (E_h = -274 mV, or $P(O_2)= 10^{-68.67}$ atm).[66-68] In the case of the COx equilibrium water — the solution A in Gaucher, *et al.*[11] of less reducing conditions than the Boom clay water (Eh = -163 mV, or $P(O_2)= 10^{-65.83}$ atm) —, the high calcium concentration ensures the predominance of the triscarbonatouranyl(VI) complexes, *i.e.*, $UO_2(CO_3)_3^{4-}$, $CaUO_2(CO_3)_3^{2-}$, only in neutral pH range at 25°C. At pH values higher than 8.5 the solution should be dominated by $U(OH)_4(aq)$ due to the lower carbonate concentrations — see Fig. 13 in Reiller and Descostes[20].

In nuclear waste management, the high-level waste (HLW) package disposal facilities are composed of multiple barriers to prevent the leaching of radionuclides from the stainless steel canisters (the primary barrier) and their contact with interstitial water. Theoretically, the thick steel overpacks wrapping the canister can protect the vitrified HLW from water corrosion for 500 years. Once the HLW packages in underground repositories, the temperature of the cell can attain around 80°C in 10-15 years due to the generated heat by radioactive decay, but the temperature between two HLW cells needs a longer period to reach the peak, *e.g.*, 40-60°C after approximately 400-500 years dependent on the types of geological formation and waste.[4]

To predict the uranium behaviour under repository conditions at temperatures higher than 25°C, the thermodynamic calculations were performed to determine the uranium speciation and to identify the mineral phases likely to precipitate using Thermochimie 10a database file,[69] in which the uranium chemistry is largely based on NEA-OECD analyses.[37-39] The thermodynamic parameters for the interactions of UO_2-CO_3 with Mg/Ca were based on the isoelectric reaction approximation because of its higher validity range of temperature that would render more reliable estimates. The thermodynamic parameters in the form of analytical expression to implement in the input PhreeqC file are listed in Table V - 3. We noted that the determined values of $\log_{10}K°$ are so sensitive to the parameters in analytical expression that they should not be rounded off in calculation.

Table V - 3 Parameters in the expression of $\log_{10}K°_{n.1.3}(T) = A_1+A_2\,T+A_3\,T^{-1}+A_4\,\log_{10}T+A_5T^{-2}$ (T in Kelvin) based on the isoelectric reaction modification in Table V - 1; the values of $\log_{10}K°_{n.1.3}$ at 70°C calculated by PhreeqC and used to perfom the uranium speciation, shown in Fig. V - 10.

Isoelectric reaction	**A_1**	**A_2**	**A_3**	**A_4**	**A_5**	**$\log_{10}K°_{n.1.3}$ at 70°C**
$CaUO_2(CO_3)_3^{2-}$	33822.8	6.01794	-1647050	-12537.7759	83260000	5.81
$Ca_2UO_2(CO_3)_3$(aq	35198.8	6.25537	-1722880	-13040.2035	88090000	9.42
$MgUO_2(CO_3)_3^{2-}$	33994.3	6.04948	-1654900	-12602.4447	83660000	4.69

Water compositions in the Boom and COx geological formations were taken from de Craen, *et al.*[9] and Gaucher *et al.*[11] The aqueous uranium concentration was set in equilibrium with the dissolution of UO_2:$2H_2O$(am) phase in both calculations — adapted from UO_2(am,hyd) in NEA-OECD analyses[38,39] that the $\Delta_r H°_m$ value is absent from Thermochimie 10a database file.[69] Fig. V - 10 shows the uranium solubility (Fig. V - 10 (a)) and speciation (Fig. V - 10 (b)) as a function of temperature for the Mol reference water. One can observe that the aqueous system undergoes a fast alteration of dominant species in the narrow temperature range of 40-50°C

while the total uranium, majorly in U(VI) from 5°C to 50°C, suffers a steep decline then an increase controlled by U(IV) in the form of $U(OH)_4(aq)$ at T > 50°C. As shown in Fig. V - S4 of the SI, the conversion of main oxidation states of Fe, S, C, and U suggests that the reducing conditions in the Boom clay at T > 50°C could be influenced by CH_4.

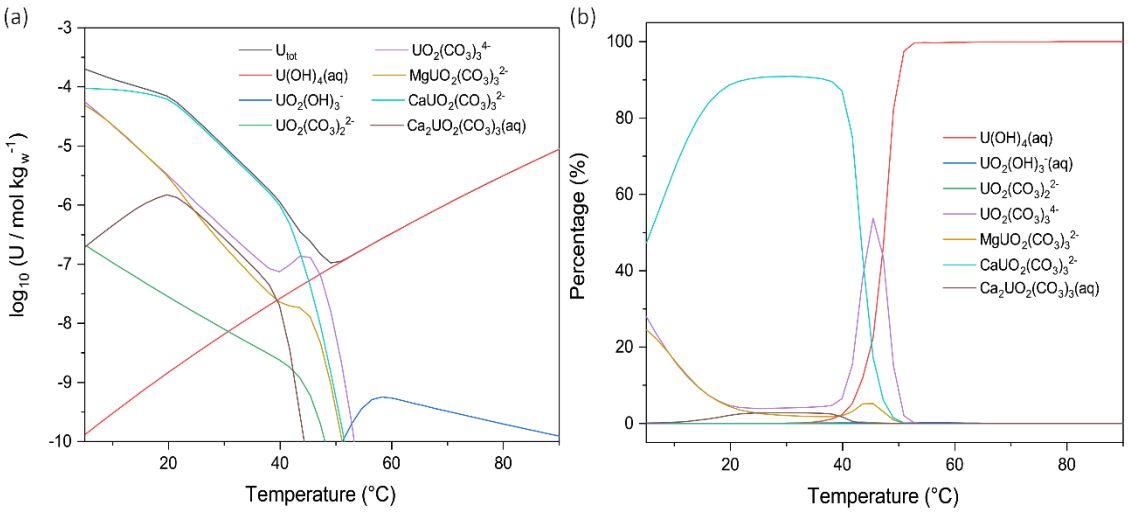

Fig. V - 10 Solubility of $UO_2{:}2H_2O(am)$ (a) and aqueous uranium speciation (b) vs. temperature for Boom clay equilibrium water ($P(O_2) = 10^{-68.67}$ atm) using thermodynamic data from the Thermochimie 10a database,[69] implementing $SrUO_2(CO_3)_3^{2-}$,[26] specific ion interaction coefficients of $Mg_n/Ca_nUO_2(CO_3)_3^{(4-2n)-}$, [34-36] and their $\Delta_r H°_m$ values determined in this work based on the isoelectric reaction approximation.

The uranium speciation and solubility in the COx solution also show sensible variations with response to temperature. As shown in Fig. V - 11 (a) and (b), $Ca_nUO_2(CO_3)_3^{(4-2n)-}$ complexes are dominant below 40°C with $Ca_2UO_2(CO_3)_3(aq)$ about three times more than $CaUO_2(CO_3)_3^{2-}$. $U(OH)_4(aq)$ becomes the only aqueous uranium species at 40°C. As temperature increases, the redox potential of water solution decreases further, which triggers the reduction of S(+VI) (mainly SO_4^{2-}) to S(-II) (mainly HS^-), and the precipitation of pyrite (FeS_2), and also the reduction of C(+IV) (mainly HCO_3^-) to C(IV) (mainly $CH_4(aq)$). These processes are consuming protons, which eventually leads to an important increase of the pH value. Fig. V - S5 of the SI displays the reduction of main oxidation states of Fe, S, C, and U, and the evolutions of pe and pH as a function of temperature. Due to the highly enriched sulphur quantity in COx in comparison to Mol reference water, the rapid increase of pH value up to 11.2 above 40°C mainly accounts for the emergence of $UO_2(OH)_3^-$ over a narrow temperature range. At the same time, Fe(II)/Fe(III) oxidation is facilitated during this short oxidizing period. When T > 70°C, the redox potential is low due to the high temperature and reduction of S and C. The sample solution only contains $U(OH)_4(aq)$ as uranium species, which is consistent with the fact that the

dipole moment of water decreases with increasing temperature and favours low or no charge species as the hydrogen bonding network weakens significantly. As the COx water is enriched in sulphur, the same calculation but without sulphur was performed in order to highlight the impacts of S(+VI)/S(-II) reduction by preventing all the unwanted S(+VI) reduction to lower oxidation states in initial input PhreeqC file. As shown in Fig. V - S6 (b) of the SI, the crossing point of $Ca_2UO_2(CO_3)_3$(aq) and $U(OH)_4$(aq) curves occurred ca. 60°C, compared to ca. 42°C in Fig. V - 11 (b) with sulphur in solution. The peak of pH value without sulphur in solution was reduced to 9.10 (Fig. V - S6 (d) of the SI) instead of 11.2 (Fig. V - S5 (b)) due to the lack of S(+VI)/S(-II) reduction. The predominance of $U(OH)_4$(aq) is maintained until 90°C and excluded the perturbation of $UO_2(OH)_3^-$.

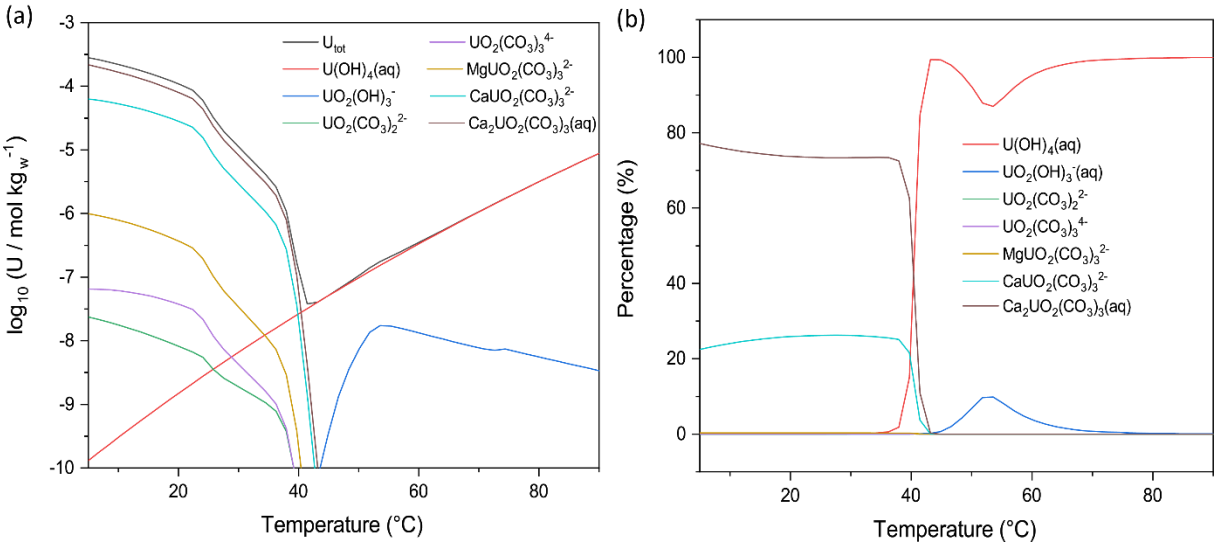

Fig. V - 11 Solubility of UO_2:2H_2O(am) (a) and aqueous uranium speciation (b) as a function of temperature for Callovo-Oxfordian clay equilibrium waters[11] $P(O_2) = 10^{-65.83}$ atm using thermodynamic data from the Thermochimie 10a database,[69] implementing $SrUO_2(CO_3)_3^{2-}$,[26] specific ion interaction coefficients of $Mg_n/Ca_nUO_2(CO_3)_3^{(4-2n)-}$,[34-36] and their $\Delta_r H°_m$ values determined in this work based on the isoelectric reaction approximation.

Hence, the formation of $U(OH)_4$(aq) may thus play an important role in reduced uranium transport. At 40-60°C, our simulation results suggest that uranium would primarily exist in the reduced state in the form of $U(OH)_4$(aq) in the COx and Mol waters and the stability of UO_2 can be sustained by the presence of pyrite (FeS_2), which consumes the oxygen supplied by infiltrating water.[70] In the very long term, the temperature in the near field of the repository will decrease to ambient temperature.[4] As hard-soft-acid-base principles suggested, the uranyl ion, a hard (high charge to radius ratio) cation, should form strong complexes with carbonate ions, which are hard anions. Thus the uranium migration would be promoted because of

$Ca_nUO_2(CO_3)_3^{(4-2n)-}$ predominance in the COx and Mol waters as suggested by previous calculations.[34-36]

Furthermore, we note that the variation of uranium solubility as a function of temperature depends on the chosen solubility controlling phase in calculation. There is an underlying assumption in HLW management that reducing conditions will prevent uranium migration due to the formation of uranium ore deposits.[71-77] The principal ore minerals includes two main types — uraninite and pitchblende, both nominally UO_2 — that differ from each other in their depositional setting and chemical constitution.[78-80] As no value of enthalpy for $UO_2{:}2H_2O$(am) selected into the Thermochimie 10a database file, special focus was put on the Mol and COx water systems in equilibrium with the dissolution of uraninite UO_2(cr) for which the $\Delta_r H°_m$ value is available. Fig. V - S7 of the SI shows the solubility variation of UO_2(cr) as a function of temperature for Mol and COx waters. Compared with Fig. V - 10 (a) and Fig. V - 11 (a), one can observe that the uranium concentration in solution is lowered by about 10 orders of magnitude in both cases. In equilibrium with UO_2(cr), the reduction of U(VI) to U(IV) is more intensely affected by temperature as the evident stronger decrease of the dissolved uranium concentration.

V - 6 Conclusions

The present study reports the formation constants for the complexation of triscarbonatouranyl(VI) with Mg^{2+}/Ca^{2+} in 5-30°C for $MgUO_2(CO_3)_3^{2-}$ and 10-50°C for $Ca_nUO_2(CO_3)_3^{(4-2n)-}$ measured by TRLFS. The variation of $\log_{10}K°_{n.1.3}$ with temperature were fitted by several theoretical approaches: the Van't Hoff equation, the constant heat capacity model, the DQUANT equation, and the isoelectric reaction modification. In the experimental temperature ranges, these approximation models provided satisfactory matching between the experimentally derived constants and the predicted values. Nonetheless, large discrepancy has been observed between the predictions of $\log_{10}K°_{n.1.3}$ by the revised approaches, probably because of the narrow experimental temperature ranges that were limited by the quenching effects with temperature. The Van't Hoff equation and the DQUANT equation showed comparable trends of $\log_{10}K°_{n.1.3}$, while the assumption of non-zero heat capacity resulted in significant deviation at high temperatures. The modification to isoelectric reaction exhibited mildly increasing $\log_{10}K°_{n.1.3}$ with temperature. The accuracy of the experimental values of equilibrium constants at elevated temperatures for these species should be improved by further investigations. The recent thermodynamic data with response to temperature and ionic strength

for $M_nUO_2(CO_3)_3^{(4-2n)-}$ complexes are highly valuable in estimating the temperature and salinity effects on the speciation of U(VI), especially encountered in nuclear waste repositories and bridging the gaps in the thermodynamic database for the proposed important $M_nUO_2(CO_3)_3^{(4-2n)-}$ complexes.

Funding sources

This work was financed by ONDRAF-NIRAS and CEA (contract DEN4857-CCHO 2018-0456/00/00).

Acknowledgements

The authors thanks Dr. Pascal Pernot, who developed the MCR-ALS analysis code in the R environment, for his help; and Dr. Hélène Isnard who prepared the uranium(VI) solution.

V - 7 References

1. D. J. Wronkiewicz and E. C. Buck, Uranium Mineralogy and the Geologic Disposal of Spent Nuclear Fuel, in *Uranium Mineralogy and the Geologic Disposal of Spent Nuclear Fuel*, eds. C. B. Peter and J. F. Robert, De Gruyter, 2018, DOI: 10.1515/9781501509193-015, pp. 475-498.
2. V. Metz, H. Geckeis, E. González-Robles, A. Loida, C. Bube and B. Kienzler, *Radiochim. Acta*, 2012, **100**, 699-713.
3. L. Rao, G. Tian, Y. Xia, J. I. Friese, P. Zanonato and P. Di Bernardo, Bridging the Gap in the Chemical Thermodynamic Database for Nuclear Waste Repository: Studies of the Effect of Temperature on Actinide Complexation, in *Nuclear Energy and the Environment*, eds. C. M. Wai and B. J. Mincher, American Chemical Society, 2010, vol. 1046, ch. 23, pp. 299-318.
4. M. V. Villar, G. Armand, N. Conil, C. de Lesquen, P. Herold, E. Simo, J. C. Mayor, A. Dizier, X. Li, G. Chen, O. Leupin, M. Niskanen, M. Bailey, S. Thompson, D. Svensson, P. Sellin and L. Hausmannova, *Initial SotA on THM Behaviour of I) Buffer Clay Materials and of II) Host Clay Materials*, Deliverable D7.1 HITEC. EURAD Project, 2020. http://www.ejp-eurad.eu/publications/eurad-deliverable-71-initial-sota-thm-behaviour-i-buffer-clay-materials-and-ii-host
5. W. L. Marshall and E. U. Franck, *J. Phys. Chem. Ref. Data*, 1981, **10**, 295-304.
6. D. P. Fernández, A. Goodwin, E. Lemmon, J. L. Sengers and R. C. Williams, *J. Phys. Chem. Ref. Data*, 1997, **26**, 1125-1166.
7. I. Grenthe, I. Puigdomenech and B. Allard, *Modelling in Aquatic Chemistry*, OECD Publishing, Issy-les-Moulineaux, France, 1997.
8. X. Cao, L. Zheng, D. Hou and L. Hu, *Chem. Geol.*, 2019, **525**, 46-57.
9. M. de Craen, L. Wang, M. Van Geet and H. Moors, *Geochemistry of Boom Clay pore water at the Mol site*, Report SCK•CEN-BLG-990, SCK•CEN, Mol, Belgium, 2004. http://jongeren.sckcen.be/~/media/Files/Science/disposal_radioactive_waste/Geochemistry_of_Boom_Clay_pore_Status_2004.pdf
10. M. Laaksoharju, J. Smellie, E.-L. Tullborg, M. Gimeno, L. Hallbeck, J. Molinero and N. Waber, *Bedrock hydrogeochemistry Forsmark - Site descriptive modelling SDM-Site*

Forsmark, Report R-08-47, SKB, Stockholm, 2008. http://www.skb.com/publication/1841127/R-08-47.pdf
11. E. C. Gaucher, C. Tournassat, F. J. Pearson, P. Blanc, C. Crouzet, C. Lerouge and S. Altmann, *Geochim. Cosmochim. Acta*, 2009, **73**, 6470-6487.
12. A. M. Fernández, J. Cuevas and P. Rivas, *MRS Proceedings*, 2011, **663**, 573.
13. A. Fernández, M. J. Turrero, D. Sánchez Ledesma, A. Yllera de Llano, A. M. Melón, M. Sánchez, F. Peña, A. Garralón, P. Rivas, P. Bossart and P. Hernán, *Phys. Chem. Earth*, 2007, **32**, 181-195.
14. X. Cao, L. Hu, J. Wang and J. Wang, *Hum. Ecol. Risk Assess.*, 2017, **23**, 2017-2032.
15. G. Bernhard, G. Geipel, V. Brendler and H. Nitsche, *Radiochim. Acta*, 1996, **74**, 87-91.
16. E. L. Tullborg, J. Suksi, G. Geipel, L. Krall, L. Auque, M. Gimeno and I. Puigdomènech, *Proced. Earth Plan. Sci.*, 2017, **17**, 440-443.
17. O. Prat, T. Vercouter, E. Ansoborlo, P. Fichet, P. Perret, P. Kurttio and L. Salonen, *Environ. Sci. Technol.*, 2009, **43**, 3941-3946.
18. F. Endrizzi and L. F. Rao, *Chem.-Eur. J.*, 2014, **20**, 14499-14506.
19. M. Maloubier, P. L. Solari, P. Moisy, M. Monfort, C. Den Auwer and C. Moulin, *Dalton Trans.*, 2015, **44**, 5417-5427.
20. P. E. Reiller and M. Descostes, *Chemosphere*, 2020, **251**, 126301.
21. G. Bernhard, G. Geipel, T. Reich, V. Brendler, S. Amayri and H. Nitsche, *Radiochim. Acta*, 2001, **89**, 511-518.
22. J. Y. Lee, M. Vespa, X. Gaona, K. Dardenne, J. Rothe, T. Rabung, M. Altmaier and J.-I. Yun, *Radiochim. Acta*, 2017, **105**.
23. S. N. Kalmykov and G. R. Choppin, *Radiochim. Acta*, 2000, **88**, 603-606.
24. G. Geipel, S. Amayri and G. Bernhard, *Spectrochim. Acta, A*, 2008, **71**, 53-58.
25. C. Götz, G. Geipel and G. Bernhard, *J. Radioanal. Nucl. Chem.*, 2010, **287**, 961-969.
26. W. Dong and S. C. Brooks, *Environ. Sci. Technol.*, 2006, **40**, 4689-4695.
27. W. Dong and S. C. Brooks, *Environ. Sci. Technol.*, 2008, **42**, 1979-1983.
28. Y. Jo, A. Kirishima, S. Kimuro, H.-K. Kim and J.-I. Yun, *Dalton Trans.*, 2019, **48**, 6942-6950.
29. Y. Jo, H.-K. Kim and J.-I. Yun, *Dalton Trans.*, 2019, **48**, 14769-14776.
30. S. D. Kelly, K. M. Kemner and S. C. Brooks, *Geochim. Cosmochim. Acta*, 2007, **71**, 821-834.
31. S. Amayri, T. Reich, T. Arnold, G. Geipel and G. Bernhard, *J. Solid State Chem.*, 2005, **178**, 567-577.
32. A. O. Tirler and T. S. Hofer, *J. Phys. Chem. B*, 2014, **118**, 12938-12951.
33. A. O. Tirler and T. S. Hofer, *Dalton Trans.*, 2016, **45**, 4983-4988.
34. C. Shang and P. E. Reiller, *Dalton Trans.*, 2020, **49**, 466-481.
35. C. Shang, P. E. Reiller and T. Vercouter, *Dalton Trans.*, 2020, **49**, 15443-15460.
36. C. Shang and P. E. Reiller, *Dalton Trans.*, 2021, **50**, 4363-4379.
37. I. Grenthe, L. Fuger, R. G. M. Konings, R. J. Lemire, A. B. Muller, C. Nguyen-Trung and H. Wanner, *Chemical Thermodynamics 1. Chemical Thermodynamics of Uranium*, *Chemical Thermodynamics Series*, North Holland Elsevier Science Publishers B. V., Amsterdam, The Netherlands, 1992.
38. R. Guillaumont, T. Fanghänel, V. Neck, J. Fuger, D. A. Palmer, I. Grenthe and M. H. Rand, *Update of the Chemical Thermodynamics of Uranium, Neptunium, Plutonium, Americium and Technetium*, OECD Nuclear Energy Agency, Data Bank, Issy-les-Moulineaux, France, 2003.
39. I. Grenthe, X. Gaona, A. V. Plyasunov, L. Rao, W. H. Runde, B. Grambow, R. J. M. Koning, A. L. Smith and E. E. Moore, *Chemical Thermodynamics 14. Second Update on the Chemical Thermodynamics of Uranium, Neptunium, Plutonium, Americium and*

Technetium, *Chemical Thermodynamics Series*, OECD Nuclear Energy Agency Data Bank, Eds., OECD Publications, Paris, France, 2020.
40. F. M. S. Maia, S. Ribet, C. Bailly, M. Grivé, B. Madé and G. Montavon, *Appl. Geochem.*, 2021, **124**.
41. L. N. Plummer and E. Busenberg, *Geochim. Cosmochim. Acta*, 1982, **46**, 1011-1040.
42. R. A. Robie and B. S. Hemingway, *Thermodynamic Properties of Minerals and Related Substances at 298.15 K and 1 bar (10^5 Pascal) Pressure and at Higher Temperatures*, Report 2131, US Geological Survey, Denver, CO, USA, 1995. http://pubs.usgs.gov/bul/2131/report.pdf
43. Y. C. Wu, W. F. Koch and R. A. Durst, *Standardization of pH measurements*, Report 260-53, US Department. of Commerce, National Bureau of Standards, 1988. http://nvlpubs.nist.gov/nistpubs/Legacy/SP/nbsspecialpublication260-53e1988.pdf
44. A. Ringböm, *Complexation in Analytical Chemistry: A Guide for the Critical Selection of Analytical Methods Based on Complexation Reactions*, Interscience Publishers, New York, NY, USA, 1963.
45. E. Giffaut, P. Vitorge and H. Capdevila, *Corrections de température sur les coefficients d'activité calculés selon la TIS*, Report CEA-N-2737 (ISSN 0429-3460), Commissariat à l'Energie Atomique, Fontenay-aux-Roses, France, 1993. http://www.vitorge.name/pierre/publis/93gif_vi.pdf
46. I. Grenthe, A. V. Plyasunov and K. Spahiu, Chapter IX. Estimations of medium effects on thermodynamic data, in *Modelling in Aquatic Chemistry*, eds. I. Grenthe and I. Puigdomènech, OECD, Paris, France, 1997, ch. IX, pp. 325-426.
47. I. Puigdomènech, A. V. Plyasunov, J. A. Rard and I. Grenthe, Chapter X. Temperature correction to thermodynamic data and enthalpy calculations, in *Modelling in Aquatic Chemistry*, eds. I. Grenthe and I. Puigdomènech, OECD, Paris, 1997, pp. 427-493.
48. H. C. Helgeson, *J. Phys. Chem.*, 1967, **71**, 3121-3136.
49. C. Götz, G. Geipel and G. Bernhard, Thermodynamical data of uranyl carbonate complexes from absorption spectroscopy, in *Uranium, Mining and Hydrogeology*, eds. B. J. Merkel and A. Hasche-Berger, Springer, Berlin, Heidelberg, Germany, 2008, DOI: 10.1007/978-3-540-87746-2_118, pp. 907-914.
50. C. S. Patterson, G. H. Slocum, R. H. Busey and R. E. Mesmer, *Geochim. Cosmochim. Acta*, 1982, **46**, 1653-1663.
51. C. S. Patterson, R. H. Busey and R. E. Mesmer, *J. Solution Chem.*, 1984, **13**, 647-661.
52. H. Oher, T. Vercouter, F. Réal, C. Shang, P. E. Reiller and V. Vallet, *Inorg. Chem.*, 2020, **59**, 15036-15049.
53. M. Viard, J. Gallay, M. Vincent, O. Meyer, B. Robert and M. Paternostre, *Biophys. J.*, 1997, **73**, 2221-2234.
54. G. H. Golub and C. F. Van Loan, *Matrix computations*, *Johns Hopkins studies in the mathematical sciences*, The Johns Hopkins University Press, Baltimore, 4th edn., 2013.
55. C. Ruckebusch, M. Sliwa, P. Pernot, A. de Juan and R. Tauler, *Journal of Photochemistry and Photobiology C: Photochemistry Reviews*, 2012, **13**, 1-27.
56. J. Ma, P. Archirel, U. Schmidhammer, J.-M. Teuler, P. Pernot and M. Mostafavi, *J. Phys. Chem. A*, 2013, **117**, 14048-14055.
57. J. Ma, P. Archirel, P. Pernot, U. Schmidhammer, S. Le Caër and M. Mostafavi, *J. Phys. Chem. B*, 2016, **120**, 773-784.
58. J. Bonin, I. Lampre, P. Pernot and M. Mostafavi, *J. Phys. Chem. A*, 2007, **111**, 4902-4913.
59. S. Kerisit and C. Liu, *Geochim. Cosmochim. Acta*, 2010, **74**, 4937-4952.
60. S. Kimuro, A. Kirishima, Y. Kitatsuji, K. Miyakawa, D. Akiyama and N. Sato, *J. Chem. Thermodynamics*, 2019, **132**, 352-362.
61. B. Li, J. Zhou, C. Priest and D. E. Jiang, *J. Phys. Chem. B*, 2017, **121**, 8171-8178.

62. R. D. Shannon, *Acta Crystallogr., Sect. A*, 1976, **32**, 751-767.
63. Y. Marcus, *Ion Solvation*, Wiley, Chichester, UK, 1985.
64. F. Claret, B. A. Sakharov, V. A. Drits, B. Velde, A. Meunier, L. Griffault and B. Lanson, *Clays Clay Miner.*, 2004, **52**, 515-532.
65. A. Dauzères, P. Le Bescop, C. Cau-Dit-Coumes, F. Brunet, X. Bourbon, J. Timonen, M. Voutilainen, L. Chomat and P. Sardini, *Cem. Concr. Res.*, 2014, **58**, 76-88.
66. G. Meinrath, *Aquatic Chemistry of Uranium. A Review Focusing on Aspects of Environmental Chemistry*, Technische Universität Freiberg - Bergakademie, Freiberg, Germany, 1994. http://www.geo.tu-freiberg.de/fog/FOG_Vol_1.pdf
67. D. A. Atwood, *Radionuclides in the Environment*, *EIC Books*, Wiley, Chichester, West Sussex, U.K. ; New York, 2010.
68. Y. H. Wang, M. Frutschi, E. Suvorova, V. Phrommavanh, M. Descostes, A. A. A. Osman, G. Geipel and R. Bernier-Latmani, *Nature Communications*, 2013, **4**.
69. J. N. Brönsted, *J. Am. Chem. Soc.*, 1922, **44**, 877-898.
70. J. Janeczek, Uranium : mineralogy, geochemistry and the environment, in *Mineralogy and Geochemistry of Natural Fission Reactors in Gabon*, eds. P. C. Burns and R. Finch, De Gruyter, Washington, DC, USA, 1999, vol. 38, pp. 321-392.
71. M. Grivé, L. Duro, E. Colàs and E. Giffaut, *Appl. Geochem.*, 2015, **55**, 85-94.
72. R. J. Baker, *Coord. Chem. Rev.*, 2014, **266-267**, 123-136.
73. T. Thoenen, W. Hummel, U. Berner and E. Curti, *The PSI/Nagra Chemical Thermodynamic Database 12/07*, Report PSI Bericht Nr 14-04 (ISSN 1019-0643), Paul Scherrer Institute, Villigen, Switzerland, 2014. http://www.psi.ch/les/database
74. J. B. Maynard, *Geol. Mag.*, 1983, **121**, 370-371.
75. G. H. Taylor, Past oxygen levels: some evidence from uranium deposits, in *Biogeochemistry of Ancient and Modern Environments*, eds. P. A. Trudinger, M. R. Walter and B. J. Ralph, Springer, Berlin, Heidelberg, 1980, DOI: 10.1007/978-3-642-48739-2_7, pp. 65-71.
76. P. B. Hostetler and R. M. Garrels, *Econ. Geol.*, 1962, **57**, 137-167.
77. M. L. Jensen, *Econ. Geol.*, 1958, **53**, 598-616.
78. R. A. Rich, H. D. Holland and U. Petersen, *Hydrothermal Uranium Deposits*, Elsevier, New York, 1977.
79. S. J. Kimberley and M. M. Kimberley, *Uranium Deposits, Their Mineralogy and Origin*, University of Toronto Press, Mineral Association of Canada, 1978.
80. J. Janeczek, R. C. Ewing and L. E. Thomas, *J. Nucl. Mater.*, 1993, **207**, 177-191.

V - 8 Supporting Information

Number of pages: 12

Number of Tables: 8

Number of Figures: 5

Table V - S1 Composition and properties of standard buffer solutions.

pH value at 25°	1.68	4.01	6.87	9.18
Composition[1]	0.05m potassium tetraoxalate ($KH_3C_4O_8$)	0.05 m potassium hydrogen phthalate ($KHC_8H_4O_4$)	0.025 m KH_2PO_4 and 0.025 m (Na_2HPO_4)	0.01 m $Na_2B_4O_7$:$10H_2O$
Temperature range	0-95	0-95	0-95	0-50
Temperature coefficient *d*pH/*dt*	--	+0.0012	-0.0028	-0.0028

Table V - S2 Recalculated pH values of buffer solutions at investigated temperatures and potential values E_{mes} read on pH-meter.

Temp	pH	E_{mes}(m V)	pH	E_{mes}(m V)	pH	E_{mes}(m V)	pH	E_{mes}(m V)	Slope	Intercept
5°	1.67	299.1	4.00	166.9	6.95	1.8	9.39	-133.4	-56.01	391.81
10°	1.67	299.5	4.00	166.2	6.92	0.8	9.33	-135.1	-56.72	393.69
15°	1.67	302.2	4.00	165.5	6.90	-0.5	9.28	-135.2	-57.45	396.79
22°	1.68	304.2	4.00	164.9	6.88	-1.4	9.23	-136.1	-58.24	400.18
30°	1.68	308.2	4.01	165.6	6.85	-3.3	9.14	-138.8	-59.86	407.39
35°	1.69	311.2	4.02	167.1	6.84	-3.2	9.11	-139.5	-60.70	412.58
40°	1.69	314	4.03	168.7	6.84	-3	9.07	-140.2	-61.49	417.38
45°	1.70	318.2	4.04	171.4	6.83	-3.1	9.04	-140	-62.44	423.97
50°	1.71	321.2	4.06	171.9	6.83	-3.3	9.02	-140.4	-63.16	428.74

Table V - S3 Stability constants of the U(VI) complexes at 25°C and I_m = 0, used in this work.

Reaction	$\log_{10}K^{\circ}$	$\Delta_rH_m°$ (kJ mol^{-1})	References
$CO_2(g) + H_2O \rightleftarrows CO_3^{2-} + 2H^+$	-18.15 ± 0.06	4.11 ± 0.28	Guillaumont, *et al.*[2]
$CO_3^{2-} + 2H^+ \rightleftarrows CO_2(aq) + H_2O$	16.68 ± 0.05	-23.86 ± 0.14	Guillaumont, *et al.*[2]
$CO_3^{2-} + H^+ \rightleftarrows HCO_3^-$	10.33 ± 0.05	-14.70 ± 0.15	Guillaumont, *et al.*[2]
$UO_2^{2+} + H_2O \rightleftarrows UO_2(OH)^+ + H^+$	-5.25 ± 0.24	43.46 ± 5.55	Guillaumont, *et al.*[2]
$UO_2^{2+} + 2H_2O \rightleftarrows UO_2(OH)_2(aq) + 2H^+$	-12.15 ± 0.07	111.16 [3]	Guillaumont, *et al.*[2]
$3UO_2^{2+} + 5H_2O \rightleftarrows (UO_2)_3(OH)_5^+ + 5H^+$	-15.55 ± 0.12	123.70 ± 0.60	Guillaumont, *et al.*[2]
$UO_2^{2+} + CO_3^{2-} \rightleftarrows UO_2(CO_3)(aq)$	9.94 ± 0.03	5.0 ± 2.0	Guillaumont, *et al.*[2]
$UO_2^{2+} + 2CO_3^{2-} \rightleftarrows UO_2(CO_3)_2^{2-}$	16.61 ± 0.09	18.50 ± 4.0	Guillaumont, *et al.*[2]
$UO_2^{2+} + 3CO_3^{2-} \rightleftarrows UO_2(CO_3)_3^{4-}$	21.84 ± 0.04	-39.20 ± 4.10	Guillaumont, *et al.*[2]
$2UO_2^{2+} + CO_2(g) + 4H_2O \rightleftarrows (UO_2)_2CO_3(OH)_3^- + 5H^+$	-19.01 ± 0.50	–	Guillaumont, *et al.*[2]
$2UO_2^{2+} + CO_3^{2-} + 3H_2O \rightleftarrows (UO_2)_2CO_3(OH)_3^- + 3H^+$	-0.86 ± 0.50		Recalculated from Guillaumont, *et al.*[2]
$UO_2(CO_3)_3^{4-} + 4H^+ \rightleftarrows UO_2(CO_3)(aq) + 2CO_2(g) + 2H_2O$	24.40 ± 0.19	35.98 ± 3.64	Recalculated from Guillaumont, *et al.*[2]
$UO_2(CO_3)_3^{4-} + 2H^+ \rightleftarrows UO_2(CO_3)_2^{2-} + CO_2(g) + H_2O$	12.92 ± 0.13	53.59 ± 1.05	Recalculated from Guillaumont, *et al.*[2]
$2UO_2(CO_3)_3^{4-} + 7H^+ \rightleftarrows (UO_2)_2CO_3(OH)_3^- + 5CO_2(g) + 2H_2O$	46.22 ± 0.30	–	Recalculated from Guillaumont, *et al.*[2]

Table V - S4 Main specific ion interaction coefficients used in this work.

Specific ion interaction coefficient	**Value (± 1σ)**	**Ref.**
$\varepsilon(H^+, Cl^-)$	0.12 ± 0.01	Guillaumont, *et al.*[2]
$\varepsilon(Na^+, CO_3^{2-})$	-0.08 ± 0.03	Guillaumont, *et al.*[2]
$\varepsilon(UO_2^{2+}, Cl^-)$	0.46 ± 0.03	Guillaumont, *et al.*[2]
$\varepsilon(Mg^{2+}, Cl^-)$	0.19 ± 0.02	Guillaumont, *et al.*[2]
$\varepsilon(UO_2(CO_3)_2^{2-}, Na^+)$	-0.02 ± 0.09	Guillaumont, *et al.*[2]
$\varepsilon(UO_2(CO_3)_3^{4-}, Na^+)$	-0.01 ± 0.11	Guillaumont, *et al.*[2]
$\varepsilon(MgUO_2(CO_3)_3^{2-}, Na^+)$ (in NaCl)	0.31 ± 0.02	Shang *et al.*[4]
$\varepsilon(CaUO_2(CO_3)_3^{2-}, Na^+)$ (in NaCl)	0.29 ± 0.11	Shang *et al.*[5]
$\varepsilon(Ca_2UO_2(CO_3)_3$, NaCl)	0.66 ± 0.22	Shang *et al.*[5]

Table V - S5 (a) Experimental sample information: pH values, calculated Ringböm coefficients α — see Shang et al.[4-6] for details —, [Mg^{2+}] (mol kg_w^{-1}) and deduced F_0; the sample solutions giving the slope of 1 are set in italics.

T (°C)	5				10			
Sample	pH value	α	[Mg^{2+}] (mol·kg_w^{-1})	F_0 (counts)	pH value	α	[Mg^{2+}] (mol·kg_w^{-1})	F_0 (counts)
1	8.92	1.00	0	1.46E+08	8.99	1.00	1.00E-05	1.26E+08
2	8.59	1.00	1.57E-04	1.16E+08	8.61	1.00	1.57E-04	1.45E+08
3	8.29	1.01	2.37E-04	1.23E+08	8.30	1.01	2.37E-04	1.29E+08
4	8.24	1.02	5.31E-04	1.16E+08	8.26	1.01	5.31E-04	1.66E+08
5	*8.13*	*1.08*	*7.50E-04*	*1.11E+08*	8.18	1.03	1.18E-03	1.35E+08
6	*7.99*	*1.48*	*1.18E-03*	*1.13E+08*	8.05	1.19	1.18E-03	1.24E+08
7	*7.88*	*2.57*	*1.82E-03*	*6.41E+07*	*7.89*	*1.31*	*1.82E-03*	*1.06E+08*
8	*7.82*	*3.78*	*2.21E-03*	*1.11E+08*	*7.82*	*2.63*	*2.21E-03*	*1.42E+08*
9	*7.79*	*4.65*	*3.38E-03*	*1.23E+08*	*7.79*	*5.13*	*3.38E-03*	*1.04E+08*
10	*7.72*	*7.74*	*4.58E-03*	*1.14E+08*	*7.72*	*7.96*	*4.58E-03*	*1.16E+08*
11	*7.69*	*9.70*	*8.89E-03*	*1.37E+08*	*7.69*	*12.55*	*8.89E-03*	*1.77E+08*
12	*7.64*	*14.25*	*1.34E-02*	*1.32E+08*	*7.64*	*16.95*	*1.34E-02*	*2.06E+08*
13	*7.61*	*17.99*	*1.51E-02*	*1.28E+08*	*7.61*	*25.30*	*1.51E-02*	*2.39E+08*
14	*7.54*	*31.21*	*3.02E-02*	*1.29E+08*	*7.54*	*34.37*	*3.02E-02*	*2.26E+08*
T (°C)	15				22[4]			
Sample	pH value	α	[Mg^{2+}] (mol·kg_w^{-1})	F_0 (counts)	pH value	α	[Mg^{2+}] (mol·kg_w^{-1})	F_0 (counts)
1	8.97	1.00	1.00E-05	7.97E+07	9.17	1.00	0	2.61E+07
2	8.80	1.00	1.57E-04	6.20E+07	8.26	1.09	3.48E-04	2.82E+07
3	8.42	1.01	2.37E-04	6.38E+07	8.22	1.12	7.32E-04	2.37E+07
4	8.38	1.01	5.31E-04	5.52E+07	*8.07*	*1.49*	*1.25E-03*	*2.23E+07*
5	*8.26*	*1.04*	*1.18E-03*	*5.04E+07*	*8.05*	*1.64*	*1.49E-03*	*2.49E+07*
6	*8.10*	*1.22*	*1.18E-03*	*5.38E+07*	*8.00*	*2.08*	*2.38E-03*	*2.62E+07*
7	*8.05*	*1.41*	*1.82E-03*	*5.74E+07*	*7.90*	*3.80*	*4.16E-03*	*2.90E+07*
8	*7.90*	*3.00*	*2.21E-03*	*6.08E+07*	*7.87*	*4.80*	*6.36E-03*	*3.30E+07*
9	*7.86*	*3.90*	*3.38E-03*	*5.95E+07*	*7.78*	*8.90*	*1.56E-02*	*3.51E+07*
10	*7.78*	*6.88*	*4.58E-03*	*6.21E+07*	*7.74*	*12.13*	*2.50E-02*	*4.59E+07*
11	*7.72*	*10.80*	*8.89E-03*	*7.20E+07*				

T (°C)	30			
Sample	pH value	α	$[Mg^{2+}]$ $(mol \cdot kg_w^{-1})$	F_0 (counts)
1	8.97	1.00	1.00E-05	9.65E+07
2	8.80	1.00	1.57E-04	4.32E+07
3	8.42	1.03	2.37E-04	8.18E+07
4	8.38	1.04	5.31E-04	3.85E+07
5	*8.25*	*1.10*	*1.18E-03*	*5.23E+07*
6	*8.09*	*1.55*	*1.18E-03*	*5.59E+07*
7	*8.05*	*1.84*	*2.21E-03*	*4.96E+07*
8	*7.90*	*4.49*	*3.38E-03*	*4.24E+07*
9	*7.81*	*8.56*	*4.58E-03*	*6.01E+07*
10	*7.78*	*10.72*	*1.34E-02*	*1.04E+08*
11	*7.75*	*13.48*	*1.51E-02*	*1.23E+08*
12	*7.72*	*16.98*	*3.02E-02*	*1.95E+08*

Table V – S5 (b). Experimental sample information – pH values, calculated Ringböm coefficients α, $[Ca^{2+}]$ $(mol\ kg_w^{-1})$ and deduced F_0; the sample solutions giving the slope of 1 are set in italics; the sample solutions giving the slope of 2 are set in ***bold****.*

T (°C)	10				15			
Sample	pH value	α	$[Ca^{2+}]$ $(mol \cdot kg_w^{-1})$	F_0 (counts)	pH value	α	$[Ca^{2+}]$ $(mol \cdot kg_w^{-1})$	F_0 (counts)
1	8.97	1.00	0	3.42E+08	8.97	1.00	0	5.22E+08
2	8.50	1.00	5.72E-05	2.92E+08	8.50	1.01	5.72E-05	3.75E+08
3	8.48	1.00	6.18E-05	3.10E+08	8.48	1.01	6.18E-05	3.65E+08
4	8.36	1.01	6.48E-05	3.15E+08	8.36	1.02	6.46E-05	3.91E+08
5	8.30	1.01	8.06E-05	3.42E+08	*8.20*	*1.07*	*8.72E-05*	*4.21E+08*
6	*8.22*	*1.03*	*9.87E-05*	*3.50E+08*	*8.16*	*1.11*	*1.19E-04*	*4.43E+08*
7	*8.18*	*1.05*	*1.23E-04*	*3.66E+08*	*8.12*	*1.18*	*1.56E-04*	*4.44E+08*
8	*8.08*	*1.18*	*1.57E-04*	*3.80E+08*	*8.05*	*1.41*	*1.74E-04*	*4.92E+08*
9	*7.99*	*1.55*	*2.31E-04*	*4.29E+08*	*8.00*	*1.72*	*2.45E-04*	*5.19E+08*
10	*7.92*	*2.17*	*4.80E-04*	*4.51E+08*	*7.93*	*2.49*	*4.34E-04*	*5.30E+08*
11	*7.82*	*4.08*	*7.41E-04*	*5.25E+08*	*7.87*	*3.64*	*6.65E-04*	*5.35E+08*
12	**7.78**	**5.43**	**1.12E-03**	**5.28E+08**	**7.83**	**4.80**	**1.15E-03**	**5.42E+08**
13	**7.75**	**6.75**	**1.33E-03**	**5.68E+08**	**7.76**	**7.98**	**1.76E-03**	**5.78E+08**
14	**7.70**	**9.82**	**2.00E-03**	**6.02E+08**	**7.70**	**12.59**	**1.96E-03**	**5.94E+08**
15	**7.62**	**18.17**	**2.63E-03**	**6.13E+08**	**7.62**	**23.45**	**2.26E-03**	**6.58E+08**
16	**7.56**	**29.13**	**3.34E-03**	**6.84E+08**	**7.57**	**34.79**	**3.86E-03**	**6.74E+08**
17	**7.51**	**43.34**	**4.40E-03**	**7.77E+08**	**7.50**	**60.70**	**4.28E-03**	**7.12E+08**
T (°C)	22^5				25			
Sample	pH value	α	$[Ca^{2+}]$ $(mol \cdot kg_w^{-1})$	F_0 (counts)	pH value	α	$[Ca^{2+}]$ $(mol \cdot kg_w^{-1})$	F_0 (counts)
1	9.90	1.00	0	1.70E+08	8.97	1.00	0	3.77E+08
2	8.66	1.06	2.78E-05	1.66E+08	8.36	1.03	6.48E-05	3.04E+08
3	8.42	1.04	9.09E-05	1.29E+08	8.16	1.19	1.39E-04	3.27E+08
4	8.26	1.10	1.76E-04	1.75E+08	*8.12*	*1.30*	*1.96E-04*	*3.44E+08*
5	8.23	1.12	2.22E-04	2.25E+08	*8.05*	*1.65*	*2.87E-04*	*3.70E+08*
6	8.15	1.24	3.06E-04	2.40E+08	*8.00*	*2.10*	*4.71E-04*	*4.10E+08*
7	8.11	1.37	4.04E-04	2.27E+08	*7.93*	*3.19*	*8.44E-04*	*3.91E+08*
8	*8.10*	*1.34*	*4.93E-04*	*2.18E+08*	*7.87*	*4.76*	*1.09E-03*	*3.84E+08*
9	*8.08*	*1.51*	*6.00E-04*	*2.74E+08*	**7.83**	**6.33**	**1.87E-03**	**3.69E+08**
10	*8.00*	*2.06*	*9.03E-04*	*2.47E+08*	**7.76**	**10.64**	**2.69E-03**	**3.88E+08**
11	*7.97*	*2.52*	*1.22E-03*	*3.08E+08*	**7.70**	**16.88**	**3.02E-03**	**4.00E+08**
12	*7.92*	*3.30*	*1.72E-03*	*3.12E+08*	**7.62**	**31.61**	**4.07E-03**	**4.19E+08**
13	*7.87*	*4.79*	*2.08E-03*	*3.32E+08*	**7.57**	**46.99**	**5.72E-03**	**3.92E+08**
14	*7.85*	*5.51*	*2.64E-03*	*3.55E+08*	**7.50**	**82.02**	**8.23E-03**	**4.33E+08**

15	**7.81**	**7.07**	**3.42E-03**	**3.08E+08**				
16	**7.75**	**11.55**	**4.70E-03**	**3.53E+08**				
17	**7.63**	**28.25**	**6.25E-03**	**3.43E+08**				
18	**7.60**	**37.08**	**8.55E-03**	**3.74E+08**				
19	**7.55**	**53.34**	**1.04E-02**	**3.84E+08**				
20	**7.52**	**70.02**	**1.53E-02**	**4.25E+08**				
21	**7.50**	**79.91**	**1.74E-02**	**4.30E+08**				
22	**7.48**	**96.30**	**2.49E-02**	**5.85E+08**				
T (°C)	35				40			
Sample	pH value	α	$[Ca^{2+}]$ ($mol \cdot kg_w^{-1}$)	F_0 (counts)	pH value	α	$[Ca^{2+}]$ ($mol \cdot kg_w^{-1}$)	F_0 (counts)
1	8.97	1.00	0	3.86E+08	8.97	1.00	0	2.85E+07
2	8.58	1.01	2.69E-05	1.71E+08	8.36	1.08	1.94E-04	5.43E+07
3	8.55	1.02	4.67E-05	1.04E+08	*8.16*	*1.42*	*2.98E-04*	*5.78E+07*
4	8.50	1.02	5.72E-05	3.66E+08	*8.12*	*1.62*	*4.19E-04*	*5.89E+07*
5	8.48	1.03	6.18E-05	3.49E+08	*8.05*	*2.23*	*6.13E-04*	*6.24E+07*
6	*8.36*	*1.06*	*6.48E-05*	*2.07E+08*	*8.00*	*2.96*	*1.01E-03*	*6.27E+07*
7	*8.16*	*1.33*	*1.39E-04*	*2.90E+08*	*7.93*	*4.66*	*1.80E-03*	*7.83E+07*
8	*8.12*	*1.50*	*1.96E-04*	*2.98E+08*	*7.87*	*7.11*	*2.56E-03*	*7.96E+07*
9	*8.05*	*2.02*	*2.87E-04*	*3.20E+08*	**7.81**	**11.09**	**3.30E-03**	**8.15E+07**
10	*8.00*	*2.65*	*4.71E-04*	*3.03E+08*	**7.78**	**13.93**	**4.25E-03**	**9.20E+07**
11	*7.93*	*4.13*	*8.44E-04*	*3.19E+08*	**7.75**	**17.53**	**5.59E-03**	**1.29E+08**
12	*7.87*	*6.28*	*1.09E-03*	*3.09E+08*	**7.71**	**23.90**	**7.04E-03**	**1.43E+08**
13	**7.78**	**12.24**	**1.80E-03**	**3.11E+08**	**7.68**	**30.21**	**7.77E-03**	**1.58E+08**
14	**7.70**	**22.69**	**2.15E-03**	**3.73E+08**				
15	**7.62**	**42.54**	**3.25E-03**	**3.37E+08**				
16	**7.57**	**80.28**	**4.50E-03**	**3.41E+08**	8.48			
17	**7.49**	**119.6**	**7.20E-03**	**3.79E+08**				
T (°C)	*45*				50			
Sample	pH value	α	$[Ca^{2+}]$ ($mol \cdot kg_w^{-1}$)	F_0 (counts)	pH value	α	$[Ca^{2+}]$ ($mol \cdot kg_w^{-1}$)	F_0 (counts)
1	8.97	1.00	0	2.64E+07	8.97	1.00	0	2.76E+07
2	8.48	1.05	1.10E-04	3.20E+07	*8.16*	*1.64*	*2.98E-04*	*2.79E+07*
3	8.36	1.10	1.94E-04	4.81E+07	*8.12*	*1.92*	*4.19E-04*	*3.01E+07*
4	*8.16*	*1.52*	*2.98E-04*	*3.08E+07*	*7.98*	*4.20*	*6.13E-04*	*3.02E+07*
5	*8.12*	*1.76*	*4.19E-04*	*3.82E+07*	*7.95*	*5.14*	*1.01E-03*	*3.99E+07*
6	*8.05*	*2.47*	*6.13E-04*	*4.30E+07*	*7.92*	*6.33*	*1.80E-03*	*5.58E+07*
7	*8.00*	*3.31*	*1.01E-03*	*4.34E+07*	*7.88*	*8.42*	*2.56E-03*	*5.14E+07*
8	*7.93*	*5.24*	*1.80E-03*	*5.57E+07*	**7.85**	**10.50**	**3.30E-03**	**5.58E+07**
9	**7.82**	**8.04**	**2.56E-03**	**5.64E+07**	**7.80**	**15.29**	**4.25E-03**	**6.60E+07**
10	**7.78**	**15.78**	**3.30E-03**	**7.19E+07**	**7.75**	**22.42**	**5.59E-03**	**7.22E+07**
11	**7.72**	**19.87**	**4.25E-03**	**7.94E+07**	**7.73**	**26.18**	**7.70E-03**	**8.28E+07**
12	**7.69**	**27.09**	**5.59E-03**	**1.00E+08**	**7.70**	**33.06**	**9.09E-03**	**9.48E+07**
13	**7.65**	**34.25**	**7.70E-03**	**1.00E+08**				
14	**7.62**	**43.35**	**9.09E-03**	**1.20E+08**				

Table V - S6 Values of the Debye-Hückel parameters A(T) at different temperatures, taken from the NEA-TDB reviews.[7]

t/°C (p = 1bar)	A(T) / $kg^{1/2}$ $mol^{-1/2}$
5	0.494
10	0.497
15	0.501
20	0.505
25	0.509
30	0.513
35	0.518
40	0.523
50	0.533
75	0.564

Table V - S7 The formation constants of $log_{10}K_{013}°$, $log_{10}Q_1$ and $log_{10}Q_2$ in the temperature range of 5-90°C, calculated using the exiting general formula; the global formation constants of $log_{10}\beta_{113}°$(Ca), $log_{10}\beta_{213}°$(Ca) and $log_{10}\beta°_{113}$ (Mg) were estimated with the Van't Hoff Equation; the formation constants of $log_{10}K°_{113}$ (Ca), $log_{10}K°_{213}$(Ca), $log_{10}K°_{113}$ (Mg) were finally determined by subtracting the sum of $log_{10}K°_{013}$, $log_{10}Q_1$ and $log_{10}Q_2$ from the global equilibrium constants $log_{10}\beta°_{113}$ (Ca), $log_{10}\beta°_{213}$ (Ca) and $log_{10}\beta°_{113}$ (Mg).

T (°C)	$log_{10}K°_{013}$ Götz, *et al.*[8]	$log_{10}Q_1$ Patterson, *et al.*[9]	$log_{10}Q_2$ Patterson, *et al.*[10]	$log_{10}\beta°_{113}$(Ca)	$log_{10}\beta°_{213}$(Ca)
5	22.48	-6.51	-10.56	-6.06	-19.35
10	22.28	-6.46	-10.49	-6.04	-19.29
15	22.11	-6.41	-10.43	-6.03	-19.23
20	21.95	-6.38	-10.38	-6.02	-19.18
22	21.93	-6.37	-10.36	-6.02	-19.16
25	21.81	-6.35	-10.34	-6.01	-19.13
35	21.58	-6.31	-10.26	-5.99	-19.08
40	21.48	-6.29	-10.23	-5.98	-18.98
45	21.40	-6.28	-10.20	-5.98	-18.94
50	21.33	-6.28	-10.18	-5.97	-18.89
55	21.27	-6.28	-10.16	-5.96	-18.85
60	21.22	-6.28	-10.15	-5.95	-18.80
65	21.18	-6.29	-10.13	-5.94	-18.76
70	21.15	-6.29	-10.12	-5.94	-18.72
75	20.96	-6.30	-10.12	-5.93	-18.69
80	20.88	-6.32	-10.11	-5.92	-18.65
85	20.81	-6.33	-10.11	-5.91	-18.61
90	20.73	-6.35	-10.11	-5.91	-18.58
T (°C)	$log_{10}\beta°_{113}$(Mg)	$log_{10}K°_{113}$(Ca)	$log_{10}K°_{213}$(Ca)	$log_{10}K°_{113}$°(Mg)	
5	-6.93	5.60	9.37	4.72	
10	-6.95	5.57	9.27	4.67	
15	-6.96	5.55	9.20	4.63	
20	-6.97	5.55	9.15	4.60	
22	-6.97	5.51	9.10	4.55	
25	-6.98	5.55	9.12	4.58	
35	-6.99	5.56	9.18	4.57	
40	-7.00	5.58	9.11	4.56	
45	-7.01	5.60	9.13	4.55	

50	-7.02	5.62	9.16	4.56	
55	-7.03	5.65	9.20	4.56	
60	-7.04	5.68	9.25	4.57	
65	-7.05	5.71	9.31	4.58	
70	-7.05	5.75	9.38	4.60	
75	-7.06	5.96	9.62	4.62	
80	-7.07	6.06	9.77	4.82	
85	-7.08	6.17	9.92	4.90	
90	-7.09	6.29	10.09	5.00	

K_{013}: $UO_2^{2+} + 3CO_3^{2-} \rightleftarrows UO_2(CO_3)_3^{4-}$ (Eq. V - 14 in the manuscript)

Q_1: $CO_2(aq) + H_2O \rightleftarrows H^+ + HCO_3^-$

Q_2: $HCO_3^- \rightleftarrows H^+ + CO_3^{2-}$ ($Q_1 + Q_2$ = Eq. V - 14 in the manuscript)

$\beta_{113}°(Ca)$: $Ca^{2+} + UO_2^{2+} + 2CO_2(aq) + CO_3^{2-} + 2H_2O\ (l) \rightleftarrows CaUO_2(CO_3)_3^{2-} + 4H^+$ (Eq. V - 15 in the manuscript)

$\beta_{213}°(Ca)$: $2Ca^{2+} + UO_2^{2+} + 3CO_2(aq) + 3H_2O(l) \rightleftarrows Ca_2UO_2(CO_3)_3(aq) + 6H^+$ (Eq. V - 16 in the manuscript)

$\beta_{113}°(Mg)$: $Mg^{2+} + UO_2^{2+} + 2CO_2(aq) + CO_3^{2-} + 2H_2O(l) \rightleftarrows MgUO_2(CO_3)_3^{2-} + 4H^+$ (Eq. V - 15 in the manuscript)

$K_{113}°(Ca)$: $Ca^{2+} + UO_2(CO_3)_3^{4-} \rightleftarrows CaUO_2(CO_3)_3^{2-}$ (Eq. V - 2 in the manuscript)

$K_{213}°(Ca)$: $2Ca^{2+} + UO_2(CO_3)_3^{4-} \rightleftarrows Ca_2UO_2(CO_3)_3$ (Eq. V - 2 in the manuscript)

$K_{113}°(Mg)$: $Mg^{2+} + UO_2(CO_3)_3^{4-} \rightleftarrows MgUO_2(CO_3)_3^{2-}$ (Eq. V - 2 in the manuscript)

Table V - S8 Characteristic decomposition parameters of the pure spectra of $Ca_nUO_2(CO_3)_3^{(4-2n)-}$ and $MgUO_2(CO_3)_3^{2-}$ shown in Fig. V - S2 and Fig. V - S3.

Peak index $CaUO_2(CO_3)_3^{2-}$	Peak Type	FWHM	Center	Area IntgP
1	Gaussian	23.10	479.58	14.98
2	Gaussian	17.97241	496.618	28.22
3	Gaussian	17.17688	514.51	24.26
4	Gaussian	23.7694	533.45	16.11
5	Gaussian	52.32048	552.16	16.42
Peak index $Ca_2UO_2(CO_3)_3(aq)$	Peak Type	FWHM	Center	Area IntgP
1	Gaussian	13.65	465.01	14.54
2	Gaussian	13.69	484.14	27.03
3	Gaussian	15.97	504.62	28.42
4	Gaussian	17.37	525.98	17.13
5	Gaussian	23.51	548.13	9.13
6	Gaussian	34.64	576.52	3.76
Peak index $MgUO_2(CO_3)_3^{2-}$	Peak Type	FWHM	Center	Area IntgP
1	Gaussian	24.15	465.60	21.44
2	Gaussian	15.45	484.98	21.17
3	Gaussian	17.89	502.85	22.221
4	Gaussian	26.34	523	16.81
5	Gaussian	59.05	545.93	18.38

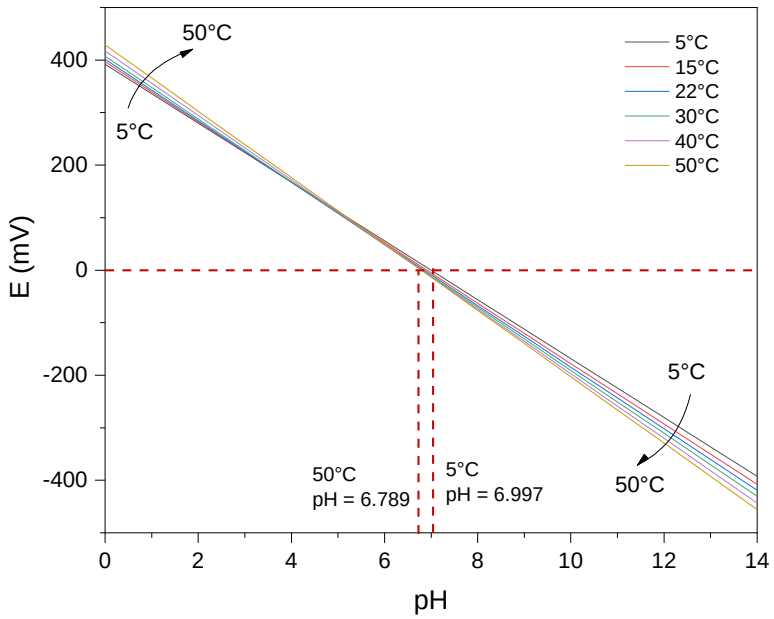

Fig. V - S1. Calibration lines in the temperature range of 5-50°C and the pH values corresponding to the zero point of electrode at 5°C and 50°C.

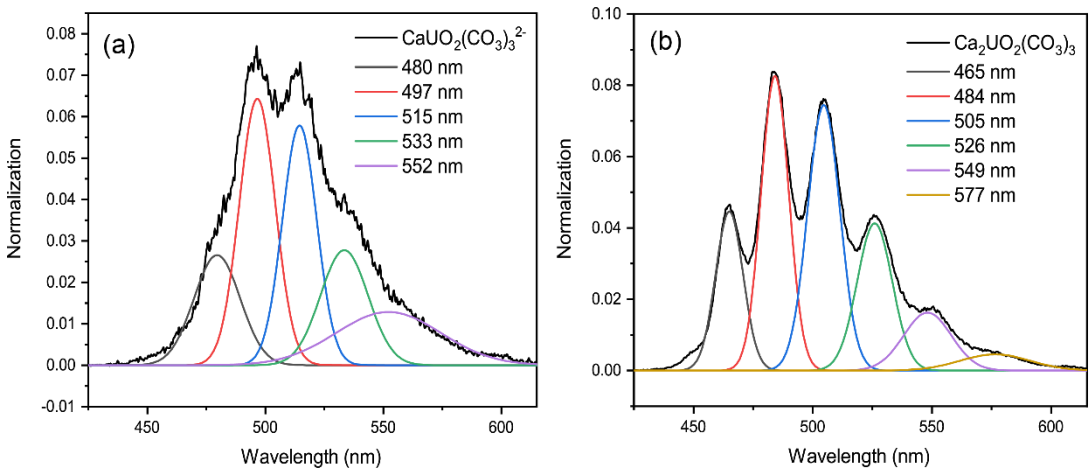

Fig. V - S2 Gaussian decomposition of the luminescence spectrum of the pure spectra of (a) $CaUO_2(CO_3)_3^{2-}$ and (b) $Ca_2UO_2(CO_3)_3(aq)$ normalized to the same area by the MCR-ALS analysis

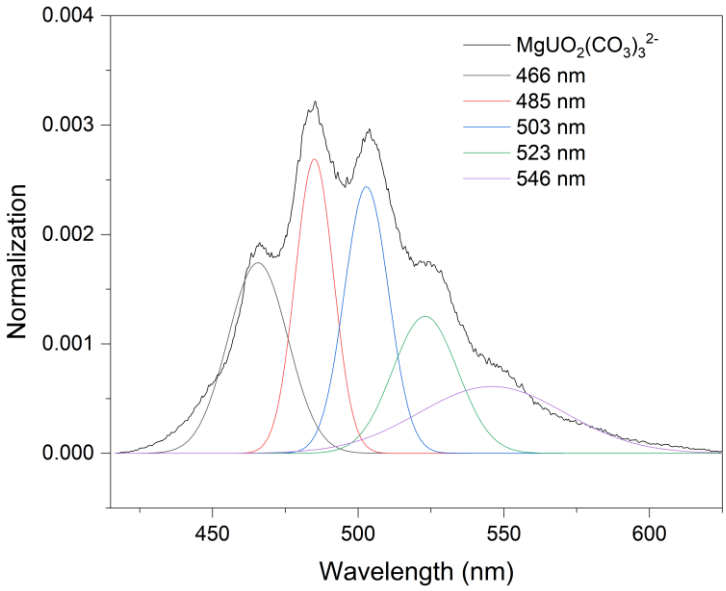

Fig. V - S3 Gaussian decomposition of the luminescence spectrum of the pure spectra of $MgUO_2(CO_3)_3^{2-}$ normalized to the same area by the MCR-ALS analysis.

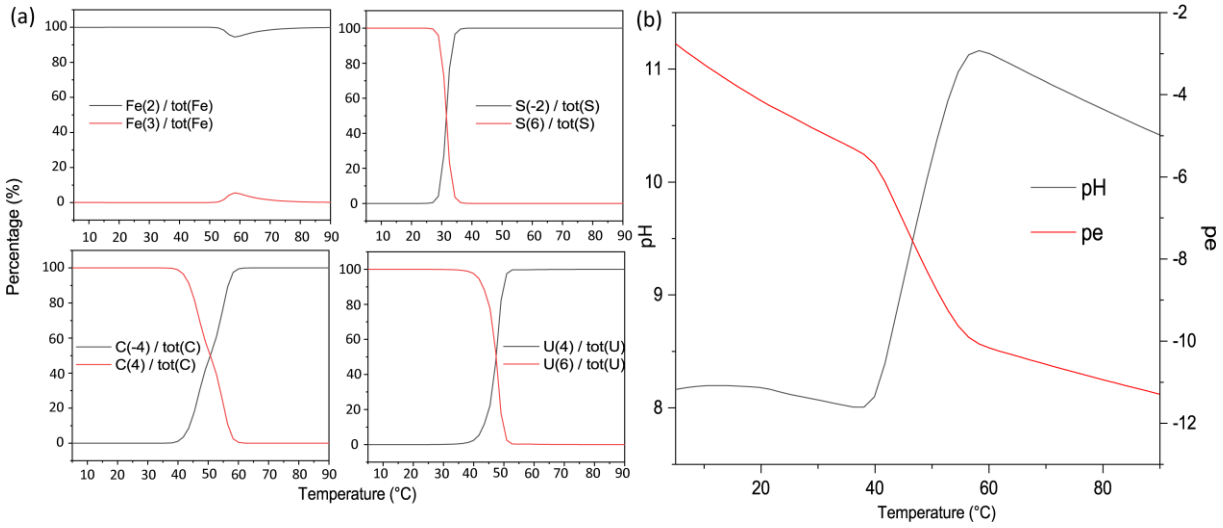

Fig. V - S4 Change in main oxidation states of Fe, S, C, U (a) and variation of pH and pe (b) as a function of temperature for Boom clay equilibrium waters,[11] $P(O_2) = 10^{-68.67}$ atm using thermodynamic data from the Thermochimie 10a database,[12] implementing $SrUO_2(CO_3)_3^{2-}$,[13] specific ion interaction coefficients of $Mg_n/Ca_nUO_2(CO_3)_3^{(4-2n)-,4-6}$ and their $\Delta_r H°_m$ values determined in this work based on the isoelectric reaction approximation.

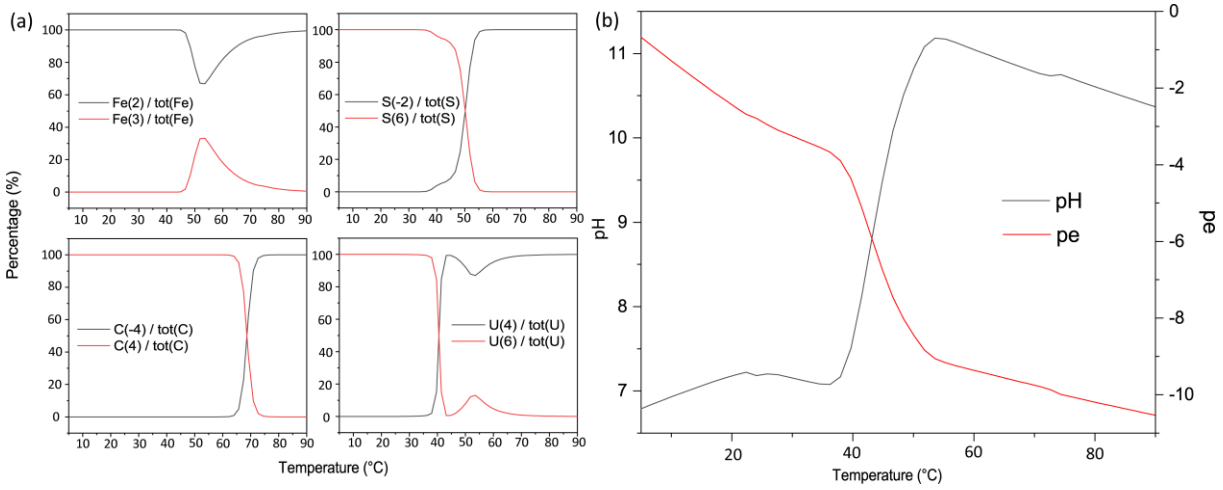

Fig. V - S5 Change in main oxidation states of Fe, S, C, U (a) and variation of pH and pe (b) as a function of temperature for Callovo-Oxfordian clay equilibrium water,[14] $P(O_2) = 10^{-65.83}$ atm using thermodynamic data from the Thermochimie 10a database,[12] implementing $SrUO_2(CO_3)_3^{2-}$,[13] specific ion interaction coefficients of $Mg_n/Ca_nUO_2(CO_3)_3^{(4-2n)-,4-6}$ and their $\Delta_r H°_m$ values determined in this work based on the isoelectric reaction approximation.

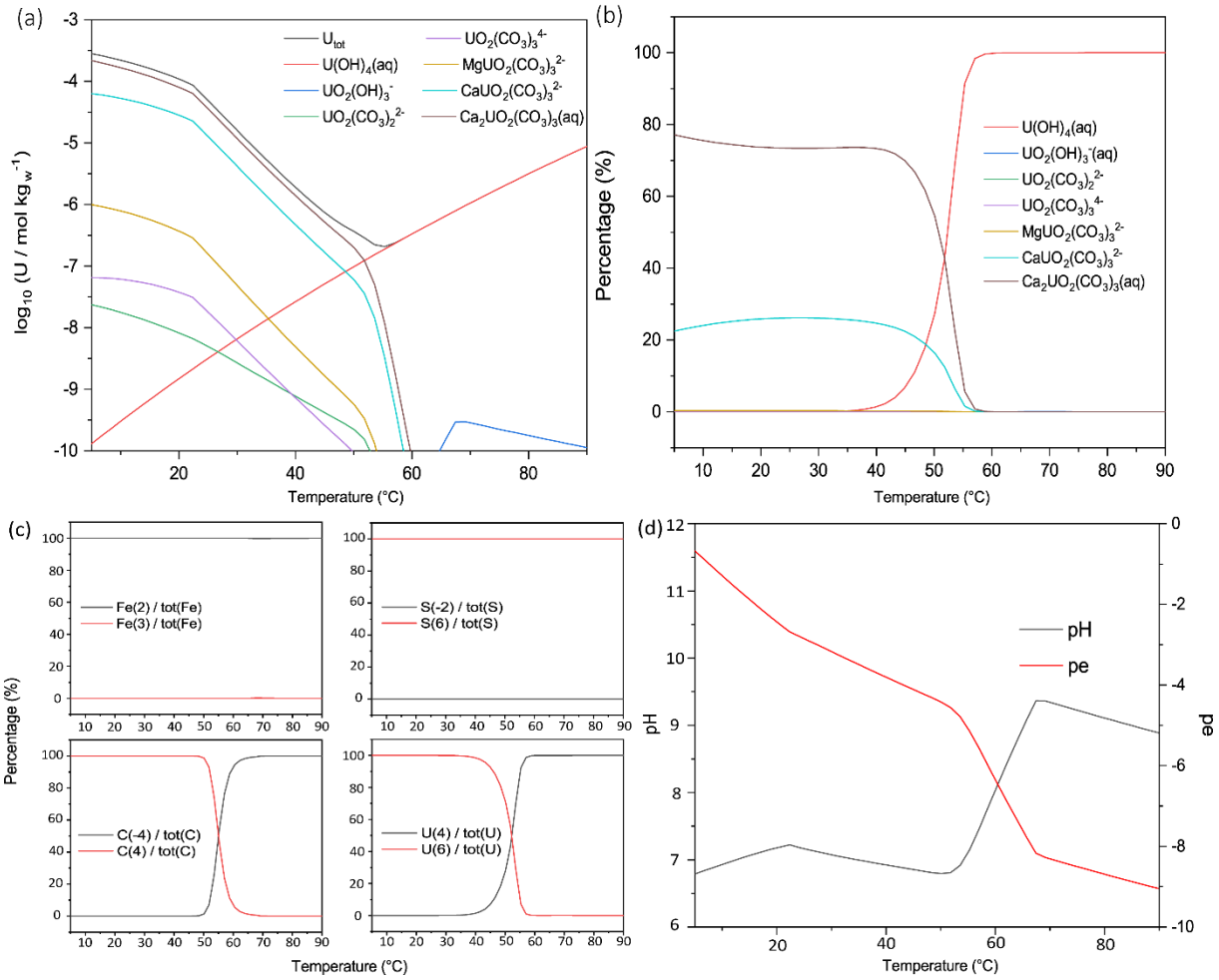

Fig. V - S6 Solubility of UO_2:2H_2O(am) (a) and aqueous uranium speciation (b) change in main oxidation states of Fe, S, C, U (c) and variation of pH, pe (d), as a function of temperature for Callovo-Oxfordian clay equilibrium waters,[14] $P(O_2) = 10^{-65.83}$ atm using thermodynamic data from the Thermochimie 10a database,[12] implementing $SrUO_2(CO_3)_3^{2-}$,[13] specific ion interaction coefficients of $Mg_nCa_nUO_2(CO_3)_3^{(4-2n)-}$ 4-6 and their $\Delta_r H°_m$ values determined in this work based on the isoelectric reaction approximation. The reduction reactions of S(+VI) to lower oxidations states were prevented in the input PhreeqC file.

(a) (b)

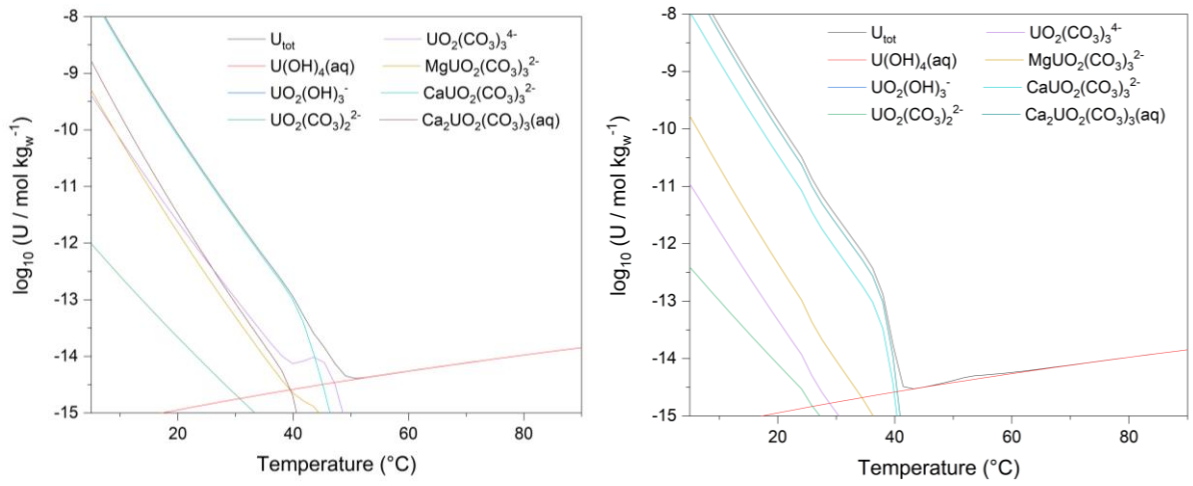

Fig. V - S7 Solubility of UO_2(cr) as a function of temperature (a) for Boom clay equilibrium waters,[11] $P(O_2) = 10^{-68.67}$ atm and (b) for Callovo-Oxfordian clay equilibrium waters,[14] $P(O_2) = 10^{-65.83}$ atm using thermodynamic data from the Thermochimie 10a database,[12] implementing $SrUO_2(CO_3)_3^{2-}$,[13] specific ion interaction coefficients of $Mg_n/Ca_nUO_2(CO_3)_3^{(4-2n)-}$ [4-6] and their $\Delta_r H°_m$ values determined in this work based on the isoelectric reaction approximation.

References

1. Y. C. Wu, W. F. Koch and R. A. Durst, *Standardization of pH measurements*, Report 260-53, US Department. of Commerce, National Bureau of Standards, 1988. http://nvlpubs.nist.gov/nistpubs/Legacy/SP/nbsspecialpublication260-53e1988.pdf
2. R. Guillaumont, T. Fanghänel, V. Neck, J. Fuger, D. A. Palmer, I. Grenthe and M. H. Rand, *Update of the Chemical Thermodynamics of Uranium, Neptunium, Plutonium, Americium and Technetium*, OECD Nuclear Energy Agency, Data Bank, Issy-les-Moulineaux, France, 2003.
3. D. D. Wagman, W. H. Evans, V. B. Parker, R. H. Schumm and I. Halow, *The NBS tables of chemical thermodynamic properties. Selected values for inorganic and C1 and C2 organic substances in SI units*, National Standard Reference Data System, 1982
4. C. Shang and P. E. Reiller, *Dalton Trans.*, 2021, **50**, 4363-4379.
5. C. Shang and P. E. Reiller, *Dalton Trans.*, 2020, **49**, 466-481.
6. C. Shang, P. E. Reiller and T. Vercouter, *Dalton Trans.*, 2020, **49**, 15443-15460.
7. R. J. Lemire, J. Fuger, H. Nitsche, P. Potter, M. Rand, J. Rydberg, K. Spahiu, J. C. Sullivan, W. J. Ullman, P. Vitorge and H. Wanner, *Chemical Thermodynamics 4. Chemical Thermodynamics of Neptunium and Plutonium*, *Chemical Thermodynamics*, North Holland Elsevier Science Publishers B. V., Amsterdam, The Netherlands, 2001.
8. C. Götz, G. Geipel and G. Bernhard, Thermodynamical data of uranyl carbonate complexes from absorption spectroscopy, in *Uranium, Mining and Hydrogeology*, eds. B. J. Merkel and A. Hasche-Berger, Springer, Berlin, Heidelberg, Germany, 2008, DOI: 10.1007/978-3-540-87746-2_118, pp. 907-914.
9. C. S. Patterson, G. H. Slocum, R. H. Busey and R. E. Mesmer, *Geochim. Cosmochim. Acta*, 1982, **46**, 1653-1663.
10. C. S. Patterson, R. H. Busey and R. E. Mesmer, *J. Solution Chem.*, 1984, **13**, 647-661.

11. M. de Craen, L. Wang, M. Van Geet and H. Moors, *Geochemistry of Boom Clay pore water at the Mol site*, Report SCK•CEN-BLG-990, SCK•CEN, Mol, Belgium, 2004. http://jongeren.sckcen.be/~/media/Files/Science/disposal_radioactive_waste/Geochemistry_of_Boom_Clay_pore_Status_2004.pdf
12. J. N. Brönsted, *J. Am. Chem. Soc.*, 1922, **44**, 877-898.
13. W. Dong and S. C. Brooks, *Environ. Sci. Technol.*, 2006, **40**, 4689-4695.
14. E. C. Gaucher, C. Tournassat, F. J. Pearson, P. Blanc, C. Crouzet, C. Lerouge and S. Altmann, *Geochim. Cosmochim. Acta*, 2009, **73**, 6470-6487.

Chapter VI. Implications of Newly Derived Thermodynamic Data on the Predominance Diagrams of the Ca-U(VI)-CO_3 Systems at Room Temperature.

VI - 1 Context

In a previous study, Reiller and Descostes[1] proposed predominance ranges — in a activity of SO_4^{2-}–pH domain at constant $\log_{10}a(Ca^{2+})$ $\log_{10}a(Mg^{2+})$ and $P(CO_2)$ — of the $(Mg/Ca)_nUO_2(CO_3)_3^{(4-2n)-}$ complexes, based on speciation calculation of water compositions relevant of uranium mining activities and of other varying occurrences, using PhreeqC database output file from PRODATA 1.1.0.4 database. In the framework of PRODATA, the values of formation constants for $Ca_nUO_2(CO_3)_3^{(4-2n)-}$, $SrUO_2(CO_3)_3^{2-}$ and $Ba_nUO_2(CO_3)_3^{(4-2n)-}$ were taken from Dong and Brooks[2], and the one of $MgUO_2(CO_3)_3^{2-}$ was chosen from Dong and Brooks.[3] In chemical modelling, the evolution of $\log_{10}\beta(M_nUO_2(CO_3)_3^{(4-2n)-})$ as a function of ionic strength is important to be specified as the final speciation results can show significant differences due to different choices of activity corrections. However, the determination of specific ion interaction coefficients ε for these ternary complexes — particularly $(Mg/Ca)_nUO_2(CO_3)_3^{(4-2n)-}$ complexes — did not receive sufficient attention and only the value of $\varepsilon(MgUO_2(CO_3)_3^{2-}, Na^+)$ was reported at the time of publication.[3] Therefore, $\varepsilon(MgUO_2(CO_3)_3^{2-}, Na^+)$ = -3.2 kg_w mol^{-1} — based on Dong and Brooks[3] — and $\varepsilon(Ca_nUO_2(CO_3)_3^{(4-2n)-}, Na^+) = 0$ — because of non-availability — were taken in the theoretical speciation calculations in Reiller and Descostes.[1]

The main objective of this chapter is to examine the main species in the natural water compositions linked to radioactive waste management (RWM), uranium mining activity, and of other more general interest related to natural uranium with the newly determined thermodynamic data for $(Mg/Ca)_nUO_2(CO_3)_3^{(4-2n)-}$ complexes obtained in previous chapters. The selected water conditions particularly cover those reported for:

(a) waters in underground research laboratories (URL) for RWM, *e.g.*, clay porewaters (Boom clay in Belgium,[4] Callovo-Oxfordian[5] and Tournemire[6] clays in France, Mont-Terri clay in Switzerland[7,8]) and granitic groundwaters (Äspö site, the Forsmark and the Laxemar-Simpevarp areas in Sweden[9-11]);

(b) groundwaters in an In Situ Recovery (ISR) context from ORANO mining sites,[1] in Al-Batin Alluvial Fan (southern Iraq),[12] and in the Lodève basin (France)[13];

(c) waters crossing the Cigar Lake mining site (Saskatchewan, Canada),[14] and in the Oklo uraninite deposit area[15,16];

(d) well waters as local sources of drinking sources in Finland,[17] around the Semipalatinsk Nuclear Test Site in Kazakhstan[18], as well as near-surface Canadian aquitards considered as underlying groundwater[19,20];

(e) waters sampled upstream, downstream and within uranium mining sites, *e.g.*, Cluff Lake in Canada[21], Lac Saint-Clément in France[22];

(f) standard seawater[23,24];

(g) several waters compositions issued from the general dataset generated through the European project FOREGS (Forum of European Geological Surveys[*])[25];

VI - 2 Description of studied water compositions

The chemical composition of natural water is a result of the physical, chemical, and biochemical processes that occur in the atmosphere-soil-rock water system. A wide range of chemical elements can dissolve in natural waters due to interactions with the atmosphere, the surrounding environment, soil, and bedrock. In particular, the rock-mineral solubility has a decisive influence on the chemical composition of natural water. Type and amount of major, secondary, and minor elements, as listed in Table VI - 1, are considerably variable and reflect the nature and effects of geochemical processes on groundwater composition. Groundwaters usually have much higher concentrations of principal constituents than surface waters. Those in contact with rock tend to be more concentrated than shallow waters.

[*] http://weppi.gtk.fi/publ/foregsatlas/

Table VI - 1 Occurrence of inorganic dissolved constituents in groundwater.[26]

Major constituents (1.0 to 1000 mg L^{-1})	Secondary constituents (0.01 to 10 mg L^{-1})	Minor constituents (0.0001 to 0.1 mg L^{-1})
Sodium	Potassium	Arsenic
Calcium	Iron	Barium
Magnesium	Aluminium	Bromide
Bicarbonate	Carbonate	Cadmium
Sulphate	Nitrate	Chromium
Chloride	Fluoride	Cobalt
Silica	Boron	Copper
	Selenium	Iodide
		Lead
		Lithium
		Manganese
		Nickel
		Phosphate
		Strontium
		Uranium
		Zinc

For this exercise, a number of natural water compositions were collected from the literature available. The measurement of the geochemical parameters — *i.e.* pH value, redox potential, salinity, alkalinity, temperature, *etc.* — important characteristics for speciation modelling were taken for each collected sample. Generally, these natural waters are dominated by the following ions: Na^+, Ca^{2+}, Mg^{2+}, K^+, Cl^-, NO_3^-, HCO_3^-, CO_3^{2-}, and SO_4^{2-} that may be attributed to the chemical weathering process and the leaching of minerals. Among these ions, chloride concentration is the most suitable parameter to describe water salinity because it is weakly lost from solution by precipitation or adsorption. The concentration of uranium in the collected samples highly depends on the sampling regions. In most natural waters, uranium concentration is between $4.2\ 10^{-10}$ M and $4.2\ 10^{-9}$ M.[27] In Europe, the average uranium concentration in continental surface water is estimated to be on the order of 0.3 µg L^{-1} (≈ $1.26\ 10^{-9}$ M) while it is on the order of 0.5 µg L^{-1} (≈ $2.1\ 10^{-9}$ M) worldwide.[28] In river waters, it can extend over four orders of magnitude with average content from 0.02 to 6 µg L^{-1} (≈ $8.40\ 10^{-11}$ to $2.52\ 10^{-8}$ M).[29,30] In France, the uranium concentration in river waters is about 0.44 µg L^{-1} (≈ $1.85\ 10^{-9}$ M) in sedimentary areas, and expected to be a little lower than 0.15 µg L^{-1} in the Hercynian shelf and alpine areas.[31] However, in mines the uranium concentration in groundwater can range from $6.3\ 10^{-8}$ to $1.68\ 10^{-6}$ M.[32]

Two water samples were collected from the Lodève site by ORANO Mining and their chemical compositions were analyzed. With this information, it is possible to perform a theoretical speciation calculation and then compared with the luminescence of the dominant

species experimentally observed by TRLFS. Table VI - 2 lists the chemical constituents for the investigated water samples: one was the "untreated" water initially at pH = 8.2 and the other one was initially acidified to pH 6.5 after sampling.

Table VI - 2 Chemical constituents for the investigated water samples

Samples (mmol L^{-1})	pH value measured on 9/7/2021	F^-	Cl^-	SO_4^{2-}	Alkalinity	Na^+	K^+	Mg^{2+}	Ca^{2+}
"untreated" water	8.3	< LD (10^{-5} mol L^{-1})	0.66 ± 0.01	5.51 ± 0.01	4.51	8.17 ± 0.03	0.49 ± 0	2.74 ± 0.03	0.78 ± 0
acidified water	8.16	< LD (10^{-5} mol L^{-1})	0.65 ± 0	6.84 ± 0	5.16	8 ± 0	0.5 ± 0	2.82 ± 0.02	2.54 ± 0

VI - 3 Description of calculations of uranium speciation in the selected samples

The choices of the chosen software, the database file and activity correction would have a particular effect on the simulation results. The calculations in this chapter were performed using the PHREEQC version 3.4.0.14000[33,34] for the speciation calculation and Phreeplot 1.0[35,36] for the predominance diagrams. According to the SIT definition in PhreeqC, activity correction adopted in this work, the formation constants at infinite dilution $\log_{10}\beta°$, the thermodynamic functions $\Delta_f H_m°$ and SIT parameters, specific ion interaction coefficients ε for $(Mg/Ca)_nUO_2(CO_3)_3^{(4-2n)-}$ complexes, were implemented in the input file, and the Thermochimie 9b database,[37] which shares the same body of thermodynamic data with PRODATA 1.1.0.4 database was used.

VI - 4 Description of activity predominance diagrams

Fig. VI - 1 illustrates the evolution of predominance diagrams obtained using Phreeplot[36] for the system Ca^{2+}-U(IV/VI)-Na^+-Cl^--OH^--HCO_3^--H_2O(l) as a function of partial pressure of oxygen. The activity diagrams $\log_{10}(a(HCO_3^-)\, a(H^+))$ *vs.* $\log_{10}(a(Mg^{2+})^{0.5}\, a(Ca^{2+})^{0.5}/a(H^+)^2)$ have been chosen for the presentation due to the number of variables affecting this system and the non-linear relationship among them. It allows to represent the variation of H_2CO_3 and (Mg-Ca)$Ca(OH)_2$. The calculations were conducted at fixed uranium concentration of 10^{-8} mol kg_w^{-1} at I_m = 0.1 mol kg_w^{-1} NaCl with $P(O_2)$ varying from 10^{-73} to 10^{-51} atm, which covers a wide range of actual underground research laboratory for the radioactive waste management — *e.g.*, of $P(O_2) = 10^{-73}$ atm for the Äspö site in Sweden up to, $P(O_2) = 10^{-67}$ atm for the Callovo-

Oxfordian site in France. One can observe that the partial pressure of oxygen has a significant impact on the aqueous speciation of uranium as well as its oxidation state. Because of the redox sensitivity of uranium, the oxidation-reduction reactions are very important in the assessment of uranium mobility. Uranium exists in the form of $U(OH)_4$, under its +IV redox state, at low $P(O_2)$ (10^{-73} atm, 10^{-67} atm) and $\log_{10}(a(HCO_3^-)\ a(H^+))$ at the expenses of $Ca_nUO_2(CO_3)_3^{(4-2n)-}$ complexes. When increasing the $P(O_2)$, the formation of $Ca\text{-}UO_2\text{-}CO_3$ ternary complexes takes place within larger range at higher values of $\log_{10}(a(HCO_3^-)\ a(H^+))$ and $\log_{10}(a(Mg^{2+})^{0.5}\ a(Ca^{2+})^{0.5}/a(H^+)^2)$. In spite of the predominant role of $Ca_nUO_2(CO_3)_3^{(4-2n)-}$ complexes, the borderlines between two different species remain almost unaffected at $P(O_2) \geq 10^{-55}$ atm. As observed in this exercise, the great impact of $P(O_2)$ on the aqueous speciation of U(IV)/(VI) can strongly affects its solubility under conditions relevant for nuclear waste disposal.

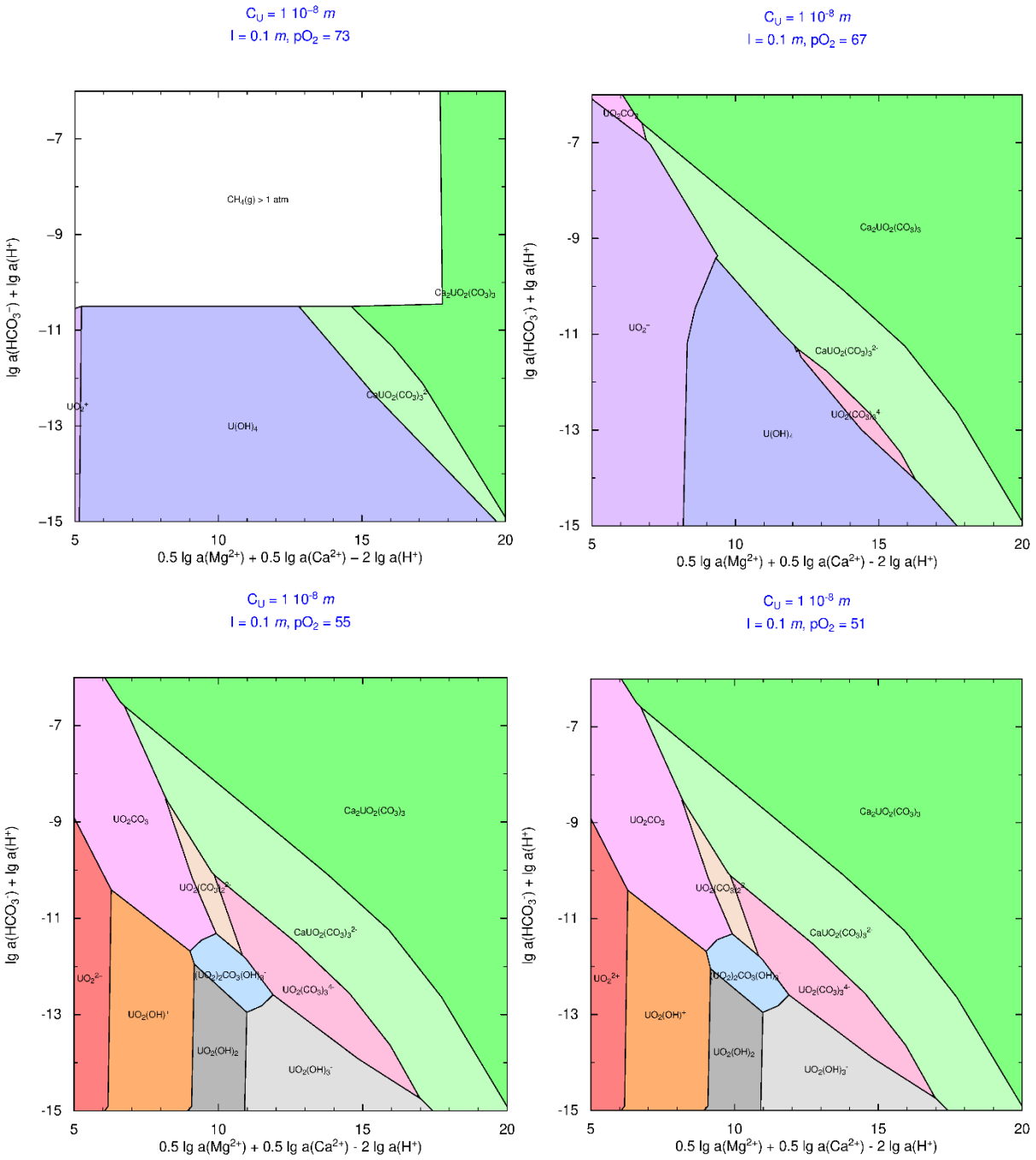

Fig. VI - 1 Predominance diagrams obtained using Phreeplot[36] of Mg-Ca-U-CO_3 and U-OH calculated for I_m = 0.1 mol kg_w^{-1} NaCl using the thermodynamic data and SIT coefficients determined in this work. Calculations performed for $C(U)_{tot} = 10^{-8}$ mol kg_w^{-1}, $P(O_2)$ from 10^{-73} to 10^{-51} atm.

VI - 5 Analysis of results

Fig. VI - 2 shows the repartition of the reported uranium concentration for the selected water compositions in this study. The measured uranium concentration varies widely from 10^{-11} to 5 10^{-3} mol kg_w^{-1}. The ionic strength ranges from 0.6 to 83.1 mmol kg_w^{-1} with an average of 12.5 mmol kg_w^{-1}. Some water samples represent the uranium concentration lower than 15 µg L^{-1}

(≈ 6.30 10^{-8} M) — the World Health Organization-proposed restrictive guideline[38] — around the Cigar Lake mining site (Saskatchewan, Canada),[14] the Oklo uranium ore deposits, from several ORANO mining sites in an ISR context,[39,40] from the European project FOREGS, and sampled in the Semipalatinsk nuclear test site.[18] However, concentrations greater than 10^{-6} M even up to the order of 10^{-4} M can occur in several water compositions associated with uranium ore deposits, such as in the former uranium mine at Cluff lake (Canada),[21] in the U ore deposits within the Lodève Basin in South Central France,[6,13] and in Kazakhstan.[18]

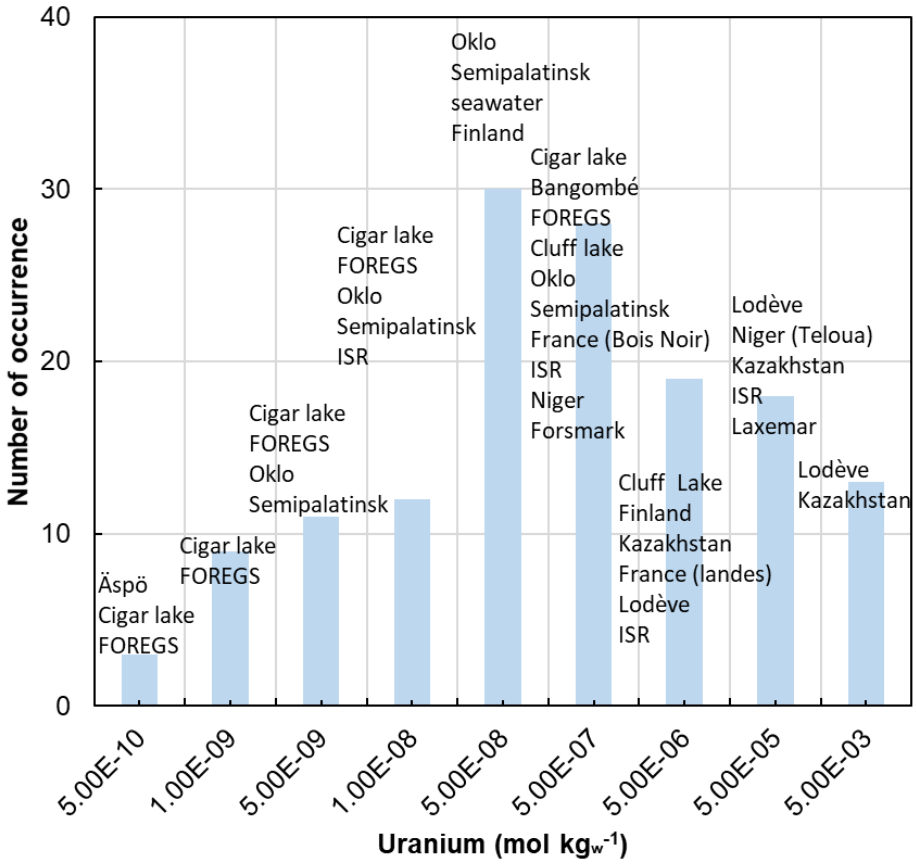

Fig. VI - 2 Frequency distribution of the uranium concentration from literature.

Some of these groundwaters containing high uranium concentration are strongly reducing, and contain important sulphide but very low calcium concentrations. The speciation distribution for the selected aqueous solutions was carried out using PhreeqC. The activity of important ions — $\log_{10}a(HCO_3^-)$, $\log_{10}a(H^+)$, $\log_{10}a(Ca^{2+})$, $\log_{10}a(Na^+)$ — and the percentage of the major species were generated in the output files. Saturation index of calcite and schoepite was also calculated, which is key parameters in geochemical studies and indicates how far the solution is from thermodynamic equilibrium with respect to these minerals. In this study, we only consider the water compositions that are showing $Ca_nUO_2(CO_3)_3^{(4-2n)-}$ as major complex. The

selected water compositions are plotted in $\log_{10}(a(HCO_3^-)\ a(H^+))$ *vs.* $\log_{10}(a(Ca^{2+})/a(H^+)^2)$ and $\log_{10}(a(Na^+)/a(H^+))$ *vs.* $\log_{10}(a(Ca^{2+})/a(H^+)^2)$ activity predominance diagrams calculated at fixed uranium concentration of 100 μmol kg_w^{-1} and $P(O_2) = 10^{-0.6788}$ atm at 25°C considering the activity of water to be unity. The choice of axis ranges in Fig. VI - 3 is based on the analysis of the frequency of the $\log_{10}(a(Ca^{2+})/a(H^+)^2)$–$\log_{10}(a(HCO_3^-)\ a(H^+))$–$\log_{10}(a(Na^+)/a(H^+))$ parameters. The most of selected samples within the range of $\log_{10}(a(Ca^{2+})/a(H^+)^2)$ from 10 to 13, of $\log_{10}(a(HCO_3^-)\ a(H^+))$ from -11 to -9.5, and of $\log_{10}(a(Na^+)/a(H^+))$ from 4 to 6. The precipitation of calcite and dolomite is not requested in calculation because several water compositions are oversaturated respective to these phases. (*cf.* Fig. II - S7) The precipitation region of calcite, limited by the blue dashed line in predominance diagrams (Fig. VI - 4 – Fig. VI - 9), is separately calculated by imposing the equilibrium between the atmospheric $CO_2(g)$ and the aqueous solution. The mineral field boundaries of calcite were found using the "hunt and track" (*i.e.* ht.1) algorithm in Phreeplot, which represents $[Ca^{2+}] = [CO_3^{2-}]$ in solubility products. The use of minstab calculation method, which can be adopted in constructing the mineral stability diagram, would definitely make the borderlines move towards lower $\log_{10}(a(Ca^{2+})/a(H^+)^2)$ because it indicates the conditions where the mineral begins to precipitate. The basic principles involved in these two algorithms are detailed in Kinniburgh and Cooper.[35,36]

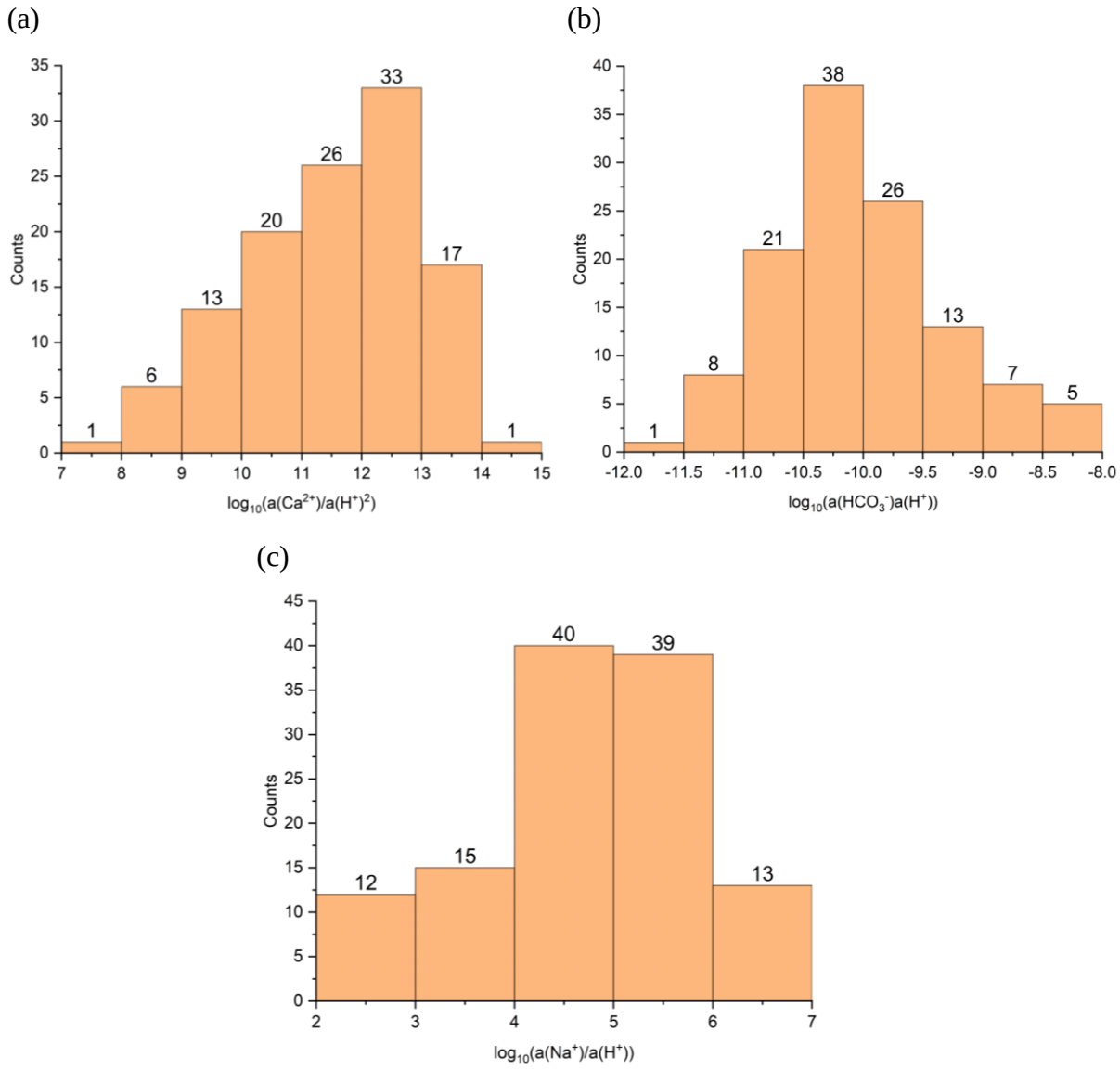

Fig. VI - 3 Frequency distributions of the (a) $log_{10}(a(Ca^{2+})/a(H^+)^2)$, (b) $log_{10}(a(HCO_3^-)\ a(H^+))$, and (c) $log_{10}(a(Na^+)/a(H^+))$ parameters for the selected sample solutions.

There are limitations in comparing all the chemical analyses of selected water compositions of different origins and types in one diagram. As shown in Fig. VI - 4, $log_{10}(a(HCO_3^-)\ a(H^+))$ *vs.* $log_{10}(a(Ca^{2+})/a(H^+)^2)$ predominance diagram plotted at $log_{10}(a(Na^+)/a(H^+)) = 5$, the positions of the points in the diagram correspond to chemistry of the studied water samples, regardless of their real values of $log_{10}(a(Na^+)/a(H^+))$. By color of points, the calculated major species in each water sample is presented. However, expression of natural water chemistry with the two parameters, *i.e.* $log_{10}(a(HCO_3^-)\ a(H^+))$ and $log_{10}(a(Ca^{2+})/a(H^+)^2)$, is a disadvantage because the value of $log_{10}(a(Na^+)/a(H^+))$ for a number of water samples differs from 5 units, and the borderlines of predominance regions of different complexes are closely related to this parameter. Fig. VI - 5 shows a three-dimensional repartition of the selected water samples with

their values of $\log_{10}(a(Na^+)/a(H^+))$ projected to the surface parallel to the z-axis of $\log_{10}(a(Na^+)/a(H^+))$ ranging from 2 to 7. Most of the data points plot around $\log_{10}(a(Na^+)/a(H^+))$ = 5. A few data points are of around $\log_{10}(a(Na^+)/a(H^+))$ = 4 and 6. For this reason, $\log_{10}(a(HCO_3^-)\ a(H^+))$ *vs.* $\log_{10}(a(Ca^{2+})/a(H^+)^2)$ predominance diagrams are plotted at the three most common values of $\log_{10}(a(Na^+)/a(H^+))$, *i.e.* 4, 5, and 6.

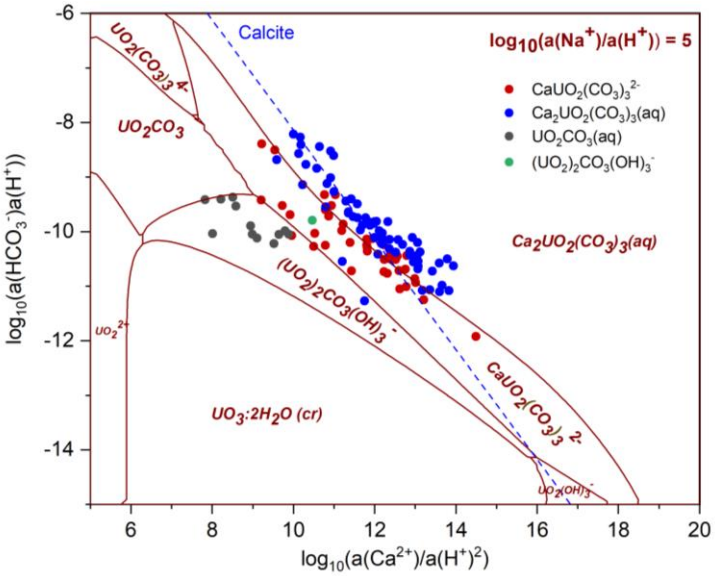

Fig. VI - 4 $\log_{10}(a(HCO_3^-)\ a(H^+))$ vs. $\log_{10}(a(Ca^{2+})/a(H^+)^2)$ predominance plot at [U(VI)] = 100 μmol kg_w^{-1}, $P(O_2)$ = 0.2095 atm and fixed values of $\log_{10}(a(Na^+)/a(H^+))$ = 5. The selected sample solutions having different major species are distinguished by color.

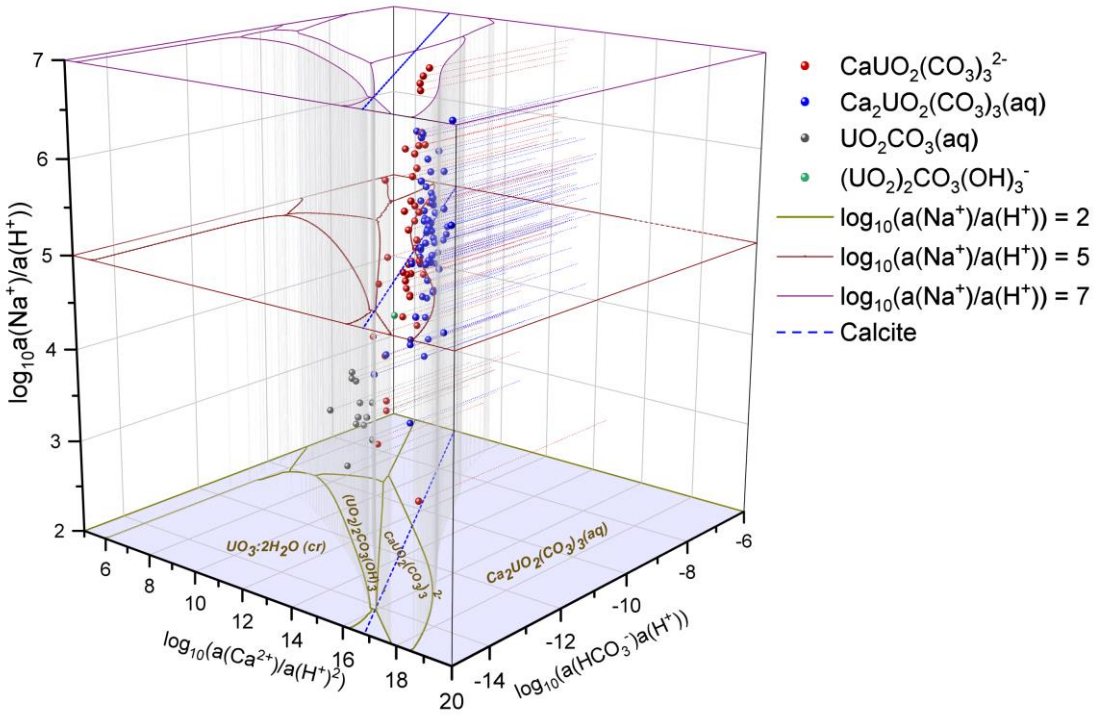

Fig. VI - 5 Repartition of the major species in the speciation calculations of the selected water compositions in a $\log_{10}(a(Ca^{2+})/a(H^+)^2)$-$\log_{10}(a(HCO_3^-)\ a(H^+))$-$\log_{10}(a(Na^+)/a(H^+))$ diagram. The values of $\log_{10}(a(Na^+)/a(H^+))$ were respectively fixed to 2, 5, and 7 to deduce the $\log_{10}(a(Ca^{2+})/a(H^+)^2)$–$\log_{10}(a(HCO_3^-)\ a(H^+))$ predominance diagrams of Ca-UO_2-CO_3 system at [U(VI)] = 100 μmol kg_w^{-1}, $P(O_2)$ = 0.2095 atm.

The water compositions are divided into groups according to their value of $\log_{10}(a(Na^+)/a(H^+))$ and separately presented in the diagram having the nearest value of $\log_{10}(a(Na^+)/a(H^+))$, as shown in Fig. VI - 6. $Ca_2UO_2(CO_3)_3(aq)$ can be identified in a large field at high $\log_{10}(a(HCO_3^-)\ a(H^+))$ and high $\log_{10}(a(Ca^{2+})/a(H^+)^2)$ in the predominance diagram with $\log_{10}(a(Na^+)/a(H^+))$ varying from 2 to 7. Actually, the variable $\log_{10}(a(Na^+)/a(H^+))$ partially reflects the ionic strength of the water samples as their pH values are comparable and sodium represents one of the major cations in these water samples. That is to say, there is close relationship between ionic strength and $\log_{10}(a(Na^+)/a(H^+))$ for the selected water solutions. It is worthy to point out that the dominant species calculated for several water samples do not strictly correspond to their position in the diagram because the predominance diagrams are calculated taking only NaCl as background electrolyte.

One can observe that the predominance regions of $UO_2(CO_3)_3^{4-}$ and $CaUO_2(CO_3)_3^{2-}$ enlarge with increasing $\log_{10}(a(Na^+)/a(H^+))$ as a result of increasing interionic attraction between Ca^{2+} and other major anions. When viewed as a function of $\log_{10}(a(Na^+)/a(H^+))$ in the predominance

diagram, the field of $Ca_2UO_2(CO_3)_3(aq)$ confined by the precipitation of calcite narrows with increasing $\log_{10}(a(Na^+)/a(H^+))$. Fig. VI - 6 (a) shows that nearly all water samples in the range $3.5 < \log_{10}(a(Na^+)/a(H^+)) < 4.5$ are under saturated with respect to calcite. Most of the selected water compositions are in the range of $4.5 < \log_{10}(a(Na^+)/a(H^+)) < 5.5$, as shown in Fig. VI - 6 (b). In particular, in the samples having $Ca_2UO_2(CO_3)_3(aq)$ as major species calcite is oversaturated or near to the saturation line, while those dominated by $CaUO_2(CO_3)_3^{2-}$ in the aqueous phase are under saturated, or slightly oversaturated, with respect to calcite. In the diagram where $\log_{10}(a(Na^+)/a(H^+)) = 6$, the region of $Ca_2UO_2(CO_3)_3(aq)$ is completely limited by the calcite precipitation. All the samples with predominant $Ca_2UO_2(CO_3)_3(aq)$ are oversaturated with respect to calcite and those with predominant $CaUO_2(CO_3)_3^{2-}$ are close to the saturation line. This observation reveals a key feature for this system: the $Ca_2UO_2(CO_3)_3(aq)$ complex is controlling the U(VI) speciation in the aqueous phase saturated with calcite depending on the value of $\log_{10}(a(Na^+)/a(H^+))$, or approximately on the ionic strength. It is worth noting that the samples with $UO_2CO_3(aq)$ as major species are filtered out in these predominance diagrams as their values $2.08 \leq \log_{10}(a(Na^+)/a(H^+)) \leq 3.38$ are too low to be represented.

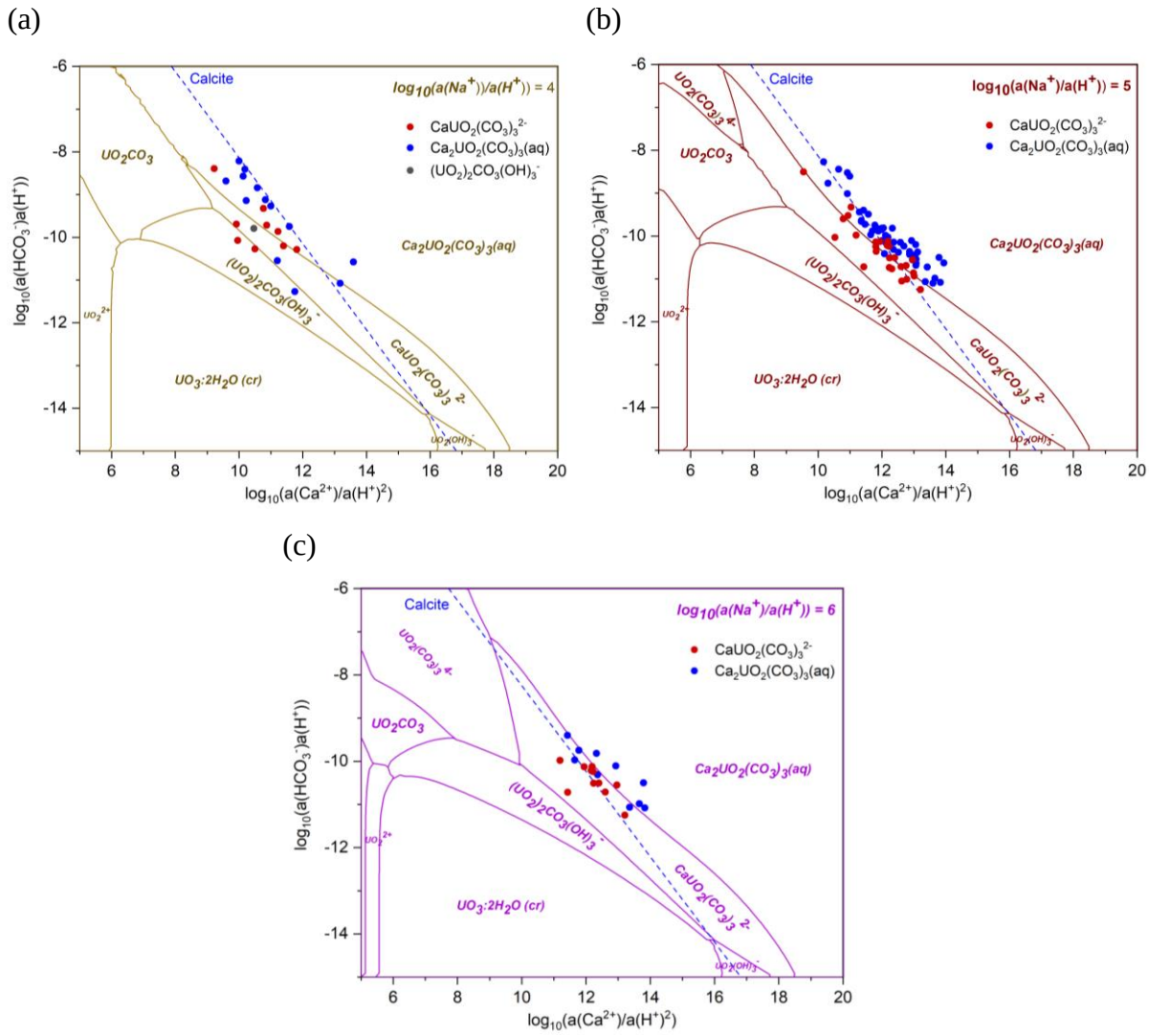

Fig. VI - 6 Major uranium species obtained in the speciation calculations of the selected water compositions of which (a) 3.5 < $log_{10}(a(Na^+)/a(H^+))$ < 4.5, (b) 4.5 < $log_{10}(a(Na^+)/a(H^+))$ < 5.5, and (c) 5.5 < $log_{10}(a(Na^+)/a(H^+))$ < 6.5.

Fig. VI - 7 focuses on the repartition of the selected water samples in a $log_{10}(a(Ca^{2+})/a(H^+)^2)$–$log_{10}(a(Na^+)/a(H^+))$–$log_{10}(a(HCO_3^-)\ a(H^+))$ diagram with the z-axis varying from -12 to -8. Most of the data points are in the range of -11 < $log_{10}(a(HCO_3^-)\ a(H^+))$ < -9.

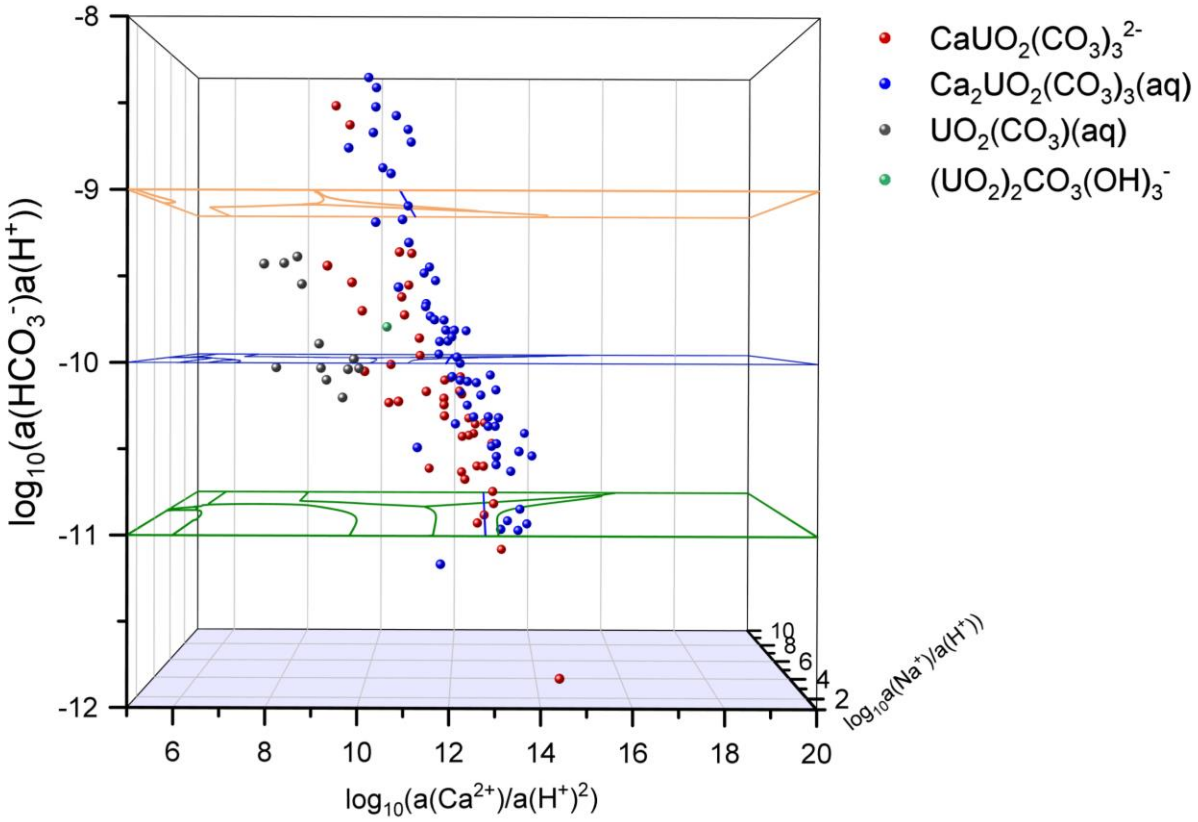

Fig. VI - 7 Repartition of the major species in the speciation calculations of the selected water compositions in a $log_{10}(a(Ca^{2+})/a(H^+)^2)$–$log_{10}(a(Na^+)/a(H^+))$–$log_{10}(a(HCO_3^-)\ a(H^+))$ diagram. The values of $log_{10}(a(HCO_3^-)\ a(H^+))$ were respectively fixed to -11, -10, -9 to deduce the $log_{10}(a(Ca^{2+})/a(H^+)^2)$–$log_{10}(a(Na^+)/a(H^+))$ predominance diagrams.

The diagrams of $log_{10}(a(Ca^{2+})/a(H^+)^2)$ *vs.* $log_{10}(a(Na^+)/a(H^+))$ with $log_{10}(a(HCO_3^-)\ a(H^+))$ = -11, -10.5, -10 and -9.5 were chosen for the representation in Fig. VI - 8. The data points were categorized based on their values of $log_{10}(a(HCO_3^-)\ a(H^+))$ and presented in the diagram having the nearest value of $log_{10}(a(HCO_3^-)\ a(H^+))$. The water sample symbols are contoured by black squares when calcite is under saturated in solution under their individual and specific conditions, and by red squares when the calcite is oversaturated in solution. Again, the saturation state with respect to calcite and the dominant species in several water samples during the calculation do not correspond to their position in the diagram because the predominance diagrams are constructed taking only NaCl as background electrolyte. Nonetheless, these particular samples are all near to the borderlines. Fig. VI - 8 again highlights the importance of calcite saturation in this system. At $log_{10}(a(HCO_3^-)\ a(H^+))$ = -11, the solution would easily be oversaturated with respect to calcite while high values of $log_{10}(a(HCO_3^-)\ a(H^+))$ promote the predominance of uranyl-carbonate complexes. The predominance of the binary/ternary complexes UO_2CO_3/$CaUO_2(CO_3)_3^{2-}$/$Ca_2UO_2(CO_3)_3(aq)$ depends on the activity of calcium

owing to the close pH values in the selected water samples. High concentration of calcium in system leads to the precipitation of calcite before having the $Ca_2UO_2(CO_3)_3(aq)$ as major species in the aqueous phase.

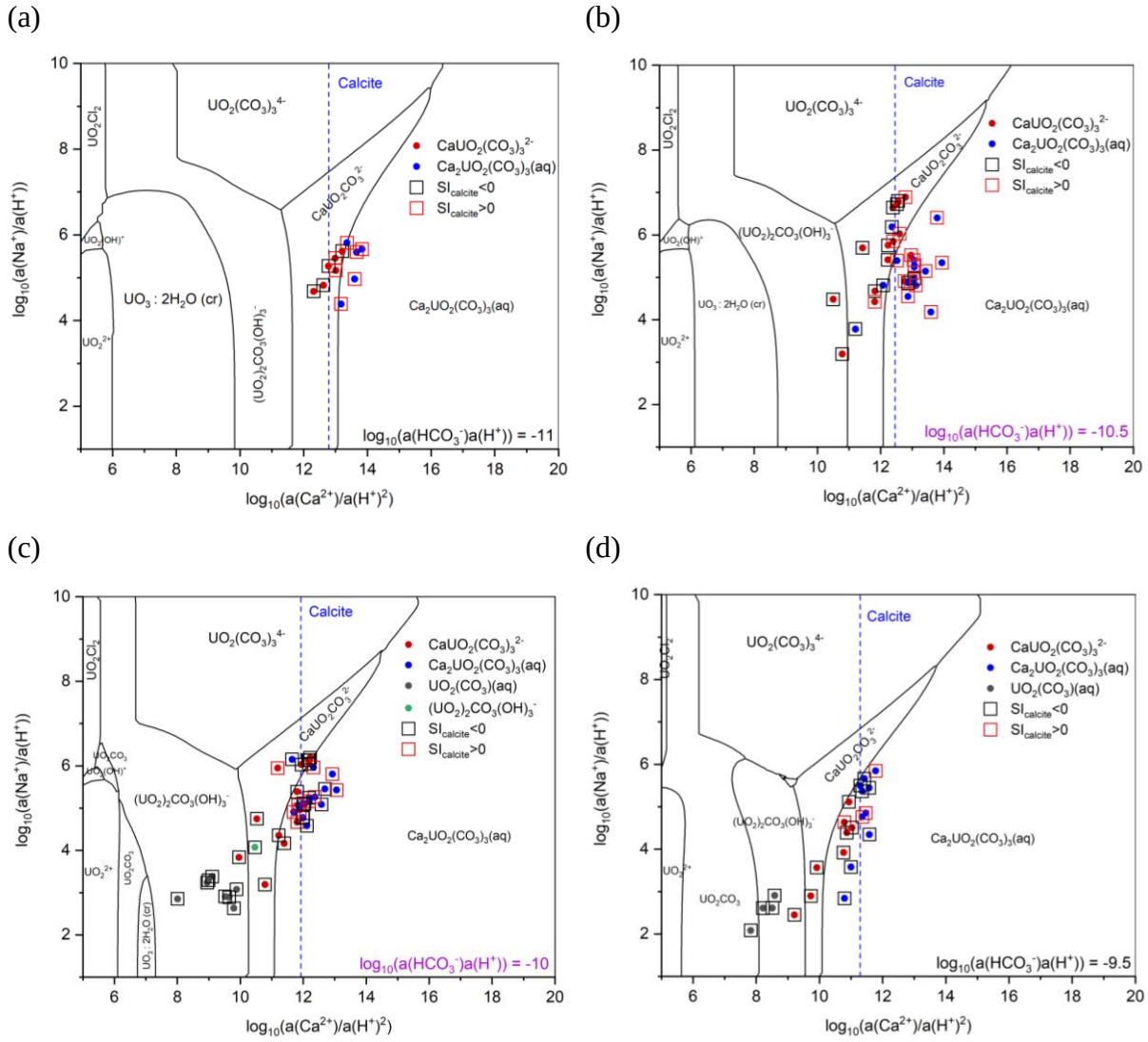

Fig. VI - 8 Major uranium species obtained in the speciation calculations of the selected water compositions in ranges of: (a) -11.5 < $log_{10}(a(HCO_3^-)\, a(H^+))$ < -10.5; (b) -11 < $log_{10}(a(HCO_3^-)\, a(H^+))$ < -10; (c) -10.5 < $log_{10}(a(HCO_3^-)\, a(H^+))$ < -9.5; and (d) -10 < $log_{10}(a(HCO_3^-)a(H^+))$ < -9.

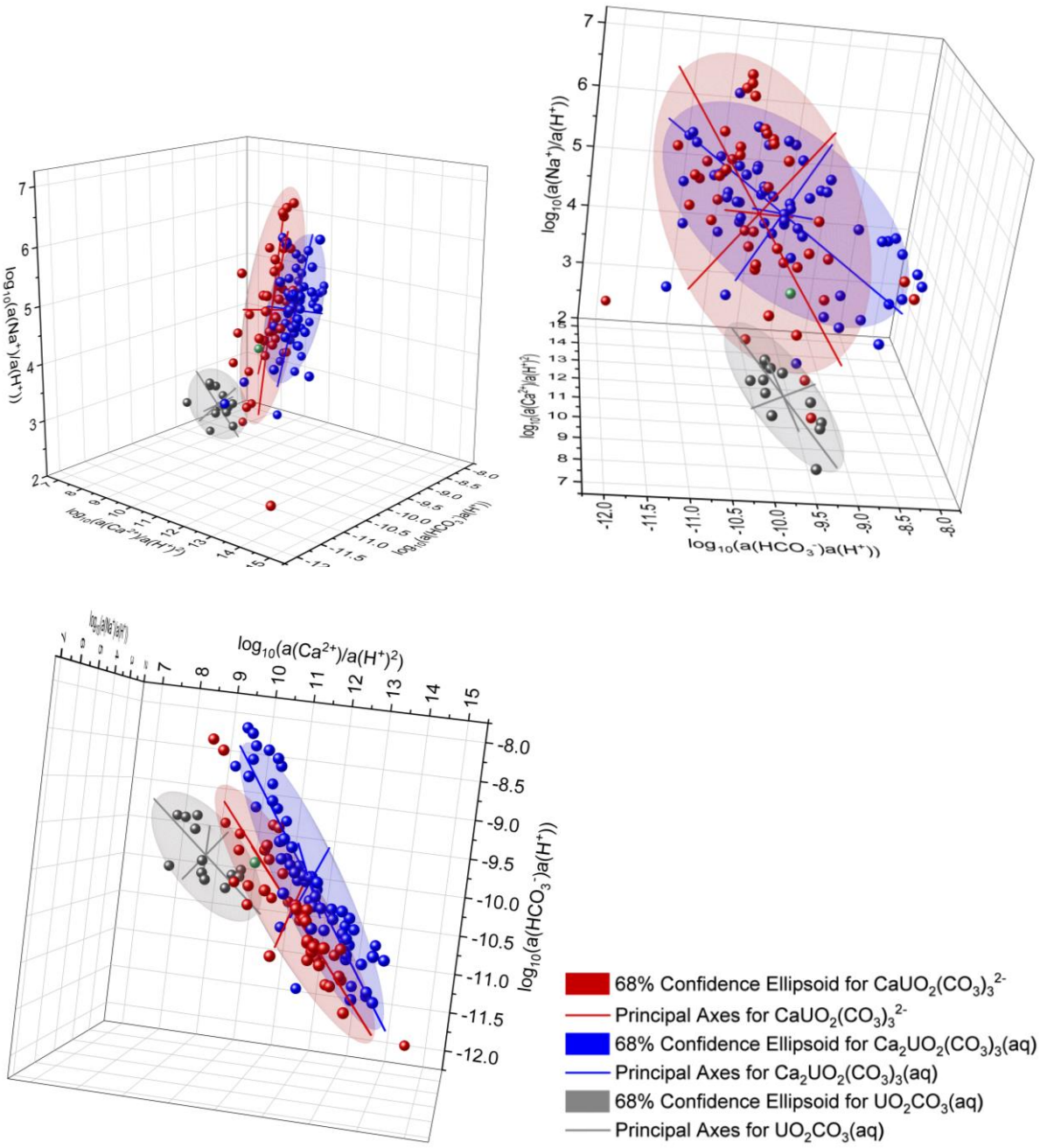

Fig. VI - 9 Ellipsoidal predominance regions of $UO_2CO_3(aq)$ (blue), $CaUO_2(CO_3)_3^{2-}$ (black), and $Ca_2UO_2(CO_3)_3(aq)$ (red) in $log_{10}(a(Ca^{2+})/a(H^+)^2)$–$log_{10}(a(Na^+)/a(H^+))$–$log_{10}(a(HCO_3^-)\,a(H^+))$ space determined from the sample point-clouds with the interval confidence of 68%. Viewings from three different angles.

The selected water solutions are colored according to their predominant species in Fig. VI - 8. For each group, an ellipsoid containing most of the data points belonging to that group is constructed using Hotelling's T-squared (T^2) distribution,* as shown in Fig. VI - 9. For this reason, the ellipsoidal boundaries of $UO_2CO_3(aq)$, $CaUO_2(CO_3)_3^{2-}$, and $Ca_2UO_2(CO_3)_3(aq)$

* https://www.originlab.com/fileExchange/details.aspx?fid=280

were determined from the distribution of sample points in $\log_{10}(a(Ca^{2+})/a(H^+)^2)$–$\log_{10}(a(Na^+)/a(H^+))$–$\log_{10}(a(HCO_3^-)\ a(H^+))$ diagram with the interval confidence of 68%, corresponding to 1σ. Using a higher confidence level, *i.e.* 95% or 98%, would generate wider ellipsoids, which tend to produce a larger intersection between the two ellipsoids of $CaUO_2(CO_3)_3^{2-}$ and $Ca_2UO_2(CO_3)_3(aq)$, thus a less clear distinction of their concentration domain.

To allow representation, Fig. VI - 9 illustrates the confidence ellipsoids for three species using 2D images in different view angles. One can note that the ellipsoid of $Ca_2UO_2(CO_3)_3(aq)$ is slightly narrower and more elongated then that of $CaUO_2(CO_3)_3^{2-}$. The overlap of the calculated ellipsoids of $CaUO_2(CO_3)_3^{2-}$, and $Ca_2UO_2(CO_3)_3(aq)$ can nearly extend to the half of their individual volumes. Furthermore, the ellipsoid of $Ca_2UO_2(CO_3)_3(aq)$ is located in the regions of higher calcium and carbonate concentrations compared with that of $CaUO_2(CO_3)_3^{2-}$, which is consistent with the evaluation of equilibrium constants. Regarding to the concentration region of $UO_2CO_3(aq)$, its ellipsoid exists at low $\log_{10}(a(Na^+)/a(H^+))$ and low $\log_{10}(a(Ca^{2+})/a(H^+)^2)$, underlining that the occurrence of major $UO_2CO_3(aq)$ in aqueous phase is due to an insufficient calcium concentration in solution of low ionic strength. Nevertheless, it is noteworthy that the pH value is also an important parameter as the samples with $UO_2CO_3(aq)$ as major species are all slightly acidic of pH value between 6 and 7, which is unfavorable to the formation of $CaUO_2(CO_3)_3^{2-}$, and $Ca_2UO_2(CO_3)_3(aq)$ especially at low calcium concentration.

VI - 6 Comparison of modelling and experimental results for the water samples collected from the Lodève site

6.1 Modelling

With the detailed chemical compositions for the "untreated" water and the acidified water sampled from the Lodève site (Table VI - 2), their uranium speciation calculations were performed using $\log_{10}\beta°$, $\Delta_f H_m°$ and SIT parameters ε for $(Mg/Ca)_nUO_2(CO_3)_3^{(4-2n)-}$ complexes implemented in the input file for PhreeqC and using Thermochimie 9b database. The percentages of major uranium carbonate species, the activity of important ions as well as the values of $\log_{10}(a(Ca^{2+})/a(H^+)^2)$, $\log_{10}(a(Na^+)/a(H^+))$, and $\log_{10}(a(HCO_3^-)\ a(H^+))$ are listed in Table VI - 3. As displayed in Fig. VI - 10, the position of the investigated samples are well included in the previously determined ellipsoids for $CaUO_2(CO_3)_3^{2-}$ (black) and $Ca_2UO_2(CO_3)_3(aq)$ (red). As with the "untreated" water sample, the black point is actually

located in the overlap between ellipsoids of $CaUO_2(CO_3)_3^{2-}$ (black) and $Ca_2UO_2(CO_3)_3(aq)$ (red), indicating that the dominant species cannot be unambiguously assigned without thermodynamic calculation. One can observe that the red point representing the acidified water is solely included in the ellipsoids of $Ca_2UO_2(CO_3)_3(aq)$ (red), suggesting a predominance of $Ca_2UO_2(CO_3)_3(aq)$ in aqueous solution. According to the thermodynamic modelling, $CaUO_2(CO_3)_3^{2-}$ is expected to be the most abundant species in "untreated" water with percentage of 50.6%, while $Ca_2UO_2(CO_3)_3(aq)$ is the principal species in the acidified water with percentage of 50.8% (Table VI - 3). It is shown that the verification of dominant complexes for the Lodève samples corroborates the results of the speciation calculation. One can conclude that the determination of ellipsoids for $Ca_nUO_2(CO_3)_3^{(4-2n)-}$ complexes is a suitable tool for quickly identifying the major (calcium) uranyl carbonate species for a given natural water sample once its chemical composition is available. In a later stage, the calculation results will be compared with the uranium speciation identified by the TRLFS analyses.

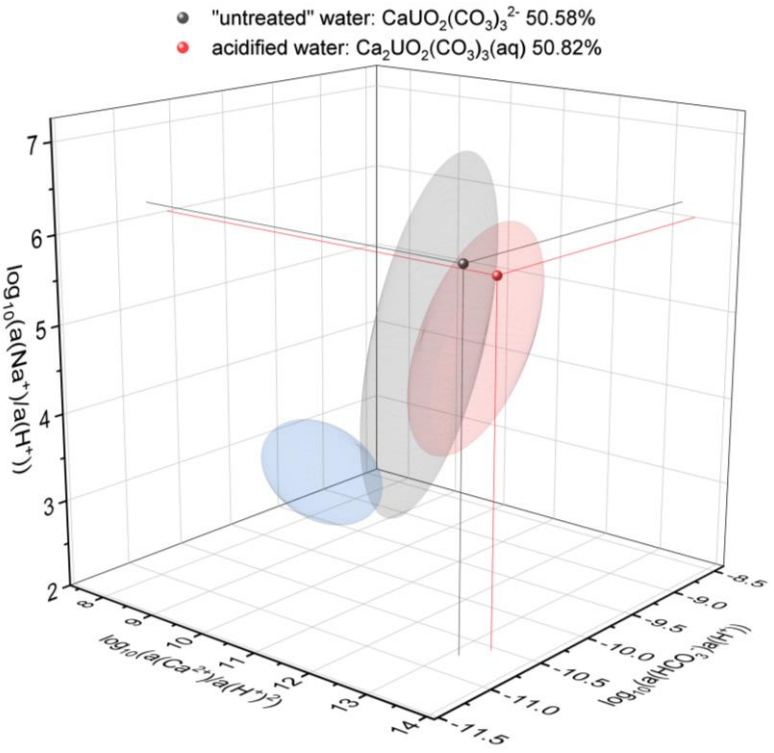

Fig. VI - 10 Position of the two Lodève water samples in a $log_{10}(a(Ca^{2+})/a(H^+)^2)$–$log_{10}(a(Na^+)/a(H^+))$–$log_{10}(a(HCO_3^-)\,a(H^+))$ diagram. Ellipsoidal predominance regions of $UO_2CO_3(aq)$ (blue), $CaUO_2(CO_3)_3^{2-}$ (black), and $Ca_2UO_2(CO_3)_3(aq)$ (red) space determined from the sample point-clouds with the interval confidence of 68%.

Table VI - 3 Percentages of major uranium carbonate species and the activity of important ions

Samples	**"untreated" water**	**acidified water at pH 6.5**
$CaUO_2(CO_3)_3^{2-}$	50.6%	41.6%
$MgUO_2(CO_3)_3^{2-}$	26.1%	6.7%
$Ca_2UO_2(CO_3)_3(aq)$	19.7%	50.8%
$UO_2(CO_3)_3^{4-}$	3.5%	0.9%
Total	99.89%	99.97%
lg $P(CO_2(g))$	-2.92	-2.73
lg $a(Ca^{2+})$	-3.446	-2.946
lg $a(Mg^{2+})$	-2.934	-2.941
lg $a(HCO_3^-)$	-2.44	-2.386
lg $a(Na^+)$	-2.15	-2.164
lg $a(H^+)$	-8.3	-8.16
lg $a(Ca^{2+})$ - 2 lg $a(H^+)$	13.15	13.37
lg $a(Mg^{2+})$ - 2 lg $a(H^+)$	13.67	13.38
n = $a(Ca^{2+})/(a(Ca^{2+}) + a(Mg^{2+}))$	0.76	0.50
nlg $a(Mg^{2+})$ + (1-n) lg $a(Ca^{2+})$ - 2 lg $a(H^+)$	13.55	13.38
lg $a(HCO_3^-)$ + lg $a(H^+)$	-10.74	-10.55
lg $a(Na^+)$ - lg $a(H^+)$	6.15	6.00
I (mol kg_w^{-1})	0.022	0.027

6.2 TRLFS measurement

TRLFS can be a useful technique to elucidate the speciation of uranium in water because of the very low detection limits, a high sensitivity with respect to U(VI) complex, and its triple selectivity — *i.e.*, selectivity in excitation wavelength, emission spectrum, and time-resolved acquisition. In general, TRLFS provides two important spectroscopic information: characteristic luminescence decay time and positions of the emission maxima. In a fingerprinting procedure, the recorded TRLFS spectra can be identified with the help of previously acquired reference complexes. In the preceding chapters, we have obtained these primary spectroscopic information for $(Mg/Ca)_nUO_2(CO_3)_3^{(4-2n)-}$ complexes under varying conditions — type of electrolyte, ionic strength and temperature — that will be compared with the recorded spectra of Lodève water samples.

As previously described, the acquisition were completed with a 355 nm tripled Nd:YAG laser (Surelite, Continiuum, USA) delivering about 170 mJ of energy, pulsed at 10 Hz with 5 ns pulse. An optical parametric oscillator system (Horizon, Continiuum, USA) is set at λ_{ex} = 450 nm. At this excitation wavelength, the luminescence quantum yield for uranium(VI) is favourable. The fluorescence signal is focused into a monochromator spectrometer (Acton) using a 300 lines mm^{-1} grating. Emission spectra are recorded as a function of gate delay *D*

≥ 25 ns, minimum for preventing the Raman scatter peak of H_2O, at the fixed gate width W = 1 µs.

The two natural occurring water samples in Lodève both delivered a measurable luminescence signal, which is characteristic for uranyl carbonate luminescence. Fig. VI - 11 (a) shows the emission spectra normalized to their total area for each sample with initial delay time of D =25 ns during the gate width W = 1 µs, in comparison with a reference solution of known composition in which U(VI) principally exists in the form of $Ca_nUO_2(CO_3)_3^{(4-2n)-}$ complexes. Hypsochromic-shifted peak positions compared with those of uranyl ions (470.07, 487.31, 509.31, 533.38 and 559.86 nm) in acidic conditions provide evidence for formation of uranyl carbonate complexes in aqueous solution. The characteristic peak positions are the same with the reference solution. Nevertheless, the water from the sample site represents an obvious distortion in the spectrum. This distortion does not seem to be identical for the two water samples: the adjustment to the value of pH 6.5 seems to have a slight influence on the initial spectrum. An acquisition of the same solutions was also made at a longer delay time (D = 100 ns), in order to verify whether the distortion is due to the luminescence of another U(VI) complex having a different decay time. As illustrated in Fig. VI - 11 (b), the luminescence spectra of the two water samples with D = 100 ns are identical to that of $Ca_nUO_2(CO_3)_3^{(4-2n)-}$ complexes. It is therefore possible to hypothesize that two decay functions of U(VI) are involved in the water samples: a fast decay function not yet identifiable and a slow decay function of which the spectrum is characteristic of $Ca_nUO_2(CO_3)_3^{(4-2n)-}$ complexes.

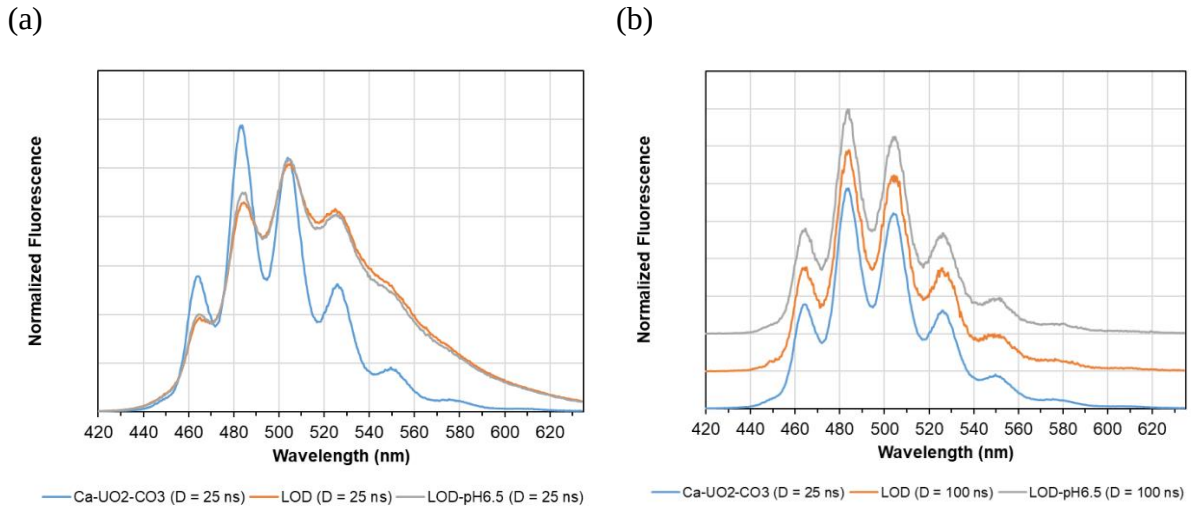

Fig. VI - 11 Comparison of luminescence spectra of uranium in a known solution (blue), in the "untreated" water sample (orange) and in the adjusted water at pH 6.5 (grey) from the Lodève site. (a) initial delay time of D = 25 ns and gate width W = 1 µs (b) initial delay time of D =100 ns and gate width W = 1 µs.

The luminescence decay of the "untreated" water sample was acquired by recording the luminescence spectra as a function of delay time. Fig. VI - 12 (a) shows the spectra normalized to the same area for the delay time ranging from 20 to 215 ns in steps of 5 ns with gate width W = 50 ns, which is more favourable to distinguish the spectra of different species. Fig. VI - 12 (b) shows the exponential fits of integrated time-resolved luminescence intensities in the wavelength range from 420 to 635 nm using the trapezoid method. A mono-exponential luminescence decay (dashed curve in Fig. VI - 12 (b)) is clearly not satisfactory to describe the decay process with τ = (31 ± 1) ns, while a bi-exponential function can better fit the luminescence decay curves with τ_1 = (11 ± 1) ns (dotted curve) and τ_2 = (38 ± 1) ns (dash-dot curve).

(a) (b)

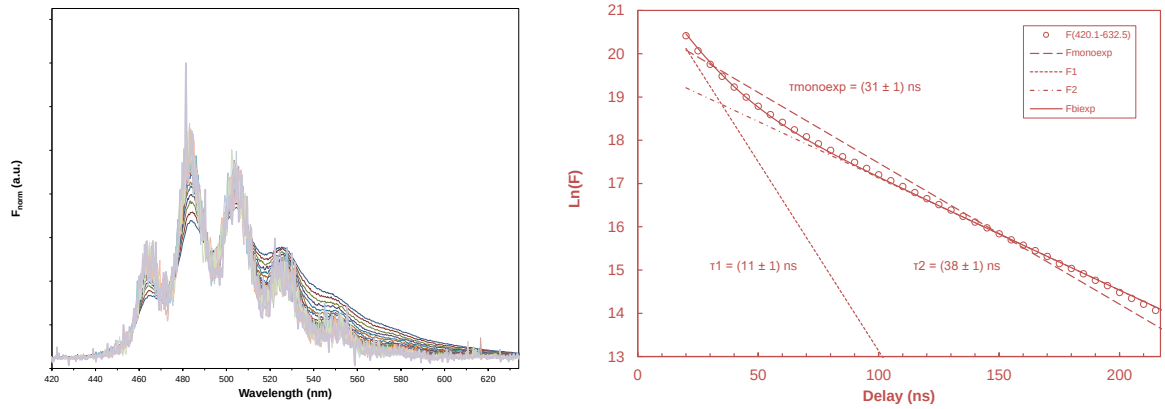

Fig. VI - 12 (a) Normalized luminescence spectra of uranium at varying delay time for the "untreated" water from the Lodève site (b) Mono-exponential and bi-exponential fits of luminescence intensity decay between 420 and 635 nm

The bi-exponential decay of the TRLFS-signals for the "untreated" water sample revealed that either two luminescent species were observed, or the rate of de-excitation process is slower than that of ligand exchange. However, for such complicated fluorophores, luminescence decay behaviour cannot be simply settled. With the determined parameters in bi-exponential function, it is possible to estimate the spectral contributions of the individual species, *e.g.*, the second component contributes 29% at D = 20 ns, and 98% at D = 100 ns and the first component represents 71% of the luminescent signal at D = 20 ns. This allows the spectral decomposition of the experimental spectrum at D = 20 ns, as shown in Fig. VI - 13.

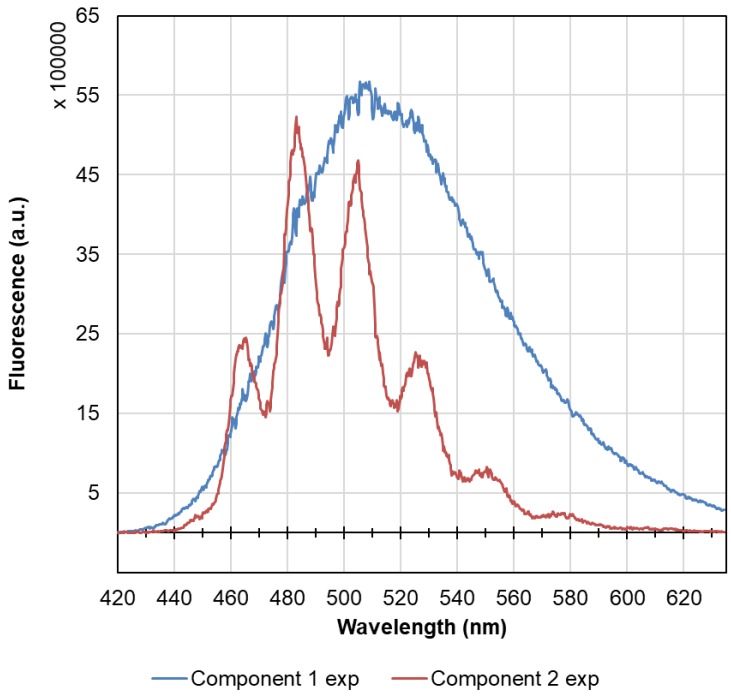

Fig. VI - 13 Decomposition of uranium luminescence signal as a function of delay time in acquisition for the "untreated" water from the Lodève site

In experiments, we observed that the luminescence spectra for the same water sample under identical measurement conditions have undergone evident spectral modification after long time laser excitation, as shown in Fig. VI - 14. It is well known that the dissolved organic matter present in natural waters can impair the detection of total uranium because of the complexation of organic species, such as humic substances, with uranyl ion. Furthermore, one can expect luminescence emission of these ligands if they contain delocalized p-electron system, like in aromatic compounds.[41] The previous determination of decay times using bi-exponential fits (Fig. VI - 12) implies the possible existence of organic ligands in the aqueous system due to the very short decay time of $\tau_1 = (11 \pm 1)$ ns.

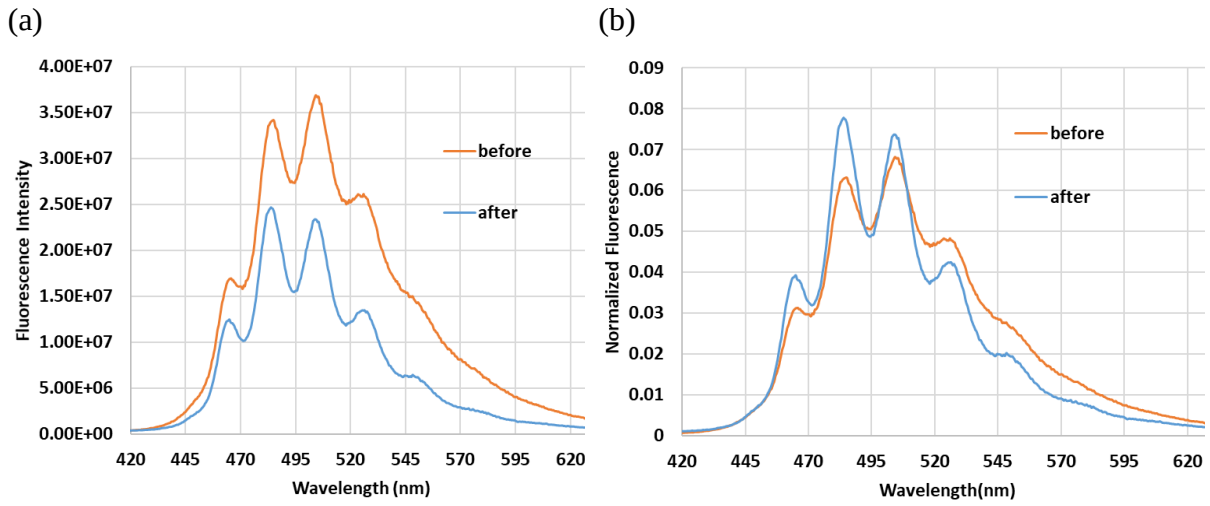

Fig. VI - 14 Comparison of (a) luminescence spectra of uranium in the "untreated" water sample from the Lodève site at 25°C with delay time of D *= 15 ns and gate width W = 50 ns before and after long period (≈5h) laser excitation of 450 nm. (b) Normalized spectra to the same area.*

A set of luminescence decays was recorded for the longtime-excited Lodève water sample at 25°C. As shown in the fitting results in the Fig. VI - 15, the luminescence decays bi-exponentially within the delay range studied. The equation: Intensity = $A_1\exp(-x/tau_1)$ + $A_2\exp(-x/tau_2)$ + y_0 was applied in the fitting procedure where A_1, A_2 represent the luminescence intensity of components 1 and 2 at D = 0, tau_1, tau_2 (also τ_1, τ_2) correspond to their decay times and y_0 is an adjustable noise term.

One can note that long period laser excitation at 25°C causes a decrease in the luminescence intensity for the first minor luminescent component 1 with τ_1 = (11 ± 1) ns from A_1 = 7.32 10^9 to 2.49 10^9 while little changes in other parameters, *i.e.* A_2, tau_1, tau_2 were observed. Our results suggest that the first minor luminescent component was photolysed due to the laser excitation with static quenching patterns since its decay time did not change. Additionally, UV/Vis absorption spectra of the Lodève water samples were collected from 200 nm to 400 nm in order to detect any changes of potentially degraded organic components after laser excitation. As seen in Fig. VI-16, the absorption spectra for the original Lodève water and the water samples subjected to long period laser excitation of 450 nm at 25 and 50°C exhibit subtle differences that are impossible to distinguish using peak decomposition because the values of peak parameters are approximately identical for different spectra taking into account the interval uncertainties. Further information on the first minor luminescent complex is difficult to obtain.

(a)

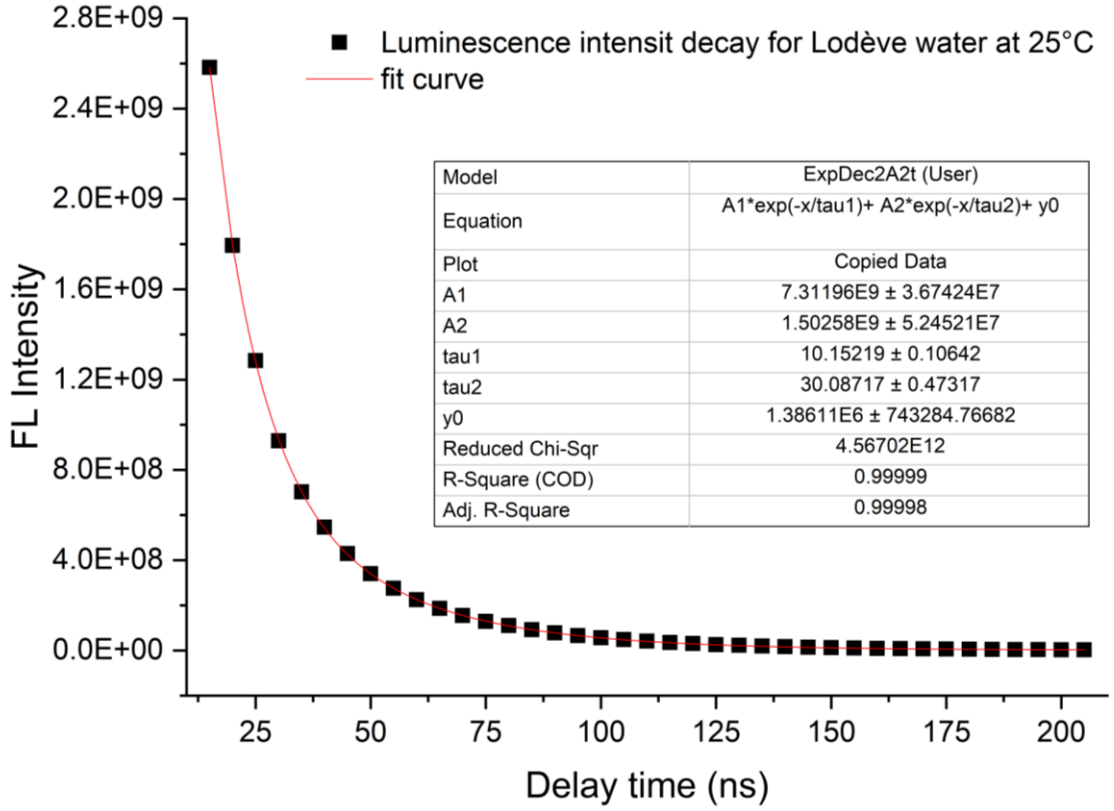

Model	ExpDec2A2t (User)
Equation	A1*exp(-x/tau1)+ A2*exp(-x/tau2)+ y0
Plot	Copied Data
A1	7.31196E9 ± 3.67424E7
A2	1.50258E9 ± 5.24521E7
tau1	10.15219 ± 0.10642
tau2	30.08717 ± 0.47317
y0	1.38611E6 ± 743284.76682
Reduced Chi-Sqr	4.56702E12
R-Square (COD)	0.99999
Adj. R-Square	0.99998

(b)

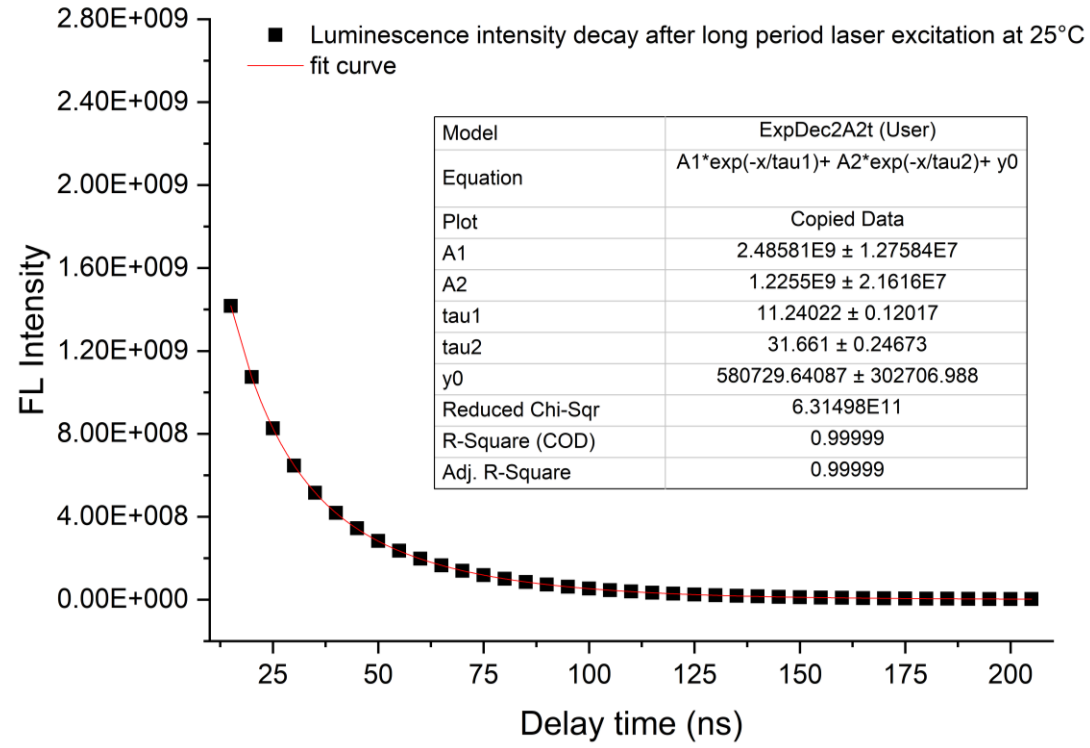

Model	ExpDec2A2t (User)
Equation	A1*exp(-x/tau1)+ A2*exp(-x/tau2)+ y0
Plot	Copied Data
A1	2.48581E9 ± 1.27584E7
A2	1.2255E9 ± 2.1616E7
tau1	11.24022 ± 0.12017
tau2	31.661 ± 0.24673
y0	580729.64087 ± 302706.988
Reduced Chi-Sqr	6.31498E11
R-Square (COD)	0.99999
Adj. R-Square	0.99999

Fig. VI - 15 Bi-exponential fits of luminescence intensity decay from D = 15 ns to 210 ns for Lodève water (a) before and (b) after long period laser excitation of 450 nm

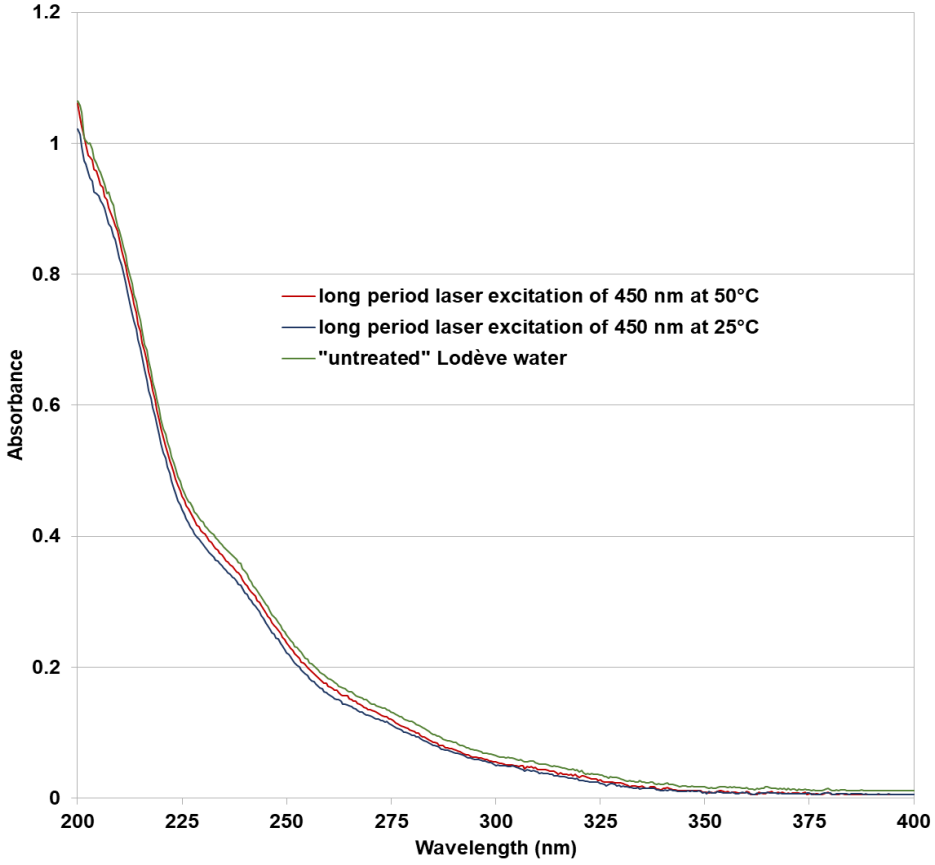

Fig. VI - 16 UV/Vis absorption of "untreated" water samples from the Lodève site in the rage 200 to 400 nm. Green: original Lodève water exempt from interruption of temperature and laser excitation. Blue: water sample subjected to long period (≈ 5h) laser excitation of 450 nm at 25°C. Red: water sample subjected to long period (≈ 5h) laser excitation of 450 nm at 50°C

Despite that the band positions of the second component correspond most likely to the $Ca_nUO_2(CO_3)_3^{(4-2n)-}$ complexes, the longer lifetime of τ_2 = (38 ± 1) ns from the investigated "untreated" water sample cannot be directly assigned to either $CaUO_2(CO_3)_3^{2-}$ or $Ca_2UO_2(CO_3)_3(aq)$. Moreover, distinguishing the $Ca_nUO_2(CO_3)_3^{(4-2n)-}$ complexes based on the band positions is always difficult because of their very similar positions of main emission bands, thus the assignment by characteristic decay time is more tenable. The value of τ_2 is present in the interval of decay times measured for $CaUO_2(CO_3)_3^{2-}$ ($\tau \approx 28$ ns) and $Ca_2UO_2(CO_3)_3(aq)$ ($\tau \approx 48$ ns) at I_m = 0.1 mol kg_w^{-1} NaCl.[42] One should note that the decay time of luminescent species is related to the presence of luminescence quenchers in different concentration ratios. Due to quenching effects of chloride, it is reasonable to suppose that $CaUO_2(CO_3)_3^{2-}$ should have a longer decay time ($\tau > 28$ ns) in natural and diluted medium, such as in the "untreated" water sample of I_m = 0.022 mol kg_w^{-1}. Therefore, the second lifetime observed for the "untreated" water sample approaches the characteristic lifetime of $CaUO_2(CO_3)_3^{2-}$, indicating a predominance of this species in aqueous solution. The thermodynamic modelling with detailed

chemical compositions convincingly verifies this conclusion as 50.6% uranium exists in the form of $CaUO_2(CO_3)_3^{2-}$ in the "untreated" water sample.

VI - 7 Interim conclusion

This chapter examines the speciation calculation of uranium in actual situations covering radioactive waste management (RWM), uranium mining activity, and other natural water samples with the previously determined thermodynamic data for $(Mg/Ca)_nUO_2(CO_3)_3^{(4-2n)-}$ complexes in this study implemented in ThermoChimie 9b database. It further represents a comprehensive and the most updated thermodynamic dataset, including the formation constants at infinite dilution $\log_{10}\beta°$, the thermodynamic functions $\Delta_fH_m°$ and SIT parameters — specific ion interaction coefficients ε for $(Mg/Ca)_nUO_2(CO_3)_3^{(4-2n)-}$ complexes —, which can be applied in geochemical calculations covering a wide range of conditions relevant to nuclear waste disposal. Compared with previous thermodynamic modelling executed with the old data in literature, data gaps can be identified in this study concerning the assessment of U(VI) chemistry under high ionic strength or high temperature as those expected in disposal environment and deserve further attention.

Based on the repartition of major uranium species obtained in the speciation calculations for the selected water compositions, three ellipsoidal predominance regions of $Ca_nUO_2(CO_3)_3^{(4-2n)-}$ complexes were constructed from the sample point-clouds in $\log_{10}(a(Ca^{2+})/a(H^+)^2)$–$\log_{10}(a(Na^+)/a(H^+))$–$\log_{10}(a(HCO_3^-)\,a(H^+))$ three-dimension space. The determination of ellipsoids for $(Ca_n)UO_2(CO_3)_3^{(4-2n)-}$ complexes allows a quick identification of the major (calcium) uranyl carbonate species for a given natural water sample once its chemical composition is available. Thermodynamic calculations and TRLFS analyses were performed for two water samples collected from the Lodève site. The calculated dominant species corroborates well the experimental observations in terms of important luminescence characteristics: band positions and decay time. The measured luminescent properties for $(Mg/Ca)_nUO_2(CO_3)_3^{(4-2n)-}$ complexes under different conditions — type of electrolyte, ionic strength, and temperature — detailed in preceding chapters and partly verified by the in-situ samples, surely enrich the reference catalog of Mg/Ca-UO_2-CO_3 luminescence spectral fingerprints.

VI - 8 References

1. P. E. Reiller and M. Descostes, *Chemosphere*, 2020, **251**, 126301.
2. W. Dong and S. C. Brooks, *Environ. Sci. Technol.*, 2006, **40**, 4689-4695.

3. W. Dong and S. C. Brooks, *Environ. Sci. Technol.*, 2008, **42**, 1979-1983.
4. M. de Craen, L. Wang, M. Van Geet and H. Moors, *Geochemistry of Boom Clay pore water at the Mol site*, Report SCK•CEN-BLG-990, SCK•CEN, Mol, Belgium, 2004. http://jongeren.sckcen.be/~/media/Files/Science/disposal_radioactive_waste/Geochemistry_of_Boom_Clay_pore_Status_2004.pdf
5. E. C. Gaucher, C. Tournassat, F. J. Pearson, P. Blanc, C. Crouzet, C. Lerouge and S. Altmann, *Geochim. Cosmochim. Acta*, 2009, **73**, 6470-6487.
6. C. Beaucaire, J. L. Michelot, S. Savoye and J. Cabrera, *Appl. Geochem.*, 2008, **23**, 2182-2197.
7. A. Courdouan Merz, Nature and Reactivity of Dissolved Organic Matter in Clay Formations Evaluated for the Storage of Radioactive Waste, ETH Zürich, 2008.
8. M. F. Thury and P. J. Bossart, *Mont Terri Rock Laboratory: Results of the Hydrogeological, Geochemical and Geotechnical Experiments Performed in 1996 and 1997*, Report Rapport Géologique Nr. 23, Swiss National Hydrological and Geological Survey, Bern, Switzerland, 1999. http://www.mont-terri.ch/content/mont-terri-internet/en/documentation/publications-from-swisstopo.download/mont-terri-internet/en/publications/publications-swisstopo/GBD-23.pdf
9. A. T. Emrén, R. Arthur, P. D. Glynn and J. McMurry, *MRS Proceedings*, 2011, **556**, 559.
10. E. L. Tullborg, J. Suksi, G. Geipel, L. Krall, L. Auque, M. Gimeno and I. Puigdomènech, *Proced. Earth Plan. Sci.*, 2017, **17**, 440-443.
11. M. Laaksoharju, J. Smellie, E.-L. Tullborg, M. Gimeno, L. Hallbeck, J. Molinero and N. Waber, *Bedrock hydrogeochemistry Forsmark. Site descriptive modelling SDM-Site Forsmark*, Sweden, 2008. http://www.osti.gov/etdeweb/servlets/purl/951442
12. M. Alkinani, W. Kanoua and B. Merkel, *Environ. Earth. Sci.*, 2016, **75**, 869.
13. C. Beaucaire and P. Toulhoat, *Appl. Geochem.*, 1987, **2**, 417-426.
14. P. Toulhoat and C. Beaucaire, *Can. J. Earth Sci.*, 1993, **30**, 754-763.
15. I. Gurban, M. Laaksoharju, B. Madé and E. Ledoux, *J. Contam. Hydrol.*, 2003, **61**, 247-264.
16. J. Salas and C. Ayora, *J. Contam. Hydrol.*, 2004, **69**, 115-137.
17. O. Prat, T. Vercouter, E. Ansoborlo, P. Fichet, P. Perret, P. Kurttio and L. Salonen, *Environ. Sci. Technol.*, 2009, **43**, 3941-3946.
18. M. Yamamoto, J. Tomita, A. Sakaguchi, Y. Ohtsuka, M. Hoshi and K. N. Apsalikov, *J. Radioanal. Nucl. Chem.*, 2010, **284**, 309-314.
19. J. F. Ranville, M. J. Hendry, T. N. Reszat, Q. L. Xie and B. D. Honeyman, *J. Contam. Hydrol.*, 2007, **91**, 233-246.
20. M. J. Hendry and L. I. Wassenaar, *Water Resour. Res.*, 2000, **36**, 503-513.
21. K. von Gunten, T. Warchola, M. W. Donner, M. Cossio, W. Hao, C. Boothman, J. Lloyd, T. Siddique, C. A. Partin, S. L. Lloyd, A. Rosaasen, K. O. Konhauser and D. S. Alessi, *Can. J. Earth Sci.*, 2018, **55**, 463-474.
22. L. Stetten, A. Mangeret, J. Brest, M. Seder-Colomina, P. Le Pape, M. Ikogou, N. Zeyen, A. Thouvenot, A. Julien, G. Alcalde, J. L. Reyss, B. Bombled, C. Rabouille, L. Olivi, O. Proux, C. Cazala and G. Morin, *Geochim. Cosmochim. Acta*, 2018, **222**, 171-186.
23. M. Maloubier, P. L. Solari, P. Moisy, M. Monfort, C. Den Auwer and C. Moulin, *Dalton Trans.*, 2015, **44**, 5417-5427.
24. F. J. Millero, R. Feistel, D. G. Wright and T. J. McDougall, *Deep-Sea Res. Pt. I*, 2008, **55**, 50-72.
25. J. E. Lartigue, B. Charrasse, B. Reile and M. Descostes, *Chemosphere*, 2020, **251**, 126302.
26. D. K. Todd and L. W. Mays, *Groundwater Hydrology*, Wiley, Hoboken, NJ, 3rd edn., 2005.

27. J. K. Osmond, J. B. Cowart and M. Ivanovich, *The International Journal of Applied Radiation and Isotopes*, 1983, **34**, 283-308.
28. W. De Vos, T. Tarvainen, R. Salminen, S. Reeder, B. De Vivo and A. Demetriades, *FOREGS Geochemical Atlas of Europe, Part 2: Interpretation of Geochemical Maps, Additional Tables, Figures, Maps, and Related Publications*, Espoo: Geological Survey of Finland, 2005.
29. B. Bonin and P. L. Blanc, L'uranium dans le milieu naturel, des origines jusqu'à la mine, in *L'Uranium, de l'Environnement à l'Homme*, ed. H. Métivier, EDP Science, Les Ulis, France, 2001, p. 340.
30. J. Garnier-Laplace, C. Colle and M. Morello, *Natural Uranium and the Environment*, Institut de Radioprotection et de Süreté Nucléaire, 2010. http://www.irsn.fr/EN/Research/publications-documentation/radionuclides-sheets/environment/Documents/Uranium_UK.pdf
31. I. Salpeteur and J.-M. Angel, *Environnement, Risques & Santé*, 2010, **9**, 121-135.
32. P. F. Fix, *U.S. Geological Survey Professional Paper* 1956, **300**, 667-672.
33. D. L. Parkhurst and C. A. J. Appelo, *User's Guide to PHREEQC (Version 2) — A Computer Program for Speciation, Batch-Reaction, One-Dimensional Transport, and Inverse Geochemical Calculations*, Report 99-4259, U.S. Geological Survey, Water-Resources Investigations, Lakewood, Colorado, USA, 1999. http://wwwbrr.cr.usgs.gov/projects/GWC_coupled/phreeqci/
34. D. L. Parkhurst and C. A. J. Appelo, *Description of Input and Examples for PHREEQC Version 3 — A Computer Program for Speciation, Batch-Reaction, One-Dimensional Transport, and Inverse Geochemical Calculations. Chapter 43 of Section A, Groundwater Book 6, Modeling Techniques*, U.S. Geological Survey, Denver, Colorado, USA, 2013. http://pubs.usgs.gov/tm/06/a43/pdf/tm6-A43.pdf
35. D. G. Kinniburgh and D. M. Cooper, *Environ. Sci. Technol.*, 2004, **38**, 3641-3648.
36. D. G. Kinniburgh and D. M. Cooper, *PhreePlot: Creating Graphical output with PHREEQC*, http://www.phreeplot.org, 2011.
37. Thermochimie, http://www.thermochimie-tdb.com/.
38. WHO, *Guidelines for drinking-water quality: fourth edition incorporating first addendum*, World Health Organization, Geneva, 2017.
39. IAEA, *Manual of Acid in Situ Leach Uranium Mining Technology*, IAEA, Vienna, Austria, 2001. http://www-pub.iaea.org/MTCD/Publications/PDF/P1741_web.pdf
40. IAEA, *Situ Leach Uranium Mining: an Overview of Operations*, IAEA, Vienna, Austria, 2016. http://www-pub.iaea.org/MTCD/Publications/PDF/P1741_web.pdf
41. G. Geipel, M. Acker, D. Vulpius, G. Bernhard, H. Nitsche and T. Fanghanel, *Spectrochim. Acta, Part. A*, 2004, **60**, 417-424.
42. C. Shang and P. E. Reiller, *Dalton Trans.*, 2020, **49**, 466-481.

Chapter VII. General Conclusions

VII - 1 Determination of $\log_{10}\beta°$ and ε for $Ca_nUO_2(CO_3)_3^{(4-2n)-}$ complexes in NaCl

The detection of luminescence signal for uranyl carbonate complexes by TRLS was successful in the first investigation at room temperature, regardless of the quenching effect of carbonates. Hypsochromic-shifted peak positions compared with those of uranyl ions in acidic conditions provided evidence for the inner-sphere substitution of carbonate groups for water molecules. The complexation of calcium with uranyl carbonate moiety was then studied by titration of calcium at varying pH values where the Ringböm coefficients were introduced to describe the variation of $UO_2(CO_3)_3^{4-}$ relative to pH and $CO_2(g)$. The degree of complexation was estimated by the variation of fluorescence intensity as a function of the free Ca^{2+} concentration. By these means, the stoichiometry of ternary species was identified by the slope analysis, which provided an approach to investigate separately their properties.

Due to the noticeable quenching effects of chloride ions, the upper limit of aqueous electrolyte concentration was imposed to 1 mol kg_w^{-1} NaCl. The characteristic luminescent properties—spectrum and decay time—were recorded for all the prepared samples at each investigated ionic strength. It was observed that successive complexation of Ca^{2+} with $UO_2(CO_3)_3^{4-}$ resulted in gradually enhanced fluorescence intensity, better-resolved spectrum, and slower luminescence decay-time. In addition, the luminescence spectra were strikingly similar for $CaUO_2(CO_3)_3^{2-}$ and $Ca_2UO_2(CO_3)_3(aq)$, except slightly narrowed peak widths for $Ca_2UO_2(CO_3)_3(aq)$. The distinctive differences between $CaUO_2(CO_3)_3^{2-}$ and $Ca_2UO_2(CO_3)_3(aq)$ were from their decay times. It was assessed that in 0.1 mol kg_w^{-1} NaCl medium, $CaUO_2(CO_3)_3^{2-}$ was showing a fast decay-time of $\tau(CaUO_2(CO_3)_3^{2-}) = (28.30 \pm 0.57)$ ns, compared with $\tau(Ca_2UO_2(CO_3)_3(aq)) = (46.7 \pm 2.7)$ ns.

The extrapolation to infinite dilution using the SIT gave $\log_{10}\beta°_{1.1.3} = 27.20 \pm 0.04$, $\varepsilon(CaUO_2(CO_3)_3^{2-},Na^+) = (0.29 \pm 0.11)$ $kg_w\ mol^{-1}$ for $CaUO_2(CO_3)_3^{2-}$ and $\log_{10}\beta°_{2.1.3} = 30.49 \pm 0.05$, $\varepsilon(Ca_2UO_2(CO_3)_3(aq),NaCl) = (0.66 \pm 0.12)\ kg_w\ mol^{-1}$. for $Ca_2UO_2(CO_3)_3(aq)$. The stability constants are consistent with previously reported data. Conversely, the values of the specific ion interaction coefficients $\varepsilon(CaUO_2(CO_3)_3^{2-},Na^+)$ and $\varepsilon(Ca_2UO_2(CO_3)_3(aq),NaCl)$ are strongly positive and markedly different from the previous estimation by analogy from like-charged ions.

This work highlighted the interference of the background ions in the formation of $Ca_nUO_2(CO_3)_3^{(4-2n)-}$ (n = {1;2}) and explained the importance of knowing their roles.

VII - 2 Study of $Ca_nUO_2(CO_3)_3^{(4-2n)-}$ complexes in $NaClO_4$

Similar study at higher ionic strength was thus performed in $NaClO_4$ medium owing to its less important quenching effect than NaCl on triscarbonatouranyl units. The range of ionic strength was extended to 2.46 mol kg_w^{-1}, while a high [ClO_4^-] *ca.* 3.50 mol kg_w^{-1} could still induce quenching effects towards $Ca_nUO_2(CO_3)_3^{(4-2n)-}$ complexes. The specific ion interaction coefficients were estimated to be $\varepsilon(CaUO_2(CO_3)_3^{2-},Na^+)$ = (0.02 ± 0.04) $kg_w\ mol^{-1}$ and $\varepsilon(Ca_2UO_2(CO_3)_3(aq),NaClO_4)$ = (0.18 ± 0.07) $kg_w\ mol^{-1}$. These latter values were different from the ones obtained in NaCl.

Several modified models based on the SIT approach were applied to better represent our experimental data and examine the dependence of interaction coefficients on ionic strength. We estimated a reliable prediction of thermodynamic constants up to 3 mol kg_w^{-1}. In a larger range of ionic strength, the ion associations, *e.g.*, Na^+-$UO_2(CO_3)_3^{4-}$, Na^+-$CaUO_2(CO_3)_3^{2-}$, and Ca^{2+}-ClO_4^-/Cl^-, could contribute to increasing ion-pairing formations where the activity coefficient should be estimated by the Pitzer model with better accuracy. This work provides valuable information to address the interaction effects between Ca-UO_2-CO_3 species and 1:1 type electrolytes. The differences in $\Delta\varepsilon$ in NaCl and $NaClO_4$ may partly be explained by the ion triplet interactions of Na^+-Ca^{2+}-ClO_4^-/Cl^- that could reduce the activity of Ca^{2+} to different degrees depending on the kind of anion with increasing ionic strengths. It is suggested that the affinity of the cation in background electrolyte with $Ca_nUO_2(CO_3)_3^{(4-2n)-}$ (n = {1;2}) are to be taken into consideration at high ionic strengths, especially for the globally non-charged species.

VII - 3 Study of $MgUO_2(CO_3)_3^{2-}$ complex in $NaClO_4$ and NaCl and applications to different geochemical contexts.

As the $\log_{10}\beta_{n.1.3}$ *vs.* I_m functions displayed remarkably different patterns for $Ca_nUO_2(CO_3)_3^{(4-2n)-}$ complexes in NaCl and $NaClO_4$, we proposed new determinations of thermodynamic constants for $Mg_nUO_2(CO_3)_3^{(4-2n)-}$ complexes in these two media by the same method. A slope *ca.* 1 was obtained in the linear correlation at ionic strength 0.1 to 1 mol kg_w^{-1} NaCl and 0.1 to 2.21 mol kg_w^{-1} $NaClO_4$, indicating the formation of $MgUO_2(CO_3)_3^{2-}$, while the expected presence of $Mg_2UO_2(CO_3)_3(aq)$ cannot be identified.

The simultaneous fitting with a common value of $\log_{10}\beta°_{1.1.3}$ was performed on the two datasets of (I_m, $\log_{10}\beta_{1.1.3} + 16D_H$) in NaCl and $NaClO_4$. The common formation constant was determined as $\log_{10}\beta°_{1.1.3} = 26.40 \pm 0.07$ with $\varepsilon(MgUO_2(CO_3)_3^{2-}, Na^+) = 0.19 \pm 0.11$ $kg_w\ mol^{-1}$ in $NaClO_4$ and $\varepsilon(MgUO_2(CO_3)_3^{2-},Na^+) = 0.09 \pm 0.16$ $kg_w\ mol^{-1}$ in NaCl. The decay-times were determined for $MgUO_2(CO_3)_3^{2-}$ in different electrolyte conditions and compared with those for $Ca_nUO_2(CO_3)_3^{(4-2n)-}$ complexes. The steric hindrance effects of Mg^{2+} in complexation with $UO_2(CO_3)_3^{4-}$ draw our attention.

As a result, the binding processes of Mg^{2+} and Ca^{2+} with $UO_2(CO_3)_3^{4-}$ should not be estimated to the binary stage alone. Still, the ion-pairs formations between Mg^{2+}/Ca^{2+} and the medium anion were supposed to have comparable quantitative effects on the complexation of Mg^{2+}/Ca^{2+} with $UO_2(CO_3)_3^{4-}$, resulting in the close values of interaction coefficients for $MUO_2(CO_3)_3^{2-}$ in a given electrolyte.

Then the applications of the determined data for $MUO_2(CO_3)_3^{2-}$ to several representative geochemical contexts stressed out the necessity to account for the $MgUO_2(CO_3)_3^{2-}$ complex in theoretical speciation calculation. Particularly when the ratio of magnesium over calcium approaches or overpasses the ratio of the formation constants.

VII - 4 Effect of temperature on the formation of $MUO_2(CO_3)_3^{2-}$

The complexation of triscarbonatouranyl(VI) with Ca^{2+} and Mg^{2+} were then studied by TRLFS at I_m = 0.1 mol kg_w^{-1} NaCl in the temperature range 10-50°C and 5-30°C, respectively. At a specified temperature, the spectra showed an increase in the emission intensity with increasing alkaline earth metal concentrations, which indicated the successive complexation of Mg^{2+}/Ca^{2+} to $UO_2(CO_3)_3^{4-}$ and allowed the determination of their formation constants. As temperature increases, the global amplitude of intensity suffered a pronounced decrease and in particular, at high temperatures, *i.e.*, 40, 45, and 50°C, the spectra showed slight shifts to higher wavelengths at the beginning of the complexation that allowed sorting out individual spectra of involved species using singular value decomposition (SVD) and supplemental calculation.

Different approximation models were adjusted to the evolution of formation constants of $M_nUO_2(CO_3)_3^{(4-2n)-}$ as a function of temperature. We concluded that the entropy term contributes primarily to the formation of $MgUO_2(CO_3)_3^{2-}$ and $CaUO_2(CO_3)_3^{2-}$ and the enthalpy contribution to these reactions may be both assumed to be almost nil due to the high uncertainties in fitting results. The second complexation of $CaUO_2(CO_3)_3^{2-}$ by Ca^{2+} contributed to an exothermic process with a less important entropy value for molecular structural reasons.

Coupled influence of temperature and ionic strength on $M_nUO_2(CO_3)_3^{(4-2n)-}$ complexation were analyzed for nuclear waste repositories scenarios—the Boom clay and the Callovo-Oxfordian (COx) clay in combination with previous data. Our simulation results suggested the predominance of $U(OH)_4(aq)$ in the temperature range of 40-60°C in the COx and Mol reference waters. In a longer term, the temperature around the cell would decrease to around 20°C, thus the uranium migration would be promoted because of $Ca_nUO_2(CO_3)_3^{(4-2n)-}$ predominance in the COx and Mol waters.

VII - 5 Analysis of $M_nUO_2(CO_3)_3^{(4-2n)-}$ in the natural water compositions

A number of natural water compositions were collected from the literature available on the subject of uranium mining and environmental monitoring activities. We only considered the water compositions that are showing $Ca_nUO_2(CO_3)_3^{(4-2n)-}$ as major complex after speciation calculation using the PHREEQC with all the previously determined thermodynamic constants $-\log_{10}\beta°$, $\Delta_fH_m°$ and SIT parameters, ε for $Mg/Ca_nUO_2(CO_3)_3^{(4-2n)-}$ complexes implemented in PRODATA 1.1.0.4 database. The ellipsoidal boundaries of $UO_2CO_3(aq)$, $CaUO_2(CO_3)_3^{2-}$, and $Ca_2UO_2(CO_3)_3(aq)$ were determined from the distribution of sample points in $\log_{10}(a(Ca^{2+})/a(H^+)^2)-\log_{10}(a(Na^+)/a(H^+))-\log_{10}(a(HCO_3^-)\,a(H^+))$ diagram. The determination of ellipsoids for $Ca_nUO_2(CO_3)_3^{(4-2n)-}$ complexes is a suitable tool for quickly identifying the dominant species for a given natural water sample once its chemical composition is available.

Two water samples were collected from the Lodève site by ORANO Mining. The two natural occurring water samples both delivered a measurable luminescence signal, which is characteristic for uranyl carbonate luminescence. With their detailed chemical compositions, the dominant species determined by theoretical speciation calculations corroborated well the measured luminescent properties by TRLFS.